Com SIS
Computer Science and Information Systems
Volume 22, Number 1, January 2025

Contents

ISSN: 2406-1018 (Online)

Computer Science and Information Systems
Vol 22, No 1, January 2025

Com SIS

Computer Science and Information Systems

Published by ComSIS Consortium

Volume 22, Number 1
January 2025

ComSIS is an international journal published by the ComSIS Consortium

ComSIS Editorial Office:
University of Novi Sad, Faculty of Sciences,
Department of Mathematics and Informatics
Trg Dositeja Obradovića 4, 21000 Novi Sad, Serbia
Phone: +381 21 458 888; **Fax:** +381 21 6350 458
www.comsis.org; Email: comsis@uns.ac.rs

Volume 22, Number 1, 2025
Novi Sad

Computer Science and Information Systems

ISSN: 2406-1018 (Online)

The ComSIS journal is sponsored by:

Ministry of Education, Science and Technological Development of the Republic of Serbia
http://www.mpn.gov.rs/

Computer Science and Information Systems

AIMS AND SCOPE

Computer Science and Information Systems (ComSIS) is an international refereed journal, published in Serbia. The objective of ComSIS is to communicate important research and development results in the areas of computer science, software engineering, and information systems.

We publish original papers of lasting value covering both theoretical foundations of computer science and commercial, industrial, or educational aspects that provide new insights into design and implementation of software and information systems. In addition to wide-scope regular issues, ComSIS also includes special issues covering specific topics in all areas of computer science and information systems.

ComSIS publishes invited and regular papers in English. Papers that pass a strict reviewing procedure are accepted for publishing. ComSIS is published semiannually.

Indexing Information

ComSIS is covered or selected for coverage in the following:

- Science Citation Index (also known as SciSearch) and Journal Citation Reports / Science Edition by Thomson Reuters, with 2023 two-year impact factor 1.2,
- Computer Science Bibliography, University of Trier (DBLP),
- EMBASE (Elsevier),
- Scopus (Elsevier),
- Summon (Serials Solutions),
- EBSCO bibliographic databases,
- IET bibliographic database Inspec,
- FIZ Karlsruhe bibliographic database io-port,
- Index of Information Systems Journals (Deakin University, Australia),
- Directory of Open Access Journals (DOAJ),
- Google Scholar,
- Journal Bibliometric Report of the Center for Evaluation in Education and Science (CEON/CEES) in cooperation with the National Library of Serbia, for the Serbian Ministry of Education and Science,
- Serbian Citation Index (SCIndeks),
- doiSerbia.

Information for Contributors

The Editors will be pleased to receive contributions from all parts of the world. An electronic version (LaTeX), or three hard-copies of the manuscript written in English, intended for publication and prepared as described in "Manuscript Requirements" (which may be downloaded from http://www.comsis.org), along with a cover letter containing the corresponding author's details should be sent to official journal e-mail.

Criteria for Acceptance

Criteria for acceptance will be appropriateness to the field of Journal, as described in the Aims and Scope, taking into account the merit of the content and presentation. The number of pages of submitted articles is limited to 20 (using the appropriate LaTeX template).

Manuscripts will be refereed in the manner customary with scientific journals before being accepted for publication.

Copyright and Use Agreement

Computer Science and Information Systems

Volume 22, Number 1, January 2025

CONTENTS

Computer Science and Information Systems 22(1): i–iii https://doi.org/10.2298/CSIS250100iI

Editorial

Mirjana Ivanović, Miloš Radovanović, and Vladimir Kurbalija

University of Novi Sad, Faculty of Sciences
Novi Sad, Serbia
{mira,radacha,kurba}@dmi.uns.ac.rs

Starting the new year of 2025, this first issue of Volume 22 of Computer Science and Information Systems consists of 17 regular articles. We are grateful for the continuing hard work and enthusiasm of all our authors and reviewers, without whom the publication of the current issue and the journal itself would not be possible.

The first regular article, "Segmentation of COVID-19 CT Lesions in CT Scans through Transfer Learning" by Symeon Psaraftis-Souranis et al., propose a novel deep learning framework designed for the segmentation of lesions evident in Computed Tomography (CT) scans. The results suggest that the incorporation of transfer learning, combined with appropriate pre-processing techniques, can contribute to achieving state-of-the-art performance in the segmentation of lesions associated with SARS-CoV-2 infections.

In the second regular article, "Topic-oriented Sarcasm Detection via Entity Knowledge-based Prompt Learning," Yuhao Zhou et al. investigate an Entity Knowledge-based Prompt Learning (EKPL) model that combines prompt learning and entity knowledge from knowledge graphs for topic-oriented sarcasm detection. Experimental results illustrate that the EKPL model exhibits good performance in the topic-oriented sarcasm detection task.

"A New Course Difficulty Index (*CDf*): Framework and Application," by Konstantinos Kelesidis et al. proposes new framework for the quantification of course difficulty in academic curricula. For each course, course difficulty index value (*CDf*) is computed using difficulty indicators that characterize the course as a whole. The difficulty indicators can be tailored to reflect the academic domain considered. The proposed framework and analysis represent a useful tool for academic policy-making and quality assurance.

Zhimin Feng et al., in "Anomalous Traffic Identification Method for POST Messages Based on Gambling Website Templates," propose a POST traffic classification method based on website templates to identify abnormal traffic from gambling websites. POST message data is collected from several gambling sites, extracting features and creating a Gambling Website Single POST Message Dataset (GSPD). Word2Vec, TF-IDF, hierarchical clustering, support vector machines and particle swarm optimization are utilized to achieve excellent performance on the evaluated test set.

"Formal Transformation of OWL Ontology to a FOKI Generic Meta-Model," authored by Bogumila Hnatkowska et al. presents a meta-model and a set of transformation rules for bi-directional transformation between ontologies expressed in the authors' FOKI framework (which does not use OWL) from previous work, and the OWL standard. The meta-model serves as a bridge in the transformation process. The correctness of the obtained transformation rules was verified on widely available ontologies expressed in OWL.

The article "Multilingual Pretrained based Multi-feature Fusion Model for English Text Classification," by Ruijuan Zhang proposes a novel multilingual pre-training based

multi-feature fusion method for English text classification (MFFMP-ETC) to tackle two challenges faced by current deep-learning approaches: (1) effectively capturing long-range contextual structure information within text sequences, and (2) adequately integrating linguistic knowledge into representations. Results on three datasets show that MFFMP-ETC introduces a new baseline in terms of accuracy, sensitivity, and precision.

In their article entitled "TPBoxE: Temporal Knowledge Graph Completion based on Time Probability Box Embedding," Song Li et al. address the challenges in temporal graph completion of making effective use of special relationships between relations and time series information, and difficulties in fully representing the complex relationships existing in the graph. The proposed model based on time probability box embedding, TPBoxE, is experimentally shown to exhibit better performance than existing state-of-the-art models.

Yong Ren et al., in their article "A Lightweight defect classification Method for Latex Gloves Based on Image Enhancement," present a glove defect classification method that integrates image enhancement techniques with a lightweight model to enhance the efficiency and accuracy of glove defect classification in industrial manufacturing. Experimental results demonstrate that the proposed MobileNetV2 model achieves excellent accuracy, effectively mitigating overfitting phenomena, and exhibits significantly faster training speed compared to the ResNet34 and ResNet50 models.

In "ASAM: Asynchronous Self-Attention Model for Visual Question Answering," Han Liu et al. propose the asynchronous self-attention model (ASAM) that makes use of an asynchronous self-attention component and a controller, integrating the asynchronous self-attention mechanism and collaborative attention mechanism effectively to leverage the rich semantic information of the underlying visuals in addition to textual information, for the task of visual question answering. Experimental evaluation demonstrates that the proposed model outperforms the state-of-the-art, without increasing model complexity and the number of parameters.

In their article "Medical Images Anomaly Detection for Imbalanced Datasets with Multi-scale Normalizing Flow," Yufeng Xiao et al. propose a novel unsupervised medical image detection model named Multi-Scale Normalizing Flow (MS-NF), in order to tackle the large number of features and parameters for the task of anomaly detection in medical images. After extracting multi-scale feature maps and normalizing flow to transfer the anomalies into a normal distribution in the latent space, channel and spatial convolutional attention mechanisms are integrated into the model. Experimental results show that MS-NF improves the pixel-level AUC index by 9% compared to existing medical image detection models.

"PSBD-EWT-EGAN: Heart Sound Denoising Using PSBD-EWT and Enhancement Generative Adversarial Network," by Jianqiang Hu et al., presents a heart sound signal (HSS) denoising method which uses Parameterless Scale-space Boundary Detection (PSBD), the Empirical Wavelet Transform (EWT) and Enhanced Generative Adversarial Network (EGAN) to remove noise signals that corrupt HSSs. Experimental results show that the proposed method achieves significant improvements over the state-of-the-art.

In their article entitled "Academic Research on Fuzzy Systems: A Country and Regional Analysis from its Origins in 1965 to 2023," Carlos J. Torres-Vergara et al. present a bibliometric study encompassing 185,673 documents from the Web of Science, that explores tendencies and trends, and identifies the most prolific and important countries in

fuzzy systems research and its evolution. Since its inception in 1965, the field has grown significantly, with its epicentre originally in the USA and England, and moving first to Europe and then to Asia, following global trends in other fields of study.

The article "Mapping-Based Approach to Integration of Technical Spaces," by Vladimir Dimitrieski et al. address software integration issues and introduce a novel mapping-based approach for structured, automated, and reusable integration of software components and systems. An automated development process for the integration adapters at a higher level of abstraction is presented, based on model-driven software development principles. A tool called AnyMap is introduced, as well as a visual domain-specific modeling language for specifying mappings and generating adapters, with the approach demonstrated on a practical use case.

Congyin Cao et al., in their article "Linear Projection-Based Noise Filtering Framework for Image Denoising," tackle the challenges of image denoising approaches related to incorporating crucial structural information from perspectives other than local space, such as local manifolds and global structures, by proposing a novel linear projection-based noise filtering (LPNF) framework grounded in linear projection learning theory. The framework learns a linear projection for noise filtering by incorporating multiple structural information sources: local spatial, local manifold, and global structures.

In "Multimodal Deep Learning-based Feature Fusion for Object Detection in Remote Sensing Images," Shoulin Yin et al. propose a multimodal deep learning-based feature fusion for object detection in remote sensing images. In the new model, a cascade region-based convolutional neural network (RCNN) is the backbone network, while a parallel cascade RCNN network is utilized for feature fusion to enhance feature expression ability. In order to solve the problem of different segmentation shapes and sizes, the central part of the network adopts multi-coefficient cascaded hollow convolution to obtain multi-receptive field features without using pooling and preserving image information.

In their article "Improved Session Recommendation Using Contrastive Learning based Tail Adjusted Repeat Aware Graph Neural Network," Daifeng Li et al. study the interactions between users and items in session-based recommender systems from a new perspective. A novel contrastive learning based tail adjusted repeat aware graph neural network (CLTAR-GNN) is proposed to tackle the problems of long-range dependencies, order information loss, and data sparsity. A tail adjusted repeat (TAR) mechanism captures users' repeat-explore behaviors in both short-head and long-tail session items, while a self-attention (SA) network with position embedding is incorporated to overcome sequence information loss issues.

Finally, "Unraveling the Organisational Debt Phenomenon in Software Companies," by Muhammad Ovais Ahmad et al. assesses the extent of knowledge, factors, and consequences of organizational maladjustment in software organizations. A survey performed in three organizations identified several highly visible issues such as complex code, inconsistent UI, unclear requirements, and outdated processes. These themes often emerge due to exponential growth, prioritizing speed over quality, lack of cooperation and coordination, and outdated processes.

Computer Science and Information Systems 22(1):1–32 https://doi.org/10.2298/CSIS240229066P

Segmentation of COVID-19 Lesions in CT Scans through Transfer Learning

Symeon Psaraftis-Souranis[1], Christos Troussas[1], Athanasios Voulodimos[2], and Cleo Sgouropoulou[1]

[1] Department of Informatics and Computer Engineering,
University of West Attica, Egaleo 12243, Greece
{cs141049, ctrouss, csgouro}@uniwa.gr
[2] School of Electrical and Computer Engineering,
National Technical University of Athens, Athens 15780, Greece
thanosv@mail.ntua.gr

Abstract. Since its emergence at the end of 2019, SARS-CoV-2 has infected millions worldwide, challenging healthcare systems globally. This has prompted many researchers to explore how machine learning can assist clinicians in diagnosing infections caused by SARS-CoV-2. Building on previous studies, we propose a novel deep learning framework designed for segmenting lesions evident in Computed Tomography (CT) scans. For this work, we utilized a dataset consisting of 20 CT scans annotated by experts and performed training, validation, and external evaluation of the deep learning models we implemented, using a 5-fold cross-validation scheme. When splitting data by slice, our optimal model achieved noteworthy performance, attaining a Dice Similarity Coefficient (DSC) and Intersection over Union (IoU) score of 0.8644 and 0.7612 respectively, during the validation phase. In the external evaluation phase, the model maintained strong performance with a DSC and an IoU score of 0.7211 and 0.5641, respectively. When splitting data by patient, our optimal model achieved a DSC score of 0.7989 and an IoU score of 0.6686 during the validation phase. During the external evaluation phase, the model maintained strong performance with a DSC and IoU score of 0.7369 and 0.5837, respectively. The results of this research suggest that incorporating transfer learning along with appropriate preprocessing techniques, can contribute to achieving state-of-the-art performance in the segmentation of lesions associated with SARS-CoV-2 infections.

Keywords: computer vision, machine learning, deep learning, transfer learning, convolutional neural networks, COVID-19, semantic segmentation, medical imaging, computed tomography.

1. Introduction

According to the World Health Organization, since the first detection of SARS-CoV-2, there have been more than 771 million confirmed cases of COVID-19 infection, of which nearly 7 million cases have resulted in death [1]. Early detection and diagnosis of COVID-19 are key factors in limiting the spread of the virus [2]. Diagnostic tests remain the most common method to detect SARS-CoV-2, with Reverse Transcription

Polymerase Chain Reaction (RT-PCR) tests being the most reliable. However, the fact that they are time-consuming is a significant disadvantage, especially regarding this particular virus, where early diagnosis plays a vital role in successful treatment [2].

The study of medical images, such as CT scans, constitutes a valuable approach for identifying COVID-19 by detecting pathological findings associated with lower respiratory tract infections (pneumonia) [3]. Medical imaging is widely used by specialists as a diagnostic tool for SARS-CoV-2 associated pneumonia, with CT scans providing much higher diagnostic accuracy, as they can identify incipient lesions in the lung parenchyma that cannot be discerned on plain chest X-rays [4].

Through the review of medical images, clinicians can assess the health status of each patient and, if concerning findings are discovered, make the correct diagnosis and follow the appropriate treatment. However, while the process of reviewing medical images by healthcare professionals often leads to correct and timely detection, diagnosis, and treatment, 40-54% of malpractice cases attributable to medical radiologists are associated with errors in interpreting medical images [5].

Given these challenges, leveraging machine learning techniques for the analysis of medical images can be a valuable tool for the early and accurate detection and diagnosis of COVID-19 infections.

The COVID-19 outbreak has resulted in increased interest in how machine learning techniques can contribute to the process of analyzing medical images to detect COVID-19 infections. Consequently, since the start of the COVID-19 pandemic, a multitude of scientific papers featuring noteworthy results have been consistently published by experts in the field of machine learning. The large volume of relevant papers indicates that this research area remains active, which is understandable given the ongoing presence of COVID-19. The opportunities for research in this area, along with the continued interest of the scientific community, motivated our engagement with this specific research topic.

In this work, we investigate the applicability of deep learning techniques for detecting and isolating lesions associated with COVID-19 pneumonia. Our contributions can be enumerated as follows:

- We utilized a segmentation architecture called U-Net [6], which we trained and evaluated using a publicly available dataset. Subsequently, we applied transfer learning principles to train and evaluate variations of the U-Net architecture, replacing the encoder with a pre-trained CNN model. Finally, we compared their performance with the basic U-Net architecture.
- We evaluated the impact of data preprocessing on the performance of the models used in this work. Specifically, we trained the selected architectures on CT slices that were normalized in terms of contrast and brightness, and then segmented to retain only the information within the lung parenchyma for each slice. While contrast and brightness normalization are standard practices, our contribution lies in the systematic integration of these techniques within a deep learning framework tailored for detecting lesions associated with COVID-19 pneumonia. This preprocessing approach proved crucial in achieving state-of-the-art results, demonstrating its effectiveness in enhancing model accuracy and reliability.

The rest of the article is organized as follows: Section 2 provides an overview of related work on COVID-19 lesion segmentation. Section 3 explains the methodology used in this research. In Section 4, we present and discuss the results of the conducted

experiments and compare them with state-of-the-art approaches. Finally, in Section 5, we draw conclusions from this research.

2. Related Work

This section provides an overview of the related literature on COVID-19 lesion segmentation in CT scans. To better present the findings, Table 1 summarizes the work conducted by other researchers that is relevant to this research paper. It can be seen that the U-Net architecture is the most popular approach used to address this problem. Furthermore, it is noteworthy that among the approaches detailed in Table 1, only three make use of the transfer learning technique. This observation underscores that the utilization of transfer learning in the context of COVID-19 lesion segmentation on CT scans has not been extensively explored within the existing literature.

Table 1. Summary of the existing literature related to our proposed work

Model Architecture	Training and Validation Dataset	External Evaluation Dataset	Preprocessing & Transfer Learning	Validation Results	External Evaluation Results
Ma et al. [7] 2D U-Net	COVID-19-CT-Seg [8] (5-fold cross-validation Train: 20% Val: 80%)	-	HU Clipping [-1250, 250], No Transfer Learning	DSC: 60.80%	-
Ma et al. [7] nnU-Net [9]	COVID-19-CT-Seg (5-fold cross-validation Train: 20% Val: 80%)	MosMed [10]	HU Clipping [-1250, 250], No Transfer Learning	DSC: 67.30%	DSC: 58.80%
Müller et al. [11] 3D U-Net [12]	COVID-19-CT-Seg (5-fold cross-validation Train: 80% Val: 20%)	-	HU Clipping [-1250, 250], No Transfer Learning	DSC: 76.10%	-
Müller et al. [13] 3D U-Net	COVID-19-CT-Seg (5-fold cross-validation Train: 80% Val: 20%)	An et al. [14]	HU Clipping [-1250, 250], Data Augmentation, No Transfer Learning	DSC: 80.40%	DSC: 66.10%
Owais et al. [15] DAL-Net	Experiment 1: COVID-19-CT-Seg (5-fold cross-validation Train: 80% Val: 20%) Experiment 2: MosMed (5-fold cross-validation Train: 80% Val: 20%) Experiment 3: COVID-19-CT-Seg	Experiment 3: MosMed	Experiment 3: Reinhard Transformation [16], No Transfer Learning	Experiment 1: DSC: 83.23% IoU: 74.86% Experiment 2: DSC: 68.63% IoU: 61.35%	Experiment 3: DSC: 74.93% IoU: 66.50%

Zheng et al. [17] 3D CU-Net	COVID-19-CT-Seg (5-fold cross-validation Train: 80% Val: 20%)	MosMed	HU Clipping [-1250, 250], Data Augmentation, No Transfer Learning	DSC: 77.80%	DSC: 66.80%
Yixin Wang et al. [18] 3D U-Net	COVID-19-CT-Seg (5-fold cross-validation Train: 20% Val: 80%)	-	No Transfer Learning	DSC: 70.04%	-
Singh et al. [19] LungINFSeg	COVID-19-CT-Seg (Train: 70% Val: 10% Test: 20%)	-	Data Augmentation, No Transfer Learning	DSC: 80.34% IoU: 68.77%	-
Amara et al. [20] O-Net	COVID-19-CT-Seg (Only 10 CT) (Train: 70% Val: 30%)	MosMed	Image Cropping, Data Augmentation, No Transfer Learning	DSC: 86.60% IoU: 76.40%	DSC: 58.40% IoU: 42.80%
Aswathy et al. [21] 3D U-Net	COVID-19-CT-Seg (Train: 60% Val: 20% Test: 20%)	-	Lung Parenchyma Segmentation, Patchwise Data Augmentation, No Transfer Learning	DSC: 82.00%	
Xiaoyan Wang et al. [22] SSA-Net	Experiment 1: COVID-19-CT-Seg (5-fold cross validation) Experiment 2: MedSeg Dataset [23] (Only 98 CT Slices) (5-fold cross validation)	-	HU Clipping [-1250, 250], No Transfer Learning	Experiment 1: DSC: 65.22% Experiment 2: DSC: 75.40%	-
Krinski et al. [24] Various CNN Models	COVID-19-CT-Seg (5-fold cross validation Train: 80% Val: 20%)	-	Transfer Learning (ImageNet [25])	Best Model DSC: 73.67% Best Model IoU: 70.91%	-
Mahmoudi et al. [26] 2D U-Net	COVID-19-CT-Seg (4-fold cross validation Train: 70% Val: 30%)	-	CLAHE, Image Cropping, Data Augmentation, No Transfer Learning	DSC: 91% IoU: 85%	-
Qiblawey et al. [27] Various CNN Models	COVID-19-CT-Seg (10-fold cross validation Train: 60% Val: 20% Test: 20%)	-	HU Normalization, Lung Parenchyma Segmentation, Data Augmentation, Transfer Learning (ImageNet)	Best Model DSC: 94.13% Best Model IoU: 91.85%	-
Enshaei et al. [28] COVID-Rate	Private Dataset + COVID-19-CT-Seg (Only 10 CT) (10-fold cross-validation Train: 60% Val: 10% Test: 30%)	MedSeg Dataset (Only 9 CT) + COVID-CT-MD [29]	Lung Parenchyma Segmentation, Data Augmentation, No Transfer Learning	DSC: 80.69%	DSC: 79.98%
Uçar et al. [30] U-Net + Various CNN Models as Encoders	MedSeg Dataset (Train: 80% Val: 20% Test: 10% of Training Data)	-	Transfer Learning (ImageNet)	Best Model DSC: 84.04% Majority Voting DSC: 85.03%	-

Building upon the research summarized in Table 1, it becomes apparent that deep learning methods, particularly those employing the U-Net architecture, are widely recognized for their effectiveness in segmenting lesions within CT scans. During our experimental phase, we followed this approach and utilized a 2D U-Net architecture, along with variations where the encoder of the U-Net model was substituted with pre-trained convolutional neural networks.

Each of the previously mentioned research papers employs various methods and pre-processing techniques to provide a more reliable assessment and enhance the performance of the models on the given task. Notably, in [7], [11], [13], [17] and [22], the authors normalize the CT slices by clipping pixel intensities. In [13], [17], [19], [20], [21], [26], [27] and [28], data augmentation is applied. Moreover, in [21], [27] and [28], segmentation of the lung parenchyma is performed and in [24] and [30], the authors leverage transfer learning.

In this work, we combine methods and pre-processing techniques from the aforementioned research papers, to achieve state-of-the-art performance. Specifically, we adopt a technique similar to the one used in [7], [11], [13], [17] and [22] to normalize CT slices in terms of contrast and brightness. Moreover, we apply data augmentation strategies analogous to those performed in [13], [17], [19], [20], [21], [26], [27] and [28]. Additionally, following the approaches in [21], [27] and [28], we perform lung parenchyma segmentation on CT slices. Furthermore, inspired by [24] and [30], we utilize a transfer learning method to train variations of the U-Net model, where the encoder of the network is replaced with a pre-trained convolutional neural network.

3. Materials and Methods

Analyzing medical images to aid in the diagnosis of COVID-19 pneumonia can be framed as a semantic image segmentation problem. In this type of problem, deep learning methods, such as convolutional neural networks, are provided with CT slices alongside corresponding “masks”, which are images where the regions of the CT slices containing lung lesions have been annotated by experts. The networks are then trained using the input data to map the pixels of each CT slice into distinct categories based on the presence or absence of lesions associated with COVID-19 pneumonia.

The framework proposed in this study is illustrated in Figure 1. In the first step, the selected dataset is preprocessed before being fed into each deep learning model. Subsequently, the deep learning models to be used in this work are selected. For our experiment, we chose to employ pre-trained neural networks as the backbone of a classic U-Net model. Following that, the implemented models undergo training and validation. Finally, after the training process is completed, the models’ ability to perform semantic image segmentation is evaluated. Appropriate performance evaluation metrics are used to assess their performance.

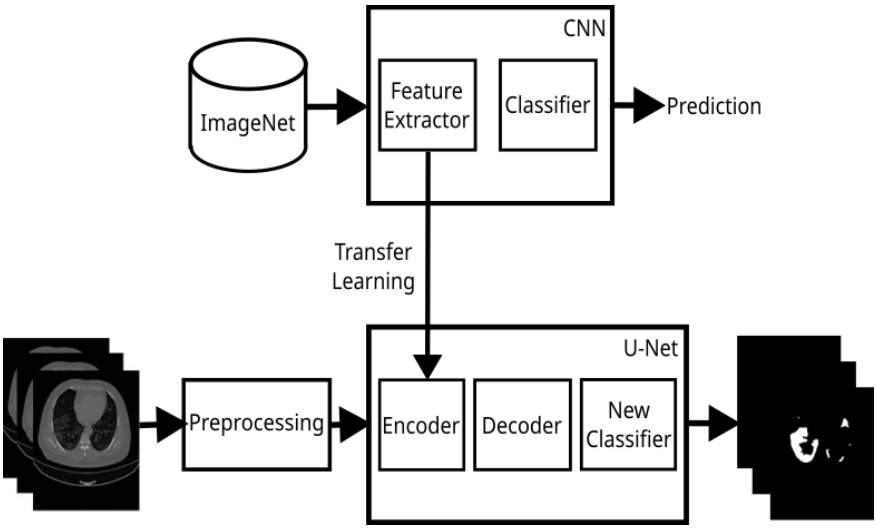

Fig. 1. Block diagram of the proposed method

3.1. Dataset Selection

For this work, we opted to use a publicly available dataset called COVID-19-CT-Seg [7], [8]. This dataset consists of 3,520 CT slices collected from the Coronacases.org [31] and Radiopaedia.org [32] repositories, comprising data from 20 distinct patients [7], [8]. Specifically, 2,581 CT slices originate from 10 patients within the Coronacases.org repository, with the remaining 939 CT slices attributed to the other 10 patients and taken from the Radiopaedia.org repository. Figure 2 illustrates the distribution of CT slices in the two subsets of the COVID-19-CT-Seg dataset.

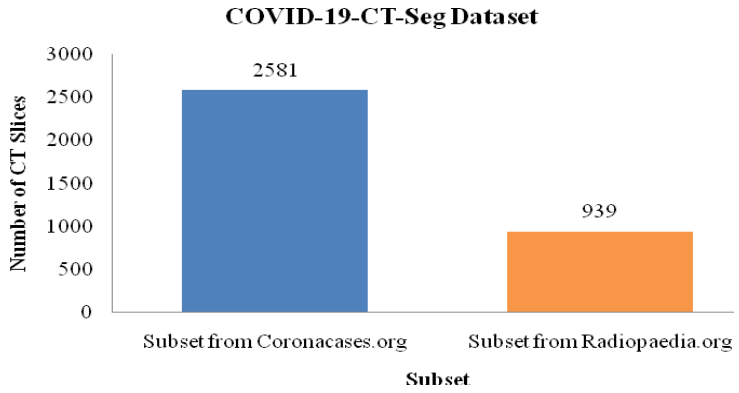

Fig. 2. Bar graph depicting the number of CT slices in the COVID-19-CT-Seg dataset

The creators of this dataset have provided a set of 3,520 masks, in which the lung parenchyma is outlined bilaterally. In addition, they have included another set of 3,520 masks outlining lesions attributed to SARS-CoV-2.

The initial outlining procedure was carried out by two radiologists with 1-5 years of experience [7], [8]. It was then optimized by radiologists with 5-10 years of experience and finally validated and further optimized by a radiologist with over 10 years of experience in respiratory radiology [7], [8].

Each patient's slices are stored in the Neuroimaging Informatics Technology Initiative (NifTI) format. A visual representation of a subset of the COVID-19-CT-Seg dataset, alongside corresponding masks outlining lesions attributed to SARS-CoV-2, is depicted in Figure 3.

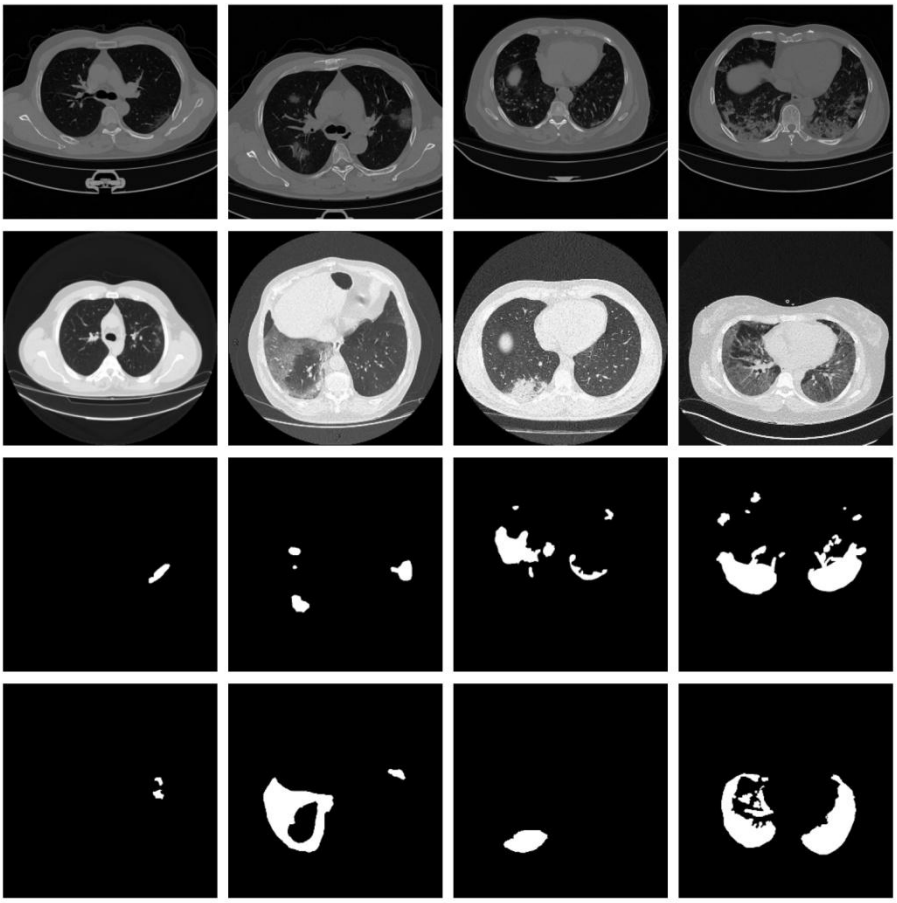

Fig. 3. A subset of CT slices from the COVID-19-CT-Seg dataset, along with their corresponding masks in which areas where lesions attributed to SARS-CoV-2 have been outlined

3.2. Preprocessing

In this section, we list the preprocessing techniques applied to the data before feeding it as input to each of the deep learning models for training and validation. The primary purpose of pre-processing the data is to improve data quality, reduce training time, and produce better results.

In the CT slices, the pixels containing lesions (positive samples) are far fewer than those that do not contain lesions (negative samples). This, combined with the relatively small size of the dataset used in this study, results in class imbalance. To alleviate this problem, we removed CT slices that do not contain lesions.

Therefore, 1,844 slices are retained in the dataset, with 1,351 slices from the Coronacases.org repository and the remaining 492 from the Radiopaedia.org repository. The distribution of CT slices in the two subsets of the COVID-19-CT-Seg dataset is shown in Figure 4. Additionally, since not all CT slices are of the same dimensions, we resize them to 256x256.

The CT slices in the dataset used in this work present significant difference in terms of contrast and brightness. This difference makes the detection of important features for accurate semantic image segmentation difficult. To address this problem, we normalize the CT slices in terms of contrast and brightness. This is achieved by applying a method called “windowing,” where we adjust the parameters Window Width and Window Level of the CT slices to 1400 HU and -500 HU respectively. The choice of these values is not random. According to [33], adjusting Window Width and Window Level to these specific values enhances the visibility of features inside the lung parenchyma, which in turn improves lesion detectability. Moreover, by standardizing the appearance of CT images through the method of “windowing,” variability can be reduced, which improves the generalization and performance of deep learning models. Figure 5 shows a CT slice before and after applying contrast and brightness normalization.

In addition, we normalize the pixel values of the CT slices to the range [0, 1], which is a common practice in deep learning applications. This preprocessing step facilitates convergence during training by ensuring that all pixel values are within a standardized range. This is achieved by dividing the pixel values of the CT slices by 255, which is the maximum pixel value.

The region of interest in a CT slice, examined for lesions attributed to the SARS-CoV-2 virus, is the lung parenchyma. A beneficial practice that enhances the efficiency of the deep learning models used in this work involves the segmentation of CT to preserve only the lung parenchyma in each slice. This can be achieved by utilizing the masks in which the lung parenchyma has been outlined bilaterally. Figure 6 shows a CT slice before and after the segmentation of the lung parenchyma.

To mitigate the risk of overfitting, data augmentation is applied to the data before it is fed into the neural network. Data augmentation is achieved by making slight modifications to the existing data. These modifications consist of combinations of rotation within the range of 0 to 15 degrees, horizontal flipping, and horizontal and vertical translation within the range of 0 to 15%.

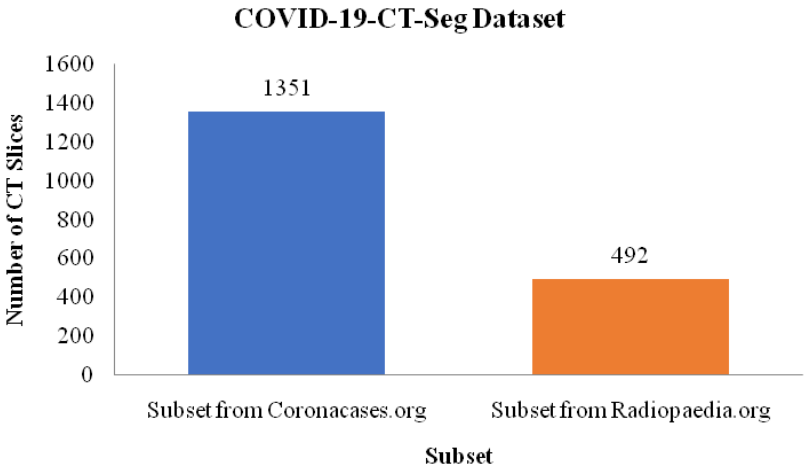

Fig. 4. Number of CT slices in the COVID-19-CT-Seg dataset after removing the slices without lesions

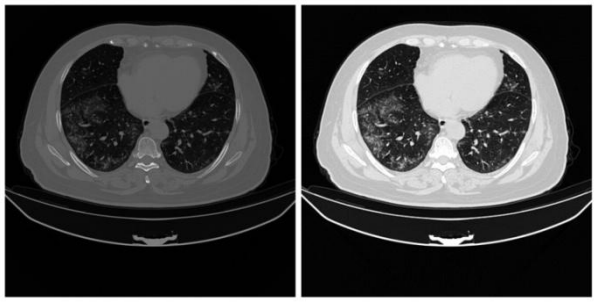

Fig. 5. A CT slice before and after applying contrast and brightness normalization

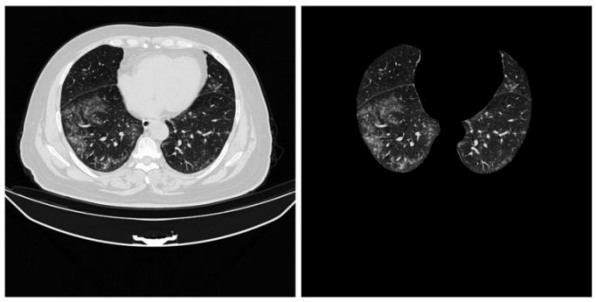

Fig. 6. A CT slice before and after segmenting the lung parenchyma

3.3. Data Splitting

For the purposes of this research paper, we leveraged the 20 CT scans provided in the COVID-19-CT-Seg dataset. Initially, our intention was to train our models using two separate datasets, as exposure to diverse datasets during training can improve a model's robustness. However, due to limited access to public datasets, we chose an alternative approach and opted to use a single dataset sourced from two distinct repositories. To explore this, we employed two different scenarios:

- In the first scenario, a set of 10 CT scans from the Coronacases.org repository, comprising of 2,581 slices, was utilized to construct the training and validation sets for training and evaluation of the deep learning models, respectively. Concurrently, another set of 10 CT scans from the Radiopaedia.org repository encompassing 939 slices, was used as an external evaluation set.
- In the second scenario, the allocation of CT scans was reversed. Here, 10 CT scans from the Radiopaedia.org repository were used to form the training and validation sets, while 10 CT scans from the Coronacases.org repository were designated for the external evaluation set.

The partitioning of data into training and validation subsets was accomplished through a 5-fold cross validation scheme. It is worth mentioning that the splitting into training and validation sets was performed using two distinct approaches:

- At the slice level, where CT slices were randomly split into training and validation sets without any predefined criteria.
- At the patient level, where CT slices were allocated into training and validation sets based on the patient they belonged to.

3.4. Model Selection

This section introduces the deep learning models employed in this research. The models used include the classic U-Net model and variations of it with different "backbones".

Specifically, these U-Net architectures replace the contractive path, or encoder, with convolutional neural networks pre-trained on the ImageNet [25] dataset, thereby leveraging transfer learning. The pre-trained convolutional neural networks selected as the encoder for the U-Net model are the VGG16 [34] and DenseNet121 [35] architectures.

U-Net Architecture. The U-Net architecture, introduced in 2015 by Ronneberger et al., is a convolutional neural network designed for biomedical image segmentation tasks [6]. This network consists of three main components: the contracting path, the bottleneck level, and the expansive path [6]. The contracting path, which acts as the encoder of the network, follows the typical structure of a convolutional neural network [6]. In each block of this path, the spatial dimensions of the images are halved, while the number of the feature channels is doubled [6]. The bottleneck level connects the contracting path to the expansive path [6]. The expansive path, or decoder, consists of blocks where, in each, the spatial dimensions of the images are doubled, and the number of feature channels is halved [6]. The output of each block in the contracting path is concatenated with the input of the corresponding block in the expansive path [6]. This

enables the network to preserve high-resolution features from the contracting path [6]. The implementation of the U-Net model allows it to leverage both high-level and low-level features, contributing to improved segmentation accuracy [6]. Another advantage of the U-Net architecture is that it has a relatively small number of parameters, which results in reduced execution time compared to alternative segmentation methods [6].

U-Net Architecture with the VGG-16 Model as Encoder. In this architectural variation, the traditional encoder is replaced with a pre-trained VGG16 model. The VGG16 model consists of 21 layers organized into five blocks [34]. The bottleneck level of the network acts as the intermediary link connecting the VGG16 model with the decoder. The decoder itself consists of five blocks of layers. Notably, the outputs from the last four blocks of the encoder are concatenated with the inputs of the corresponding first four blocks of the decoder.

U-Net Architecture with the DenseNet121 Model as Encoder. In this architectural variation, the traditional encoder is replaced with a pre-trained DenseNet121 model. The DenseNet121 model begins with a convolutional layer followed by a max pooling layer [35]. It then includes four dense blocks, separated by transition blocks [35]. The decoder consists of five blocks of layers. Notably, the outputs from the convolutional layer and the first three dense blocks of the encoder are concatenated with the inputs of the corresponding first four blocks of the decoder.

3.5. Model Training

The training of the implemented architectures was conducted using the Kaggle [36] platform, leveraging the computational capabilities of an Nvidia Tesla P100 GPU with 16 GB of memory. The models were trained on grayscale images of size 256x256 for 200 epochs, with a learning rate of 0.001. Due to memory constraints, the data were divided into batches and incrementally loaded into memory during each epoch. A batch size of 32 was chosen for this purpose. Additionally, Adam [37] was selected as the optimizer. Regarding fine-tuning, we chose not to freeze any layers of the encoder part of the models during training. This decision was motivated by two reasons: First, the problem addressed in this research significantly differs from the original task for which the CNN models were pre-trained. Training all layers from scratch allows the models to better adapt to the specific characteristics of the new problem. Second, since the dataset used is relatively small, freezing layers might limit the models' ability to learn important features specific to the dataset.

3.6. Model Evaluation

In this section, we detail the methodologies used to evaluate the performance of the models described in the previous section. To assess the models' ability to segment lesions in CT slices and detect overfitting, we implemented a 5-fold cross-validation scheme. Additionally, we used graphical representations to monitor the training and validation processes, aiming to identify the presence of underfitting or overfitting and investigate the models' generalization capabilities. The evaluation also includes key

metrics, namely Precision, Recall, Dice Similarity Coefficient, and Intersection over Union.

Precision, in the context of semantic image segmentation, is defined as the ratio of true positive pixels to the total number of pixels included in the segmentation by the model, as shown in Equation (**1**).

$$\text{Pr}ecision = \frac{TP}{TP + FP} \tag{1}$$

Recall, in the context of semantic image segmentation, is defined as the ratio of true positive pixels to the total of pixels that should have been included in the segmentation by the model, as shown in Equation (**2**).

$$\text{Re}call = \frac{TP}{TP + FN} \tag{2}$$

The Dice Similarity Coefficient, a fundamental metric for evaluating semantic segmentation tasks, is calculated as the harmonic mean of Precision and Recall. This metric measures the spatial overlap between two segmentation regions, A and B, as shown in Equation (**3**).

$$DSC(A,B) = \frac{2|A \cap B|}{|A| + |B|} = \frac{2TP}{2TP + FP + FN} \tag{3}$$

Intersection over Union, another fundamental metric for evaluating semantic segmentation tasks, measures the spatial overlap between two segmentation regions, A and B, as shown in Equation (**4**).

$$IoU(A,B) = \frac{|A \cap B|}{|A \cup B|} = \frac{TP}{TP + FP + FN} \tag{4}$$

4. Results and Discussion

To assess the impact of transfer learning on the performance of the U-Net model, we conducted an ablation experiment. This involved training three variants of the U-Net architecture: the standard U-Net model and two modified versions, where the original encoder was replaced with pre-trained models, specifically VGG16 and DenseNet121.

4.1. Results when Splitting Data by Slice

For our initial experiment, we chose to use 10 CT scans obtained from Coronacases.org for both training and validation, while reserving the remaining CT scans from Radiopaedia.org for external evaluation. This split into training and validation sets was performed at the slice level. Table 2 presents the metrics used to assess the performance of the trained models in semantically segmenting lesions associated with COVID-19 pneumonia.

Among the models evaluated, the U-Net + DenseNet121 model demonstrated superior performance on both the validation and external validation datasets, as indicated by higher mean DSC and IoU values. Despite some decline in performance on the external validation set, all models maintained competitive results.

When comparing the models' performance on the validation data with their performance on the external evaluation data, it is evident that the evaluation metric values are higher in the former than in the latter. This outcome is expected, considering that the external validation dataset contains previously unseen data. Therefore, it is reasonable that the models do not perform as well on this "unknown" dataset. Moreover, the validation set is used during the training process to tune each network's parameters, which may lead the models to learn features specific to that set and, thus perform better on it, despite not being explicitly trained on that specific dataset.

Notably, all models achieved high mean Precision and Recall on the validation set. Higher Precision indicates a lower false positive rate, meaning the model is less likely to incorrectly identify non-lesion regions as lesion-containing areas. Higher Recall implies that the model can effectively identify actual lesions.

In the case of external evaluation, a notable difference between Precision and Recall values is apparent. Although Precision slightly decreased compared to the validation set, Recall exhibited a more significant reduction. A lower Recall suggests that the model is more likely to miss identifying actual lesion regions.

Table 2. Ablation study results when evaluating variations of the U-Net architecture on the validation and external validation sets, with data split at the slice level. Training and validation utilized 10 CT scans sourced from the Coronacases.org repository, while the external validation set comprised the remaining 10 CT scans from the Radiopaedia.org repository

Model	Validation Mean DSC	Validation Mean IoU	Validation Mean Precision	Validation Mean Recall	External Mean DSC	External Mean IoU	Externa Mean Precision	External Mean Recall
U-Net	0.8423 ± 0.0131	0.7277 ± 0.0194	0.8312 ± 0.0267	0.8545 ± 0.0195	0.6587 ± 0.0396	0.4921 ± 0.0435	0.8321 ± 0.0269	0.5487 ± 0.0631
U-Net + VGG16	0.8573 ± 0.0072	0.7503 ± 0.0111	0.8489 ± 0.0120	0.8661 ± 0.0140	0.7118 ± 0.0165	0.5528 ± 0.0200	0.8190 ± 0.0171	0.6305 ± 0.0325
U-Net + DenseNet121	0.8644 ± 0.0091	0.7612 ± 0.0143	0.8597 ± 0.0112	0.8691 ± 0.0094	0.7211 ± 0.0197	0.5641 ± 0.0238	0.8071 ± 0.0450	0.6566 ± 0.0584

Table 3 presents the training and inference times for the models discussed in Table 2. The results show that the U-Net model exhibits the shortest runtime, while the U-Net + DenseNet121 model required the most time. This observation aligns with expectations, as the U-Net + DenseNet121 model includes DenseNet121 as its encoder, a deep and complex model that requires more time to run compared to the standard U-Net model.

Figure 7 illustrates the training and validation curves for the models, the results of which are shown in Table 2. Examination of these curves reveals that all models converge, showing no signs of overfitting.

Table 3. Running times of different variations of the U-Net architecture evaluated with the data split at the slice level. Training and validation used 10 CT scans sourced from the Coronacases.org repository, while the external validation set comprised the remaining 10 CT scans from the Radiopaedia.org repository

Model	Training Time	Validation Time	External Validation Time
U-Net	4577.40 ± 51.57 seconds	1.47 ± 0.08 seconds	2.62 ± 0.15 seconds
U-Net + VGG16	4633.48 ± 17.83 seconds	1.63 ± 0.02 seconds	2.90 ± 0.01 seconds
U-Net + DenseNet121	7807.70 ± 218.71 seconds	2.58 ± 0.05 seconds	4.50 ± 0.098 seconds

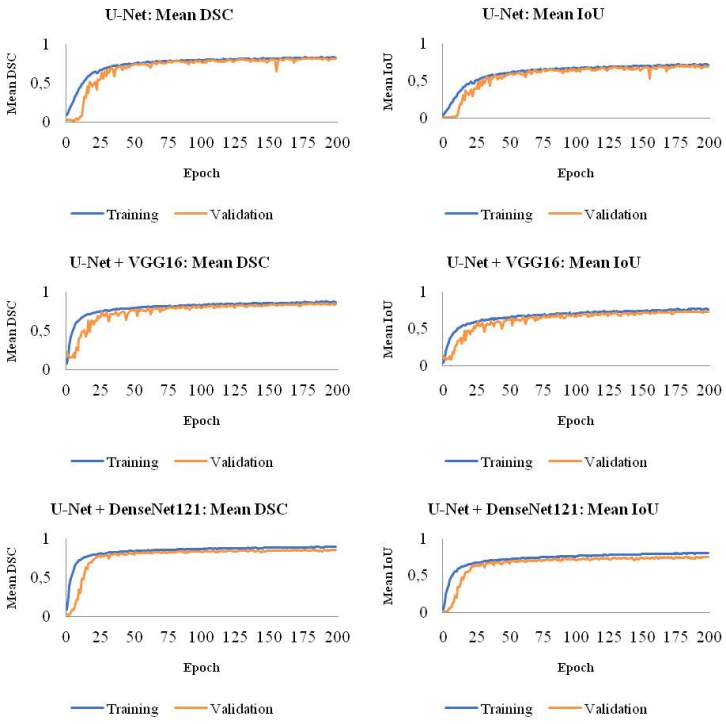

Fig. 7. Training and validation curves for the models trained and evaluated on data split at the slice level. Training and validation used 10 CT scans sourced from the Coronacases.org repository, while the external validation set comprised the remaining 10 CT scans from the Radiopaedia.org repository

In our second experiment, we maintained the data splitting by slice approach, but this time utilized the 10 CT scans taken from Radiopaedia.org for training and validation, and the 10 CT scans from Coronacases.org for external validation.

Upon comparing the model performances, it becomes apparent that the U-Net + DenseNet121 model once again exhibits the highest performance across all metrics in both the validation and external evaluation cases. Notably, a distinct observation arises: the difference in performance between U-Net + DenseNet121 and the other variants is more apparent compared to the corresponding models in Table 2. Given that the dataset sourced from Radiopaedia.org is significantly smaller than the one sourced from Coronacases.org, it seems that U-Net + DenseNet121 performs better than the other two models, particularly in scenarios with limited data availability.

Interestingly, the difference between Precision and Recall values during external evaluation appears to be smaller compared to what was demonstrated in Table 2. This suggests that using the subset sourced from Radiopaedia.org for training and validation, and the subset sourced from Coronacases.org for external evaluation, may lead to models with improved ability to generalize.

Table 4. Ablation study results when evaluating variations of the U-Net architecture on the validation and external validation sets, with data split at the slice level. Training and validation utilized 10 CT scans sourced from the Radiopaedia.org repository, while the external validation set comprised the remaining 10 CT scans from the Coronacases.org repository

Model	Validation Mean DSC	Validation Mean IoU	Validation Mean Precision	Validation Mean Recall	External Mean DSC	External Mean IoU	External Mean Precision	External Mean Recall
U-Net	0.7909 ± 0.0051	0.6541 ± 0.0070	0.7962 ± 0.0253	0.7864 ± 0.0154	0.6546 ± 0.0161	0.4867 ± 0.0180	0.6565 ± 0.0411	0.6559 ± 0.0379
U-Net + VGG16	0.8062 ± 0.0055	0.6753 ± 0.0078	0.7935 ± 0.0241	0.8201 ± 0.0155	0.7152 ± 0.0132	0.5568 ± 0.0159	0.7341 ± 0.0381	0.6991 ± 0.0239
U-Net + DenseNet121	0.8586 ± 0.0068	0.7523 ± 0.0105	0.8568 ± 0.0166	0.8609 ± 0.0158	0.7553 ± 0.0065	0.6069 ± 0.0084	0.7879 ± 0.0235	0.7261 ± 0.0185

Table 5. Running times of different variations of the U-Net architecture evaluated with the data split at the slice level. Training and validation used 10 CT scans sourced from the Radiopaedia.org repository, while the external validation set comprised the remaining 10 CT scans from the Coronacases.org repository

Model	Training Time	Validation Time	External Validation Time
U-Net	1596.20 ± 26.73 seconds	0.53 ± 0.04 seconds	6.47 ± 0.03 seconds
U-Net + VGG16	1805.55 ± 43.33 seconds	0.64 ± 0.05 seconds	7.88 ± 0.02 seconds
U-Net + DenseNet121	3075.20 ± 62.63 seconds	1.15 ± 0.04 seconds	12.17 ± 0.14 seconds

Table 5 showcases the training and inference times for the models discussed in Table 4. The results reveal that, as expected, the U-Net model exhibited the shortest runtime, while the U-Net + DenseNet121 model required the most time. Moreover, the training

and validation times in this case are shorter, and the external validation time is longer compared to those in Table 3. This is expected, as the dataset used for training and validation, sourced from Radiopaedia.org, is notably smaller than the one used for external evaluation.

Figure 8 depicts the training and validation curves corresponding to the models whose results are displayed in Table 4. Upon examining these curves, it is evident that all the models converge, indicating no signs of overfitting.

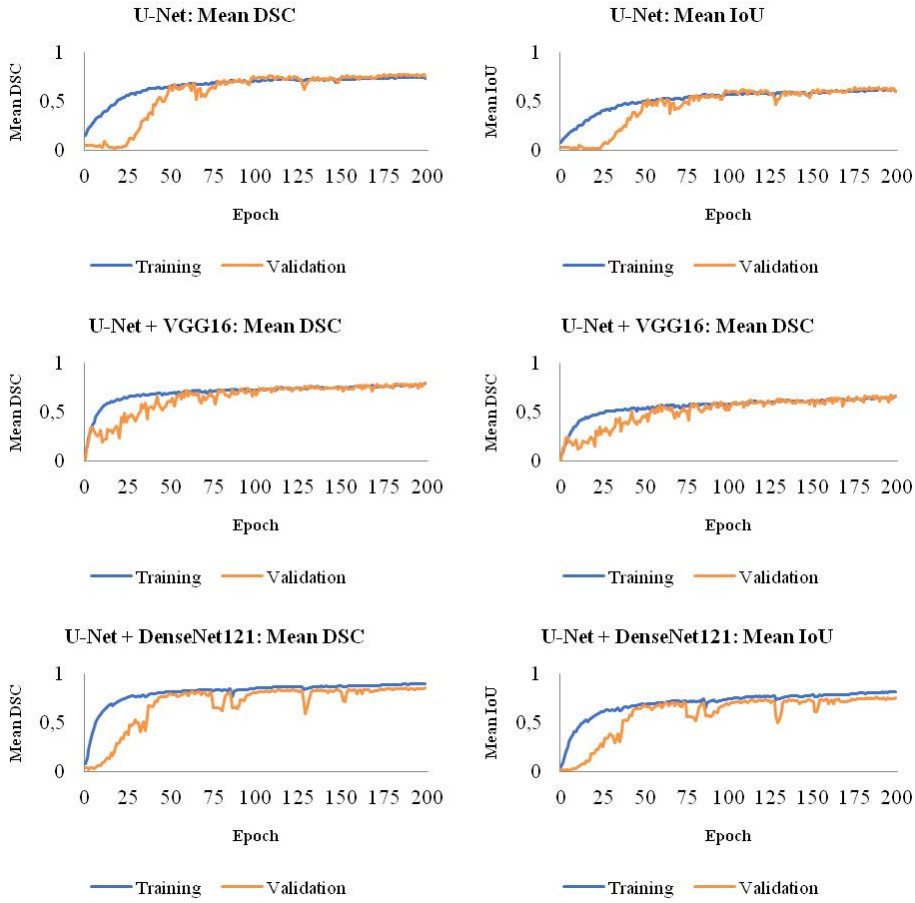

Fig. 8. Training and validation curves for the models trained and evaluated on data split at the slice level. Training and validation utilized 10 CT scans sourced from the Radiopaedia.org repository, while the external validation set comprised the remaining 10 CT scans from the Coronacases.org repository

4.2. Results when Splitting Data by Patient

In this section, we assess the performance of the selected models under a patient-wise data split. For the first experiment, we utilized 10 CT scans from Coronacases.org for training and validation, while 10 CT scans originating from Radiopaedia.org were used for external evaluation. The performance metrics achieved during validation and external evaluation are summarized in Table 6.

Once again, the U-Net + DenseNet121 model exhibits superior performance on both the validation and external evaluation sets. Although the model's performance does not reach the levels observed when trained on data split by slice, it remains satisfactory.

Table 6 shows lower performance metrics compared to Table 2. It is important to note that Table 2 contains performance metrics obtained from models trained using a slice-wise data split, whereas here we have opted for a patient-wise data split. When data are split by slice, the training and validation sets contain more diverse data, which often leads to improved generalization during training. In contrast, when splitting data by patient, the limited number of patients poses challenges due to insufficient training data for the model to learn patterns and relationships. Furthermore, lower performance metrics when splitting by slice could be associated with data leakage [38], a phenomenon where information from the validation or test set is used during the training phase, potentially overestimating model performance [38].

Consistent with the findings in Table 2, all models achieve similar mean Precision and Recall on the validation set, although these values are lower than the corresponding ones reported in Table 2. Notably, the performance on the external evaluation dataset is significantly lower, with Recall being lower than Precision, mirroring the results observed when using a slice-wise data split.

Table 6. Ablation study results when evaluating variations of the U-Net architecture on the validation and external validation sets, with data split at the patient level. Training and validation utilized 10 CT scans sourced from the Coronacases.org repository, while the external validation set comprised the remaining 10 CT scans from the Radiopaedia.org repository

Model	Validation Mean DSC	Validation Mean IoU	Validation Mean Precision	Validation Mean Recall	External Mean DSC	External Mean IoU	External Mean Precision	External Mean Recall
U-Net	0.7637 ± 0.0678	0.6216 ± 0.0883	0.7394 ± 0.0894	0.7912 ± 0.0442	0.6613 ± 0.0372	0.4940 ± 0.0404	0.7302 ± 0.1209	0.6392 ± 0.1431
U-Net + VGG16	0.7669 ± 0.0629	0.6253 ± 0.0830	0.7591 ± 0.0675	0.7759 ± 0.0673	0.7022 ± 0.0217	0.5414 ± 0.0258	0.7592 ± 0.0974	0.6654 ± 0.0639
U-Net + DenseNet121	0.7889 ± 0.0541	0.6540 ± 0.0738	0.8219 ± 0.0521	0.7603 ± 0.0706	0.7079 ± 0.0123	0.5480 ± 0.0146	0.8037 ± 0.0558	0.6369 ± 0.0466

The training and inference times of the models, whose metrics are presented in Table 6, are detailed in Table 7. Similar to the experiments presented in the previous section, the results demonstrate that the U-Net model had the shortest runtime, while the U-Net + DenseNet121 model required the longest time.

The training and validation curves for the models, whose results are depicted in Table 6, are shown in Figure 9. Upon examining these curves, it is notable that all models exhibit convergence. However, unlike the curves presented in the case of data split by

slice, it is apparent that the models show signs of overfitting. This could be attributed to the potential lack of diversity in the data when splitting by patient. Furthermore, the reduced incidence of overfitting when splitting by slice could be linked to data leakage.

Within Table 8, we present the metrics used to assess the ability of models trained with a patient-based split approach to accurately segment lesions attributed to SARS-CoV-2. For this evaluation, 10 CT scans sourced from Radiopaedia.org were used for training and validation, while the remaining CT scans from Coronacases.org were used for external evaluation.

In line with all previous experiments, the U-Net + DenseNet121 model demonstrates superior overall performance. Similar to our previous experiment, where we trained and validated using data from the Radiopaedia.org repository, we note that the difference between Precision and Recall values during external evaluation is smaller compared to instances where our models were trained on data from the Coronacases.org repository.

Table 7. Running times of different variations of the U-Net architecture evaluated with the data split at the patient level. Training and validation used 10 CT scans sourced from the Coronacases.org repository, while the external validation set comprised the remaining 10 CT scans from the Radiopaedia.org repository

Model	Training Time	Validation Time	External Validation Time
U-Net	4176.32 ± 143.44 seconds	1.36 ± 0.28 seconds	2.41 ± 0.02 seconds
U-Net + VGG16	4684.79 ± 157.58 seconds	1.64 ± 0.35 seconds	2.92 ± 0.01 seconds
U-Net + DenseNet121	7613.26 ± 223.34 seconds	2.45 ± 0.50 seconds	4.45 ± 0.10 seconds

Table 8. Ablation study results when evaluating variations of the U-Net architecture on the validation and external validation sets, with data split at the patient level. Training and validation utilized 10 CT scans sourced from the Radiopaedia.org repository, while the external validation set comprised the remaining 10 CT scans from the Coronacases.org repository

Model	Validation Mean DSC	Validation Mean IoU	Validation Mean Precision	Validation Mean Recall	External Mean DSC	External Mean IoU	External Mean Precision	External Mean Recall
U-Net	0.7631 ± 0.0813	0.6224 ± 0.1035	0.7845 ± 0.0842	0.7568 ± 0.1285	0.6724 ± 0.0380	0.5075 ± 0.0428	0.6975 ± 0.0746	0.6621 ± 0.0890
U-Net + VGG16	0.7755 ± 0.0079	0.6387 ± 0.1032	0.7680 ± 0.0699	0.7872 ± 0.1056	0.6895 ± 0.0437	0.5275 ± 0.0512	0.7227 ± 0.0433	0.6631 ± 0.0690
U-Net + DenseNet121	0.7989 ± 0.0615	0.6686 ± 0.0835	0.7905 ± 0.0762	0.8146 ± 0.0925	0.7369 ± 0.0189	0.5837 ± 0.0238	0.7642 ± 0.0420	0.7152 ± 0.0484

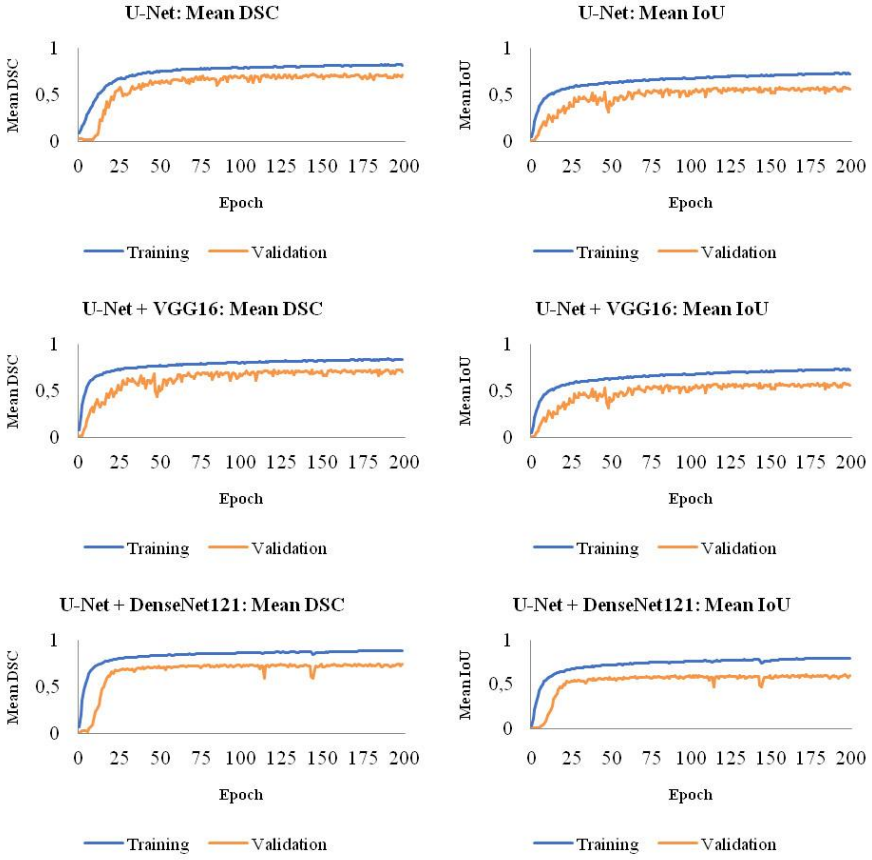

Fig. 9. Training and validation curves for the models trained and evaluated on data split at the patient level. Training and validation utilized 10 CT scans sourced from the Coronacases.org repository, while the external validation set comprised the remaining 10 CT scans from the Radiopaedia.org repository

Table 9. Running times of different variations of the U-Net architecture evaluated with the data split at the patient level. Training and validation used 10 CT scans sourced from the Radiopaedia.org repository, while the external validation set comprised the remaining 10 CT scans from the Coronacases.org repository

Model	Training Time	Validation Time	External Validation Time
U-Net	1581.43 ± 97.51 seconds	0.50 ± 0.18 seconds	6.48 ± 0.02 seconds
U-Net + VGG16	1799.78 ± 83.24 seconds	0.63 ± 0.24 seconds	7.90 ± 0.04 seconds
U-Net + DenseNet121	3101.80 ± 144.39 seconds	1.06 ± 0.36 seconds	12.13 ± 0.21 seconds

Table 9 provides a breakdown of the training and inference times for the models that achieved the performance metrics displayed in Table 8. Once again, the U-Net model had the shortest runtime, in contrast to the U-Net + DenseNet121 model, which required the longest time for training, validation and external evaluation.

In Figure 10, the training and validation curves for the models, whose results are shown in Table 8, are presented. In the experiment conducted for this section, all trained models converge. However, it is evident that each model exhibits some degree of overfitting.

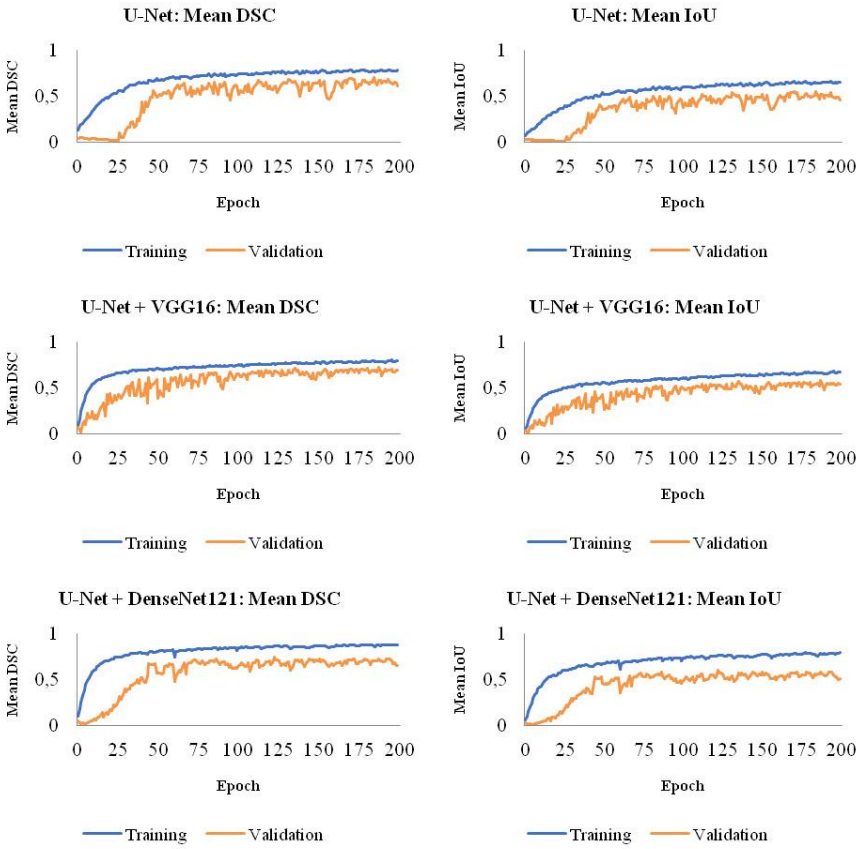

Fig. 10. Training and validation curves for the models trained and evaluated on data split at the patient level. Training and validation utilized 10 CT scans sourced from the Radiopaedia.org repository, while the external validation set comprised the remaining 10 CT scans from the Coronacases.org repository

4.3. Results of the Application of Semantic Segmentation on a Subset of the Validation and External Validation Datasets

Figures 11 and 12 illustrate the results of applying semantic segmentation to subsets of the validation and external evaluation datasets, respectively. Upon examining these results, it is evident that all models effectively isolate lesions present in the CT slices.

In addition, a quantitative analysis was conducted, and the results are presented in Tables 10 and 11. Notably, the U-Net + DenseNet121 demonstrated the most accurate segmentation among the models on both the validation and external evaluation datasets, as evidenced by its superior DSC and IoU values in Tables 10 and 11.

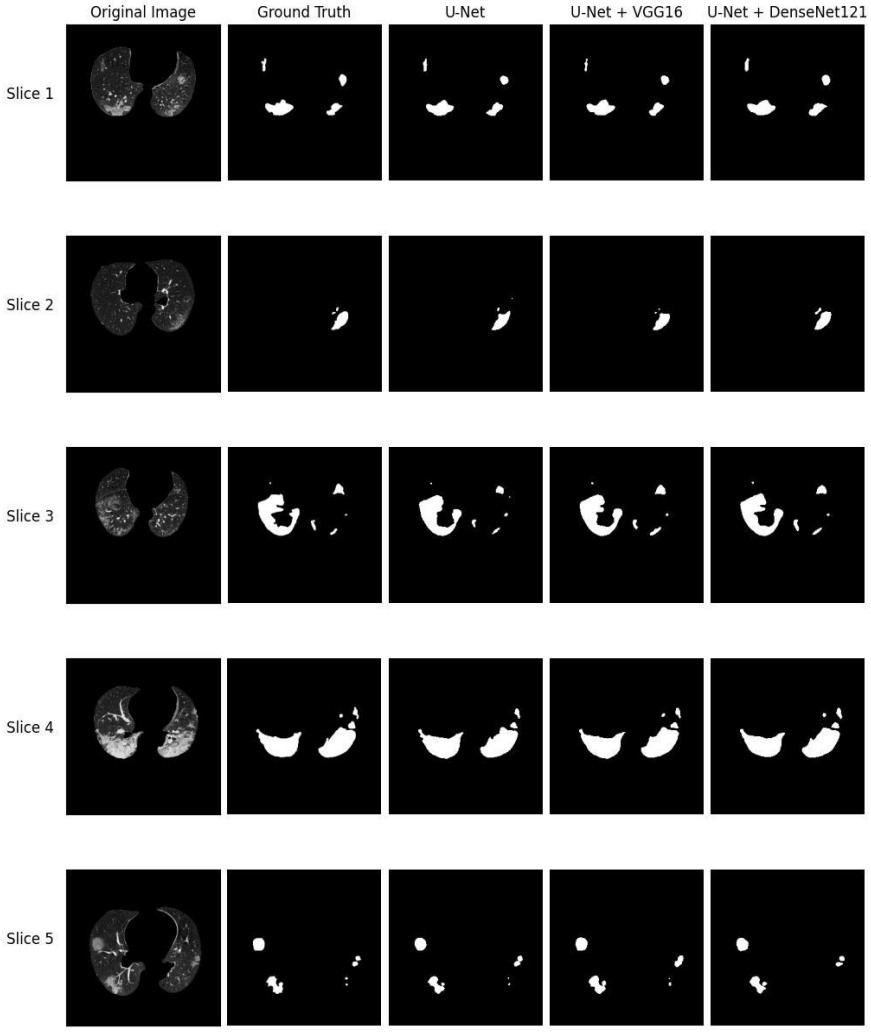

Fig. 11. Semantic segmentation results on a subset of the validation dataset

Table 10. Quantitative analysis of the results displayed in Figure 11

Slice	U-Net		U-Net + VGG16		U-Net + DenseNet121	
	DSC	IoU	DSC	IoU	DSC	IoU
Slice 1	0.8622	0.7577	0.8818	0.7886	0.8830	0.7905
Slice 2	0.8170	0.6906	0.8475	0.7353	0.8927	0.8062
Slice 3	0.8460	0.7331	0.8828	0.7901	0.8988	0.8162
Slice 4	0.9071	0.8300	0.9448	0.8953	0.9461	0.8977
Slice 5	0.8638	0.7602	0.8585	0.7521	0.8653	0.7626

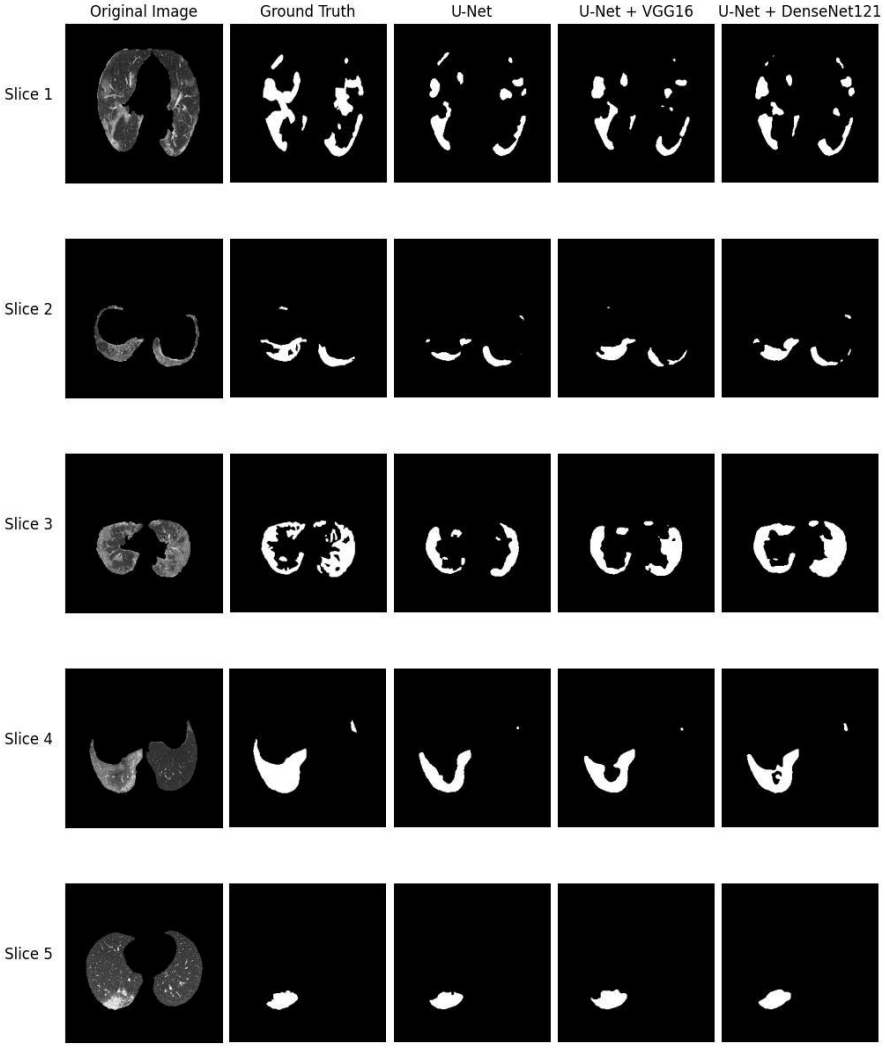

Fig. 12. Semantic segmentation results on a subset of the external validation dataset

Table 11. Quantitative analysis of the results displayed in Figure 12

Slice	U-Net		U-Net + VGG16		U-Net + DenseNet121	
	DSC	IoU	DSC	IoU	DSC	IoU
Slice 1	0.6218	0.4511	0.6417	0.4724	0.6627	0.4955
Slice 2	0.6537	0.4856	0.7074	0.5472	0.7283	0.5726
Slice 3	0.6624	0.4952	0.7595	0.6122	0.8020	0.6695
Slice 4	0.7669	0.6219	0.8131	0.6851	0.8444	0.7307
Slice 5	0.8521	0.7423	0.8704	0.7705	0.8853	0.7942

4.4. Statistical Test Analysis of the Results

In this section, we conduct a comprehensive statistical analysis of the results derived from our experiments. Our goal is to compare the performance of the best and worst models, namely U-Net + DenseNet121 and U-Net, respectively. To assess the performance of our models across different cross-validation data partitions, we employed a statistical test called t-test.

A t-test is used to compare the means of two groups [39]. There are two types of t-tests: the independent t-test, which compares the means of two groups that are unrelated to each other, and the paired t-test which compares the means of two groups that are related to each other [39].

Since we compare two CNN models that have been trained and evaluated on the same data using a 5-fold cross-validation scheme, the appropriate t-test to use is the paired t-test. This is because the same data folds are used for evaluating both models, meaning the results from each fold are paired. The aim of an analysis using a paired t-test is to discern whether there exists a statistically significant difference in the models' mean performance scores.

The paired t-test employs two contradictory research hypotheses: the null hypothesis and the alternative hypothesis [40]. The null hypothesis states that the mean difference between the paired observations is zero [40]. The alternative hypothesis states that the mean difference between the paired observations is not zero [40].

The steps to compute the paired t-test are summarized below:

1. Calculate the difference between each pair of observations:

$$d_i = y_i - x_i \tag{5}$$

2. Calculate the mean difference:

$$\bar{d} = \frac{1}{n}\sum_{i=1}^{n} d_i \tag{6}$$

3. Calculate the standard deviation of the differences:

$$s_d = \sqrt{\frac{1}{n-1}\sum_{i=1}^{n}(d_i - \bar{d})} \tag{7}$$

4. Calculate the t-statistic:

$$t = \frac{\bar{d}}{s_d}\sqrt{n} \quad (8)$$

Under the null hypothesis, this statistic follows a t-distribution with n-1 degrees of freedom

5. Find the p-value corresponding to the calculated t-statistic.

6. Compare the p-value to the chosen significance level:

- If the p-value is less than the significance level (commonly 0.05), reject the null hypothesis.
- If the p-value is greater than the significance level, fail to reject the null hypothesis.

Table 12 presents the p-values obtained from the paired t-test. In cases where the p-values are less than 0.05, there exists a statistically significant difference in the performance of the compared models. By examining Table 12, we can see that all p-values are less than 0.05. This indicates a statistically significant difference in the performance between U-Net and U-Net + DenseNet121.

Table 12. Statistical test analysis of the U-Net and U-Net + DenseNet121 models. Training and validation utilized 10 CT scans sourced from the Coronacases.org repository, while the external validation set comprised the remaining 10 CT scans from the Radiopaedia.org repository.

Split by Slice				Split by Patient			
Validation		External Validation		Validation		External Validation	
DSC	IoU	DSC	IoU	DSC	IoU	DSC	IoU
0.0026	0.0022	0.0231	0.0202	0.0263	0.0175	0.0093	0.0080

4.5. Comparison of our Results with the Results of other Researchers

In this paper, we employed deep learning methods, specifically convolutional neural networks, to assess their efficacy, after appropriate training, in detecting and outlining lesions in CT slices caused by COVID-19 pneumonia. This proved to be a challenging task for two primary reasons. Firstly, collecting a large enough dataset posed difficulties due to the necessity of annotations provided by medical experts. Secondly, the prevalence of the negative class in medical images contributed to evident class imbalance within the data. To address these issues, we proposed leveraging transfer learning by replacing the encoder of a standard U-Net model with a pre-trained model.

Results indicate that the quality and quantity of the utilized dataset, as well as the use of ideal preprocessing techniques, were critical for our models' performance. Segmentation of the lung parenchyma and normalization in terms of contrast and brightness helped achieve better overall performance. On the other hand, data augmentation was not that helpful.

Employing two different splitting techniques provided us with the opportunity to compare our method with the literature, as some authors chose to split by patient instead of by slice and vice versa.

Verifying our approach using both subsets of the dataset for training, validation and external evaluation showed similar performance. This observation indicates the robustness of the models and their strong generalization capabilities.

Upon observing the performance of the selected models during semantic segmentation on both the validation and external validation datasets, it becomes evident that the standard U-Net model achieves significantly improved performance when transfer learning is applied. Moreover, the results on the external evaluation datasets demonstrate high generalization ability.

Table 13. Comparison of our work with other scientific papers where the data were split by slice.

Model Architecture	Training and Validation Dataset	External Evaluation Dataset	Preprocessing & Transfer Learning	Validation Results	External Evaluation Results
Xiaoyan Wang et al. [22] SSA-Net	Experiment 1: COVID-19-CT-Seg (5-fold cross validation) Experiment 2: MedSeg Dataset [23] (Only 98 CT Slices) (5-fold cross validation)	-	HU Clipping [-1250, 250], No Transfer Learning	Experiment 1: DSC: 65.22% Experiment 2: DSC: 75.40%	-
Krinski et al. [24] Various CNN Models	COVID-19-CT-Seg (5-fold cross validation Train: 80% Val: 20%)	-	Transfer Learning (ImageNet [25])	Best Model DSC: 73.67% Best Model IoU: 70.91%	-
Mahmoudi et al. [26] 2D U-Net	COVID-19-CT-Seg (4-fold cross validation Train: 70% Val: 30%)	-	CLAHE, Image Cropping, Data Augmentation, No Transfer Learning	DSC: 91% IoU: 85%	-
Qiblawey et al. [27] Various CNN Models	COVID-19-CT-Seg (10-fold cross validation Train: 60% Val: 20% Test: 20%)	-	HU Normalization, Lung Parenchyma Segmentation, Data Augmentation, Transfer Learning (ImageNet)	Best Model DSC: 94.13% Best Model IoU: 91.85%	-
Our Approach U-Net + DenseNet121	Experiment 1: COVID-19-CT-Seg (10 CT from Coronacases) (5-fold cross-validation) Experiment 2: COVID-19-CT-Seg (10 CT from Radiopaedia) (5-fold cross-validation)	Experiment 1: COVID-19-CT-Seg (10 CT from Radiopaedia) Experiment 2: COVID-19-CT-Seg (10 CT from Coronacases)	HU Normalization WW: 1400 WL: -500, Lung Segmentation, Data Augmentation Transfer Learning (ImageNet)	Experiment 1: DSC: 86.44% IoU: 76.12% Experiment 2: DSC: 85.86% IoU: 75.23%	Experiment 1: DSC: 72.11% IoU: 56.41% Experiment 2: DSC: 75.53% IoU: 60.69%

Through our experiments, we found that increasing the batch size results in better overall model performance, while increasing the depth of the U-Net model by adding extra layers or changing layer parameters increases the model complexity without significant performance gains.

Another distinctive aspect of our approach that sets it apart from the works of other researchers is the utilization of 2D U-Nets instead of 3D U-Net architectures, which are less computationally expensive. Upon reviewing Tables 13 and 14 it is evident that our best model outperforms the majority of the models featured in other works, demonstrating enhanced performance. Analytically, when splitting by slice and training on the data from the Coronacases.org repository, our best model achieves a DSC and IoU score of 0.8644 and 0.7612 during the validation phase and a DSC and IoU score of 0.7211 and 0.5641 during the external evaluation phase. When splitting by slice and training on the data from the Radiopaedia.org repository, our best model achieves a DSC and IoU score of 0.8586 and 0.7523 during the validation phase and a DSC and IoU score of 0.7553 and 0.6069 during the external evaluation phase. When splitting by patient and training on the data from the Coronacases.org repository, our best model achieves a DSC and IoU score of 0.7889 and 0.6540 during the validation phase and a DSC and IoU score of 0.7079 and 0.5480 during the external evaluation phase. When splitting by patient and validating on the data from the Radiopaedia.org repository, our best model achieves a DSC and IoU score of 0.7989 and 0.6686 during the validation phase and a DSC and IoU score of 0.7369 and 0.5837 during the external evaluation phase. This improvement is crucial for clinical applications, as accurate segmentation of COVID-19 lesions can lead to better monitoring of disease progression and response to treatment. Automated and reliable identification of affected lung regions can help radiologists quantify the extent of disease more efficiently, enabling timely adjustments in patient management strategies. This could potentially reduce diagnostic errors and improve patient outcomes by ensuring that critical cases are identified and treated promptly.

By further examining the results in Table 13, it is evident that our best model is surpassed by the models trained in studies [26] and [27] in terms of performance. While our work demonstrates lower DSC and IoU scores compared to [27], it is important to consider the difference in our data preprocessing strategies. In [27], the authors applied data augmentation techniques before splitting the dataset into training and validation sets. This approach may introduce a risk of data leakage, as slightly modified images could be present in both training and validation sets potentially overestimating model performance during evaluation. In contrast, our method follows a better practice by performing data augmentation after the data split and exclusively on the training set. Regarding [26], their strategy of cropping the CT slices to the size 256x256 likely contributed to their models achieving higher DSC and IoU scores, as it may have helped them better focus on anatomical features relevant to the task. As shown in the results of Table 14, our best model is slightly outperformed by the model presented in [13], as well as by the model implemented in [15].

Table 14. Comparison of our work with other scientific papers where the data were split by patient

Model Architecture	Training and Validation Dataset	External Evaluation Dataset	Preprocessing & Transfer Learning	Validation Results	External Evaluation Results
Ma et al. [7] 2D U-Net	COVID-19-CT-Seg [8] (5-fold cross-validation Train: 20% Val: 80%)	-	HU Clipping [-1250, 250], No Transfer Learning	DSC: 60.80%	-
Ma et al. [7] nnU-Net [9]	COVID-19-CT-Seg (5-fold cross-validation Train: 20% Val: 80%)	MosMed [10]	HU Clipping [-1250, 250], No Transfer Learning	DSC: 67.30%	DSC: 58.80%
Müller et al. [11] 3D U-Net [12]	COVID-19-CT-Seg (5-fold cross-validation Train: 80% Val: 20%)	-	HU Clipping [-1250, 250], No Transfer Learning	DSC: 76.10%	-
Müller et al. [13] 3D U-Net	COVID-19-CT-Seg (5-fold cross-validation Train: 80% Val: 20%)	An et al. [14]	HU Clipping [-1250, 250], Data Augmentation, No Transfer Learning	DSC: 80.40%	DSC: 66.10%
Owais et al. [15] DAL-Net	Experiment 1: COVID-19-CT-Seg (5-fold cross-validation Train: 80% Val: 20%) Experiment 2: MosMed (5-fold cross-validation Train: 80% Val: 20%) Experiment 3: COVID-19-CT-Seg	Experiment 3: MosMed	Experiment 3: Reinhard Transformation [16], No Transfer Learning	Experiment 1: DSC: 83.23% IoU: 74.86% Experiment 2: DSC: 68.63% IoU: 61.35%	Experiment 3: DSC: 74.93% IoU: 66.50%
Zheng et al. [17] 3D CU-Net	COVID-19-CT-Seg (5-fold cross-validation Train: 80% Val: 20%)	MosMed	HU Clipping [-1250, 250], Data Augmentation, No Transfer Learning	DSC: 77.80%	DSC: 66.80%
Yixin Wang et al. [18] 3D U-Net	COVID-19-CT-Seg (5-fold cross-validation Train: 20% Val: 80%)	-	No Transfer Learning	DSC: 70.04%	-
Our Approach U-Net + DenseNet121	Experiment 1: COVID-19-CT-Seg (10 CT from Coronacases) (5-fold cross-validation) Experiment 2: COVID-19-CT-Seg (10 CT from Radiopaedia) (5-fold cross-validation)	Experiment 1: COVID-19-CT-Seg (10 CT from Radiopaedia) Experiment 2: COVID-19-CT-Seg (10 CT from Coronacases)	HU Normalization WW: 1400 WL: -500, Lung Segmentation, Data Augmentation Transfer Learning (ImageNet)	Experiment 1: DSC: 78.89% IoU: 65.40% Experiment 2: DSC: 79.89% IoU: 66.86%	Experiment 1: DSC: 70.79% IoU: 54.80% Experiment 2: DSC: 73.69% IoU: 58.37%

5. Conclusions and Future Work

The primary goal of this study was to investigate the ability of deep learning methods to accurately segment lesions in CT slices caused by pneumonia attributed to SARS-CoV-2. Our focus was on evaluating the performance of a U-Net architecture and two variations of it, where the encoder was replaced with pre-trained convolutional neural networks. The outcomes, presented in Section 4 and compared with the literature in Section 2, indicate that the objectives of this research have been achieved.

This study lays the groundwork for potential future extensions aimed at enhancing the robustness and applicability of the proposed models. Future work could involve collecting more diverse data, featuring variations in patient age, gender and ethnicity from various healthcare facilities. This would allow for further training of the models using more varied datasets. Additionally, training the models on higher-resolution images could enhance segmentation precision and overall model performance. Another potential direction could involve adapting our segmentation method for other respiratory diseases where accurate lesion segmentation is equally critical. Moving our method from research to clinical practice is also a promising prospect. This would require further steps, including extensive clinical trials and validation studies to ensure the robustness and reliability of the segmentation tool in real-world scenarios. Collaborating with healthcare providers to integrate our tool into hospital information systems and workflows will be essential for practical implementation.

Tuning the hyperparameters of the deep learning models automatically using methods such as Grid Search and Random Search could potentially improve model performance. These methods were omitted in this work due to their computational expense. Implementing regularization techniques, such as Lasso and Ridge Regression, could help address the overfitting phenomenon observed when data are split by patient.

References

1. WHO Coronavirus (COVID-19) Dashboard. [Online]. Available: https://covid19.who.int/ (current July 2023)
2. Chen, Y. J., Jian, W. H., Liang, Z. Y., Guan, W. J., Liang, W. H., Chen, R. C., Tang, C. L., Wang, T., Liang, H. R., Li Y. M., et al.: Earlier diagnosis improves COVID-19 prognosis: a nationwide retrospective cohort analysis. Annals of Translational Medicine, Vol. 9, No. 11, 941. (2021)
3. Machnicki, S., Patel, D., Singh, A., Talwar, A., Mina, B., Oks, M., Makkar, P., Naidich, D., Mehta, A., Hill, N. S., et al.: The Usefulness of Chest CT in Patients with Suspected or Diagnosed COVID-19: A Review of Literature. Chest, Vol. 60, No. 2, 652-670. (2021)
4. Borakati, A., Perera, A., Johnson, J., Sood, T.: Diagnostic accuracy of X-ray versus CT in COVID-19: a propensity matched database study. BMJ Open, Vol. 10, No. 11. (2020)
5. Pinto, A., Brunese, L.: Spectrum of diagnostic errors in radiology. World Journal of Radiology, Vol. 2, No. 10, 377-383. (2010)
6. Ronneberger, O., Fischer, P., Brox, T.: U-Net: Convolutional Networks for Biomedical Image Segmentation. In Proceedings of the 18th International Conference on Medical Image Computing and Computer-Assisted Intervention. Springer-Verlag, Munich, Germany, 234-241. (2015)

7. Ma, J., Wang, Y., An, X., Ge, C., Yu, Z., Chen, J., Zhu, Q., Dong, G., He, J., He, Z., et al.: Toward data-efficient learning: A benchmark for COVID-19 CT lung and infection segmentation. Medical Physics, Vol. 48, No. 3, 1197-1210. (2021)
8. Ma, J., Ge, C., Wang, Y., An, X., Jiantao, G., Ziqi, Y., Zhang, M., Liu, X., Deng., X., Cao, S., et al.: COVID-19 CT Lung and Infection Segmentation Dataset. (2020). [Online]. Available: https://zenodo.org/records/3757476 (current July 2023).
9. Isensee, F., Jaeger, P. F., Kohl, S. A. A., Petersen, J., Maier-Hein, K. H.: nnU-Net: a self-configuring method for deep learning-based biomedical image segmentation. Nature Methods, Vol. 18, 203-211. (2021)
10. Morozov, S. P., Andreychenko, A. E., Blokhin, I. A., Gelezhe, P. B., Gonchar, A. P., Nikolaev, A. E., Pavlov, N. A., Chernina, V. Y., Gombolevskiy, V. A.: MosMedData: data set of 1110 chest CT scans performed during the COVID-19 epidemic. Digital Diagnostics, Vol. 1, No. 1, 49-59. (2020)
11. Müller, D., Rey, I. S., Kramer, F.: Automated Chest CT Image Segmentation of COVID-19 Lung Infection based on 3D U-Net. (2020). [Online]. Available: https://arxiv.org/abs/2007.04774 (current July 2023)
12. Çiçek, Ö., Abdulkadir, A., Lienkamp, S. S., Bronx, T., Ronnebeger, O.: 3D U-Net: Learning Dense Volumetric Segmentation from Sparse Annotation. In Proceedings of the 19th International Conference on Medical Image Computing and Computer-Assisted Intervention. Springer-Verlag, Athens, Greece, 424-432. (2016)
13. Müller, D., Rey, I. S., Kramer, F.: Robust chest CT image segmentation of COVID-19 lung infection based on limited data. Informatics in Medical Unlocked, Vol. 25, 100681. (2021)
14. An, P., Xu, S., Harmon, S. A., Turkbey, E.B., Sanford, T. H., Amalou, A., Kassin, M., Varble, N., Blain, M., Anderson, V., et al.: CT Images in COVID-19. [Online]. Available: https://wiki.cancerimagingarchive.net/display/Public/CT+Images+in+COVID-19 (current December 2023).
15. Owais, M., Baek, N. R., Park, K. R.: Domain-Adaptive Artificial Intelligence-Based Model for Personalized Diagnosis of Trivial Lesions Related to COVID-19 in Chest Computed Tomography Scans. Journal of Personalized Medicine, Vol. 11, No. 10, 1008. (2021)
16. Reinhard, E., Adhikhmin, M., Gooch, B., Shirley, P.: Color transfer between images. IEEE Computer Graphics and Applications, Vol. 21, No. 5, 34-41. (2001)
17. Zheng, R., Zheng, Y., Dong-Ye, C.: Improved 3D U-Net for COVID-19 Chest CT Image Segmentation. Scientific Programming, Vol. 2021, No. 1. (2021)
18. Wang, Y., Zhang, Y., Liu, Y., Tian, J., Zhong, C., Shi, Z., Zhang, Y., He, Z.: Does non-COVID-19 lung lesion help? Investigating transferability in COVID-19 CT image segmentation. Computer Methods and Programs in Biomedicine, Vol. 202, 106004. (2021)
19. Singh, V. K., Abdel-Nasser, M., Pandey, N., Puig, D.: LungINFseg: Segmenting COVID-19 Infected Regions in Lung CT Images Based on a Receptive-Field-Aware Deep Learning Framework. Diagnostics, Vol. 11, No. 20, 158. (2021)
20. Amara, K., Aouf, A., Kennouche, H., Djekoune A. O., Zenati, N., Kerdjidj, O.; Ferguene, F.: COVIR: A virtual rendering of a novel NN architecture O-Net for COVID-19 Ct-scan automatic lung lesions segmentation. Computers & Graphics, Vol. 104, 11-23. (2022)
21. Aswathy, A.L., Chandra, S. S. V.: Cascaded 3D UNet architecture for segmenting the COVID-19 infection from lung CT volume. Scientific Reports, Vol. 12, 3090. (2022)
22. Wang, X., Yuan, Y., Guo, D., Huang, X., Cui, Y., Xia, M., Wang, Z., Bai, C., Chen, S.: SSA-Net: Spatial self-attention network for COVID-19 pneumonia segmentation with semi-supervised few-shot learning. Medical Image Analysis, Vol. 79, 102459. (2022)
23. COVID-19 – Medical segmentation. [Online]. Available: http://medicalsegmentation.com/covid19 (current July 2023)
24. Krinski, B. A., Ruiz, D. V., Todt, E.: Spark in the Dark: Evaluating Encoder-Decoder Pairs for COVID-19 CT's Semantic Segmentation. In Proceedings of the 2021 Latin American

Robotics Symposium (LARS), 2021 Brazilian Symposium on Robotics (SBR), and 2021 Workshop on Robotics in Education (WRE). IEEE, Natal, Brazil. (2021)
25. Deng, J., Dong, W., Socher, R., Li, L.-J., Li, K., Fei-Fei, L.: ImageNet: A large-scale hierarchical image database. In Proceedings of the 2009 IEEE Conference on Computer Vision and Pattern Recognition (CVPR). IEEE, Miami, Florida, USA, 248-255. (2009)
26. Mahmoudi, R., Benameur, N., Mabrouk, R., Mohammed M. A., Gacia-Zapirain, B., Bedoui, M. H.: A Deep Learning-Based Diagnosis System for COVID-19 Detection and Pneumonia Screening Using CT Imaging. Applied Sciences, Vol. 12, No. 10, 4825. (2022)
27. Qiblawey, Y., Tahir, A., Chowdhury, M. E. H., Khandakar, A., Kiranyaz, S., Rahman, T., Ibtehaz, N., Mahmud, S., Maadeed, S. A., Musharavati, F. et al: Detection and Severity Classification of COVID-19 in CT Images Using Deep Learning. Diagnostics, Vol. 11, No. 5, 893. (2021)
28. Enshaei, N., Oikonomou, A., Rafiee, M. J., Afshar, P., Heidarian, S., Mohammadi, A., Plataniotis, K. N., Naderkhani, F.: COVID-rate: an automated framework for segmentation of COVID-19 lesions from chest CT images. Scientific Reports, Vol. 12, No. 1, 3212. (2022)
29. Afshar, P., Shahin, H., Enshaei, N., Naderkhani, F., Rafiee, M. J., Oikonomou, A., Fard, F. B., Samimi, K., Plataniotis, K. N., Mohammadi, A.: COVID-CT-MD, COVID-19 computed tomography scan dataset applicable in machine learning and deep learning. Scientific Reports, Vol. 8, 121. (2021)
30. Uçar, M.: Automatic segmentation of COVID-19 from computed tomography images using modified U-Net model-based majority voting approach. Neural Computing and Applications, Vol. 34, No. 24, 21927-21938. (2022)
31. CORONACASES.ORG – by RAIOSS.com. [Online]. Available: https://coronacases.org/ (current February 2023).
32. Playlist 'COVID-19 pneumonia' by Dr Yaïr Glick. [Online]. Available: https://radiopaedia.org/playlists/25887/ (current February 2023)
33. Chau, S., Hayre, C. M.: Computed Tomography: A Primer for Radiographers. CRC Press, Boca Raton, Florida, USA. (2022)
34. Simonyan, K., Zisserman, A.: Very Deep Convolutional Networks for Large-Scale Image Recognition. In Proceedings of the 3rd International Conference on Learning Representations. San Diego, California, USA. (2015)
35. Huang, G.. Liu, Z.. van der Maaten, L.. Weinberger, K. Q.: Densely Connected Convolutional Networks. In Proceedings of the 2017 IEEE Conference on Computer Vision and Pattern Recognition (CVPR). IEEE, Honolulu, Hawaii, USA, 4700-4708. (2017)
36. Kaggle: your machine learning and data science community. [Online]. Available: https://www.kaggle.com/ (current February 2023).
37. Kingma, D. P, Ba, J.: Adam: A Method for Stochastic Optimization. In Proceedings of the 3rd International Conference on Learning Representations. San Diego, California, USA. (2015)
38. Yagis, E., Atnafu, S. W., García Seco de Herrera, A., Marzi, C., Scheda, R., Giannelli, M., Tessa, C., Citi, L., Diciotti, S.: Effect of data leakage in brain MRI classification using 2D convolutional neural networks. Scientific Reports, Vol. 11, No. 1, 22544. (2021)
39. Kim, T. K.: T test as a parametric statistic. Korean Journal of Anesthesiology, Vol. 68, No. 6, 540-546. (2015)
40. Hasija, Y.: All About Bioinformatics: From Beginner to Expert. Academic Press, London, UK. (2023)

Symeon Psaraftis-Souranis received his M.Eng. degree from the Department of Informatics and Computer Engineering at the University of West Attica in 2023. During his studies, he worked on several academic projects, gaining hands-on experience in

applying artificial intelligence across various fields, including medicine. He has developed strong proficiency in programming languages and artificial intelligence applications, with a keen interest in computational biology. His research interests include artificial intelligence, machine learning, image processing, natural language processing, data mining, and bioinformatics.

Christos Troussas is currently an Assistant Professor in the Department of Informatics and Computer Engineering at the University of West Attica. He has been PostDoc Researcher in the field of Software Engineering and Applied Artificial Intelligence at the same Department. He has received a PhD degree in Informatics, a MSc degree with specialization in “Intelligent Technologies of Human-Computer Interaction” and a BSc degree in Informatics from the Department of Informatics, University of Piraeus. He has participated in national and international research projects. His academic influence is indicated by thousands of citations of his work and by having received best paper awards in international conferences in the field of computer science. His current research interests are in the areas of personalized software technology, human-computer interaction and applied artificial intelligence. He is among the world’s top 2% of scientists, according to the Stanford University ranking for the years 2020, 2021 and 2022 (Ioannidis, John P.A. (2023), “October 2023 data-update for "Updated science-wide author databases of standardized citation indicators"”, Elsevier Data Repository, V6, doi: 10.17632/btchxktzyw.6). Additionally, he holds the position of Research Fellow at INTI International University, Malaysia.

Athanasios (Thanos) Voulodimos is currently an Assistant Professor in the School of Electrical and Computer Engineering at the National Technical University of Athens (NTUA). He received his Dipl.-Ing., MSc, and PhD degrees from the same institution with the highest honors. His research interests include machine learning, artificial intelligence, image and signal processing, multimedia, and multimodal data fusion, management, and analysis. He has participated in more than 15 European and national research and development projects as a researcher, senior researcher, and/or technical manager. Dr. Voulodimos has co-authored more than 140 papers in refereed international journals, conference proceedings, and books, with his work receiving over 7,000 citations. He has served as an Organizing and Program Committee member at various international conferences and workshops and has guest-edited collective book volumes and special issues in international journals. He is a member of IEEE and ACM.

Cleo Sgouropoulou holds a Ph.D. in Electrical and Computer Engineering from the National Technical University of Athens (NTUA) and is currently a Professor in the Department of Informatics and Computer Engineering at the University of West Attica (UNIWA). Her research focuses on software engineering, with emphasis on the design, development, and standardization of Learning Technology and Research Information Systems. She has coordinated numerous national and European projects related to e-Learning, Open Educational Resources (OER), and skills modeling. Prof. Sgouropoulou has published over 140 articles and has received more than 3000 citations. She plays a key role in European Learning Technologies Standardization, leading the Greek delegation to CEN Technical Committees and contributing to projects on learning outcomes, digital skills, and learner mobility. Her work has resulted in several European

Norms, including the EuroLMAI, and she has been widely recognized within the field for her contributions.

Received: February 29, 2024; Accepted: September 09, 2024.

Computer Science and Information Systems 22(1):33–57 https://doi.org/10.2298/CSIS240320067Z

Topic-oriented Sarcasm Detection via Entity Knowledge-based Prompt Learning

Yuhao Zhou[1], Shunxiang Zhang[1,*], Caiqin Wang[1], Yanhui Wang[1], Xiaolong Wang[1] and KuanChing Li[2,*]

[1] School of Computer Science and Engineering,
Anhui University of Science & Technology, 232001 Huainan, China
1303496845@qq.com
sxzhang@aust.edu.cn
1976499113@qq.com
2457172801@qq.com
1556282598@qq.com
[2] Department of Computer Science and Information Engineering (CSIE),
Providence University, 43301 Taizhong, Taiwan
kuancli@pu.edu.tw

Abstract. The extensive spread of sarcasm on social media has attracted great attention to sarcasm detection. Topic-oriented sarcasm detection aims to determine the sarcastic tendency of a comment on a specific topic. Existing methods focus on using topics as contextual information to enhance comprehension of comment semantics. However, when topics and comments contain entities with knowledge information, accurately understanding the comment semantics becomes challenging. To this end, we investigate an Entity Knowledge-based Prompt Learning (EKPL) model that combines prompt learning and entity knowledge from knowledge graphs for topic-oriented sarcasm detection. Specifically, we use prompt learning to transform topic-oriented sarcasm detection from a classification task to a mask prediction task, while we incorporate entity knowledge into the prompt representation to enhance the expressiveness of its predictive mask words and the model's understanding of text semantics. Experimental results on the public *ToSarcasm*[†] dataset illustrate that our EKPL model has a significant performance in topic-oriented sarcasm detection task.

Keywords: Sarcasm detection, Entity knowledge, Prompt Learning, Knowledge graph, EKPL.

1. Introduction

As a crucial medium for online communication, social media platforms' real-time nature and convenience allow people to stay updated on trending topics and make comments at

* Corresponding authors

† https://github.com/HITSZ-HLT/ToSarcasm/tree/main

any time. This has led to rich and diverse expressions of social media comments, such as irony, sarcasm, and humor. Sarcasm is a rhetorical device widely used by people and is characterized by indirectness [1]. The characteristic often leads to a significant contrast between the literal meaning of comments and the true emotions of users, resulting in misunderstandings of the comments. This brings huge challenges to user opinion mining and sentiment analysis [2].

With the advancement of deep learning, numerous deep learning-based methods have been proposed [3-4], greatly improving the detection performance. Most of the current research on sarcasm detection for social media comments focuses on sentence-level text sarcasm detection. However, social media users' comments typically revolve around specific topics or events. A topic may have multiple comments, which are intended to describe or subjectively reflect users' opinions on the topic. In light of this phenomenon, the study [5] proposed a topic-oriented sarcasm detection task. This task requires judging whether a comment is a sarcastic expression (i.e., sarcasm or non-sarcasm) on a specific topic, which is different from traditional sentence-level text sarcasm detection. To solve this task, they built a topic-oriented sarcastic expression prompt learning model. This model leverages prompt learning to utilize the Pretrained Language Model (PLM) and achieves better performance than models that utilize PLM based on features and fine-tuning, thereby effectively modeling the topic-oriented sarcasm detection task.

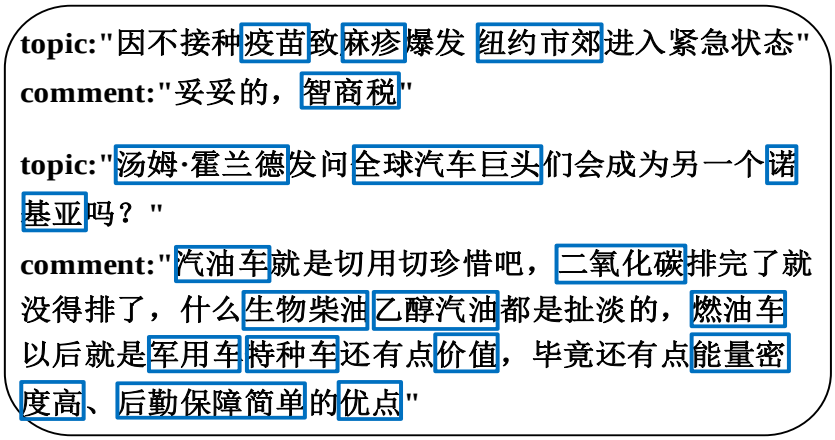

Fig. 1. Two examples of topic-comment text pairs on *ToSarcam*

As a new paradigm for utilizing PLM, prompt learning aims to effectively use pre-training information by aligning the learning process with pre-training objectives. This approach overcomes the data starvation problem of fine-tuning. Previous PLM utilization methods, especially fine-tuning, have achieved great success under data-sufficient conditions, but they tend to perform poorly in low-resource scenarios. Unlike methods that utilize PLM to directly output class distributions based on features and fine-tuning, prompt learning methods mask specific label words and make predictions like a cloze problem. (e.g., *“这是一条针对话题1的<_>评论。”* This is a <_> comment for Topic 1.). This greatly reduces the disparity between pre-training and target task. Additionally, in low-resource environments with a limited number of training

examples, prompt learning has also shown significant effectiveness [6-8]. Therefore, prompt learning is anticipated to enhance topic-oriented sarcasm detection task in real-world scenarios.

In addition, knowledge graphs can benefit topic-oriented sarcasm detection task through entity representation. Generally, topics are condensed, comments are subjectively tendentious, and both are filled with entities. These entities may appear in a variety of forms, such as aliases, abbreviations, and alternative spellings. Figure 1 shows two topic-comment text pairs in the *ToSarcam* dataset, which include entities such as *"纽约市郊"* (suburbs of New York City), *"智商税"* (IQ tax), *"汤姆·霍兰德"* (Tom Hollander), *"诺基亚"* (Nokia), and *"汽油车"* (gasoline car). In the comment *"妥妥的，智商税"* (Sure enough, IQ tax), the entity *"智商税"* (IQ tax) is a slang or metaphorical term. It refers to the consequences of not getting *"疫苗"* (vaccinated) leading to an outbreak of *"麻疹"* (measles) in the *"纽约市郊"* (suburbs of New York City). In another topic-comment text pair, the entity *"汽油车"* (gasoline car) is another name for the entity *"燃油车"* (fuel car), and they both refer to cars that need to use oil. In addition, the entity *"生物柴油"* (biodiesel) and the entity *"乙醇汽油"* (ethanol gasoline) refer to one type of diesel and gasoline respectively. These entities usually contain a lot of semantic information and background knowledge. Therefore, we can help the model understand these different entities by introducing external knowledge, thereby improving the model's accuracy in judging sarcastic comments.

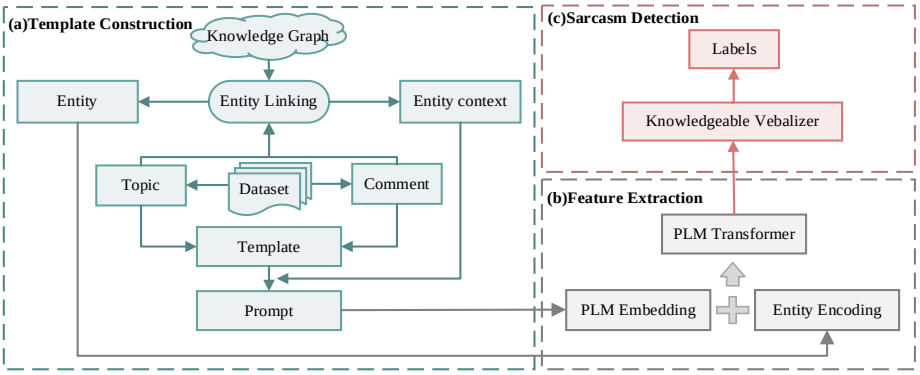

Fig. 2. The frame diagram of the EKPL model

For the model to understand these entities, we use the knowledge graph to obtain the corresponding entity information. The knowledge graph is a multi-relationship graph, which is composed of entity nodes and entity relationship edges. The relationship edges can describe the directional relationship between two entity nodes. The knowledge-level judgments and connections are beneficial to understanding the content of topics and comments because: (1) ambiguity can be avoided by linking each entity in topics and comments to its corresponding entity in the knowledge graph, and the problem of ambiguous entity mentions can be solved. (2) the knowledge graph can also provide more background information about entities, that is, entity context information. It helps to learn knowledge-level relationships among entities in topics and comments and

improves the performance of sarcasm detection. Therefore, the incorporation of external knowledge is crucial for topic-oriented sarcasm detection.

In this paper, we propose an entity knowledge-based prompt learning model for the topic-oriented sarcasm detection task. The frame diagram of the model is shown in Figure 2. First, we design a topic-oriented prompt template for topics. Then we identify entities in topics and comments and obtain the corresponding entities using the knowledge graph *Wikidata* [9]. Next, we extract each entity's directly connected neighbor entities in the knowledge graph as entity context information. Finally, the entity context information and entity information are integrated into prompt learning as external knowledge to enhance prompt guidance for topic-oriented sarcasm detection.

To assess the EKPL model, we conducted experiments on the *ToSarcasm* dataset. The model proves effective in low-resource small sample environments and also achieves good performance when there are enough training examples. The primary contributions of this paper are as follows:

(1) We propose an entity knowledge-based prompt learning model (EKPL), which effectively utilizes PLM through prompt learning for topic-oriented sarcasm detection.

(2) We integrate entity knowledge and entity context knowledge extracted from the knowledge graph into prompt learning to enhance prompt guidance.

(3) We carry out comprehensive experiments on publicly available datasets, with the experimental results showcasing the effectiveness and superior performance of our proposed model in both low-resource and data-rich scenarios.

The rest of this paper is organized as follows: we introduce related work in section 2. In section 3, we explain our target task. And we introduce the details of EKPL in section 4. Section 5 introduces the experimental content and provides a detailed analysis. In section 6 we conclude and look toward future work.

The preparation of manuscripts which are to be reproduced by photo-offset requires special care. Papers submitted in a technically unsuitable form will be returned for retyping, or canceled if the volume cannot otherwise be finished on time.

2. Related Work

2.1. Sarcasm detection

In recent years, scholars have increasingly focused on sarcasm detection in social media comments. Sarcasm detection for social media comments is a challenging task, which is related to multiple factors such as the authenticity of the comment, the author's intention, and the form of text. Following previous works [10-11], we define sarcastic comments as comments that convey sentiments or thoughts opposite to the user's genuine emotions or intentions. The rule-based and dictionary-based method requires researchers to manually design language rules [12] or extract simple statistical patterns from the corpus [13], and then learn through the statistical machine-learning method [14-15] to distinguish the sarcastic tendency of comments.

Thanks to its powerful data-independent modeling capabilities and excellent performance, deep learning technology has recently garnered significant attention in the realm of sarcasm detection. For example, the study [16] proposed a retrieval detection method for verbal sarcasm by retrieving implicit knowledge in the open domain. In [17], Wang et al. proposed a multi-modal mutual learning network for multi-modal sarcasm detection. In addition, transformer-based models have also been applied to sarcasm detection [18-19]. In fact, the determination of sarcasm depends heavily on the topic information. In [20], Lin et al. used the Latent Diliket Allocation (LDA) topic model to build a key feature vocabulary based on consumer topic reviews and discovered sarcastic feature words based on consumer review topics. In response to the problem that topic information cannot be used in multi-label emotion detection tasks, the study [21] proposed a topic-enhanced capsule network to learn the underlying topic information. In [22], Wu et al. performed topic modeling on input images and text and combined latent multi-modal topic features to enrich context.

Topic-oriented sarcasm detection is a type of sarcasm detection, and they all need to detect the sarcastic tendency of sentences. The difference is that the former requires a specific topic to determine whether the sentence is a satirical expression for that topic. This means that the same sentence may have different sarcastic labels when the topic is different. Therefore, compared with traditional sarcasm detection, topic-oriented sarcasm detection is closer to real scenes and more challenging [5]. Inspired by the topic-oriented sarcasm detection task, this paper proposes an Entity Knowledge-based Prompt Learning (EKPL) model. Different from existing methods for this task, we utilize an external knowledge base to link entities in topics and comments, and we introduce entity context information to provide a better explanation of topics and comments.

2.2. Prompt Learning

Existing PLMS have demonstrated their strong performance in various classification tasks, such as ELMo [23], BERT [24], and Roberta [25]. Many studies are also exploring how to better utilize these PLMs. Previous studies are mainly divided into two ways to leverage PLMs: feature-based and fine-tuning. The feature-based approach regards the PLM as a feature extractor, while the fine-tuning approach treats the PLM as an initialized backbone for continued training on downstream tasks [26]. Despite the great success of the above methods, there is an inevitable huge disparity between the language model pre-training and the target task fine-tuning process [27-28].

Fortunately, many studies have explored another reliable paradigm for leveraging PLMs, called prompt learning. Prompt learning can show the potential to further improve performance by narrowing the disparity between language model pre-training and target task training [29-30]. Later, the study [7] proposed the Pattern Exploration Training (PET) method for few-shot learning. This method replaces labels with [MASK] tokens in a manually constructed template, converts the original classification task into a cloze form, and relies on the language model to predict the words filled in at [MASK]. In response to the problem that previous prompt learning-based methods did not consider external information, the study [31] proposed a knowledge-based prompt learning method. This method improves the coverage of labels by integrating external

knowledge bases and demonstrates the effectiveness of knowledge tuning in zero-shot and few-shot text classification tasks. In [32], Xie et al. proposed a method to extract prior knowledge from pre-trained language models using prompts. This method enables the model to effectively extract relevant information from a huge language knowledge base for different relationship types by designing specific query instructions. We leverage prompt learning to use Roberta for topic-oriented sarcasm detection, where the template combines entity knowledge information and learnable tokens.

2.3. Knowledge information utilization

In recent years, external knowledge information has attracted widespread attention in several natural language processing tasks [33-36], including sarcasm detection tasks. Some studies assist in judging the sarcastic tendency of a given text by introducing contextual information [37]. From a multimodal perspective, many studies utilize multimodal data such as images and videos to help with sarcasm detection [38-40]. In addition, some researchers have used knowledge graphs to extract information from text for sarcasm detection [10-11]. The good flexibility of knowledge graphs allows them to be used without external information (such as contextual information and image data). Therefore, we use knowledge graphs for topic-oriented sarcasm detection.

The knowledge graph is composed of multiple entity nodes and edges describing entity relationships, which can provide rich auxiliary information for learning the semantic features of the context. Knowledge graphs are widely used in various fields through entity linking [41-43]. In [44], Hu et al. proposed a method to align knowledge representation with text representation by applying entity-linking technology. In [45], Dun et al. utilize attention mechanisms to adjust word representations and entity knowledge representations. In addition, some studies propose integrating knowledge information into prompt learning. In [16], Wen et al. used prompt learning to identify texts with connotative knowledge related to a given text, thereby improving the model's ability to understand text semantics.

Different from the above methods, our EKPL model integrates knowledge information obtained from the knowledge graph into PLM and further enhances the comprehension of comment content by fusing knowledge information sequences to explore its application in topic-oriented sarcasm detection task.

3. Task Modeling

The topic-oriented sarcasm detection task is a binary classification task. Our research goal is to detect the sarcastic tendency of social media comments on specific topics. We formally define this task as follows: The input is a topic-comment text pair, which contains a topic text and a comment text. The topic text $T = \{t_1, t_2, t_3, \mathrm{L}\ , t_m\}$ consists of m words, and the comment text $C = \{c_1, c_2, c_3, \mathrm{L}\ , c_n\}$ consists of n words. Topic-oriented sarcasm detection aims to predict the label $y \in \{0,1\}$ of a comment C on a

specific topic T, where 1 represents sarcasm comments and 0 represents non-sarcasm comments.

4. Methodology

In this section, we first elaborate on the method for acquiring knowledge, then introduce the method of leveraging PLM through prompt learning in our topic-oriented sarcasm detection task. Finally, we detail its knowledge enhancement method.

The overall architecture of the EKPL model is shown in Figure 3. The input of EKPL is the topic and comment text, and its output is the predicted probability of the labels. Specifically, we first leverage prompt learning to build a topic-oriented template and add learnable tokens to this template. Entity knowledge and entity context knowledge are then extracted from the knowledge graph and their representations are integrated into the template. Finally, we map the labels of sarcastic comments to corresponding words and predict them through a module called Veralizer.

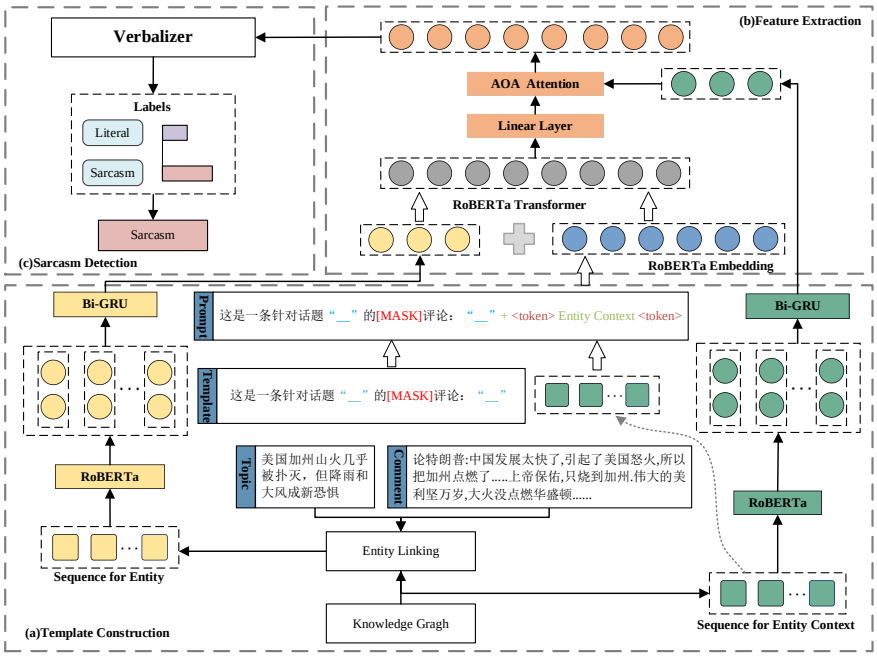

Fig. 3. The overall architecture of the EKPL model

4.1. Knowledge Acquisition

Entity knowledge acquisition. The utilization of external knowledge to enhance the performance of PLM has been extensively researched [46-47]. The purpose of this part is to obtain relevant entity knowledge in topics and comments by knowledge graphs. The model can better comprehend the expression of topic and comment content in this way. Entity linking is the most common method of leveraging knowledge graphs. We use the *TagMe* [48] tool to distinguish entities in topics and comments as shown in Figure 4. Then we align the entities with the corresponding entities in the knowledge graph *Wikidata* [9]. For example, the topic mentions the entity *"特朗普"* (Trump), we link it to and align it with the entity *"唐纳德特朗普"* (Donald Trump) in *Wikidata*. Through this step, we get entity sequence $EN = \{en_1, en_2, en_3, \text{L}\ , en_n\}$.

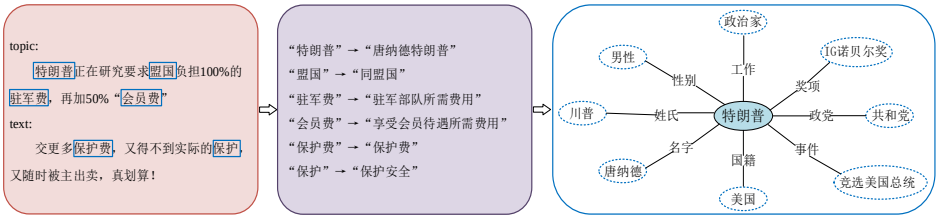

Fig. 4. The process of knowledge extraction

Entity context knowledge acquisition. The entity context is obtained based on the corresponding entities aligned above. For entity en_i, we define the entity context as the entity node adjacent to en_i in the knowledge graph. Therefore, we extract the entity node en_j that is related to the current entity en_i and has a distance of $ec(en_i)$ as the entity context r:

$$ec(en_i) = \left\{ en_i \middle| (en_i, r, en_j) \in K \wedge \left(\left| d_{en_j} - d_{en_j} \right| \right) = 1 \right\} \tag{1}$$

where r is the relationship between entity en_i and entity en_j, K is the knowledge graph, and d is the distance between entity en_i and entity en_j. For example, the entity nodes adjacent to the entity *"唐纳德特朗普"* (Donald Trump) are *"美国总统"* (President of the United States), *"IG诺贝尔奖"* (IG Nobel Prize), *"政治家"* (Politician), *"共和党"* (Republican Party) and so on. These adjacent entity nodes form the entity context of entity *"唐纳德特朗普"* (Donald Trump). Then we can get the entity context sequence: $EC = \{ec(en_1), ec(en_2), ec(en_3), \text{L}\ , ec(en_n)\}$.

4.2. Prompt Learning

To address the challenge of data scarcity during fine-tuning, we use a different PLM utilization paradigm, namely prompt learning. Similar to pre-training, prompt learning uses a cloze-style approach to the tuning process. Therefore, it makes more effective use of pre-training information, thereby further improving performance in data-scarce conditions [8]. In this section, we introduce in detail the proposed entity knowledge-based prompt learning model, which uses entity knowledge in prompt learning to complete the topic-oriented sarcasm detection task.

In the topic-oriented sarcasm detection task, the input to our model is a topic-comment text pair that contains a topic text and a comment text. Assume that the topic contains m words and the comment contains n words. We denote the topic text sequence as $T=\{t_1,t_2,t_3,\mathrm{L}\ ,t_m\}$ and the comment text sequence as $C=\{c_1,c_2,c_3,\mathrm{L}\ ,c_n\}$. To be aligned with the pre-training process, we use a task-related template te to encapsulate the input. This template is carefully designed and summarized based on the characteristics of the topic-oriented sarcasm detection task. We mask a keyword in the template and then add topics and comments to this template. The specific content and representation of the template are as follows:

这是一条针对话题 "T" *的* [MASK] *评论* "C"

(This is a [MASK] comment "C" for topic "T")

$$te=\left[z_1^{te},\mathrm{L}\ ,T,z_i^{te},\langle mask\rangle,\mathrm{L}\ ,z_w^{te},C\right] \tag{2}$$

Meanwhile, the use of entity information and entity context information containing rich knowledge can effectively promote the topic-oriented sarcasm detection task. Therefore, we propose a method to incorporate entity knowledge representations that are extracted from knowledge graphs into prompt learning. We add the obtained entity context to the template that we constructed as a supplementary explanation of the entities in the template, thereby forming a new interpretable template to advance our prompt learning model.

4.3. Entity knowledge utilization

First, we add the entity context sequence EC obtained from the knowledge graph to the template te to explain the large number of entities contained in the topics and comments in the template, thereby enhancing the guidance performance of the template.

We splice the entity context sequence EC after the template te to form a new prompt p:

这是一条针对话题 "T" *的* [MASK] *评论* "C"$|EC$

(This is a [MASK] comment "C" for topic "T"$|EC$)

Inspired by [49], prompt with special learnable tokens can make prompt learning more effective. Therefore, we further add learnable tokens to the prompt p. We insert two special learnable tokens "<ht>" (head token) and "＜tt＞" (tail token) into the head and tail of the entity context sequence EC. The special learnable tokens are randomly initialized and updated during training. The specific content and expression of the prompt are as follows:

这是一条针对话题 "*T* "*的*[MASK] *评论* "*C* "|<ht> *EC* ＜tt＞
(This is a [MASK] comment " *C* " for topic " *T* "|<ht> *EC* ＜tt＞)

$$p = \left[z_1^{te}, \mathrm{L}\ , T, z_i^{te}, \langle mask \rangle, \mathrm{L}\ , z_w^{te}, C \middle| \langle ht \rangle, EC, \langle tt \rangle \right] \tag{3}$$

Then, we divide Roberta's encoder into two parts: embedding and transformer. As shown in formula (4):

$$RoBERTa\_Encoder(p) = RoBERTa\_Transformer\left(RoBERTa\_Embedding(p)\right) \tag{4}$$

We input the prompt p into the embedding layer of Roberta for prompt embedding. As shown in formula (5):

$$e_1^{te}, \mathrm{L}\ , e^T, e_i^{te}, e_{mask}^{te}, \mathrm{L}\ , e_w^{te}, e^C \middle| e_{ht}, e^{EC}, e_{tt} = RoBERTa\_Embedding\left(p\right) \tag{5}$$

where e_i^{te} is the embedding of the i-th word in template te. e^T, e^C and e^{EC} are the embeddings of topic text sequence, comment text sequence, and entity context sequence respectively. e_{mask}^{te}, e_{ht} and e_{tt} are the embeddings of mask <mask>, learnable tokens <ht> and <tt> respectively.

Next, we encode the entity sequence EN and entity context sequence EC separately. We encode entity sequence EN and entity context sequence EC with Roberta to obtain entity encoding $EN' = \left(r_1^{EN}, r_2^{EN}, \mathrm{L}\ , r_n^{EN}\right)$ and entity context encoding $EC' = \left(r_1^{EC}, r_2^{EC}, \mathrm{L}\ , r_n^{EC}\right)$:

$$r_1^{EN}, \mathrm{L}\ , r_n^{EN} = RoBERTa\left(en_1, \mathrm{L}\ , en_n\right) \tag{6}$$

$$r_1^{EC}, \mathrm{L}\ , r_n^{EC} = RoBERTa\left(ec\left(en_1\right), \mathrm{L}\ , ec\left(en_n\right)\right) \tag{7}$$

We utilize the Bidirectional Gated Recurrent Unit (Bi-GRU) to perform feature extraction on entity encoding EN' and entity context encoding EC'. Bi-GRU utilizes gating mechanisms to capture long-term information of sequences and is less complex than Bidirectional Long Short-Term Memory (Bi-LSTM). The formulas are as follows:

$$h_1^{EN}, \mathrm{L}\ , h_n^{EN} = Bi-GRU\left(r_1^{EN}, \mathrm{L}\ , r_n^{EN}\right) \tag{8}$$

$$h_1^{EC}, \mathrm{L}\ , h_n^{EC} = Bi-GRU\left(r_1^{EC}, \mathrm{L}\ , r_n^{EC}\right) \tag{9}$$

where h_i^{EN} and h_i^{EC} are feature vectors containing entity sequence information and entity context sequence information respectively.

Knowledge integration. We choose the head feature h_1^{EN} and tail feature h_n^{EN} in the feature vector $h_1^{EN}, \mathrm{L}\ , h_n^{EN}$ that contains long-term and bidirectional entity sequence information output through Bi-GRU as the representation of entity knowledge. These two vectors are then added to the learnable tokens e_{ht} and e_{tt} in the prompt embedding:

$$\hat{e}_{ht} = e_{ht} + h_1^{EN} \tag{10}$$

$$\hat{e}_{tt} = e_{tt} + h_n^{EN} \tag{11}$$

Next, we extract features from the prompt embedding containing entity knowledge to obtain prompt features through Roberta's transformer:

$$l_1^{te}, \mathrm{L}\ , l^C \middle| l_{ht}, \mathrm{L}\ , l_{tt} = RoBERTa\_Transformer\left(e_1^{te}, \mathrm{L}\ , e^C \middle| \hat{e}_{ht}, \mathrm{L}\ , \hat{e}_{tt}\right) \tag{12}$$

After getting the prompt features, we perform a linear transformation on them:

$$L = \left(l_1^{te}, \mathrm{L}\ , l^C \middle| l_{ht}, \mathrm{L}\ , l_{tt}\right) \cdot W^T + b \tag{13}$$

where W is the weight matrix with dimension [256,768], b is the bias vector with dimension [1,256] and L is the output matrix.

To better learn the relevant information between prompt and entity context, we introduce an Attention-over-Attention (AOA) mechanism after the output matrix L. This mechanism can further refine the relationship between hints and entity context by calculating the word pair correlation matrix, thereby improving the performance of the model. Firstly, we calculate an interaction matrix I:

$$I = L \cdot \left(h_i^{EC}\right)^T \tag{14}$$

where $\left(h_i^{EC}\right)^T$ is the transpose of the entity context feature vector.

Each row or column of this interaction matrix I represents the word pair correlation between topic and comment. We perform *softmax* normalization on each row to obtain an attention matrix α of the prompt relative to the entity context. Then we perform *softmax* normalization on each column to obtain an attention matrix β of the entity context relative to the prompt. Then we average β by column to get the EC-level attention representation $\bar{\beta}$, and do the dot multiplication with $\boldsymbol{\alpha}$ to get the prompt-level attention representation γ:

$$\gamma = \alpha \cdot \bar{\beta}^T \tag{15}$$

Finally, the correlation representation s between the prompt and the entity context is the weighted sum of the output matrix L and the attention representation γ:

$$s = L^T \cdot \gamma \tag{16}$$

Veralizer. We use a module called Veralizer to simulate the process of predicting mask words in pre-training. This module maps labels to corresponding words, which are called mapping words. Inspired by [26], we convert each label into words with similar meanings through a similar translation method. For example, the label *“讽刺”* (sarcasm) can be similarly translated as *“反讽”* (irony) and *“讥讽”* (satire). Figure 5 shows the mapping details between the label *“讽刺”* (sarcasm) and its mapping words. As shown in Figure 6, the topic-oriented sarcasm detection is a binary classification task, we set the label opposite to the label *“讽刺”* (sarcasm) as *“字面”* (literal) based on the template content *“这是一条针对话题“T”的* [MASK] *评论“C””*.

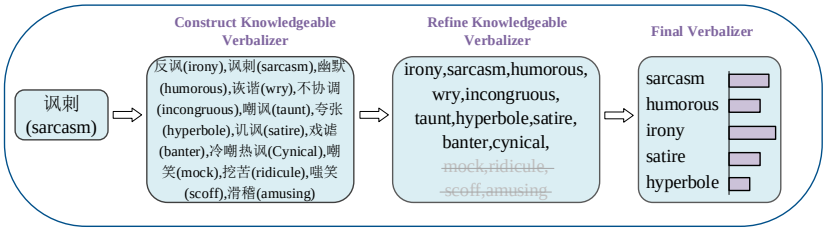

Fig. 5. Mapping words corresponding to the label *“讽刺”* (sarcasm)

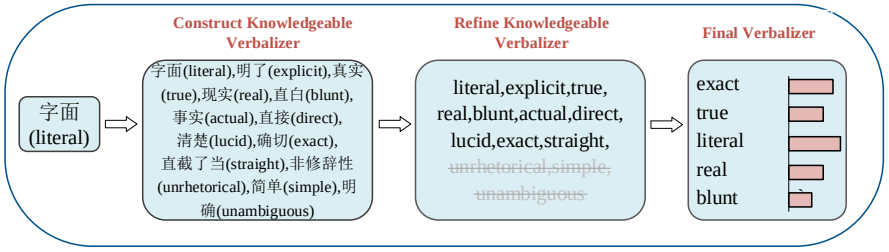

Fig. 6. Mapping words corresponding to the label *"字面"* (literal)

First, we use *Related Words*[‡] and *Google Translation*[§] to obtain words with similar meanings to the labels. *Related Words* is a knowledge graph that integrates various resources, including word embeddings, *ConceptNet*, etc. Then we select 10 mapping words based on the word similarity provided by *Related Words* and *Google Translation*.

Finally, we use MLP to predict the distribution probability of the <mask> position mapping word:

$$P\left(mw|p\right)=MLP\left(s_{mask}^{te}\right) \tag{17}$$

where mw is the mapping word, $P\left(mw|p\right)$ is the probability distribution of the mapping word mw, s_{mask}^{te} is the feature of the mask <mask> in the correlation representation s.

Since each mapping word has a different importance in the corresponding label, we allocate a learnable weight q_{mw} to each mapping word. The label probability $P\left(y|p\right)$ can be obtained through the learnable weight q_{mw} and the probability distribution of the mapping word $P\left(mw|p\right)$:

$$P\left(y|p\right)=sigmoid\left(\sum_{mw\in S_y}q_{mw}P\left(mw|p\right)\right) \tag{18}$$

where S_y is the mapping word set corresponding to the label.

We use cross-entropy loss and L2 loss function to train and optimize our EKPL model. In addition, we use dropout to prevent model overfitting, thereby enhancing the model's generalization ability and robustness:

$$Loss=-\sum_{i=1}^{N}\sum_{j=1}^{K}y_i^j\log P\left(y_i^j|p\right)+\lambda\left\|\Theta\right\|^2 \tag{19}$$

where N is the total number of training samples and K is the total number of categories. y_i^j is the true label of training sample i belonging to category j. $P\left(y_i^j|p\right)$ is the probability that training sample i belongs to category j. λ is the L2 regularization coefficient. Θ represents a trainable parameter in the model (e.g. Weight_decay).

[‡] https://relatedwords.org
[§] https://translate.google.com

5. Experiment

In this section, we will verify the validity of the model through experiments. We first present the details of the dataset and related parameter settings. Then, we present and summarize the results of our model on test data. Finally, we analyze the stability and visualization of the model.

Table 1. Dataset information

Label	Train	Validation	Test	Total	Ratio (%)
irony	1464	486	486	2436	50.01
literal	1461	487	487	2435	49.99
total	2925	973	973	4871	100

5.1. Experiment Setup

To verify the effectiveness of our model, we conduct experiments on the publicly available *ToSarcasm* dataset. *ToSarcasm* is a dataset consisting of 4871 topic-comment text pairs, including 707 topics and 4871 comments. These topics and comments come from the *Guanchazhe*[**] website, and are mostly related to political news and humanities and social science. The statistics of the dataset are shown in Table 1.

Due to the scarcity of public Chinese sarcasm detection datasets, *ToSarcasm* is the only existing publicly known topic-oriented sarcasm detection Chinese dataset. Therefore, we set up "Few-shot" and "Full-scale" in the comparison experiment and ablation experiment to simulate low-resource scenario and sufficient-resource scenario.

Few-shot. We randomly select (5, 10, 20, 50, 100) samples from the original training set as the training set to simulate the real low-resource scenario. Then we create the development set of the same size, and the test set still uses the original test set. Considering that the training set and development set with different sample sizes in low-resource scenarios significantly affect model performance, we repeated the above sampling method on 10 random seeds for the experiment. The results of the experiments were averaged after removing the maximum and minimum values.

Full-scale. We directly use the original training set, development set and test set in the *ToSarcasm* dataset. The ratio of the three sets is 6:2:2 and they are all balanced sets.

Model settings. We use Roberta-base [25] as our PLM. The hidden vector dimension of Roberta-base is 768, and the hidden layer dimension of Bi-GRU is 256. We have set the hidden layer size to 200 for MLP. To prevent overfitting, we use dropout to reduce the density of the model, and we set dropout to 0.2. During the training process, if the learning performance of the model does not improve after more than 10 times, the training will end early. We use the *Adam* optimizer [50] to optimize the parameters of the model.

[**] https://www.guancha.cn/

Considering that our goal is to detect sarcastic comments, we set *“讽刺”* (sarcasm) as a positive example and *“字面”* (literal) as a negative example. We use precision (P), recall (R), accuracy (Acc), and F1-score (F1) to evaluate the model's classification performance. The calculation formula for each evaluation indicator is as follows:

$$Accuracy = \frac{TP + TN}{TP + TN + FP + FN} \tag{20}$$

$$Precision = \frac{TP}{TP + FP} \tag{21}$$

$$Recall = \frac{TP}{TP + FN} \tag{22}$$

$$F1 - score = \frac{2 \times P \times R}{P + R} \tag{23}$$

where TP represents the number of samples where the predicted label and the actual label both are *“讽刺”* (sarcasm); FP represents the number of samples where the predicted label is *“讽刺”* (sarcasm) but the actual label is *“字面”* (literal); FN represents the number of samples where the predicted label is *“字面”* (literal) but the actual label is *“讽刺”* (sarcasm); TN represents the number of samples where the predicted label and the actual label both are *“字面”* (literal).

5.2. Comparative Methods

In this section, we compare our EKPL model with traditional word vector models (1-3), which do not use PLM. Furthermore, we compare our EKPL model with feature-based models (4-5) and standard fine-tuned models (6-7). We further compare our EKPL model with several other powerful models for prompt learning (8-9). The details are as follows:

(1) **Bi-LSTM** [51]: Use bidirectional LSTM to extract features from sentences and targets respectively, and then concatenate the extracted hidden layer features, which are finally used as classification features for sarcasm detection.

(2) **MIARN** [52]: Effectively captures the contextual semantics of multi-dimensional information through the attention mechanism and Bi-LSTM, and then learns the inconsistency of sarcastic expressions in topics and comments, ultimately achieving accurate sarcasm detection.

(3) **ADGCN** [53]: Utilizes external sentiment knowledge and adaptive dynamic graph convolutional networks to model sentiment inconsistencies in topics and comments to detect sarcastic expressions.

(4) **BERT** [24]: The pre-trained language model BERT-base-Chinese can semantically represent target sentences and capture contextual semantic relationships through pre-training and fine-tuning.

(5) **ADGCN-BERT** [53]: Combines the Adaptive Dynamic Graph Convolution Network (ADGCN) and the pre-trained language model BERT-base-Chinese.

(6) **KL-BERT** [54]: A sarcasm detection model based on BERT and incorporating common sense knowledge.

(7) **KC-ISA-BERT** [55]: An implicit sentiment analysis model that uses a joint attention mechanism to integrate external common sense and contextual features.

(8) **PET** [7]: Use the "[CLS]s[SEP]t[SEP] this is [MASK]" template as the input of the pre-trained language model BERT-base-Chinese, and predict whether the [MASK] position corresponds to "sarcasm" or "non-sarcasm"

(9) **TOSPrompt** [5]: Prompt learning is used to construct a topic-oriented sarcastic expression prompt template to determine the sarcastic tendency of comments on specific topics.

5.3. Experimental Results and Analysis

Our experiments on the *ToSarcasm* dataset are shown in Table 2 and Table 3. From Table 2 and Table 3 we can derive the following results:

Table 2. Comparison between our model and other models in **Few-shot**. The best results among the comparison models are marked with "*"

Model	Few-shot									
	5		10		20		50		100	
	Acc	F1	Acc	F1	Acc	F1	Acc	F1	Acc	F1
Bi-LSTM	23.17	26.06	28.27	30.76	35.56	37.58	31.60	33.36	39.67	41.43
MIARN	24.89	26.54	26.23	27.76	19.52	20.45	18.45	20.84	40.67	42.25
ADGCN	27.53	29.30	30.09	31.98	31.91	33.56	34.03	35.94	41.90	43.57
BERT	35.24	36.75	33.71	36.32	35.90	37.70	38.57	40.38	47.23	50.65
KL-BERT	35.89	36.27	34.66	36.71	35.41	37.83	38.72	40.59	48.17	50.90
ADGCN-BERT	30.94	32.75	36.04	38.61	42.38	44.97	50.57	52.30	58.16	60.98
KC-ISA-BERT	29.06	30.97	36.75	38.32	42.88	44.80	50.79	51.80	58.23	61.23
PET	36.67	37.80	37.07	38.78	43.44*	45.20	50.08	52.63	59.87	61.57
TOSPrompt	37.52*	39.61*	41.67*	43.22*	43.02	45.68*	51.16*	53.39*	60.22*	62.88*
EKPL	40.83	41.25	42.77	43.92	46.40	48.34	52.52	54.60	61.29	63.51

Comparison with Word Vector Models. First, we analyze the results between traditional word vector models and our entity knowledge-based prompt learning model. We used Chinese Word Vectors [56] to initialize word vectors for the three comparison models of Bi-LSTM, MIARN, and ADGCN. According to the experimental results, our entity knowledge-based prompt learning model has significantly improved the four evaluation indicators of precision, recall, accuracy, and F1-score compared to the traditional word vector models. Because the traditional word vector models have shortcomings in text semantic representation. In addition, the PLM-based models have also improved their indicators compared with the traditional word vector models. It can be shown that in the topic-oriented sarcasm detection task, the PLM-based models have better results.

Table 3. Comparison between our model and other models in **Full-scale**. The best results among the comparison models are marked with "*"

Model	Full-scale	
	Acc	F1
Bi-LSTM	63.72	66.65
MIARN	65.32	68.25
ADGCN	65.90	69.19
BERT	69.17	69.09
KL-BERT	69.66	70.14
ADGCN-BERT	70.40	70.83
KC-ISA-BERT	70.57	71.88
PET	70.70	71.44
TOSPrompt	71.76*	73.20*
EKPL	73.77	74.04

Comparison with other PLM utilization models. Second, we compare our prompt learning model with feature and fine-tuning based PLM utilization models (KL-BERT, BERT, KC-ISA-BERT, ADGCN-BERT). It can be seen that our prompt learning model achieves better performance. It proves that our prompt learning model can better utilize PLM information. In addition, through the comparison of the above four PLM utilization models and prompt learning models (PET, TOSPrompt), we found that prompt learning has better results in topic-oriented sarcasm detection tasks. A simple sentence-level sarcasm detection model cannot complete the topic-oriented sarcasm detection task well, but this problem can be better solved with the help of the topic information prompt.

Comparison with conventional prompt learning models. Finally, we validate the contribution of external knowledge to prompt learning. We compared our entity knowledge-based prompt learning model with conventional prompt learning models (PET, TOSPrompt). Compared with PET, our EKPL model improves accuracy and F1-score by 2.01% and 0.84% respectively. Compared with TOSPrompt, our EKPL model improves accuracy and F1-score by 3.07% and 2.60% respectively. This shows that external knowledge can effectively guide prompt learning, thereby improving model performance.

The above results show that our EKPL model achieves the best classification performance when the training data is sufficient. Our EKPL model still has good performance when training data is insufficient. Therefore, this model is suitable for topic-oriented sarcasm detection tasks in real scenarios. We summarize the reasons for the good performance of the EKPL model into the following two points: 1) EKPL uses prompt learning to model topic-oriented sarcasm detection tasks, and by designing a topic-oriented sarcastic expression prompt learning template, it can better learn the sarcastic expression information in comments. 2) EKPL uses entity knowledge and entity context knowledge to eliminate ambiguity caused by entities in topics and comments. It uses the attention mechanism to effectively integrate entity information into prompt learning.

Comparison with EKPL variants. We conducted ablation experiments to verify the effectiveness of each part of the EKPL model. Variants of EKPL are as follows:

EKPL-EC: EKPL-EC is a variant of EKPL without entity context knowledge. The specific method is to remove the entity context sequence in the prompt and remove the AOA mechanism and the entity context features input to the AOA mechanism.

EKPL-EN: EKPL-EN is a variant of EKPL without entity knowledge. We remove learnable tokens so that entity sequence features cannot be added to the corresponding positions of the learnable tokens in the prompt embedding.

EKPL-EC-EN: EKPL-EC-EN is a variant of EKPL without entity knowledge and entity context knowledge. This variant only uses a manually designed template for prompt learning and is equivalent to the regular prompt learning model.

EKPL-LW: EKPL-LW is a variant of EKPL without learnable weight for mapping words.

EKPL-PT: EKPL-PT is a variant of EKPL that does not use prompt learning. We feed topics and comments directly into the model and keep only two learnable tokens.

EKPL-TM: EKPL-TM is a variant of EKPL without template. We do not use templates for prompt learning, only keeping <mask> and entity knowledge injection.

EKPL-AOA: EKPL-AOA is a variant of EKPL without the AOA mechanism.

Table 4. Ablation study in **Few-shot**

variants	Few-shot									
	5		10		20		50		100	
	Acc	F1	Acc	F1	Acc	F1	Acc	F1	Acc	F1
-PT	32.14	33.49	33.98	34.21	33.90	34.00	35.61	36.37	37.78	38.82
-TM	32.85	33.76	32.47	33.95	34.35	35.49	35.69	36.21	39.21	40.21
-EC-EN	35.25	36.30	35.92	36.53	37.34	38.57	38.60	39.08	43.51	44.73
-EN	37.80	38.54	38.78	39.59	44.20	45.03	50.63	51.41	59.73	60.51
-EC	37.48	38.74	39.57	40.14	45.37	46.07	51.64	52.16	60.43	61.17
-LW	38.12	39.68	40.50	41.16	45.69	46.90	51.41	52.20	60.74	61.90
-AOA	39.51	40.17	41.48	42.43	46.39	47.53	52.12.	53.37	61.29	62.10
EKPL	40.83	41.25	42.77	43.92	46.40	48.34	52.52	54.60	61.96	63.51

As shown in Table 4 and Table 5, the variants of EKPL show varying degrees of performance degradation, which indicates that each part of EKPL is effective. Variant EKPL-PT and variant EKPL-TM have the most significant performance degradation. One possible reason is that after losing the guidance of the prompt, it is difficult for the model to understand the comment content based on the topic, resulting in more errors when predicting the meaning of the <mask> position. The result proves the importance of prompt learning and the construction of a template for prompt learning. When we remove entity context knowledge, the Acc and F1 of EKPL-EC decrease by 2.40% and 1.28% respectively. This shows that comprehensive entity context knowledge is helpful for understanding entities in topics and comments. When we ignore entity knowledge, the Acc and F1 of EKPL-EN decrease by 2.54% and 1.39% compared with EKPL. The result shows that entity knowledge plays an important role in entity disambiguation. It also provides a basis for effectively combining entity context knowledge. When we remove external knowledge from EKPL, the indicators of EKPL-EC-EN decrease. For example, there is a 2.29% drop compared to EKPL in terms of F1-score. The research

result shows that entity knowledge is instructive for EKPL to detect sarcasm. Furthermore, we observe that the variant EKPL-LW performs comparably to fine-tuning without learnable weight for mapped words. Probably because PLM has a fixed prior preference for [MASK] prediction, which is determined by the pre-training process. The learnable weights of mapping words map the mapping words to the label through weighted summation to obtain more accurate results.

Table 5. Ablation study in Full-scale

variants	Full-scale	
	Acc	F1
-PT	68.48	69.06
-TM	69.56	70.49
-EC-EN	70.44	71.75
-EN	71.23	72.65
-EC	71.37	72.76
-LW	72.18	73.30
-AOA	72.32	73.93
EKPL	73.77	74.04

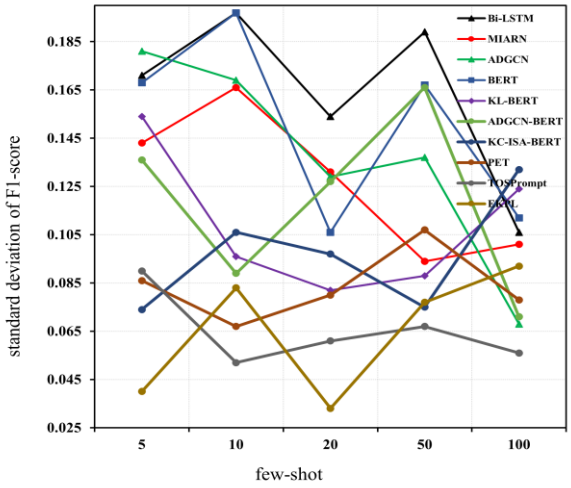

Fig. 7. The standard deviation of F1-score in few-shot settings

5.4. Stability Analysis

The stability of a model is also an important indicator for evaluating model performance, so we measured and analyzed the stability of our EKPL model. Model stability is measured as the standard deviation of F1-score. As shown in Figure 7, we compared the standard deviations of the 10 experimental results of each model under

few-shot in the comparative experiment. It can be found that our EKPL model is more stable than feature-based, fine-tuning and other prompt learning models in most cases through comparison. This proves that our model has great stability.

In addition, we found that the standard deviation of the model will show a downward trend as the few-shot increases. We noticed that the word vector-based models tend to be more stable than various PLM utilization models in the case of smaller few-shots. It may be that PLM-based models are prone to overfitting when there is insufficient data, resulting in poor generalization ability and high randomness of the model.

5.5. Visualization of mapping word weights

We analyze the weight of each answer word after training. We average the answer weights under few-shot settings.

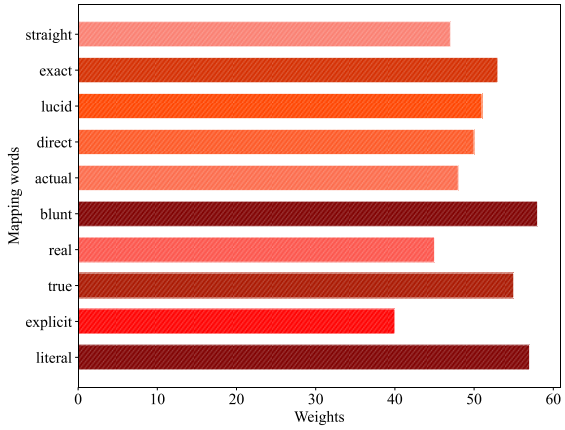

Fig. 8. The mapping word weights of literal label

Among the mapping words corresponding to the label *“字面”* (literal), *“直白”* (blunt) has the highest weight, while *“明了”* (explicit) has the smallest weight. As shown in Figure 8, it may be that PLM has a strong preference for the word *“直白”* (blunt). This result suggests that PLM's perception and understanding of words may be different from humans. As shown in Figure 9, we performed a visual analysis of the weight of each mapped word after training. Among the mapping words corresponding to the label *“讽刺”* (sarcasm), *“讽刺”* (sarcasm) and *“反讽”* (irony) have higher weights, which is in line with our predictions.

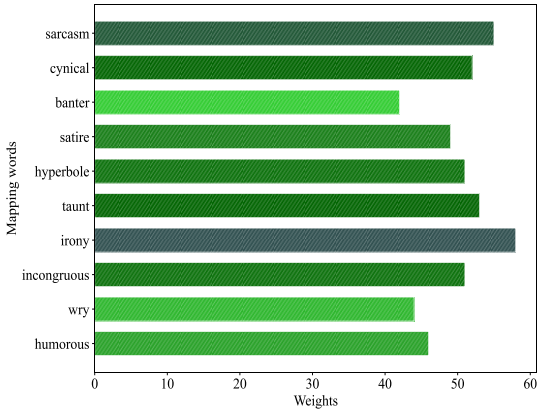

Fig. 9. The mapping word weights of sarcasm label

6. Conclusion

In this paper, we propose an entity knowledge-based prompt learning model (EKPL) to solve the topic-oriented sarcasm detection task. The core idea of the model is to use prompt learning to guide PLM. It adopts the same goal as the language model pre-training, significantly narrowing the gap between pre-training and target task training. In addition, we inject entity knowledge into our well-designed template to refine the prompt representation. This can further enhance our sarcasm detection model. To the best of our knowledge, this is the first work to combine prompt learning and knowledge graphs for topic-oriented sarcasm detection.

To evaluate our model, we conduct experiments on the publicly available *ToSarcasm* dataset. Comparison with different PLM utilization methods and other prompt learning models fully illustrates the superiority of our prompt learning method and the effectiveness of external knowledge on our prompt learning model. Furthermore, we conduct a detailed discussion and analysis of the results for a comprehensive understanding of our model.

In future work, we will look for better knowledge representations and incorporate them as explicit features into prompt learning and deep neural networks to further improve the performance of sarcasm detection models.

Acknowledgments. This work was supported by the National Natural Science Foundation of China (Grant NO.62076006), the Opening Foundation of the State Key Laboratory of Cognitive Intelligence, iFLYTEK (Grant NO.COGOS-2023HE02), and the University Synergy Innovation Program of Anhui Province (Grant NO.GXXT-2021-008).

References

1. Kanakam, R., & Nayak, R. K. (2021, June). Sarcasm Detection on Social Networks using Machine Learning Algorithms: A Systematic Review. In 2021 5th International Conference on Trends in Electronics and Informatics (ICOEI) (pp. 1130-1137). IEEE.
2. Zhang, S., Zhao, T., Wu, H., Zhu, G., & Li, K. (2023). TS-GCN: Aspect-level sentiment classification model for consumer reviews. Computer Science and Information Systems, 20(1), 117-136.
3. Khan, M., & Malviya, A. (2020, February). Big data approach for sentiment analysis of twitter data using Hadoop framework and deep learning. In 2020 International Conference on Emerging Trends in Information Technology and Engineering (ic-ETITE) (pp. 1-5). IEEE.
4. Wang Z, Hu S, Liu W. Product feature sentiment analysis based on GRU-CAP considering Chinese sarcasm recognition[J]. Expert Systems with Applications, 2024, 241: 122512.
5. Liang, B., Lin, Z., Qin, B., & Xu, R. (2022, October). Topic-Oriented Sarcasm Detection: New Task, New Dataset and New Method. In Proceedings of the 21st Chinese National Conference on Computational Linguistics (pp. 557-568).
6. Feng K, Huang L, Wang K, et al. Prompt-based learning framework for zero-shot cross-lingual text classification[J]. Engineering Applications of Artificial Intelligence, 2024, 133: 108481.
7. Schick, T., & Schütze, H. (2021, April). Exploiting Cloze-Questions for Few-Shot Text Classification and Natural Language Inference. In Proceedings of the 16th Conference of the European Chapter of the Association for Computational Linguistics: Main Volume (pp. 255-269).
8. Schick, T., & Schütze, H. (2021, June). It's Not Just Size That Matters: Small Language Models Are Also Few-Shot Learners. In Proceedings of the 2021 Conference of the North American Chapter of the Association for Computational Linguistics: Human Language Technologies (pp. 2339-2352).
9. Vrandečić, D., & Krötzsch, M. (2014). Wikidata: a free collaborative knowledgebase. Communications of the ACM, 57(10), 78-85.
10. Wen, Z., Gui, L., Wang, Q., Guo, M., Yu, X., Du, J., & Xu, R. (2022). Sememe knowledge and auxiliary information enhanced approach for sarcasm detection. Information Processing & Management, 59(3), 102883.
11. Ren, Y., Wang, Z., Peng, Q., & Ji, D. (2023). A knowledge-augmented neural network model for sarcasm detection. Information Processing & Management, 60(6), 103521.
12. Pavan Kumar, M. R., & Jayagopal, P. (2023). Context-sensitive lexicon for imbalanced text sentiment classification using bidirectional LSTM. Journal of Intelligent Manufacturing, 34(5), 2123-2132.
13. Ortega-Bueno, R., Rosso, P., & Pagola, J. E. M. (2022). Multi-view informed attention-based model for Irony and Satire detection in Spanish variants. Knowledge-Based Systems, 235, 107597.
14. Vinoth, D., & Prabhavathy, P. (2022). An intelligent machine learning-based sarcasm detection and classification model on social networks. The Journal of Supercomputing, 78(8), 10575-10594.
15. Govindan, V., & Balakrishnan, V. (2022). A machine learning approach in analysing the effect of hyperboles using negative sentiment tweets for sarcasm detection. Journal of King Saud University-Computer and Information Sciences, 34(8), 5110-5120.
16. Wen, Z., Wang, R., Chen, S., Wang, Q., Ding, K., Liang, B., & Xu, R. (2023). RDVI: A Retrieval–Detection Framework for Verbal Irony Detection. Electronics, 12(12), 2673.
17. Wang J, Yang Y, Jiang Y, et al. Cross-modal incongruity aligning and collaborating for multi-modal sarcasm detection[J]. Information Fusion, 2024, 103: 102132.

18. Mohan, A., Nair, A. M., Jayakumar, B., & Muraleedharan, S. (2023). Sarcasm Detection Using Bidirectional Encoder Representations from Transformers and Graph Convolutional Networks. Procedia Computer Science, 218, 93-102.
19. Lu Q, Long Y, Sun X, et al. Fact-sentiment incongruity combination network for multimodal sarcasm detection[J]. Information Fusion, 2024, 104: 102203.
20. Lin, H. C. K., Wang, T. H., Lin, G. C., Cheng, S. C., Chen, H. R., & Huang, Y. M. (2020). Applying sentiment analysis to automatically classify consumer comments concerning marketing 4Cs aspects. Applied Soft Computing, 97, 106755.
21. Fei, H., Ji, D., Zhang, Y., & Ren, Y. (2020). Topic-enhanced capsule network for multi-label emotion classification. IEEE/ACM Transactions on Audio, Speech, and Language Processing, 28, 1839-1848.
22. Wu, S., Fei, H., Cao, Y., Bing, L., & Chua, T. S. (2023). Information Screening whilst Exploiting! Multimodal Relation Extraction with Feature Denoising and Multimodal Topic Modeling. arXiv preprint arXiv:2305.11719.
23. Peters, M., Neumann, M., Iyyer, M., Gardner, M., Clark, C., Lee, K., & Zettlemoyer, L. (2018). Deep contextualized word representations. In Proceedings of the 2018 conference of the north american chapter of the association for computational linguistics: human language technologies, Volume 1 (Long Papers) (pp. 2227–2237).
24. Devlin, J., Chang, M.-W., Lee, K., & Toutanova, K. (2019). BERT: Pre-training of deep bidirectional transformers for language understanding. In Proceedings of the 2019 conference of the north american chapter of the association for computational linguistics: human language technologies, volume 1 (long and short papers) (pp. 4171–4186).
25. Liu, Y., Ott, M., Goyal, N., Du, J., Joshi, M., Chen, D., ... & Stoyanov, V. (2019). Roberta: A robustly optimized bert pretraining approach. arXiv preprint arXiv:1907.11692.
26. Jiang, G., Liu, S., Zhao, Y., Sun, Y., & Zhang, M. (2022). Fake news detection via knowledgeable prompt learning. Information Processing & Management, 59(5), 103029.
27. Zhang, Z., Han, X., Liu, Z., Jiang, X., Sun, M., & Liu, Q. (2019). ERNIE: Enhanced language representation with informative entities. arXiv preprint arXiv:1905.07129.
28. Liu, W., Zhou, P., Zhao, Z., Wang, Z., Ju, Q., Deng, H., & Wang, P. (2020, April). K-bert: Enabling language representation with knowledge graph. In Proceedings of the AAAI Conference on Artificial Intelligence (Vol. 34, No. 03, pp. 2901-2908).
29. Liu, X., & Zheng, Y. (2021). Zhengxiao Du, Ming Ding, Yujie Qian, Zhilin Yang, and Jie Tang. 2021. Gpt understands, too. arXiv preprint arXiv:2103.10385, 6(2).
30. Han, X., Zhao, W., Ding, N., Liu, Z., & Sun, M. (2022). Ptr: Prompt tuning with rules for text classification. AI Open, 3, 182-192.
31. Hu, S., Ding, N., Wang, H., Liu, Z., Wang, J., Li, J., ... & Sun, M. (2021). Knowledgeable prompt-tuning: Incorporating knowledge into prompt verbalizer for text classification. arXiv preprint arXiv:2108.02035.
32. Xie, S., Pan, Q., Wang, X., Luo, X., & Sugumaran, V. (2024). Combining prompt learning with contextual semantics for inductive relation prediction. Expert Systems with Applications, 238, 121669.
33. Zhu, C., Chen, M., Zhang, S., Sun, C., Liang, H., Liu, Y., & Chen, J. (2023). SKEAFN: Sentiment knowledge enhanced attention fusion network for multimodal sentiment analysis. Information Fusion, 100, 101958.
34. Jain, P. K., Quamer, W., Saravanan, V., & Pamula, R. (2023). Employing BERT-DCNN with sentic knowledge base for social media sentiment analysis. Journal of Ambient Intelligence and Humanized Computing, 14(8), 10417-10429.
35. Zhang, B., Hu, Y., Xu, D., Li, M., & Li, M. (2022). SKG-Learning: a deep learning model for sentiment knowledge graph construction in social networks. Neural Computing and Applications, 34(13), 11015-11034.
36. He, Z., Wang, H., & Zhang, X. (2023). Multi-Task Learning Model Based on BERT and Knowledge Graph for Aspect-Based Sentiment Analysis. Electronics, 12(3), 737.

37. Yu, Z., Jin, D., Wang, X., Li, Y., Wang, L., & Dang, J. (2023, August). Commonsense knowledge enhanced sentiment dependency graph for sarcasm detection. In Proceedings of the Thirty-Second International Joint Conference on Artificial Intelligence pp. 2423-2431.
38. Chauhan, D. S., Singh, G. V., Arora, A., Ekbal, A., & Bhattacharyya, P. (2022). An emoji-aware multitask framework for multimodal sarcasm detection. Knowledge-Based Systems, 257, 109924.
39. Bedi, M., Kumar, S., Akhtar, M. S., & Chakraborty, T. (2021). Multi-modal sarcasm detection and humor classification in code-mixed conversations. IEEE Transactions on Affective Computing.
40. Yue, T., Mao, R., Wang, H., Hu, Z., & Cambria, E. (2023). KnowleNet: Knowledge fusion network for multimodal sarcasm detection. Information Fusion, 100, 101921.
41. Cheng, L., Wu, D., Bing, L., Zhang, Y., Jie, Z., Lu, W., & Si, L. (2020, November). ENT-DESC: Entity Description Generation by Exploring Knowledge Graph. In Proceedings of the 2020 Conference on Empirical Methods in Natural Language Processing (EMNLP) pp. 1187-1197.
42. Li, Y., Zou, B., Li, Z., Aw, A., Hong, Y., & Zhu, Q. (2021, November). Winnowing knowledge for multi-choice question answering. In Findings of the association for computational linguistics: EMNLP 2021 pp. 1157-1165.
43. Wei, X., Huang, H., Nie, L., Zhang, H., Mao, X. L., & Chua, T. S. (2016). I know what you want to express: sentence element inference by incorporating external knowledge base. IEEE Transactions on Knowledge and Data Engineering, 29(2), 344-358.
44. Hu, L., Yang, T., Zhang, L., Zhong, W., Tang, D., Shi, C., ... & Zhou, M. (2021, August). Compare to the knowledge: Graph neural fake news detection with external knowledge. In Proceedings of the 59th Annual Meeting of the Association for Computational Linguistics and the 11th International Joint Conference on Natural Language Processing (Volume 1: Long Papers) pp. 754-763.
45. Dun, Y., Tu, K., Chen, C., Hou, C., & Yuan, X. (2021, May). Kan: Knowledge-aware attention network for fake news detection. In Proceedings of the AAAI conference on artificial intelligence Vol. 35, No. 1, pp. 81-89.
46. Guan, J., Huang, F., Zhao, Z., Zhu, X., & Huang, M. (2020). A knowledge-enhanced pretraining model for commonsense story generation. Transactions of the Association for Computational Linguistics, 8, 93-108.
47. Yang, A., Wang, Q., Liu, J., Liu, K., Lyu, Y., Wu, H., ... & Li, S. (2019, July). Enhancing pre-trained language representations with rich knowledge for machine reading comprehension. In Proceedings of the 57th Annual Meeting of the Association for Computational Linguistics pp. 2346-2357.
48. Ferragina, P., & Scaiella, U. (2010, October). Tagme: on-the-fly annotation of short text fragments (by wikipedia entities). In Proceedings of the 19th ACM international conference on Information and knowledge management pp. 1625-1628.
49. Hambardzumyan, K., Khachatrian, H., & May, J. (2021, August). WARP: Word-level Adversarial ReProgramming. In Proceedings of the 59th Annual Meeting of the Association for Computational Linguistics and the 11th International Joint Conference on Natural Language Processing (Volume 1: Long Papers) pp. 4921-4933.
50. Kingma, D. P., & Ba, J. (2014). Adam: A method for stochastic optimization. arXiv preprint arXiv:1412.6980.
51. Graves, A., & Graves, A. (2012). Long short-term memory. Supervised sequence labelling with recurrent neural networks, 37-45.
52. Tay, Y., Luu, A. T., Hui, S. C., & Su, J. (2018, July). Reasoning with Sarcasm by Reading In-Between. In Proceedings of the 56th Annual Meeting of the Association for Computational Linguistics (Volume 1: Long Papers) pp. 1010-1020.

53. Lou, C., Liang, B., Gui, L., He, Y., Dang, Y., & Xu, R. (2021, July). Affective dependency graph for sarcasm detection. In Proceedings of the 44th International ACM SIGIR Conference on Research and Development in Information Retrieval pp. 1844-1849.
54. Li, J., Pan, H., Lin, Z., Fu, P., & Wang, W. (2021). Sarcasm detection with commonsense knowledge. IEEE/ACM Transactions on Audio, Speech, and Language Processing, 29, 3192-3201.
55. Xu, M., Wang, D., Feng, S., Yang, Z., & Zhang, Y. (2022, October). Kc-isa: An implicit sentiment analysis model combining knowledge enhancement and context features. In Proceedings of the 29th International Conference on Computational Linguistics pp. 6906-6915.
56. Li, S., Zhao, Z., Hu, R., Li, W., Liu, T., & Du, X. (2018, July). Analogical Reasoning on Chinese Morphological and Semantic Relations. In Proceedings of the 56th Annual Meeting of the Association for Computational Linguistics (Volume 2: Short Papers) pp. 138-143.

Yuhao Zhou received his Bachelor's degree from the School of Computing Science and Engineering, Anhui University of Science and Technology in 2022, China. At present, he is a MS degree majoring in Computer Science and Technology from the School of Computing Science and Engineering, Anhui University of Science and Technology. His current research interests include natural language processing, sentiment analysis, and complex network.

Shunxiang Zhang received the Ph.D. degree from the School of Computing Engineering and Science, Shanghai University, Shanghai, China, in 2012. He is a Professor at the Anhui University of Science and Technology, Huainan, China. His current research interests include web mining, semantic search, and complex network.

Caiqing Wang received his Bachelor's degree from the School of Computing Science and Engineering, Anhui University of Science and Technology in 2022, China. At present, he is a MS degree majoring in Computer Science and Technology from the School of Computing Science and Engineering, Anhui University of Science and Technology. His current research interests include natural language processing, web intelligent information processing, and calculation theory.

Yanhui Wang received her Bachelor's degree from the School of Computing Science and Engineering, Anhui University of Science and Technology in 2022, China. At present, she is a MS degree majoring in Computer Science and Technology from the School of Computing Science and Engineering, Anhui University of Science and Technology. Her current research interests include natural language processing, web intelligent information processing, and sentiment analysis.

Xiaolong Wang received his Bachelor's degree from the School of Computing Science and Engineering, Anhui University of Science and Technology in 2022, China. At present, he is a MS degree majoring in Computer Technology from the School of Computing Science and Engineering, Anhui University of Science and Technology. His current research interests include natural language processing, web intelligent information processing, and semantic search.

Kuan-Ching Li is currently a Distinguished Professor at Providence University, where he also serves as the Director of the High-Performance Computing and Networking Center. He published more than 450 scientific papers and articles and is the coauthor or coeditor of more than 50 books published by well-known publishers. He is the Editor-in-Chief of IJCSE and IJES and serves as an associate editor for several leading journals. His research interests include parallel and distributed computing, big data, and emerging technologies. He is a fellow of the IET and a Senior Member of the IEEE.

Received: March 20, 2024; Accepted: September 22, 2024.

Computer Science and Information Systems 22(1):59–78 https://doi.org/10.2298/CSIS240420068K

A New Course Difficulty Index (*CDf*): Framework and Application

Konstantinos Kelesidis, Leonidas Karamitopoulos, and Dimitris A. Dervos

Dept. of Information and Electronic Engineering, International Hellenic University, Sindos, Greece
kelesidis@iee.ihu.gr
karamitopoulos@ihu.gr
dad@ihu.gr

Abstract. A new framework for the quantification of course difficulty in academic curricula is proposed. The originality of the approach lies in its course-centric nature. A course difficulty index value is calculated (*CDf*), using difficulty indicators that characterize the course as a whole. The difficulty indicators can be tailored to reflect the academic domain considered. A weighting percentage is calculated and it is assigned to each course difficulty indicator, by systematically conducting Principal Component Analysis (PCA) on students' assessment data. Next, the weighted difficulty indicators are used to calculate *CDf* in the form of a composite indicator. In general, the value of the latter varies across courses, and across different offerings of a given course. The *CDf* framework is applied in the case of a university in Greece by utilizing course difficulty indicators which are objective in their nature, like course mean and median grades, passing grade percentages, etc. The dataset used spans a period of thirteen (13) academic years. The findings are used to identify courses that represent "bottlenecks" in student study paths. Subjective course difficulty indicators may also be used, like students' questionnaire data. It is worth noting that the quantification of course difficulty by means of a single index can be used in the calculation of adjusted student scores and, as such, facilitate data mining operations on students' assessment data. All in all, the proposed *CDf* framework and analysis comprise a useful tool for academic policy-making and quality assurance.

Keywords: course difficulty, difficulty index, learning analytics, principal component analysis, exploratory data analysis, composite indicator.

1. Introduction and Motivation

The present research is motivated by the need to analyze student assessment data in order to devise effective policies for educational development. At the Information and Electronic Engineering (*IEE*) department of the International Hellenic University (*IHU*) in Greece, the task comprises the responsibility of the department's Internal Evaluation Group (*IEG*). Exploratory data analysis and mining operations are conducted on student assessment records, i.e. grades assigned to students in course modules (*courses*, for brevity). A valuable outcome is the identification of courses that present notable challenges for students, equivalently: courses that students find difficult to pass, or achieve a high grade in. Such information is useful in many aspects, from designing course curricula (especially in the context of the new online learning paradigms, like smart education

[1]), and helping students identify their preferred course of study [33], to rating students with respect to their academic performance.

The way course difficulty perplexes the task of rating students on the basis of their performance in courses is best illustrated by an example in [9]: nine courses C_i (*i*=1,...,9) and four students S_i (*i*=1,...,4) are listed in Table 1 alongside with grades assigned to the latter in courses they have been assessed in. When a student has not been assessed in a specific course, the corresponding (*Course*, *Student*) cell is left blank.

Table 1. Student Assessment Scores Example ([9])

Course	Student				Average Course Grade
	S_1	S_2	S_3	S_4	
$\mathbf{C}_1$	93			90	91.5
$\mathbf{C}_2$	85		80		82.5
$\mathbf{C}_3$			100	95	97.5
$\mathbf{C}_4$	80	75			77.5
$\mathbf{C}_5$		97		95	96.0
$\mathbf{C}_6$	93			85	89.0
$\mathbf{C}_7$		92	89		90.5
$\mathbf{C}_8$	92	91	90	88	90.3
$\mathbf{C}_9$		91	89		90.0
Average Student Grade	88.6	89.2	89.6	90.6	

For the example considered, using *Average Course Grade*, the nine courses are ranked in descending order of difficulty as follows: $C_4 > C_2 > C_6 > C_9 > C_8 > C_7 > C_1 > C_5 > C_3$. Each one of the four students is seen to have been assessed in five of the nine courses. In accordance with their *Average Student Grade* values, the four students are ordered as follows: $S_4 > S_3 > S_2 > S_1$. However, when compared to each other and ranked on the basis of their grades in courses they have both enrolled in, the students are ordered as follows: $S_1 > S_2 > S_3 > S_4$. This is exactly the opposite to their *Average Student Grade* based ordering. Evidently, it does not suffice to evaluate student performance by just considering grades obtained in courses. It is important to take into account the difficulty of each one course a student has been assessed in.

In Greece, the academic year consists of the *Fall*- and the *Spring*- semesters. Course offerings are semester based. Each semester, students enroll in courses and they participate in two (2) final examinations periods: *examinations Period-A*, and *examinations Period-B*. Upon completion of each final examinations period, students are awarded an overall grade for each course in which they have been assessed. Examinations Period-A for the Fall semester courses runs from January to February. Likewise, June is the month for the Spring semester's examinations Period-A. In September one common examinations Period-B is held for all courses offered during the academic year (Fall- and Spring-semesters, alike). Student performance grades lie in the [0,10] range. Five (5.0) comprises the minimum grade requirement for passing a course. In the *CDf* framework that is to be considered next, when a student is assessed twice in a given course during the same academic year, both grades are accounted for.

Course difficulty may vary due to, for example, a new instructor stepping in, when there are significant updates to the course's educational and training content, or when the instructor of a given course attempts to address a backlog of students who haven't passed the exam in previous attempts. In this respect, course difficulty need be measured per course offering. Once quantified, it can be used for calculating adjusted student scores that incorporate the difficulty of the course at the time of assessment.

One may argue at this point that percentile-based standard scores like the $T-$ and $z-$scores comprise the means to rate/rank the performance of a student without sticking to a raw x grade [27]. The research herewith presented aims for extending the standard scores paradigm (a) by considering the relative difficulty of a course with respect to other courses of a given academic curriculum, and (b) by allowing room for the difficulty of a given course to vary from one of its offerings to the next.

The present treatise is organised as follows: the research goal is considered in the context of the relevant bibliography in Section 2 (*Related Work*). Five (5) objectives that pertain to the set aims and goals are outlined in Section 3 (*Research Objectives*). The academic dataset used is outlined in Section 4 (*The Dataset*). Section 5 (*Methodology*) comprises a detailed presentation of the proposed *CDf* framework and its application in the case of the *IEE* department at *IHU*. The results obtained are presented and discussed in Sections 6 (*Results*) and 7 (*Discussion*). The treatise concludes by summing up and identifying new potential research goals in Section 8 (*Conclusion and Future Work*).

2. Related Work

Higher education establishments exploit course difficulty relating information to shape and implement educational policies with the aim to (a) increase success rates in exams [2,24,28,31], (b) minimize the prolongation of the typical student's study period [10], and (c) promote fairness in student performance evaluation and ranking [36]. Fair student ranking has long attracted the interest of researchers because academic performance is used in most high-stakes decisions as in the determination of eligibility for scholarships, or job employment [36].

Academic analytics involves a wide range of methodologies and techniques utilized by higher education institutions, alongside with their quality assurance procedures and strategic policies for educational development [24]. In academic analytics, course difficulty arises as an issue in methodologies aimed at improving student performance evaluation, curriculum design, and course sequencing. Yet another analytical outcome of great interest is the prediction of student performance in courses that lie ahead in their study path [3,21]. The relevant data analysis and data mining tasks are expected to benefit from the adoption and use of a (single) difficulty index that characterizes each course offering. However, there appears to be no single approach on the quantification of course difficulty in the relevant research literature.

One approach to quantifying course difficulty is to use instruments like questionnaires that utilize Likert-type prompts to collect the students' perceptions of a course's level of difficulty [7][25]. To better assess the perceived course difficulty, questionnaires are also used to collect demographic information that can be combined with Grade Point Average (GPA) scores, and course-related details (workload, assignments, etc.).

The authors in [23] investigate the correlation between course difficulty and student stress during course selection scheduling. The determination of course difficulty comprises a milestone in fulfilling their research objective. They propose four methods for the classification of courses with respect to their degree of difficulty: pairwise comparison, an Analytic Hierarchy Process (*AHP*), *GPA*, and physiological measurements.

A number of studies propose methods for improving the *GPA* score in order to provide a fairer measure of a student's academic performance [9][36][37]. In this respect, adjusted *GPA* scores are calculated for university students, scores that correlate better with pre-admission measures like high school *GPA* and *SAT* scores. The flaws of the (unadjusted) *GPA* scores relate to the fact that grading standards and practices tend to vary from instructor to instructor, and from department to department within the university. The proposed methods involve a predictive model of student grades based on parameters such as the ability of a student, the difficulty, and the discrimination of a course.

More specifically, the authors in [9] have investigated several models for adjusting a student's *GPA* score to account for the difficulty of the courses they have been assessed in. In the simplest and perhaps most useful approach, the model predicts a student's grade in a course as the difference between two parameters: the student's ability and the grading standard index that corresponds to the course (i.e. the course's difficulty), plus an error term. The two parameters are estimated for each one student and for each one course, in a way that minimizes the error term. An analogous linear model is proposed by Vanderbei et al. in [37], with the student's intrinsic overall aptitude and the course's inherent difficulty as parameters. The authors calculate the values of the two parameters in the case where each student has been assessed in each and every one course, as well as in the case where students enrol in selected courses. In [36], the authors utilize a two-parameter logistic model that predicts the grade of a student in a course. Their approach involves one student parameter (*ability*) and two course parameters (*difficulty* and *discrimination*). For each student, grades are predicted for all the courses in the academic curriculum, even for those that the student in question has not enrolled in. A modelled *GPA* value is computed based on the predicted grades. The approach is shown to remove the course-choice drawback of the (unadjusted) *GPA* scores.

In addition, several methodologies have been devised within the framework of Item Response Theory (*IRT*) [22][30], generating measures that have been demonstrated to be more reliable than conventional *GPA* scores in capturing student performance [16][38][39]. *IRT* is used extensively in the field of education to assess and calibrate items within tests, questionnaires, and other instruments. It is also used to score individuals based on their abilities, attitudes, or other underlying traits. In this regard, *IRT* models are used to calculate adjusted *GPA* scores, aiming to provide a more accurate estimation of students' performance (ability) in academic courses.

In [38] the author uses an *IRT* model called the *Graded Response Model* (*GRM*) on undergraduate student assessment data [32]. A number of K ($K > 2$) ordinal grade categories are assumed to apply. In *GRM*, the probability of a student to achieve a specific grade or higher in one course is expressed as a function of the student's ability, plus the course's difficulty (referred as *grade category boundary*), and discrimination. An important feature of *GRM* is its explicit parameterization of grade category boundaries for each course. In theory, this enables the model to account for variations in instructor grading patterns [16]. The model proposed in [16] can be regarded as a Bayesian extension to

GRM. The primary motivation behind the adjustment is to utilize the relative rankings of students within courses (instead of absolute grades) as a means for evaluating student performance.

3. Research Objectives

All the approaches discussed in Section 2 (*Related Work*) adopt a student-centric approach when assessing course difficulty. More specifically, course difficulty is calculated (a) by considering student responses to questionnaires, or (b) as a model parameter alongside the student's ability and course discrimination, or (c) through a hybrid combination of (a) and (b). This is achieved by assuming that course difficulty remains consistent across the dataset used. To be exact, some approaches allow for course difficulty to vary, say from one course offering to the next, at the cost of increased model complexity, and processing overhead.

The research herewith reported aims to quantify course difficulty from a course-centric (as opposed to student-centric) perspective. In this context, the intended research objectives are set as follows:

1. Course difficulty is to be quantified by means of a single measure (index)
2. The measure will be calculated using a set of course difficulty indicators
3. The mix of the indicators used may vary across different academic environments and systems
4. Course difficulty may vary from one specific course offering to the next
5. Strong emphasis to be given on the visual presentation of the results

Commenting on objective number one, the need for a single measure aims to facilitate further analytical processing such as the calculation of adjusted student scores, and the prediction of students' performance in courses that lie ahead in their study path. In this respect, the calculation of the course difficulty index is seen to comprise a task of the data preparation for data mining stage.

Objective number two relates directly to the course-centric nature of the approach: the measure need be calculated on the basis of parameters that characterize the course as a whole, not on parameters that characterize each individual student assessed.

Objective number three highlights the need for the relevant framework to seamlessly adapt to diverse application domains. Course difficulty indicators may vary significantly in number and/or nature across different academic establishments or systems.

Objective number four is established to account for course difficulty dependence on instructor teaching and/or grading styles, assessment types (e.g., remote testing necessitated by unforeseen circumstances like the COVID-19 lockdown), etc.

Objective number five stresses the need to visualize the results in order to facilitate exploratory analysis and strategic policy planning.

4. The Dataset

As stated in Section 1 (*Introduction and Motivation*) above, in Greece the academic year comprises two semesters. The academic curriculum delineates the courses that are

taught during each semester. Students are assessed based on their performance during the semester and in the final examination. There are two final examination periods to each academic semester. Consequently, a student may receive up to two grades for a course during the academic year.

Table 2 outlines the dataset used. It comprised a total of 199,813 grades assigned to 3,737 students in relation to their enrollment in 81 courses at the *IHU IEE* department. The dataset spans a period of thirteen (13) academic years: from 2009-10 to 2021-22. Several elective courses were added to and/or removed from the department's undergraduate academic curriculum over this 13-year period. To maintain consistency, analysis proceeded by focusing on nineteen (19) core STEM courses comprising the *STEM courses subset*. Still, data from all the courses offered over the 13-year period was used in order to better analyze longitudinal trends and student performance patterns for the STEM courses considered.

Table 2. Students' assessment data: 2009-2021

	All courses	**STEM courses subset**
Assessment scores	199,813	123,850
Courses	81	19
Students	3,737	3,721
(*Course, Academic Year*) instances	565	247

5. Methodology

For the undergraduate program of the *IEE* department at *IHU*, the six indicators listed in Table 3 are taken to shape a course's difficulty profile in the academic year.

Table 3. Six (6) course difficulty indicators

Indicator	**Description**
δ_1	Percentage of course grades in the [0,1] range
δ_2	Average course grade
δ_3	Median course grade
δ_4	Average number of attempts a student makes to achieve a passing grade in the course
δ_5	Percentage of passing grades in the course
δ_6	Percentage of active students in the course: enrolled and assessed vs. enrolled

Table 4 lists two (2) measures used per each one indicator: (a) *Course in ac. year*, the value of which is calculated for the (*course, academic year*) pair considered, and (b) *All courses, all ac. years* which is calculated as an average for the given indicator over all courses and all academic years in the dataset. Alongside with the previous two, the

table lists two more variables that will be defined next: the indicator's *Bias (b)*, and its normalized difficulty value (*N_Value*) as calculated for the (*course, academic year*) pair in question.

Beginning with the (binary) *Bias (b)*, its value is set to "0" ("1") to indicate the positive(negative) impact the corresponding δ_i represents to course difficulty. A positive bias implies that as the value of δ_i increases, the course in question becomes more difficult. For example, δ_4 represents a positive bias (*b*=0), since the higher the average number of attempts students make to achieve a passing grade, the more difficult the course is perceived to be. On the other hand, δ_2 represents a negative bias (*b*=1), since the higher the average grade students achieve in a course, the less difficult the latter is perceived to be.

$$d_i = (-1)^b \times 100 \times \frac{x - X}{X} \qquad i = 1, \ldots, 6 \tag{1}$$

where

- x is the value of the given indicator's *Course in ac. year* measure
- X is the value of the given indicator's *All courses, all ac. years* measure, and
- b is the indicator's *Bias (b)* value

For the STEM courses in Table 2, an indicator percent variation (d_i) value per (δ_i, *course*, *academic year*) triplet is calculated as follows:

For example, d_5 is calculated as $d_5 = (-1)^1 \times 100 \times \frac{\mu - M}{M}$, μ and *M* being the percentage of passing grade values for a given STEM course in the academic year considered, and that of the average course across the entire dataset, respectively.

Table 4. Course difficulty indicators: measures, plus bias and normalized values

Indicator	**Measures**		**Bias (*b*)**	**N_Value**
	Course in ac. year	**All courses, all ac. years**		
δ_1	α	A	0	Δ_1
δ_2	β	B	1	Δ_1
δ_3	γ	Γ	1	Δ_3
δ_4	ε	E	0	Δ_4
δ_5	μ	M	1	Δ_5
δ_6	ν	N	1	Δ_6

Next, the Δ_i values listed under *N_Value* in Table 4 are calculated by constructing a d_i-standings list for each δ_i. The list registers all (*course*, *academic year*) instances sorted in descending order, based on their d_i values. Considering the positioning of each (*course*, *academic year*) pair in the d_i-standings list, and using the *Rainbow Ranking* equation from [34], Δ_i is calculated to resume values in the (0,100] range:

$$\Delta_i = 100 - 100 \left(\frac{N_{above(c)}}{C} + \frac{N_{tie(c)}}{2C} \right) \tag{2}$$

where

- c refers to a given (*course*, *academic year*) pair, herewith said to comprise a c instance

- C is the total number of c instances in the d_i-standings list
- $N_{above(c)}$ is the number of c instances ranked higher than the given c in the list, and
- $N_{tie(c)}$ is the number of ties (if any, otherwise: 0) c is involved in, not counting c

Along the lines with the research goals outlined in Section 3 (*Research Objectives*), a single course difficulty value for a given course in a specific academic year can be calculated as a linear combination of the Δ_i (i=1,...,6) values calculated via Equation 2, provided that the latter are weighted appropriately:

$$CDf = \sum_{i=1}^{6} \Delta_i \times w_i \tag{3}$$

At this point, it is noted that the introduction of Δ_i (i=1,...,6) complies with objective numbers 3 and 4 outlined in *Research Objectives*. Moreover, a single *CDf* value for a course in a specific academic year is calculated via Equation 3, given the corresponding Δ_i (i=1,...,6) values and their w_i (i=1,...,6) weights. The latter is inline with objective numbers 1 and 2 of the *Research Objectives* section. Remaining to be done is the calculation of the w_i (i=1,...,6) weight values. This is achieved by conducting Principal Component Analysis (*PCA*) as described in the following.

Principal Component Analysis (*PCA*) is a multivariate statistical technique commonly used for dimensionality reduction and data simplification. Its input comprises an $n \times p$ matrix where p is the number of measured variables X_i, and n is the number of observations recorded. The initial correlated variables are transformed into a smaller number of uncorrelated variables ($m < p$), called principal components (*PC*s). This is done by preserving as much as possible of the variation (information) present in the original dataset. For a detailed treatise on *PCA* the reader is referred to [17].

Initially, the number of *PC*s of the *PCA* output is equal to the number of variables p present in the original dataset:

$$PC_j = \sum_{i=1}^{p} \alpha_{ij} X_i \qquad j = 1, \ldots, p \tag{4}$$

The difference made by the *PCA* transformation is that the *PC*s are ordered so that the first few retain most of the variance of the initial variable set X_i. More specifically, PC_1 captures most of the variation in all of the initial variables, PC_2 captures most of the remaining variation, and so on. The a_{ij} coefficients are called *loadings* [5].

In the present study the w_i weight values are calculated on the basis of the loadings derived from applying *PCA* on the academic dataset outlined in Section 4 (*The Dataset*). More specifically, *CDf* is calculated as a composite indicator which constitutes a compilation of individual indicators in order to form a single index the value of which quantifies the multidimensional concept as a whole [26]. The use of *PCA* in the construction of composite indicators enjoys applicability in scientific fields ranging from economics [6][14], and environmental engineering and management [11][13], to road safety [12].

Section 6 (*Results*) details the application of the aforementioned methodology in the current study. The determination of the w_i (i=1,...6) weights proceeds in four steps, as follows:

In **step number one** the correlation structure of the dataset is examined to assess its suitability for *PCA*. First, the Bartlett's test of sphericity [4] is applied in order to

test whether the correlations in the dataset (as a whole) are strong enough to justify the application of *PCA*. Next, Spearman's correlation coefficient (r_s) is calculated for every pair of Δ_i (*i*=1,...6) variables. This is done in order to ensure that the *PCA* output can be used for calculating reliable weight (w_i) values for Equation 3.

Step number two involves the application of *PCA* on the academic dataset. Considering Equation 4, the Δ_i (*i*=1,...6) variables are used to derive the principal components PC_j (*j*=1,...,6):

$$PC_j = \sum_{i=1}^{6} \alpha_{ij} \Delta_i \qquad j = 1, \ldots, 6 \tag{5}$$

In Equation 5, the loading (α_{ij}) represents the correlation between PC_j and Δ_i. Equivalently, the squared loading (${\alpha_{ij}}^2$) expresses the variance in Δ_i explained by PC_j [6]. Next, the number (*m*) of *PC*s to be retained need be determined. The relevant literature provides a number of guidelines for determining the number of components to retain without experiencing any significant information loss: the Kaiser criterion [18], *Scree plot* [8], and the variance explained criteria [15], to name a few. More than one criteria are typically used in practice and in this respect.

In **step number three**, the retained principal components are rotated to enhance their interpretability. Rotation comprises a transformation to achieve a *simple structure*, namely one where (i) each variable has a high loading on only one of the retained components, and (ii) each retained component represents high loadings for only some of the variables [29]. This way, the most important variables emerge in the rotated principal component: they are the ones with the larger absolute values for their loadings. At the other end, the least important variables emerge with near zero loadings. In the present study, the *varimax rotation* is applied, as it is the one most commonly used [35].

Step number four involves the utilization of the *PCA* output to calculate the w_i (*i*=1,...,6) weights. Denoting *m* the number of retained components from step two, the total variance of Δ_i explained by all *m PC*s is called *communality* (${h_i}^2$) and it is calculated as follows [15]:

$${h_i}^2 = \sum_{j=1}^{m} \alpha_{ij}^2 \qquad i = 1, \ldots, 6 \tag{6}$$

Δ_i's weight (w_i) is calculated as the ratio of Δ_i's communality over the sum of communalities of all Δ_i (*i*=1,...,6) variables:

$$w_i = \frac{h_i^2}{\sum_{i=1}^{6} h_i^2} \qquad i = 1, \ldots, 6 \tag{7}$$

Summarizing, the w_i component in Equation 3 is taken to represent the proportion of Δ_i's variance explained relative to the variance of all Δ_i (*i*=1,...,6) variables explained by the retained components. This is along the lines of the approach reported to have been implemented in the literature, for example [6] and [26].

6. Results

For the dataset used, the correlations among all pairs of the Δ_i (i=1,...,6) variables were calculated and they are presented in Table 5. It is noted that pairs involving variables from the $\{\Delta_2, \Delta_3, \Delta_4, \Delta_5\}$ set exhibited significant correlations, as measured by the Spearman rank correlation coefficient (r_S), the latter varying from 0.34 to 0.87. Notably, the Δ_1 variable is seen exhibit significant correlations with all other variables, with the exception of Δ_4. In addition, the Δ_6 variable correlates significantly only with Δ_1 (r_S =0.23). Bartlett's sphericity test results (χ^2=757.48, df=15, and p <0.001) implied the presence of correlation patterns among the Δ_i (i=1,..,6) variables. In this respect, the results obtained led to the rejection of the null hypothesis, namely that of an identity correlation matrix.

Considering the above, the Δ_i (i=1,...,6) variables turned out to be suitable for subsequent PCA analysis. In addition, it was decided to consider two more configurations by omitting Δ_6 and Δ_1, respectively. Thus, three PCA configurations were implemented: (a) PCA_{1-6} with Δ_i (i=1,...,6), (b) PCA_{1-5} with Δ_i (i=1,..,5), and (c) PCA_{2-6} with Δ_i (i=2,..,6). This was done for two reasons: (a) PCA_{1-5} is a direct analogue to the heuristic approach reported in [19], and (b) in Table 5, Δ_1 is seen to correlate significantly with Δ_2, Δ_3, Δ_5, and Δ_6, while Δ_6 correlates significantly only with the Δ_1 variable.

Table 5. Spearman's rank correlation coefficient (r_s) values for all (Δ_i, Δ_j) (i, j=1,..,6)

	Δ_1	Δ_2	Δ_3	Δ_4	Δ_5	Δ_6
Δ_1	-	r_s=0.34 (p<0.01)	r_s=0.30 (p<0.01)	r_s=0.07 (p=0.30)	r_s=0.22 (p=0.01)	r_s=0.23 (p<0.01)
Δ_2	-	-	r_s=0.81 (p<0.01)	r_s=0.40 (p<0.01)	r_s=0.87 (p<0.01)	r_s=0.12 (p=0.06)
Δ_3	-	-	-	r_s=0.34 (p<0.01)	r_s=0.70 (p<0.01)	r_s=0.11 (p=0.10)
Δ_4	-	-	-	-	r_s=0.48 (p<0.01)	r_s=0.06 (p=0.37)
Δ_5	-	-	-	-	-	r_s=0.05 (p=0.42)
Δ_6	-	-	-	-	-	-

Beginning with PCA_{1-6}, Table 6 lists the eigenvalues and the corresponding explained variances for all six principal components (PCs) in the PCA outcome. In accordance with Kaiser's criterion, the first two components (PC_1 and PC_2 in Table 6) need be retained since their eigenvalues are greater than 1. The *Scree plot* in Figure 1 is indicative of the notably sharp drop from the first eigenvalue to the second, the rate of decrease remaining small thereafter. For PCA_{1-6}, the findings suggest that analysis may safely proceed by considering only PC_1 and PC_2 which together account for 69.52% of the variance present in the original dataset (the *Cumulative Variance Explained* column in Table 6).

Table 6. Eigenvalues and variance explained for the six PCs in PCA_{1-6}

Component	Eigenvalue	Variance Explained (%)	Cumulative Variance Explained (%)
PC_1	3.05	50.89	50.89
PC_2	1.12	18.63	69.52
PC_3	0.82	13.60	83.12
PC_4	0.65	10.75	93.87
PC_5	0.28	4.66	98.53
PC_6	0.09	1.47	100.00
Total	6.00	100.00	

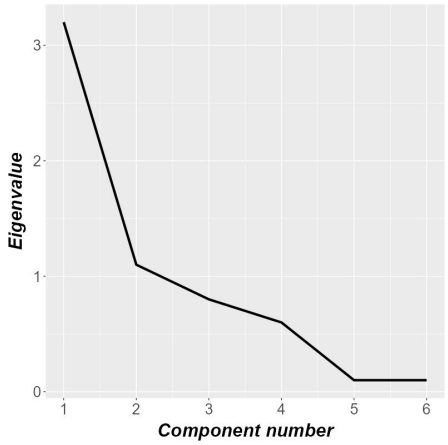

Fig. 1. Eigenvalues of the six principal components (PCs) in PCA_{1-6} (*Scree plot*)

Table 7 presents the PCA_{1-6} findings in the form of loadings associated to the given Δ_i (i=1,...,6) variables when the first two principal components are used, alongside with the corresponding communalities and w_i (i=1,...6) weights. The *varimax rotation* method was applied on the original PCA_{1-6} outcome. The communality (h^2) for each Δ_i (i=1,...,6) is the sum of the squared loadings of the two retained components (cf. Equation 6) For each Δ_i, the corresponding w_i value is calculated by Equation 7. The percentage of cumulative variance explained (information) of the two principal components (PC_1 and PC_2) is also listed under the PCA_{1-6} label.

Table 8 is analogous to Table 7 and summarizes the findings for PCA_{1-5} and PCA_{2-6}. Again, the first two principal components are used. One notes the increase in the cumulative variance explained values: 79.16% and 77.75% for PCA_{1-5} and PCA_{2-6}, respectively, next to 69.52% in the case of PCA_{1-6}. An observation that applies to all PCA outcomes in Tables 7 and 8, is that Δ_2, Δ_3, Δ_4 and Δ_5 are seen to maximize their (information) contribution values in PC_1, whereas Δ_1 and Δ_6 maximize theirs in PC_2 (column: *Loadings*).

Table 7. PC_1 and PC_2 loadings, communalities, and weights for PCA_{1-6}

	PCA_{1-6} (*cumulative variance explained: 69.52%*)			
Variables	**Loadings**		**Communalities**	**Weights**
	PC_1	**PC_2**	**(h^2)**	**(w_i)**
Δ_1	0.27	0.70	0.56	0.13
Δ_2	0.92	0.22	0.90	0.22
Δ_3	0.85	0.23	0.77	0.18
Δ_4	0.63	-0.08	0.41	0.10
Δ_5	0.92	0.08	0.84	0.20
Δ_6	-0.08	0.83	0.69	0.17
Total			4.17	1.00

Table 8. PC_1 and PC_2 loadings, communalities, and weights for PCA_{1-5} and PCA_{2-6}

	PCA_{1-5} (*cumulative variance explained*: 79.16%)				***PCA_{2-6}*** (*cumulative variance explained*: 77.75%)			
Variables	**Loadings**		**Communalities**	**Weights**	**Loadings**		**Communalities**	**Weights**
	PC_1	**PC_2**	**(h^2)**	**(w_i)**	**PC_1**	**PC_2**	**(h^2)**	**(w_i)**
Δ_1	0.12	0.90	0.83	0.21				
Δ_2	0.87	0.39	0.90	0.23	0.94	0.07	0.90	0.23
Δ_3	0.79	0.39	0.77	0.20	0.87	0.08	0.77	0.20
Δ_4	0.74	-0.26	0.61	0.16	0.61	0.00	0.37	0.10
Δ_5	0.89	0.21	0.84	0.21	0.92	0.00	0.85	0.22
Δ_6					0.04	1.00	1.00	0.26
Total			3.96	1.00			3.89	1.00

Table 9 summarizes on Equation 3's w_i (*i*=1,...,6) weights as calculated using Equation 7 for PCA_{1-6}, PCA_{2-6}, and PCA_{1-5}, and set heuristically in [19]. PCA_{1-6} and PCA_{2-6} are seen to exhibit similar weighting patterns for Δ_i (i =1,...,5). Comparing PCA_{1-5} to PCA_{1-6}, the weight w_1 for Δ_1 increases from 0.13 to 0.21, incorporating the majority of the contribution from the Δ_6 variable (0.17), which is present in PCA_{1-6} but not in PCA_{1-5}. Analogously for PCA_{2-6} and PCA_{1-6}, the weight w_6 for Δ_6 increases from 0.17 to 0.26, incorporating the majority of the contribution from the Δ_1 variable (0.13), which is present in PCA_{1-6} but not in PCA_{2-6}. In all three PCA configurations, the w_4 value for Δ_4 is notably smaller from the rest of the weight values. Consequently, the δ_4 indicator (*Average number of attempts a student makes to achieve a passing grade*) emerges to possess the smallest relative impact on course difficulty. Regarding the weights heuristically assigned to the Δ_i (i =1,...,5) variables in [19], there are notable deviations in w_1, w_4, and w_5 compared to those calculated for the three PCA configurations.

Table 9. PCA_{1-6}, PCA_{2-6}, PCA_{1-5} and $Heuristic$ weight values

Variables	**Weights** w_i (i=1,...,6)			
	$\boldsymbol{PCA}_{1-6}$	$\boldsymbol{PCA}_{2-6}$	$\boldsymbol{PCA}_{1-5}$	***Heuristic***
Δ_1	0.13		0.21	0.05
Δ_2	0.22	0.23	0.23	0.20
Δ_3	0.18	0.20	0.20	0.20
Δ_4	0.10	0.10	0.16	0.05
Δ_5	0.20	0.22	0.21	0.50
Δ_6	0.17	0.26		
Total	1	1	1	1

7. Discussion

As stated previously, PCA_{1-5} and *Heuristic* in Table 9 both involve the same set of course difficulty indicators. Their difference lies in the way the w_i (i =1,...,5) weights are determined. In the *Heuristic* configuration, weight values are set heuristically, whereas in PCA_{1-5} weight values are calculated by conducting *PCA* and using Equation 7. The heuristic approach is seen to deviate significantly from PCA_{1-5} in three of the five weights assigned to the Δ_i (i=1,...,5) variables. More specifically: (a) Δ_1 (*percentage of grades in the [0,1] range for the given course in the academic year considered*) is rated to be nearly four times as important in PCA_{1-5} (w_1=0.21) as in the heuristic approach (w_1=0.05), (b) Δ_4 (*the average number of attempts a student makes to achieve a passing grade in the course*) turns out to be nearly three times more important in PCA_{1-5} (w_4=0.16) compared to what it is set heuristically (w_4=0.05), and Δ_5 (*percentage of passing grades for the course in the academic year considered*) is nearly half as important in PCA_{1-5} (w_5=0.21) as in the heuristic approach (w_5=0.5).

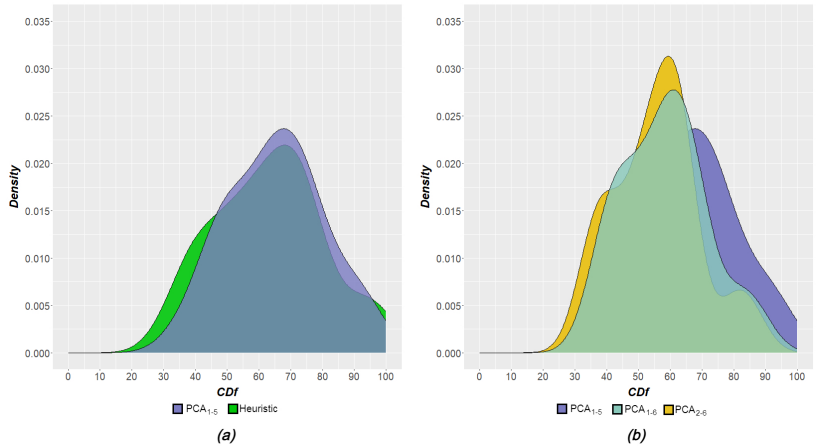

Fig. 2. *CDf* density plots (19 core STEM courses, all years)

Figure 2 presents the *CDf* distribution (density) curves for the nineteen (19) core STEM courses over the 13-year period: PCA_{1-5} and *Heuristic* in Fig.2*a*, PCA_{1-5}, PCA_{1-6}, and PCA_{2-6} in Fig.2*b*. All are left-skewed, with PCA_{1-6} and PCA_{2-6} seen to involve a smaller degree of left-skewness as compared to PCA_{1-5} and *Heuristic*. PCA_{1-5} is seen to lie notably closer to *Heuristic* relative to both PCA_{1-6} and PCA_{2-6}. It is also narrower than the *Heuristic*, i.e. it involves a smaller variance. PCA_{1-6} and PCA_{2-6} appear to be slightly shifted towards smaller *CDf* scores, relatively to the other two. This could be taken to indicate that the δ_6 indicator (*percentage of enrolled students who have been assessed*) represents a lesser impact on course difficulty compared to the δ_1 indicator (*percentage of course grades in the [0,1] range*). This is further supported by the fact that PCA_{1-5} (where δ_6 is not used) represents the highest cumulative variance explained (79.16%) compared to PCA_{2-6} (77.75%) and PCA_{1-6} (69.5%), as shown in Tables 7 and 8. Given these findings, the remainder of this section will exclusively focus on the PCA_{1-5} configuration.

Using PCA_{1-5}, Figure 3 presents two *CDf* distribution curves: one for all courses (the 19 core STEM courses included) and one for the 19 core STEM courses, both over the 13 academic years period considered. The former is significantly more uniform compared to the latter. The STEM courses curve exhibits a notable degree of left-skewness, plus it is clearly shifted towards higher *CDf* scores. This is taken to mean that students tend to face more challenges with the 19 core STEM courses, compared to the other (81-19=62, mostly: elective) courses in the undergraduate curriculum.

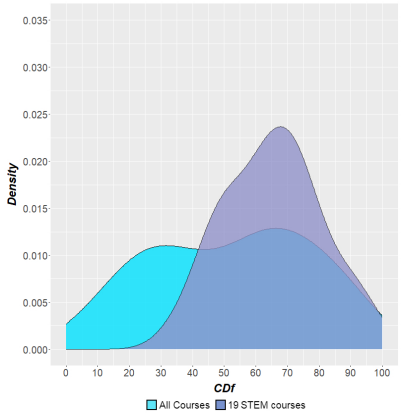

Fig. 3. *CDf* density plots (all years): 19 core STEM courses vs. all courses

The proposed *CDf* framework can effectively identify specific courses that present increased challenges for students. Such courses act as "bottlenecks" that hinder student progress, and prolong the study period. For example, focusing on course C_1, its *CDf* value is marked as a dot on the STEM courses' *CDf* distribution curve in Figure 4, during the 2021-22 academic year. The C_1 dot is seen to be positioned well past the curve's dominant inflexion point. Thus, for the academic year considered (2021-22), with a *CDf* score close to 85, C_1 is undoubtedly ranked among the most challenging core STEM courses.

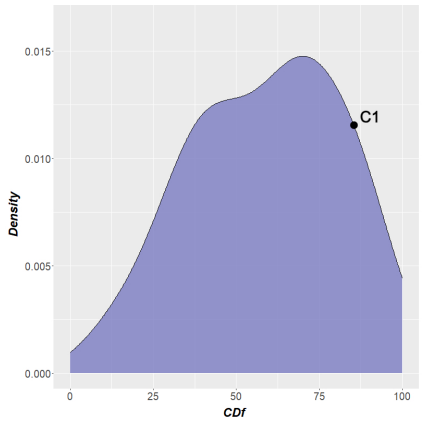

Fig. 4. Course C_1 on the 19-STEM courses' *CDf* curve during the 2021-22 academic year

To obtain a feeling of how C_1's *CDf* has varied during the 2017-2022 period, Figure 5 combines in one graph all five *CDf* distribution curves of the 19 core STEM courses for the academic years considered. It is noted that C_1 has shown a steady increase in difficulty, rising from 52.74 in 2017-18 to 85.36 in 2021-22.

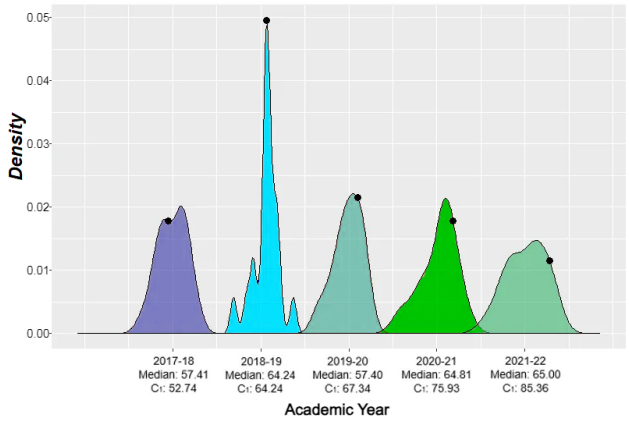

Fig. 5. Course C_1 on the 19-STEM courses' *CDf* curves during the 2017-22 period

Better yet, Figure 6 encapsulates in one graph all the information on the variation of *CDf* scores for two courses (C_1: red, and C_2: green dots on the graph) over the entire 13-year period. With one box plot per academic year the C_1 and C_2 *CDf* scores positioned relative to the former, the reader has a complete picture of how the two courses' difficulty has varied over the 13-year period. Moreover, the graph reveals information on how the difficulty of the 19 core STEM courses (as a group) has varied from one academic year

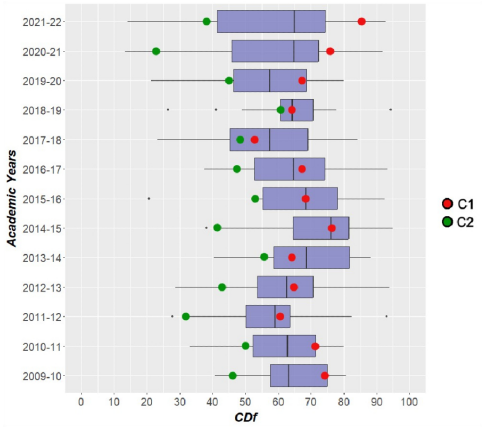

Fig. 6. 13-academic years period: Courses C_1 and C_2 positioned on all 19 core STEM courses' *CDf* box plots

to the next. For instance, by examining their median *CDf* scores, the core STEM courses are seen to have posed the greatest challenge to undergraduate students during the 2014-15 academic year. Also, 2018-19 has been the academic year with the largest number of outliers among the 19 core STEM courses: two (2) in the low (less difficult), and one (1) in the high (most difficult) ends of the corresponding box plot.

Focusing on C_1 in Figure 6, the course's *CDf* score is seen to lie in the right whisker region of the box plot only during the last two academic years (2020-21 and 2021-22). Prior to 2020-21, C_1 consistently remained below or on the Q3 boundary of the STEM courses' box plot. More precisely, C_1 comprised an outlier (in terms of its difficulty) STEM course during the 2020-21 and 2021-22 academic years. This may be indicative of C_1's tendency to gradually evolve into a "bottleneck" course for students. In this context, Figure 6 signals an alert to course instructors and the department regarding the increasing challenge associated with C_1. In response to this, possible actions may include (a) a review of the student assessment procedures, and (b) the identification of one or more other courses in the curriculum that could be designated to comprise prerequisites for C_1. On the other hand, and with the exception of the 2017-18 academic year, course C_2 is seen to always comprise an outlier in the left (less difficult) whisker region of the corresponding box-plots in Figure 6. This too deserves the department's attention.

As stated already, the results herewith presented and commented upon relate to the case of a typical university in Greece. In accordance with research objective number three in Section 3 (*Research Objectives*), the mix of the course difficulty indicators used may vary across different academic environments and systems. Indicators like expected study hours, number of course prerequisites, and independent study requirements also comprise potential candidates to be used as difficulty indicators. U.K. and U.S. universities closely monitor student dropout rates and class sizes for course offerings; these too tend to relate to course difficulty. Last but not least, student feedback and course evaluation survey outcomes can be used in the form of one or more course difficulty indicators, provided

that student response rates are consistently high, as in the case of the National Student Survey (N.S.S.) scores in the U.K.

8. Conclusion and Future Work

A new framework for the quantification of course difficulty in academic curricula is proposed. A course-centric index (*CDf*) is calculated using difficulty indicators per course offering. Each indicator is assigned a weight which is determined systematically by conducting Principal Component Analysis (PCA) on student and/or course assessment data. The course difficulty indicators may be either objective (e.g. the percentage of assessed students who achieved a passing grade, the course's mean and median scores, etc.), or subjective (e.g. student questionnaires data). The approach differs from its predecessors in that (a) it is course-centric (instead of student-centric) in nature, (b) the difficulty of a course is assumed to vary from one of its offerings to the next, and (c) the course difficulty indicators can be defined flexibly both in number and type, in order to seamlessly adapt to diverse application domains (universities, schools, and departments).

The proposed *CDf* framework and methodology have been applied in the case of the *IEE* department of the International Hellenic University (*IHU*), where each course is offered once per academic year, in either the Fall or Spring semester. A maximum of six course difficulty indicators were used, all objective in nature. Three PCA configurations were considered, using students' assessment data from nineteen (19) core STEM courses over thirteen (13) academic years. For each (*course*, *academic year*) pair, a single *CDf* score was calculated as a linear combination of the (normalized) course difficulty indicator values, using a matching set of (PCA calculated) weights. As a result, *CDf* density distribution curves were constructed. In relation with research objective number five in Section 3: *Research Objectives*, which dictates that strong emphasis be given on the visual presentation of the results obtained, each course's *CDf* score was positioned on the density distribution curve and on the box plot of all courses in each academic year. This type of graphical output facilitates exploratory analysis and has already proven valuable for the department's Internal Evaluation Group (*IEG*) in identifying potential "bottleneck" courses that may prolong a typical student's study period.

In the future stages of the research, the plan is to:

1. evaluate the proposed *CDf* framework in data mining operations that predict a student's future performance on the basis of their past assessment records [20],
2. consider additional course difficulty indicators (both objective and subjective) and their impact on the efficacy of the *PCA/CDf* output, and
3. develop and offer *CDf* as a prototype open source web service to be used by academic units in Greece and abroad.

Potential improvements of the proposed framework include, for example: (a) the monitoring of an instructor's difficulty profile in cases where the same course is measured to involve a notably different *CDf* value when it is taught by more than one instructors, or when the same instructor teaches both core STEM and elective courses (the former tending to be more challenging to the students, as suggested by Figure 3), and (b) the inclusion of subjective indicators based on data from student feedback and course evaluation surveys with consistently high response rates. The use of such subjective difficulty indicators could unveil hidden insights often missed by objective indicators.

Acknowledgments. The authors thank the anonymous reviewers for their comments and suggestions which have significantly enhanced the readability and integrity of this report.

References

1. Al-Turjman, F., Ivanovic, M.: Guest editorial: Interactive and innovative technologies for smart education. Computer Science and Information Systems 19, vii–x (2022)
2. Arnold, K.E., Pistilli, M.D.: Course signals at purdue: Using learning analytics to increase student success. In: Proceedings of the 2nd International Conference on Learning Analytics and Knowledge. p. 267–270. Association for Computing Machinery, New York, NY, USA (2012)
3. Baepler, P., Murdoch, C.: Academic analytics and data mining in higher education. International Journal for the Scholarship of Teaching and Learning 4(2) (2010)
4. Bartlett, M.S.: A note on the multiplying factors for various $\chi 2$ approximations. Journal of the Royal Statistical Society. Series B (Methodological) 16(2), 296–298 (1954)
5. Berlage, L., Terweduwe, D.: The classification of countries by cluster and by factor analysis. World Development 16(12), 1527–1545 (1988)
6. Boylaud, O., Nicoletti, G., Scarpetta, S.: Summary indicators of product market regulation with an extension to employment protection legislation. SSRN Electronic Journal (2000)
7. Bradley, G.: Factors that influence course difficulty. Doctoral dissertation, Iowa State University (1992), https://lib.dr.iastate.edu/rtd/9820
8. Cattell, R.B.: The scree test for the number of factors. Multivariate Behavioral Research 1(2), 245–276 (1966)
9. Caulkins, J., Larkey, P., Wei, J.: Adjusting gpa to reflect course difficulty (1996)
10. Chalaris, M., Gritzalis, S., Maragoudakis, M., Sgouropoulou, C., Lykeridou, K.: Examining students' graduation issues using data mining techniques - The case of TEI of Athens. AIP Conference Proceedings 1644(1), 255–262 (2015)
11. Gine, R., Pérez-Foguet, A.: Improved method to calculate a water poverty index at local scale. Journal of Environmental Engineering 136, 1287–1298 (2010)
12. Gitelman, V., Doveh, E., Hakkert, S.: Designing a composite indicator for road safety. Safety Science 48, 1212–1224 (2010)
13. Gomez-Limon, J., Riesgo, L.: A composite indicator to measure agricultural sustainability: Alternative approaches. Decision Support Systems in Agriculture, Food and the Environment: Trends, Applications and Advances (2008)
14. Gomez-Limon, J., Sanchez-Fernandez, G.: Empirical evaluation of agricultural sustainability using composite indicators. Ecological Economics 69(5), 1062–1075 (2010)
15. Hair, J.F., Black, W.C., Babin, B.J., Anderson, R.E.: Multivariate Data Analysis. Pearson Education Limited, Upper Saddle River, NJ, 7th edition edn. (2013)
16. Johnson, V.E.: An alternative to traditional GPA for evaluating student performance. Statistical Science 12(4), 251–269 (1997)
17. Jolliffe, I.T.: Principal Component Analysis. Springer Science & Business Media, New York, 2nd edition edn. (2002)
18. Kaiser, H.F.: The application of electronic computers to factor analysis. Educational and Psychological Measurement 20(1), 141–151 (1960)
19. Kelesidis, K., Dervos, D., Sidiropoulos, A.: Quantifying the Difficulty of Academic Course Modules. In: 24th Pan-Hellenic Conference on Informatics. pp. 245–249. ACM, Athens Greece (2020)
20. Kelesidis, K., Fotopoulou, N., Dervos, D.: Correlation as an arm interestingness measure for numeric datasets. In: 27th Pan-Hellenic Conference on Informatics. pp. 1–7. ACM, Athens Greece (2023)

21. Komenda, M., Víta, M., Vaitsis, C., Schwarz, D., Pokorná, A., Zary, N., Dušek, L.: Curriculum mapping with academic analytics in medical and healthcare education. PLOS ONE 10(12), 1–18 (2015)
22. Lord, F., Novick, M.: Statistical Theories of Mental Test Scores. Addison-Wesley series in behavioral sciences: Quantitative methods, Information Age Publishing, Incorporated (2008)
23. Ma, S., Akgunduz, A., Zeng, Y.: Course scheduling according to student stress. Proceedings of the Canadian Engineering Education Association (2015)
24. Mat, U.b., Buniyamin, N., Arsad, P.M., Kassim, R.: An overview of using academic analytics to predict and improve students' achievement: A proposed proactive intelligent intervention. 2013 IEEE 5th Conference on Engineering Education (ICEED) pp. 126–130 (2013)
25. Mundfrom, D.: Estimating course difficulty. Doctoral dissertation, Iowa State University (1991), https://doi.org/10.31274/RTD-180813-11387
26. Nardo, M., Saisana, M., Saltelli, A., Tarantola, S., Hoffman, A., Giovannini, E.: Handbook on Constructing Composite Indicators and User Guide. OECD Publishing (2008)
27. Neukrug, E., Fawcett, R.C.: The essentials of testing and assessment: a practical guide for counselors, social workers, and psychologists. Cengage Learning, Stanford, CT, 3rd edn edn. (2015)
28. Palmer, S.: Modelling engineering student academic performance using academic analytics. International Journal of Engineering Education 29, 132–138 (2013)
29. Pedhazur, E., Schmelkin, L.: Measurement, Design, and Analysis: An Integrated Approach. Lawrence Erlbaum Associates (1991)
30. Rasch, G.: Studies in mathematical psychology: I. Probabilistic models for some intelligence and attainment tests. Nielsen & Lydiche, Danmarks Paedagogiske Institut, Copenhagen (1960)
31. Romero, C., Ventura, S.: Educational data mining and learning analytics: An updated survey. Wiley Interdisciplinary Reviews: Data Mining and Knowledge Discovery 10(3) (2020)
32. Samejima, F.: Estimation of latent ability using a response pattern of graded scores. Psychometrika Monograph Supplement 34(4) (1969)
33. Savic, M., Ivanovic, M., Luković, I., Delibašić, B., Protic, J., Janković, D.: Students' preferences in selection of computer science and informatics studies: A comprehensive empirical case study. Computer Science and Information Systems 18, 54–54 (2020)
34. Sidiropoulos, A., Stoupas, G., Katsaros, D., Manolopoulos, Y.: The rainbow over the greek departments of computer science/engineering: a bibliometric study. In: 21st Pan-Hellenic Conference on Informatics. pp. 1–6. ACM (2017)
35. Tabachnick, B.G., Fidell, L.S.: Using multivariate statistics. Pearson, New York, 7 edn. (2019)
36. Tomkin, J.H., West, M., Herman, G.L.: An improved grade point average, with applications to CS undergraduate education analytics. ACM Transactions on Computing Education 18(4) (2018)
37. Vanderbei, R.J., Scharf, G., Marlow, D.: A regression approach to fairer grading. SIAM Review 56(2), 337–352 (2014)
38. Young, J.W.: Adjusting the cumulative GPA using item response theory. Journal of Educational Measurement 27(2), 175–186 (1990)
39. Young, J.W.: Gender bias in predicting college academic performance: A new approach using item response theory. Journal of Educational Measurement 28(1), 37–47 (1991)

Konstantinos Kelesidis is a Ph.D. candidate with the Department of Information and Electronic Engineering at the International Hellenic University. His research focuses on academic student assessment data analytics. He holds a B.Sc. degree (2009) from the Department of Information Technology of the Alexander Technological Educational Institute of Thessaloniki, and an M.Sc. degree in Web Intelligence (2020) from the Department of Information and Electronic Engineering at the International Hellenic University

in Thessaloniki. Mr. Kelesidis is a highly experienced software developer, working in the software engineering domain since 2011.

Leonidas Karamitopoulos is a lecturer (Laboratory Teaching Staff) with the Department of Information and Electronic Engineering at the International Hellenic University. He holds a B.A. degree in Mathematics from the Aristotle University of Thessaloniki, a M.Sc. degree in Operations Research from the George Mason University, Virginia, and a Ph.D. degree in Time Series Data Mining from the University of Macedonia. His current main research interests lie in the areas of time series data mining and recommendation systems.

Dimitris A. Dervos is Professor Emeritus of Information and Electronic Engineering at the International Hellenic University (I.H.U.) in Thessaloniki, Greece. He holds a B.Sc. in Physics (1979) and a Ph.D. in Computer Science (2000) from the Aristotle University of Thessaloniki, as well as an M.Sc. in Computer Engineering (1982) from the University of Southern California. He has taught Database Technologies and Predictive Data Analytics in Greece and the U.K. A founding member of the Database Technologies Network (DBTechNet), he has lectured on database technologies in Finland, Germany, and Spain. He is a recipient of the 2015 Thomson ISI/ASIS&T Citation Analysis Research Grant. Since retiring in 2023, he supervises Ph.D. candidates and lectures on Predictive Data Analytics at I.H.U. and the University of Macedonia.

Received: April 20, 2024; Accepted: September 20, 2024.

Computer Science and Information Systems 22(1):79–103 https://doi.org/10.2298/CSIS240728069F

Anomalous Traffic Identification Method for POST Messages Based on Gambling Website Templates

Zhimin Feng[1], Dezhi Han[1], Songyang Wu[2,⋆], Wenqi Sun[2], and Shuxin Shi[1]

[1] College of information Engineering, Shanghai Maritime University
201306 Shanghai, China
fengzhimin@stu.shmtu.edu.cn
dzhan@shmtu.edu.cn
shishuxin@stu.shmtu.edu.cn
[2] Network Security Center, The Third Research Institute of the Ministry of Public Security
200031 Shanghai, China
wusongyang@stars.org.cn
sunwenqi@gass.ac.cn

Abstract. Malicious websites pose significant social risks, necessitating automatic, efficient, and accurate identification methods. This paper proposes a POST traffic classification method based on website templates to identify abnormal traffic from gambling websites. Using Fiddler, POST message data is collected from several gambling sites, extracting features like URLs, cookie parameters, and request body parameters to create a Gambling Website Single POST Message Dataset (GSPD). These features are converted into vector representations with Word2Vec and TF-IDF techniques. Hierarchical clustering identifies template-generated types, achieving unsupervised template recognition. Using clustering results, individual POST messages are labeled and features are extracted using TF-IDF and mutual information methods. The parameters of a Support Vector Machine (SVM) are then optimized with the Particle Swarm Optimization (PSO) algorithm for optimal classification. Experimental results show the model's excellent performance, with a test set accuracy of 0.9985 and high precision, recall, and F1-scores, effectively identifying gambling and other illegal websites.

Keywords: Template recognition, Illegal Website Detectio, feature extraction, POST traffic classification.

1. Introduction

The Internet has become the primary source of information for people today. However, it is also inundated with malicious content, particularly gambling websites, which are closely linked to cybercrime and pose significant harm to society. Statistics from 2023 reveal that 26% of the global population is involved in online gambling. Manual identification is impractical because of the vast number of gambling websites and their continual updates. Consequently, there is an urgent need to develop an automatic, efficient, and accurate method for identifying abnormal traffic from gambling websites.

⋆ Corresponding author

Current methods for identifying gambling websites can be categorized into several groups: Blocklists, URLs, web content, and hybrid features. Blocklisting methods, which rely on collecting malicious URLs or domain names, are helpful but costly to maintain and inefficient. URL-based methods[5] classify websites by extracting features from URLs, but their accuracy is limited due to the minimal URL information. Web content methods[25,16,17,15,8,7,23,14] analyze content features such as HTML text, images, links, and JavaScript code to perform recognition. Hybrid feature methods [3,22,4,1,9,24,21,26] combine multiple features to enhance classification accuracy. Currently, in the field of cybersecurity, deep learning has been proven to be effective in improving the detection of complex traffic[11,12,13], which provides strong support for the optimisation of gambling site identification techniques . In addition, the combination of federated learning and blockchain technology opens up new ways for the construction of distributed and privacy-preserving gambling site detection systems[10], thus enhancing the security and robustness of the system . And for the problem of inconsistent data distribution, the latest research proposes a feedback semi-supervised learning method[2], which shows better robustness in dealing with highly polluted data, which is important for improving the detection accuracy of gambling website traffic.However, web content and hybrid feature approaches struggle with accurately recognizing gambling websites due to the complexity of dealing with images.

While researching gambling websites, this paper finds that most gambling website operators use site-building script technology[18] to automatically generate websites to reduce costs and simplify creation and management. By analyzing the HTTP POST behavioural data submitted by users, this study identifies similar characteristics in the HTTP POST data of gambling websites generated using the same template. It is observed that the cookie parameters in the request headers of these sites are remarkably similar. While some cookie parameter names are commonly used for specific purposes, such as authentication and session management (e.g., session, auth_token), these names are not mandatory, and web developers can choose names freely, For example, the parameter 'isAutoPay' is used to identify whether a user has auto-pay enabled, and the parameter 'hasPhone' is used to identify whether a user has bound or verified a mobile phone number. Furthermore, the analysis reveals that web developers specify many cookie parameter names rather than being strictly defined. Additionally, there is a high degree of similarity in the URL segments following the domain name for the same behaviours on gambling websites generated under the same template in POST messages. The parameters in the request body also exhibit a significant level of similarity.

Based on the HTTP POST data, this paper employs a pre-trained Word2Vec model, converting the data into vector representations using a TF-IDF weighted average, and applies hierarchical clustering to group websites generated from the same template into a single class. While this method can identify gambling website templates, it is insufficient for recognizing anomalous traffic based on the overall website behaviour. Therefore, this paper uses templates to classify individual POST messages. The process involves TF-IDF feature vectorization, feature re-extraction using the mutual information method, and classification using a support vector machine (SVM) optimized with the particle swarm algorithm (PSO) to find the optimal model parameters. The main contributions of this paper are as follows:

1. In this paper, we utilize the Fiddler tool to capture POST messages associated with various behaviours such as login, registration, adding bank cards, and betting on gambling websites that use existing templates. We process the contents of their request headers, request lines, and request bodies to create a Gambling Website Single POST Message Dataset (GSPD). To facilitate the clustering of gambling websites, we then integrate the POST data from the same websites to form a Gambling Website POST Message Merge Dataset (GPMD).
2. In this paper, by analyzing user-submitted HTTP POST behavioural data, we find that gambling websites generated by the same template exhibit high similarity in cookie parameters within the request headers, parameters in the request body, and word similarity following the URL domain name. Feature pattern discovery using unsupervised clustering. The pre-trained Word2Vec model converts the POST messages into vector representations using a TF-IDF weighted average. The hierarchical clustering technique in unsupervised clustering is applied to cluster the gambling websites generated from the same template.
3. In this paper, we develop a template-based classification method for POST messages that employs TF-IDF feature vectorization and the mutual information method for feature extraction. When classifying a single POST message, we use Support Vector Machines (SVMs) for classification and Particle Swarm Optimization (PSO) to optimize the model parameters, enhancing classification accuracy. This method effectively handles large-scale datasets, quickly and accurately identifies gambling sites, reduces the cost of human intervention, and demonstrates strong adaptability and robustness in dealing with constantly evolving gambling sites.

The remainder of this paper is organized as follows: Section 2 introduces related work on identifying gambling websites. Section 3 details the POST message classification process for the dataset used in this study, including the dataset's creation, the clustering of gambling websites, and the method for classifying individual POST messages. Section 4 validates the proposed method through experiments. Finally, Section 5 concludes the paper and suggests directions for future research.

2. Related Work

Wang et al.[20] classified web page screenshots by integrating visual features and textual content. They extracted visual features using a fine-tuned pre-trained ResNet 34 model, employed OCR (Optical Character Recognition) techniques for text extraction from images, and utilized a Bi-LSTM model for semantic feature extraction from the text. These features were fused using a self-attention mechanism and integrated using a post-fusion method for classification. Chen et al.[4] introduced PG-VTDM (visual and textual content using a decision mechanism), an automated detection system for identifying pornographic and gambling websites based on visual and textual content. The system utilized Doc2Vec to learn textual features from HTML source codes, represented visual features of web page screenshots with a modified bag of visual words (BoVW) algorithm incorporating local spatial relationships of feature points, and trained text and image classifiers. A logistic regression-based data fusion algorithm was designed to integrate the classification results from both features. Sun et al.[16] proposed CT-GDNC (certificated and textual

analysis-based classification), a method for classifying gambling domain names (GDNs). This method enhanced classification accuracy through BERT fine-tuning using 10,000 benign data samples from GDNs and the Alexa Top 1 million list. Wang et al.[19] developed a co-training approach combining visual and semantic features of web screenshots to identify gambling websites. They utilized OCR for text extraction, trained CNN and TextRNN classifiers separately, and used a co-training algorithm to retrain unlabeled data. Gu et al.[6] introduced HeCGamb (Heterogeneous Communication Graph-based method to enhance the Gambling app detection performance), a method for detecting mobile gambling applications through encrypted traffic analysis. They analyzed communication features of 175 popular gambling apps in China, identified server domain randomization and inter-application family features, modelled inter-flow relationships from traffic streams, and constructed inter-application relationships for application-level family feature extraction.

In contrast to Wang et al.[20] and Chen et al.[4], whose methods rely on visual features and textual content extracted from webpage screenshots, the approach in this paper starts directly from user-submitted HTTP POST behavioural data. This method captures specific user interaction behaviours by analyzing the cookie parameters in the request headers, the parameters in the request body, and the word features following the URL domain name in the POST messages. HTTP POST messages directly reflect user actions on a website, eliminating the need for intermediate steps involving screenshots and text content. This approach is more efficient and real-time, leveraging the more straightforward structure and reduced noise of POST messages to enhance recognition accuracy.

Unlike the multimodal data fusion methods of Wang et al. [19], which combined images and text, and Sun et al.[16], which also utilized images and text, the method proposed in this paper focuses solely on single-modality POST data. This approach simplifies the model complexity and reduces the time and resource consumption for data processing. Despite this focus on a single modality, the method in this paper achieves exceptionally high recognition accuracy on unimodal data through deep mining and optimization of POST data.

In contrast to other methods, the approach in this paper excels in meticulously analyzing and detecting specific operational behaviours of gambling websites, thereby offering comprehensive monitoring and protection. Compared to Gu et al.[6], whose method relies on complex multi-view semantic information fusion and graph analysis, the method presented here is more concise and efficient in feature extraction and classification. It processes large-scale datasets quickly and accurately, significantly enhancing recognition efficiency and reducing the need for human intervention.

3. Method

This paper presents a method for identifying POST requests related to gambling website traffic, illustrated in Fig. 1 (Overall structure diagram). Firstly, the paper preprocesses the collected POST request data by extracting features from request lines, request bodies, and cookies. For request lines, the complete URL is extracted and segmented into words. For cookies and request bodies, all parameters are extracted. Subsequently, the paper compiles and stores each website's URL vocabulary, cookie parameters, and body parameters from all associated POST requests into a file.

Next, the paper uses the extracted URL vocabulary, cookie, and body parameters to train the Word2Vec model. The TF-IDF weighted average transforms Each website's data into vector representations. Subsequently, hierarchical clustering is conducted using the Ward linkage method to categorize the websites, where each cluster corresponds to a gambling website template. Finally, the clustering results are added to the original data, the Gambling Site Single POST Message Dataset (GSPD), as class labels for each POST request.

Then, this paper proceeds to classify each POST request based on its request line, cookie parameters, and request body parameters. Initially, the paper applies the mutual information method to select features most pertinent to the assigned labels. Subsequently, the Particle Swarm Algorithm (PSO) is employed to optimize the hyperparameters of the support vector machine (SVM) for optimal classification performance. Next, feature unions merge and process the selected features through TF-IDF vectorization. Finally, the paper trains the support vector machine model using the optimized parameters.

This paper will provide detailed descriptions of the dataset production, data vector representation, clustering of gambling sites, and classification based on POST messages in the subsequent subsections.

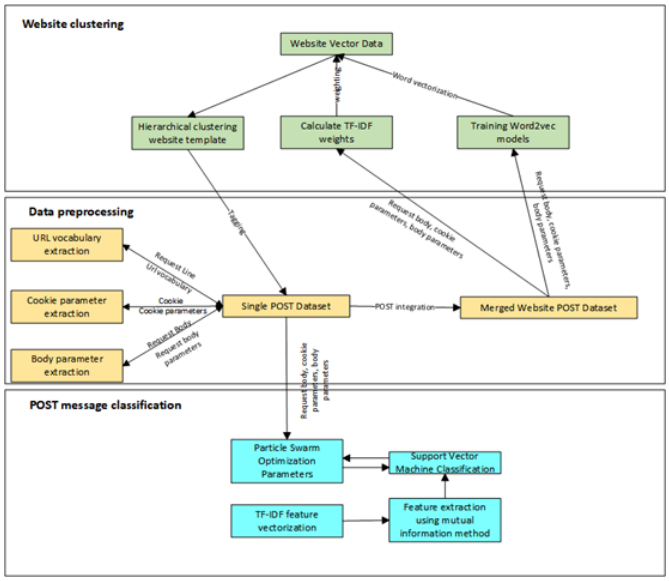

Fig. 1. The overall flowchart outlines the three main parts of achieving the final classification in this thesis, including data preprocessing, website clustering, and single-article POST classification. It also specifically refines the detailed processing of each part

3.1. Data set production

HTTP POST message. For a website, common HTTP behaviours include GET and POST requests. GET requests retrieve information from the server, while POST requests are used to submit data to a specified resource, altering the server's state upon execution. Parameters in a GET request are usually appended to the URL as part of the query string. Because URL lengths are limited, GET requests can pass a relatively small amount of data, and POST requests include the data in the request's body rather than in the URL. A POST request can pass significantly since the request body can contain a large amount of data. Hence, this paper selects HTTP POST as the basis for detection. An HTTP POST message typically comprises the following components.

1. The Request Line in an HTTP message follows the "HTTP method URL HTTP version" format. The HTTP method indicates the action the client intends to perform, such as GET for retrieving resources from the server, POST for sending data to the server, PUT for replacing a resource on the server, DELETE for requesting deletion of a server resource, and other methods like HEAD, OPTIONS, PATCH, and TRACE. The URL (Uniform et al.) specifies the target resource of the request, typically including the protocol (e.g., HTTP, HTTPS), the domain name (e.g., www.example.com), path (e.g., /path/to/resource), and optional query parameters (e.g., ?key1=value1&key2=value2). The HTTP version specifies the version of HTTP being used, commonly HTTP/1.1, HTTP/2, etc.
2. Request Header: The request header consists of multiple lines of key-value pairs, each line of "key: value" The request header field conveys some of the client's configuration information and the nature of the request so that the server can correctly understand and process the request. The following is the meaning of some of the keys in the request header: Host specifies the domain name of the target server for the request, and Connection indicates that the client wishes to maintain a connection with the server in order to send subsequent requests. Content-Length specifies the length of the request body in bytes. sec-ch-ua indicates the client's user-agent information, including the browser and version. Accept specifies the type of content that the client can handle. Content-Type specifies the media type of the request body. The referer specifies the URL of the facet that initiated the request. Accept-Encoding specifies the content encoding format supported by the client. Accept-Language specifies the client's preferred language. A cookie contains all the cookies the client previously stored on the same server. A cookie contains all cookies stored by the client before the same server.
3. Request Body: This section is located at the end of the HTTP request message, immediately after the request headers. Its structure is simply a piece of data in the format specified by the Content-Type in the request header. The request body is usually closely related to the request line (containing the request method, URL, and HTTP version) and the request headers, but the actual data content is stored entirely in the request body. The request body is the core of the data transfer and can carry complex, structured data in various formats (e.g., form data, JSON, XML, etc.). The data is usually in JSON format if the Content-Type is application/JSON.

GSPD dataset production. By examining the POST messages of the captured gambling websites, this paper finds that for gambling websites that are in the same template con-

structed by the same template, there is a significant similarity in the URLs, the cookies in the request header, and the body of the request and that the URLs of these websites contain the exact words, and similar parameters and values are passed under the same behaviour. Cookie parameters in the request headers of gambling websites created from the same template tend to be similar. However, some of the parameter names in the cookies are widely received and used for specific purposes, with common authentication cookie names such as session, auth_token, and so on commonly used for authentication, session management, and so on. These are not mandatory specifications; web developers can choose the parameter names. According to the analysis of the data captured in this paper, many of the cookie parameter names are specified by the web developers themselves rather than being strictly regulated. In addition, according to the data analysed in this paper, there is a high degree of similarity in the request body parameters of gambling websites created from the same template. The following is a treatment of the above three components.

1. For the request line, the complete URL is extracted and split into words; when splitting the URL, this paper extracts words from the part of the URL after the domain name and also extracts words from the keys and values in its query parameters.
2. For cookies in the request header, extract the parameters in the cookie, i.e. the part to the left of the equals sign, and do not process the values.
3. For the request body, extract its parameters; if the request body is in the form of "parameter=value", extract the part to the left of the equals sign; if the request body is in the form of "key: value", extract the critical part.

Fiddler is a robust network debugging tool mainly used to capture and analyse HTTP and HTTPS traffic. It intercepts all network requests and responses from a client (such as a browser or application) to a server and helps users view, modify and debug network data. In this paper, we utilize the Fiddler tool to capture POST message information from various templates of multi-class gambling websites. We segment and compile data from request headers, request lines, and request bodies, including URLs associated with website names, POST behaviours, cookies, and request body parameters. The processed results, including segmented URL words, cookie parameters, and request body parameters, are saved into a file to form the Gambling Site Single POST Message Dataset (GSPD).

GPMD dataset integration. In the data captured for this paper, each gambling website involves multiple POST messages related to actions such as registration, login, adding bank cards, topping up, and betting. Given the focus on website templates for classification and single POST messages for identifying gambling traffic, analysing the features across all POST messages within each gambling website is essential. Based on the Gambling Site Single POST Message Dataset (GSPD), this paper analyses and finds that URL vocabulary information, cookie parameters and parameters in Request Body can be used for website feature pattern discovery. To facilitate this analysis, the paper extracts and compiles URL vocabulary, cookie parameters, and request body parameters from the POST messages obtained from each website. These features are then saved into a file to create a comprehensive Website Merge Dataset (GPMD). Unlike the GSPD, which focuses on the individual behaviours of each gambling site, the GPMD consolidates data

from a single website, including only the URL vocabulary, cookie parameters, and request body parameters from the GSPD. Therefore, the Gambling Site POST Message Merge Dataset (GPMD) exclusively includes URL vocabulary, cookie parameters, and request body parameters extracted from the Gambling Site Single POST Dataset (GSPD).

3.2. Data Vector Representation

Word2Vec. Word2Vec is a prominent method for converting natural language into distributed vector representations. It effectively captures word relationships within a multi-dimensional space and is a crucial preprocessing step in predictive modelling, semantic analysis, and information retrieval tasks. Fig. 2 (Word2vec models) illustrates the Word2Vec process, which includes two primary components: a continuous bag of words (CBOW) and a skip-gram. The CBOW component predicts the target word based on the surrounding context words, whereas the skip-gram component predicts the context words given an input word. These components enable Word2Vec to generate meaningful vector embeddings that reflect semantic relationships and contextual similarities among words in text data.

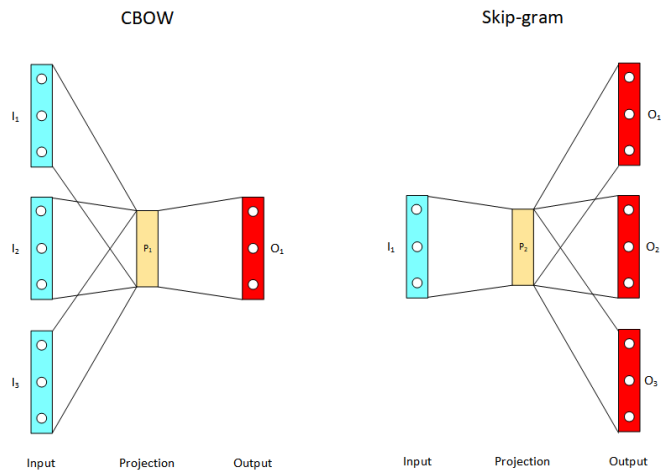

Fig. 2. Word2vec models (including CBOW, Skip-gram)

The Skip-gram component used in this paper is the Skip-gram model, which predicts the context word given the target word, calculates the conditional probability using the softmax function, and trains the word vector by maximising this probability.

In the Skip-gram model, Suppose we have a target word w_t and a window size c,Then the goal of the Skip-gram model is to pass the w_t and its contextual words w_{t+j},The goal of the Skip-gram model is to maximise the following conditional probabilities:

$$P(w_{t+j} \mid w_t)\,. \tag{1}$$

On the corpus as a whole, this goal can be expressed as follows:

$$\prod_{t=1}^{T} \prod_{-c \leq j \leq c, j \neq 0} P\left(w_{t+j} | w_t\right). \tag{2}$$

Where T is the total number of words in the corpus and c is the window size
To calculate this conditional probability, the softmax function is applied:

$$P\left(w_O | w_I\right) = \frac{exp\left(v_{w_O} \bullet v_{w_I}\right)}{\sum_{w=1}^{V} exp\left(v_w \bullet v_{w_I}\right)}. \tag{3}$$

Where w_O is the context word, w_I is the target word, v_{w_O} and v_{w_I} are the word vector representations of the words w_O and w_I, respectively, V is the size of the vocabulary list, and " $\bullet$ " denotes the vector dot product.

The model updates the word vectors during training by maximising the above conditional probabilities. The specific steps are as follows:

1. Randomly initialise word vectors for all words.
2. For each word w_t in the corpus, take a context word whose surrounding window size is c.
3. Use the softmax function to calculate $P\left(w_{t+j} | w_t\right)$.
4. Maximise the conditional probability by gradient descent and update the word vectors v_{w_O} and v_{w_O}.

Due to the computational intensity of the softmax function, practical applications often resort to methods like Hierarchical Softmax and Negative Sampling to expedite training processes. In this paper, Hierarchical Softmax is employed.

Hierarchical Softmax leverages a Huffman Tree to mitigate computational complexity. This approach reduces the softmax function, which is the computational burden from $O(V)$ to $O\left(\log V\right)$, significantly enhancing efficiency in processing large vocabulary.

TF-IDF. TF-IDF is a widely utilized technique in text analysis and information retrieval for assessing the significance of words within a document. It computes the product of term frequency (TF) and inverse document frequency (IDF), thereby emphasizing words that are particularly distinctive to the document's content.

The primary role of TF-IDF:

1. TF-IDF effectively emphasises crucial words that distinguish documents by diminishing the importance of common words and amplifying the significance of words appearing in a limited number of documents.
2. TF-IDF serves as a valuable text feature extraction method in tasks such as text classification, clustering, and topic modelling. It transforms textual data into a vector representation conducive to subsequent machine learning processing.
3. In search engines, TF-IDF plays a crucial role in measuring the relevance of document queries. It aids in identifying and returning the most pertinent documents by assessing the importance of terms within documents relative to the entire corpus.

The TF-IDF value is obtained by calculating the product of word frequency (TF) and inverse document frequency (IDF). The specific steps are as follows:

1. Calculate word frequency (TF) Word frequency indicates how often a word appears in a document. Word frequency can be calculated in a number of ways; the most common way is to count the number of times a word appears in a document and normalise it:

$$TF\left(t,d\right)=\frac{f_{t,d}}{N_d}\,. \tag{4}$$

   Where $f_{t,d}$ denotes the number of occurrences of word t in document d, and N_d denotes the total number of words in document d.
2. Calculating the Inverse Document Frequency (IDF) The inverse document frequency is used to reduce the weight of words that occur commonly in multiple documents and is defined as follows:

$$IDF\left(t,D\right)=\log\left(\frac{N}{|\{d\in D:t\in d\}|}\right). \tag{5}$$

   where N denotes the total number of documents and $\{d\epsilon D:t\epsilon d\}$ denotes the number of documents containing the word t.
3. Calculation of TF-IDF values Finally, the TF-IDF value is obtained by multiplying TF and IDF:

$$TF\text{-}IDF\left(t,d,D\right)=TF\left(t,d\right)\times IDF\left(t,D\right)\,. \tag{6}$$

Web Feature Vectorisation. This paper compiles a comprehensive dataset of POST messages from gambling websites, referred to as the Gambling Website POST Message Site Merge Dataset (GPMD). This dataset comprises three components: a list of URL words, a list of cookie parameter words in the request header, and a list of parameter words in the request body.

Firstly, the list of words in the URL of each website in the dataset, the list of words in the Cookie parameter in the request header, and the list of words in the request body parameter are extracted, and the three-word lists are integrated. The integration is the union of sets to ensure that all relevant words from each website are included in the final complete word list. These lists are then combined to calculate the global TF-IDF weights. Analyzing the website data reveals that gambling websites generated by the same template have nearly identical cookie parameters, and the cookie parameters for different behaviours on the same website are also broadly consistent. Therefore, the weight of the cookie parameters is increased when training the Word2Vec model.

The input data consists of a list of URL words for each website, cookie parameter words in the request header, and parameter words in the request body. The structure of this data is shown in Table 1 below.

The data from the above table is used as input. The data is subdivided, the lists are merged, and the TF-IDF weights are calculated. The Word2Vec model is trained, and the word list of each POST message is converted into a TF-IDF-weighted average word vector, which is then saved as a CSV file. The structure of the output data is shown in Table 2.

Table 1. Input data

WebName	RequestLineKey	BodyParam	CookieParam
Name1	['word1','word2', ···]	['param1','param2', ···]	['cookie1','cookie2', ···]
Name2	['word3','word4', ···]	['param3','param4', ···]	['cookie3','cookie4', ···]
···	···	···	···

Table 2. Output data

Dim_0	Dim_1	Dim_2	···	Dim_499	WebName
0.0750426	0.1420163	0.2485222	···	-0.1477123	Name1
0.0622372	0.1342609	0.1215802	···	-0.0396667	Name2
···	···	···	···	···	···

3.3. Web Site Clustering

Hierarchical Clustering. Hierarchical clustering is a powerful method for uncovering hierarchical structures and intrinsic relationships in data. It effectively groups similar data points by calculating a distance matrix, gradually merging the most similar clusters, and updating the distance matrix. In practice, hierarchical clustering is widely used in data analysis, grouping, pattern recognition, and simplification.

There are two main types of hierarchical clustering:

1. Agglomerative Hierarchical Clustering (AHC) is a bottom-up approach where each data point starts as its cluster. The most similar clusters are progressively merged until all data points are combined into a single cluster or a predetermined number of clusters is reached.
2. Divisive Hierarchical Clustering (DHC) is a top-down approach where all data points initially form one cluster. This cluster is progressively split into smaller clusters until each data point stands alone as its cluster or a predefined number of clusters is reached.

The following are the detailed implementation steps for cohesive hierarchical clustering:

1. Calculate the distance matrix: Calculate the distance or similarity among all data points. Commonly used distance metrics include Euclidean distance, Manhattan distance and cosine similarity.

$$d_{ij} = \sqrt{\sum_{k=1}^{n} \left(x_{ik} - x_{jk}\right)^2}. \tag{7}$$

   Where d_{ij} denotes the Euclidean distance between data points i and j, and x_{ik} and x_{jk} denote the values of i and j in the kth dimension, respectively.
2. Merge the most similar clusters: At each step, find the two closest clusters and merge them into a new cluster.

$$d\left(A \bigcup B, C\right) = \min\left\{d\left(a, c\right) : a \in A, c \in C\right\}. \tag{8}$$

Where A and B are the two clusters to be merged, and $d(A \cup B, C)$ is the distance between the new cluster and the other clusters.

3. Update Distance Matrix: Update the distance matrix to reflect the distance between the new cluster and all other clusters.
   a. Single Linkage method: The distance between a new cluster and other clusters is the smallest distance between any two points in its constituent clusters.

$$d(A \cup B, C) = \min\{d(a, c) : a \in A, c \in C\}. \tag{9}$$

   b. Complete Linkage: The distance of a new cluster from other clusters is the maximum distance between any two points in its constituent clusters.

$$d(A \cup B, C) = \max\{d(a, c) : a \in A, c \in C\}. \tag{10}$$

   c. Average Linkage: The distance between a new cluster and other clusters is the average of the distances between all pairs of points in its constituent clusters.

$$d(A \cup B, C) = \frac{1}{|A||C|} \sum_{a \in A, c \in C} d(a, c). \tag{11}$$

   d. Ward's Method: Ward's method defines the distance between clusters by minimising the Sum of Squared Errors (SSE) within the merged cluster.

$$\triangle SSE = \frac{|A||B|}{|A| + |B|} \|\overline{x}_A - \overline{x}_B\|^2. \tag{12}$$

   Where $|A|$ and $|B|$ are the number of data points in clusters A and B, and $\overline{x}_A$ and $\overline{x}_B$ are the centres of mass of clusters A and B. Ward's method tends to generate clusters that are similar in size and regular in shape
4. Repeat steps 2 and 3 until all data points are combined into a single cluster or a predetermined number of clusters is reached.

Clustered Website Templates. In this paper, the text data is represented as high-dimensional vectors using the Word2Vec model, which effectively captures the data's structure. By applying TF-IDF weighting, the importance of keywords is enhanced, reducing the influence of common but non-discriminatory words. This approach improves the accuracy of clustering the websites.

Because this paper cannot accurately distinguish which class of template a gambling website belongs to based on its visible form, there are no template-based labels in the Gambling Site POST Message Merge Dataset (GPMD). Hierarchical clustering, particularly agglomerative hierarchical clustering, does not require a predetermined number of clusters. Instead, clustering is controlled through a distance threshold, allowing the identification of natural clusters by analyzing the structure of the data at different scales.

Using the Ward linkage method minimizes the variance of the clusters at each merge. This approach ensures that each merge aims to preserve the tightness within the cluster, thereby promoting the formation of more compact clusters.

Calculating the distance matrix using Euclidean distance ensures that the distance metric in the clustering process is standardized and valid in high-dimensional space. The following are the specific data processing steps.

Firstly, the preprocessed data was loaded, where each text was converted into a high-dimensional vector, as shown in the table. We extracted 500 columns as features to capture the primary information of the text. These high-dimensional vectors reflect the structure of the data well, and by applying TF-IDF weighting, we further enhance sensitivity to critical words. This weighting method helps mitigate the impact of frequently occurring but non-discriminative words, thereby improving the accuracy of clustering.

In the clustering process, the distance matrix of the data was first calculated using Euclidean distance as the metric. This ensures that the distance metric used in the clustering process is standardized and valid in high-dimensional spaces. Hierarchical clustering through the Ward linkage method allows us to minimize the intra-cluster variance at each merge, thereby maintaining the tightness of the clusters. After clustering is complete, we incorporate the clustering results into the raw data and output the WebName tags in each class. The format is shown in Table 3. This helps us understand the composition of each cluster and its characteristics. To better understand the clustering results, we further reduce the dimensionality of the high-dimensional data to 2D using the t-SNE (t-Distributed Stochastic Neighbor Embedding) method and plot a scatter plot. t-SNE effectively preserves the local structure of high-dimensional data, enabling us to visualize the distribution and relationships among different clusters. In the two-dimensional scatterplot generated after t-SNE reduction, each point is colour-coded according to the cluster to which it belongs. This allows clear visualization of the internal structure and relationships between clusters.

Table 3. Web site clustering

Cluster	Website Name
Cluster 0	‘WebName1’ ‘WebName2’ · · ·
Cluster 2	‘WebName3’ ‘WebName4’ · · ·
· · ·	· · ·
Cluster N	‘WebName 174’ ‘WebName175’ · · ·

3.4. Abnormal Website POST Classification

Mutual Information Act. The mutual information method is a statistical measure used to quantify the amount of information one random variable provides about another. It assesses the dependence or correlation between two variables, making it valuable in various fields such as feature selection, feature engineering, image processing, and information retrieval.

In machine learning, the mutual information method is crucial in evaluating and selecting features that strongly correlate with the target variable. By identifying such features, models can achieve improved performance and generalization capabilities. In image registration, mutual information can assess the similarity between two images, aiding their alignment by quantifying how much information is shared. Moreover, the mutual information method helps evaluate the relevance between documents and queries in information retrieval tasks. This evaluation enhances the accuracy of retrieval results by identifying documents that contain information most closely related to the user’s query.

Mutual information quantifies the interdependence between two random variables X and Y, defined as:

$$I(X;Y) = \sum_{y \in Y} \sum_{x \in X} p(x,y) \log \left(\frac{p(x,y)}{p(x)p(y)} \right). \tag{13}$$

Where $p(x,y)$ is the joint probability distribution of X and Y, and $p(x)$ and $p(y)$ are the marginal probability distributions of X and Y, respectively.

Particle Swarm Algorithm(PSO). Particle Swarm Algorithm (PSO) is an optimisation algorithm based on group intelligence and is mainly used to solve complex optimisation problems. It is inspired by group behaviours such as flocks of birds foraging for food and schools of fish swimming.PSO finds the optimal solution to a problem by simulating individuals (particles) moving and collaborating in the search space.

PSO is widely used in machine learning to optimise model parameters, function optimisation, path planning, engineering optimisation, etc. The PSO algorithm searches for the optimal solution by updating the velocity and position of each particle. Each particle is represented in the search space as a position vector x_i and a velocity vector v_i. The particle adjusts its velocity and position at each step based on its own experience and the experience of its neighbours. Following is the procedure of the particle swarm algorithm PSO:

1. Initialisation
   Initialise the position and velocity of the particles and set the initial parameters such as the number of particles, maximum number of iterations, individual learning factor and social learning factor.

$$x_i(0) \sim U(x_{min}, x_{max}) . \tag{14}$$

$$v_i(0) = U(v_{min}, v_{max}) . \tag{15}$$

   Where U denotes a uniform distribution, x_{min} and x_{max} are position ranges, and v_{min} and v_{max} are ranges of velocities.
2. Speed Update
   The velocity of each particle is updated according to the following equation:

$$v_i(t+1) = w \times v_i(t) + c_1 \times r_1 \times (p_i - x_i(t)) + c_2 \times r_2 \times (g - x_i(t)) . \tag{16}$$

   w is the inertia weight, which controls the effect of the particle's previous velocity; c_1 and c_2 are the individual learning factor and the social learning factor, respectively, which control the extent to which the particle moves towards its optimal position and the global optimal position. r_1 and r_2 are random numbers between [0,1]. p_i is the historical optimal position of the particle i. g is the global optimal position found amongst all particles.
3. Location Updates
   The position of the particle is updated according to the following equation:

$$x_i(t+1) = x_i(t) + v_i(t+1) . \tag{17}$$

4. Evaluating and updating optimal solutions
   Each particle's fitness is evaluated at each step, and the particle's historical best position p_i and global best position g:

$$if \;\; f\left(x_i\left(t+1\right)\right) < f\left(p_i\right) \;\; then \;\; p_i = x_i\left(t+1\right), if \;\; f\left(p_i\right) < f(g) \;\; then \;\; g = p_i \,. \tag{18}$$

Support Vector Machine (SVM). Support Vector Machine (SVM) is a supervised learning algorithm widely used in classification and regression problems. The basic idea of SVM is to find an optimal hyperplane to maximise the classification interval (Margin) to achieve good classification performance.

SVMs were initially designed for binary classification problems but can be extended to multiclassification problems using various strategies. Common approaches are One-vs-Rest (OvR) and One-vs-One (OvO).

1. One-vs-Rest(OvR):
   The OvR method bisects each category with other categories to build K classifiers (for a K-class problem)—for each classifier.

$$f_k(x) = sign\left(w_k \times x + b_k\right) \,. \tag{19}$$

2. One-vs-One (OvO):
   The OvO method builds one classifier for every two categories, for a total of $\frac{K(K-1)}{2}$ classifiers. Each classifier $f_{i,j}(x)$ distinguishes category i from category j.

$$f_{ij}(x) = sign\left(w_{i,j} \times x + b_{i,j}\right) \,. \tag{20}$$

   The final decision is determined through a voting mechanism where each classifier votes for its category, and the category with the most votes is the final classification result:

$$Class(x) = \arg\max_k \sum_{i,j} \delta\left(f_{i,j}(x) = k\right). \tag{21}$$

Support Vector Machines are powerful classification algorithms particularly suitable for high-dimensional data. By introducing kernel functions, SVMs can handle linearly indivisible problems.

Single POST Classification. Based on the cluster analysis of gambling websites, this paper assigns labels to each POST request in the single POST dataset (GSPD) of gambling websites. Analysis reveals that cookie parameters in the request headers of different behaviours within the same gambling website are broadly consistent, and those of websites sharing the same template exhibit high similarity. Therefore, using the TF-IDF method, this study utilizes the request line, cookie parameters from the request header, and request body parameters as input for textual feature extraction. These components collectively form a comprehensive feature vector. Subsequently, the mutual information method is

employed for feature selection, retaining features with mutual information scores greater than 0.

After the feature selection is completed, in order to optimise the parameters c and gamma of the Support Vector Machine (SVM) model, this paper adopts the Particle Swarm Optimisation (PSO) algorithm to perform parameter tuning by minimising the negative accuracy on the training data. The specific processing steps are as follows:

1. It reads data from a single POST dataset and extracts features and labels. The dataset contains request lines, request body parameters, cookie parameters, and labels. To evaluate the model performance, the dataset is divided into a training set and a test set, with 80% and 20%, respectively. The format of the dataset is shown in Table 4.

Table 4. POST dataset format

POST Name	RequestLine	CookieParam	BodyParam	Flag
Name1	HTTP Method URL1 HTTP Version	[‘cookie1’,···]	[‘param1’,···]	1
Name2	HTTP Method URL2 HTTP Version	[‘cookie2’,···]	[‘param2’,···]	2
...	...	...	...	...
NameN	HTTP Method URLN HTTP Version	[‘cookieM’,···]	[‘paramM’,···]	m

   In Table 4, RequestLine denotes the request line, CookieParam denotes the cookie parameter in the request header, and BodyParam denotes the request body parameter.CookieParam and BodyParam contain word lists, and Flag is the class label labelled according to the website clustering. In addition to the above four parts, the POST dataset also includes the behaviour of the POST message, the name of the website to which it belongs, the Cookie, the request body, etc. Table 4 only lists the content required for classification in this paper.
2. Textual features from request lines, request body parameters and cookie parameters are extracted using the TF-IDF method. A FeatureUnion is constructed to facilitate processing where TF-IDF transformation is separately applied to each component. Subsequently, the mutual information method is employed for feature selection, retaining features with mutual information scores greater than 0. This approach aims to reduce feature redundancy and enhance the model's overall performance.
3. Parameter tuning is conducted using the Particle Swarm Optimization (PSO) method to find the optimal SVM parameters. The objective function used is the negative accuracy of the SVM model on the training set. The PSO algorithm simulates the flight of particles in the solution space to search for the best combination of SVM parameters, aiming to maximize the model's accuracy on the training data.
4. The SVM model is trained using the optimised parameters, and predictions are made using a divided test set to evaluate the model's performance.

Through the above steps, this paper effectively classifies POST requests for gambling websites, confirming the significance of the clustering effect and demonstrating high model performance.

4. Experiments and Analysis

In this section, experiments are conducted to evaluate the performance of the proposed method for identifying anomalous POST traffic based on website templates. The experiments were performed on a server with an AMD EPYC 7T83 64-core processor, 90 GB of RAM, and an NVIDIA RTX 4090 GPU with 24 GB of video memory. The system has a 30 GB capacity for the system disk and 50 GB for the data disk. It runs Ubuntu 20.04 with Python 3.8 installed, PyTorch 2.0.0, and CUDA 11.8 support.

Dataset: This paper uses Fiddler, a web debugging proxy tool, to capture POST messages about gambling websites' logins, registrations, bank card additions, betting, and other behaviours. Since some POST messages are repeated, this paper removes duplicate and noisy data. It collates each POST message into tabular data by removing the request line, cookies in the request header, and the empty request body. Data, and finally, 6525 POST data and 175 gambling websites are collated. Then, the complete URL is extracted from the request line, and the words after the URL domain name are extracted for saving, the cookie parameters are extracted and saved, and the parameters in the request body are extracted and saved.

Evaluation metrics: In this paper, four evaluation metrics, accuracy, precision, recall, and F1-score, are used, and the confusion matrix for the experiments in this paper is shown in Table 5. The confusion matrix consists of four values: true positive (*TP*), true negative (*TN*), false positive (*FP*), and false negative (*FN*). Where *TP* denotes the number of samples that were correctly classified as that class for a given class a, *FP* denotes the number of samples that were incorrectly classified as that class for a given class a (i.e., samples belonging to other classes were predicted to be in that class), *FN* denotes the number of samples that were incorrectly classified as other classes for a given class a (i.e., samples actually belonging to that class were predicted to be in that other class), and *FN* denotes the number of samples that were correctly classified as other (i.e., the number of samples that belonged to other classes and were not predicted to be that class). *TN* denotes the number of samples correctly classified as other for a class a (i.e., the number of samples that belonged to that class and were not predicted to be that class).

Table 5. Output data

	Predicted 0	Predicted 1	Predicted 2	···	Predicted N
Actual 0	*TP*	*FP*	*FP*	···	*FP*
Actual 1	*FN*	*TP*	*FP*	···	*FP*
Actual 2	*FN*	*FN*	*TP*	···	*FP*
···	···	···	···	···	···
Actual N	*FN*	*FN*	*FN*	···	*TP*

Accuracy is the proportion of total samples that the classifier predicts correctly. The formula is:

$$Accuracy = \frac{TP + TN}{TP + TN + FP + FN}. \tag{22}$$

The precision rate is the proportion of all samples predicted to be in the positive category that are actually in the positive category. The formula is:

$$Precision = \frac{TP}{TP + FP}\,. \tag{23}$$

Recall is the proportion of all samples in the positive category that are correctly predicted to be in the positive category. The formula is:

$$Recall = \frac{TP}{TP + FN}\,. \tag{24}$$

The F1 score is the reconciled average of precision and recall and is used to assess the precision and recall of the model in a combined manner. The formula is:

$$F1\text{-}score = \frac{2 \times Precision \times Recall}{Precision + Recall}\,. \tag{25}$$

The above four evaluation metrics, accuracy, precision, recall, and F1, are important; the closer to 1 the four metrics are, the better the model's performance in this paper.

Web site clustering evaluation. Firstly, this paper calculates the TF-IDF weights for the whole dataset, and the IDF values for each word are stored in a dictionary, which is once again used for subsequent use in generating word vectors.

In this paper, a Word2Vec model is trained on a curated dataset of gambling websites. The word vectors are configured with a dimensionality of 500, and a context window size of 2 is employed. Due to the dataset's preprocessing, which involved removing duplicates, the minimum word frequency threshold is set to 1. The training process iterates over 80 rounds, employing the Skip-gram method with hierarchical softmax for training the Word2Vec model.

This paper utilizes three main components: the URL vocabulary from the dataset, cookie parameters in the request header (given twice the weighting), and parameters from the request body. The vector representation of each sentence synthesized from these components is computed using TF-IDF weights, where the weights of the parameters are also considered in the calculation.

Save the file using the trained Word2Vec model and the generated sentence vectors.

Using the saved vector file mentioned earlier, this paper clusters 175 gambling websites from the dataset using hierarchical clustering. Specifically, Agglomerative Clustering is employed with Ward's method as the linkage criterion. The clustering results are depicted in Fig. 3 (Website Template Clustering).

According to Figure 3, this paper clusters 175 websites into ten classes: Cluster 0 contains 14 websites, Cluster 1 contains 16 websites, Cluster 2 contains 45 websites, Cluster 3 contains 6 websites, Cluster 4 contains 16 websites, Cluster 5 contains 11 websites, Cluster 6 contains 10 websites, Cluster 7 contains 13 websites, Cluster 8 contains 33 websites, and Cluster 9 contains 11 websites. The paper analyzes the data and identifies several clusters that contain similar templates, such as Wanjiao.com, Fujiao.com, Dejiao.com, Xiangjiao.com, Longjiao.com, and various lottery websites, as well as similar sports gambling websites, following the processing described in the paper.

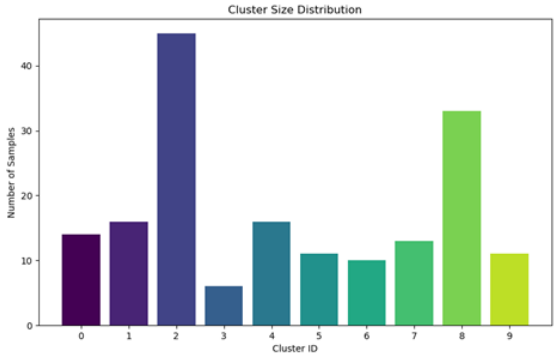

Fig. 3. Cluster Size Distribution

Based on the clusters clustered by the above hierarchical clustering, Fig. 4 (Cluter 3 homepage) and Fig. 5 (Cluter 4 homepage) are screenshots of the websites' home pages under the same class templates selected above.

Fig. 4. Cluter 3 homepage

Screenshots of the home pages of two randomly selected websites from Cluster 3 are presented in Figure 4: The first shows the home page of DeColour, and the second displays the home page of FooColour. Similarly, screenshots of two randomly selected websites from Cluster 4 are shown in Figure 5: the first depicts the home page of BoyeSports.com, and the second shows the home page of FourSeasonsSports4.vip.com. By comparing the screenshots in Fig. 4 and Fig. 5, it becomes evident that DeColour and FooColour share the same template, as do BoyeSports and FourSeasonsSports4.vip.com. This illustrates the effectiveness of our clustering approach in correctly grouping websites that utilize identical templates.

The 500-dimensional data was downscaled to 2 dimensions using t-SNE to visualise the effect of the above clustering of gambling sites, as shown in Fig. 6 (Clustered scatter-plot).

Fig. 5. Cluter 4 homepage

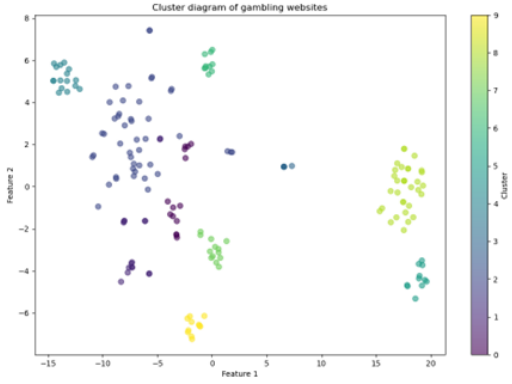

Fig. 6. Cluster diagram of gambling websites

In the t-SNE scatterplot, each point's position reflects its relationships within the 500-dimensional feature space. Different colours in Figure 6 represent distinct clustering results. The plot reveals that a few points are situated near the boundaries of multiple clusters, possibly indicating feature ambiguity or noise that complicates clear distinction after dimensionality reduction. However, multiple clearly defined clusters in Figure 6 indicate significant feature similarity among points in the original high-dimensional space, underscoring the effectiveness of the clustering.

Evaluation of POST traffic classification. Based on the websites' clustering results, this paper annotates each POST in the crawled dataset with a corresponding cluster label. The dataset comprises 6525 POST entries collated from the websites.

This paper applies an 80%-20% split to the dataset, with 80% used for training and 20% for testing. The dataset includes three components: the request line, cookie parameters in the request header, and parameters from the request body, which are selected as input data. Additionally, three feature extraction pipelines are employed to process each feature column and transform the text into TF-IDF feature vectors. Subsequently, mutual information between each feature and the label is computed, and features with mutual information scores greater than 0 are selected for further analysis.

Define the objective function of PSO optimisation to assess the parameter combination's goodness using the SVM model's accuracy. PSO defines the support vector machine model 'c' parameter range to be [0.01,10]. The parameter range of 'gamma' is [0.0001,1]; by PSO optimising the objective function, the best parameters are obtained as 4.2414 and 0.0790, respectively. Using the best parameters to train the SVM model, the test set is predicted, and the classification test results are shown in Table 6.

Table 6. Message classification results

Cluter	Precision	Recall	F1 Score	Actual sample size
0	1.0000	1.0000	1.0000	211
1	1.0000	1.0000	1.0000	397
2	1.0000	1.0000	1.0000	34
3	0.9820	1.0000	0.9909	109
4	1.0000	1.0000	1.0000	230
5	1.0000	1.0000	1.0000	7
6	1.0000	1.0000	1.0000	51
7	1.0000	1.0000	1.0000	60
8	1.0000	0.9887	0.9943	177
9	1.0000	1.0000	1.0000	29
Accuracy			0.9985	1305
Macro avg	0.9982	0.9989	0.9985	1305
Weighted avg	0.9985	0.9985	0.9985	1305

As shown in Table 6, the overall accuracy (Accuracy) is 0.9985, indicating that only a few of the 1305 test samples were misclassified. The proportion of all samples predicted to be in the positive class that was actually in the positive class, i.e., the precision rate, is almost always 1, indicating that the model predicts very accurately. The proportion of

all samples that were positively classified and correctly predicted to be positive, i.e., the recall, was also almost always 1, indicating that the model identified positively classified samples very well. The harmonic mean of precision and recall, or F1 score, is also close to 1, indicating that the model performs very well in all categories.

Table 7 shows the results after applying the dataset's Random Forest, K-Nearest Neighbors (KNN), Naive Bayes, XGBoost and NODE (Neural Oblivious Decision Ensembles) deep learning models. Results of the classification performed.

Table 7. Classification results by model

Model	Accuracy	Precision	Recall	F1-Score
SVC	0.9985	0.9985	0.9985	0.9985
Random Forest	0.9900	0.9900	0.9900	0.9897
KNN	0.9785	0.9792	0.9785	0.9784
Naive Bayes	0.9456	0.9429	0.9456	0.9415
XGBoost	0.9885	0.9886	0.9885	0.9883
NODE	0.9862	0.9900	0.9900	0.9900

As depicted in Table 7, aggregating all metrics, the Support Vector Machine (SVC) with optimized parameters demonstrates superior performance in this classification task, achieving the highest accuracy, precision, recall, and F1 score. The experimental outcomes underscore its efficiency in processing and classifying data, effectively adapting to accurately categorizing POST message traffic from individual gambling websites based on features such as the request line, request header cookie parameters, and request body parameters.

5. Conclusions and Outlook

This paper proposes and validates a method for classifying abnormal POST traffic based on website templates. Our experiments demonstrate the method's effectiveness and high performance in identifying and classifying abnormal traffic on gambling websites. Firstly, using the Fiddler tool, we capture POST messages related to login, registration, adding bank cards, betting, and other behaviours on gambling websites. After removing duplicates and noisy data, we compile 6525 POST entries. We perform feature extraction on URLs, cookie parameters in the request header, and parameters in the request body using TF-IDF and Word2Vec, assigning appropriate weights to different features for efficient representation. Secondly, we use Agglomerative Clustering with Ward's method to cluster 175 gambling websites. The results show that websites with similar templates and structures are successfully grouped, verifying the effectiveness of our method in recognizing website templates. Based on these clustering results, we label the POST data and optimize the classification model's parameters using a Support Vector Machine (SVM) combined with Particle Swarm Optimization (PSO). The experimental results indicate that the classification accuracy on the test set is 0.9985, with precision, recall, and F1-score all close to 1, demonstrating the model's excellent performance across all categories. Finally, we

experimentally verify that the SVM model is better suited to classify the traffic of individual gambling website POST messages based on the request line, request header cookie parameters, and request body parameters compared to other models. This highlights the method's high practical value in effectively identifying and classifying anomalous network traffic. In summary, the method presented in this paper shows excellent performance and application potential in classifying gambling website POST traffic. Future research will optimize feature extraction and model training methods and extend their application to other web traffic classification tasks.

In this paper, we have collected data from various existing gambling websites, covering all known types of gambling website templates. However, to address the emergence of new gambling website templates in the future, we propose further investigation into recognition methods using unsupervised learning techniques to tackle these new challenges.

Acknowledgments. This work was Supported by Key Lab of Information Network Security, Ministry of Public Security,the National Natural Science Foundation of China under Grants 61672338, the Natural Science Foundation of Shanghai under Grant 21ZR1426500.

References

1. Auer, M., Griffiths, M.D.: Using artificial intelligence algorithms to predict self-reported problem gambling with account-based player data in an online casino setting. Journal of Gambling Studies 39(3), 1273–1294 (2023)
2. Cai, S., Han, D., Li, D.: A feedback semi-supervised learning with meta-gradient for intrusion detection. IEEE Systems Journal 17(1), 1158–1169 (2022)
3. Cernica, I., Popescu, N.: Computer vision based framework for detecting phishing webpages. In: 2020 19th RoEduNet Conference: Networking in Education and Research (RoEduNet). pp. 1–4. IEEE (2020)
4. Chen, Y., Zheng, R., Zhou, A., Liao, S., Liu, L.: Automatic detection of pornographic and gambling websites based on visual and textual content using a decision mechanism. Sensors 20(14), 3989 (2020)
5. Fan, Y., Yang, T., Wang, Y., Jiang, G.: Illegal website identification method based on url feature detection. Comput. Eng 44, 171–177 (2018)
6. Gu, Z., Gou, G., Liu, C., Yang, C., Zhang, X., Li, Z., Xiong, G.: Let gambling hide nowhere: Detecting illegal mobile gambling apps via heterogeneous graph-based encrypted traffic analysis. Computer Networks 243, 110278 (2024)
7. Gupta, J., Pathak, S., Kumar, G.: Aquila coyote-tuned deep convolutional neural network for the classification of bare skinned images in websites. International Journal of Machine Learning and Cybernetics 13(10), 3239–3254 (2022)
8. Jain, A.K., Gupta, B.B.: A machine learning based approach for phishing detection using hyperlinks information. Journal of Ambient Intelligence and Humanized Computing 10, 2015–2028 (2019)
9. Kairouz, S., Costes, J.M., Murch, W.S., Doray-Demers, P., Carrier, C., Eroukmanoff, V.: Enabling new strategies to prevent problematic online gambling: A machine learning approach for identifying at-risk online gamblers in france. International Gambling Studies 23(3), 471–490 (2023)
10. Li, D., Han, D., Weng, T.H., Zheng, Z., Li, H., Liu, H., Castiglione, A., Li, K.C.: Blockchain for federated learning toward secure distributed machine learning systems: a systemic survey. Soft Computing 26(9), 4423–4440 (2022)

11. Li, D., Han, D., Zheng, Z., Weng, T.H., Li, K.C., Li, M., Cai, S.: Does short-and-distort scheme really exist? a bitcoin futures audit scheme through birch & bpnn approach. Computational Economics 63(4), 1649–1671 (2024)
12. Li, J., Han, D., Weng, T.H., Wu, H., Li, K.C., Castiglione, A.: A secure data storage and sharing scheme for port supply chain based on blockchain and dynamic searchable encryption. Computer Standards & Interfaces 91, 103887 (2025)
13. Li, J., Han, D., Wu, Z., Wang, J., Li, K.C., Castiglione, A.: A novel system for medical equipment supply chain traceability based on alliance chain and attribute and role access control. Future Generation Computer Systems 142, 195–211 (2023)
14. Li, L., Gou, G., Xiong, G., Cao, Z., Li, Z.: Identifying gambling and porn websites with image recognition. In: Advances in Multimedia Information Processing–PCM 2017: 18th Pacific-Rim Conference on Multimedia, Harbin, China, September 28-29, 2017, Revised Selected Papers, Part II 18. pp. 488–497. Springer (2018)
15. Liu, D., Lee, J.H., Wang, W., Wang, Y.: Malicious websites detection via cnn based screenshot recognition. In: 2019 International Conference on Intelligent Computing and its Emerging Applications (ICEA). pp. 115–119. IEEE (2019)
16. Sun, G., Ye, F., Chai, T., Zhang, Z., Tong, X., Prasad, S.: Gambling domain name recognition via certificate and textual analysis. The Computer Journal 66(8), 1829–1839 (2023)
17. Syahputra, H., Wibowo, A.: Comparison of support vector machine (svm) and random forest algorithm for detection of negative content on websites. Jurnal Ilmiah Teknik Elektro Komputer dan Informatika (JITEKI) 9(1), 165–173 (2023)
18. Urvoy, T., Chauveau, E., Filoche, P., Lavergne, T.: Tracking web spam with html style similarities. ACM Transactions on the Web (TWEB) 2(1), 1–28 (2008)
19. Wang, C., Xue, P., Zhang, M., Hu, M.: Identifying gambling websites with co-training. In: SEKE. pp. 598–603 (2022)
20. Wang, C., Zhang, M., Shi, F., Xue, P., Li, Y.: A hybrid multimodal data fusion-based method for identifying gambling websites. Electronics 11(16), 2489 (2022)
21. Yang, P., Zhao, G., Zeng, P.: Phishing website detection based on multidimensional features driven by deep learning. IEEE access 7, 15196–15209 (2019)
22. Zhang, W., Jiang, Q., Chen, L., Li, C.: Two-stage elm for phishing web pages detection using hybrid features. World Wide Web 20, 797–813 (2017)
23. Zhao, J., Shao, M., Peng, H., Wang, H., Li, B., Liu, X.: Porn2vec: A robust framework for detecting pornographic websites based on contrastive learning. Knowledge-Based Systems 228, 107296 (2021)
24. Zhou, S., Ruan, L., Xu, Q., Chen, M.: Multimodal fraudulent website identification method based on heterogeneous model ensemble. China Communications 20(5), 263–274 (2023)
25. Zhou, S., Xu, C., Xu, R., Ding, W., Chen, C., Xu, X.: Image recognition model of fraudulent websites based on image leader decision and inception-v3 transfer learning. China Communications 21(1), 215–227 (2024)
26. Zuhair, H., Selamat, A.: Phishing hybrid feature-based classifier by using recursive features subset selection and machine learning algorithms. In: Recent Trends in Data Science and Soft Computing: Proceedings of the 3rd International Conference of Reliable Information and Communication Technology (IRICT 2018). pp. 267–277. Springer (2019)

Zhimin Feng is currently pursuing the M.S.degree with the School of Information Engineering, Shanghai Maritime University, Pudong, China. His current research interest is network security.

Dezhi Han received the B.S. degree in applied physics from the Hefei University of Technology, Hefei, China, in 1990, and the M.S. and Ph.D. degrees in computing science from the Huazhong University of Science and Technology, Wuhan, China, in 2001 and 2005,

respectively. He is currently a Professor with the Department of Computer, Shanghai Maritime University, Pudong, China, in 2010. His current research interests include cloud and outsourcing security, blockchain, wireless communication security, network, and information security.

Songyang Wu is a researcher and director of the Cyber Security Center of the Third Research Institute of the Ministry of Public Security (MPS) and also serves as the deputy director of the National Engineering Research Center for Network Security Level Protection and Security Technologies and the executive deputy director of the Key Laboratory of the Ministry of Public Security of the Ministry of Information Network Security, etc. He received his B.S. degree in Computer Science and Technology from Tongji University in 2005 and his Ph.D. in Computer Application from Tongji University in 2011. He joined the Center of the Ministry of Public Security in the same year. He received his PhD in Computer Application from Tongji University in 2011. He joined the Network Security Center of the Third Research Institute of the Ministry of Public Security in the same year. His research interests include cybercrime investigation, electronic data forensics, ample data security, and artificial intelligence security.

Wenqi Sun, Associate Researcher and Research Engineer at the Cyber Security Center of the Third Research Institute of the Ministry of Public Security; she received her B.S. degree in Computer Science and Technology from Northeastern University in 2010 and her Ph.D. degree in Computer Science and Technology from Tsinghua University in 2016. She joined the Cyber Security Center of the Third Research Institute of the Ministry of Public Security in 2018; her current research interest is in cybercrime investigation.

Shuxin Shi received an M.S. in Computer Science and Technology from Shanghai Maritime University, Pudong, China, in 2024 and is currently pursuing a Ph.D. in the School of Information Engineering. His current research interest is network security.

Received: July 28, 2024; Accepted: September 17, 2024.

Computer Science and Information Systems 22(1):105–131 https://doi.org/10.2298/CSIS240227002H

Formal Transformation of OWL Ontology to a FOKI Generic Meta-model

Bogumila Hnatkowska, Adrianna Kozierkiewicz, and Marcin Pietranik

Wroclaw University of Science and Technology,
Wybrzeże Wyspiańskiego 27, 50-370, Wrocław, Poland
{bogumila.hnatkowska, adrianna.kozierkiewicz, marcin.pietranik}@pwr.edu.pl

Abstract. Ontology integration is merging a set of ontologies to provide a single, unified ontology, which contains all of the knowledge from input ontologies. Most solutions described in the literature are based on the OWL format and incorporate its strengths and weaknesses. In our previous research, we developed the ontology integration framework FOKI, which does not use the OWL. Collected experimental data using prepared ontologies proved its usefulness. However, the lack of OWL support makes it challenging to use the FOKI framework in practical applications. This paper presents a meta-model and a set of transformation rules for bi-directional transformation between ontologies expressed in our framework and the OWL standard. The meta-model serves as a bridge in the transformation process. Transformation rules are built by referencing an abstract syntax element of OWL2 and an appropriate mathematical formalism from FOKI. Their correctness was verified on widely available ontologies expressed in OWL provided, e.g., by the Ontology Alignment Evaluation Initiative.

Keywords: FOKI, ontology integration, OWL, transformation

1. Introduction

Ontology integration, a well-explored area within the field of knowledge management, addresses the challenge of merging multiple source ontologies into a unified target ontology, encapsulating the collective knowledge of the input sources. This process involves selecting elements from source ontologies representing the same aspects of a modeled universe of discourse and integrating them into a cohesive entity while preserving unique, non-conflicting elements. Formally, it can be defined as: *for the given n ontologies* $O_1, O_2, ..., O_n$ *one should determine an ontology* O^*, *which is the best representation of the given input ontologies*.

The topic is widely discussed in literature. In [20], authors examine the challenge of semantic heterogeneity in ontologies on the Semantic Web, emphasizing the importance of ontology alignment and merging for achieving interoperability. It categorizes existing merging approaches into three types—single-strategy, multiple-strategy, and those utilizing external semantic resources—and introduces a novel framework that leverages multiple knowledge bases to address semantic discrepancies and enhance ontology merging.

For example, in [6], authors address the need for effective methodologies to integrate and reuse ontologies, which are vital for standardizing information and fostering knowledge-based digital ecosystems. The paper introduces an approach that employs heterogeneous matching techniques to automate the process of building ontologies, thereby

simplifying the creation of digital ecosystems. The method has been successfully applied to the food production domain, demonstrating its practical utility.

The article [24] discusses the integration of biomedical ontologies using Semantic Web standards, specifically addressing the challenges posed by structural differences that can lead to inconsistencies when merging. It introduces a framework that uses a seed ontology for iterative enrichment with new sources, employing a novel fine-grained approach for mapping repair and alignment conservativity supported by both theoretical formalization and practical algorithms. The framework has been applied to integrate multiple medical ontologies, enhancing real-world healthcare services provided by Babylon Health, and shows promising results when compared with leading ontology integration systems.

The academic literature is replete with various approaches to address this topic, each offering unique insights and methodologies. A comprehensive review of these diverse strategies and an exploration of ongoing research avenues that have yet to be fully explored is described in detail in ([22]). This work not only aggregates the different available solutions but also critically examines their effectiveness and potential for further development.

While the concept of ontology integration is straightforward conceptually, it presents significant semantic and computational complexities. Most existing solutions are restricted to a specific ontology representation format, typically OWL (Web Ontology Language), particularly its second version, OWL2. Despite OWL's robustness, it imposes limitations on the expressiveness of concept attributes. For instance, once an attribute is associated with a concept, it cannot be reused with the same name in another context within the ontology, leading to rigid and unnatural naming conventions to circumvent this limitation.

Our research has identified that attributes often acquire varied meanings across different concepts. For example, the attribute "number" might represent different data in the "Book" and "Address" contexts. This observation inspired us to develop a novel ontology expression and management approach based on a solid formal foundation that ensures flexible domain modeling and determinism. We proved in [23] that an approach to ontology alignment (and later into ontology integration) based on analyzing attributes semantics gives good results.

This research led to the development of the Framework for Ontological Knowledge Integration (FOKI), which offers a formally grounded, theoretically robust tool for ontology management. The FOKI framework allows for a detailed examination of ontological elements and their interrelationships, providing a comprehensive perspective on ontology structure. Moreover, our approach provides a broad perspective on ontologies, allowing a deep analysis of their internal elements and their relationships.

The developed framework has many advantages, such as limiting human participation in the integration process to a minimum, resolving issues related to a diversity of semantic relations, and enabling proper identification of mappings between the ontologies. Additionally, the FOKI framework can express changes that appear while maintained ontologies evolve. Informally speaking – a FOKI model can answer the question "What changed when". Several applications showed the usefulness of our approach in both the tasks of ontology integration and ontology alignment ([18], [19], [17]).

Despite its advantages, the primary limitation of FOKI is its incompatibility with OWL, particularly for practical applications that rely on standard ontology formats like

those provided by the Ontology Alignment Evaluation Initiative (OAEI) [1] – a state-of-the-art dataset used to test the usefulness of many ontology-related applications. Therefore, we need to transform the FOKI model into the OWL standard for experimental verification and comparison of our approach with other solutions.

This paper, therefore, focuses on establishing a set of transformation rules that facilitate the conversion between OWL (OWL2 specifically) and the FOKI formalism, aiming to bridge the gap between these two frameworks and enhance the practical deployment of FOKI. Every rule must be built by referencing an abstract syntax element of OWL2 and an appropriate mathematical formalism of the FOKI framework (obviously if such exists and is applicable).

Preparing the aforementioned transformations presents several challenges. The first significant challenge arises from the assumption in FOKI that attributes and relations are annotated with logical sentences, explicitly defining their intended semantics. This requirement substantially increases the complexity of maintaining the FOKI ontology. Each logical sentence must be meticulously crafted and maintained to preserve the intended semantics, which can be time-consuming and error-prone. The explicit annotation of semantics also demands higher expertise from ontology developers, making developing and maintaining FOKI-based ontologies more demanding compared to other frameworks.

Secondly, the OWL standard operates under the premise of an open-world domain, where it is assumed that the absence of information does not imply falsehood. In contrast, FOKI assumes a closed-world domain, where what is unknown as true is considered false. This fundamental difference in assumptions can lead to an OWL ontology built using FOKI formalism being overly restrictive. For example, OWL provides mechanisms to express that two concepts are equivalent, implying that their sets of instances cannot be disjointed. In FOKI, it is straightforward to check whether two sets of instances are disjoint; however, this does not necessarily mean that the ontology developer intended these concepts to be equivalent. This mismatch in assumptions can result in unintended interpretations and constraints within the OWL ontology, complicating its application and potentially leading to incorrect inferences.

Eventually, we introduce a meta-model that encapsulates the essential concepts of FOKI. This meta-model is built on a dual foundation: it functions both as a simplified version of the OWL2 meta-model and as an extension that includes elements unique to FOKI. This dual nature facilitates bi-directional translation between OWL2 and FOKI, allowing for the transformation of ontologies in both directions with minimal information loss.

Our goal is to develop procedures that enable these transformations while preserving the integrity and semantics of the original ontologies. This involves addressing the significant semantic differences between OWL and FOKI, such as the open-world assumption in OWL versus the closed-world assumption in FOKI, as well as the unique name assumption in OWL and its reproduction in FOKI. By carefully considering these differences, we aim to create a robust and reliable method for ontology translation that maintains the fidelity of the original data.

The developed meta-model is a versatile solution that accommodates varying semantic definitions and relationships inherent in different ontologies, making it universally applicable. Its design allows it to adapt to and integrate diverse ontological structures and

[1] http://oaei.ontologymatching.org

semantics, ensuring that the FOKI framework is not limited to any specific domain or ontology structure. This flexibility supports a broad range of ontology types and integration scenarios, enhancing its utility across various applications.

By accommodating different semantic definitions, the meta-model ensures that the FOKI framework can handle the complexities of integrating multiple ontologies with differing structures and semantics. This universality is particularly beneficial for projects requiring data synthesis from disparate sources, enabling seamless interoperability and more comprehensive data analysis. Consequently, the FOKI framework becomes a powerful tool for a diverse range of applications, from academic research to industry-specific solutions, ensuring robust and efficient ontology management and integration.

The paper is organized as follows. Section 2 contains an overview of similar research found in the literature. Section 3 provides base mathematical definitions used throughout the paper. A motivating example is presented in Section 4 The core contribution is given in Section 5, and the accepted evaluation procedure with its results can be found in Section 6. Section 7 summarizes the paper and overviews our upcoming research plans.

2. Related Works

In real situations, there is a need to transform one model or standard into another. This paper is devoted to ontology transformation, which can be defined as changing one ontology format into another with the same semantics. In other words, we will define rules that allow us to run transformation between an OWL ontology and FOKI.

There exists different ontology representation approaches like Suo-Kif [21], OWL (expressed by many concrete syntaxes, e.g., functional, Manchester, XML, RDF Turtle, RDF/XML), database schema, different mathematical representations or UML. In many practical solutions ontologies, especially expressed in OWL2, are subjects of transformations to/from different notations [27], UML [8], [9], [27], [28],[7], description logic [5], programming languages [4], [12], database (schema) [1], [2], [14] or business vocabularies and rules [15], [16].

Many approaches exist to the definition of transformation rules, depending on their formality level and paradigms used. It is possible to represent transformation rules in natural language [1], [4], [8], [9], [12], [25]. The alternative approach is a semi-formal method that can be based, e.g., on structured tables [14], or patterns with placeholders [16]. The most precise method is based on a mathematical apparatus [2], [27]. It reduces the risk of misinterpretation but could be hard to understand. So the formal representations are typically extended with simple explanations.

The second division is based on how the transformation rules are written – one can use either a declarative ([28]) or operational language ([8]). Sometimes a hybrid method is used, e.g. [15]. When the ordering of transformation rules matters, their ordering is also provided [27].

We can also differ transformations based on the direction (one or two ways) and the loss of information (lossy transformation vs. lossless). Authors of [1] developed the OWLMap tool for the automatic and lossless ontology transformation into a relational database. Similarly, [25] proposed a transformation system providing a lossless roundtrip mapping for OBO and OWL ontologies. Rule-based transformations presented by [3] and [29] are lossy as some OWL axioms are not considered, e.g., property restrictions.

Similarly, in [8], only some features of UML class diagrams have been preserved in the transformation to OWL. Xu and et.all [27] manage to propose a semantics-preserving approach for extracting OWL ontologies from existing UML class diagrams, however, it cannot support several new syntaxes (including the Functional-Style syntax and the Manchester syntax) and richer datatypes of OWL2 language. Authors of [26] proposed an algorithm for transforming OWL ontology into a relational database that works without a loss of information; however, authors are aware of limitations to represent more advanced OWL features.

The created FOKI meta-model and transformation procedures allow us to transform ontologies (OWL2 – FOKI) in both directions almost losslessly, which is a major advantage. This issue is discussed in more detail in Section 5. The transformation procedures are defined in an operational manner.

3. Basic Notions

Framework for Ontological Knowledge Integration (FOKI) is built on mathematical foundations [23]. We assume that a real world is defined as a triple (A, V, P) where: A is a finite set of attributes that can be used to describe objects, V is a set of their valuations (domains) such that $V = \bigcup_{(a \in A)} V_a$, where V_a is a domain of a particular attribute a and P is a set of predicates that can be used to define integrity constraints. The following sextuple defines an ontology in FOKI as a (A, V, P)-based ontology:

$$O = (C, H, R^C, I, R^I, Z) \tag{1}$$

where: C is a set of concepts; H is a concepts' hierarchy; R^C is a set of relations between concepts, $R^C = \{r_1^C, r_2^C, ..., r_n^C\}$, $n \in N$, such that $r_i^C \in R^C (i \in [1, n])$ is a subset of $C \times C$; I is a set of instance identifiers; $R^I = \{r_1^I, r_2^I, ..., r_n^I\}$ is a set of relations between concepts' instances, Z is a set of first-order logic sentences, built over predicates from P. Each concept $c \in C$ is defined as:

$$c = (id^c, A^c, V^c, I^c) \tag{2}$$

where: id^c is an identifier of the concept c, A^c is a set of its attributes, such that $A^c \subseteq A$, V^c is a set of attributes domains (formally: $V^c = \bigcup_{(a \in A^c)} V_a$), I^c is a set of instances of the concept c. We write $a \in c$ to denote that an attribute a belongs to concept c set of attributes A^c. It is worthy of notice that attributes from set A have no semantics. They can be only interpreted if they are part of the chosen concept [10].

By D_A we denote a set containing of words that can be used to define the sublanguage L_S^A of the propositional calculus composed of D_A elements and logical operators of conjunction, disjunction, and negation. By their own, elements of D_A. can be interpreted as atomic descriptions of attributes. Formally, we can define a function S_A that assigns a logical sentence from L_S^A to attributes A^c within a specific concept c. The function S_A has a following signature $S_A : A \times C \to L_S^A$ and allows us to formally define relation: *equivalency* (denoted as $\equiv$), *generalization* (denoted as $\leftarrow$) and *contradiction* (denoted as $\sim$) between attributes:

- Two attributes $a \in A^{c_1}, b \in A^{c_2}$ are *semantically equivalent*, denote by $a \equiv b$, if the formula $S_A(a, c_1) \Leftrightarrow S_A(b, c_2)$ is a tautology for any two $c_1 \in C_1$ and $c_2 \in C_2$.

- The attribute $a \in A^{c_1}$ in concept $c_1 \in C_1$ is *more general* than the attribute $b \in A^{c_2}$ in concept $c_2 \in C_2$ (denoted by $a \leftarrow b$) if the formula $S_A(b, c_2) \Rightarrow S_A(a, c_1)$ is a tautology for any two $c_1 \in C_1$ and $c_2 \in C_2$.
- Two attributes $a \in A^{c_1}, b \in A^{c_2}$ are in *semantical contradiction*, denoted by $a \sim b$, if the formula $\neg(S_A(a, c_1) \wedge S_A(b, c_2))$ is a tautology for any two $c_1 \in C_1$ and $c_2 \in C_2$.

Instances are closely related to the concepts because they are their physical materialization. Thus, we can write $i \in c$, which can be read that the instance i belongs to the concept c. Formally, an instance i which belongs to the set I_C is defined as a pair $i = (id^i, v_c^i)$ where:

- id^i is an instance identifier,
- v_c^i is a function with a signature $v_c^i : A^c \rightarrow V^c$

Instances can belong to many different concepts, therefore, a set of instances' identifiers from Equation 1 is defined as $I = \bigcup_{c \in C} \{id^i | (id^i, v_c^i) \in I^c\}$. We also define an auxiliary function $Ins(c) = \{id^i | (id^i, v_c^i) \in I^c\}$ which for a given concept *c* returns a set containing identifiers of instances assigned to it.

By analogy to D_A we define a set D_R and a sub-language L_S^R to give relations semantics. Formally, we can define a function $S_R : R^C \rightarrow L_S^R$ that assigns a logical sentence from L_S^R to a relation from the set R^C. As a consequence, we can define formal criteria for relationships between relations, analogical to criteria for relationships between attributes. However, within L_S^R we distinguish elements: *is_symmetric*, *is_transitive* and *is_reflexive* that for some selected relation *r* can be used to describe their properties:

- $\big(S_R(r_1^C) \implies is\_symmetric\big) \Rightarrow (\forall(c_1, c_2) \in r_1^C : c_1 = c_2) \wedge \forall(i_1, i_2) \in r_1^I \; \exists(i_2, i_1) \in r_1^I$, where $c_1, c_2 \in C, r_1^C \in R^C, r_1^I \in R^I, i_1 \in c_1 \vee c_2, i_2 \in c_1 \vee c_2)$
- $\big(S_R(r_1^C) \implies is\_transitive\big) \Rightarrow (\forall(c_1, c_2) \in r_1^C : c_1 = c_2) \wedge \forall(i_1, i_2), (i_2, i_3) \in r_1^I$: $(i_1, i_3) \in r_1^I)$ where $c_1, c_2 \in C, r_1^C \in R^C, r_1^I \in R^I, i_1 \in c_1 \vee c_2, i_2 \in c_1 \vee c_2)$
- $\big(S_R(r_1^C) \implies is\_reflexive\big) \Rightarrow (\forall(c_1, c_2) \in r_1^C : \exists(c_1, c_1) \in r_1^C \wedge \exists(c_2, c_2) \in r_1^C)$ $\wedge \forall(i_1, i_2) \in r_1^I : \exists(i_1, i_1) \in r_1^I \wedge \exists(i_2, i_2) \in r_1^I)$

In the above conditions, we utilize the $\implies$ symbol to denote the implication that occurs within logical sentences built from elements from L_S^R. The symbol $\Rightarrow$ denotes the implication in the context of the ontology definition and its elements. To simplify the notation, we will use predicates (e.g., $is\_asymmetric\,(r)$)) to denote properties defined above.

The hierarchy of concepts *H* is simply defined as a subset of a cartesian product of a set of concepts $H \subset C \times C$. A pair of concepts (c_1,c_2) such that $c_1 = (id^{c_1}, A^{c_1}, V^{c_1}, I^{c_1})$ and $c_2 = (id^{c_2}, A^{c_2}, V^{c_2}, I^{c_2})$ may be included in the hierarchy (to represents the fact that c_1 is an ancestor of c_2) only if all of the following postulates are met:

1. $|A^{c_2}| \geq |A^{c_1}|$
2. $\forall a \in A^{c_1} \exists a' \in A^{c_2} : (a \equiv a') \vee (a \leftarrow a')$
3. $Ins(c_2) \subseteq Ins(c_1)$

The set of relations R^C allows us to describe which concept instances can be connected. The actual materialization of these connections is described by the set of instance relations marked as R^I which must satisfy the following formal criteria:

1. $r_j^I \subseteq \bigcup_{(c_1,c_2)\in r_j^C} (Ins(c_1) \times Ins(c_2))$
2. $(i_1, i_2) \in r_j^I \implies \exists (c_1, c_2) \in r_j^C : (c_1 \in Ins^{-1}(i_1)) \wedge (c_2 \in Ins^{-1}(i_2))$ which describes that two instances may be connected by some relation only if there is a relation connecting concepts they belong to
3. $(i_1, i_2) \in r_j^I \implies \neg\exists r_k^I \in R^I : ((i_1, i_2) \in r_k^I) \wedge (r_j^C \sim r_k^C)$ which concerns a situation in which two instances cannot be connected by two contradicting relations
4. $(i_1, i_2) \in r_j^I \wedge \exists r_k^I \in R^I : r_k^C \leftarrow r_j^C \implies (i_1, i_2) \in r_k^I$ which denotes that if two instances are in a relation and there exists a more general relation, then they are also connected by it.

4. Motivating example

As was mentioned before, FOKI lacks a formal syntax but delivers – at the meta-model level – the necessary means for ontology integration. The semantics of attributes and relations are defined as logic formulas in FOKI, which is the main difference between FOKI and OWL. Zero-order logic is a mechanism used in FOKI to define alignment rules ([11]) and integration rules ([10]).

There are plenty of ontologies expressed in OWL, including those dedicated to ontology integration (e.g., OEAI benchmarks). To be able to process these ontologies in FOKI, a translation mechanism from OWL to FOKI meta-model is necessary. The translation must be two-directional, as the result of ontology integration should be comparable with existing benchmarks expressed in OWL. Translation FOKI-OWL is performed on the syntax level only. The semantics of particular elements (attributes, relations) are defined later by an expert.

To motivate our work and explain the source of the problems mentioned in the introduction, we use a simple example of ontology integration. Let's assume there are two ontologies, O1 and O2, to be integrated into OWL – see Table 1.

Each ontology introduces only one concept *Person* with a few attributes. These ontologies could be represented using our FOKI formal model as:

O_1 = { $Person$ ($name$: $string$, $birthdate$: $dateTime$) }

O_2 = {$Person$ ($first\_name$: $string$, $last\_name$: $string$,
age : $nonNegativeInteger$)}

For the ontologies' integration, the value of the S_A function has to be defined for each attribute. The semantics are later stored separately in CSV files. Having the semantics defined, the integration process can be run. The integration results could be, e.g. as follows:

$O_1\_O_2$ = {$Person$ ($name$: $string$, $birthdate$: $dateTime$,
age : $nonNegativeInteger$) }

Now, to make the results readable, and useful for further processing, a transformation from FOKI to OWL is necessary. It could produce an ontology in the form given in Listing 1.1.

Table 1. Ontologies to be integrated in OWL format

O_1	O_2
<Declaration> <Class IRI="#Person"/> </Declaration> <Declaration> <DataProperty IRI="#name"/> </Declaration> <DataPropertyDomain> <DataProperty IRI="#name"/> <Class IRI="#Person"/> </DataPropertyDomain> <DataPropertyRange> <DataProperty IRI="#name"/> <Datatype abbreviatedIRI="xsd:string"/> </DataPropertyRange> <Declaration> <DataProperty IRI="#birthdate"/> </Declaration> <DataPropertyDomain> <DataProperty IRI="#birthdate"/> <Class IRI="#Person"/> </DataPropertyDomain> <DataPropertyRange> <DataProperty IRI="#birthdate"/> <Datatype abbreviatedIRI="xsd:dateTime"/> </DataPropertyRange>	<Declaration> <Class IRI="#Person"/> </Declaration> <Declaration> <DataProperty IRI="#first_name"/> </Declaration> <Declaration> <DataProperty IRI="#age"/> </Declaration> <Declaration> <DataProperty IRI="#last_name"/> </Declaration> <DataPropertyDomain> <DataProperty IRI="#age"/> <Class IRI="#Person"/> </DataPropertyDomain> <DataPropertyDomain> <DataProperty IRI="#first_name"/> <Class IRI="#Person"/> </DataPropertyDomain> <DataPropertyDomain> <DataProperty IRI="#last_name"/> <Class IRI="#Person"/> </DataPropertyDomain> <DataPropertyRange> <DataProperty IRI="#age"/> <Datatype abbreviatedIRI ="xsd:nonNegativeInteger"/> </DataPropertyRange> <DataPropertyRange> <DataProperty IRI="#first_name"/> <Datatype abbreviatedIRI="xsd:string"/> </DataPropertyRange> <DataPropertyRange> <DataProperty IRI="#last_name"/> <Datatype abbreviatedIRI="xsd:string"/> </DataPropertyRange>

Listing 1.1. Integrated ontology

```
<Declaration><Class IRI="#Person"/></Declaration>
<Declaration><DataProperty IRI="#name"/></Declaration>
<Declaration><DataProperty IRI="#age"/></Declaration>
<Declaration><DataProperty IRI="#birthdate"/></Declaration>

<DataPropertyDomain>
<DataProperty IRI="#name"/><Class IRI="#Person"/>
</DataPropertyDomain>

<DataPropertyRange>
<DataProperty IRI="#name"/>
<Datatype abbreviatedIRI="xsd:string"/>
</DataPropertyRange>

<DataPropertyDomain>
<DataProperty IRI="#age"/><Class IRI="#Person"/>
</DataPropertyDomain>

<DataPropertyRange>
<DataProperty IRI="#age"/>
<Datatype abbreviatedIRI="xsd:nonNegativeInteger"/>
</DataPropertyRange>

<DataPropertyDomain>
<DataProperty IRI="#birthdate"/>
<Class IRI="#Person"/>
</DataPropertyDomain>

<DataPropertyRange>
<DataProperty IRI="#birthdate"/>
<Datatype abbreviatedIRI="xsd:dateTime"/>
</DataPropertyRange>
```

5. Transformation Procedure

This section presents detailed transformation procedures to convert ontologies between FOKI and the OWL2 standard. These two frameworks exhibit fundamental differences in their treatment of unknown facts. To bridge these differences, we designed a set of precise transformation rules to preserve the semantic integrity of the ontologies.

The intricacies of translating OWL's complex, expressive capabilities, particularly its data properties and logical constructs, into the formal structure of FOKI are explained. This includes handling equivalence, disjointness, and cardinality constraints in a closed-world context. Next, the rigorous testing and validation of our procedures using benchmark datasets provided by the Ontology Alignment Evaluation Initiative and the Ontology

Lookup Service is presented. The aim of our experimental research is to confirm the reliability and consistency of our transformation rules in practical ontology management applications.

5.1. Assumptions

The primary contribution of this paper is the development of transformation procedures that facilitate the conversion between two fundamentally distinct ontology representation notations: the newly developed FOKI formalism and the widely adopted OWL2 standard.

The critical difference between these frameworks lies in their approaches to managing unknown facts within a given domain. OWL2 operates under an open-world assumption, meaning that the absence of explicit information does not imply falsehood. In contrast, FOKI follows a closed-world assumption, where any statement not explicitly included in the ontology is considered false.

To bridge these conceptual differences effectively, we have established a detailed set of transformation rules. These rules are designed to be repeatable and concise, ensuring that the semantics of the input ontology are preserved as accurately as possible despite the inherent constraints of the differing frameworks. This transition involves careful consideration of OWL's non-functional data properties and open-world assumption, as well as FOKI's functional attributes and closed-world perspective. The meticulous design of these transformation rules aims to minimize information loss and maintain the integrity of the original ontology's semantics.

Furthermore, our approach addresses the challenges of converting OWL's rich, expressive capabilities into the more rigid structure required by FOKI. This includes handling equivalence, disjointness, and other logical constructs that may have different interpretations in a closed-world context. Our transformation procedures have been rigorously tested to ensure that they provide reliable and consistent results, facilitating the interoperability between systems using OWL2 and those based on the FOKI framework. This advancement not only supports seamless data integration across diverse ontological systems but also enhances the robustness and flexibility of ontology management practices.

The other difference relates to data properties. In OWL, an instance may have many valuations (literals) of a specific data property unless the property is marked as functional. In FOKI, an attribute (the equivalent of OWL data property) may have, at most, one value assigned independently on the case. No mechanism in FOKI allows combining attribute domains. It is why almost all OWL axioms referring to data properties (e.g., *DataUnionOf*, *DataComplementOf*) are not taken into consideration, including new data types declaration. Some other axioms, e.g., *DataMinCardinality*, are considered with specific restrictions (the cardinality must be equal to 1). At that moment, only OWL primitive types (declared in e.g., owl, RDF namespaces) are translated. For the unknown type, a special *anyURI* is assigned, which can be treated as a parent for all types.

Given the profound semantic differences between OWL2 and FOKI, achieving an utterly lossless transformation is impractical. Instead, our approach focuses on providing the best possible approximation by narrowing the transformation scope to the most frequently utilized elements in real-world ontologies. This decision was informed by extensive analysis of datasets provided by the Ontology Alignment Evaluation Initiative (OAEI) and the Ontology Lookup Service (OLS), which serve as benchmarks and repositories for state-of-the-art ontology applications and biomedical ontologies, respectively.

These platforms provide invaluable resources for validating and refining our transformation procedures, ensuring they meet the practical demands of ontology management and application in diverse domains. The former, OAEI (Ontology Alignment Evaluation Initiative), is a non-profit organization that has organized (since 2004) public campaigns aimed at evaluating ontology matching technologies. For this reason, it provides benchmark datasets with pre-prepared ontologies. These datasets are frequently treated as a state of the art benchmark data used to test various ontology-related applications. The latter, the Ontology Lookup Service (OLS), is a repository for biomedical ontologies that provides a single point of access to the latest ontology versions.

We tested more than 250 ontologies (first level only, without counting imported elements), and based on them, created a frequency distribution for all axioms. The obtained results are presented in Table 2. The table contains all axioms found in processed ontologies. Some axioms represent constructs that cannot be considered in transformations to FOKI formalism (e.g., annotations). These are written in italics. Out of the remaining axioms we have selected to implement in transformation rules those with at least 1% occurrence. As one can observe, the *DataPropertyRange* is the last axiom directly translated to FOKI (it represents an attribute domain) with 239 occurrences (more than 99.99% of axiom instances are above that limit).

5.2. FOKI Meta-model

Figures 1, 2, and 3 present the FOKI meta-model, which enables bi-directional translation between OWL2 and FOKI. Both OWL and FOKI ontologies can be represented as meta-model instances expressed in an abstract way (syntax agnostic).

The meta-model includes all elements specific to FOKI and those of OWL, which can be translated into FOKI. On one side, it is a limited version of the OWL2 meta-model, and – on the other side – it is an extension of the OWL2 meta-model as it contains elements presented in FOKI only (e.g., the semantics part). Because of its flexibility, we call it generic or universal.

The ontology, according to its formal definition (see chapter 3), is defined as a composition of concepts (C), generalization relationships between concepts (H), relations (R_C), instances of concepts (I), instances of relations (R_I), and predicates (Z) – see Figure 1. The predicates are specific to FOKI and are skipped in the meta-model. The other ontology components are directly visible in the meta-model, represented by associations and compositions written in blue.

There exists an apparent connection between OWL2 and the meta-model. The OWL2 class is represented by the *Concept* meta-class while the OWL2 instance – by the *Instance* meta-class.

OWL2 class is a container of data properties represented by the *Attribute* meta-class. Each attribute should have a domain defined. The domain is perceived as a set of primitive types defined in namespaces owl, RDF, XSD). Additionally, the attribute can be set as functional.

Each attribute is functional by default in FOKI (one can have at most one value assigned). Here, it is used to mark the fact that the translation OWL2-meta-model-FOKI can be potentially lossy (when *isFunctional* = false). However, instances are rarely defined in ontologies, and an attribute has extremely rarely more than one value (see Table 2).

Table 2. The frequency of the axioms occurring in ontologies provided by OAEI and OLS

Axioms' name	Count	Axioms' name	Count	Axioms' name	Count	Axioms' name	Count
[*AnnotationAssertion*]	11398600	[DataPropertyAssertion]	5637	[Declaration(DataProperty)]	530	[InverseFunctionalObjectProperty]	38
[SubClassOf]	2541198	[ObjectAllValuesFrom]	3920	[EquivalentObjectProperties]	419	[DisjointUnion]	33
[Declaration(Class)]	1725507	[ObjectHasValue]	3705	[ObjectOneOf]	379	[ReflexiveObjectProperty]	28
[ObjectPropertyAssertion]	1676802	[ObjectPropertyDomain]	3135	[DataPropertyRange]	239	[*DataIntersectionOf*]	23
[ObjectSomeValuesFrom]	1314347	[ObjectPropertyRange]	3068	[SymmetricObjectProperty]	230	[DisjointObjectProperties]	20
[Declaration(NamedIndividual)]	489422	[*SameIndividual*]	2721	[FunctionalObjectProperty]	152	[*DataAllValuesFrom*]	16
[ObjectIntersectionOf]	400322	[ObjectPropertyChain]	2391	[IrreflexiveObjectProperty]	106	[DataMaxCardinality]	14
[EquivalentClasses]	191466	[InverseObjectProperties]	2071	[*Declaration(Datatype)*]	103	[*AnnotationPropertyDomain*]	11
[ClassAssertion]	46979	[TransitiveObjectProperty]	1490	[*FunctionalDataProperty*]	82	[*DataOneOf*]	3
[*DataHasValue*]	14339	[*SubAnnotationPropertyOf*]	1462	[*SubDataPropertyOf*]	77	[*DatatypeDefinition*]	1
[ObjectExactCardinality]	12522	[*DataSomeValuesFrom*]	1196	[*AnnotationPropertyRange*]	75	[*DataUnionOf*]	1
[SubObjectPropertyOf]	11275	[*DatatypeRestriction*]	1191	[*DifferentIndividuals*]	71	[*DataComplementOf*]	0
[Declaration(ObjectProperty)]	11171	[ObjectMaxCardinality]	910	[AsymmetricObjectProperty]	67	[*EquivalentDataProperties*]	0
[*Declaration(AnnotationProperty)*]	9521	[ObjectComplementOf]	639	[ObjectHasSelf]	65	[*DisjointDataProperties*]	0
[DisjointClasses]	6916	[ObjectMinCardinality]	619	[DataExactCardinality]	58	[NegativeObjectPropertyAssertion]	0
[ObjectUnionOf]	6353	[ObjectInverseOf]	589	[DataMinCardinality]	40	[NegativeDataPropertyAssertion]	0

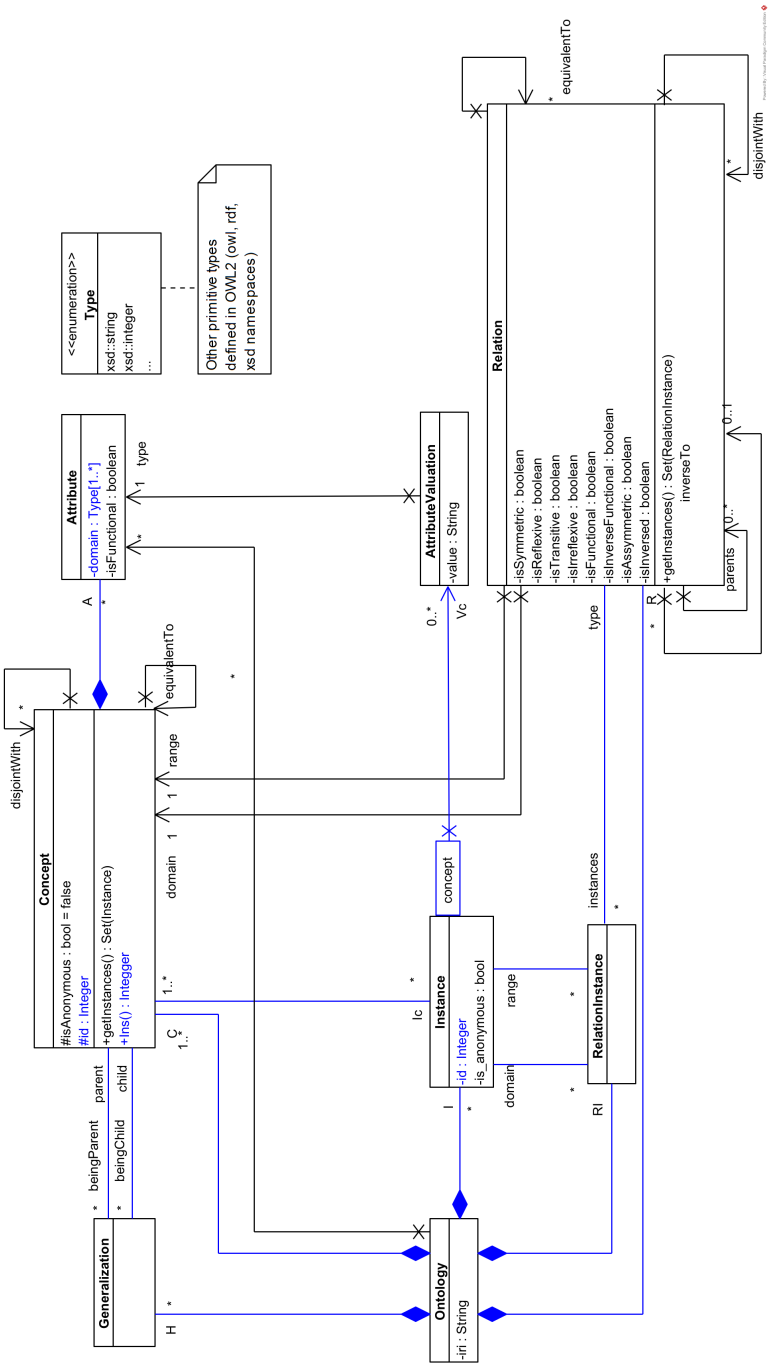

Fig. 1. FOKI meta-model – ontology basic structure

How OWL2 class expression axioms are represented in the meta-model depends strongly on its type. *SubClassOf* axiom is represented by *Generalization* meta-class, which directly links the parent and its child. Self-associations with the representative role names *equivalentTo, disjointWith* represent OWL *EquivalentClass* and *DisjointClass* axioms.

The meta-model *Relation* class represents an OWL2 object property. Such a relation can be marked as transitive, reflexive, symmetric, etc. It can also refer to its inverse version (a result of the translation of *InverseObjectProperty*). Essential axioms define the domain and range of a property. In the meta-model, both are represented by directional associations with specific roles (domain, range) from *Relation* to *Concept* meta-class. Similarly to classes, axioms about object properties equivalence, or the fact some are disjoint or inverse, are represented by directional self-associations with *Relation* meta-class on both ends. A relation can also store a list of its parents (if any).

The OWL2 concept instances are represented by the *Instance* meta-class. The qualifier *concept* represents this at the end of the association, linking the *Instance* meta-class with *AttributeValuation* meta-class (representation of the OWL2 Literal, e.g., 'John'). Similarly, instances of object properties are represented by the *RelationInstance* meta-class. The instance of the *Relation* meta-class remembers its features, i.e., if it is symmetric, reflexive, functional, etc.

Concepts and instances are named elements, i.e., they can be identified by an IRI (Internationalized Resource Identifier) from which the resource's name can be extracted (the name attribute) – see Figure 2. The name can include the package name, while its short version (the *shortName* attribute) is only limited to the resource name. For an anonymous instance, the *is_anonymous* attribute is set to false. As an instance can belong to many classes (concepts), their attributes can be split into groups (one group per concept).

Let us demonstrate the correspondence between the OWL ontology from Section 4 and our meta-model. In this example:

- O_1, O_2 are instances of the *Ontology* meta-class
- *Person* is an instance of the FOKI *Concept* meta-class (all the properties inherited from *NamedElement* meta-class, i.e. *name*, *iri* and *shortName* are set for *Person*, the concept is not anonymous); *Person* is a part of the proper ontology
- *name*, *birthdate* etc. are instances of the *Attribute* meta-class with properly set domain (*string* for *name*, *dateTime* for *birthdate*). The concept instance keeps attributes via composition relationship. The functional property for attributes is set to false.

Attributes (parts of *Concepts*) and *Relations* are elements to which semantics can be assigned in the form of a first-logic predicate sentence – see Figure 2. Such sentences are represented by instances of the *Semantics* class and its children (*Label, Operator*). Assuming that Person's *name* has semantics defined as $first\_name$ and $last\_name$, the semantics (associated with the *name* attribute) will be represented as two instances of the *Label* meta-classes, one for *first_name*, and one for *last_name*, connected by an instance of the *Operator* meta-class with the *type* property set to 'and'. The semantic part is not considered in the OWL2 to FOKI translation because this part is absent in OWL.

The core of every ontology is formed by a concept's definition and concept hierarchy – see Figure 3.

Any concept in OWL2 can be directly declared and have a name or be introduced indirectly as a combination of other concepts, e.g., union, intersection, etc. The combinations

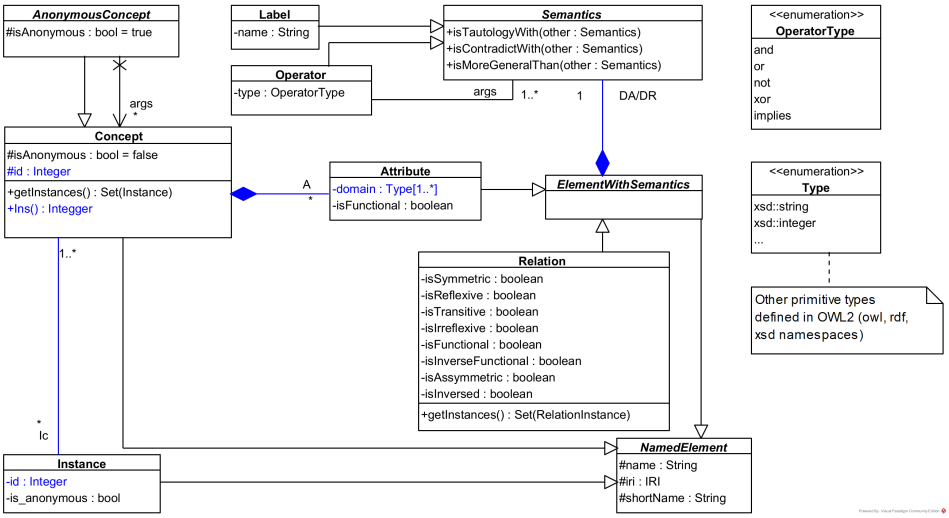

Fig. 2. FOKI meta-model – ontology named elements and elements with semantics

are represented as children of *AnonymousConcept* meta-class working on arguments (*args* role). The concrete children of *AnonymousConcepts* can be easily linked to the proper class expressions in OWL2, e.g. *ObjectIntersectionOf (ObjectIntersection)* in the meta-model), *ObjectUnionOf (ObjectUnion), ObjectComplementOf (ObjectComplement), ObjectSomeValuesFrom (ObjectValuesFrom, type*=some), *ObjectAllValuesFrom (ObjectValuesFrom, type*=all), *ObjectMinCardinality (ObjectCardinality, type* = min), *ObjectMaxCardinality (ObjectCardinality, type*=max), *ObjectExactCardinality (ObjectCardinality, type*=exact), *ObjectHasSelf*,*ObjectHasValue*, *ObjectOneOf*.

Such a solution enables the representation of complex structures, e.g., *UnionOf(IntersecionOf(A, B), C)* – see Figure 4. As one can notice, the names for anonymous concepts are created by the FOKI tool, and they reflect the intended semantics of the way the concept's arguments are combined.

DisjointUnion OWL axiom introduces a separate anonymous class – *DisjointUnion* in the meta-model.

5.3. Transformation Rules from OWL

The input ontology O, in OWL, can contain elements that are not explicitly defined. It means that some of its content must be inferred before any operations on reading ontology are possible. For the sake of consistency, the elements that can be inferred include:

- domain/ranges of relations if they are known for one of the parent relations
- instances of concepts/relations (a result of *getInstance* operation).

Examples of transformation procedures are presented below. The meta-model is a proxy between OWL2 and FOKI translation. Therefore, translation procedures are split

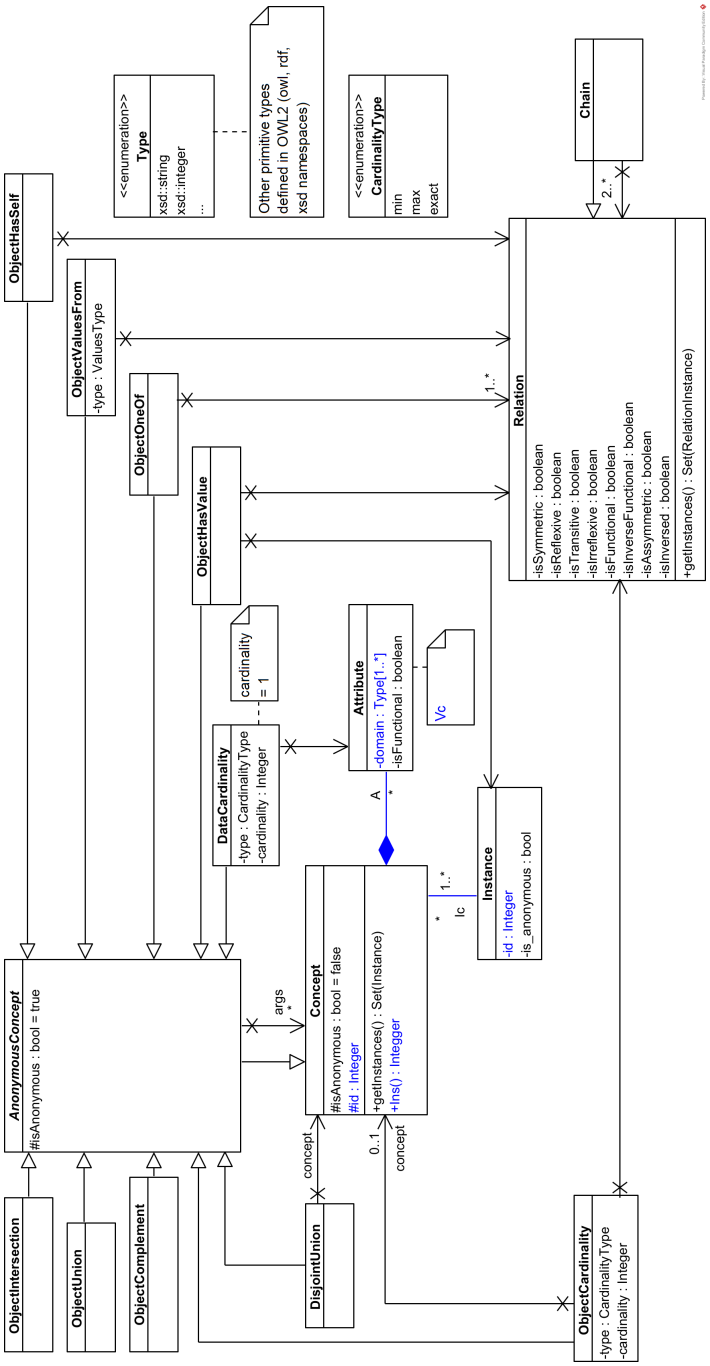

Fig. 3. FOKI meta-model – ontology concept heierarchy

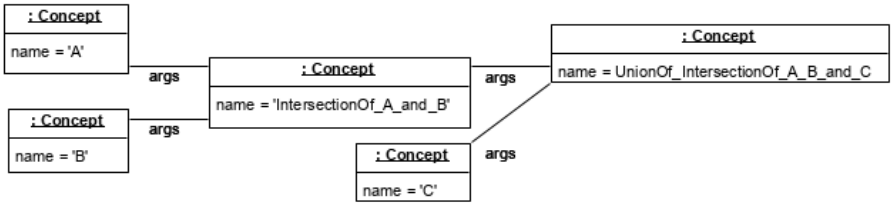

Fig. 4. Exemplary instance of a complex concept

into two groups. The first takes an OWL2 ontology and produces an instance of the meta-model. The second goes further and translates an instance of the meta-model into an instance of FOKI (the mathematical formalism). The opposite transformations, i.e., from FOKI formalisms to the instance of the meta-model and farther to the OWL are straightforward (defined indirectly by the existing transformation rules).

Let O_{OWL} represent an ontology expressed in OWL2, O_{MM} represent the same ontology as an instance of the meta-model, and O_{FOKI} represent the ontology O expressed in FOKI formalism (abstract syntax). These three representations are globally available for every formulated procedure. To select a specific element from one of the ontologies, a dot notation is used, e.g., $O_{FOKI}.C$ which represents the set of concepts *C* from the O_{FOKI} ontology. If the element belongs to the meta-model, the meta-class name proceeded by a '_' (to represent an instance) is used instead, e.g., *_Attribute*, *_Instance*, *_Relation*. The valuation of attributes for meta-class instances, if necessary, will be described with a dot notation, e.g. *_AttributeValuation.value* ='5'. In the same manner, the association ends will be referred, e.g., *_Ontology.I* = new *Set(Instance)* – where *I* is the association end representing a set of instances being part of the ontology.

Due to the limited space available for this paper, we present only some representatives of transformation procedures and divide them into two sections. The first shows how basic ontology elements are created. These elements are classes, attributes, relations between concepts, and relations between instances. The second demonstrates how relation properties are translated using a symmetry feature as an example. The last example concentrates on so-called *AnonymousConcepts*, i.e., concepts without a specific name constructed as a composition, e.g., a union or an intersection of other concepts.

OWL2 to meta-model translations The first transformation algorithm 1 shows how a new concept is created. When a new instance of a meta-model class is created, all its association ends are also initialized as empty collections (sets). For example, when an *Attribute* is created, then it is connected with an empty set of *AttributeValuations*. For simplicity, that fact is skipped in the transformation procedures.

The next four transformations 2, 3, 4, 5 present how axioms connected with *data property* are processed. The procedure 2 translates a data property declaration that introduces a data property name only. On that basis, a new attribute is created and stored (as a part of meta-model ontology) for further processing.

Algorithm 1 CreateConcept in meta-model.
OWL syntax: *Class(c)*

1: **Input:** $c \in O_{OWL}$
2: create new $\_Concept$
3: generate unique id
4: $\_Concept.id = id$
5: $\_Concept.name = c.name$
6: $\_Concept.IRI = c.IRI$
7: add $\_Concept$ to $O_{OWL}.\_Ontology.C$

Algorithm 2 CreateAttribute in meta-model.
OWL syntax: *Declaration(DataProperty(p))*

1: **Input:** $p(roperty) \in O_{OWL}$
2: create new $\_Attribute$
3: $\_Attribute.isFunctional = false$
4: $\_Attribute.name = p.name$
5: $\_Attribute.IRI = p.IRI$
6: add $\_Attribute$ to $O_{OWL}.\_Ontology.attribute$

The *FindOrCreateAttribute* function 3 is an auxiliary element, used later for translation of other axioms. The existence of similar functions, e.g. *FindOrCreateConcept*, *FindOrCreateRelation* etc., is assumed. These functions look for an element with a specific name. If it does not exist, the element is created.

Algorithm 3 FindOrCreateAttribute in meta-model

1: **Input:** a, O_{OWL}
2: **Result:** An attribute $\_Attribute$ – meta-model representation of a in OWL2
3: **if** $O_{MM}.\_Ontology.attribute$ **contains** $\_Attribute : \_Attribute.name = a.name$ **then**
4: **return** $\_Attribute$
5: **end if**
6: **return** CreateAttribute(a, O_{OWL})

Translation of *DataPropertyDomain* axiom 4 results in finding or creation (if it does not exist) of an attribute that is assigned to the proper class (also found or created).

Translation of *DataPropertyRange* axiom 5 requires the proper attribute to be found (or created). After that, its feature *domains* are modified by adding a new range.

The procedure 6 shows the creation of complex concepts (by the example of *ObjectIntersectionOf*).

The next procedure 7 shows the creation of a concept instance, assuming that the instance is not an anonymous one (a result of the processing of *ClassAssertion* axiom).

Data property in OWL2 may have a value assigned to an instance that is a proper class member. In the meta-model, the data property value is represented by an instance of $AttributeValuation$ class. The instance uses a qualifier (concept) to split attribute values into manageable pieces (Algorithm 8).

Algorithm 4 Assign an attribute to a concept in meta-model
OWL syntax: *DataPropertyDomain(p, c)*

1: **Input:** $p(roperty), c(lass) \in O_{OWL}$
2: $\_Attribute$ = FindOrCreateAttribute($p, O_{MM}.\_Ontology$);
3: $\_Concept$ = FindOrCreateConcept($c, O_{MM}.\_Ontology$);
4: add $\_Attribute$ to $\_Concept.attribute$

Algorithm 5 Assign an attribute's domain in meta-model
OWL syntax: *DataPropertyRange(p, r)*

1: **Input:** $p(roperty), r(ange) \in O_{OWL}$
2: $\_Attribute$ = FindOrCreateAttribute($p, O_{MM}.\_Ontology$);
3: add r to $\_Attribute.domains$

Algorithm 6 Create an anonymous concept
OWL syntax: *ObjectIntersectionOf*$(c_1, c_2, \ldots, c_n)$

1: **Input:** $c_1[OWL], c_2[OWL], \ldots, c_n[OWL] \in O_{OWL}$
2: create new $\_ObjectIntersection$
3: add $\_ObjectIntersection$ to $O_{MM}.\_Ontology.concepts$
4: $\_ObjectIntersection.name = ObjectIntersectionOf\_+c_1.name+\_and\_+\cdots+\_and\_+c_n.name$
5: **for** $c_i \in \{c_1, \ldots, c_n\}$ **do**
6: add c_i to $\_ObjectIntersection.args$
7: **end for**

Algorithm 7 Create an instance
OWL syntax: *ClassAssertion(c i)*

1: **Input:** $c(lass), i(nstance) \in O_{OWL}$
2: $\_Instance$ = FindOrCreateInstance($i, O_{MM}.\_Ontology$);
3: generate unique id;
4: $\_Instance.id = id$;
5: $\_Instance.is\_anonymous = false$;
6: $\_Concept$ = FindOrCreateConcept($c, O_{MM}.\_Ontology$);
7: add $\_Instance$ to $\_Concept.instances$;
8: add $\_Concept$ to $\_Instance.concept$;

Algorithm 8 Create an instance valuation
OWL syntax: *DataPropertyAssertion(p i v)*

1: **Input:** $p(roperty), i(nstance), v(alue) \in O_{OWL}$
2: create new $\_AttributeValuation$;
3: $\_AttributeValuation.value = v$;
4: $\_Instance$ = FindOrCreateInstance($i, O_{OWL}.\_Ontology$);
5: add $\_AttributeValuation$ to $\_Instance.attributes$; ▷ Assuming $\_Instance[c]$ means to add to instance's attributes

Meta-model relation is created during the processing of *ObjectProperty* axioms (declarations, domain definition, range definition). These axioms are processed similarly to *DataProperty* axioms and therefore are skipped. Relation in OWL could have many features, e.g., be symmetric, reflexive, etc. The processing of *SymmetricObjectProperty* axiom is presented in Algorithm 9.

Algorithm 9 Create a symmetric relation
OWL syntax: *SymmetricObjectProperty(p)*

1: **Input:** $p(roperty) \in O_{OWL}$
2: $\_Relation =$ FindOrCreateRelation$(p, O_{MM}._Ontology)$;
3: $\_Relation.isSymmetric =$ true;

Transformation rules from meta-model to FOKI This section presents some procedures for translating elements taken from the presented meta-model into mathematical constructs defined according to the formal foundations presented in Section 3. Such transformation requires an auxiliary procedure, which takes as an input an instance for *Semantics* class from the meta-model. It recursively creates a logic sentence built from atomic literals and logic operators (negation, conjunction, disjunction, implication, and exclusive disjunction). This procedure is presented as Algoritm 10.

Algorithm 10 Create_Semantics

1: **Input:** $\_s \in O_{MM}.Semantics$
2: **if** $\_s$ is $O_{MM}.Label$ **then**
3: **return** $\_s.name$;
4: **else**
5: **if** $\_s.type =$ 'not' **then**
6: **return** $\neg$ + Create_Semantics($\_s.args[0]$);
7: **else if** $\_s.type =$ 'and' **then**
8: **return** Create_Semantics($\_s.args[0]$) + $\wedge$ + Create_Semantics($\_s.args[1]$);
9: **else if** $\_s.type =$ 'or' **then**
10: **return** Create_Semantics($\_s.args[0]$) + $\vee$ + Create_Semantics($\_s.args[1]$);
11: **else if** $\_s.type =$ 'xor' **then**
12: **return** Create_Semantics($\_s.args[0]$) + $\oplus$ + Create_Semantics($\_s.args[1]$);
13: **else if** $\_s.type =$ 'implies' **then**
14: **return** Create_Semantics($\_s.args[0]$) + $\implies$ + Create_Semantics($\_s.args[1]$);
15: **end if**
16: **end if**

The first transformation 11 shows how a concept's definition is built from an instance of a Concept. If the concept is anonymous, an additional predicate is stored in FOKI. The procedure also shows how the defined earlier procedure for creating logic sentences is used in the context of attributes' semantics.

Algorithm 11 Transformation of a concept

Input:O_{MM}, $\_c \in O_{MM}.C$
create new concept $c = (\_c.id, A^c = \emptyset, V^c = \emptyset, I^c = \emptyset)$;
for $\_a \in \_c.A$ **do**
    create an attribute a named $\_a.name$;
    add a to A^c;
    $O_{FOKI}.S_A(a, c)$ = Create_Semantics($\_a.DA/DR$);
    add $\_a.domain$ to V^c;
end for
add c to $O_{FOKI}.C$;
if $\_c.isAnonymous$ **then**
    add $is\_anonymous(c)$ to $O_{FOKI}.Z$;
end if

The next procedure 12 addresses the transformation of instances. It allocates attributes' values to the particular instance created accordingly to the template enforced by a concept to which it will be eventually assigned. Similarly to the previous procedure (11), the situation in which a particular instance is not explicitly defined in OWL is handled by adding $is\_anonymous$ predicate.

Algorithm 12 Transformation of a concept's instance

Input: O_{MM}, $\_c \in O_{MM}.C$, $\_i \in O_{MM}.I \wedge \_i \in c.Ic$
create new instance $i = (\_i.id, v_c^i = \emptyset)$;
find $c \in O_{FOKI}.C$ such that $c.id = \_c.id$;
for $a \in \_i.V_c$ **do**
    add $a.value$ to v_c^i;
end for
$I^c = I^c \cup \{i\}$;
if $\_i.is\_anonymous$ **then**
    add $is\_anonymous(i.id)$ to $O_{FOKI}.Z$;
end if

The procedure 13 shows how a transformation of concepts hierarchy is performed. According to Equation 1 the generalization of concepts is expressed as an ordered pair of concepts included in the set *H*. Therefore, the transformation takes as input an instance of a *Generalization* class, which has two attributes pointing to two *Concept* class instances. Then, these concepts are extracted, the generalization representation is created, which is eventually added to the set *H* according to the mathematical definition.

Algorithm 13 Transformation of a concept's generalization

Input: O_{MM}, $\_h \in O_{MM}.H$
find $c_1 \in O_{FOKI}.C$ such that $\_h.parent.id = c_1.id$;
find $c_2 \in O_{FOKI}.C$ such that $\_h.child.id = c_2.id$;
add (c_1, c_2) to $O_{FOKI}.H$;

The last two procedures (14, 15) focus on translating concepts and instances relations. The first ((Algorithm 14) addresses relations between concepts. It is a similar approach to the transformation of concept generalization, but it requires a *Relation* class instance as an input to extract participating concepts. It then utilizes a procedure for creating logic sentences to generate relation's semantics, which is eventually expanded with descriptions of particular relations features (e.g. its transitivity or reflexivity).

Algorithm 14 Transformation of a concept's relation

1: **Input:** O_{MM}, $\_r \in O_{MM}.R$
2: find $c_1 \in O_{FOKI}.C$ such that $\_r.domain.id = c_1.id$;
3: find $c_2 \in O_{FOKI}.C$ such that $\_r.range.id = c_2.id$;
4: find $r^C \in O_{FOKI}.R^C$ such that $r^C = \_r.name$;
5: add (c_1, c_2) to r^C;
6: $O_{FOKI}.S_R(r)$ = $Create\_Semantics(\_r.DA/DR)$;
7: **if** $\neg r.isSymmetric$ **then**
8: concatenate $' \wedge is\_symmetric'$ to $S_R(r)$
9: **end if**
10: **if** $\neg r.isReflexive$ **then**
11: concatenate $' \wedge is\_reflexive'$ to $S_R(r)$
12: **end if**
13: **if** $\neg r.isTransitive$ **then**
14: concatenate $' \wedge is\_transitive'$ to $S_R(r)$
15: **end if**
16: **if** $\neg r.isIrreflexive$ **then**
17: concatenate $' \wedge is\_irreflexive'$ to $S_R(r)$
18: **end if**
19: **if** $\neg r.isFunctional$ **then**
20: concatenate $' \wedge is\_functional'$ to $S_R(r)$
21: **end if**
22: **if** $\neg r.isInverseFunctional$ **then**
23: concatenate $' \wedge is\_inverse\_functional'$ to $S_R(r)$
24: **end if**
25: **if** $\neg r.isAssymetric$ **then**
26: concatenate $' \wedge is\_assymetric'$ to $S_R(r)$
27: **end if**

The last procedure 15 performs a translation of relations between instances. It accepts an instance of *RelationInstance* class from the meta-model. Then it extracts two participating instances, which are eventually included in the appropriate relation taken from the set $O_{FOKI}.R^I$ according to Equation 1.

6. Evaluation Procedure

The meta-model and bi-directional transformation procedure were implemented in a prototype tool written in Java 1.8, and available in executable version (jar file) at [13].

The following testing procedure was used to check the correctness and completeness of the transformation process. After reading an input ontology, it was saved without

Algorithm 15 Transformation of instances relation

1: **Input:** O_{MM}, $\_r \in O_{MM}.RI$
2: find $r^I \in O_{FOKI}.R^I$ such that $r^I = \_r.name$;
3: find $i_1 \in O_{FOKI}.I$ such that $\_r.domain.id = i_1.id$;
4: find $i_2 \in O_{FOKI}.I$ such that $\_r.range.id = i_2.id$;
5: add (i_1, i_2) to r^I

any change in the functional syntax for further comparison. Next, the input ontology was transformed into a meta-model instance. This instance was later saved under another name in the functional syntax. Such an approach made a textual comparison of two files possible (the original input ontology and the result of its processing) with generally available tools. We used the $diff$ tool that computes and displays the differences between the contents of two files. When any textual difference was identified, it was checked if the FOKI translation was semantically different from the original version.

The testing procedure was run for commonly available ontologies of different sizes and natures. The results are presented in Table 3. The first column contains information about the ontology processed, the second – about the number of axioms and annotations (not translated) in the ontology, the third – about not translated axioms, and the fourth some notes/explanations of the results.

In most places when syntax differences were identified, the semantics were preserved, e.g. *InverseObjectProperties*(:forEvent :hasCall) is an equivalent for *InverseObjectProperties* (:hasCall :forEvent)). Once it occurred that the original ontology was redundant – some axioms could be eliminated without changing the semantics (they can be inferred from existing axioms). The translation didn't contain the redundant axioms. And once, the axiom *InverseObjectProperties*(:parallel_with :parallel_with) is replaced with the equivalent one *ReflexiveObjectProperty*(:parallel_with).

7. Future Works and Summary

In this paper, we introduced a meta-model and a comprehensive set of rules designed to facilitate the translation of ontologies between the FOKI framework's internal mathematical formalism and the widely used OWL2 standard. Utilizing UML notation, we meticulously defined the meta-model and outlined transformation procedures that effectively bridge these distinct frameworks. Each transformation procedure was crafted to align an abstract syntax element of OWL2 with its corresponding representation in the FOKI framework using specific meta-model elements.

The meta-model and the bi-directional transformation procedures, a result of our research, were implemented in Java. This practical implementation allowed us to rigorously test our translation method against ontologies primarily sourced from the Ontology Alignment Evaluation Initiative. These ontologies, serving as a benchmark dataset, are essential for validating many ontology-related tools.

The input ontology was initially preserved in its original functional syntax as a baseline for subsequent comparisons. It was then transformed into a meta-model instance and saved under a new identifier in the functional syntax. This approach facilitated a detailed textual comparison between the original input ontology and its processed counterpart

Table 3. The results of transformation

Ontology name and source	**Axiom number Annotation number**	**Percentage of correctly transformed axioms**	**Not transformed axioms or transformed with some changes**	**Comments**
Shop	92/0	92 (100%)	-	The FOKI translation contains one additional axiom: Declaration(Class(owl:Thing))
EDAS[2]	194/0	193 (99.9%)	DifferentIndividuals (1)	
Sigkdd [2]	892/11	891 (99.9%)		ObjectPropertyRange(:award :Award) – redundancy
ConfOf [2]	270/65	269 (99.9%)		Instead of: InverseObjectProperties(:parallel_with :parallel_with) It is: ReflexiveObjectProperty(:parallel_with)
Conference [2]	408/0	399 (97.7%)	Declaration(Datatype(xsd:date)) (1) Usage of datatype (8)	Instead of: DataPropertyRange(:is_an_ending_date xsd:date) It is: DataPropertyRange(:is_an_ending_date xsd:anyURI)
Movie Ontology [3]	870/0	861 (98.9%)	DifferentIndividuals (6) Declaration(Datatype(xsd:date)) (1) Usage of datatype (1)	Declaration(Datatype(xsd:date)) ObjectPropertyDomain (movieontology:hasActress www:Movie) ObjectPropertyDomain (movieontology:hasMaleActor www:Movie) – axioms can be inferred from definition of hasActor object property.
Sabine_target [4]	2896/784	2894 (99.9%)	DataPropertyAssertion (s///abine:hasTopicID :EU ”130”8sd:int) DataPropertyAssertion(sabine:hasTopicID :Politica_sociale ”300”8sd:int) (2)	In FOKI all attributes are functional by definition, and it is why only the last value assigment is remembered.
Sabine _source [4]	2582/784	2580 (99.9%)	DataPropertyAssertion (sabine:hasTopicID :EU ”164”8sd:int) DataPropertyAssertion(sabine:hasTopicID :Immigration ”281”8sd:int) (2)	In FOKI all attributes are functional by definition, and it is why only the last value assigment is remembered.
Human [5]	14857/15507	14854 (99.9%)	Declaration (AnnotationProperty(...)) (3)	.
Mouse [5]	7592/3451	7588 (99.9%)	Declaration (AnnotationProperty(...)) (4)	.

using standard tools. The transformation accuracy, a key measure of our methodology, consistently exceeded 95% across all tested ontologies. The minor losses observed were primarily due to inherent differences between the OWL and FOKI frameworks. Despite this, the results were highly satisfactory, demonstrating that OWL2 ontologies can now be effectively processed using the FOKI framework. Non-functional attributes are adeptly managed within the transformation, which is primarily lossy only in rare cases where an attribute is assigned multiple values. Addressing this issue could be achieved by enhancing the complexity of the transformation, possibly by representing a non-functional attribute domain as a collection in FOKI.

In the future, our efforts will concentrate on developing a concrete syntax and a query language for FOKI, as currently, the framework is equipped only with an abstract syntax. For FOKI to be utilized in practical applications, it is imperative to either adapt an existing ontology syntax or devise a new one tailored to its unique requirements.

References

1. Afzal, H., Waqas, M., Naz, T.: Owlmap: fully automatic mapping of ontology into relational database schema. International journal of advanced computer science and applications 7(11) (2016)
2. Andon, P., Reznichenko, V., Chistyakova, I.: Mapping of description logic to the relational data model. Cybernetics and Systems Analysis 53, 963–977 (2017)
3. Astrova, I., Korda, N., Kalja, A.: Storing owl ontologies in sql relational databases. International Journal of Electrical, Computer and Systems Engineering 1(4), 242–247 (2007)
4. Athanasiadis, I.N., Villa, F., Rizzoli, A.E.: Ontologies, javabeans and relational databases for enabling semantic programming. In: 31st Annual International Computer Software and Applications Conference (COMPSAC 2007). vol. 2, pp. 341–346. IEEE (2007)
5. Baader, F.: The description logic handbook: Theory, implementation and applications. Cambridge university press (2003)
6. Caldarola, E.G., Picariello, A., Rinaldi, A.M.: An approach to ontology integration for ontology reuse in knowledge based digital ecosystems. In: Proceedings of the 7th International Conference on Management of computational and collective intElligence in Digital EcoSystems. pp. 1–8 (2015)
7. De Paepe, D., Thijs, G., Buyle, R., Verborgh, R., Mannens, E.: Automated uml-based ontology generation in oslo 2. In: The Semantic Web: ESWC 2017 Satellite Events: ESWC 2017 Satellite Events, Portorož, Slovenia, May 28–June 1, 2017, Revised Selected Papers 14. pp. 93–97. Springer (2017)
8. El Hajjamy, O., Alaoui, K., Alaoui, L., Bahaj, M.: Mapping uml to owl2 ontology. Journal of Theoretical and Applied Information Technology 90(1), 126 (2016)
9. Hnatkowska, B.: Automatic sumo to uml translation. e-Informatica Software Engineering Journal 10(1) (2016)
10. Hnatkowska, B., Kozierkiewicz, A., Pietranik, M.: Semi-automatic definition of attribute semantics for the purpose of ontology integration. IEEE Access 8, 107272–107284 (2020)
11. Hnatkowska, B., Kozierkiewicz, A., Pietranik, M.: Fuzzy based approach to ontology relations alignment. In: 2021 IEEE International Conference on Fuzzy Systems (FUZZ-IEEE). pp. 1–7. IEEE (2021)
12. Hnatkowska, B., Woroniecki, P.: Transformation of owl2 property axioms to groovy. In: SOFSEM 2018: Theory and Practice of Computer Science: 44th International Conference on Current Trends in Theory and Practice of Computer Science, Krems, Austria, January 29-February 2, 2018, Proceedings 44. pp. 269–282. Springer (2018)

13. Hnatkowska, B.: Owl2 to foki translator. https://github.com/bhnatkowska/OWL2FOKI (2020)
14. Jiménez-Ruiz, E., Kharlamov, E., Zheleznyakov, D., Horrocks, I., Pinkel, C., Skjæveland, M.G., Thorstensen, E., Mora, J.: Bootox: Practical mapping of rdbs to owl 2. In: The Semantic Web-ISWC 2015: 14th International Semantic Web Conference, Bethlehem, PA, USA, October 11-15, 2015, Proceedings, Part II 14. pp. 113–132. Springer (2015)
15. Karpovic, J., Nemuraite, L., Stankeviciene, M.: Requirements for semantic business vocabularies and rules for transforming them into consistent owl2 ontologies. In: Information and Software Technologies: 18th International Conference, ICIST 2012, Kaunas, Lithuania, September 13-14, 2012. Proceedings 18. pp. 420–435. Springer (2012)
16. Kendall, E., Linehan, M.H.: Mapping sbvr to owl2. Tech. rep., IBM Research Report, RC25363 (WAT1303-040) March (2013)
17. Kozierkiewicz, A., Pietranik, M.: The knowledge increase estimation framework for integration of ontology instances' relations. In: Databases and Information Systems: 13th International Baltic Conference, DB&IS 2018, Trakai, Lithuania, July 1-4, 2018, Proceedings 13. pp. 172–186. Springer (2018)
18. Kozierkiewicz-Hetmańska, A., Pietranik, M.: The knowledge increase estimation framework for ontology integration on the concept level. Journal of Intelligent & Fuzzy Systems 32(2), 1161–1172 (2017)
19. Kozierkiewicz-Hetmańska, A., Pietranik, M., Hnatkowska, B.: The knowledge increase estimation framework for ontology integration on the instance level. In: Intelligent Information and Database Systems: 9th Asian Conference, ACIIDS 2017, Kanazawa, Japan, April 3-5, 2017, Proceedings, Part I 9. pp. 3–12. Springer (2017)
20. Maree, M., Belkhatir, M.: Addressing semantic heterogeneity through multiple knowledge base assisted merging of domain-specific ontologies. Knowledge-Based Systems 73, 199–211 (2015)
21. Niles, I., Pease, A.: Towards a standard upper ontology. In: Proceedings of the international conference on Formal Ontology in Information Systems-Volume 2001. pp. 2–9 (2001)
22. Osman, I., Yahia, S.B., Diallo, G.: Ontology integration: approaches and challenging issues. Information Fusion 71, 38–63 (2021)
23. Pietranik, M., Nguyen, N.T.: A multi-attribute based framework for ontology aligning. Neurocomputing 146, 276–290 (2014)
24. Stoilos, G., Geleta, D., Shamdasani, J., Khodadadi, M.: A novel approach and practical algorithms for ontology integration. In: The Semantic Web–ISWC 2018: 17th International Semantic Web Conference, Monterey, CA, USA, October 8–12, 2018, Proceedings, Part I 17. pp. 458–476. Springer (2018)
25. Tirmizi, S.H., Aitken, S., Moreira, D.A., Mungall, C., Sequeda, J., Shah, N.H., Miranker, D.P.: Mapping between the obo and owl ontology languages. Journal of biomedical semantics 2(1), 1–16 (2011)
26. Vysniauskas, E., Nemuraite, L.: Transforming ontology representation from owl to relational database. Information technology and control 35(3) (2006)
27. Xu, Z., Ni, Y., He, W., Lin, L., Yan, Q.: Automatic extraction of owl ontologies from uml class diagrams: a semantics-preserving approach. World Wide Web 15, 517–545 (2012)
28. Zedlitz, J., Jörke, J., Luttenberger, N.: From uml to owl 2. In: Knowledge Technology Week, pp. 154–163. Springer (2011)
29. Zina, N., Kaouther, N.: Automatically building database from biomedical ontology. In: International Work-Conference on Bioinformatics and Biomedical Engineering. pp. 1403–1411 (2014)

Adrianna Kozierkiewicz received the M.Sc. degree in computer science and the Ph.D. degree in 2007 and 2011, respectively. She is currently an associate professor at the Fac-

ulty of Information and Communication Technology at Wrocław University of Science and Technology. She is the author or co-author of over 80 scientific publications, including articles in journals from the Journal Citation Report (JCR) list. She is also the editor of 4 books published by the prestigious Springer publishing house. Her research interests focus on knowledge processing techniques and artificial intelligence, which are integral to modern computer systems. Her research work has been funded by the National Centre for Research and Development or the National Science Centre. She also conducts her research in cooperation with multiple business partners. In addition, she is the Editor in Chief of the International Journal of Intelligent Information and Database System and a member of the Computational Collective Intelligence research group - IEEE SMC. For several years, she has been involved in the organization of international scientific conferences, including ICCCI: International Conference on Computational Collective Intelligence and ACIIDS: Asian Conference on Intelligent Information and Database Systems. She has also organized several special sessions and given numerous presentations at international conferences, including keynote lectures.

Marcin Pietranik is an assistant professor at Wrocław University of Science and Technology since 2016. He obtained his M.Sc and Ph.D. degrees in computer science in 2008 and 2014, respectively. Dr. Pietranik is passionate about knowledge integration and is interested in ontology management, particularly ontology evolution and alignment. He has published more than 45 articles and has co-organized several conferences, demonstrating his significant contribution to the field. In addition to his academic pursuits, Dr. Pietranik has a practical background in modern web technologies, especially in the context of medical and telecommunication projects, which provides him with a unique perspective in his research.

Bogumiła Hnatkowska received an M.Sc. and Ph.D. in computer science from the Wrocław University of Science and Technology, Poland, in 1992 and 1997, respectively. Her Ph.D. dissertation was associated with using formal methods in software engineering. Since 2024, she has worked as a Professor at the Faculty of Information and Communication Technology. She has over 120 publications in international journals and conference proceedings from different areas of software engineering. Her main scientific interests include but are not limited to software development processes, modeling languages, model-driven development (also with the use of ontologies), and the quality of the software products. She is a member of program committees at several international conferences.

Received: February 27, 2024; Accepted: August 29, 2024.

Computer Science and Information Systems 22(1):133–152 https://doi.org/10.2298/CSIS240630004Z

Multilingual Pretrained based Multi-feature Fusion Model for English Text Classification

Ruijuan Zhang

School of Foreign Languages, Zhengzhou University of Science and Technology
Zhengzhou, 450064, China
ruijzhang2024@163.com

Abstract. Deep learning methods have been widely applied to English text classification tasks in recent years, achieving strong performance. However, current methods face two significant challenges: (1) they struggle to effectively capture long-range contextual structure information within text sequences, and (2) they do not adequately integrate linguistic knowledge into representations for enhancing the performance of classifiers. To this end, a novel multilingual pre-training based multi-feature fusion method is proposed for English text classification (MFFMP-ETC). Specifically, MFFMP-ETC consists of the multilingual feature extraction, the multi-level structure learning, and the multi-view representation fusion. MFFMP-ETC utilizes the Multilingual BERT as deep semantic extractor to introduce language information into representation learning, which significantly endows text representations with robustness. Then, MFFMP-ETC integrates Bi-LSTM and TextCNN into multilingual pre-training architecture to capture global and local structure information of English texts, via modelling bidirectional contextual semantic dependencies and multi-granularity local semantic dependencies. Meanwhile, MFFMP-ETC devises the multi-view representation fusion within the invariant semantic learning of representations to aggregate consistent and complementary information among views. MFFMP-ETC synergistically integrates Multilingual BERT's deep semantic features, Bi-LSTM's bidirectional context processing, and TextCNN local feature extraction, offering a more comprehensive and effective solution for capturing long-distance dependencies and nuanced contextual information in text classification. Finally, results on three datasets show MFFMP-ETC conducts a new baseline in terms of accuracy, sensitivity, and precision, verifying progressiveness and effectiveness of MFFMP-ETC in the text classification.

Keywords: Multi-feature fusion, multilingual pretrained model, English text classification, multi-level structure learning.

1. Introduction

As the scale of the internet expands, vast amounts of data inundate various platforms [21,12,7]. Behind this seemingly chaotic data lies immeasurable value [14]. For example, shopping platforms categorize products into different types, making it easier for users to make purchases. News media accurately classify texts, enabling users to quickly find the information they need, saving time and improving work efficiency. Therefore, the ability to quickly and accurately obtain target information and uncover the potential value behind data has become crucial [6,5]. Text classification technology, as a key solution for

information categorization, has attracted significant attention. Text classification involves mining the semantics of texts and grasping the main topics to categorize texts under predefined labels. Specifically, text classification uses labeled data to train and teach the model. Through training and learning, the model learns certain classification rules, and finally, an established classifier is used to predict and categorize unknown texts. As a fundamental technology in natural language processing, text classification is the cornerstone of many NLP tasks. It is widely applied in fields such as news classification, spam filtering, sentiment analysis, and public opinion analysis [22].

In recent years, deep learning-based text classification methods have emerged one after another, significantly improving classification efficiency [13,2,30,9]. Neural network models such as convolutional neural networks, self-attention models, generative adversarial networks, and recurrent neural networks have been widely applied to text classification tasks. Compared to traditional statistical learning methods like support vector machines (SVMs), deep learning models generally exhibit superior performance in classification. This is because deep learning models can automatically extract high-level features from large datasets, reducing the reliance on manual feature engineering while possessing strong representation learning capabilities. For instance, Multilingual BERT, based on the self-attention mechanism and large-scale pretraining, can capture contextual information, handle long-distance dependencies, and enhance the generalization ability of the model through multitask learning.

Despite the strong performance of deep learning-based text classification models in various scenarios, challenges remain in capturing semantic information related to long-distance dependencies within texts. Researchers have proposed several innovative methods to address this issue. For instance, Mundra et al. developed the hierarchical attention network, which improves text structure understanding by introducing two levels of attention mechanisms—sentence and word levels—using bidirectional recurrent neural networks for encoding [18]. Liu et al. introduced the MEANI model, which employs an attention mechanism to integrate emotional language features into the neural network, thereby enhancing the model ability to handle complex emotional expressions [16]. While self-attention-based models have made significant progress in addressing long-distance dependency issues, they have not entirely solved the problem. A key limitation is that many models focus primarily on sentence or document-level processing without explicitly incorporating linguistic knowledge, which is essential for grasping nuanced semantic relationships across different contexts. This shortcoming can lead to suboptimal performance in certain scenarios. Take, for example, the sentence: “Although the plot of this film may seem somewhat monotonous and indistinct, it uniquely captivates our perception in a manner that few contemporary films achieve.” At first glance, the sentence appears to criticize the film’s plot. However, considering the context—especially the phrase “in a manner that few contemporary films achieve”—the sentence is actually offering high praise. If a model fails to incorporate linguistic knowledge effectively, it might misclassify this sentence as a negative review, illustrating the limitations of current self-attention models in capturing subtle semantic relationships.

To this end, a novel multilingual pre-training based multi-feature fusion method is proposed for English text classification (MFFMP-ETC). Specifically, MFFMP-ETC consists of the multilingual feature extraction, the multi-level structure learning, and the multi-view representation fusion. Specifically, multilingual feature extraction utilizes the power

of Multilingual BERT to extract rich semantic features from English texts. By capturing both contextual and nuanced language details, it provides a solid foundation for precise text classification, which ensures that even subtle linguistic cues are effectively identified and leveraged. Then, multi-level structure learning combines the strengths of Bi-LSTM and TextCNN to capture both global and local features of the text. The Bi-LSTM focuses on understanding long-term dependencies in both directions, ensuring that contextual relationships within the text are thoroughly explored. Meanwhile, TextCNN is responsible for identifying important local features using convolutional techniques, capturing finer details that might be missed by global models. Furthermore, multi-view representation fusion merges the features extracted by the previous components into a unified and comprehensive representation. By fusing global and local insights, it creates a more robust and holistic understanding of the text which enhances the model sensitivity to both the overall context and detailed features, resulting in superior classification performance. Finally, experiment results prove the model advantages in recognizing complex semantic structures and enhancing classification precision, setting a new baseline for English text classification tasks.

The contributions of MFFMP-ETC are threefold:

- A multi-level structure learning within the deep multilingual feature extraction architecture is proposed via modelling bidirectional contextual semantic dependencies and multi-granularity local semantic dependencies, which captures global and local structure information of English texts.
- An invariant semantic learning is devised to aggregate consistent and complementary information among representations of views for obtaining a more robust and holistic understanding of the text which enhances the model sensitivity to both the overall context and detailed features, resulting in superior classification performance.
- Experiment results illustrate the efficacy of MFFMP-ETC in comparison to existing methods, highlighting its superior accuracy across three English text classification datasets.

Next, Section 2 reviews related research on text classification methods based on deep learning, including methods based on convolutional neural networks, methods based on recurrent neural networks, methods based on feedforward neural networks, methods based on graph neural networks, and methods based on pre-trained language models. Section 3 provides a detailed introduction to the structure and working principles of the MFFMP-ETC model, including the input layer, multilingual BERT pre-trained language model layer, (Bi-LSTM layer, TextCNN layer, multi-feature fusion layer, and classifier layer. Section 4 presents the experimental results on the MR, SST-2, and CoLA datasets, demonstrating the significant improvement in classification accuracy of the MFFMP-ETC model compared to existing models. Finally, Section 5 summarizes the main contributions of this paper and discusses potential future research directions, including exploring more complex attention mechanisms, integrating domain knowledge, and applying the model to other related tasks to further enhance text classification performance.

2. Related Works

Deep learning-based text classification model refer to a model that utilizes deep neural network architectures to extract features from textual data and classify the text. This model

learns from a large amount of training data to automatically capture semantic information in the text and categorize it into one or more predefined classes. It is primarily divided into five branches: methods based on convolutional neural networks (CNNs), methods based on recurrent neural networks (RNNs), methods based on feedforward neural networks (FNNs), methods based on graph neural networks (GNNs), and methods based on pre-trained language models (PLMs).

Methods based on CNNs: CNNs are initially used for image processing. With further research, they began to be applied in the field of text classification. Kim et al. proposed the classic TextCNN model, which was the first to combine CNNs with text classification tasks [2]. The TextCNN first utilized word2vec for word vector initialization, then used multiple kernels of different sizes to extract key information from sentences, helping the model better capture local features. Finally, the model fed the acquired data into a fully connected layer for final classification and output. Although this model can better capture text features, it loses lexical order and positional information during convolution and pooling operations, and can only capture local word order information, which is detrimental to the final classification results. In addition to the TextCNN model, there are also classic text classification models such as CharCNN [30], DPCNN [9], and CCRCNN [27]. CharCNN transforms the input text into individual characters, representing the text using strings without relying on syntactic and semantic features of the text. This approach has a good fault tolerance rate and can improve classification accuracy. The DPCNN model further refines and improves upon TextCNN by increasing the network depth to enhance text feature extraction, thereby improving text classification accuracy. The CCRCNN model is suitable for short text classification. It extracts contextual features of the text through the network, uses attention mechanisms to capture contextual concepts, and integrates these conceptual features, thereby strengthening the model's ability to capture semantic information and improving classification accuracy.

Methods based on RNNs: Text is sequential in nature, and understanding it requires connecting words in a specific sequence rather than interpreting each word in isolation. For example, the meaning of "I," "eat," and "banana" changes depending on their order. RNNs are designed to handle sequential data, making RNN-based text classification models widely applicable [19]. RNNs can capture positional information and long-distance dependencies in sequences, enhancing the model's ability to capture semantic information in text. However, RNNs suffer from the issues of gradient vanishing and exploding, which prevent parallel computation and result in high computational costs. Despite these challenges, many excellent RNN-based text classification models have been developed. TextRNN is one of the classic RNN-based text classification models. It is a multi-task learning model that can be used in scenarios with limited sample data and has achieved good results on many datasets. Other classic RNN-based text classification models include the MT-LSTM model [17] and the HAN model [24]. The MT-LSTM model leverages LSTM, a variant of RNN, by categorizing the hidden states of LSTM into several groups and activating or updating them at different intervals, making the model suitable for long text classification. The HAN model divides the text into sentences, encodes words and sentences using bidirectional LSTMs, and then employs an attention mechanism to strengthen feature capture. Finally, it uses a softmax layer for text classification prediction, achieving excellent results in long text classification tasks. The semi-supervised text classification model based on bidirectional LSTM, proposed in 2019, integrates various

loss functions such as cross-entropy, which also enhances the accuracy of text classification to some extent [20].

Methods based on FNNs: Models based on feedforward neural networks are also applied to text classification tasks. By modifying word embeddings, feedforward neural network models enhance the extraction of text features, significantly improving text classification accuracy. One of the most classic models is the fastText model [10]. This model introduces the concept of n-grams, summing and averaging the input word vectors before feeding them into a softmax layer for classification. By converting multi-class tasks into binary classification tasks, the model maintains low complexity and few parameters, enabling fast and efficient text classification. Additionally, the SWEM model also demonstrates excellent performance in long text classification [23]. This model captures the maximum value of each dimension in word embeddings through max pooling, thereby extracting key feature information from each word embedding. It then performs hierarchical pooling by averaging all windows, and finally uses global max pooling to sample text features, capturing the most prominent text features. This process enhances the model's ability to extract text features, allowing it to achieve good results in text classification.

Methods based on GNNs: To address the limitations of traditional deep learning models in long-distance information transfer and comprehensive text semantics extraction, recent research has shifted attention to Graph Neural Networks (GNNs). GNNs were initially designed for applications in graph-structured data. Nowadays, with deeper research, GNNs have been applied to the field of text classification. Graph Neural Networks can define relationships between multiple concepts and preserve global structural information. They can transform text classification tasks into graph node classification tasks. Due to their unique properties, many classic text classification models based on GNNs have been developed. Firstly, the graph-CNN model was proposed to convert text into graphs before classification [3]. The model transforms text into a text graph and uses graph convolution operations to capture long-distance text semantics, enhancing the model's ability to capture semantic information. TextGCN is another classic text classification model based on GNNs [28]. This model constructs a text graph for the corpus based on word co-occurrence and semantic relationships between words. The special properties of the graph structure allow long-distance information transmission, improving the accuracy of text classification. Zhang et al. proposed a heterogeneous graph neural network based on transformers [29]. This model introduces additional structural encoding to account for node heterogeneity, and the integration within the transformer allows for learning node representations. Lin et al. proposed BertGCN, which integrates BERT with GCN to capture text features [15]. However, this model has a narrow focus on text feature information and does not consider text features from multiple perspectives. Xie et al. proposed the TV-GAE model, which captures feature information using GNNs [26]. This model integrates a topic model into the graph structure to capture semantic information between text and words, enhancing the model's ability to learn text semantics and improving text classification accuracy. Wang et al. proposed GLHG, a new graph construction method capable of distinguishing different word documents, which is a new cross-language heterogeneous graph neural network model [25]. Li et al. proposed the TextGTL model, which uses a non-heterogeneous graph construction method [11]. This model constructs semantic text graphs, context text graphs, and syntactic text graphs, and jointly trains multiple graphs to capture significant feature information.

Methods based on PLMs have also achieved great success in text classification tasks by enhancing the extraction of text features through extensive pre-training. One of the most classic models is the BERT pre-trained model, proposed in 2018. BERT is trained on a large amount of unlabeled data to extract general features, which are then used to complete classification tasks [4]. Specifically, the BERT model utilizes the encoder structure of the Transformer and is trained through two tasks. The first task is Masked Language Modeling (Masked LM), where some tokens are masked and the model predicts the masked tokens. The second task is Next Sentence Prediction, which involves randomly selecting sentence pairs (sentence A and sentence B) and predicting whether sentence B follows sentence A. This approach allows BERT to deeply learn word-level and sentence-level features, improving its performance in subsequent classification tasks. In addition to BERT, VAMPIRE is another classic pre-trained language model [8]. This model first inputs unlabeled text into a variational autoencoder (VAE) to learn general features through pre-training. The data is then fine-tuned within the VAE model to obtain corresponding word vector representations, which are then concatenated with GloVe word vectors. Finally, the text classification is completed using an encoder and an MLP. MitText, proposed in 2021, is another pre-trained language model [1]. This model uses BERT to predict mixed labeled sample data, generating pseudo-labels. It then performs TMix training and combines TMix with other data, enhancing the data through back-translation, thereby improving the model's classification accuracy.

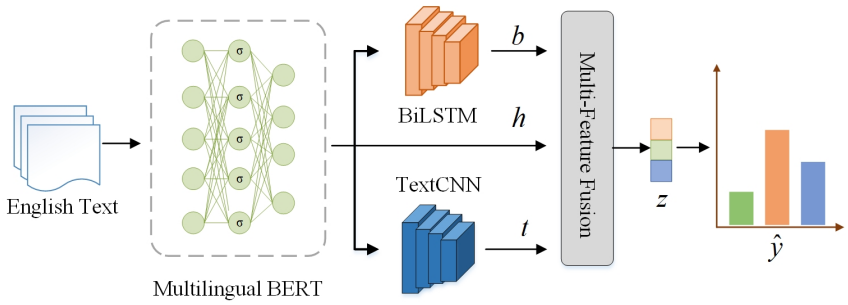

Fig. 1. The illustration of MFFMP-ETC, containing the multilingual feature extraction, the multi-level structure learning, and the multi-view representation fusion

MFFMP-ETC stands out from traditional text classification methods due to its unique integration of advanced techniques. Unlike CNNs that primarily capture local features and often lose positional information, MFFMP-ETC combines the strengths of Multilingual BERT, Bi-LSTM, and TextCNN to address both local and global semantic contexts. While RNNs like TextRNN handle sequential data and long-distance dependencies, they struggle with issues like gradient vanishing, which MFFMP-ETC overcomes through its multi-feature fusion approach. FNNs, such as fastText, efficiently process text but may lack depth in capturing complex semantic relationships. GNNs enhance long-distance information transfer through graph structures but may not fully leverage linguistic knowledge. Pre-trained Language Models PLMs like BERT provide deep contextual features

but often do not integrate other feature extraction techniques. MFFMP-ETC synergistically integrates Multilingual BERT's deep semantic features, Bi-LSTM's bidirectional context processing, and TextCNN local feature extraction, offering a more comprehensive and effective solution for capturing long-distance dependencies and nuanced contextual information in text classification.

3. Multilingual Pretrained based Multi-feature Fusion Model for English Text Classification

A novel English text classification model is proposed via integrating multi-view features within the multilingual pre-training optimization framework (MFFMP-ETC), as shown in Fig. 1. MFFMP-ETC consists of the multilingual feature extraction, the multi-level structure learning, and the multi-view representation fusion. The main mathematical notations in MFFMP-ETC are listed in Table 1.

Table 1. Frequently used notations

Notations	Description
x_i	the i-th word in the sentence.
h_i	the i-th word embedding vector
b	the feature generated by BiLSTM
t	the feature generated by TextCNN
z	the fusion feature
MLP	the multi-layer perceptron
L_{pos}	positive Pair Loss
L_{neg}	negative Pair Los
L_{cross}	the cross-entropy loss
λ,β	the balance coefficients

3.1. Multilingual feature extraction

In general, multilingual pre-trained encoders address the challenge of capturing long-range contextual semantic information within text sequences by leveraging their training across multiple languages. These models have learned to understand diverse sentence structures and linguistic patterns, enabling them to better capture long-distance dependencies in text. By being exposed to languages with varying syntactic and grammatical rules, multilingual encoders develop a more flexible and comprehensive approach to understanding context, which enhances their ability to model relationships between distant words in a sentence.

Hence, MFFMP-ETC utilizes the multilingual BERT to extract features from English texts for enhancing representation discriminability. Firstly, the preprocessing is conduced on each sentence, that is, a [CLS] token, indicating the beginning of the sentence, is added to the start, and a [SEP] token, indicating the end of the sentence, is inserted at the end. After preprocessing, the input English sentence is converted into three types of input vector

embeddings: word embeddings, segment embeddings, and position embeddings. The final input is the sum of these three types of embeddings. In this process, segment embeddings are mainly used to differentiate between pairs of sentences by connecting the sentences in the input text using the [CLS] token, which helps determine the order of two different sentences during pre-training. Position embeddings are primarily used to distinguish the semantic differences of words in different positions within the text sequence.

Specifically, given an input English sentence x composed of k words, which can be formalized as:

$$x = [x_1, x_2, x_3, \ldots, x_k] \tag{1}$$

where x_i represents the i-th word in the sentence.

In the experiments, the masked language model pre-training strategy is used to enable the model to learn contextual features of sentences. In this task, a random 15% of the words in the text are masked with a special token, [MASK], and the model is then tasked with predicting the masked words based on the final hidden output vectors obtained through softmax functions. Here's an example of the masking operation:

Original sentence: After watching the movie, I think it is better than the one I saw last week.

Masked sentence: After watching the movie, I think it is [MASK] than the one I saw last week.

However, since the input vectors do not include the [MASK] token as mentioned earlier, a mask strategy is needed to address this issue. For words to be randomly masked with the [MASK] token, the mask strategy is as follows: (1) 80% of the words are directly replaced with [MASK]. (2) 10% of the original words are replaced with any other word. (3) The remaining 10% are left unchanged. This strategy ensures varied input for the model training, enhancing its understanding of context. For instance: (1)"After watching the movie, I think it is [MASK] than the one I saw last week." (2) "After watching the movie, I think it is no than the one I saw last week." (3) "After watching the movie, I think it is better than the one I saw last week."

After pre-training, using the sum of three embedding vectors generated by Multilingual BERT as the input for both the BiLSTM layer and the TextCNN layer:

$$h = [h_1, h_2, h_3, \ldots, h_k] \tag{2}$$

where the dimension of h_i is 768.

3.2. Multi-level structure learning

To capture multi-level structure information for learning robust and comprehensive fusion representations, MFFMP-ETC integrates BiLSTM and TextCNN into a multi-feature fusion module. TextCNN is responsible for extracting local features, such as key phrases and n-gram patterns, while BiLSTM captures global contextual information and long-range dependencies within the text. By combining these two approaches, the fusion module generates a rich representation that balances local and global structures, leading to improved generalization and robustness across different types of text data.

BiLSTM feature extraction: BiLSTM involves processing the text in both forward and backward directions, capturing global structure features from the entire sequence. The

BiLSTM learns long-range dependencies and contextual relationships by using hidden state vectors at each time step. Specifically, the input to the BiLSTM network at time step t is the concatenation of the hidden state from the previous time step h_{t-1} and the current input vector x_t. This enables the BiLSTM to integrate information from both past and future contexts, refining the structure features produced by Multilingual BERT. As a result, BiLSTM captures global dependencies within the text:

$$\vec{h}_t = \sigma(W_t[\vec{h}_{t-1}, x_t] + b) \tag{3}$$

The output vector of the hidden state of the LSTM network from back to front is:

$$\overleftarrow{h}_t = \sigma(W_t[\overleftarrow{h}_{t-1}, x_t] + b) \tag{4}$$

where W_t and b represent the weight matrix and bias vectors of the forward and backward LSTM networks. $\vec{h}_{t-1}$ and $\overleftarrow{h}_{t-1}$ denote the forward and backward hidden state vectors at time step $t-1$, respectively. Finally, at time step t, the hidden state vector of the Bi-LSTM layer is the concatenation of the forward and backward hidden state vectors:

$$b_t = [\vec{h}_{t-1}, \overleftarrow{h}_{t-1}] \tag{5}$$

After processing all time steps, a collection of hidden layer vectors that encapsulate long-range contextual semantic information is obtained, denoted as:

$$B = [b_1, b_2, b_3, \ldots, b_k] \tag{6}$$

TextCNN feature extraction: TextCNN excels at extracting local features and captures different N-gram features through convolution windows of various sizes. A piece of text contains local semantic features of different granularities, thus necessitating the extraction of features at different scales. By designing convolution kernels of various sizes to extract text information and integrating features of different granularities, a comprehensive local feature representation can be achieved. Using the convolution structure of TextCNN, local features of the text can be extracted, facilitating text classification. The outputs of all encoders in multilingual BERT are fed into the TextCNN layer. By adjusting the sizes of convolution kernels, local text features are obtained at different widths. Convolution operations are performed on the text sequence using convolution kernels with sizes of 2, 3, and 4. The resulting vectors are passed through the ReLU activation function to capture important sentence information. The feature vectors obtained after pooling are concatenated to form the output of the TextCNN layer.

Convolution operation formula: For a text sequence $h = [h_1, h_2, h_3, \ldots, h_k]$ and a convolution kernel of size s, the feature c_i extracted by the i-th convolution kernel is:

$$c_i = f(\mathbf{w} \cdot \mathbf{h}_{i:i+s-1} + b) \tag{7}$$

where $\mathbf{h}_{i:i+s-1}$ denotes the concatenation of word vectors from position i to $i+s-1$, $\mathbf{w}$ is the weight matrix, b is the bias, and f is the activation function (e.g., ReLU). After the convolution operation, max-pooling is applied to extract the most significant feature from each feature map. For a feature map $\mathbf{c} = [c_1, c_2, \ldots, c_{n-k+1}]$, the pooled feature p is:

$$p = \max([c_1, c_2, \ldots, c_{n-k+1}]) \tag{8}$$

In the MFFMP-ETC, Using multiple convolution kernels of different sizes (e.g., 2, 3, and 4), the final output feature vector t of the TextCNN layer is obtained by concatenating the outputs from all convolution and pooling operations:

$$t = concat[p_2, p_3, p_4] \tag{9}$$

where concat[] denotes concatenating function.

3.3. Multi-view representation fusion

The benefits of contrastive learning for learning fusion representations lie in its ability to effectively utilize information from multiple views, thereby enhancing the model performance and generalization ability. By merging representations from different views, richer and more accurate semantic information can be obtained, which helps to improve the quality of text representations and the effectiveness of the model.

The fusion representation is obtained through an MLP fusion layer, where the input consists of the concatenation of three features. This process can be expressed by the following formula:

$$z = f(h, t, b) = \text{MLP}\left([\text{Concatenate}(h, t, b)]\right) \tag{10}$$

Here, h, t, and b represent the feature representations from the multilingual BERT feature extraction, the textCNN feature extraction, and the BiLSTM feature extraction, respectively. $[\cdot]$ denotes vector concatenation, and MLP represents a multi-layer perceptron.

In the contrastive learning framework, the goal is to maximize the similarity between the fused representation z and the feature representations while minimizing the similarity between these representations.

$$\mathcal{L}_{\text{pos}} = -(\cos(z, h) + \cos(z, t) + \cos(z, b)) \tag{11}$$

$$\mathcal{L}_{\text{neg}} = \cos(h, t)) + \cos(h, b) + \cos(t, b) \tag{12}$$

$$\mathcal{L}_{\text{contra}} = \mathcal{L}_{\text{pos}} + \lambda \mathcal{L}_{\text{neg}} \tag{13}$$

where λ is the parameter for balancing $\mathcal{L}_{\text{pos}}$ and $\mathcal{L}_{\text{neg}}$. $\cos(,)$ denotes the similarity function.

Meanwhile, MFFMP-ETC uses a fully connected classification layer as the classification head to transform the fusion representation z into scores for each class, and then uses the softmax function to convert these scores into probabilities.

The output y of the classification head can be represented as:

$$y = \text{softmax}(W_{\text{class}} z + b_{\text{class}}) \tag{14}$$

Here, W_{class} is the weight matrix of the the classification head, b_{class} is the bias vector, and softmax is the softmax function. y is a vector of size K, representing the probability distribution over each class.

Then, the cross-entropy loss for K classes is utilized to achieve pattern mining of English text, which can be expressed as:

$$\mathcal{L}_{cross} = -\frac{1}{N}\sum_{i=1}^{N}\sum_{k=1}^{K} y_{i,k}\log(\hat{y}_{i,k}) \tag{15}$$

Where N is the number of samples, $y_{i,k}$ is the true label indicating whether the i-th sample belongs to the k-th class, and $\hat{y}_{i,k}$ is the predicted probability by the model for the i-th sample belonging to the k-th class. This process transforms the fused representation z into a probability distribution over each class, enabling text classification.

3.4. Overall Objective Function

The MFFMP-ETC model employs an integrated objective function that combines three distinct types of losses to optimize its performance comprehensively. The overall objective function incorporates the following components:

$$\mathcal{L} = \mathcal{L}_{\text{pos}} + \lambda\mathcal{L}_{\text{neg}} + \beta\mathcal{L}_{\text{cross}}, \tag{16}$$

where λ and β are balancing parameters that control the influence of the negative pair loss and cross-entropy loss, respectively.

The choice of this integrated objective function is driven by several key advantages:

- Enhanced semantic representation: By incorporating the positive pair loss, the model benefits from a more comprehensive and enriched semantic representation. This fusion of information from multiple feature sources allows the MFFMP-ETC model to better capture and represent the nuanced meanings within the text, enhancing its overall expressiveness.
- Reduced information redundancy: The negative pair loss contributes to minimizing redundancy by maximizing the mutual information between the fused representation and individual viewpoints. This reduction in redundancy not only improves the efficiency of the model but also enhances its generalization capability, making it more effective in diverse classification scenarios.
- Improved model robustness: The combination of contrastive learning losses helps the model handle noise and errors more effectively. By focusing on both positive and negative pairs, and aligning predictions with true labels through cross-entropy loss, the model becomes more robust and stable, which is crucial for achieving reliable performance in practical applications.

Overall, this multi-faceted loss function allows MFFMP-ETC to balance feature fusion, differentiation, and classification accuracy, leading to significant performance improvements in English text classification tasks compared to traditional single-loss or less integrative approaches.

4. Experiments

4.1. Set up

Dataset and metric: The following three common English text datasets, i.e., MR dataset, SST-2 dataset, and CoLA dataset, are primarily employed for training and testing MFFMP-ETC:

- MR dataset is constructed based on brief movie review texts. The training set mainly includes 5,331 negative samples and 3,610 positive samples.
- SST-2 dataset is a variant of the MR dataset. It should be noted that very positive and affirmative review texts are labeled as positive samples, while negative and extremely negative review texts are labeled as negative samples. Overall, the training set is divided into 3,310 negative samples and 3,610 positive samples.
- CoLA dataset is a dataset used for binary single-sentence classification tasks, which contains 8,551 training data and 1,043 test data, totaling 6,744 positive samples and 2,850 negative samples. The average text length of the dataset is 7.7 words. Since the test set of CoLA is not annotated, this paper allocates 5% of the samples from the training set as the validation set and uses the original validation set as the test set.

For evaluation metrics, MFFMP-ETC mainly uses accuracy, sensitivity, and precision to measure and assess the effectiveness and performance of MFFMP-ETC and comparative models. Accuracy is calculated using the following formula:

$$\text{Accuracy} = \frac{TP + TN}{TP + TN + FP + FN} \tag{17}$$

where TP, TN, FP, and FN represent the number of positive samples correctly identified, negative samples correctly identified, negative samples incorrectly identified as positive, and positive samples incorrectly identified as negative, respectively. Sensitivity is calculated using the following formula:

$$\text{Sensitivity} = \frac{TP}{TP + FN} \tag{18}$$

This metric measures the proportion of actual positives that are correctly identified by the test. Precision is calculated using the following formula:

$$\text{Precision} = \frac{TP}{TP + FP} \tag{19}$$

This metric measures the proportion of positive identifications that are actually correct.

Implementation Details: In the experiments, MFFMP-ETC is meticulously constructed on the NVIDIA GeForce RTX 3080 Ti graphics card, leveraging the capabilities of the PyTorch framework within the Visual Studio Code as the development environment, where Python version 3.6.8 is deployed. Word2Vec vectors, each with a dimension of 300, are employed to represent textual data, accommodating a maximum text length of 150 characters.Bi-LSTM network layer within MFFMP-ETC is tailored with 16 nodes to effectively capture the dynamics of sequential information. MFFMP-ETC undergoes a structure training regimen comprising 10 epochs and a batch size of 32, parameters

chosen to balance thorough training with the risk of overfitting. The Adam optimizer is engaged for its adaptive learning rate mechanism, initiated with a learning rate of 0.001 and accompanied by a decay rate of 0.1 to strategically taper the learning rate throughout the training process. To augment the model generalization capabilities and mitigate overfitting, Dropout with a 0.3 probability is seamlessly integrated into the MFFMP-ETC model training phase. This method introduces an element of randomness by deactivating a subset of neurons during training, compelling the model to develop a more diverse and robust set of features. Furthermore, MFFMP-ETC benefits from the incorporation of word embeddings derived from the pre-trained multilingual BERT model, which, with a dimensionality of 768, provides a comprehensive semantic representation. This integration allows MFFMP-ETC to capitalize on the nuanced language understanding expertise acquired by BERT during its pre-training.

Table 2. Comparison results of methods on different datasets in terms of accuracy (Acc), precision (Prec), and sensitivity (Sens)

Method	MR dataset			SST-2 dataset			CoLA dataset		
	Acc	Prec	Sens	Acc	Prec	Sens	Acc	Prec	Sens
SVM	0.745	0.715	0.744	0.794	0.777	0.789	0.572	0.499	0.556
MLP	0.759	0.726	0.749	0.808	0.810	0.799	0.608	0.612	0.576
CNN-non-static	0.815	0.815	0.812	0.872	0.877	0.874	0.617	0.613	0.631
LSTM	0.804	0.799	0.800	0.859	0.866	0.864	0.612	0.632	0.605
Bi-LSTM	0.813	0.812	0.812	0.882	0.888	0.898	0.625	0.666	0.625
Multilingual Bert	0.816	0.815	0.822	0.912	0.910	0.901	0.811	0.804	0.802
MFFMP-ETC	**0.862**	**0.866**	**0.859**	**0.915**	**0.920**	**0.919**	**0.832**	**0.818**	**0.820**

4.2. Comparison with baselines

Comparison methods: To thoroughly evaluate the capability of MFFMP-ETC to accurately capture both local and global advanced contextual semantic information, a series of comparative and evaluative experiments are conducted with MFFMP-ETC against several benchmark models. In addition to the original Bert pre-trained language model being directly applied to English text classification tasks, several relevant deep learning network models are selected for comparative experiments. The detailed information on the selected benchmark models is described as follows: SVM: To ensure the comprehensiveness of the comparative experiment, the traditional classification model SVM is specifically chosen as a benchmark for comparison in MFFMP-ETC. MLP: The multi-layer perceptron, a traditional model, has two hidden layers comprising 512 and 100 hidden units, respectively. This perceptron is utilized with bag-of-words vectors that are weighted by term frequency (TF). CNN-non-static: The input vectors for this model are kept consistent with those of the MLP, with the model original training parameters remaining unaltered. LSTM: The hidden layer output vectors of the Bert model are served as inputs to a unidirectional Long Short-Term Memory network. Bi-LSTM: The bidirectional LSTM network is provided with inputs that are consistent with those of the unidirectional network. Multilingual Bert: In the experiments, the original pre-trained multilingual Bert model is utilized. To

guarantee that the comparative experiments represent a fair comparison, all models have been trained from scratch.

Comparison results: As shown in Table 2, MFFMP-ETC outperforms all other models across all datasets and evaluation metrics, demonstrating advantage in extracting both local and global high-level contextual semantic information. On the MR dataset, MFFMP-ETC achieved the highest scores among all models in terms of Acc, Prec, and Sens, with values of 0.862, 0.866, and 0.859, respectively. On the SST-2 dataset, MFFMP-ETC once again demonstrated the best performance across all evaluation metrics, with Acc, Prec, and Sens, being 0.915, 0.920, and 0.919, respectively. On the CoLA dataset, the MFFMP-ETC performance was also the best among all compared models, with an Acc of 0.832, a Prec of 0.818, and a Sens of 0.820. The reasons are twofold: (1) Utilization of multilingual pretrained models. MFFMP-ETC leverages a multilingual BERT model as one of its core components. This pretrained model has been trained on a variety of languages, capturing cross-linguistic semantic information, thereby enhancing the model's comprehension and classification capabilities for English texts. This cross-linguistic semantic understanding is a capability that traditional monolingual models lack, giving MFFMP-ETC an advantage when dealing with English texts that are multilingual or have complex semantic structures. (2) Multi-feature fusion strategy. MFFMP-ETC employs a multi-feature fusion strategy, effectively combining the deep semantic features from the BERT model, the bidirectional contextual features from Bi-LSTM, and the local n-gram features from TextCNN. This fusion strategy not only enhances the model's ability to capture a wide range of textual information but also improves the accuracy and robustness of classification through the complementary nature of the features.

In addition, in the realm of text classification, the ability to discern and utilize semantic information is paramount. The Multilingual Bert model's success over traditional models such as SVM, MLP, and LSTM is a testament to its advanced capability to capture and process linguistic nuances. This pre-trained model, with its exposure to a diverse range of languages, has honed a deep understanding of language constructs that transcends the limitations of models trained solely on local context. The Bi-LSTM model's enhancement over its unidirectional counterpart is particularly noteworthy. By processing information in both forward and backward sequences, Bi-LSTM is able to develop a more comprehensive representation of the text, thus enhancing its predictive accuracy. This bidirectional capability is crucial for understanding the context in which words are used, as the meaning of a sentence can be significantly altered by the words that precede or follow it. Despite the Bi-LSTM model showing a slight dip in performance when compared to the CNN-non-static model on the MR dataset, this is not indicative of a weakness. Instead, it highlights the potential for hybrid models that can leverage the strengths of various architectures. The CNN-non-static model, with its ability to capture local features through convolution operations, complements the Bi-LSTM's contextual prowess. The combination of the Bi-LSTM with the Multilingual Bert model is a case in point. This synergy not only bolsters the model's ability to express and extract semantic information but also significantly amplifies the overall performance of the classification task. The Multilingual Bert model's pre-training on a vast corpus of text endows it with a rich vocabulary of linguistic patterns and structures, which, when combined with the Bi-LSTM's temporal insights, results in a model that is both sensitive to local features and attuned to broader contextual elements.This integrated approach to text classification is a step to-

wards more sophisticated models that can handle the intricacies of natural language with greater finesse. It opens up avenues for further research and development, encouraging the exploration of additional hybrid models and the refinement of existing architectures. As we continue to push the boundaries of what is possible with text classification models, the fusion of diverse methodologies will undoubtedly play a key role in shaping the future of natural language processing.

4.3. Ablation Study

Table 3. Ablation experiments of each component on MR

L_{pos}	L_{neg}	L_{cross}	Accuracy	Precision	Sensitivity
		√	0.798	0.780	0.794
√		√	0.842	0.842	0.840
	√	√	0.814	0.812	0.820
√	√	√	**0.862**	**0.866**	**0.859**

Three ablation experiments about L_{pos}, L_{neg}, and L_{cross} are conducted to prove the effectiveness of each component. Specifically, (1) MFFMP-ETC utilizes L_{cross} to train the network. This configuration serves as a baseline where only the cross-entropy loss is used. The results show an accuracy of 0.798, precision of 0.780, and sensitivity of 0.794. This indicates the performance when contrastive components are not used. (2) MFFMP-ETC utilizes L_{pos} and L_{cross} to train the network. In this setup, the positive sample pair loss is included along with the cross-entropy loss, resulting in improved performance with an accuracy of 0.842, precision of 0.842, and sensitivity of 0.840. This demonstrates the effectiveness of maximizing the similarity between the fused representation and feature representations. (3) MFFMP-ETC utilizes L_{neg} and L_{cross} to train the network. Here, the negative sample pair loss is included along with the cross-entropy loss, leading to an accuracy of 0.814, precision of 0.812, and sensitivity of 0.820. This shows the benefit of minimizing the similarity between different feature representations. These results indicate that both L_{pos} and L_{neg} contribute significantly to the model's performance. Including all three components (L_{pos}, L_{neg}, and L_{cross}) achieves the best results, demonstrating the effectiveness of the proposed framework.

As shown in Table 3, there are three conclusions: (1) The inclusion of L_{pos} significantly improves performance. Comparing the results with and without L_{pos}, we observe that accuracy increases from 0.798 to 0.842, precision from 0.780 to 0.842, and sensitivity from 0.794 to 0.840 when L_{pos} is added. This demonstrates the effectiveness of maximizing the similarity between the fused representation and the individual feature representations. (2) The addition of L_{neg} also enhances the model's performance. When L_{neg} is included, accuracy improves from 0.798 to 0.814, precision from 0.780 to 0.812, and sensitivity from 0.794 to 0.820. This indicates the benefit of minimizing the similarity between different feature representations to improve overall performance. (3) Combining all three components (L_{pos}, L_{neg}, and L_{cross}) yields the best results. The model achieves the highest accuracy of 0.862, precision of 0.866, and sensitivity of 0.859 when all components are included. This confirms that the proposed contrastive learning framework, which

incorporates both positive and negative sample pair losses along with the cross-entropy loss, is the most effective configuration for optimizing performance.

4.4. The impact of different maximum sentence lengths

In an effort to understand how the maximum lengths of text in various datasets affect the performance of machine learning models, a series of ablation studies were conducted on the MFFMP-ETC. These studies were meticulously carried out across three distinct datasets to provide a comprehensive insight into the influence of text length on model outcomes. The findings, as presented in Fig. 2, reveal an intriguing pattern. Initially, the performance of the model was observed to improve consistently across all three datasets as the maximum length of the text was incrementally increased. This improvement suggests that longer texts, up to a certain point, enable the model to capture more contextual information, which contributes to more accurate predictions. However, this trend of improvement does not persist beyond a certain text length. The data indicates that when the length of the text surpasses 150 tokens, the performance gains of the model are curtailed, and a slight decline in performance is noted. This could be due to the model's capacity to process information reaching saturation, or the inclusion of noise or irrelevant information that may dilute the signal-to-noise ratio. Recognizing this inflection point, it was concluded that extending the text length beyond 150 tokens does not yield significant performance improvements and may even be detrimental. This insight is crucial for optimizing the model's efficiency and effectiveness. A maximum text length of 150 tokens was selected as the optimal value, striking a balance that maximizes the model's predictive power while minimizing computational expenses.

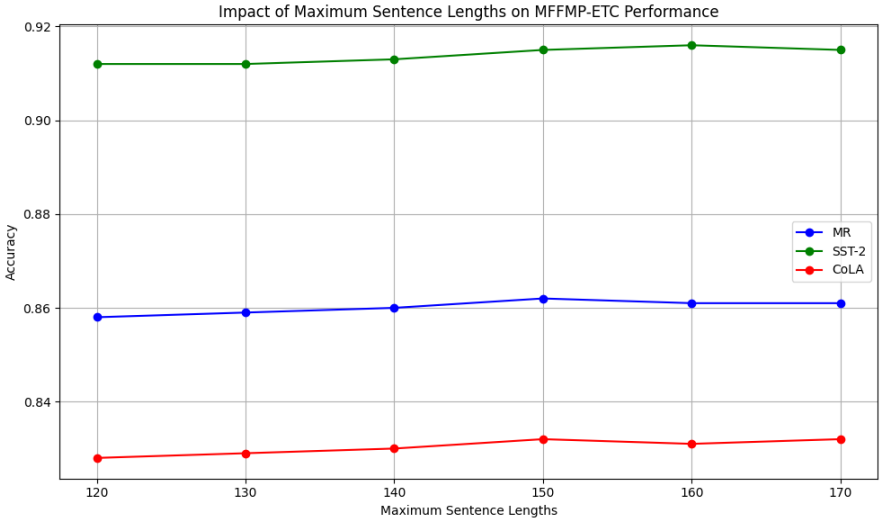

Fig. 2. The impact of different maximum sentence lengths on the performance of MFFMP-ETC

4.5. Parameter Analysis

Fig. 3 illustrates the sensitivity analysis of parameters λ and β on three datasets for MFFMP-ETC. Specifically, in the experiments, λ and β are constrained within the set $\{0, 0.0001, 0.001, 0.01, 0.1, 1\}$ where one parameter was kept constant while the other was systematically varied. The results depicted in Fig. 3 illustrate MFFMP-ETC's robustness across varying values of λ and β. The performance consistently remains satisfactory, particularly when λ is set to 0.01 and β is set to 0.001. As a result, for the three datasets, MFFMP-ETC is configured with $\lambda = 0.01$ and $\beta = 0.001$ in the experiments. This configuration is empirically determined to yield a high level of accuracy, suggesting that it effectively weights the different components of the network loss function in a manner that is conducive to learning robust action recognition features. The parameters λ and β play a crucial role in the network by controlling the balance between certain regularization terms and the overall loss. The optimal values provide a valuable reference for future research and applications of MFFMP-ETC, as they offer a blueprint for achieving high performance with a reasonable computational cost.

4.6. Comparison and analysis of different feature fusion

To validate the effectiveness of the multi-feature fusion model in English text classification, MFFMP-ETC designs three types of feature fusions: (1) fusion of features extracted by multilingual BERT and BiLSTM, (2) fusion of features extracted by multilingual BERT and TEXTCNN, and (3) fusion of features extracted by TEXTCNN and BiLSTM. Based on the results in Table 4, three key observations can be made. First, the fusion of multilingual BERT and TEXTCNN demonstrates higher accuracy, precision, and sensitivity (0.850, 0.854, and 0.852, respectively) compared to the other two feature fusion methods involving multilingual BERT and BiLSTM or TEXTCNN and BiLSTM. Second, while the TEXTCNN and BiLSTM fusion performs slightly better than the multilingual BERT and BiLSTM fusion in terms of precision (0.844 vs. 0.845) and sensitivity (0.847 vs. 0.845), it has a marginally lower accuracy (0.841 vs. 0.847). Third, MFFMP-ETC outperforms all other methods across all metrics, achieving the highest accuracy (0.862), precision (0.866), and sensitivity (0.859), indicating its superior effectiveness in feature fusion for English text classification.

Table 4. Comparison and analysis of different feature fusion on MR

Fusion	Accuracy	Precision	Sensitivity
multilingual BERT and BiLSTM	0.847	0.845	0.845
multilingual BERT and TEXTCNN	0.850	0.854	0.852
TEXTCNN and BiLSTM	0.841	0.844	0.847
MFFMP-ETC	**0.862**	**0.866**	**0.859**

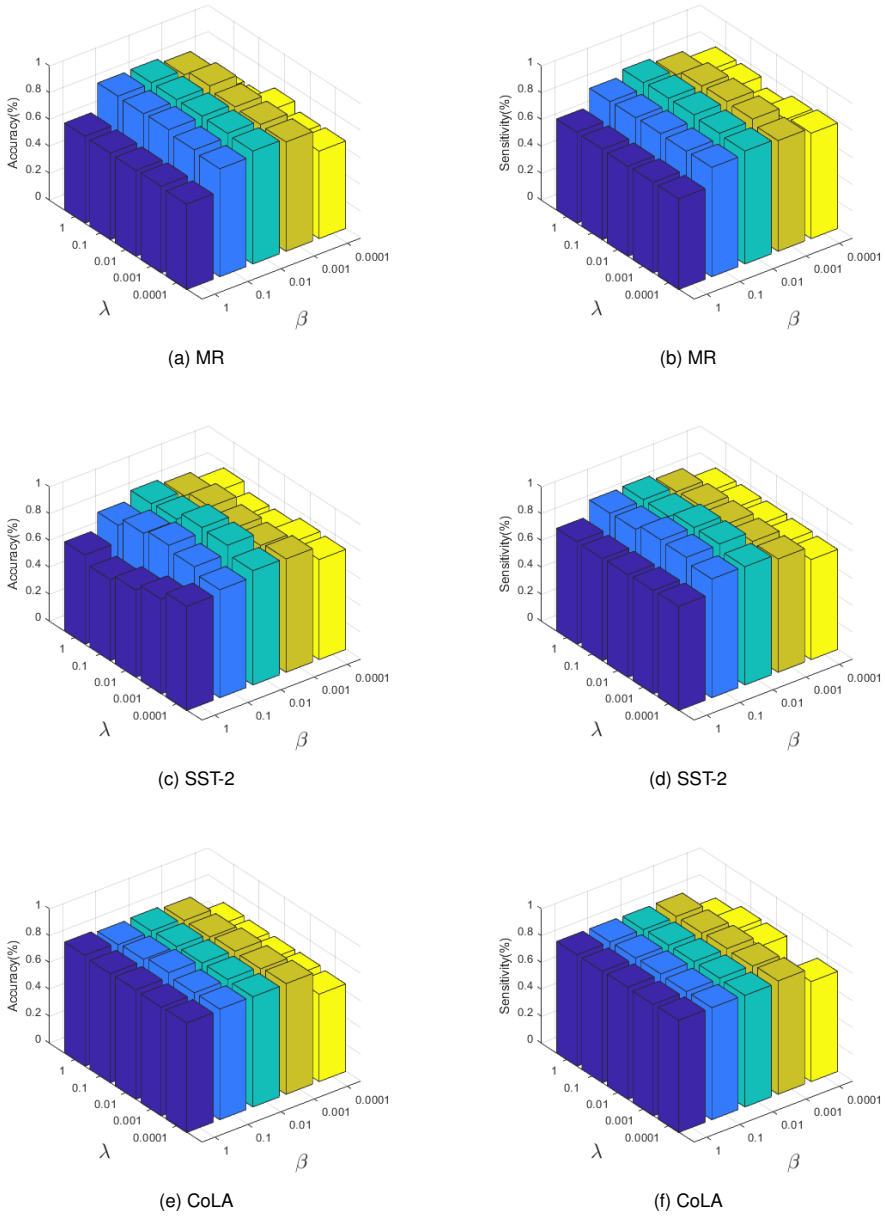

(a) MR (b) MR

(c) SST-2 (d) SST-2

(e) CoLA (f) CoLA

Fig. 3. The sensitivity analysis of parameters λ and β on three datasets for MFFMP-ETC

5. Conclusion

The paper introduces a novel English text classification model known as Multilingual Pre-trained based Multi-feature Fusion Model (MFFMP-ETC), which represents a significant advancement in natural language processing. By integrating the strengths of Multilingual BERT, Bi-LSTM, and TextCNN, MFFMP-ETC effectively captures both local and global contextual structure information in texts. Its innovative approach to feature fusion and the use of a multilingual pre-trained language model are crucial for enhancing the recognition of long-distance dependencies and contextual information. MFFMP-ETC achieves state-of-the-art results on the MR, SST-2, and CoLA datasets, with accuracies of 86.2%, 91.5%, and 83.2%, respectively, highlighting its superior accuracy and robustness in managing complex semantic structures and improving classification precision. Future work could further expand by exploring other multilingual pre-trained models, integrating additional contextualized features, handling multimodal data, conducting real-world application tests, improving scalability and efficiency, and enhancing model interpretability. These directions promise to push the boundaries of text classification technology and address a broader range of linguistic and contextual challenges.

References

1. Chen, J., Yang, Z., Yang, D.: Mixtext: Linguistically-informed interpolation of hidden space for semi-supervised text classification. arXiv preprint arXiv:2004.12239 (2020)
2. Chen, Y.: Convolutional neural network for sentence classification (2015)
3. Defferrard, M., Bresson, X., Vandergheynst, P.: Convolutional neural networks on graphs with fast localized spectral filtering. Advances in neural information processing systems 29 (2016)
4. Devlin, J., Chang, M.W., Lee, K., Toutanova, K.: Bert: Pre-training of deep bidirectional transformers for language understanding. arXiv preprint arXiv:1810.04805 (2018)
5. Gao, J., Li, P., Laghari, A.A., Srivastava, G., Gadekallu, T.R., Abbas, S., Zhang, J.: Incomplete multiview clustering via semidiscrete optimal transport for multimedia data mining in iot. ACM Transactions on Multimedia Computing, Communications and Applications 20(6), 1–20 (2024)
6. Gao, J., Liu, M., Li, P., Laghari, A.A., Javed, A.R., Victor, N., Gadekallu, T.R.: Deep incomplete multi-view clustering via information bottleneck for pattern mining of data in extreme-environment iot. IEEE Internet of Things Journal (2023)
7. Gao, J., Liu, M., Li, P., Zhang, J., Chen, Z.: Deep multiview adaptive clustering with semantic invariance. Transactions on Neural Networks and Learning Systems (2023)
8. Gururangan, S., Dang, T., Card, D., Smith, N.A.: Variational pretraining for semi-supervised text classification. arXiv preprint arXiv:1906.02242 (2019)
9. Johnson, R., Zhang, T.: Deep pyramid convolutional neural networks for text categorization. In: Proceedings of the 55th Annual Meeting of the Association for Computational Linguistics (Volume 1: Long Papers). pp. 562–570 (2017)
10. Joulin, A., Grave, E., Bojanowski, P., Mikolov, T.: Bag of tricks for efficient text classification. arXiv preprint arXiv:1607.01759 (2016)
11. Li, C., Peng, X., Peng, H., Li, J., Wang, L.: Textgtl: Graph-based transductive learning for semi-supervised text classification via structure-sensitive interpolation. In: IJCAI. pp. 2680–2686 (2021)
12. Li, P., Chen, Z., Yang, L.T., Gao, J., Zhang, Q., Deen, M.J.: An incremental deep convolutional computation model for feature learning on industrial big data. Transactions on Industrial Informatics 15(3), 1341–1349 (2018)

13. Li, P., Gao, J., Zhang, J., Jin, S., Chen, Z.: Deep reinforcement clustering. Transactions on Multimedia (2022)
14. Li, P., Laghari, A.A., Rashid, M., Gao, J., Gadekallu, T.R., Javed, A.R., Yin, S.: A deep multimodal adversarial cycle-consistent network for smart enterprise system. IEEE Transactions on Industrial Informatics 19(1), 693–702 (2022)
15. Lin, Y., Meng, Y., Sun, X., Han, Q., Kuang, K., Li, J., Wu, F.B.: Transductive text classification by combining gcn and bert. arxiv 2021. arXiv preprint arXiv:2105.05727
16. Liu, C., Wang, X.: Quality-related english text classification based on recurrent neural network. Journal of Visual Communication and Image Representation 71, 102724 (2020)
17. Liu, P., Qiu, X., Chen, X., Wu, S., Huang, X.J.: Multi-timescale long short-term memory neural network for modelling sentences and documents. In: conference on empirical methods in natural language processing. pp. 2326–2335 (2015)
18. Mundra, S., Mittal, N.: Fa-net: fused attention-based network for hindi english code-mixed offensive text classification. Social Network Analysis and Mining 12(1), 100 (2022)
19. Peng, H., Li, J., He, Y., Liu, Y., Bao, M., Wang, L., Song, Y., Yang, Q.: Large-scale hierarchical text classification with recursively regularized deep graph-cnn. In: world wide web conference. pp. 1063–1072 (2018)
20. Sachan, D.S., Zaheer, M., Salakhutdinov, R.: Revisiting lstm networks for semi-supervised text classification via mixed objective function. In: Proceedings of the aaai conference on artificial intelligence. vol. 33, pp. 6940–6948 (2019)
21. Shabestanı, S., Geçikli, M.: Machine learning use for english texts' classification (a mini-review). Osmaniye Korkut Ata Üniversitesi Fen Bilimleri Enstitüsü Dergisi 7(1), 414–423 (2024)
22. Taha, K., Yoo, P.D., Yeun, C., Taha, A.: Text classification: A review, empirical, and experimental evaluation. arXiv preprint arXiv:2401.12982 (2024)
23. Wang, G., Li, C., Wang, W., Zhang, Y., Shen, D., Zhang, X., Henao, R., Carin, L.: Joint embedding of words and labels for text classification. arXiv preprint arXiv:1805.04174 (2018)
24. Wang, X., Ji, H., Shi, C., Wang, B., Ye, Y., Cui, P., Yu, P.S.: Heterogeneous graph attention network. In: The world wide web conference. pp. 2022–2032 (2019)
25. Wang, Z., Liu, X., Yang, P., Liu, S., Wang, Z.: Cross-lingual text classification with heterogeneous graph neural network. arXiv preprint arXiv:2105.11246 (2021)
26. Xie, Q., Huang, J., Du, P., Peng, M., Nie, J.Y.: Inductive topic variational graph auto-encoder for text classification pp. 4218–4227 (2021)
27. Xu, J., Cai, Y., Wu, X., Lei, X., Huang, Q., Leung, H.f., Li, Q.: Incorporating context-relevant concepts into convolutional neural networks for short text classification. Neurocomputing 386, 42–53 (2020)
28. Yao, L., Mao, C., Luo, Y.: Graph convolutional networks for text classification. In: Proceedings of the AAAI conference on artificial intelligence. vol. 33, pp. 7370–7377 (2019)
29. Zhang, H., Zhang, J.: Text graph transformer for document classification. In: Conference on empirical methods in natural language processing (EMNLP) (2020)
30. Zhang, X., Zhao, J., LeCun, Y.: Character-level convolutional networks for text classification. Advances in neural information processing systems 28 (2015)

Ruijuan Zhang is an outstanding scholar in the field of computational linguistics and natural language processing, with a particular focus on multilingual pre-trained models and text classification. She holds a position at the School of Foreign Languages, Zhengzhou University of Science and Technology in Zhengzhou, China. Ruijuan Zhang has a rich background in both linguistics and computer science, and has made significant contributions to the development and understanding of algorithms that enhance the accuracy and efficiency of multi-feature fusion models in English text classification tasks.

Received: June 30, 2024; Accepted: November 20, 2024.

Computer Science and Information Systems 22(1):153–180 https://doi.org/10.2298/CSIS240820006L

TPBoxE: Temporal Knowledge Graph Completion based on Time Probability Box Embedding

Song Li[1], Qi Wang[1], Zheng Li[2], and Liping Zhang[1,⋆]

[1] Harbin University of Science and Technology,
150080 Harbin, China
lisongbeifen@hrbust.edu.cn
wangqi441329@163.com
[2] Heilongjiang University, China

Abstract. Temporal knowledge graph completion is a technique that uses existing knowledge to predict or infer the missing information in the temporal knowledge graph. It combines the technical features of knowledge graph completion and time series analysis to deal with entities and relationships that change over time. The existing temporal knowledge graph completion technology fails to make effective use of the special relationship between relations and time series information, and it is difficult to fully represent the complex relationships existing in the graph. In order to solve the above problems, the model based on time probability box embedding (TPBoxE) was proposed. Firstly, the entities and relationships in the temporal knowledge graph are represented in the vector space by box embedding, so as to complete the static part of the temporal knowledge graph. Secondly, the head and tail entities that exist at the same time in a given time period are selected, and the completed static parts are filtered according to the time information of the entities. Finally, the Bayesian classification method is used to fully mine the time features hidden in the relationship, and the completion results are obtained by combining the confidence scores of the static parts. The link prediction task test of the proposed model on YAGO11k, WIKIdata12k, ICEWS18 and GDELT datasets shows that the proposed model has better performance than the existing excellent models, which proves the effectiveness and advancement of TPBoxE.

Keywords: Temporal knowledge graph, Knowledge graph completion, Temporal information, Link prediction, Bayesian classification.

1. Introduction

In 2012, Google launched the Google Knowledge Graph, which began to apply knowledge graph to search engines, marking the widespread application of knowledge graph technology. A knowledge graph is a vast knowledge base that contains information about entities (such as people, places, organizations, etc.), their relationships, and their attributes, which are structured and organized together to form an integrated knowledge graph. At present, the more complete knowledge graphs include DBpedia [10], Freebase [22], Wikidata [30], and YGAO [13]. Temporal knowledge graph (TKG) is formed into a time-stamped quadruple. Compared with the traditional knowledge graph, the temporal knowledge graph can express richer information.

⋆ Corresponding author

Nowadays, knowledge graphs have been widely used in natural language processing, search engines, question answering systems, and recommendation systems [21,2,23,31]. Baidu baike is an example of an applied knowledge graph, where users can search for keywords to obtain rich information including entity definitions, attributes, relationships, and various related knowledge.

However, real-world data is often incomplete and insufficient, and there may be missing or wrong information, which will inevitably lead to missing entities or relationships in the TKG. The above problems will reduce the reliability and application value of the TKG, and bring trouble and limitations to downstream application tasks. Therefore, it is of great significance to improve the data quality and content of the TKG.

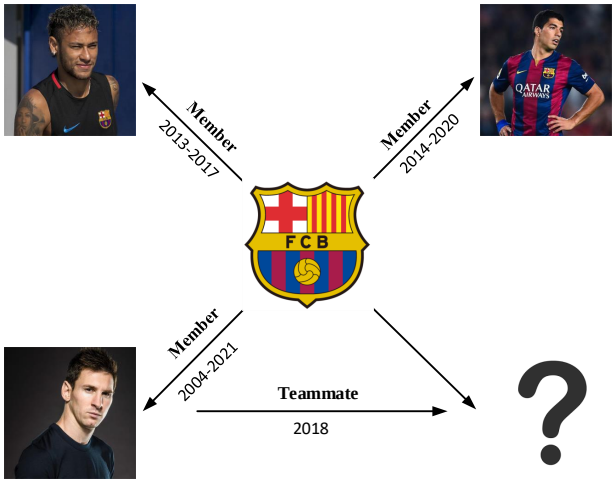

Fig. 1. An example of subgraph completion in a temporal knowledge graph

In order to improve the accuracy and completeness of the temporal knowledge graph, scholars have proposed various completion tasks. Temporal Knowledge Graph Completion (TKGC) refers to the filling or prediction of missing entities and relationships in an incomplete time series knowledge graph through inference, so as to make the TKG more complete and comprehensive. Compared with the traditional knowledge graph completion(KGC), the completion of the TKG needs to consider the consistency of time, that is, the existing TKG and the completed entity or relationship need to be logically consistent in time. In addition, the dynamic evolution of entities and relationships in the temporal knowledge graph is also very important. The completed entity or relationship needs to be able to satisfy the temporal correlation between the facts of the time series, including the order in which the facts occur, the time interval, and so on. As shown in Figure 1, the relationship between the connected entities has time information, indicating the point in time or time period when the fact is established. When the static knowledge graph completion method is adopted, it can lead to confusion in the semantic information of entities

or relationships. For example, when completing a missing entity (Messi, teammate, ?, 2018), ignoring the given timestamp 2018 may confuse Luis Suárez with the rest of the Barcelona team, giving the wrong answer.

TKGC holds significant application value for time-related prediction, recommendation, inference tasks, and describing the development patterns of entities. Since the concept of TKGC was introduced, the technology for completing temporal knowledge graphs has rapidly advanced in response to practical application needs. However, most existing TKGC methods have one or more problems:

- Embedding the time series information into the entities or completely separating them, and ignoring the special connection between the relationship between the entities and the time series information, will lead to the loss of part of the information. These connections usually contain a wealth of knowledge, which can provide more accurate and reliable auxiliary information for reasoning, so as to improve the correctness of knowledge graph completion.
- The representation of time information is unreasonable, and only how to represent time information in the form of a point in time (e.g., [2022-12-25]) is not considered, but how to represent time information in the form of time period (e.g., [2022, 2023]) is not considered.
- The complex relationship between entities cannot be fully represented, such as: 1-n, n-n, etc, relationship.
- There are few studies on the relationship between entities and temporal information, and the importance of relationships is ignored in the process of completion.

In order to solve these problems and better improve the ability of KGC, this paper proposes a Temporal Knowledge Graph Completion based on Time Probability Box Embedding (TPBoxE). The model is based on the box embedding technology, which embeds the entities and relationships in the temporal knowledge graph into the vector space, and sets regular functions to capture the complex relationships between the entities. At the same time, a time scoring method is designed to filter out the correct static facts in a given time period according to the time series information of the entity. The model also has excellent universal applicability, and other static KGC models can be migrated to the TKGC task. The main contributions of this paper are briefly described as:

- In order to solve the problem of missing entities or relationships in the temporal knowledge graph, a temporal knowledge graph completion model TPBoxE based on time probability box was proposed, which improved the ability to learn the static part of the temporal knowledge graph through box embedding, and screened the static facts of the completion based on the time information as the evaluation basis, which solved the problem of applying the static knowledge graph completion method to the completion task of the TKG.
- The relationship between entities and temporal information is studied and verified by experiments. The feature-weighted frequency naïve Bayes classification method is used to integrate this feature into the screening process of static facts, which improves the accuracy of the completion results.

The proposed TPBoxE model is end-to-end in the TKG completion task, and the missing temporal facts can be automatically predicted by learning the existing TKG data as

background knowledge, without the need to manually segment and label the data. For the missing temporal facts, different models output tasks are selected based on the type of missing data, such as entities, relations, or time information. The missing parts of the temporal fact quadruple are marked, and the final answer is found by following the scores of the TPBoxE model. In the completion process, the model will automatically learn the vector representations of entities and relations and their temporal information from the TKG background knowledge, and deduce the missing parts of the temporal knowledge through the above learned information. In this study, experiments are carried out on four public datasets extracted from the real time series knowledge graph WIKIdata, YAGO, ICEWS and GDELT, and the results in the link prediction task show that the performance of the TPBoxE model has obvious advantages over other models. It is compared with the existing excellent models, which shows that it has low time and space complexity. The superiority of the model in TKGC tasks was demonstrated.

2. Related Works

Knowledge graphs provide a structured way to organize and store data [25], correlate and represent a large amount of knowledge and information in the form of graphs, and provide a rich data foundation for artificial intelligence. However, there are still some problems with the completeness of the TKG itself, resulting in low availability. Therefore, scholars have carried out a lot of research on knowledge graph completion, which is divided into KGC and TKGC according to whether there is timing information inside the graph.

2.1. Knowledge Graph Completion

The model based on the translation approach embeds the entities in the KG into the vector space and encodes the relationships as translation work between the entities in the vector space. Representatives include TransE[4], and RotatE[26]. The classical TransE model embeds entities as vectors and represents relationships as displacements between entity vectors. This approach is easy to understand and implement but performs poorly when dealing with 1-n or n-n relationships. To better represent entities and relationships, RotatE embeds them in complex vector spaces and employs rotation operations to handle the complexity between relationships. This rotation operation allows it to better represent binary relations such as symmetry and self-inverse relations in the knowledge graph.

With the advances in artificial intelligence, many deep learning techniques are also being used to solve the KGC problem. ConvE [9] model is based on the convolutional neural network, which represents the KG as a two-dimensional matrix, and uses a multi-layer convolutional neural network to perform feature extraction on the matrix. By using convolutional layers and fully connected layers, ConvE can capture complex non-linear interactions between entities and relationships. DistMult [36] noticed the particularity of the relationship between entities, by representing the relationships as elements on the diagonal of the corresponding matrices, which makes it more advantageous in dealing with the task of KGC with symmetric relationships. Building on DistMult, ComplEx [27] uses more complex vectors to represent entities and uses complex inner products to predict the scores of triples, enabling it to represent and reason about more complex relationships. In recent years, with the wide application of attention mechanism [28], K-Bert [18] based on

Transformer architecture has been proposed to be applied to KGC tasks. It learns generic entity and relationship representations by large-scale pre-training on knowledge graph data with high quality. These representations capture the semantic information between entities and relationships well but cannot learn the structural information between entities and relations.

Knowledge graphs are a technical approach to describing knowledge and establishing relationships between everything in the world using graphical models [25]. The traditional KGC model cannot make good use of the graphic structure features in KG, which results in the loss of a large amount of information, including contextual information and entity features. For this reason, researchers have proposed some models to solve such problems, among which the representative ones are JGAN [14] based on graph convolutional neural networks, and GAT [29], which is a graph attention mechanism that applies the attention mechanism to graphs. The core of the JGAN and GAT model lies in its ability to learn the representation of a node in the graph by aggregating the features of the node and its neighboring nodes using a graph convolution model. This enables better use of information about nodes and edges in the graph structure data to learn the local features of entities. The Melo [34] model obtains meta-information and ontological information based on the contextual structure of entities, and infers high-confidence triples by mining logical rules within KG knowledge. This approach enables the model to understand how to represent KG appropriately.

2.2. Temporal Knowledge Graph Completion

Due to the inability of knowledge graphs to represent changes in entities over time, an increasing number of scholars are turning their attention to the task of TKGC. It is common practice to accomplish TKGC tasks by adding an embedded representation of temporal information [16] on top of existing KGC tasks.

Leblay et al. proposed the TTransE [17] model, which introduced the time dimension into the vector representation of entities and relations respectively based on TransE so that they could change dynamically according to the time interval. However, the shortcomings of TransE are also inherited, and the representation of entity, relationship, and time information is relatively isolated, resulting in some missing information. For this reason, Dasgupta et al. proposed HyTE [7], which is a hyperplane-based embedding method. The model gets the connection between entities, relationships, and temporal information by defining temporal information as a hyperplane and relationships as embedded as normal vectors in a hyperplane onto which entities are projected. Compared with TTransE, it has a better ability to deal with 1-n and n-n relationships but has some problems in the processing tasks of continuous dynamic graphs, large-scale knowledge graphs, and sparse data. TBoxE [20] proposed by Johannes Messner et al., based on the BoxE [1] model, embedded timing information into two transfer vectors to find the connection between entities again. By doing so, the missing relationships in the TKG can be predicted more accurately, and more complete temporal information can be provided. Existing TKGC methods embedding knowledge into Euclidean space often have the problem of high-dimensional nonlinear data and complex geometric structures. To solve this problem, Wang et al. proposed a multi-curvature adaptive embedding model MADE [33]. MADE models TKG with multiple geometries in multi-curvature spaces and assigns different weights to different curvature spaces through data-driven. In order to realize information

interaction in multiple different geometric spaces, the model independently represents the embedding of entity, relationship and time information in a specific space, so as to fully capture semantic information and construct a quadruple distribution network to promote information aggregation and reasonable distribution between information.

The deep learning model has strong expressive ability and can learn more complex features and patterns of temporal knowledge graphs [5]. To capture the changes in the global characteristics of TKG, Mingsheng He et al. proposed a query-aware embedding model ConvTKG [11] based on convolutional neural network to execute TKGE, thus solving the TKGC task. In this model, a new temporal information encoder based on gated recurrent unit and attention mechanism is used to learn the query-aware representation of temporal information. For the positional semantic information of entities, the model assigns two independent vectors to each entity and makes use of inverse relations to allow them to be learned dependently.In order to deal with the problem of interdependence between timetable features and temporal facts, Yue et al. proposed the CEC-BD [37] model, which is based on tensor decomposition technology, which uses two-factor matrix and core tensor embedding to learn the entities and relationships in the temporal knowledge graph, and proposes a temporal smoothing function to represent the temporal information. The existing TKGC tasks still have the problems of ignoring the importance of temporal information and ignoring the location semantic information of entities, so Hao Wang et al. proposed a linear multi-view representation model MvTuckER [32]. The model treats various features in TKG as independent views and uses tensor operations to capture the relationship between different views, which greatly improves the model's ability to learn large knowledge graphs.

3. Proposed method: TPBoxE

The existing methods have not paid enough attention to the connection between the relationships and temporal information, resulting in insufficient utilization of knowledge and low accuracy of completion. Moreover, excellent KGC models cannot be directly applied to TKGC tasks. To improve the correctness of the complementation task and increase the generality of the method, this paper investigates the temporal characterization and embedding methods of entities and relations and proposes the TPBoxE model.

3.1. Basic Definition

Definition 1: TKG is usually stored as a quadruple [12], and for each fact of the quadruple, it is represented using $(h, r, t, [\tau_1, \tau_2])$. The head entity and tail entity are represented as h and t respectively, with r representing the relationship between entities, and τ_1, τ_2 indicating the start time and end time of the fact. where $h, t \in E, r \in R, \tau_1, \tau_2 \in T$. The temporal knowledge graph can be expressed as $G = \{(h, r, t, [\tau_1, \tau_2])|h, t \in E, r \in R, \tau_1, \tau_2 \in T\}$. Fact G is valid only from the start time τ_1 to the end time τ_2, if and only if $\tau_1 = \tau_2$ means that the fact is valid only at τ_1 or τ_2 time-point.

Definition 2: TKG is typically represented as a collection of entities, relationships, and time points, denoted as E, R, and T respectively. Where $E = e_1, e_2, ..., e_n$ represents the set of entities, $R = r_1, r_2, ..., r_n$ represents the set of relationships between entities, and $T = \tau_1, \tau_2, ..., \tau_n$ represents the set of time points.

Definition 3: The head-time and tail-time of an entity in TKG denote the start time and end time of the entity's existence in the time dimension, respectively. For each entity, the set of time information can be represented as $T_e = \{\tau_1, \tau_2, ..., \tau_n | e, \tau_i \in G\}$, where head-time$= min(T_e)$, tail-time $= max(T_e)$.

3.2. The Overall Architecture of The TPBoxE Model

Firstly, the model represents knowledge by embedding entities as boxes and representing relationships as affine transformations between entity boxes. At the same time, the regular definition of relationships is carried out in this paper to enhance the learning of complex relationships, such as combinatorial, transitive and reflective relations. In addition, the negative sampling technique is used to optimize the training process of the model, further optimize the representation of entities and relationships, and obtain the answer set independent of time information. Secondly, a scoring approach for temporal information is proposed, which is mainly for evaluating how closely entities and temporal facts are linked in time. At the same time, we propose a method to categorize the connection between different relationships and temporal information. Filter the abnormal answers that contradict each other in time by the degree of dependence of the relationship on temporal information, keep compressing the size of the time-independent answer set, and ultimately obtain the set of answers to be complemented with the TKG. Finally, a score function for ranking quaternion confidence is designed to rank the set of answers.

The TPBoxE model proposed in this paper based on the assumption of translation invariance, models the entities in the TKG using high-dimensional vectors over the entire feature space for display modeling is represented as entity vector boxes, and relationships are represented as transfer vectors between entity vector boxes. In this process, the size and position of entity boxes are two important features of the entity representation process. The model determines the degree of correlation between the head and tail entities by the size and position of the head entity vector box after being updated by the relationship vector transfer and the size of the overlap interval of the tail entity vector box. At the global level, the goal of the TPBoxE model is to minimize the prediction error of all correct TKG static triples and to find the optimal entity and relation vector representations to be able to accurately reconstruct the TKG triples. The model scores of the triples and their temporal relevance are used as the main features, and the posterior probabilities of belonging to positive and negative samples in the static training samples are computed through a classification method. Finally, the samples are classified into the category with the highest a posterior probability. For the classification method proposed in this paper, the judgment on the classification of TKG complementary results can be continuously updated or adjusted by the training set data. This process is dynamic, and with the accumulation of data, the classification results continue to be accurate and reasonably inferred even in the case of scarce data.

The architecture of the TKG complementary model proposed in this paper is shown in Fig. 2 Subgraph (a) in the figure above represents the entities, relationships, and temporal information in the space of real temporal knowledge graphs. Subgraph (b) represents the correspondence of entities in the embedded vector space. Subgraph (c) represents the answer set without temporal information obtained by ignoring the time information and using the KGC method for the task "What buildings did China construct from year t_1 to year t_2?" for which the temporal knowledge is to be complemented. The temporal

characteristics of the temporal facts in the TKGC task make it impossible to directly use the KGC method to complete the temporal facts. In TPBoxE model, the KGC method is used to obtain the static partial completion answer set of temporal facts in TKG. In order to select the correct answers that meet the constraints of time information from the answer set, TPBoxE learns the distribution probability of all entities in the TKG in the time dimension, and verifies each candidate temporal fact in the answer set according to the close relationship between the distribution probability and the relationship with the time information, and then obtains the time score of the temporal fact. The value range of the time score is between 0 and 1, and its size means the degree of matching of entities and relationships in the time dimension, and the higher the value, the greater the probability that the temporal fact is true. By setting a reasonable time scoring threshold by the proposed Bayesian classification method, the size of the answer set can be continuously compressed until the missing temporal fact completion result in the final TKG is obtained. In subgraph (d), the final answer is obtained by incorporating temporal information and continuously compressing the set size, which is represented using shaded areas.

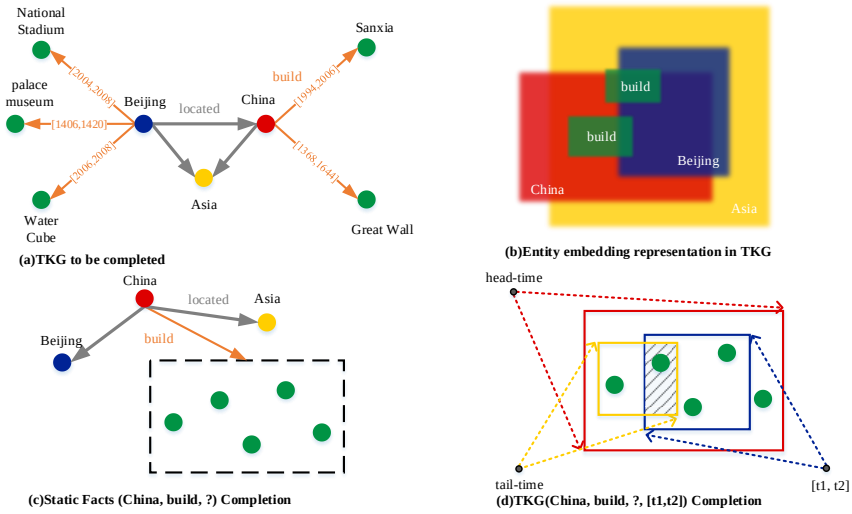

Fig. 2. Overall architecture of the TPBoxE Model

3.3. Knowledge Graph Embedding Method Based on Box Model

The traditional approach embeds entities and relations as vector dot products in a vector space, but the simplicity of the structure makes it limited in the relationships it can express. It lacks efficacy in dealing with relations expressing relationships with transitive properties such as $(A, r, B) \wedge (B, r, C) \Longrightarrow (A, r, C)$, and the geometry of the box can

make it better to model the relations between entities. Therefore, in this paper, we utilize the Box Embedding Model to make the entities in the TKG embedded as boxes and learn each relationship between entities as shape and position transformations between boxes. The formalization of a box embedding is defined as an n-dimensional hyperrectangle, which is the product between vectors:

$$Box(X) = \prod_{i=1}^{n} [x_i^{min}, x_i^{max}]. \tag{1}$$

Where $Box(X) \subseteq \mathbb{R}$, in some cases, two different boxes may have similar local structures, leading to the disappearance of their gradient signals, which in turn makes it difficult to train with gradient descent methods. In this paper, the Gumbel Boxes method [8,3] is used to train entity boxes, where the maximum and minimum coordinates of the box are denoted as:

$$x_i^{min} \sim MinGumbel(u_i^{min}, \beta), x_i^{max} \sim MaxGumbel(u_i^{max}, \beta). \tag{2}$$

In formula 2, u_i is a position parameter that determines the distribution location of the entity box. The exponential function in the Gumbel expectation formula is expanded using the first-order Taylor expansion as:

$$E(Box(X)) \approx \prod_{i=1}^{d} \beta log(2 + \frac{2len(Box(E))}{\beta} - 2\gamma). \tag{3}$$

In Formula 3, the $len(Box(E))$ parameter represents the length of the entity box E. The β represents the variance of the box and γ is the hyperparameter. In this research, by using $cen(Box(X)) \subseteq \mathbb{R}^d$ to denote the center point of the box, $len_h(Box(X)), len_t(Box(X)) \in \mathbb{R}^d$ to denote the offsets of the boxes of the head and tail entities, respectively. For the two cases where the same entity appears at the head or tail of the fact, we use the same box center, different box positions, and offsets to represent it. The resulting relationship between the position, center point, and offset of the entity boxes is:

$$\begin{aligned} u_i^{min} &= cen(Box(X) - len_h(Box(X))), \\ u_i^{max} &= cen(Box(X) + len_h(Box(X))), \\ u_j^{min} &= cen(Box(X) - len_t(Box(X))), \\ u_j^{max} &= cen(Box(X) + len_t(Box(X))). \end{aligned} \tag{4}$$

For head and tail entities in the same fact, $f_r(Box(X))$ is used as the mapping function of the relation, as follows:

$$f_r(Box(X)) = \begin{cases} len(Box(X)) \circ \alpha_r, \\ cen(Box(X)) \pm \Delta_e. \end{cases} \tag{5}$$

Considering that even if the same entity will have different semantic information at different positions, this paper adds the translation vector parameter Δ_e in the process of

training the box representation vector, which is responsible for adapting to the semantic information transformation brought about by the transformation of the position of the entity. In order to avoid the problem that the entity representation in the TKG depends too much on the transformation of the relationship and cannot capture the nonlinear relationship, the model can learn a variety of semantic relationships of entities under different relations, and proposes the offset vector parameter α_r of the entity representation box according to the characteristics of the relationship, and enlarges or shrinks the size of the entity embedded in the box. The above parameters, together with the box vector embedded in the entity and the transfer vector of the relationship, constitute the representation of the temporal facts in TKG. The parameters α_r and Δ_e are initialized as all 1 and all 0 tensors, respectively, and the shape is consistent with the box vector and participates in the training with it. In summary, the scoring function formula for the model on entity or relation completion tasks is as follows:

$$score(h,r,t) = \frac{E[f_r(Box(h)) \bigcap Box(t)] * E[f_r(Box(t)) \bigcap Box(h)]}{E[Box(h)] * E[Box(t)]} \tag{6}$$

The score function simultaneously verifies the correctness of the static part completion results of temporal facts from both forward and inverse relation perspectives. The numerator represents the intersection of the head entity box and tail entity box in the binary random variable set after relation transition vector calculation. The denominator is the distribution set of binary random variables for the head entity box and tail entity box.

3.4. Regularized Constraints on Relationships

In the temporal knowledge graph, the relationship between entities is the core component, which determines the semantic information and structural relationship between entities. The representation of complex relationships has always been a major problem in the existing TKGC methods, and when the TKGC model often has the risk of overfitting in order to learn a reasonable relationship representation, the regular constraints of the relationship are helpful to simplify the model and improve the training efficiency of the model. In order to solve the above problems and ensure that the representation of complex relations in the temporal knowledge graph satisfies the specific semantic relations, and at the same time improve the robustness and generalization ability of the model, the regular constraints of relations are added to the training process of the model. The additional rules and constraints are imposed on special relationships, and relationship transfer between entities is achieved based on the similarity degree between them. Compared to previous work, the proposed method in this paper is more comprehensive and defines different rule constraints when treating multiple complex relationships. In addition, the method in this research is more robust and less affected by sparse and incomplete TKG data. Finally, it is possible to infer from the training dataset that the entities themselves have, but are not shown to express, implicit relationships in the TKG.

The work of Chen et al. [3] proves that the rule constraints of relationships are effective in improving the performance of the model, so this paper conducts further research on the basis of this. Using A, B, and C to represent entities, r, $r^{'}$, $r1$, $r2$, and $r3$ to represent relationships, and $Box(X)$ to represent the box representation learned by X entity.

Hierarchical Relations. The relation r holds if it holds for A, B, then the relation $r^{'}$ holds for A, B as well. The purpose of learning the relation r is that when (A, r, B) is

true, then $(B, r^{'}, A)$ should also be predicted to be true. This objective is satisfied if for relations r and $r^{'}$ there exists entities A and B with the same probability that the facts they comprise hold. Therefore, in this paper, we constrain the relations r and $r^{'}$, with u denoting the set of embedded boxes, and the formula is expressed as follows:

$$L_e(r) = \frac{1}{|u|} \sum_{A,B \in u} \|P_{Box}(f_r(A)|f_r(B) - P_{Box}(f_{r'}(A)|f_{r'}(B)))\|^2 \tag{7}$$

Transfer Relations. The relation r can be passed between entities to each other, such that (A, r, B) holds if (A, r, C) and (B, r, C) hold, respectively. Then the following rule constraints are imposed on the boxes A, B, and C that imply the relation r:

$$L_t(r) = \frac{1}{|u|} \sum_{A,C \in u} \|P_{Box}(A|C)^{-1}\|^2 \tag{8}$$

Combinatorial Relations. The relations $r1$ and $r2$ can be deduced from $r3$, for $(A, r1, B)$ holds with $(B, r2, C)$, then $(A, r3, C)$ holds. To ensure that entities with combinatorial relationships remain unchanged after embedding into the vector space, we use the method of injecting rules to constrain the relationships as follows:

$$f_{r3} = f_{r1} \bigodot f_{r2} \tag{9}$$

Where $\bigodot$is the Hadamard product, i.e., the element-by-element multiplication. For any box $A \in u$ with a combinatorial relation, the expectation is that all have the following relation $f_{r3}(A) = f_{r1}(f_{r2}(A))$, which yields the rule constraint formula:

$$\begin{aligned} L_c(r_1, r_2, r_3) = \frac{1}{|u|} \sum_{A,B \in u} \|P_{Box}(f_{r3}(A)|f_{r1}(f_{r2}(B)))^{-1}\|^2 + \\ \|P_{Box}(f_{r1}(f_{r2}(B))|f_{r1}(A))^{-1}\|^2 \end{aligned} \tag{10}$$

In order to fully learn the background knowledge of TKG involved in learning and training, and to distinguish the correct and wrong temporal facts of the model, this paper uses the dynamic equilibrium negative sampling method for data augmentation in the process of model training. The main idea of this method is to make more negative samples of the same type in the next iteration of training to strengthen the learning of the weakness of the problem that it is difficult to distinguish specific samples in the process of each iteration of the model. Algorithm shows the specific process of the dynamic equilibrium negative sampling method:

```
Dynamic equilibrium negative sampling method (DEN_sample)
  Output The dataset that will participate in the
         training in the next iteration;
  var    Training set data S;
         Test set data T;
         Number of relationships n;
         Trained model BoxTE;
         The size of the dataset that each epoch
```

```
      participates in the training N;
begin
  // num is used to record the amount of training.
     data for each relationship
  num=Array.full(n, 1);
  for (h, r, t, [T1, T2]) in T:
      // Stores the inverse of the difference between
         the model score and the ideal score.
      num[r]=1/abs(1 - BoxTE((h, r, t, [T1, T2])))
      or BoxTE((h, r, t, [T1, T2])));
  // The reciprocal of the difference is normalized
     and the number of training samples is allocated
     according to the N-value.
  num=normalization(num)*N;
  // Initializes an empty collection to store the
     training set data.
  train_data = set();
  for i in num:
      // Generate i samples for each relationship.
      for j=0 to i:
          // Randomly destroy head-tailed entities to
             make new negative samples.
          set.add((h, r, random(t' in S && t' != t),
          [T1, T2]) or (random(h' in S && h' != h),
          r, t, [T1, T2]));
   return train_data;
end.
```

The code in Algorithm specifies the specific process of the dynamic equilibrium negative sampling algorithm, the 1 to 4 lines are to calculate the number of each type of relational data participating in the training, and the 5 to 9 lines are the negative sample making process by randomly destroying the head and tail entities according to the number of data participating in the training. For positive samples involved in the training process, positive sample loss L^+ is obtained. The loss from the negative sample is L^-. Combined with the losses arising from the logical constraints above, the expression is:

$$L_{ogic} = \omega_e \sum_{r \in R_e} L_e(r) + \omega_t \sum_{r \in R_t} L_t(r) + \omega_c \sum_{r \in R_c} L_c(r1 + r2 + r3) \tag{11}$$

Where $R_e, R_t, R_c \in R$, represent the set of hierarchical, transfer, and combinatorial relations, respectively, and the corresponding $\omega_e, \omega_t, \omega_c$ parameters are the regularization coefficients. The training loss function $L = L^+ + L^- + L_{ogic}$ for the PBoxE model is finally obtained.

3.5. A Tolerant Intersection over Union Time Information Evaluation Method

The $gIOU$ [24] and $aeIOU$ [15] are two commonly used intersection over union metrics for target detection tasks in the field of machine vision, which are also applicable to the

time prediction evaluation task and have achieved good results. Time2BOX [6] proposed the $gaeIOU$ evaluation method on this basis, and the main idea is that when the size of the prediction interval is kept constant, the metric scores of the prediction intervals decrease as the gap to the actual intervals increases in the absence of intersections, and increase as the gap to the actual intervals increases in the presence of large intersections. Using I^{gold} to denote the actual time interval and I^{pred} to denote the predicted time interval, $gaeIOU$ can be expressed as:

$$gaeIOU(I^{gold}, I^{pred}) = \begin{cases} \dfrac{D(I^{gold} \bigcap I^{pred})}{D(I^{gold} \biguplus I^{pred})}, D(I^{gold} \bigcap I^{pred}) > 0 \\ \dfrac{D^{'}(I^{gold} \bigcap I^{pred})^{-1}}{D(I^{gold} \biguplus I^{pred})}, otherwise. \end{cases} \tag{12}$$

Where $D^{'}(I^{gold}, I^{pred}) = max(I^{gold}_{min}, I^{pred}_{min}) - min(I^{gold}_{max}, I^{pred}_{max}) + 1$ denotes the size of the gap between the predicted and the actual intervals. The $gaeIOU$ makes some improvements for the case where the gap between the predicted interval and the actual interval is very large, but it does not take into account issues such as the size of the gap between the actual and prediction interval widths. To solve this problem, this paper proposes the tolerant Intersection over Union ($tIOU$). The main idea is to reduce the influence of the size of the prediction interval range on the $tIOU$ value when the prediction interval intersects with the actual interval. The Intersection over Union (IoU) metric in existing machine vision is strict regarding the difference between the predicted image size and the target image size for accurate target recognition, which is not applicable in the TKGC task. The reason is that when the predicted time information and the actual time information do not intersect in the TKGC task, the confidence of the time of the completed time series fact depends not only on the difference between the time information and the real time series fact, but also on the difference between the predicted time interval and the actual time interval. In order to solve the above problems, we use the tolerance coefficient λ to dynamically adjust the size of the predicted interval in the tIOU. The magnitude of λ depends on the difference between the predicted time interval and the actual time interval, $\lambda = 1$ when the two are equal, and tends to $\lambda = 0$ when the difference between the two is large, so as to realize the constraint of the predicted size of the time interval. When the predicted time interval intersects with the actual time interval, the influence from the size of the predicted time interval should be reduced. In order to achieve this requirement, the union of the two types of time intervals in the gaeIOU formula is converted to the size of the actual time interval only. Through the above methods, the constraints on the predicted time interval are more tolerant when the predicted time interval is similar to the actual time interval, and the constraints are stricter when the two types of intervals are quite different, so as to realize the dynamic adjustment of time confidence. When the predicted interval does not intersect with the actual interval, the influence from the size of the predicted interval range is enlarged. Based on $gaeIOU$, it is generalized to $tIOU$, which is denoted by the formula:

$$tIOU(I^{gold}, I^{pred}) = \begin{cases} \dfrac{D(I^{gold} \bigcap I^{pred})}{I^{gold}}, D(I^{gold} \bigcap I^{pred}) > 0 \\ \lambda \dfrac{D^{'}(I^{gold}, I^{pred})^{-1}}{D(I^{gold} \bigcup I^{pred})}, otherwise. \end{cases} \tag{13}$$

Where the coefficient $\lambda = [abs(I_{max}^{pred} - I_{min}^{pred} - I_{max}^{gold} + I_{min}^{gold}) + 1]^{-1}$ represents the difference between the predicted and actual interval widths. For the predicted intervals of [2015,2018], [2020,2022], [2016,2023], [2016,2017], and [2024,2028], respectively, and the actual interval I^{gold} is [2018,2022], the results of the three-time scoring methods are shown in Table 1 below. It can be seen that the difference between the results of the three scoring methods is small when the time interval is small, while when treating the interval with the largest time [2016,2023], there is a large difference in the performance of the three scoring methods, in which the results of both the aeIOU and $gaeIOU$ methods are 0.857, whereas the result of the $tIOU$ method is 1. Therefore, the $tIOU$ method has a better performance when treating time intervals spanning a wide range of predictions.

Table 1. Comparison of time-scoring methods

prediction interval	aeIOU	gaeIOU	tIOU	intersection
[2015,2018]	0.125	0.125	0.167	T
[2020,2022]	0.8	0.8	0.667	T
[2016,2023]	0.857	0.857	1.0	T
[2016,2017]	0.142	0.071	0.014	F
[2024,2028]	0.1	0.05	0.025	F

3.6. Temporal Filters for Feature-weighted Frequency-based Naive Bayesian Classification Methods

Bayesian classification [35] is a statistical classification method based on Bayes' theorem, which can predict the labels of test set data (data to be predicted) according to the statistical distribution of training set samples. The Naive Bayesian classification is a special form of Bayesian classification. It assumes that the dependencies between relationships are "naive", i.e., that each attribute is independent of the other attributes given the conditions, which greatly reduces the complexity of the problem. The naive Bayesian classification method achieves good performance in many cases. It can be expressed as:

$$h_{nb}(x) = argmaxP(c)_{c\in y} \prod_{i=1}^{d} P(x_i|c). \tag{14}$$

Where d is the number of attributes, x_i is the value of x on the ith attribute, and c is a sample of a class.

To select the correct temporal facts from the static fact set, this paper proposes a feature-weighted frequency-based naive Bayesian classification method to compute the confidence score C between the facts to be tested and the temporal information. For the temporal fact G and the static fact S, whether G is correct or not is jointly influenced by the size of the intersection of the temporal scope of action of the entities in G and the temporal scope of the query about G, and the confidence scores of the static fact S. In addition, considering that different relationships between entities do not have the same

level of sensitivity to time, the time scores are integrated according to the different entity relationships.

When a certain attribute value does not exist simultaneously with other attributes in the training set, the classifier will get a probability value of 0. Data in temporal knowledge graphs are often missing, which leads to the absence of certain attribute values in the training set alongside other attribute values. For example, the distribution probability interval of the time score for the temporal facts formed by the relation r in the training dataset is $[0.7, 1]$. When the time score $t_i \in [0, 0.7)$ of a temporal fact containing relation r in the test set needs to be predicted, the $P(t_i|c)$ probability part value in the classifier is 0. Even if the static part of the temporal fact is true, the classifier will still judge the temporal fact as an incorrect completion result, leading to reduced completion accuracy. To solve the above defect in the effect of one attribute value being completely erased by other attributes, we introduce the Laplacian correction method. Specifically, denote N as the number of features that affect the temporal fact G, N_i as the number of possible categories in a given feature, D as the size of the training set data volume, D_c as a given feature in the training set, x_i as the possible values in a given feature, and f_i as the frequency of occurrence of this value in D_c. The prior probability $P(x_i|c)$ and the conditional probability $P(x_i|c)$ are defined as equation (15):

$$P(x_i|c) = \frac{\sum_{i=1}^{D} f_i|D_c, x_i| + 1}{|D_c + N_i|}, P(x_i) = \frac{\sum_{i=1}^{D} |D_c, x_i| + 1}{|D| + N_i}. \tag{15}$$

Although the Naive Bayes classification method has achieved good results in some tasks, it assumes that all features are independent, which is rarely the case in reality. For this reason, this paper proposes a new feature weighting method, W_i, which is used to improve classification accuracy. The relationship between the confidence scores of the static triples, the temporal information features of entities, and relationships must be positively correlated, so in this research, we use the Chi-square statistics feature weighting method to calculate the weights W_i.

Specifically, the weight size is indicated by the difference between the actual frequency T_p and the predicted frequency F_p. The larger the difference represents that the feature has a greater impact on the classification result, and the larger the weight it occupies. The procedure for calculating the influence weights of the score sizes of the triples on the establishment of the temporal facts is shown below. In this paper, we use c_{tt}, c_{tf}, c_{ft}, and c_{ff} to represent the four cases of fact true and score within a certain interval, fact true and score not within a certain interval, fact false and score within a certain interval, fact false and score not within a certain interval, respectively. The prediction frequency F_p and the weight W_i can be defined in the following form:

$$\begin{aligned} F_p &= \frac{(c_{tt} + c_{tf})(c_{tt} + c_{ft}) - c_{ff}}{N_i} \\ W_i &= \sum_{G} \sum_{D_c} \frac{(T_p - F_p)^2}{F_p}. \end{aligned} \tag{16}$$

Also, the probability values are converted to exponential form to prevent the numerical lower bound from overflowing. Finally, the above equation (14) can be rewritten as:

$$h_{nb}(x) = argmax_{c \in y}[logP(x_i) + \sum_{i=1}^{N} W_i f_i logP(x_i|c)]. \tag{17}$$

For the treatment of timestamps, in this research, we use $T(e)$ to denote the temporal range of action of an entity, and for every fact G for which there exists an entity $e, T(e)$ will completely contain its temporal interval, as defined by Eq:

$$T(e_i) = \begin{cases} T(e_i)_{min} = \sum\limits_{e_i \in G_j}^{i<m,j<n} min(T(e_i)_{min}, G_j^{\tau 1}) \\ T(e_i)_{max} = \sum\limits_{e_i \in G_j}^{i<m,j<n} max(T(e_i)_{max}, G_j^{\tau 2}). \end{cases} \tag{18}$$

The final formula to derive the confidence score C is:

$$C(S, t_{pre}) = h_{nb}(tIOU(T(S), t_{pre}), r_i|True) + h_{nb}(score(S)|True). \tag{19}$$

Where S stands for the static triples and $T(S) = T(e_h) \bigcap T(e_t)$ denotes the time horizon of action of the static triples. Whether the completion of the temporal series facts is true depends on the size of the confidence score. The confidence formula is mainly composed of two parts, namely the probability value score based on the static fact and the probability value score based on the time series information. For the probability value of the static fact, the confidence score of the static part of the completed time series fact is obtained through the KGE model, and then the probability of the static fact being true under the confidence score is obtained by using the proposed Bayesian classification method (formula 17), which can bridge the performance gap of different KGE models. The probability value of the temporal series fact composed of the temporal information and relationship of the entity in the temporal dimension (formulas 13 and 18) is obtained by Bayesian classification method. The confidence score composed of the above two important parts can comprehensively consider whether the completion of the timing facts is correct or not. Finally, the algorithm gives the learning process of the TPBoxE model.

```
Training the TPBoxE model
  Output Confidence ranking of the embedding vectors e
         for all entities and relations and all to be
         complementary temporal quaternions;
  const  Tbatch = 2000;
  var    Training dataset S;
         Entity dataset E;
         Relation dataset R;
         Timestamps dataset T;
         Number of training iterations N;
         Batch size batch;
         Embedding dimension d;
         Number of negative samples n;
         Relation regularisation coefficients;
```

```
begin
 e = [xmin, xmax] in Gumbel(x, y) for each e in E;
 r = init_embedding() for each r in R;
 for i = 1 to N do
     for each batch S in Strain do
        data = DEN_sample(S, T, n, BoxTE, N);
        Tbatch =Union {data, (h,r,t)};
     Calculate the score function score(Tbatch);
     Update embeddings e, r, t;
     end for
 end for
 for S = (h, r, ?, T), e in E do
     // Calculating confidence model is added
        to the answer set.
     Sc = C(S, T);
     // The score of the quadruple prediction
        result and the confidence level of the
        model is added to the answer set.
     Map = Map intersection {S, Sc};
 end for
 Sort(Map);
end.
```

The algorithm is the whole model training process. Lines 1 and 2 are embedding initialization of entities and relations. Lines 3 to 14 are for representation training of the model using the static part of the temporal facts to get a fuller representation. The algorithm in lines 15 to 20 obtains the final set of supplementary results by replacing entities, filtering wrong answers, and categorizing them.

3.7. Hyperparameter Selection and Its Time and Space Complexity Analysis

In this research, the Stochastic Gradient Descent (SGD) method is used to train the TPBoxE model. The $batch$ value is 2048, the learning rate l_r is 0.0001, the embedding dimension d is 300, and the number of iterations N is 1000. 25 negative samples are constructed for each positive sample, and the GUMBEL-BETA of the training gumbel box is set to 1. The regularized constraint parameters are 0.1, 0, 0 for the YAGO11k dataset; 0.1, 0, 0 for the WIKIdata12k dataset; 0.1, 0.1, 0.1 for the complex ICEWS18 dataset and 0.3, 0.2, 0.2 for the GDELT dataset.

Time complexity and space complexity are important indicators to measure the performance of a model. Traditional models such as RotatE and TComplex introduce the concept of complex numbers to obtain a better representation of entities or relationships, but this greatly increases the computational effort and the complexity of the model. Other models, such as HyTE's representation of temporal information, are imperfect in some respects, and the complexity of the model increases steeply when the data is denser. Complex models usually have greater expressive and learning capabilities. The uniqueness of the TPBoxE model proposed in this paper is that it strikes a good balance between expressive power and model complexity, i.e., the model still has excellent expressive power without requiring too much computational resources.

We analyze and compare the space complexity and time complexity of the TPBoxE model and several existing state-of-the-art TKGC models. In terms of space complexity, the number of most model parameters is related to the number of embedding dimensions, entities, relations, and timestamps, except for the T-Temp model. In TPBoxE model, time information is used as a way to filter static triples, reducing the embedding of timestamps. In addition, the number of parameters required

Table 2. Comparison of time complexity and space complexity of the TPBoxE model with other TKGC models

Model	Time Complexity	Space Complexity
TTransE	O(Nd)	d(E+R+T)
HyTE	O(Nd)	d(E+R)d(T)
TeRo	O(Nd)	2d(E+R+T)
ChronoR	O(Nd)	3d(E+R)+3(rR+T)
TIME2BoX	O(Nd)	2d(E)+d(R+T)
T-Temp	O(Nd)	2d(E+R)+(2rdR+dT)+k(2E+4R)
BoxTE	O(Nd)	d(E+R)+2d(T)
TLogic	O(Nd)	2d(E+R+T)
TPBoxE	O(Nd)+O(1)	2d(E+R)+k(E+R+T)

by the model for the way of processing temporal information is k(E+R+T). In general, k is much smaller than the embedding dimension d, and it can be ignored. Therefore, the space complexity of the TPBoxE model is much smaller than other similar TKGC models. For time complexity, the time consumption of all similar models is positively correlated with the embedding dimension and the number of iterations, so the time complexity is O(Nd). The model additionally computes the temporal information of entities and relationships than the comparable models, which requires an additional time complexity of O(1) at the constant level, so that the time complexity of the TPBoxE model is equal to that of the comparable models.

In conclusion, the TPBoxE model outperforms or equalizes its counterparts both in terms of time consumption and space consumption, and it has excellent performance. It provides new ideas for solving the problems of large-scale knowledge graph complementation tasks and models that are too large to be deployed and require massive computational resources. For detailed information, please refer to Table 2.

4. Experimental Process and Result Analysis

To evaluate the effectiveness of the TPBoxE model on the task of temporal knowledge graph complementation, four commonly used datasets are used as experimental datasets in this paper: YAGO11k, WIKIdata12k, ICEWS18, and GDELT. Cropping out edges that contain individual entities, ensures better connectivity within the temporal knowledge graph. The WIKIdata12k dataset contains 40,000 triples and 12,554 entities, which is twice the size of the YAGO11k dataset. ICEWS is a global event database and conflict prediction system widely used in international relations research, of which the ICEWS18 dataset is an updated version of the ICEWS database in 2018. The ICEWS18 dataset contains data on a wide range of events, political conflicts, social unrest, and other relevant information about the globe, and the dataset has a large number of complex relationships within it. The GDELT dataset contains events occurring at more than 200 million geographic locations worldwide from 1979 to 2012, with events updated at 15-minute intervals. The statistical information for each dataset is shown in Table 3.

4.1. Evaluation Criteria

In this paper, Mean Rank, Hits@1, Hits@3, and Hits@10 are used as evaluation metrics. The Hits@1 metric represents the number of correct answers predicted by the model to rank first. The higher the Hits@1, the better the representation model performs in learning and representing the

Table 3. Statistical information on datasets

Data set	YAGO11k	WIKIdata12	ICEWS18	GDELT
Entity	10623	12554	23032	7691
Relation	9	23	255	240
Training set	16408	32497	373018	1734399
Validation set	2050	4062	45995	238765
Test set	2051	4062	49545	305241
Interval	year	year	day	15 minutes

relatedness between entities. Hits@n is how many of the n most likely outcomes are correct in total. Its value ranges from 0 to 1, and the closer it is to 1 the better the predictive ability of the model.

$$Hits@k = \frac{1}{|S|}\sum_{i=1}^{|S|}\begin{cases} rank_i, if(rank_i < k) \\ 0, else \end{cases}(k = 1, 3, 10). \tag{20}$$

Mean Rank is a widely used evaluation indicator, which indicates the average ranking of a model in predicting the correct associated entities for a query entity. The lower the Mean Rank value, the more it indicates that the model ranks higher in predicting the correct associated entities of the query entity, that is, the model's prediction accuracy is higher. The formula is:

$$MR = \frac{1}{|S|}\sum_{i=1}^{|S|} rank_i \tag{21}$$

4.2. Experimental Settings

In this paper, the model fills entities or relations into missing positions iteratively to obtain the value of the static triplet score, and finally adds time constraint information to obtain the confidence score. The confidence score is used as the basis for fact ranking to obtain the set of predicted results.

In the YAGO11k dataset, Fig. 3 is obtained from the trained model and scoring method as follows. The horizontal coordinates represent the mapped values of the different relationships, and the vertical coordinates represent the time expectations of the relationship under the fact that it holds and the weight it carries in the data, respectively. In Fig. 3, it can be concluded that different relationships rely on temporal information to different degrees, which means that some relationships treat time leniently. For example, for Relationship 0 and Relationship 6, which have the largest gap in time expectations, the expectations are 0.98 and 0.506, respectively, nearly double the difference.

To avoid that the above phenomenon is caused by the excessive weight in the dataset where a certain relation is located. Taking out the facts containing two kinds of relationships, and two probability values are calculated by using the model and the time scoring method. The first is the probability value that the triplet model scores in the interval [0.96,1] when the timing facts hold; The second is to calculate the probability value of its time information within the interval [0.96,1] through the time scoring method, as shown in Fig. 4.

For relation 7, it can be seen that for the temporal fact that implies this relation only holds if the time score is approximately 1, and the higher the time score, the higher the probability that the fact holds. It can therefore be argued that such relationships are more demanding in terms of temporal information. For relation 8, although the temporal facts containing this relation also follow the law that the higher the temporal score, the higher the probability of the fact being true, there is also a probability of about 0.412 that the temporal fact will be true for the scoring interval [0.96, 0.99]. The requirement for temporal information is not as stringent for Relation 8 as compared to Relation

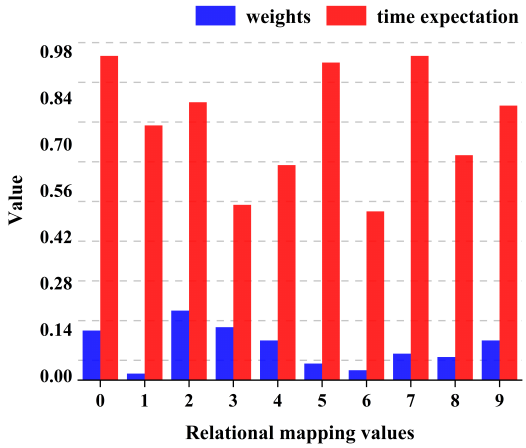

Fig. 3. The connection between relationships and temporal information in YAGO11k and their weights

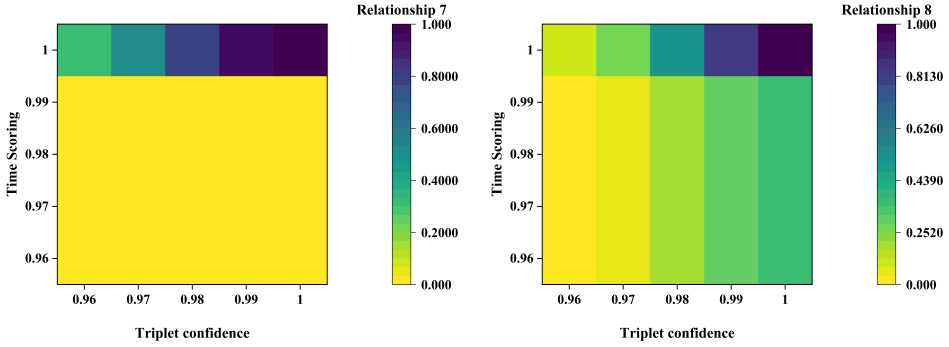

Fig. 4. Probability Plot of the effect of temporal information and static fact confidence on the establishment of temporal fact

7. We experimentally observe that the same KGC model for relations with more stringent temporal information requirements (e.g., "relation 7") lags behind that for relations with more relaxed temporal information requirements (e.g., "relation 8"), which is one of the difficulties in applying the KGC model directly to the TKGC task.

4.3. Comparison Experiment

In the selection of benchmark models, considering the TPBoxE model as a variant of the box model, this paper takes BoxTE and TIME2Box as the benchmark models and compares them together with other TKGC models that perform well. The experimental procedure is to train TPBoxE on three datasets, and the optimal results are measured against the benchmark model according to three evaluation metrics: Mean Rank, Hits@1, Hits@3, or Hits@10.

Table 4. Results of the TPBoxE model on the head and tail entity link prediction task

Model	YAGO11k			WIKIdata12k			ICEWS18			GDELT			MR mean
	MR	H@1	H@10	MR	H@1	H@10	MR	H@1	H@10	MR	H@1	H@10	
TTransE	1233	.023	.149	1107	.057	.193	1461	.052	.213	1510	035	.168	1327
HyTE	1160	.026	.161	862	.035	.212	1003	.094	.292	1145	069	.182	1042
TeRo	824	.098	.287	539	.167	.423	82	.146	.355	1052	.097	.202	849.25
TNTComplex	318	.283	.517	361	.284	.496	482	.196	.317	821	.114	.219	495.5
TIME2BoX	232	.273	.561	198	.249	.511	-	-	-	-	-	-	-
BoxTE	201	.259	.497	236	.261	.501	347	.271	.395	569	.231	.372	363.25
TLogic	112	.287	.563	152	.292	.513	441	.201	.425	398	.213	.385	291
TKGC(SOTA)	112	.287	**.563**	106	.292	**.575**	347	.271	.425	186	.293	.485	234.75
TPBoxE	**86**	**.288**	.559	**77**	**.294**	.572	**166**	**.312**	**.511**	**144**	**.326**	**.487**	**118.25**

From the table 4 above, it can be observed that the TPBoxE model achieves state-of-the-art performance on the ICEWS18 dataset, and there exists a great advantage over other models. For the MR (mean rank) evaluation index, the model in this paper improves about 200 ranks compared with the optimal model BoxTE, and for the indexes Hits@1 and Hits@10, it also improves about 4 and 9 percentage points respectively, which is a big progress. The main reason for this is that the relationships in the ICEWS18 dataset are diverse and contain a large number of complex types of relationships, such as "transfer" and "self-reversal". The other models involved in the comparison do not adequately represent complex relationships due to the simplicity of their modeling, and the TPBoxE model performs better because of the natural way in which boxes can model the particular connections between entities and relationships.

In the YAGO11k and WIKIdata12k datasets because of fewer and simpler inclusion relationships, the expressive power requirements of the models are not stringent, and therefore the gap between the TPBoxE model and the other models is not large. On the YAGO11k dataset, the MR and Hits@1 evaluation metrics achieve optimal performance, and the results under the Hits@10 evaluation metric have the same small gap with the performance of the current optimal model, which indicates that the model in this paper is competitive with the optimal model Tlogic[19].

In the WIKIdata12k dataset, the MR and Hits@1 metrics achieved optimal performance at the same time, and the Hits@10 metrics were almost identical in comparing the optimal performance.

For the GDELT dataset, which has the smallest time interval, the TPBoxE model achieves optimal performance and improves over the previous optimal results. Combining the model performances on all datasets, for the entity link prediction task, the models in this paper achieve optimal performance or are on par with the state-of-the-art.

Table 5. Results of the TPBoxE model on the relational link prediction task

Model	YAGO11k			WIKIdata12k			ICEWS18			GDELT			MR mean
	MR	H@1	H@3	MR	H@1	H@3	MR	H@1	H@3	MR	H@1	H@3	
TTransE	1.79	.775	.812	1.47	.821	.887	20.98	.233	.357	18.62	.102	.197	10.76
HyTE	1.68	.782	.836	1.42	.842	.898	20.13	.273	.329	16.91	.116	.202	10.03
TeRo	1.55	.771	.865	1.51	.841	.907	18.26	.302	.498	9.44	.269	.451	7.69
TNTComplex	1.41	.782	.862	1.39	.837	.865	17.56	.369	.502	11.64	.144	.233	8.00
TIME2BoX	1.32	.821	.924	1.22	.913	.922	-	-	-	-	-	-	-
BoxTE	1.44	.779	.839	1.41	.819	.857	16.19	.376	.513	9.62	.251	.366	7.16
TLogic	1.29	.839	.898	1.19	.901	.951	14.55	.349	.498	10.73	.207	.339	6.94
TKGC(SOTA)	1.24	.839	.924	1.19	.913	.951	14.23	.376	.513	9.62	.369	.451	6.87
TPBoxE	**1.21**	**.855**	**.967**	**1.09**	**.933**	**.991**	**11.21**	**.411**	**.579**	**7.42**	**.396**	**.457**	**5.23**

For the link prediction task of relational complementation, TPBoxE performs equally well. The Hits@10 evaluation metric was replaced with Hits@3 due to the presence of fewer relationships in the YAGO11k dataset and the WIKIdata12k dataset. For the YAGO11k dataset, this paper's model is optimal on all evaluation metrics, leading the baseline model by 0.03 on the MR metric, and by 2 and 4 percentage points for the Hits@1 and Hits3 evaluation metrics, respectively. On the WIKIdata12k dataset, the TPBoxE model is also at the optimum on all evaluation metrics, leading by about 10% on the MR metrics with a large advantage, and also leading by 2 points in Hits@1 and 4 points in Hits@3.

In the GDELT dataset, the lead is about 2 places on the MR metric, about 3 percentage points on the Hits@1 metric, and the Hits@3 metric is on par with the performance of the state-of-the-art model. Finally, on the ICEWS18 dataset, which has the most complex relationships, the model in this paper similarly leads and maintains a large advantage. It leads by about 3 places for the MR dataset, 4 percentage points for the Hits@1 metric, and 6 percentage points for Hits@3. The model in this paper achieves optimal results by performing the relational link prediction task on all the test datasets. For detailed information, please refer to Table 5.

The reason for the advanced results of the model is that the TPBoxE model has excellent portability of each component through structural modularization, and the excellent KGE model can always be used to achieve the best effect of the embedded representation of entities and relations in TKG. Based on the conclusion that the TKG completion results are a subset of the KG completion results, the model further improves the TKGC completion accuracy through the connection between entities, relationships and time series information. From the results of multiple experiments, it can be concluded that the greater the difference in time intervals, the more obvious the improvement of the TPBoxE model in the TKGC task compared with the existing KGC model and the baseline model.

4.4. Ablation Experiment

To analyze the impact of static knowledge graph complementation tasks and time-scoring methods on the model performance, this paper conducts several ablation experiments based on the model TPBoxE. First, in this paper, by replacing the static knowledge graph complementation method with other KG embedding methods, the resulting three model variants, are:

- TP-TransE: The box embedding method is replaced with TransE.
- TP-RotatE: The box embedding method is replaced with RotatE.
- TBoxE: The box embedding method is replaced with BoxE.

The above three static knowledge graph complementation methods are representative in terms of embedding method, and computational complexity. In addition, by replacing the ways of evaluation of temporal information into three ways such as gIOU, aeIOU, and gaeIOU, three variants of the model are obtained as TPBoxE (gIOU), TPBoxE (aeIOU) and TPBoxE (gaeIOU) respectively. All the above variants of the model are trained on the four datasets presented above. The variant model evaluates performance by linking prediction tasks through head and tail entities. The evaluation metric is MR^{-1}, with larger values indicating better modeling.

As can be seen in plot (a) in Fig. 5, the TPBoxE model has a large lead in the results under the MR^{-1} metrics on the four datasets. The TPBoxE model leads the state-of-the-art TBoxE model by about 30 percentage points on the YAGO11k dataset, and by 20, 10, and 20 percent on the WIKIdata12k, ICEWS18, and GDELT datasets, respectively, over the TBoxE model. On the KGC task, BoxE has a major advantage over other models in that the model expresses the complex relationships more adequately. Making it effective on the subsequent time-screening task. In Subfigure (b) of Fig. 5, for different temporal scoring methods, the tIOU method is 30 and 10 percentage points ahead of the optimal scoring method on the datasets YAGO11k and WIKIdata12k, respectively. While for the ICEWS18 dataset, the TPBoxE model is about 10 percentages behind compared to the optimal model. The reason for this is that the data within the dataset was taken from the 2018 Integrated Crisis Early Warning System (ICES) and the timeframe is from January 1, 2018, to December 31, 2018, which covers the entire 2018 timeframe, but there is a higher density of data within the same timeframe and a smaller time, so the difference in the results between the different scoring methods is smaller.

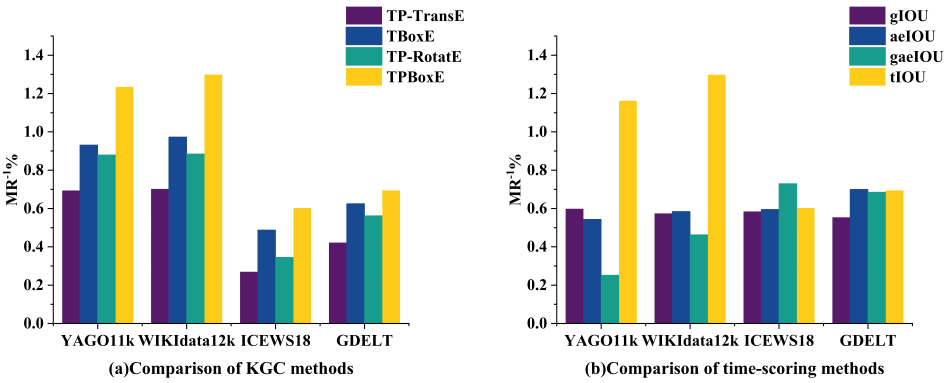

Fig. 5. Comparison chart of the results of ablation experiments

For the GDELT dataset, the fact that the start times within the dataset are all at the same moment similarly makes the difference in the results of the time scores smaller, resulting in the TPBoxE model only equaling the performance of the other similar models.

4.5. Parametric Analysis

In this section, this paper investigates the choice of parameters and their sensitivity of the TPBoxE model, including batch size, learning rate, embedding dimension, number of negative samples, Gumbel-BETA for entity box embedding, and regularization constraint parameter for relations. The variation of TPBoxE's performance on the YAGO11k dataset is demonstrated by varying the hyperparameters.

Training batch size, learning rate, and embedding dimension. The training batch size and learning rate determine how fast the model is trained, and the embedding dimension determines the accuracy and expressiveness of the model. Subplot (a) in Fig. 6 demonstrates the effect of different sizes of parameters on the model. As larger embedding dimensions are used, the initial loss of the model is larger, and the training speed slows down at the same time as the learning rate and training batch decrease. The training of the model reaches the optimal loss and levels off when the parameters chosen are 2048, 0.0001, and 300, respectively.

Gumbel-BETA. The BETA parameter of the solid box is the scale parameter of the Gumbel distribution, which controls the width of the solid box distribution. In subplot (b) of Fig. 6, it can be seen that relative to 0.01, as the BETA parameter increases or decreases, it leads to the width of the bounding box distribution becoming too large or too small, thereby reducing the model's ability to complete missing information.

Regularization Constraints for Complex Relationships. For the complex relations in the dataset, this paper provides a special treatment for them, in which the regularization constraint parameter indicates the weights occupied by the complex relations. Take the YAGO11k dataset as an example, in which there are only hierarchical relationships and the number is 1, so the weight ratio between the three complex relationships is 1:0:0. For the relationship weight settings within the dataset, as shown in subfigure (c) of Fig. 6, the model achieves an optimal representation for entities and relationships within the YAGO11k dataset at a weight of 0.1:0:0.

Number of negative samples. Manufacturing negative samples as a method of data augmentation enhances the model's ability to differentiate between positive and negative samples. Subplot (d) of Fig. 6 demonstrates that as the number of negative samples corresponding to each positive sample increases, the correctness of the model increases. However, when the number of negative samples is after 20, the model accuracy improvement effect is smaller as the number of samples increases. Therefore, considering the model complexity, the number of negative samples in this paper is chosen as 25.

5. Conclusion

Along with the wide application of temporal knowledge graphs, its complementation task has also become one of the research hotspots. Because of this situation, this paper proposes a model based on the temporal probability box for complementing the temporal knowledge graph. The model proposed in this paper utilizes the full expressive power of box embeddings and accomplishes the task of temporal knowledge graph completion by introducing a Bayesian classification approach to model the linkages among static facts, temporal information, and time-series facts. Through extensive experiments on datasets from three different domains, this paper proves practically that the model has higher efficiency and better expressive ability in handling the complementary task compared to the traditional translation model, and theoretically demonstrates the existence of lower time and space consumption of the model.

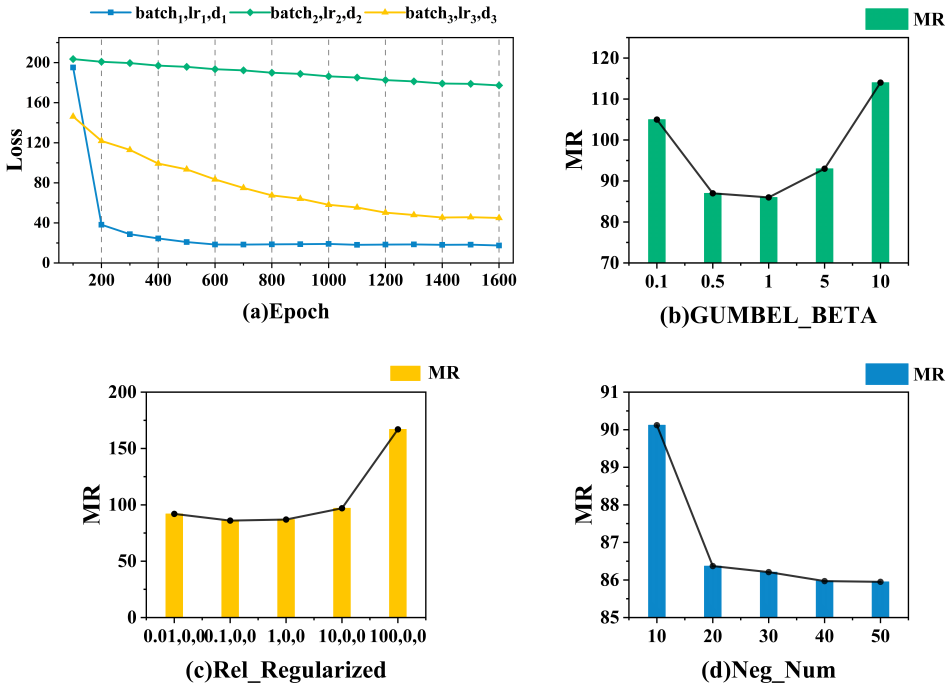

Fig. 6. Parameter sensitivity on TPBoxE

Most scholars have now noted the connection between entities and temporal information, but they have ignored the temporal properties of the relationship and the fact that it suffers from its problems of missing data and sparsity. In the future, we hope that we can further excavate the connection between entities, relationships, and temporal information to find better temporal representations and improve the expressive power of the model.

Acknowledgments. This work was supported by the National Natural Science Foundation of China under Grant No. 62072136, the Key research and development project of Heilongjiang Province No.JD2023SJ20, the National Key R&D Program of China under Grant No. 2020YFB1710200.

References

1. Abboud, R.: BoxE: A Box Embedding Model for Knowledge Base Completion. Advances in Neural Information Processing Systems 33, 9649–9661 (2020)
2. Ahmed, I.A., AL-Aswadi, F.N., Noaman, K.M., Alma'aitah, W.Z.: Arabic Knowledge Graph Construction: A close look in the present and into the future. Journal of King Saud University - Computer and Information Sciences 34(9), 6505–6523 (Oct 2022)
3. Boratko, M., Chen, M., Dasgupta, S.S., Li, X.L., McCallum, A.: Probabilistic Box Embeddings for Uncertain Knowledge Graph Reasoning. In: Proceedings of the 2021 Conference of the North American Chapter of the Association for Computational Linguistics: Human Language Technologies. pp. 882–893. Association for Computational Linguistics, Online (2021)
4. Bordes, A., Usunier, N., Garcia-Duran, A., Weston, J., Yakhnenko, O.: Translating Embeddings for Modeling Multi-relational Data. Proceedings of the 26th International Conference on Neural Information Processing Systems pp. 2787–2795 (2013)

5. Cai, B., Xiang, Y., Gao, L., Zhang, H., Li, Y., Li, J.: Temporal Knowledge Graph Completion: A Survey. In: Proceedings of the Thirty-Second International Joint Conference on Artificial Intelligence. pp. 6545–6553. International Joint Conferences on Artificial Intelligence Organization, Macau, SAR China (Aug 2023)
6. Cai, L., Janowicz, K., Yan, B., Zhu, R., Mai, G.: Time in a Box: Advancing Knowledge Graph Completion with Temporal Scopes. In: Proceedings of the 11th on Knowledge Capture Conference. pp. 121–128. ACM, Virtual Event USA (Dec 2021)
7. Dasgupta, S.S., Ray, S.N., Talukdar, P.: HyTE: Hyperplane-based Temporally aware Knowledge Graph Embedding. In: Proceedings of the 2018 Conference on Empirical Methods in Natural Language Processing. pp. 2001–2011. Association for Computational Linguistics, Brussels, Belgium (2018)
8. Dasgupta, S.S., Zhang, D., Li, X.L., Boratko, M., Vilnis, L., McCallum, A.: Improving Local Identifiability in Probabilistic Box Embeddings. advances in neural information processing systems pp. 182–192 (2020)
9. Dettmers, T., Minervini, P., Stenetorp, P., Riedel, S.: Convolutional 2D Knowledge Graph Embeddings. Proceedings of the AAAI Conference on Artificial Intelligence 32(1) (Apr 2018)
10. Färber, M., Bartscherer, F., Menne, C., Rettinger, A.: Linked data quality of DBpedia, Freebase, OpenCyc, Wikidata, and YAGO. Semantic Web 9(1), 77–129 (Nov 2017)
11. He, M., Zhu, L., Bai, L.: Convtkg: A query-aware convolutional neural network-based embedding model for temporal knowledge graph completion. Neurocomputing 588, 127680 (2024), https://www.sciencedirect.com/science/article/pii/S092523122400451X
12. He Peng, Gang, Z., Jing, C., Mengli, Z., Yuanlong, N.: Type-Enhanced Temporal Knowledge Graph Representation Learning Model. Journal of Computer Research and Development 60(4), 916–929 (2023)
13. Hoffart, J., Suchanek, F.M., Berberich, K., Weikum, G.: YAGO2: A spatially and temporally enhanced knowledge base from Wikipedia. Artificial Intelligence 194, 28–61 (Jan 2013)
14. Huang, J., Lu, T., Zhu, J., Yu, W., Zhang, T.: Multi-relational knowledge graph completion method with local information fusion. Applied Intelligence 52(7), 7985–7994 (May 2022)
15. Jain, P., Rathi, S., Mausam, Chakrabarti, S.: Temporal Knowledge Base Completion: New Algorithms and Evaluation Protocols. In: Proceedings of the 2020 Conference on Empirical Methods in Natural Language Processing (EMNLP). pp. 3733–3747. Association for Computational Linguistics, Online (2020)
16. Lacroix, T., Obozinski, G., Usunier, N.: TENSOR DECOMPOSITIONS FOR TEMPORAL KNOWLEDGE BASE COMPLETION. International Conference on Learning Representations pp. 1–12 (2020)
17. Leblay, J., Chekol, M.W.: Deriving Validity Time in Knowledge Graph. In: Companion of the The Web Conference 2018 on The Web Conference 2018 - WWW '18. pp. 1771–1776. ACM Press, Lyon, France (2018)
18. Liu, W., Zhou, P., Zhao, Z., Wang, Z., Ju, Q., Deng, H., Wang, P.: K-BERT: Enabling Language Representation with Knowledge Graph. Proceedings of the AAAI Conference on Artificial Intelligence 34(03), 2901–2908 (Apr 2020)
19. Liu, Y., Ma, Y., Hildebrandt, M., Joblin, M., Tresp, V.: TLogic: Temporal Logical Rules for Explainable Link Forecasting on Temporal Knowledge Graphs. Proceedings of the AAAI Conference on Artificial Intelligence 36(4), 4120–4127 (Jun 2022)
20. Messner, J., Abboud, R., Ceylan, I.I.: Temporal Knowledge Graph Completion Using Box Embeddings. Proceedings of the AAAI Conference on Artificial Intelligence 36(7), 7779–7787 (Jun 2022)
21. Miao, L., Li, X., Yu, D., Ren, Y., Huang, Y., Cao, S.: Integrating users' long-term and short-term interests with knowledge graph to improve restaurant recommendation. Journal of King Saud University - Computer and Information Sciences 35(9), 101735 (Oct 2023)

22. Paulheim, H.: Knowledge graph refinement: A survey of approaches and evaluation methods. Semantic Web 8(3), 489–508 (Dec 2016)
23. Peng, C., Xia, F., Naseriparsa, M., Osborne, F.: Knowledge Graphs: Opportunities and Challenges. Artificial Intelligence Review 56(11), 13071–13102 (Nov 2023)
24. Rezatofighi, H., Tsoi, N., Gwak, J., Sadeghian, A., Reid, I., Savarese, S.: Generalized Intersection Over Union: A Metric and a Loss for Bounding Box Regression. In: 2019 IEEE/CVF Conference on Computer Vision and Pattern Recognition (CVPR). pp. 658–666. IEEE, Long Beach, CA, USA (Jun 2019)
25. Song, L., Zhe, W., Liping, Z.: SL-tgStore: new temporal knowledge graph storage model. Journal of Zhejiang University (Engineering Science) 58(3), 449–458 (2024)
26. Sun, Z., Deng, Z.H., Nie, J.Y., Tang, J.: ROTATE: KNOWLEDGE GRAPH EMBEDDING BY RELA- TIONAL ROTATION IN COMPLEX SPACE. International Conference on Learning Representations pp. 1–18 (2019)
27. Trouillon, T., Welbl, J., Riedel, S.: Complex Embeddings for Simple Link Prediction. The 33rd International Conference on Machine Learning 48, 2071–2080 (2016)
28. Vaswani, A., Shazeer, N., Parmar, N., Uszkoreit, J., Jones, L., Gomez, A.N., Kaiser, Ł., Polosukhin, I.: Attention is All you Need. Advances in neural information processing systems 30, 11 (2017)
29. Velic˘kovic, P., Cucurull, G., Casanova, A., Romero, A., Lio, P., Bengio, Y.: GRAPH ATTENTION NETWORKS. stat 1050(20), 10–48550 (2018)
30. Vrandečić, D., Krötzsch, M.: Wikidata: A free collaborative knowledgebase. Communications of the ACM 57(10), 78–85 (Sep 2014)
31. Wang, F., Gai, Y., Zhang, H.: Blockchain user digital identity big data and information security process protection based on network trust. Journal of King Saud University - Computer and Information Sciences 36(4), 102031 (Apr 2024)
32. Wang, H., Yang, J., Yang, L.T., Gao, Y., Ding, J., Zhou, X., Liu, H.: Mvtucker: Multi-view knowledge graphs representation learning based on tensor tucker model. Information Fusion 106, 102249 (2024), https://www.sciencedirect.com/science/article/pii/S1566253524000277
33. Wang, J., Wang, B., Gao, J., Pan, S., Liu, T., Yin, B., Gao, W.: Made: Multicurvature adaptive embedding for temporal knowledge graph completion. IEEE Transactions on Cybernetics pp. 1–14 (2024)
34. Wang, L., Lu, J., Sun, Y.: Knowledge graph representation learning model based on meta-information and logical rule enhancements. Journal of King Saud University - Computer and Information Sciences 35(4), 112–125 (Apr 2023)
35. Wenjun, Z., Liangxiao, J., Huan, Z., Long, C.: A Two-Layer Bayes Model: Random Forest Naive Bayes. Journal of Computer Research and Development 58(9), 2040–2051 (2021)
36. Yang, B., Yih, W.t., He, X., Gao, J., Deng, L.: EMBEDDING ENTITIES AND RELATIONS FOR LEARN- ING AND INFERENCE IN KNOWLEDGE BASES. International Conference on Learning Representations pp. 1–13 (2015)
37. Yue, L., Ren, Y., Zeng, Y., Zhang, J., Zeng, K., Wan, J., Zhou, M.: Complex expressional characterizations learning based on block decomposition for temporal knowledge graph completion. Knowledge-Based Systems 290, 111591 (2024), https://www.sciencedirect.com/science/article/pii/S0950705124002260

Song Li received the Ph.D. degree in computer application technology from Harbin University of Science and Technology, Harbin, China, in 2009. He is currently a Professor with the College of Computer Science and Technology, Harbin University of Science and Technology. He is the author of two books, more than 60 articles. His research interests include spatial database, data mining, big data and information privacy protection, knowledge graph.

Qi Wang, a postgraduate student, is currently studying at the School of Computer Science and Technology, Harbin University of Science and Technology. His research interests include Temporal Knowledge Graph, Graph Neural Network, big data, and spatial database.

Zheng Li, a postgraduate student, is currently studying at the School of Information Management, Heilongjiang University. Her research interests include big data, data mining, and data analysis.

Liping Zhang received the M.S. degree in computer application technology from Harbin University of Science and Technology, Harbin, China, in 2006. She is currently a Professor with the College of Computer Science and Technology, Harbin University of Science and Technology. She is the author of two books, more than 40 articles. Her research interests include spatial database, data mining, knowledge graph, big data and information privacy protection.

Received: August 20, 2024; Accepted: November 20, 2024.

Computer Science and Information Systems 22(1):181–197 https://doi.org/10.2298/CSIS240911007R

A Lightweight Defect Classification Method for Latex Gloves Based on Image Enhancement

Yong Ren[1,⋆], Dong Liu[1] and Sanhong Gu[2]

[1] Applied Technology College Of Soochow University
215325 SuZhou,China
renyong@suda.edu.cn
flovvv@163.com
[2] Suzhou Dechuang Measurement and Control Technology Co., Ltd.
215104 Suzhou, China
threehym@163.com

Abstract. This paper presents a glove defect classification method that integrates image enhancement techniques with a lightweight model to enhance the efficiency and accuracy of glove defect classification in industrial manufacturing. A dataset comprising images of five types of gloves was collected, totaling 360 sample images, for the training and validation of a deep learning-based glove defect classification model. Image enhancement techniques, including super-pixels, exposure adjustment, blurring, and limited contrast adaptive histogram equalization, increased dataset diversity and size, improving model generalization. Based on the lightweight model MobileNetV2, the model was improved by reducing the number of input image channels through grayscale conversion and optimizing the loss function. Experimental results demonstrate that the improved MobileNetV2 model achieved an average accuracy of 97.85% on both the original and enhanced datasets, effectively mitigated overfitting phenomena, and exhibited a significantly faster training speed compared to the ResNet34 and ResNet50 models.

Keywords: glove defect classification, machine vision, image enhancement, deep learning, lightweight model, mobilenetv2.

1. Introduction

Industrial defect classification is an important technology to ensure product quality. The rapid development of new technologies in the fields of machine vision, image processing, and deep learning has also driven the significant progress of industrial defect classification technology. Currently, it can be applied to the detection of various industrial products such as metals, semiconductors, textiles, and rubber [21].

The limitations of traditional manual inspection methods, such as low efficiency, high cost, and strong subjectivity, can no longer meet the needs of modern industrial production. In the field of latex glove production, with the advancement of industrial automation and intelligence, glove defect classification technology is also gradually transitioning from traditional manual visual inspection to automated detection based on machine vision, which makes the machine vision-based defect classification technology play an

⋆ Corresponding Author

increasingly important role in product quality assurance. Therefore, the research and development of efficient defect classification technology has become particularly urgent [20].

Traditional machine vision-based defect classification methods mainly relied on image processing technologies, such as edge detection and template matching [3]. These methods performed well in handling simple or rule-based industrial images, but their performance was limited in complex scenarios. With the application of machine learning technology, researchers have begun to explore statistical learning-based methods, such as support vector machines (SVMs) and random forests, which can better handle the local features and classification problems of images [10, 24].

The rise of deep learning technology has brought new development opportunities for defect classification. Convolutional neural networks (CNNs) have been widely applied to defect classification tasks, especially in image classification, object detection, and semantic segmentation [6, 16, 30].

The main goal of glove defect classification in the industrial production process is to quickly distinguish the types of qualified and nonqualified products, so as to control product quality. Due to the variety of gloves and defect types, collecting and labeling a large amount of high-quality data is costly and challenging [27], and there are still problems such as strong data dependency and weak model generalization ability. In addition, real-time and computational resource requirements are also limiting factors. Therefore, this paper proposes a lightweight latex glove defect classification method based on image enhancement.

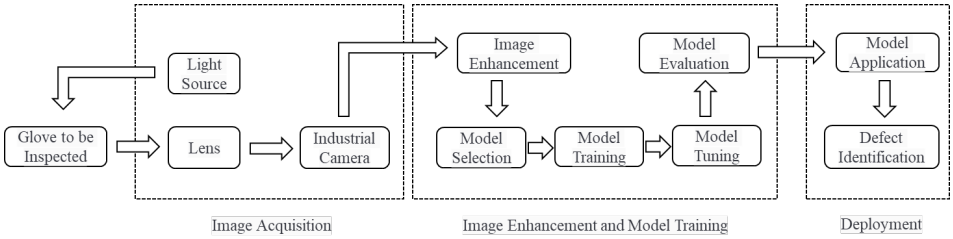

Fig. 1. The process of glove defect classification based on machine vision

2. Related Work

2.1. Defect classification based on machine vision

The typical process of defect classification based on machine vision usually includes three parts: image acquisition, image enhancement and model training, and deployment application.

Firstly, an industrial camera is used to capture high-quality images of products. The collected data is then subjected to image enhancement. Next, a suitable model is selected for training. Finally, the trained model is applied to perform defect classification. For example, The overall process of glove defect classification is illustrated in Figure 1.

Early defect detection methods relied heavily on manual inspection and basic image processing techniques. While early methods can be effective in specific scenarios, they are labor-intensive and do not scale well with increasing production volumes. To overcome these limitations, conventional image processing techniques such as thresholding, edge detection, and template matching were introduced [15]. Thresholding involves setting a gray-level threshold to segment images into foreground and background, facilitating defect identification based on pixel intensity differences [11]. Edge detection algorithms, such as Canny and Sobel, are designed to identify abrupt changes in image brightness, thereby outlining object boundaries that can indicate the presence of cracks or scratches [19]. Template matching compares a region of interest in the test image with predefined templates, allowing for the detection of deviations that signify defects [32]. Despite their simplicity and high computational efficiency, traditional methods often face challenges when dealing with complex defect patterns, varying lighting conditions, and noisy images. This has prompted the exploration of more advanced techniques, particularly those that leverage deep learning.

In recent years, deep learning has transformed defect detection by automating feature extraction and enabling the learning of intricate patterns from large datasets. Convolutional Neural Networks (CNNs) have become foundational in deep learning-based defect detection due to their capability to hierarchically learn spatial hierarchies of features from image data [6]. CNNs utilize convolutional layers that apply learnable filters to the input images, allowing them to automatically capture essential features such as edges, textures, and shapes at multiple scales. This hierarchical feature extraction process means that initial layers may learn simple patterns like edges and colors, while deeper layers can recognize more complex structures, such as patterns specific to defects [7]. Furthermore, the architecture of CNNs can be tailored to specific defect detection tasks by adjusting parameters such as the number of layers, filter sizes, and activation functions. This flexibility allows researchers to optimize CNNs for particular types of defects or image characteristics, thereby improving classification accuracy [12].

Beyond CNNs, other deep learning architectures have also been employed for defect detection. Generative Adversarial Networks (GANs), for instance, are effective for anomaly detection by training a generator to create realistic, defect-free images, while a discriminator distinguishes between real and generated images. This setup allows GANs to flag anomalies as deviations from the learned distribution [29]. Similarly, Autoencoders can be adapted for defect detection by reconstructing input images with minimal reconstruction error. Significant discrepancies between the original and reconstructed images can indicate potential defects, making Autoencoders valuable for identifying anomalies that may not be well-represented in the training data [14].

2.2. Image enhancement techniques

Image enhancement techniques play a pivotal role in enhancing the efficiency and generalization capabilities of deep learning models, especially when dealing with limited sample data [25, 8]. These techniques serve to expand the diversity and size of the dataset by simulating various changes that may occur in the real world and generating new image samples by applying a series of transformations to the original image [18].

One common approach to image enhancement is data augmentation, which involves applying a series of transformations to the original images, such as rotation, scaling, flip-

ping, and color adjustments. These transformations help the model generalize better by exposing it to a wider range of visual patterns during training. In addition to data augmentation, other image enhancement techniques, such as histogram equalization and noise reduction, can also be employed to further improve image quality and feature extraction [1, 13]. These techniques are particularly useful in scenarios where the original images are of low quality or contain significant noise. Recent advancements in generative adversarial networks (GANs) have also opened up new possibilities for image enhancement [28]. GANs can generate highly realistic synthetic images that can be used to augment the training dataset, further improving the performance of deep learning models in glove defect classification tasks.

In summary, the integration of image enhancement techniques with deep learning models has significantly advanced the field of glove defect classification. By leveraging these techniques, researchers have been able to improve classification accuracy, reduce manual inspection efforts, and enhance the robustness and generalization capabilities of their models.

3. Materials and Methods

3.1. Dataset construction

The choice and setup of the lens and industrial camera are crucial for the quality of captured images [5]. In this study, a 5 megapixel color camera and a 12mm fixed focus lens of Detron were selected, and white stripe light and black background were used for shooting. The side view of the camera is shown in Figure 2.

In this paper, a dataset containing five types of glove images, totaling 360 sample images, was collected to train and validate a glove defect classification model based on deep learning.The dataset is crucial for effectively training the model to recognize various types of defects that may occur in latex gloves, which are commonly used in industrial settings. Each type of image reflects different defect characteristics, as shown in Table 1.

The inclusion of these diverse image types allows for a comprehensive evaluation of the model's ability to detect defects that can occur in real-world scenarios. For instance, minor damage such as small cracks or wear may not render the gloves immediately unusable but could lead to issues over time, affecting the safety of users. On the other hand, major damage, including significant tears, directly impacts the gloves' usability and poses a safety risk.

To address the challenges presented by varying defect types and conditions, the following image enhancement techniques are introduced in this study: color dithering, which can simulate the effects of different lighting conditions and increase the color diversity of the dataset by randomly changing the color values in the image; brightness adjustment, which can better adapt to different ambient lighting situations by adjusting the brightness of the image so that the model can deal with a variety of scenarios ranging from bright to dim; and contrast adjustment, which enhances or reduces the contrast of the image that can help the model learn to recognize defects under different contrast conditions.

Additionally, other methods such as superpixels, blur, solarize, affine transformations, Canny edge detection, and CLAHE are utilized for image enhancement, as illustrated in Figure 3. The specific image augmentation methods and their parameters are summarized in Table 2.

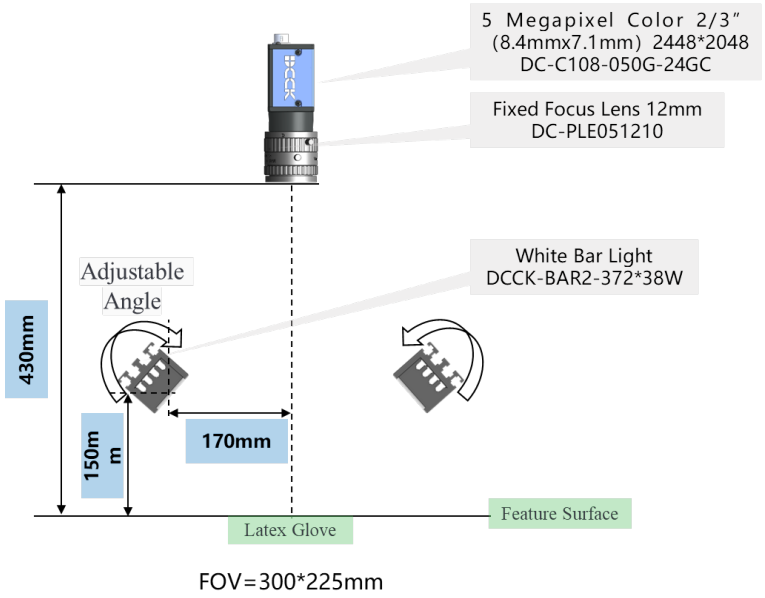

Fig. 2. Camera Side View and Parameter Description

In order to compare and analyze the impact of image enhancement on the model training effect, the dataset (Raw) is the original glove sample image set, without any image enhancement processing. The dataset (Aug) adopts 6 transformation methods for image enhancement. The above image enhancement combination builds the training dataset as shown in Table 3.

3.2. Network model structure

In this study, lightweight network MobileNetV2 was selected as the basic model architecture, and the classic ResNet34 and ResNet50 network models were used in the comparative experiment. ResNet networks [4] effectively solve the problem of gradient disappearance in deep neural networks by introducing residual connections, thus allowing the network to train deeper model structures. The difference between ResNet34 and ResNet50 lies not only in their depth and number of layers, but also in their construction of Residual blocks. ResNet34 uses the Residual Block, while ResNet50 uses a Bottleneck block, as shown in Figure 4.

ResNet34 includes a 34-layer network structure with fewer parameters, making it more efficient when computing resources are limited or on small datasets. ResNet50, which contains a 50-layer network structure, has more parameters and more complex feature extraction capabilities, and is suitable for large datasets and complex image recognition tasks. The MobileNetV2 [22] network employs an Inverted Residual Block structure (as shown in Figure 5) and Linear Bottlenecks, enhancing model efficiency and accuracy while maintaining low computational cost and minimal memory usage.

Table 1. Glove Image Types and Sample Quantities

Type	Quantity(Pieces)	Description
Normal Images (Ok)	200	Glove images without visible defects
Empty Images (Empty)	18	Blank images with no gloves captured
Minor Damage Images (Minor)	27	Glove images with small cracks or wear
Major Damage Images (Major)	72	Glove images with significant damage or tears
Dirty Images (Dirty)	43	Glove images contaminated with oil stains or similar substances

To reduce the computational complexity of the model, this study converts input sample images to grayscale, removing color information and retaining only luminance data, which means the model is trained using single-channel images. Consequently, the first input layer parameter of the MobileNetV2 model is changed from 224×224×3 to 224×224×1. The overall structure of the adjusted MobileNetV2 network is shown in Table 4, where t represents the expansion factor, c denotes the depth of the output feature map (channel), n indicates the number of repetitions of the bottleneck, and s refers to the stride.

Meanwhile, ReLU6 is used as the activation function, a Rectified Linear Unit activation function [23] with a rectified linear unit output limit of 0 to 6, which can be mathematically defined as:

$$ReLU6(x) = min(max(0, x), 6) \tag{1}$$

3.3. Loss Function Optimization

In addition, to train the model to accurately identify the defect type of gloves, the Loss function employs Multi-Class Cross-Entropy loss, which measures the difference between the probability distribution predicted by the model and the true label [31]. For each sample, the loss function can be expressed as:

$$L = \sum_{i=1}^{C} y_i log(P_i) \tag{2}$$

Where: C is the number of categories, y_i is the unique thermal coding of the real label, and p_i is the probability distribution predicted by the model.

To improve model performance, Mini-batch Gradient Descent is utilized for training, specifically using the Adam optimizer [17, 26]. The Adam optimizer combines the benefits of Momentum and adaptive learning rates, allowing for automatic adjustment of the learning rate for each parameter, thus speeding up the training process and increasing convergence speed.

Table 2. Image Augmentation Methods

Method	Parameter Settings	Operational Steps
Color Dithering	RGB values within ±10%	Use `PIL` to modify pixel values randomly.
Brightness Adjustment	Range: [0.5, 1.5]	Use `ImageEnhance.Brightness` to adjust brightness.
Contrast Adjustment	Range: [0.5, 1.5]	Use `ImageEnhance.Contrast` to adjust contrast.
Superpixels	N/A	Apply superpixel segmentation using `skimage`.
Blur	Adjustable kernel size	Use Gaussian blur to reduce noise and details.
Solarize	Threshold parameter	Invert brightness of pixels above a certain threshold.
Affine Transform	Rotation angle, scaling factors	Apply transformations to create diverse perspectives.
Canny Edge Detection	N/A	Highlight edges using the Canny algorithm.
CLAHE	Clip limit, grid size	Enhance local contrast using `CLAHE` algorithm.

Table 3. Image Enhancement Combination for Constructing the Training Dataset

Dataset	Sample Classification Quantity	Total(Pieces)
Original Dtaset(Raw)	Normal (OK) 200, Empty 18, Minor 27, Major 72, Dirty 43	360
Augmented Dtaset(Aug)	Normal (OK) 200, Empty 108, Minor 162, Major 432, Dirty 253	1155

On the basis of multi-class cross-entropy Loss function, weighted loss function and Focal Loss are introduced.The weighted loss function increases the model's attention to a few categories by assigning different weights to each category. The weights for each class can be set based on the frequency of samples in the dataset. For example:

$$\text{Weight}_i = \frac{N}{n_i}$$

Where: N is the total number of samples, and n_i is the number of samples in class i. By assigning higher weights to minority classes (e.g., Minor damage), the model focuses more on these samples during training. The weights are fine-tuned through cross-validation to find a balance that maximizes overall model accuracy.

Fig. 3. Example of Image Enhancement

The focus loss makes the model more focused on the learning of difficult classification samples by reducing the loss weights of easy classification samples. Specifically, focus loss can be expressed as

$$FL(p_i) = -\alpha_t(1-p_t)^{\gamma}(p_t) \tag{3}$$

In this formula, α_t is the class weight, p_t is the prediction probability of the model for the correct class, and γ is the regulator that adjusts the rate at which easy samples are down-weighted. A typical value for γ might be set to 2, but it can be optimized through grid search or random search techniques to determine the value that yields the best validation accuracy.

By introducing an improved loss function, the model can deal with class imbalance more effectively, thus improving the overall detection accuracy.

(a) Residual Block (b) Bottleneck

Fig. 4. Two Types of Residual Blocks in ResNet

Table 4. The overall structure of the adjusted MobileNetV2

Input	Operator	t	c	n	s
$224^2 \times 1$	conv2d	-	32	1	2
$112^2 \times 32$	bottleneck	1	16	1	1
$112^2 \times 16$	bottleneck	6	24	2	2
$56^2 \times 24$	bottleneck	6	32	3	2
$28^2 \times 32$	bottleneck	6	64	4	2
$14^2 \times 64$	bottleneck	6	96	3	1
$14^2 \times 96$	bottleneck	6	160	3	2
$7^2 \times 160$	bottleneck	6	320	1	1
$7^2 \times 320$	conv2d 1×1	-	1280	1	1
$7^2 \times 1280$	avgpool 7×7	-	-	1	-
$1 \times 1 \times 1280$	conv2d 1×1	-	-	-	-

4. Experiment and Results

4.1. Experimental environment and model training

The experiments in this paper were conducted on a cloud server equipped with an NVIDIA GPU to ensure sufficient computing power for deep learning model training. The hardware specifications are as follows:

GPU: NVIDIA RTX A4000 with 16GB of video memory
CPU: 8 × Intel(R) Xeon(R) CPU E5-2686 v4 @ 2.30GHz
Memory: 60GB
Storage: 200GB

The software environment used for the experiments includes Ubuntu 20.04, Python 3.10, PyTorch 2.0.1, and CUDA 11.8. All training and testing experiments were performed in this environment.

Three models were trained: ResNet34, ResNet50 and MobileNetV2. Each model was trained for 50 epochs on both the Raw dataset and the Aug dataset. The initial learning rate for all gradient descent algorithms was set to 1e-3, and the model training batch size was set to 4.

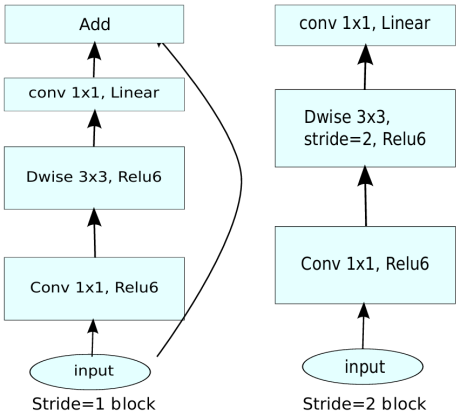

Fig. 5. Convolution block of MobilenetV2

(a) ResNet34 (b) ResNet50 (c) MobileNetV2

Fig. 6. Model Training Process on the Raw Dataset

As shown in Figure 6, it can be observed that on the original dataset (Raw), both the ResNet34 and ResNet50 models begin to overfit after 10 training epochs due to insufficient training samples. The ResNet50 model, having a stronger feature fitting capability, tends to overfit more easily, resulting in a higher validation loss. In contrast, Figure 7 indicates that on the augmented dataset (Aug), overfitting for both ResNet34 and ResNet50 occurs only after 40 epochs, with a noticeable improvement in both training and validation accuracy, and a loss value approaching zero. The MobileNetV2 model outperformed the other two models both before and after enhancement.

4.2. Confusion matrix, ROC curve and multi-classification evaluation index

In order to ensure the effectiveness and generalization performance of the experimental results, the enhanced dataset is divided, and 20% (233 images) are set aside as the test dataset, and the original proportion of various types of images is maintained as far as possible. For the model trained by ResNet34, ResNet50 and MobileNetV2 on the Raw dataset, the confusion matrix and ROC curve of the test results [9] are shown in Figure 8 and Figure 9.

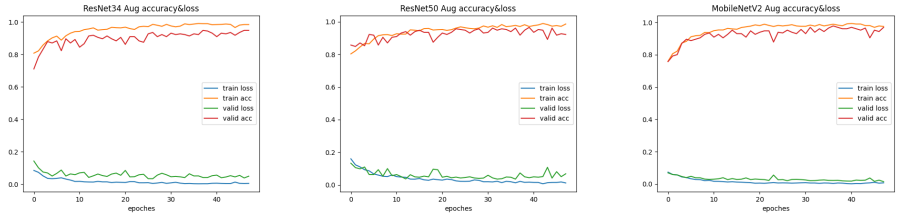

(a) ResNet34 (b) ResNet50 (c) MobileNetV2

Fig. 7. Model Training Process on the Augmented Dataset

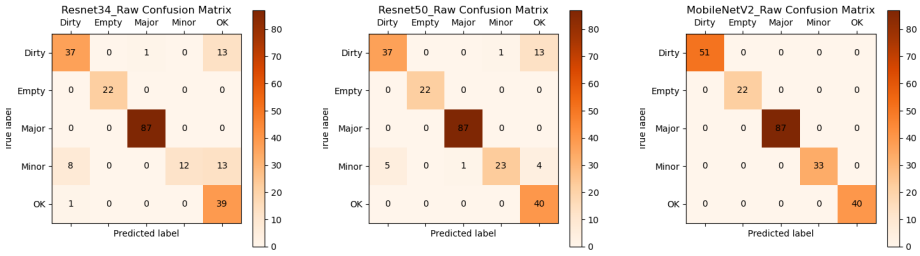

Fig. 8. Confusion Matrix of the Model on the Raw Dataset

According to the above test results, the prediction accuracy of the Minor image model is the lowest for all kinds of models, because the number of samples is relatively small and the difference between the minor image and normal image (OK) and Dirty image is not obvious. In the same case, although the Empty image has the smallest sample number, it has the most significant difference from other types of images, so it is easier to distinguish and has the highest prediction accuracy. However, due to the large number of samples and great difference from other types of images, Major image has the second highest prediction accuracy.

Training results of ResNet34, ResNet50, and MobileNetV2 models on the enhanced dataset (Aug). The confusion matrix and ROC curve tested are shown in Figure 10 and Figure 11.

It can be seen that in the enhanced dataset, the model training effect has been significantly improved, and all evaluation indicators of ResNet34 and ResNet50 models have exceeded 99%, and MobileNetV2 even reached 100%. Moreover, the Area Under Curve (AUC) of the five types of ROC curves almost reached 1, indicating good model performance.

This improvement can be attributed to increased dataset diversity from various augmentation techniques, which enable the model to learn robust features. Additionally, the use of enhanced data mitigates overfitting by encouraging the model to focus on essential features rather than memorizing specific examples. Finally, the introduction of challeng-

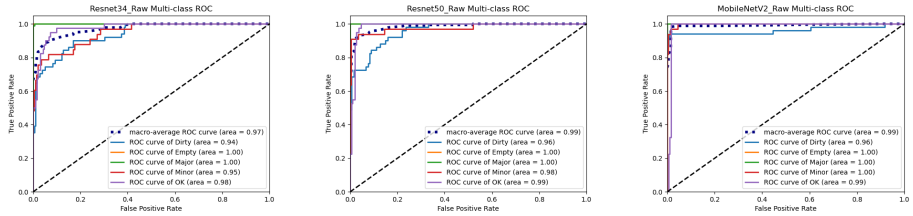

Fig. 9. ROC Curve of the Model on the Raw Dataset

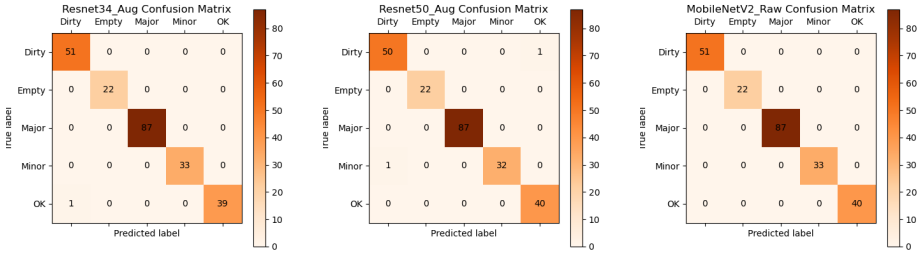

Fig. 10. Confusion Matrix of the Model on the Augmented Dataset

ing examples allows the model to better recognize subtle differences in glove defects, which is crucial for precision in industrial applications. These factors collectively demonstrate the effectiveness of image enhancement techniques in boosting detection accuracy and model reliability in glove defect classification tasks.

In addition, based on the confusion matrix of model test, Accuracy, Precision, Recall and F1 Score were calculated in this paper as evaluation indicators of model performance [2], and the experimental results were shown in Table 5.

Table 5. Model Evaluation Metrics Statistics

Evaluation Metrics	Resnet34		Resnet50		MobileNetV2	
	Raw	Aug	Raw	Aug	Raw	Aug
Accuracy	84.55	99.57	89.70	99.14	95.71	100
Precision	87.86	99.62	90.59	99.12	95.20	100
Recall	81.28	99.50	88.45	99.00	94.79	100
F1 Score	80.67	99.55	88.43	99.05	94.86	100

Comparative analysis of the experimental results shows that: In the training results on the original dataset, the four evaluation indexes of Resnet34 and Resnet50 models are

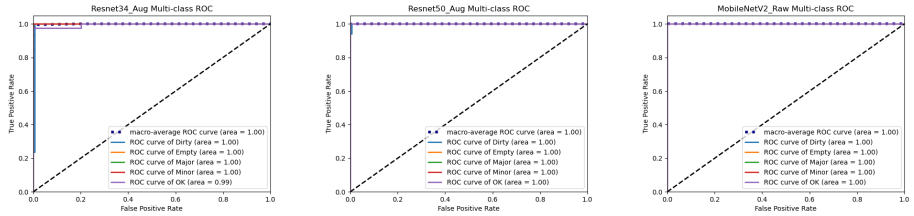

Fig. 11. ROC Curve of the Model on the Raw Dataset

between 80% and 90%, while the MobileNetV2 model is about 95%. The training results on the enhanced dataset showed that the four evaluation indexes of the three models were improved, with the Resnet34 and Resnet50 models exceeding 99%, and the improved MobileNetV2 model even reaching 100%. This shows that the combined image enhancement transform proposed in this paper can play a good role in improving the training effect of the model, and the training effect of the improved lightweight model MobileNetV2 is obviously better than that of the other two models. The glove classification detection effect under the optimal weight condition is shown in Figure 12.

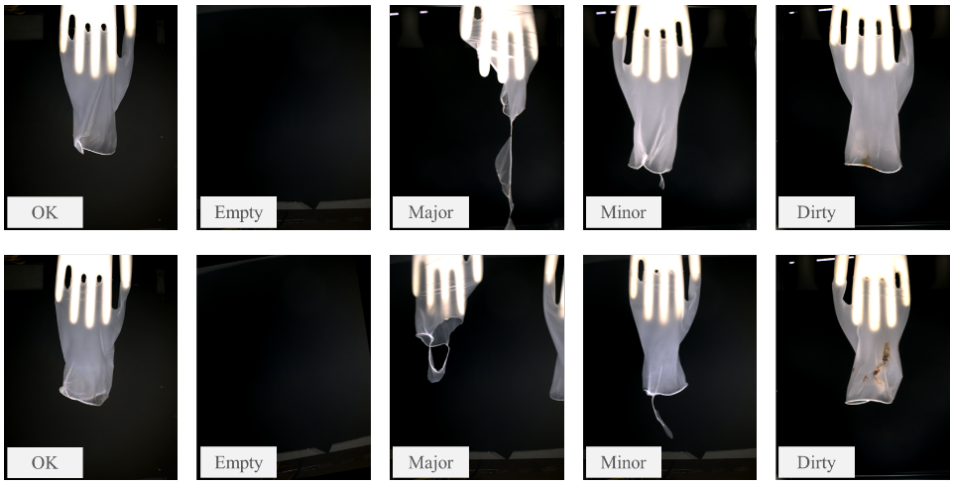

Fig. 12. Improved glove detection effect based on MobileNetV2 model

To understand the performance differences among the models, we examined key factors such as architecture, parameter count, computational complexity, and applicable scenarios. MobileNetV2 employs depthwise separable convolutions, reducing parameters and computational complexity compared to ResNet34 and ResNet50, enhancing generalization especially with limited data. With only 3.4 million parameters, MobileNetV2 offers faster training and less risk of overfitting, making it suitable for resource-constrained

environments and real-time applications. In contrast, ResNet34 and ResNet50, with approximately 21 and 25 million parameters respectively, require more computational resources but offer higher accuracy, suitable for scenarios where precision is prioritized and resources are abundant.

4.3. Model training time overhead

Under the same experimental conditions, Resnet34, Resnet50 and MobileNetV2 models do not use pre-training weights, and their respective training time costs on different datasets as shown in Figure 13.

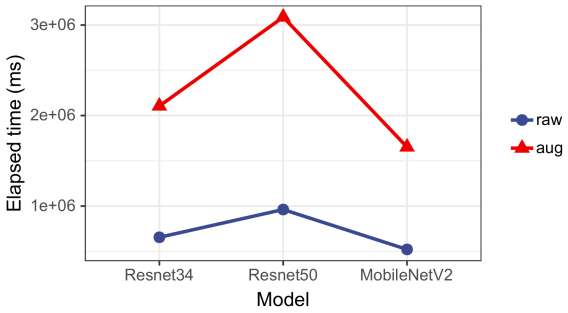

Fig. 13. Comparison of Model Training Time Costs

The experimental results indicate that the training time of the model is primarily determined by factors such as the complexity of the model structure, the number of parameters, and the size of the training dataset. Compared to the ResNet34 and ResNet50 models, the MobileNetV2 model employs depthwise separable convolutions, effectively reducing both the parameter count and computational load. This allows it to maintain high performance while offering better computational efficiency, making it suitable for resource-constrained situations.

In conclusion, the introduction of image augmentation techniques has significantly enhanced the model's performance. By simulating different perspectives and scales, image augmentation increases the diversity of the dataset, enabling the model to learn more robust feature representations. Considering the performance requirements for glove image defect classification and the trade-off between model effectiveness and time expenditure, the MobileNetV2 model trained on the augmented dataset(Aug), demonstrates superior overall performance compared to the ResNet34 and ResNet50 models.

5. Conclusion and Discussion

Aiming at glove defect classification in industrial production, a deep learning method combining image enhancement technology and lightweight model is proposed in this paper. Three network models, ResNet34, ResNet50 and MobileNetV2, were used to compare and analyze the model training effect of the original dataset and the enhanced dataset.

The experimental results demonstrate that high-quality image samples, captured using machine vision, effectively simulate the diversity of real-world scenarios when subjected to image enhancement techniques. This approach significantly improves the model's generalization ability and detection accuracy, allowing it to identify a wider range of defects with greater reliability. Specifically, the enhancements not only facilitate better recognition of subtle defects but also enable the model to perform well under varying conditions that might not be present in the original dataset. Furthermore, the lightweight MobileNetV2 model, in particular, showcases a remarkable reduction in the number of parameters and computational complexity, making it suitable for real-time applications in industrial settings. By meeting the stringent performance requirements of practical industrial applications, this method provides a novel and efficient solution for glove defect classification. Ultimately, it contributes to improving the efficiency and overall product quality in industrial production processes.

Future researches on glove defect classification can focus on exploring more efficient image enhancement techniques and deep learning models, tailored to the needs of practical application scenarios. While our study has primarily employed some augmentation methods, such as brightness and contrast adjustments, it is still potential to investigate more advanced techniques, including Generative Adversarial Networks (GANs), which could generate diverse and realistic images to augment the dataset and enhance model generalization.

Furthermore, expanding the scope of research to more complex scenarios, including varying lighting conditions, occlusions, and diverse glove materials, is essential for assessing the model's adaptability in real-world applications. By addressing these challenges, we aim to continuously optimize and improve the accuracy and efficiency of glove defect classification systems, ensuring their robustness and applicability in diverse industrial settings.

Future studies could also consider the integration of multimodal data, such as thermal imaging or depth information, to enhance detection accuracy and reliability.

Acknowledgments. Teaching research project of Basic Computer Education in national colleges and Universities (2022-AFCEC-121); Ministry of Education Industry-University Collaborative Education Project (230804471307131).

References

1. Acharya, U.K., Kumar, S.: Genetic algorithm based adaptive histogram equalization (gaahe) technique for medical image enhancement. Optik 230, 166273 (2021)
2. Cubuk, E.D., Zoph, B., Shlens, J., Le, Q.V.: Randaugment: Practical automated data augmentation with a reduced search space. In: Proceedings of the IEEE/CVF conference on computer vision and pattern recognition workshops. pp. 702–703 (2020)
3. Gaidhane, V.H., Rani, A., Singh, V., et al.: An improved edge detection approach and its application in defect detection. In: IOP conference series: materials science and engineering. vol. 244, p. 012017. IOP Publishing (2017)
4. He, K., Zhang, X., Ren, S., Sun, J.: Deep residual learning for image recognition. In: Proceedings of the IEEE conference on computer vision and pattern recognition. pp. 770–778 (2016)
5. How, Y.C., Nasir, A.F.A., Muhammad, K.F., Majeed, A.P.A., Razman, M.A.M., Zakaria, M.A.: Glove defect detection via yolo v5. Mekatronika: Journal of Intelligent Manufacturing and Mechatronics 3(2), 25–30 (2021)

6. Jha, S.B., Babiceanu, R.F.: Deep cnn-based visual defect detection: Survey of current literature. Computers in Industry 148, 103911 (2023)
7. Khanam, R., Hussain, M., Hill, R., Allen, P.: A comprehensive review of convolutional neural networks for defect detection in industrial applications. IEEE Access (2024)
8. Kim, J.S., Kang, D.S.: A study on fire data augmentation from video/image using the similar-label and f-guessed method. Computer Science and Information Systems (00), 11–11 (2024)
9. Kleiman, R., Page, D.: Aucμ: a performance metric for multi-class machine learning models. In: International Conference on Machine Learning. pp. 3439–3447. PMLR (2019)
10. Krummenacher, G., Ong, C.S., Koller, S., Kobayashi, S., Buhmann, J.M.: Wheel defect detection with machine learning. IEEE Transactions on Intelligent Transportation Systems 19(4), 1176–1187 (2017)
11. Kumar, M.P., Ashok, D.: A multi-level colour thresholding based segmentation approach for improved identification of the defective region in leather surfaces. Engineering Journal 24(2), 101–108 (2020)
12. Lee, K.H., Lee, H.W., Yun, G.J.: A defect detection framework using three-dimensional convolutional neural network (3d-cnn) with in-situ monitoring data in laser powder bed fusion process. Optics & Laser Technology 165, 109571 (2023)
13. Liu, J., Malekzadeh, M., Mirian, N., Song, T.A., Liu, C., Dutta, J.: Artificial intelligence-based image enhancement in pet imaging: Noise reduction and resolution enhancement. PET clinics 16(4), 553–576 (2021)
14. Lu, T., Wang, Z., Shen, Y., Shao, X., Tang, Y.: Defvae: A defect detection method for catenary devices based on variational autoencoder. IEEE Transactions on Instrumentation and Measurement (2023)
15. Ma, B., Zhu, W., Wang, Y., Wu, H., Yang, Y., Fan, H., Xu, H.: The defect detection of personalized print based on template matching. In: 2017 IEEE International Conference on Unmanned Systems (ICUS). pp. 266–271. IEEE (2017)
16. Mezher, A.M., Marble, A.E.: A novel strategy for improving robustness in computer vision manufacturing defect detection. arXiv preprint arXiv:2305.09407 (2023)
17. Mezher, A.M., Marble, A.E.: Computer vision defect detection on unseen backgrounds for manufacturing inspection. Expert Systems with Applications 243, 122749 (2024)
18. Nagaraju, M., Chawla, P., Kumar, N.: Performance improvement of deep learning models using image augmentation techniques. Multimedia Tools and Applications 81(7), 9177–9200 (2022)
19. Ni, X., Liu, H., Ma, Z., Wang, C., Liu, J.: Detection for rail surface defects via partitioned edge feature. IEEE Transactions on Intelligent Transportation Systems 23(6), 5806–5822 (2021)
20. Ren, Z., Fang, F., Yan, N., Wu, Y.: State of the art in defect detection based on machine vision. International Journal of Precision Engineering and Manufacturing-Green Technology 9(2), 661–691 (2022)
21. Saberironaghi, A., Ren, J., El-Gindy, M.: Defect detection methods for industrial products using deep learning techniques: A review. Algorithms 16(2), 95 (2023)
22. Sandler, M., Howard, A., Zhu, M., Zhmoginov, A., Chen, L.C.: Mobilenetv2: Inverted residuals and linear bottlenecks. In: Proceedings of the IEEE conference on computer vision and pattern recognition. pp. 4510–4520 (2018)
23. Sheng, T., Feng, C., Zhuo, S., Zhang, X., Shen, L., Aleksic, M.: A quantization-friendly separable convolution for mobilenets. In: 2018 1st Workshop on Energy Efficient Machine Learning and Cognitive Computing for Embedded Applications (EMC2). pp. 14–18. IEEE (2018)
24. Shipway, N., Barden, T., Huthwaite, P., Lowe, M.: Automated defect detection for fluorescent penetrant inspection using random forest. NDT & E International 101, 113–123 (2019)
25. Shorten, C., Khoshgoftaar, T.M.: A survey on image data augmentation for deep learning. Journal of big data 6(1), 1–48 (2019)
26. Vrbačič, G., Pečnik, Š., Podgorelec, V.: Hyper-parameter optimization of convolutional neural networks for classifying covid-19 x-ray images. Computer Science and Information Systems 19(1), 327–352 (2022)

27. Wang, H., Wang, Y.: Improved glove defect detection algorithm based on yolov5 framework. In: 2022 IEEE 6th Advanced Information Technology, Electronic and Automation Control Conference (IAEAC). pp. 1192–1197. IEEE (2022)
28. Xu, B., Zhou, D., Li, W.: Image enhancement algorithm based on gan neural network. IEEE Access 10, 36766–36777 (2022)
29. Xu, C., Li, W., Cui, X., Wang, Z., Zheng, F., Zhang, X., Chen, B.: Scarcity-gan: Scarce data augmentation for defect detection via generative adversarial nets. Neurocomputing 566, 127061 (2024)
30. Zhang, K.: Using deep learning to automatic inspection system of printed circuit board in manufacturing industry under the internet of things. Computer Science and Information Systems 20(2), 723–741 (2023)
31. Zhang, Z., Sabuncu, M.: Generalized cross entropy loss for training deep neural networks with noisy labels. Advances in neural information processing systems 31 (2018)
32. Zhou, X., Wang, Y., Xiao, C., Zhu, Q., Lu, X., Zhang, H., Ge, J., Zhao, H.: Automated visual inspection of glass bottle bottom with saliency detection and template matching. IEEE Transactions on Instrumentation and Measurement 68(11), 4253–4267 (2019)

Yong Ren is an Associate Professor with the School of Engineering, Applied Technology College of Soochow University, SuZhou, China. He received his Master's degree in Software Engineering from Soochow University. His research interests include artificial intelligence, machine vision, and image processing.

Dong Liu is a Bachelor of Computer Science from the Engineering School, Applied Technology College of Soochow University. His research interests include artificial intelligence, and machine vision.

Sanhong Gu is a Senior Engineer of Suzhou Dechuang Measurement and Control Technology Co., Ltd. His research interests include machine vision, and machine design.

Received: September 11, 2024; Accepted: November 29, 2024.

Computer Science and Information Systems 22(1):199–217 https://doi.org/10.2298/CSIS240321003L

ASAM: Asynchronous Self-Attention Model for Visual Question Answering

Han Liu[1], Dezhi Han[1], Shukai Zhang[1], Jingya Shi[1], Huafeng Wu[2,⋆], Yachao Zhou[3], and Kuan-Ching Li[4,⋆]

[1] College of Information Engineering, Shanghai Maritime University, Shanghai 201306, China
liuhanshmtu@163.com
dzhan@shmtu.edu.cn
zhang_shukai11@163.com
jingyashi00@163.com
[2] Merchant Marine College, Shanghai Maritime University, Shanghai 201306, China
hfwu@shmtu.edu.cn
[3] Shanghai Anheng Times Information Technology Co., Ltd.
Shanghai 200131, China
anna.zhou@dbappsecurity.com.cn
[4] Dept of Computer Science and Information Engr (CSIE), Providence University, Taiwan
kuancli@pu.edu.tw

Abstract. Visual Question Answering (VQA) is an emerging field of deep learning that combines image and question features and generates collaborative feature representations for classification by uniquely fusing the components. To enhance the effectiveness of models, it is crucial to fully utilize the semantic information from both text and vision. Some researchers have improved the accuracy of the model's training by either adding new features or enhancing the model's ability to extract more detailed information. However, these methods have made experimentation more challenging and expensive. We propose a model called asynchronous self-attention model (ASAM) that makes use of an asynchronous self-attention component and a controller, integrating the asynchronous self-attention mechanism and collaborative attention mechanism effectively to leverage the rich semantic information of the underlying visuals. It realizes an end-to-end training framework that can extract and exploit the rich representational information of the underlying visual images while performing coordinated attention with text features, as it does not over-emphasize fine-grained but finds a balance within it, thus allowing the model to learn more valuable information. Extensive ablation experiments were conducted on the proposed ASAM using the VQA v2 dataset to verify its effectiveness. The results of the experiments demonstrate that the proposed model outperforms other state-of-the-art models, without increasing the model complexity and the number of parameters.

Keywords: Visual Question Answering, Asynchronous Self-Attention, Deep Collaborative, Controller.

⋆ Corresponding authors

1. Introduction

With the comprehensive development of deep learning, single-modal tasks involving computer vision (CV) and natural language processing (NLP) no longer meet the demands of technological advancement. Consequently, there has been a growing emphasis on multimodal task learning involving the collaboration of image and text modalities. Among these multi-modal tasks [28,43,25], a pivotal research direction is visual question answering (VQA)[37,23].

The VQA task aims to accurately answer the natural language questions about images. This requires the model to not only comprehend the content of both the images and the questions but also to grasp the intricate relationships between them. Initially, training models of convolutional neural network developed rapidly and involved in many fields [8,5]. The research on VQA also focused on the training model using convolutional neural networks [9,29,35] and subsequently evolved to incorporate attention mechanisms which are now widely used in scientific research [6]. Several studies [27,31,44] have demonstrated that methods leveraging conventional self-attention mechanisms have provided significant impetus to advancing visual question answering (VQA) tasks. However, their performance remains limited as traditional attention mechanisms fail to effectively model the intricate relationships between the two modalities.

With the advancement of computing and communication technologies, a disruptive new architecture has emerged-the Transformer [40]. Initially devised to address problems in NLP, the Transformer has progressively found success in applications to computer vision and multimodal tasks. This success is attributed to its attention mechanism, which excels in comprehensively modeling the relationships between modalities and has been applied in various fields[5,26] Yu et al. [45] were the first to employ the transformer model in the VQA, leading to the model securing the championship in the 2019 VQA Challenge. Due to the simplicity and effectiveness of the transformer's encoder-decoder structure and attention mechanism and its ability to capture long-distance dependencies, there have been many attempts in VQA so far[3,42,48,4,12,20]. However, it has been observed that fine granularity can be used in all fields[24].If most of the work emphasizes and over-attention to it, it may lead to the loss of some effective information [24,21]. For this reason, we consider whether there can be a solution to the issue above.

Regarding fusing features from different layers, ResNet [17] introduces an identity shortcut connection structure that directly skips one or more layers and fuses features between different layers to solve the problem of gradient disappearance. Qin et al. [34] propose a Residual Weight-Sharing Attention Network (RWSAN), wherein within each attention unit of the RWSAN layer, residual learning is performed using learnable connectivity patterns and shared parameters. Drawing upon this conceptual framework, we propose an asynchronous self-attention mechanism combined with collaborative attention, resulting in the design of the Asynchronous Self-Attention Model (ASAM). ASAM can perform bottom-up connections to the attention map from the previous layer's output, thereby balancing the coarseness of the granularity in image representation. This ensures that the model focuses on crucial regions of the image without introducing additional complexity, thereby allowing the effective extraction of rich semantic information from the image. Extensive ablation experiments based on the VQA v2 benchmark dataset prove the effectiveness of our proposed models. The main contributions of this paper are as follows:

(1) An asynchronous self-attention mechanism is proposed to optimize the balance between coarse-grained and fine-grained image representations. Simultaneously, a controller is designed to optimize the features computing attention scores during the self-attention modeling process.

(2) By integrating collaborative attention with the designed self-attention mechanism, we propose an Asynchronous Self-Attention Model (ASAM). This model is capable of coordinating relationships between objects of different granularities and collaboratively attending to image features in conjunction with text.

(3) We conducted extensive experiments on the benchmark dataset VQA v2, and the results indicate that the proposed ASAM achieved favorable performance without increasing model complexity or the numbers of parameters.

The remainder of this work is organized as follows. We introduce the work related to Visual Question Answering research in section 2. Then section 3 describes the asynchronous self-attention mechanism in detail. Next, section 4 verifies the validity of the model through extensive experiments, and finally, the concluding remarks and a prospect for future directions are given in section 5.

2. Related Work

2.1. Visual Question Answering

The essence of the visual question answering task lies in the simultaneous comprehension of the input question and image, coupled with a capacity for reasoning to accurately respond to natural language inquiries about the image. Over the past few years, an increasing number of researchers have devoted themselves to investigating VQA tasks, leading to a diverse array of methods that contribute to enhancing task performance. Models based on the transformer architecture have gained more widespread application [3,16,30,15]. Mao et al. [30]proposed an approach guided by positional attention, significantly enhancing the model's performance by incorporating three distinct positional attention modules into a single transformer model. Chen et al. [2] proposed for the first time to introduce contextual information with different combinations of representations into VQA, and proposed a context-aware attention network (CAAN) to solve the problem of existential comprehension bias, marking a novel breakthrough built upon the foundation of MCAN [45]. Furthermore, visual question answering requires models to possess extensive multimodal knowledge beyond specific domains to enable models to answer more abundant questions. Consequently, some researchers leverage large-scale knowledge bases for information extraction, allowing the models to infer image content and answer questions requiring common-sense knowledge not explicitly covered in the image [47,7,41]. Building upon optimizing features, some researchers have proposed methods such as feature filtering, gating mechanisms, and stepwise refinement of features from coarse to fine. Nguyen et al. [32] extract predicates simultaneously with features, enabling dual learning of coarse-grained and fine-grained information and achieving robust reasoning. Guo et al. [13] utilized top-k filtering, explicitly selecting the most crucial information from both the image and the question to concentrate attention, proposing a novel multi-modal explicit sparse attention network. Diverging from other methods that focus on refining features, we leverage the output of the model's preceding layer to influence the input of the next

layer, thereby balancing the coarseness in granularity between feature representations. We optimize the model by integrating heterogeneous self-attention and modular co-attention networks.

2.2. Attention Model

Referring to how humans process information when seeing images, the researchers consider that the model should be able to recognize what and where the object in the images is when faced with a question. The location of the model's gaze should be the object's position in the image most relevant to the question. Due to its capability to dynamically modulate attention towards critical regions or words across multimodal modeling processes, and to allocate weights based on feature importance, the attention mechanism confers significant advantages in addressing VQA tasks. Consequently, it has been extensively adopted in this task to enhance modeling processes across diverse modalities effectively. VQA models can concentrate attention on relatively important information by incorporating attention mechanisms, thereby reducing interference from irrelevant information. Yang et al. [44] devised a multi-layer attention network to address noise induced by global features, which is the first attempt of attention mechanisms in VQA tasks, yielding promising performance. Anderson et al. [1] introduced a Bottom-up and Top-down Attention (BUTD) network to identify prominent image region features within the model. However, aside from image features, learning textual features is equally crucial. In general, visual attention assists the model in focusing on critical image regions, while textual attention attends to essential words. Consequently, dense co-attention over both images and questions is currently prevalent. Lu et al. [27] devised a hierarchical collaborative attention model, wherein the architecture constructs a collaborative attention graph at three levels: word level, phrase-level, and question level. Emphasizing mutual guidance between text and modalities, the model, however, is limited to learning coarse interactions between modalities. Nam et al. [31] introduced a dual attention network (DAN) for multimodal reasoning, employing multi-step reasoning to mutually guide visual and textual attention. Yu et al. [45] proposed a multimodal dense co-attention network by modeling dense interactions within and between modalities, representing a significant breakthrough in attention mechanisms. Chen et al. [3] designed a textual global-context module and a compact attention mechanism, introducing a multimodal vision-language paradigm that enhances the modeling dependencies capability of image tokens and the model's reasoning ability.

3. Method

3.1. Model Components

Before presenting the complete model framework, this section first introduces the essential components of the model. The collaborative asynchronous self-attention attentive layer consists of three basic units: Self-Attention unit (SA), Asynchronous Self-Attention unit (ASA), and Guided-Attention unit (GA).

As shown in Fig. 1(a), only one input, denoted as X, represent either text or visual features. In Fig. 1(b), Y_i and $Y_{(i-1)'}$, are image features, and $Y_{(i-1)'}$ is the reserved feature of the previous layer. In Fig. 1(c), X and Y denote text features and image features respectively. And Z represents output features.

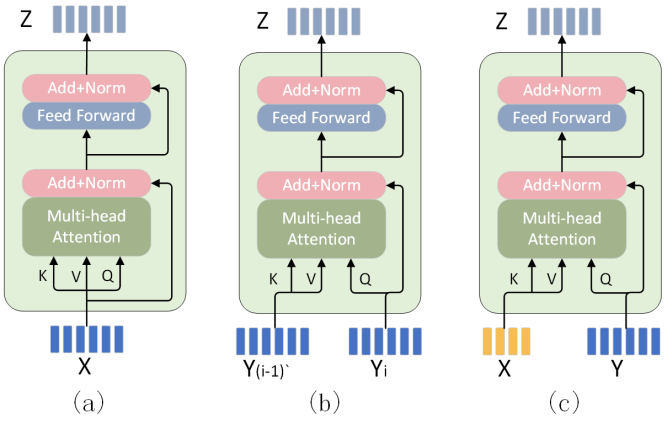

Fig. 1. Three base components in the proposed SASM model

Self-Attention, Asynchronous Self-Attention and Guided-Attention Units. The attention mechanism used in this paper is drawn from [40]. In feature processing, question and image features are transformed into queries, keys, and values feature. d_k and d_v are the dimensions of the keys and queries that make up the scaled dot-product attention's input in attention mechanisms, respectively. We calculate the dot-product of queries with all keys and divide the result by $\sqrt{d}$. Finally, we use the softmax function to obtain the attention weights on the values. In practice, to compute the attention weights on a set of queries simultaneously, we pack queries into matrix $Q \epsilon \mathbb{R}^{1\times d}$, and pack the keys and values into matrices $K \epsilon \mathbb{R}^{n\times d}$ and $V \epsilon \mathbb{R}^{n\times d}$. The calculation process of self-attention specific is shown as follows:

$$f = Attention\left(Q, K, V\right) = softmax\left(\frac{QK^T}{\sqrt{D_k}}\right)V \tag{1}$$

To improve the representational capability of the features, the attention mechanism uses a multi-head attention mechanism to enrich the feature information by jointly focusing on the representation subspace at different locations. Taking the example of h separate heads, the output feature f can be represented as follows:

$$f = MHA\left(Q, K, V\right) = Concat\left(head_1, head_2..., head_h\right)W^O \tag{2}$$

$$head_i \;=\; Attention\left(Q^i, K^i, V^i\right) \tag{3}$$

where $W_i^Q, W_i^K, W_i^V \epsilon \mathbb{R}^{d\times d_h}$ are the projection matrices of $Q,\ K\ , V$ in the i-th head, respectively. $W^O \epsilon \mathbb{R}^{h\times d_h \times d}$ is the projection parameter matrix, d_h is the dimension of each header output feature and is generally set to $d_h = d/h$. This setting aims to prevent multi-head attention models from becoming too large and consuming too many computing resources.

Based on the above description and inspiration from [45], we have independently designed an asynchronous self-attention module ASA (see Fig. 1(b)). The input feature can be flexibly represented as SA's text or image features. After the feature obtains the

attention weight in the multi-head attention layer, it guides the attention of features X, connects the output result with the residual of the original feature, and then normalizes it with the LayerNorm function to facilitate optimization. After performing the above operations, we feed the processed features into a feed-forward layer and then perform the residual and the normalization operations again, finally outputting the attention features $Z \epsilon \mathbb{R}^{m \times d}$. In GA, $X \epsilon \mathbb{R}^{m \times d_x}$ represents the text features and $Y \epsilon \mathbb{R}^{n \times d_y}$ represents the image features. Different from SA, GA uses text features to guide the attention learning of image features.

The Asynchronous Self-Attention (ASA) we designed is different from SA and GA. $Y, Y_{(i-1)} \epsilon \mathbb{R}^{n \times d_y}$ in ASA represent the same type of features, i.e., text or image features. Different from the synchronous SA (Q, K, V all come from the same component output), $Y_{(i-1)} \epsilon \mathbb{R}^{n \times d_y}$ in ASA are derived from the output of the previous component, and the $Y_{(i-1)}$, which are closer to the original features than the attended features, retain the relatively rich semantic information of the original features. Taking image features as an example, high-level image features have richer semantic information compared to the underlying features. Applying the above characteristics to multi-head attention can be represented by the following equation:

$$f_Y = Attention\left(Y_i, Y_{(i-1)}, Y_{(i-1)}\right) = softmax\left(\frac{Y_i Y_{(i-1)}^T}{\sqrt{d_y}}\right) Y_{(i-1)} \tag{4}$$

The more detailed model structure of the combined components will be described in the following sections.

Component Combination. As shown in Fig. 2, we can obtain different model structures by combining the three components in Sect.3.1, in which the text and image features are consistent with those described in Fig. 1. The figure presents the image Asynchronous Self-Attention Model ASAM-I (using asynchronous self-attention components on image features), the text Asynchronous Self-Attention Model ASAM-Q (using asynchronous self-attention components on question features), and the common Asynchronous Self-Attention Model ASAM-QI (applying asynchronous self-attention components on image and question features simultaneously). These three models are all cascade structures, and we provide a detailed description of the multi-modal feature transfer process. Image Asynchronous Self-Attention Model in Fig. 2(a) is our baseline model. The text features $X_{(i)}$ are passed to the next layer after intensive interaction with themselves in SA. In the image processing part, the image features $Y_{(i)}$ are first asynchronous self-attention with the image features $Y_{(i-1)}$ from the previous layer through the ASA component, the result features are guided by the text features X in the GA. The modelling of the image features is completed in the GA to obtain more detailed image features. In contrast to the baseline model described above, text asynchronous self-attention (Fig. 2(b)), as a contrasting model, swaps the component SA with the component ASA in the baseline and uses an asynchronous self-attention approach in the modeling of the text features to simulate the interaction process of the text features in unimodality. The model (Fig. 2(c)) also used as a comparison model, has a structure that combines the two structures described previously, using asynchronous self-attention for both image and text processing, which is guided attention for multi-modal features and interaction between unimodal features at different moments in time.

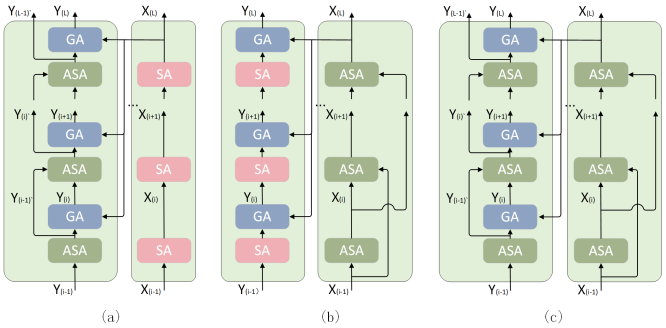

Fig. 2. Three different structures of the model. (a) denotes the image asynchronous self-attention model. (b) is the text asynchronous self-attention model. (c) is the text-image asynchronous self-attention model

3.2. Asynchronous Self-attention Model

The overall model structure of ASAM is shown in Fig. 3. ASAM contains three parts: features representation, model modeling, and features fusion and answer classifier. We improve the model in the interaction modeling part, which will be described in the subsequent sections. The above section had provided the introduction to the basic structure of the model. In this section, we will describe the entire model structure in detail. The entire framework can be specifically represented as three parts. The first is to address the way in which the image and text features that are represented as input, and the second is the separate cascade of the three models in the model section mentioned that models the features of the two modalities in a detailed interactive manner. Finally, for the output image and question features, we use a multi-modal fusion model to fuse the features and feed them to a multi-label classifier for predicting the answer.

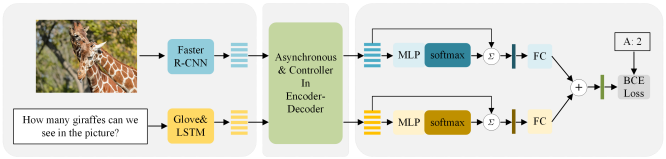

Fig. 3. The overall structure of the Asynchronous Self-Attentive Model (ASAM)

Image and Question Representations. The input question is processed first. For a question, we take the sentence into words and trim it to a maximum of 14 words. Next, we use the previous words as input, transform them into a vector using the 300-D GloVe word embedding [38] pre-trained on a large-scale corpus to obtain a words sequence of size $m \times 300$, where the maximum is 14 and the minimum is 1. Finally, we input the word

embedding sequence to a single layer 512-dimensional long short-term memory (LSTM) network to obtain the question features $X \epsilon \mathbb{R}^{m \times 512}$.

For image features, we use a Faster R-CNN [36] model with a ResNet-101 as its backbone and pre-trained on the Visual Genome dataset [19] to extract them, we can obtain objects features $Y \epsilon \mathbb{R}^{n \times 2048}$ with a dynamic number of objects,$n \epsilon [10, 100]$.

With the above description, the process of the question and image features extraction can be expressed by the following equations:

$$Y = Faster\_RCNN\,(image) \tag{5}$$

$$X = LSTM\,(Glove\,(question)) \tag{6}$$

The above describes that the images have different number of object regions and the questions also have variable number of words. To facilitate the calculation, we use the zero-padding method to fill the number of image objects and question words to the maximum, which fills the image object regions n to 100 and the number of question words m to 14. In practice, we use a linear transformation to unify the image and question dimensions, transforming the image features to the exact 512 dimensions as the question features.

Collaborative Asynchronous Self-Attention with Controller. In Sect.3.1, we have introduced our models, including the baseline model ASAM-I (Fig. 2(a)) and two comparison models ASAM-Q and ASAM-QI (Fig. 2(b)(c)). This section will focus on describing our baseline model. The asynchronous self-attention model consists of a deep cascade of modules shown in Fig. 2, where the question features X and the image features Y can be described in the deep model as $X_{(L)}$ and $Y_{(L)}$ respectively, where $Y_{(L)}$ represents the intermediate features in a hierarchy that the ASA component has processed. In all models, the first layer will uniformly use the SA component instead of ASA component, because there are no incoming features from the previous layer for the first layer of the model. In addition to the baseline model described above, we have additionally designed a controller as shown in Fig. 4 (the left half of the figure shows the processing of the features within the controller, while the right half adds the controller on the basis as indicated in Fig. 2(a)), which can provide a self-learning parameter for the features and can effectively further improve the model performance. The process can be summarized in the following equations:

$$k_1 = Linear\,(AAP\,(k)) \tag{7}$$

$$k_2 = Linear\,(ReLU\,(k)) + Linear\,(ReLU\,(k_1)) \tag{8}$$

$$k_{parm} = Linear\,(k_2) \tag{9}$$

$$k_{fin} = k_{parm} \cdot k + q \tag{10}$$

where AAP() is the AdaptiveAvgPool2d() adaptive average pooling function. We feed the processed K into a linear layer, and the result is activated simultaneously with the unprocessed K subsequently by the $ReLU()$ function. Then we pass them to another linear layer separately and finally add them together. We obtain a parameter by summing the results of the features through a linear layer, multiplying this parameter with the original K and finally, adding it to Q. The input V is treated in the same way as K. With the above processing, we can obtain more detailed features.

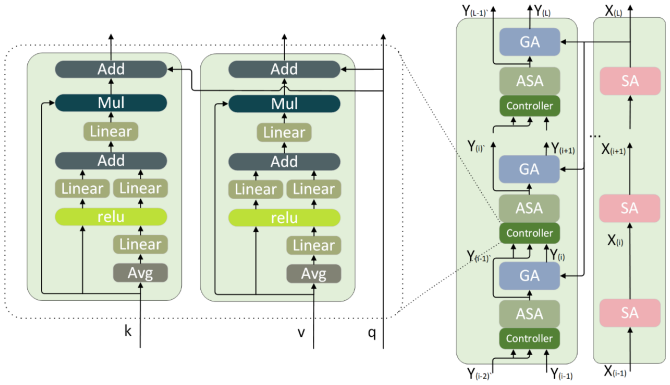

Fig. 4. Asynchronous Self-Attention with Controller

Feature Fusion and answer Classifier. With a deep collaborative asynchronous self-attention model, we obtain question features $X_{(L)}$ and image features $Y_{(L)}$ that contain rich semantic information. To fuse the features of these two modalities, we use an MLP layer consisting of two fully connected layers to transform the multi-modal features. Then the softmax function calculates the attention weight α^X (or α^Y) for the question word features X_i^m (or the image region features Y_j^n). Finally, by multiplying the attention weights with the multi-modal features separately, we can obtain the final question features $\bar{X}$ and image features $\bar{Y}$. Using the question features as an example, the above process can be summarized in the following equations:

$$\alpha^X = softmax\left(MLP\left(X_{(L)}\right)\right) \tag{11}$$

$$\bar{X} = \sum_{i}^{m} \alpha_i^X X_{(L)i} \tag{12}$$

Similarly, we can obtain image features $\bar{Y}$ by using the same method.

Next, we embed features $\bar{X}$ and $\bar{Y}$ into the same dimension and project the multi-modal features onto a vector $F \epsilon \mathbb{R}^c$ by using a linear layer, where c represents the number of features classified in the training set. Finally, the sigmoid activate function is used to obtain the final classification. The formula can be expressed as:

$$f = LN\left(W_X^T \bar{X} + W_Y^T \bar{Y}\right) \tag{13}$$

$$F = Linear\left(f\right) \tag{14}$$

$$A = sigmoid\left(F\right) \tag{15}$$

where W_X^T and W_Y^T denote two linear projection matrices. In the final training process, as similar to the paper [39], we use binary cross-entropy (BCE) as the loss function to train the model.

4. Experimental Results

In this section, we conduct a series of experiments using the collaborative asynchronous self-attention model. Experiments will be conducted on the benchmark VQA v2 dataset to validate the model's performance. We provide a brief description of the parameter settings and conduct extensive ablation experiments on the number of layers of the depth model stack and multiple variants of the model under selected parameters in this section. Then, we show the model validity using attention visualization. Finally, we compare the performance with some of the previous state-of-the-art.

4.1. Implementation Details

Following [45], we set the number of heads h of the multi-head attention mechanism to 8, such a setting makes the originally 512-dimensional intermediate dimension d evenly distributed to the 8 heads, and the dimension of each head is $d_h = 64$. In terms of the number of layers, we set the number of model layers to $L\epsilon\{2, 4, 6\}$ and performed adequate experiments. During training, we set the batch size to 64 and applied the Adam optimizer with parameters $\beta_1 = 0.9$ and $\beta_2 = 0.98$. For all model training epochs and learning rate settings, we use 13 training epochs and set the base learning rate to $1e^{-4}$. The model starts training with an initial learning rate of one quarter of the base learning rate, which is gradually increased in subsequent training epochs until the learning rate becomes $1e^{-4}$, and remains constant in the tenth training epoch. Finally, the learning rate decreases in the following training epochs at a rate of 0.2 times every two epochs.

4.2. Datasets

All experiments in this paper are based on the most commonly VQA v2 dataset [11], which uses the MS-COCO dataset as well as question and answer pairs annotated by humans. Compared to the initial version of the VQA dataset, VQA v2 minimizes linguistic bias. In the VQA v2 dataset, each image corresponds to three questions and each question will have ten answers to be answered, the answer chosen most frequently will be considered the correct answer to the question. The entire dataset is divided into three parts: training set (train), validation set (val) and test set (test). Our training process will use both the training and validation sets described above and an additional vg dataset (the additional VQA samples from Visual Genome). After completing the training, the results will be uploaded online for evaluation. The test-dev and test-standard subsets, which divided by test set, will be used for online evaluation, and all training results will be evaluated online with more excellent stability and accuracy than local testing. All test results will be divided into four sections: Yes/No (Y/N), Number, Other and Qverall (All) accuracy.

4.3. Ablation Studies

Model Layers. We first proceeded with several ablation experiments on the layers of the model, which results are depicted in Fig. 5 and Table 1. The model's validity is discussed in detail in the light of the results.

As shown in Fig. 5, with the number of layer settings increasing, the performance of all three different models steadily increases in the other three test criteria (Yes/No, Number and Overall accuracy), except for the ASAM-Q model which decreases after 4 layers in terms of other. This verifies that the use of asynchronous self-attention components is effective for modeling self-attention as the depth of the model increases. It is also not hard to notice that when setting the number of layers to 2, the effect of using asynchronous self-attention on the question self-attention modeling (ASAM-Q) are higher than the other two models. The analysis shows that the word sequences in the question features are only 14-dimensional space, compared to the 100 object dimensions in the image features, and the question features can be focused on the correct words more quickly with the asynchronous self-attention component. However, as the depth of the model increases and the attention on the image continues to be refined, the accuracy of both the ASAM-QI and ASAM-I models gradually approaches or even surpasses that of the ASAM-Q model after 4 layers. In the case of the transition from 2 to 4 layers, the model performance improves rapidly and slows down when the transition from 4 to 6 layers, which also indicates a gradual saturation of the model performance as the depth increases. Therefore, we set our baseline model layer parameter to 6 layers, which saves the time cost of model training and also controls the number of parameters in the model.

Based on 6 layers, the accuracy of each model is presented in Table 1 for comparison with the MCAN model. The experimental results indicate that the ASAM outperforms the MCAN on all other problems except in the Number type. Specifically, it improves the model performance and does not increase the number of model parameters after using the asynchronous self-attention component.

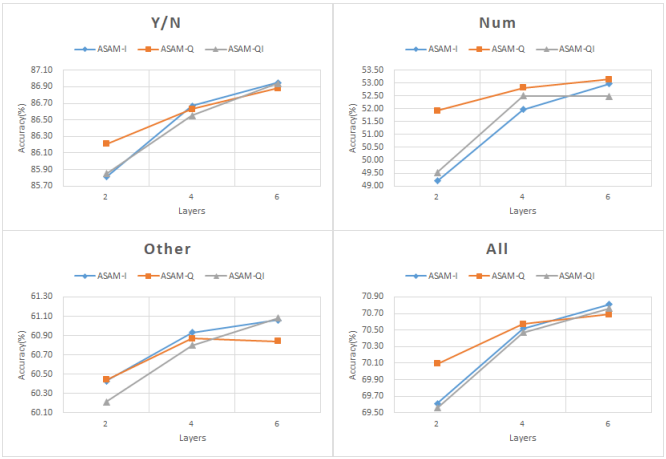

Fig. 5. Results of ablation on the ASAM-I, ASAM-QI, and ASAM-Q model layers

Model Variation. Table 2 and Fig. 6 present the results of the proposed ASAM model with a controller. As depicted in Table 2, incorporating a controller results in a further

Table 1. Accuracy of ASAM-Q, ASAM-QI and ASAM-I with six model layers on the test-dev of VQA v2

Model	Y/N	Number	Other	All
MCAN	86.82	53.26	60.72	70.63
ASAM-Q	86.88	53.15	60.84	70.69
ASAM-QI	86.94	52.48	61.08	70.76
ASAM-I	86.95	52.97	61.06	70.81

augmentation of the model's performance across various metrics, substantiating the effectiveness of the controller design. This observation highlights that the collaborative interaction between the asynchronous self-attention model and the controller can unlock more significant potential.

The performance of the basic model is compared with the performance of the model using the controller as shown in Fig. 6 (The blue part is the original model and the orange part is the model with the addition of the controller). Experimental results show that adding a controller is superior to the model without the controller in some of the test types as well as in overall accuracy, which further demonstrates that the controller we have designed optimizes the features to some extent and allows the model to locate the target location more accurately when converging on the attention. In addition, the figure also depicts the trend lines for the original model and the model with the added controller under different test contents. The results of the original model show an upward trend under all test contents except for a slight downward trend in the trend line for the original model under Y/N. This is one reason why we ended up using the model with the asynchronous self-attention component alone on the image as our baseline model.

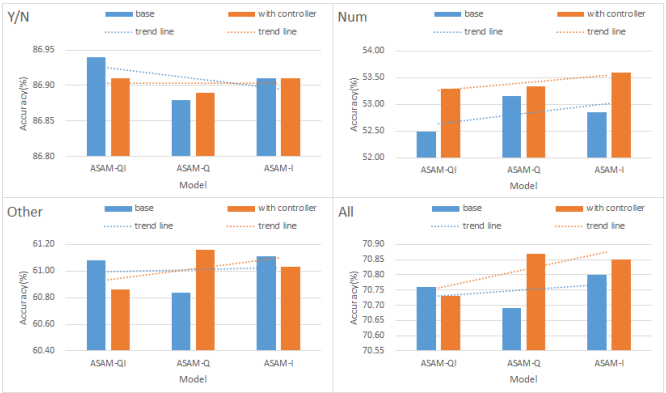

Fig. 6. Comparison between the original model and the model with the Controller

Table 2. Accuracy of ASAM-Q, ASAM-QI and ASAM-I model with controller on the test-dev and test-std set of VQA v2

	Test-dev Test-dev				**Test-std**
Model	**Y/N**	**Number**	**Other**	**All**	**All**
ASAM-QI(c)	86.91	53.29	60.86	70.73	70.96
ASAM-Q(c)	86.89	53.34	61.16	70.87	71.30
ASAM-I(c)	86.91	52.59	61.03	70.85	71.20

4.4. Comparison with State-of-the-Art

Table 3 lists the experimental results of the ASAM and the other state-of-the-art model on the benchmark dataset VQA v2. BUTD [1] used a bottom-up visual feature of attention and was the winning model in the 2017 VQA Challenge. In addition to focus on where to look, HieCoAttVQA [27] also focuses on what words to listen for, and the model was able to make joint inferences about attention to images and questions. Compared to other bilinear pooling methods, MFH [46] used generalized higher-order models to capture the more complex interactions between multi-modal features. BAN [18] effectively extends a single attention network using a bilinear attention mapping, and also keeps the computational cost constant while taking into account each pair of multimode input channels. Peng et al. [33] devised a self-guided word relation attention scheme and two problem-adaptive visual relation attention modules to explore the semantic latent relationships between words and extract precise binary relationships between objects. Qin et al. [34] propose a Residual Weight-Sharing Attention Network (RWSAN). By using a method that dynamically fuses multi-modal features with intra-modal and inter-modal information flow, DFAF [10] achieved high-level interaction between visual and language modalities. To understand the visual scene in an image, ReGAT [22] encoded the image as a graph and used the graph attention mechanism to model the objects in the graph with multiple types of relationships. Re-atten [12] reconstructs attention based on answer re-attention, which allows the model to re-learn visual objects in the image. Guo et al. [14] set thresholds for attention score to filter out the text or image features, to choose the most relevant information for predicting the correct answer and avoid the distract of unrelated question or image areas. MCAN [45] proposes a deep-modular co-attention network to address the issue of insufficient deep interactions in models, winning the 2019 VQA Challenge. MESAN [13] proposes top-k-based filter method of attention scores. From the experimental results, it is evident that the proposed method outperforms current state-of-the-art models across most metrics, except for a slight decrement in performance for Yes/No type questions. Compared to MCAN, ASAM also applied an encoder-decoder architecture and used an asynchronous self-attention (with controller) model on the images, with an overall accuracy 0.22 points higher than MCAN on test-dev and 0.3 points higher on test-std, with significant accuracy improvements on other validation metrics. This validates the superiority of our model for Visual Question Answering with leading performance.

Table 3. Accuracies of the model proposed in this paper on the Visual Question Answering Dataset VQA v2 to compare with the state-of-the-art methods

	Test-dev				Test-std
Model	**Y/N**	**Number**	**Other**	**All**	**All**
Bottom-up[1]	81.82	44.21	56.05	65.32	65.67
HieCoAttVQA[27]	79.70	40.00	59.80	65.80	66.10
MFH[46]	84.27	49.56	59.89	68.76	-
BAN[18]	85.31	50.93	60.26	69.52	-
MRA-Net[33]	85.58	48.92	59.46	69.02	69.46
RWSAN[34]	86.45	52.18	60.38	70.19	-
DFAF[10]	86.09	53.32	60.49	70.22	70.34
ReGAT[22]	86.08	54.42	60.33	70.27	70.58
Re-attn[12]	87.00	53.06	60.19	70.43	70.72
MCAN[45]	86.82	53.26	60.72	70.63	70.90
SCAVQA-I[14]	87.00	53.31	60.83	70.76	71.09
MESAN[13]	87.05	53.21	60.72	70.71	71.08
ASAM-QI	86.94	52.48	61.08	70.76	-
ASAM-Q	86.88	53.15	60.84	70.69	-
ASAM-I	86.95	52.97	61.06	70.81	-
ASAM-QI(c)	86.91	53.29	60.86	70.73	70.96
ASAM-Q(c)	86.89	53.34	61.16	70.87	71.30
ASAM-I(c)	86.91	52.59	61.03	70.85	71.20

4.5. Attention Visualization

Fig. 7 compares the visualization results of the MCAN with ASAM (The darker-colored parts are the model's attentional focus). In the Visual Question Answering task, the asynchronous self-attention mechanism proposed in this paper no longer singularly pursues fine-grained but takes a broader view of the image and retains as much information as possible. Each of the three examples in Fig. 7 combines the real situation, the situation predicted by the MCAN model, and the situation predicted by our model. The more highlighted areas in the image regions indicate that the model is focusing more attention on them. Based on the images, it is apparent that the model proposed in this paper focuses on objects from multiple perspectives, pinpointing the key objects and distracting some attention from other relevant objects. In the first instance, the man is playing a sport, and the model focuses not only on the man himself and the surfboard beneath his feet, but also the waves and ultimately get a valid answer. For the counting question in the example in the third column, our model covers all objects more comprehensively than the fine-granularity of the comparison model, and thus correctly answers the given question. It is not difficult to find that our model can always focus on more information, but this also implies another problem, which is information interference. When faced with problems requiring precise targeting of attention, MCAN reduces the interference of redundant information, which has more advantages.

5. Concluding Rewarks

This paper proposed an Asynchronous Self-Attention Model (ASAM) and a controller, balancing coarse-grained and fine-grained attention within the attention model for VQA. Its component can coordinate the relationship between the upper and lower attention layers and the VQA model using this component. The controller can retain other related object information as much as possible without reducing the attention on key objects. Experimental results and ablation studies on the benchmark dataset VQA v2 validate the effectiveness of the proposed model and demonstrate the effectiveness of coordinating the upper and lower attention layers to improve model performance. However, the choice of feature matching fusion method still needs to be continuously explored, and this is a direction for our future research. In future research, we will aim to explore more effective models and apply them to the field of Visual Question Answering to assist the models in better understanding visual and question features and to advance further the research work related to Visual Question Answering.

Fig. 7. Attention visualization result. The first row is the input images, questions and ground truth answers. The second is the baseline model MCAN. The third row is the proposed ASAM model

Acknowledgments. This work was supported in part by the National Natural Science Foundation of China (Grant No. 52331012) and the Natural Science Foundation of Shanghai under Grant 21ZR1426500.

References

1. Anderson, P., He, X., Buehler, C., Teney, D., Johnson, M., Gould, S., Zhang, L.: Bottom-up and top-down attention for image captioning and visual question answering. In: Proceedings of the IEEE conference on computer vision and pattern recognition. pp. 6077–6086 (2018)
2. Chen, C., Han, D., Chang, C.C.: Caan: Context-aware attention network for visual question answering. Pattern Recognition 132, 108980 (2022)
3. Chen, C., Han, D., Chang, C.: MPCCT: multimodal vision-language learning paradigm with context-based compact transformer. Pattern Recognit. 147, 110084 (2024)
4. Chen, C., Han, D., Shen, X.: CLVIN: complete language-vision interaction network for visual question answering. Knowl. Based Syst. 275, 110706 (2023)
5. Diao, C., Zhang, D., Liang, W., Li, K.C., Hong, Y., Gaudiot, J.L.: A novel spatial-temporal multi-scale alignment graph neural network security model for vehicles prediction. IEEE Transactions on Intelligent Transportation Systems (2022)
6. Diao, C., Zhang, D., Liang, W., Li, K., Hong, Y., Gaudiot, J.: A novel spatial-temporal multi-scale alignment graph neural network security model for vehicles prediction. IEEE Trans. Intell. Transp. Syst. 24(1), 904–914 (2023)
7. Ding, Y., Yu, J., Liu, B., Hu, Y., Cui, M., Wu, Q.: Mukea: Multimodal knowledge extraction and accumulation for knowledge-based visual question answering. In: Proceedings of the IEEE/CVF Conference on Computer Vision and Pattern Recognition. pp. 5089–5098 (2022)
8. Fan, Y., Xu, B., Zhang, L., Song, J., Zomaya, A.Y., Li, K.: Validating the integrity of convolutional neural network predictions based on zero-knowledge proof. Inf. Sci. 625, 125–140 (2023)
9. Gao, H., Mao, J., Zhou, J., Huang, Z., Wang, L., Xu, W.: Are you talking to a machine? dataset and methods for multilingual image question. Advances in neural information processing systems 28 (2015)
10. Gao, P., Jiang, Z., You, H., Lu, P., Hoi, S.C., Wang, X., Li, H.: Dynamic fusion with intra-and inter-modality attention flow for visual question answering. In: Proceedings of the IEEE/CVF conference on computer vision and pattern recognition. pp. 6639–6648 (2019)
11. Goyal, Y., Khot, T., Summers-Stay, D., Batra, D., Parikh, D.: Making the v in vqa matter: Elevating the role of image understanding in visual question answering. In: Proceedings of the IEEE conference on computer vision and pattern recognition. pp. 6904–6913 (2017)
12. Guo, W., Zhang, Y., Yang, J., Yuan, X.: Re-attention for visual question answering. IEEE Trans. Image Process. 30, 6730–6743 (2021)
13. Guo, Z., Han, D.: Multi-modal explicit sparse attention networks for visual question answering. Sensors 20(23), 6758 (2020)
14. Guo, Z., Han, D.: Sparse co-attention visual question answering networks based on thresholds. Applied Intelligence 53(1), 586–600 (2023)
15. Guo, Z., Han, D., Massetto, F.I., Li, K.C.: Double-layer affective visual question answering network. Computer Science and Information Systems 18(1), 155–168 (2021)
16. Han, D., Zhou, S., Li, K.C., de Mello, R.F.: Cross-modality co-attention networks for visual question answering. Soft Computing 25, 5411–5421 (2021)
17. He, K., Zhang, X., Ren, S., Sun, J.: Deep residual learning for image recognition. In: 2016 IEEE Conference on Computer Vision and Pattern Recognition, CVPR 2016, Las Vegas, NV, USA, June 27-30, 2016. pp. 770–778. IEEE Computer Society (2016)

18. Kim, J.H., Jun, J., Zhang, B.T.: Bilinear attention networks. Advances in neural information processing systems 31 (2018)
19. Krishna, R., Zhu, Y., Groth, O., Johnson, J., Hata, K., Kravitz, J., Chen, S., Kalantidis, Y., Li, L.J., Shamma, D.A., et al.: Visual genome: Connecting language and vision using crowdsourced dense image annotations. International journal of computer vision 123, 32–73 (2017)
20. Li, H., Han, D., Chen, C., Chang, C., Li, K., Li, D.: A visual question answering network merging high- and low-level semantic information. IEICE Trans. Inf. Syst. 106(5), 581–589 (2023)
21. Li, J., Han, D., Wu, Z., Wang, J., Li, K., Castiglione, A.: A novel system for medical equipment supply chain traceability based on alliance chain and attribute and role access control. Future Gener. Comput. Syst. 142, 195–211 (2023)
22. Li, L., Gan, Z., Cheng, Y., Liu, J.: Relation-aware graph attention network for visual question answering. In: Proceedings of the IEEE/CVF international conference on computer vision. pp. 10313–10322 (2019)
23. Li, S., Gong, C., Zhu, Y., Luo, C., Hong, Y., Lv, X.: Context-aware multi-level question embedding fusion for visual question answering. Inf. Fusion 102, 102000 (2024)
24. Liang, W., Yang, Y., Yang, C., Hu, Y., Xie, S., Li, K., Cao, J.: Pdpchain: A consortium blockchain-based privacy protection scheme for personal data. IEEE Trans. Reliab. 72(2), 586–598 (2023)
25. Lin, W., Chen, J., Mei, J., Coca, A., Byrne, B.: Fine-grained late-interaction multi-modal retrieval for retrieval augmented visual question answering. In: Oh, A., Naumann, T., Globerson, A., Saenko, K., Hardt, M., Levine, S. (eds.) Advances in Neural Information Processing Systems 36: Annual Conference on Neural Information Processing Systems 2023, NeurIPS 2023, New Orleans, LA, USA, December 10 - 16, 2023 (2023)
26. Long, J., Liang, W., Li, K.C., Wei, Y., Marino, M.D.: A regularized cross-layer ladder network for intrusion detection in industrial internet of things. IEEE Transactions on Industrial Informatics 19(2), 1747–1755 (2022)
27. Lu, J., Yang, J., Batra, D., Parikh, D.: Hierarchical question-image co-attention for visual question answering. Advances in neural information processing systems 29 (2016)
28. Ma, F., Zhou, Y., Rao, F., Zhang, Y., Sun, X.: Image captioning with multi-context synthetic data. In: Wooldridge, M.J., Dy, J.G., Natarajan, S. (eds.) Thirty-Eighth AAAI Conference on Artificial Intelligence, AAAI 2024, Thirty-Sixth Conference on Innovative Applications of Artificial Intelligence, IAAI 2024, Fourteenth Symposium on Educational Advances in Artificial Intelligence, EAAI 2014, February 20-27, 2024, Vancouver,Canada. pp. 4089–4097. AAAI Press (2024)
29. Malinowski, M., Rohrbach, M., Fritz, M.: Ask your neurons: A neural-based approach to answering questions about images. In: Proceedings of the IEEE international conference on computer vision. pp. 1–9 (2015)
30. Mao, A., Yang, Z., Lin, K., Xuan, J., Liu, Y.J.: Positional attention guided transformer-like architecture for visual question answering. IEEE Transactions on Multimedia (2022)
31. Nam, H., Ha, J.W., Kim, J.: Dual attention networks for multimodal reasoning and matching. In: Proceedings of the IEEE conference on computer vision and pattern recognition. pp. 299–307 (2017)
32. Nguyen, B.X., Do, T., Tran, H., Tjiputra, E., Tran, Q.D., Nguyen, A.: Coarse-to-fine reasoning for visual question answering. In: Proceedings of the IEEE/CVF Conference on Computer Vision and Pattern Recognition. pp. 4558–4566 (2022)
33. Peng, L., Yang, Y., Wang, Z., Huang, Z., Shen, H.T.: Mra-net: Improving vqa via multi-modal relation attention network. IEEE Transactions on Pattern Analysis and Machine Intelligence 44(1), 318–329 (2020)
34. Qin, B., Hu, H., Zhuang, Y.: Deep residual weight-sharing attention network with low-rank attention for visual question answering. IEEE Transactions on Multimedia (2022)

35. Ren, M., Kiros, R., Zemel, R.: Exploring models and data for image question answering. Advances in neural information processing systems 28 (2015)
36. Ren, S., He, K., Girshick, R., Sun, J.: Faster r-cnn: Towards real-time object detection with region proposal networks. Advances in neural information processing systems 28 (2015)
37. Shen, X., Han, D., Zong, L., Guo, Z., Hua, J.: Relational reasoning and adaptive fusion for visual question answering. Appl. Intell. 54(6), 5062–5080 (2024)
38. Sturman, D.J., Zeltzer, D.: A survey of glove-based input. IEEE Computer graphics and Applications 14(1), 30–39 (1994)
39. Teney, D., Anderson, P., He, X., Van Den Hengel, A.: Tips and tricks for visual question answering: Learnings from the 2017 challenge. In: Proceedings of the IEEE conference on computer vision and pattern recognition. pp. 4223–4232 (2018)
40. Vaswani, A., Shazeer, N., Parmar, N., Uszkoreit, J., Jones, L., Gomez, A.N., Kaiser, L., Polosukhin, I.: Attention is all you need. In: Advances in Neural Information Processing Systems 30: Annual Conference on Neural Information Processing Systems 2017, December 4-9, 2017, Long Beach, CA, USA. pp. 5998–6008 (2017)
41. Wang, Y., Yasunaga, M., Ren, H., Wada, S., Leskovec, J.: Vqa-gnn: Reasoning with multimodal knowledge via graph neural networks for visual question answering. In: Proceedings of the IEEE/CVF International Conference on Computer Vision. pp. 21582–21592 (2023)
42. Xia, H., Lan, R., Li, H., Song, S.: ST-VQA: shrinkage transformer with accurate alignment for visual question answering. Appl. Intell. 53(18), 20967–20978 (2023)
43. Yan, S., andWeifeng Chen, M.B., Zhou, X., Huang, Q., Li, L.E.: Vigor: Improving visual grounding of large vision language models with fine-grained reward modeling. CoRR abs/2402.06118 (2024)
44. Yang, Z., He, X., Gao, J., Deng, L., Smola, A.: Stacked attention networks for image question answering. In: Proceedings of the IEEE conference on computer vision and pattern recognition. pp. 21–29 (2016)
45. Yu, Z., Yu, J., Cui, Y., Tao, D., Tian, Q.: Deep modular co-attention networks for visual question answering. In: IEEE Conference on Computer Vision and Pattern Recognition, CVPR 2019, Long Beach, CA, USA, June 16-20, 2019. pp. 6281–6290. Computer Vision Foundation / IEEE (2019)
46. Yu, Z., Yu, J., Xiang, C., Fan, J., Tao, D.: Beyond bilinear: Generalized multimodal factorized high-order pooling for visual question answering. IEEE transactions on neural networks and learning systems 29(12), 5947–5959 (2018)
47. Zheng, W., Yin, L., Chen, X., Ma, Z., Liu, S., Yang, B.: Knowledge base graph embedding module design for visual question answering model. Pattern recognition 120, 108153 (2021)
48. Zhou, Y., Ren, T., Zhu, C., Sun, X., Liu, J., Ding, X., Xu, M., Ji, R.: TRAR: routing the attention spans in transformer for visual question answering. In: 2021 IEEE/CVF International Conference on Computer Vision, ICCV 2021, Montreal, QC, Canada, October 10-17, 2021. pp. 2054–2064. IEEE (2021)

Han Liu received a B.S. degree in computer networking from the Shenyang Normal University, Shenyang, China, in 2013, and the M.S. and Ph.D. degrees in computer software & theory and information management & information systems from the Shanghai Maritime University, Shanghai, China, in 2016 and 2022, respectively. He is a Postdoctoral Fellow with the Department of Logistics, Shanghai Maritime University, Pudong, China, in 2022. His main research interests include blockchain, IoT, cloud security, and machine learning.

Dezhi Han received a B.S. degree in applied physics from the Hefei University of Technology, Hefei, China, in 1990, and the M.S. and Ph.D. degrees in computing science from

the Huazhong University of Science and Technology, Wuhan, China, in 2001 and 2005, respectively. He is a Professor with the Department of Computer, Shanghai Maritime University, Pudong, China, in 2006. His research interests include cloud and outsourcing security, wireless communication security, network and information security, and visual question answering.

Shukai Zhang received an M.S. from the School of Information Engineering at Shanghai Maritime University, China. His research interest is visual question answering.

Jingya Shi is pursuing an M.S. at the School of Information Engineering at Shanghai Maritime University, China. Her current research interest is visual question answering.

Huafeng Wu received a Ph.D. degree in computer science from Fudan University in 2009, a master's degree in traffic information engineering and control from Dalian Maritime University in 2004, conducted Postdoctoral Research at Carnegie Mellon University from 2008 to 2009, and also a Visiting Scholar with Shanghai Jiao Tong University from 2012 to 2013. He is currently a Professor and a Ph.D. Supervisor with the Merchant Marine College, Shanghai Maritime University. His research interests include the Internet of Shipping, the Internet of Things, and wireless sensor networks. He also serves as an Editorial Board Member for the Computer Communications journal.

Yachao Zhou received a B.S. degree from Beijing University of Posts and Telecommunications, an M.S. from Tsinghua University, Beijing, China, and a Ph.D. from Dublin City University, Dublin, Ireland. She is the chief scientist of Technology Co., Ltd. Her specific interests include big data and cloud computing, cybersecurity, and deep packet inspection.

Kuan-Ching Li is a Life Distinguished Professor at Providence University, Taiwan. He is a recipient of distinguished and chair professorships from universities in several countries and awards and funding support from a number of agencies and high-tech companies. Besides publishing numerous journal articles, book chapters, and refereed conference papers, he is co-author/co-editor of more than 50 technical professional books published by CRC Press/Taylor & Francis, Springer, and McGraw-Hill. His research interests include parallel and distributed computing, Big Data, and emerging technologies. He is a senior member of the IEEE and a fellow of the IET.

Received: March 21, 2024; Accepted: September 17, 2024.

Computer Science and Information Systems 22(1):219–238 https://doi.org/10.2298/CSIS240227001X

Medical Images Anomaly Detection for Imbalanced Datasets with Multi-scale Normalizing Flow

Yufeng Xiao[1,2,3], Xueting Huang[1,2,3],Wei Liang[1,2,3,⋆], Jingnian Liu[1,2,3], Yuxiang Chen[1,2,3], Rui Xie[1,2,3], Kuanching Li[1,2,3,⋆] and Nam Ling[4]

[1] School of Computer Engineering and Science, Hunan University of Science and Technology, Xiangtan 411100, China
[2] Sanya Research Institute, Hunan University of Science and Technology, Sanya 572024, China
[3] Hunan Key Laboratory for Service Computing and Novel Software Technology, Xiangtan 411201, China
hnxiaoyf@hnust.edu.cn
HXuetingmail@163.com
wliang@hnust.edu.cn
jingnianl@mail.hnust.edu.cn
chenyuxiang@hnust.edu.cn
xierui54@mail.hnust.edu.cn
aliric@hnust.edu.cn
[4] Department of Computer Science and Engineering, Santa Clara University, USA
nling@scu.edu

Abstract. Due to the substantial feature extraction and end-to-end learning capability, deep learning has been widely used in intelligent medical image detection. However, amount of parameters in these models relies on the number of labeled training data, which influences the performance. Due to this reason, we propose a novel unsupervised medical image detection model named Multi-Scale Normalizing Flow (MS-NF). First, a fusion backbone network is applied to extract the multi-scale feature maps, which capture the different scale features of the anomalies. Second, normalizing flow transfers the abnormal distribution into the normal distribution hidden in the latent space, which is used for anomaly detection. To further improve the detection performance, channel and spatial convolutional attention mechanisms are integrated to make the model focus on the anomalous region by a shared network. Experimental results obtained on brain tumor MRI and ISIC2018 datasets show that MS-NF improves the pixel-level AUC index by 9% compared to existing medical image detection models, also performing well on small-scale data with efficient training and inference.

Keywords: Anomaly Detection, Unsupervised learning, Attention Mechanisms, Normalizing Flow, Medical Images.

1. Introduction

Medical image anomaly detection through image processing and deep learning can automatically detect anomalies and localize abnormal regions. It has been widely applied in assisted diagnosis, treatment, condition assessment, and medical decision support. In the

⋆ Corresponding authors

past decade, diverse machine learning models has been introduced to establish anomaly detection models, such as SVM [24], Decision Trees, and KNN. These models take the handcrafted features as the input, which heavily relies on expert knowledge. Moreover, the shallow structure of machine learning limits their capability to learn the deep representations hidden in the medical images.

Unlike traditional machine learning, Deep Learning (DL), which consists of a large number of hidden layers and nodes, can distill the complex features hidden in the data. Since it has successfully been applied in the Internet of Things [20, 3, 14], Blockchain[19, 39, 41], Quality of Service [17, 18], data recovery [16, 10], DL is also introduced to fuse low- and high-dimensional image features by jump-joining in the field of the medical image detection. Taking advantage of learning ability, it can effectively extract low- and high-resolution features of medical images when containing noise, blurred boundaries, and so on**??**. Indeed, automatic feature extraction can improve the effectiveness and performance of the training model.

Undoubtly, medical image detection is a supervised task, while DL is a data-driven model. Their performance heavily depends on the number of the training dataset. However, it is time-consuming to obtain the amount of high-quality labeled medical images that rely on professional knowledge. In other words, the procedure of the annotation is subjective and inconsistent. Worse, abnormal medical images are usually scarce compared to the normal samples. Therefore, training the medical images often faces the challenge of data imbalance in real-world application scenarios. It means that deep learning mainly learns the hidden representations of the normal samples, making it difficult to recognize the abnormal samples. Meanwhile, the location of the lesion is uncertain that has a variety of shapes and sizes.

To avoid the dependence on the labeled data, a diversity of unsupervised models are introduced to process the medical image detection, such as variational Autoencoder (VAE) [12], generative adversarial network (GAN) [4] and their variational models [11, 13]. The core idea of these models is to transform the abnormal region into a normal medical image which can generate a new abnormal medical image. The generated image is optimized by the differences between it and the original image. Therefore, the augmented medical images are helpful for lesion detection and localization. However, the performance is still affected by the inherent shortage of the generative models. For VAE, the high-dimensional data is mapped into the low-dimensional hidden feature space that may cause information loss. When performing reconstruction processing, the generated image is usually blurred, which harms medical image detection. Different from VAE, GAN directly models the distribution of the data. Nevertheless, it faces the challenges of training instability, gradient disappearance, and mode collapse. Denoising Diffusion Probabilistic Models (DDPM) is another popular generative model that generates high-quality samples without adversarial training. The self-encoder component in the DDPM denoises and restores the anomalous medical images corrupted by Gaussian noise. Since the denoising processing is carried out at each step, the model converges slowly.

Another common medical image detection method is to learn the distribution of normal data using deep learning. The anomalies are identified by distinguishing whether the distribution satisfies the normal data. It comprises two components: the feature extraction network and the distribution estimation network. The feature distribution of normal data is learned using deep convolutional networks, such as Resnet or visual architecture Vit

based on transformer [36]. Then, normalizing flow is implemented to estimate the feature distribution likelihood of the sample data, which is used for classification. Though this method has widely been applied in industrial anomaly detection, though seldom used in the medical field.

Taking advantage of the coupling layers, a novel inverse neural network is established to estimate the distribution of the abnormality. Specifically, a backbone is used to extract the feature maps in terms of different scales, which are split into two parts. A trained normalizing flow takes them as input and splices them into the output matrix. According to the matrix, the likelihood probability between anomalous and healthy data is calculated to recognize the anomalies. Several public datasets, such as ISIC 2018 and Brain MRI, are chosen to evaluate the effectiveness of the proposed model. The contributions of this work are summarized as follows.

- A novel unsupervised model with normalizing flow is proposed for medical image detection, which can automatically identify the differences between normal and abnormal data. The differences are used to generate new abnormal medical images. These generated images are implemented to train the model, which can relieve the dependence on abnormal medical images.
- The proposed model integrates the convolutional attention mechanism and normalizing flow, which makes it easy to focus on the critical features. It can improve the detection performance.
- Experiments conducted on several public datasets show that the proposed model is superior to other state-of-the-art models.

The remainder of this article is organized as follows. The related work is introduced in Section 2. The methodology of the proposed model is described in Section 3. The experiments are discussed in Section 4. Concluding remarks and future directions are drawn in Section 5.

2. Related Work

Deep learning has been widely used to learn the features hidden in medical images. To relieve the dependence on the labeled data, unsupervised models are introduced to apply in medical image detection. They can roughly divided into two categories, including feature- and reconstruction-based models.

2.1. Feature-based Unsupervised Models

Feature-based models usually aim to perform feature extraction and distribution transformation. They can learn the critical information hidden in the latent feature space used to detect anomalies. For example, some pre-training models, such as AlexNet, VGG, which train deep neural networks on the large-scale dataset Imagenet are widely implemented to extract features from the medical images. Compared with AlexNet, VGG, which has a deeper network structure and smaller convolutional kernels, achieves better performance[15]. However, it faces the challenges of gradient vanishing, gradient explosion, and degradation. He *et al.* proposed a novel model Resnet by introducing the structure

of residual connection to convolutional neural networks. It can effectively solve these problems by selecting the operation of skipping part of the layers [9]. Most of the work, anomaly detection based on unsupervised models, takes Resnet as the backbone network to extract features[29]. Some researches [21] use transformers-based visual networks Vit, DeiT, and their variations for unsupervised anomaly detection. Vit [6] and DeiT [34] use a self-attentive mechanism to extract features with better migration capabilities. Transferring learning across different visual tasks gives it better generalization to deal with multi-tasks. In addition, Vit and DeiT are more adaptable to large-scale datasets and robust to changes in data augmentation than other state-of-the-art models.

For distribution transformation, the mean and variance of normal features are used to model the normal distribution. When the probability distribution of the input data significantly deviates from the true distribution, it is recognized as an anomalous medical image. Normalizing Flows (NF) is a generative model, consisting of a series of invertible transformations[28]. It can learn probability distributions by mapping one distribution to another one. Combining these mappings forms a complete flow that can transform a complex distribution into a simple probability distribution. To address the problem of the poor efficiency of INN training and inference, Dinh et al. proposed Real-NVP by using reversible, local affine transformations to transform regularized streams of data distributions, which can improve computational efficiency[5]. Rudolph et al. presented Differnet, which accomplishes image detection through likelihoods provided by Normalizing Flow on multi-scale image features with multi-transform evaluation [30]. Compared to other models, Differnet requires fewer training samples. These works show promising results in the field of anomaly detection. Existing methods are based on reconstruction, and few works have applied them to medical image detection.

2.2. Reconstruction-based Methods for Generative Modeling

Variational Autoencoder(VAE) contains an encoder and a decoder. The encoder aims to learn the features hidden in the latent space and the decoder reconstructs the input data according to the latent features. Van et al. proposed a discretized VAE with a code book approach to learning the data distribution instead of VAE. However, it cannot generate high pixel-level samples[35]. Consequently, Razavi et al. introduced a hierarchical structure to propose VQ-VAE2[27]. It extends the number of discrete codebooks from the original thousands to millions that can capture the local features of the data in detail. Esser et al. incorporates a transformer structure, which generates millions of pixels[7]. In addition, the autoencoder is used to model the distribution of the normal data for medical image detection. The sample deviates from the distribution of the normal data that can be classified as abnormal data. Zimmerer et al. proposed a combination of density-based and reconstruction-based anomaly detection models that do not require labeled data and allow for anomaly scoring and localization of samples[43]. However, using VAE to reconstruct, the re-generated image is blurred, and anomalous regions may be retained. Nevertheless, VAE has been gradually replaced by subsequent competitive models.

The training of GAN is based on a set of neural networks that fight against each other. The generator generates the new data, which is discriminated the true or false by the discriminator [4]. The generator then adjusts its parameter weights according to the classification results of the discriminator to generate more realistic images. Based on [4], Radford et al. proposed Deep Convolutional GAN (DCGAN), which uses Convolutional

Neural Networks (CNNs) as generators and discriminators to produce higher-quality images. The experimental results show better image synthesis results[26]. Arjovsky et al. proposed Wasserstein GAN (WGAN), which uses Wasserstein distance to measure the difference between generated samples and real samples. It can overcome the instability when training GANs, which perform better image generation and speech synthesis [8]. Zhu et al. introduced CycleGAN to image translation tasks, which converts an image from one domain to an image from another domain [42]. Compared to the previously mentioned methods, CycleGAN does not require training data pairs and can be trained without matching data. Karras et al. proposed a Style-Based Generative Adversarial Network (StyleGAN), which uses a new generator architecture, including a style network and a generative network, to generate higher-resolution and more realistic images. Brock et al. proposed BigGAN, using more extensive networks and more sophisticated training strategies to generate higher-quality images, and has achieved leading results in various image-generation tasks[2].

GAN and its derived models are influential in anomaly detection. The generator can simulate the distribution of the real data. Therefore, if the input data differs significantly from the data generated by the generator, it can be considered anomalous data. Schleg et al. proposed AnoGAN, which is the first GAN-based anomaly detection method [32]. The normal sample distribution is obtained by trained DCGAN to find the abnormal region of the sample. To address the slow model speed of the technique in [32], Schleg et al. proposed an unsupervised anomaly detection method using GANS called F-AnoGAN [31], to replace the iterative optimization used in AnoGAN with a fast approximation algorithm based on Wasserstein distance. This approximation generates a latent representation of the normal data and a reconstruction loss for normal and abnormal samples. The reconstruction loss is used to score each sample and determine whether it is normal or abnormal. Bhatt et al. uses progressive GANs to improve the resolution of detecting anomalies, allowing for the processing of more detailed images [1]. However, the above adversarial generative network-based approach still suffers from training instability and difficulty in capturing the complete data distribution of the image.

Wyatt et al. first applied diffusion modeling to the field of anomaly detection and achieved good detection results in industrial, medical image detection, and other areas [38]. A more extensive range of anomalous regions can be recovered by replacing Gaussian noise with simple noise. Teng et al. applied a score-based model to visual defect detection [33]. Pinaya et al. proposed an encoder model for anomaly segmentation of medical images [23].

MRI images usually are low quality and have poor contrast due to image projection and laminar imaging processes. The boundaries between biological tissues are often blurred and difficult to detect, which makes it difficult for generative reconstruction methods to accomplish the task of pixel-level image segmentation. In contrast to the generative model, the proposed MS-FLOW can estimate the exact likelihood value. Therefore, it can accurately detect Out-Of-Distribution (OOD) samples. Moreover, it does not require a large amount of data for training and is more stable in training, with shorter convergence time and faster inference.

3. Methodology

To relieve the dependence on the label information and achieve a good performance, we propose a novel unsupervised model, MS-NF, which can detect and locate anomalous regions in medical images. The framework of the MS-NF is shown in Fig. 1, which consists of two components, including a feature extraction network and a distribution transformation network. Concretely, the first three residual blocks of Resnet18 are considered the backbone for feature extraction, whose outputs are fed into the distribution transformation network. Then, a normalizing flow transforms the feature maps into the latent space, where convolutional operation preserves the 2-dimensional information of the medical image. Moreover, a convolutional attention mechanism is applied to make the model more focused on the critical region of the medical image. This section details the proposed model's principles and presents the training and inference procedure.

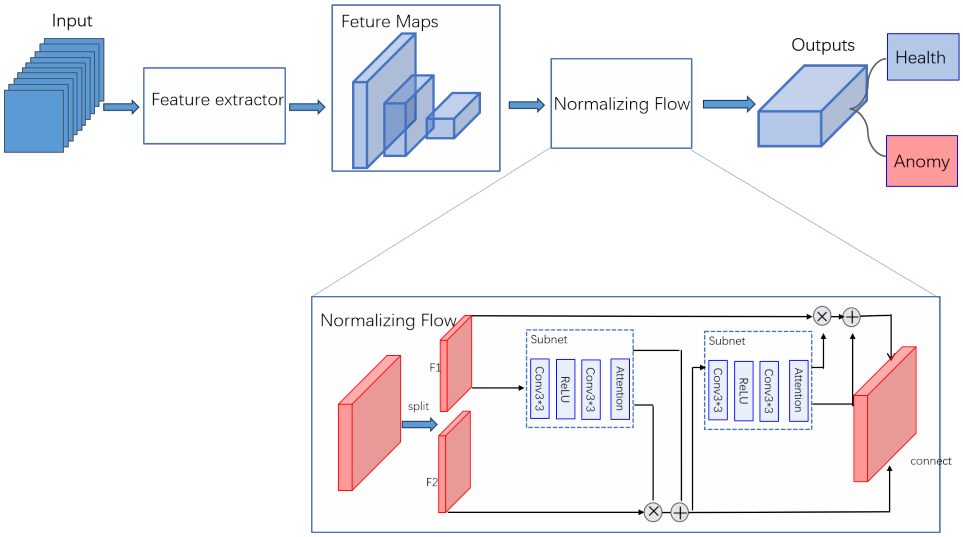

Fig. 1. The detailed view of MS-FLOW

3.1. Feature extraction network

Given a medical image, we denote it as $x \sim p(x)$, where x belongs to $X(x_1, x_2.....)$. The backbone network is formed by deep convolutional neural network, such as Resnet or visual transformer-based network model Vit. Since these pre-training models is optimized by amount of images, it can be used to extract the critical features hidden in the medical images. Assuming ex: $X \rightarrow F$, it transforms the original information hidden in the image x to the high-level feature representation. There are some lesions or tumors in the abnormal regions, which have a diversity of characteristics in different organ. Therefore, it is important to extract the global information of the medical images. In this paper, we use

the residual block of Resnet18 to extract features, which can learn the local and global information. And the last last layer of each residual block is implemented to capture the connection between local and global features. These features are fed into normalizing flow later.

3.2. Distribution transformation network

This article takes normalizing flow as the distribution transformation network, which transforms the image feature F into the latent space L. This is done to compute exactly the distributional likelihood for each feature element $f \in F$. Since the training consists entirely of normal samples, in the inference phase, the likelihood of the abnormal information in the medical images will be mapped to the edges of the distribution. At this point, a threshold is set to distinguish between abnormal and normal. The process of normalizing flow consists of a series of stacked invertible differentiable functions. The process of going from the characteristic distribution F to the Gaussian distribution L undergoes some series of flow changes. There is a one-to-one mapping relationship between the image features and the corresponding latent space features, and it can be expressed as $T : F \rightarrow L$. In other words, they are reversible. Assuming the processing stack is a series of transformation functions, it can be expressed as.

$$L = T_1(F) \circ T_2 \circ T_3 ... T_K. \tag{1}$$

Therefore, the anomalies that deviate from the distribution of the normal data can be restored to the original image according to the stacking invertible functions.

$$F = T_K(L) \circ T_{K-1} \circ T_{K-2} ... T_1, \tag{2}$$

Setting $l = T_\theta(f)$, the following expression for calculating the likelihood of the characteristic distribution can be obtained by applying variable substitution to Equation. 2:

$$\log p_\theta(f) = \log p_\theta(l) + \log \left| \det \left(\frac{\partial l}{\partial f} \right) \right| \tag{3}$$

Due to the properties of the flow-varying bijection, Equation.4 can be converted to Equation.5 by the chain rule:

$$log p_\theta(f) = \log p_\theta(l) + \sum_{i=1}^{k} \log \left| \det \left(\frac{\partial T_k(l)}{\partial T_{k-1}(l)} \right) \right| \tag{4}$$

The exact likelihood for the sample features is computed by transforming f into l. The parameters of the target distribution are optimized by maximizing the log-likelihood, where transformation network T is implemented by normalizing the flow component. The construction of the normalizing flow component is shown in Fig. 1. Therefore, the distribution transformation network stacks several normalizing flow components. Moreover, we introduce coupling layers according to [23, 40]. Concretely, the input data x is first separated into two parts x_1 and x_2. Transformations are respectively performed on x_1 and x_2 using normalizing flow. When the 2-dimensional flow layer transforms the 2-dimensional image into 1-dimensional space, it may occur the loss of medical image

information may make the distribution transformation unstable. Consequently, 3×3 convolutional kernel is used to retain the 2-dimension information. The intermediate quantity y_1 is obtained by combining x_1 to x_2 using an invertible transformation.

$$y_1 = e^{sub_1(x_1)} \odot x_2 + sub_2(x_1) \tag{5}$$

Then, continue to perform transformations on y_1 using subnet. Finally, y_1 and y_2 are combined to get the final output tensor y:

$$y_2 = e^{sub_1^{'}(y_1)} \odot x_1 + sub_2^{'}(y_1) \tag{6}$$

$$y = concat(y_1, y_2) \tag{7}$$

where sub represents the normalizing flow component consisting of convolutional and attention layers. For the separation of x and y_1, it is performed on the channel. Respectively, the symbols $\odot$ and $+$ denote multiplication and addition along the feature direction.

3.3. Convolutional Attention

Medical images suffer from problems such as blurred boundaries and unclear imaging. In this work, to enable the NF module to focus more on the image region of interest for the detection task and thus improve the detection ability of the model. Therefore, the attention mechanism based on the convolutional block is embedded between the convolutional layers [37]. The detection performance is improved without significantly increasing the number and complexity of model parameters. Convolutional attention consists of two parts: channel attention and spatial attention. The intermediate feature map F, obtained by the NF module subnet, enters the channel attention layer and the spatial attention layer successively in order. The entire process can be summarized as follows:

$$F_i = A_c(F) \otimes F \tag{8}$$

$$F_o = A_s(F_i) \otimes F_i \tag{9}$$

The channel attention layer focuses on the information that is meaningful in the features. Through average pooling and maximum pooling, two feature vectors are generated and fed into a shared network. This shared network is a Multi-Layer Perceptron (MLP) with a hidden layer. Once the two feature vectors have passed through the forward network, the features are then merged for each element at the same location:

$$A_c\left(F\right) = \sigma\left(MLP\left(AvgPool\left(F\right)\right) + MLP\left(MaxPool\left(F\right)\right)\right) \tag{10}$$

Spatial attention focuses on where the features have the most information. Two feature vectors will be generated by average pooling and maximum pooling operations. The convolution operation is performed on these two feature vectors to get the spatial attention map:

$$[A_s\left(F\right) = \sigma\left(conv^{7\times7}\left(\left[AvgPool\left(F\right); MaxPool\left(F\right)\right]\right)\right)] \tag{11}$$

where σ represents a sigmoid function, while $conv$ represents the convolution operation with a kernel size of 7×7. By combining channel attention and spatial attention, we capture inter-channel dependencies and intra-channel spatial relationships to enhance the performance of the proposed model. The two attention mechanisms can be used in parallel or a sequential order. In this work, we adopt the arrangement proposed in [37], which integrates channel attention and then incorporates spatial attention.

We use the following algorithm 1 to construct our MS-NF module as a sub-network of the feature transformation module: the details are as follows: first input the backbone features f, the convolution size $kernel\_size$, and the $reduction$ that controls the proportion of dimensionality reduction in the channel's attention mechanism. Next, the features f at the different scales are input to each nf module in order. For each module, a sequence of reversible neural networks is created. The feature f will be successively processed by the 2D convolution, the RELU, the 2D convolution, and the convolutional attention layer, and the transformed feature probabilities will continue to be sent to the next nf module until the end of the loop.

Algorithm 1: Normalizing flow with attention

Input: Image features f, kernel_size, reduction
Output:y
Procedure:
  Initialize()
    $c1 \leftarrow$ `conv2d`(in_channels, hidden, kernel_size $=$ cc)
    $ac \leftarrow$ `relu`()
    $c2 \leftarrow$ `conv2d`(hidden, out, kernel_size $= \ldots$)
    $att \leftarrow$ `Attention`(reduction $= 16$)
  for nf_i in NF_n :
    $y \leftarrow$ `conv2d`(F)
    $y \leftarrow$ `relu`(y)
    $y \leftarrow$ `conv2d`(y)
    $y \leftarrow$ `att`(y)
  end for

3.4. Training and Inference

For normalizing flow, the model is trained entirely on normal medical images. We would like to get the exact likelihood value of the sample feature distribution, but it isn't easy to solve pf directly. So the log-likelihood of the feature $f \in F$ is estimated by, *i.e.*, the potential space, as shown in Equation 12. The method aims to find suitable parameters to maximize the probability density function of the feature f extracted by the backbone. Therefore, the loss is defined as follows:

$$loss = -\log p_\theta(f) = -\log p_\theta(l) - \log \left| \det \frac{\partial l}{\partial f} \right| \tag{12}$$

Algorithm 2: Training and Inference

Input: Image image x
Output:y
Procedure:
  Feature_exactor ← create_model(resnet18,pretrained=False,features=true,
  out_indices=[1,2,3,],in_chans=1)
  f ← Feature_exactor(x)
  output,log_jac_dets ← nfblock(f)
  $loss \leftarrow \frac{\|z\|_2^2}{2} - \log \left| \det \frac{\partial z}{\partial f} \right|$
  If not training
    anomap mean(output**2,dim=1)
  return anomap

In the inference stage, because the anomalous features never appear in the training data, the probability density function of the anomalous features obtained by the model is lower than that of the normal data. When the normalization flow transforms the abnormal features into the latent space, the data distribution lies in different intervals. When T_{NF} transforms the anomalous features into the latent space, a different distribution is obtained. The likelihood of the features can be used as an anomaly score in detection. We set a threshold τ, for a normal image. The likelihood on the feature map is more significant than τ:

$$Ano = \begin{cases} 1, p_L\left(T_\theta\left(F\left(x\right)\right)\right) > \tau \\ 0, p_L\left(T_\theta\left(F\left(x\right)\right)\right) < \tau \end{cases} \tag{13}$$

When $Ano = 1$, it means there is an anomaly in the current medical image.

The following is our training and inference algorithm. It is done as follows. First, the backbone network of resnet18 is constructed for feature extraction, and the loss function for training is obtained according to Eq. (10) to optimize the parameters. If the model is in the inference stage, the likelihood of the probability distribution of each pixel point is calculated, and then an anomaly map is obtained for anomaly detection.

4. Experimental Results

In this section, we evaluate the performance of the proposed model MS-FLOW, which is compared with other state-of-the-art methods collected in the literature [31] [38] [40]. In addition, ablation experiments are performed to verify the influence of each model component.

4.1. Datasets

Normalizing flow learns the distribution of the sample data, while the abnormal data are outside the distribution. The training process is performed entirely on normal datasets. The training set is divided into two parts, including brain MRI impact and dermatologic images. The brain MRI images is NFBS dataset [25]. The test set is a neuroimaging

dataset of brain tumor patients (NIBT) [22]. NFBS dataset consists of 125 T1-weighted MRI (magnetic resonance images) with the size of $256 \times 256 \times 192$. In this paper, only single slices of the transverse axis are considered, and a single-channel image of size 256×256 is intercepted. Since most of the critical information of brain MRI images is concentrated in the middle of the brain, we randomly selected the slices from 40 to 80. Since the edge portion of the image has a black background, we perform center cropping on each medical MRI image to make the model focus on the brain region. Small rotations and translations are applied to the images to enhance image diversity. The input is uniformly resized and normalized to improve training stability. A neuroimaging dataset, brain tumor patients (NIBT) [22], is chosen as the test set, which consists of T1, T2, fMRI, and DTI MRI images for 22 brain tumor patients. The size of the images in this dataset is $256 \times 256 \times 192$. For evaluation, we also consider transverse slices. Since most brain tumors occurred in the middle, we discarded the beginning and the end. Therefore, the slices of the image are randomly selected in the range of 140 to 200 slices. Then, data enhancement operations, such as center cropping, resizing, and normalization, are performed on each medical image. For the Brats2020 dataset, we take slices from the center region. For slices with mask 0, it is treated as normal, while others are treated as abnormal.

The other part is a dataset (Task 3) from the ISIC2018 challenge, which is related to the classification and localization of dermatological images. Task 3 contains seven categories in total. We consider the nevus type as normal data and the other types as abnormal data. The training set contains 8224 nevus images and the test set contains 1514 images of other types. The data is normalized and resized to 256×256 size.

4.2. Implementation Details

We use Pytorch to implement the proposed model. The construction of the inn network is completed through the FrEIA library. Resnet18 is treated as backbone, which obtains multi-scale feature maps by fusing the outputs of the first three residual blocks. We do not choose the pre-training model due to the difference between MRI and imagenet images. The input of the model is unified as a single-channel brain MRI image with a size 256×256. The three scales' feature map channels are 64, 128, and 256, respectively. The distribution transformation model consists of 15 NF blocks. Each sub-network consists of a 3×3 2D convolutional network, a relu layer, and a convolutional attention layer (CBAM). The construction of CBAM is completed by the fightcv_attention library, and the reduction parameter that specifies the compression ratio of the number of channels is set to 16. In addition, the dimension of the hidden feature learned is set as 128.

During training, the images are subjected to random rotations ranging from -3 degrees to $+3$ degrees and random translations of width 0.02 and height 0.09. The batch size is set to 15. The Adam optimizer is used as the parameter optimizer with a learning rate of 10^{-3}. The weight decay value is set to 10^{-5}. During inference, the performance of the proposed method is evaluated against other comparative methods using the Area Under the Receiver Operating Characteristic Curve (AUROC). To evaluate the performance of the model on the test data set, we used metrics such as the area under the receiver operating characteristic curve (AUROC), accuracy (Acc), recall, average precision (AP), and F1.

4.3. Quantitative Results

We quantitatively compare the proposed model with the remaining three deep learning-based anomaly detection methods. They contain a representation-based method, Fast-flow [40], and two image reconstruction-based methods, f-AnoGan [31] and AnoDDPM [38]. For testing, we evaluate the proposed model and the compared models on two public datasets, including Brain MRI and ISIC2018. Table 1 collects the results of the quantitative analysis of the proposed model and the remaining three methods on the brain MRI dataset. Table 2 demonstrates the results of the quantitative analysis of our method and the remaining three methods on the ISIC2018 dataset.

Table 1. Quantitative analysis for different methods on Brain MRI

	Auc	Acc	Recall	Ap	F1
Ours	0.91	0.84	0.78	0.45	0.42
f-AnoGan[31]	0.84	0.75	0.81	0.10	0.14
AnoDDPM[38]	0.74	0.98	0.61	0.67	0.64
Fast-flow[40]	0.72	0.73	0.72	0.24	0.32

Table 2. Quantitative analysis for different methods on ISIC2018

	Auc	Acc	Recall	Ap	F1
Ours	0.81	0.72	0.72	0.70	0.67
f-AnoGan[38]	0.78	0.67	0.69	0.68	0.66
Fast-flow[40]	0.72	0.68	0.67	0.62	0.64
Autoencoder	0.70	0.62	0.60	0.65	0.65

Table 3. The performance of MS-NF with different backbones selected on the Brain MRI

Conv	Backbone	Metric Values				
		Auc	Acc	Recall	Ap	F1
3×3	Resnet18	0.91	0.84	0.78	0.41	0.39
	WideResnet50	0.73	0.68	0.70	0.09	0.18
	Cait	0.66	0.51	0.81	0.07	0.14
	Deit	0.65	0.35	0.90	0.08	0.12
3×3 and 1×1	Resnet18	0.77	0.73	0.81	0.10	0.23
	WideResnet50	0.54	0.46	0.68	0.05	0.11
	Cait	0.66	0.51	0.81	0.07	0.14
	Deit	0.65	0.35	0.90	0.08	0.12

We select the threshold with the slightest difference between True Positive Rate (TPR) and False Positive Rate (FPR) on the ROC curve as the accurate value for calculating other evaluation criteria. Figure 2 shows the ROC curve of this method and the other three methods on the NIBT dataset. Our method is superior to other compared models.

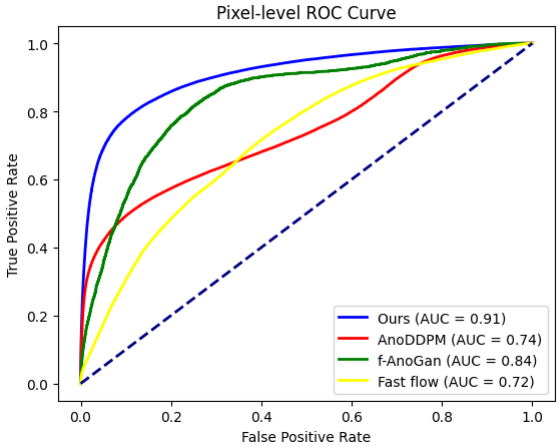

Fig. 2. Demonstration of ROC curves for different methods

MS-FLOW achieves the best results in the AUROC metric. It also performs well in ACC, recall, and so on. By transforming the feature distribution to a standard normal distribution through the NF module, abnormal data deviates from the normal distribution, completing the localization. Figure 3 shows the localization effect of MS-FLOW on brain MRI data. Columns 1 to 5 are abnormal data. The latter column is a normal brain MRI scan. For the tumor portion, MS-FLOW localizes its abnormal portion.

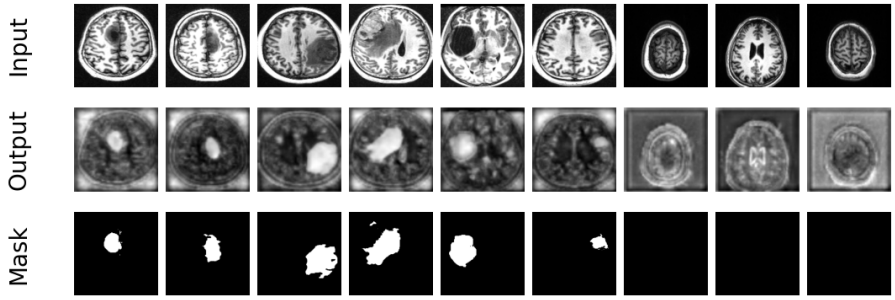

Fig. 3. Detection effect diagram. Output represents the model-predicted images, and Mask represents the ground truth

f-Anogan performs excellent in image-level anomaly detection tasks, but does not perform as well as the other methods in pixel-level medical image detection tasks. AnoDDPM performs excellent pixel-level detection tasks, though sensitive to the selected thresholds. It is much slower than other methods in training and inference time. MS-FLOW further improves pixel-level image detection through spatial and channel attention mechanisms. Normalized flow-based characterization methods are not only fast to train but also yield satisfactory results even with small datasets.

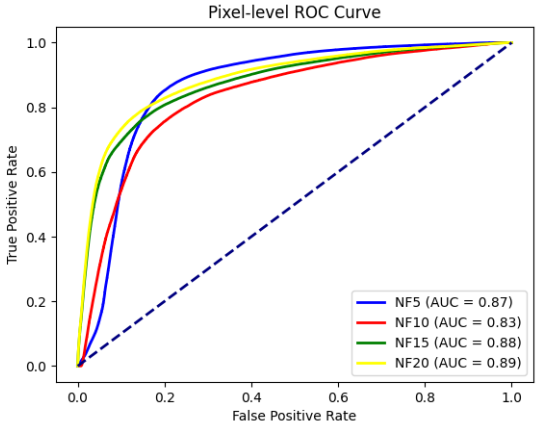

Fig. 4. a schematic diagram of the ROC curve on the NIBT data set

4.4. Ablution Study

Since the model consists of feature extraction and the NF module, we investigated the performance of the model after choosing different backbone networks and the structure of the NF module. For the backbone networks, we chose four backbone networks, including two deep convolutional networks, resnet18 and wideresnet50, and two visual transformer methods, cait and diet. For the evaluation criteria, we still use the five metrics, such as AUC, depicted in section 4.3. Table 3 shows the performance of the attentional flow when the sub-networks use different convolutions, and the backbone network is resnet18, wideresnet50, cait, and diet. Choosing a more complex convolutional neural network or employing a visual transformer does not improve performance.

The number of NF modules is also an essential hyperparameter for our method, which impacts the model's performance and efficiency. So we selected 4 different numbers of NF modules for the MS-FLOW, as a way to observe the effect it has on the model performance. Figure 4 shows the roc curves under different NF modules. We finally find that the model has the best overall performance when the number of NF modules equals 15. Figure 5 shows the Precision-Recall curves for different numbers of NF modules, and the best performance is also obtained when the number of NF modules is equal to 15.

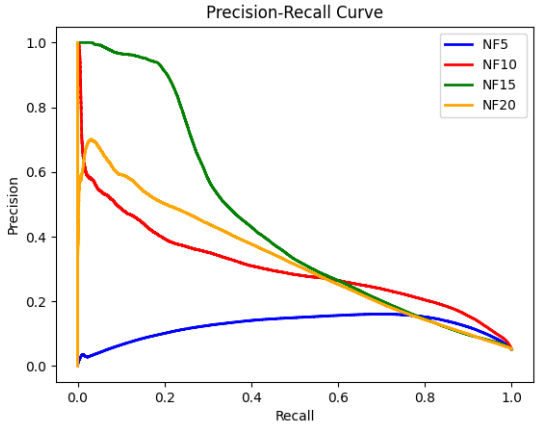

Fig. 5. a schematic diagram of the RP curve on the NIBT data set

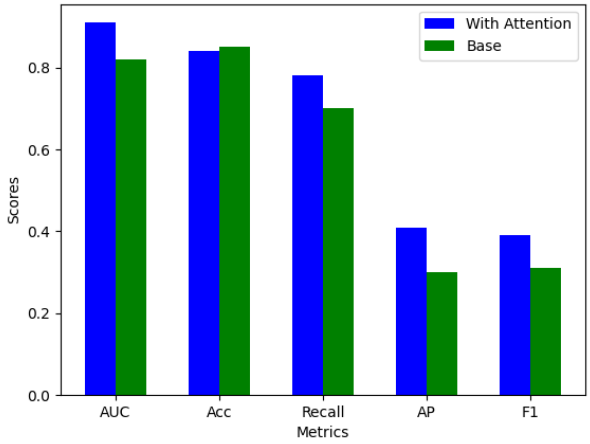

Fig. 6. Schematic representation of the attention mechanism for model performance images

To study the effectiveness of the proposed MS-NF module and observe the model performance changes after eliminating attention and adding attention mechanism in the sub-network. Figure 6 demonstrates the performance change of the model with and without the attention mechanism under the evaluation metrics such as AUC, and Acc. It can be seen that AUC, recall, AP, and F1 are improved, indicating that the attention module has a positive effect on the model.

4.5. Complexity evaluations

To analyze and evaluate the complexity of the model, we used the model parameter count and inference speed metrics to compare MS-NF with the other methods in Table 4. The comparison results are shown in Table N. MS-NF has a parameter count of 15.1M with the number of NF modules equal to 15, and a feature extraction network of resnet18, and an fps of 2.92 on the dataset. Compared to Anoddpm, MS-NF cuts the number of parameters to one-tenth of Anoddpm and improves the inference speed dramatically. Still, it is comparable to it in terms of detection effectiveness. In contrast, compared to fno-gan as well as fast-flow, the detection effect is better than the above two methods when the number of parameters is appropriately boosted.

It can be seen that the proposed MS-NF can achieve excellent performance and real-time detection with a small number of parameters, showing that the proposed work is competitive. The equipment configuration used for testing is composed of one Intel(R) Xeon(R) Silver 4314 CPU @ 2.40GHz, 128 GB memory, 4 TB storage, and one NVIDIA GeForce RTX 3090 card attached. All experiments are carried out in the operation system Linux. Pycharm is selected as the development environment. In addition, the program code of the models in this paper is implemented by Pytorch, an open-source tool that supports the agile development of deep learning models.

Table 4. Model Complexity Analysis

	parameters	time	fps
Ours	15.1M	9.26	2.92
f-AnoGan	3.93M	4.33	6.23
AnoDDPM	131M	0.04	632
fast-flow	15.0M	9.97	2.72

5. Concluding Remarks and Future Work

In this work, we propose a novel unsupervised learning model for medical image detection, which performs recognition without label information. It can avoid the subjective factors of the annotators to impact the performance of the model. Concretely, this model fuses the different scale feature maps to learn the contextual information and to detail multi-granularity information hidden in the data. Then, the normalizing flow in the model learns the distribution of the data, which is used for detection. Moreover, the convolutional attention mechanism makes the model focus on the useful regions. It can further

improve the performance without significantly increasing the number of parameters. The experimental results illustrate that the proposed model outperforms the compared models. Particularly, the training speed of the proposed model is faster than others. The proposed model aims to learn the distribution of the normal medical images, which are used to generate new abnormal medical images combined with the abnormal information through the transfer module. It can relieve the requirement of the abnormal medical images. In future directions, we aim further to introduce the GAN mechanism to the proposed model to improve the quality of the generated abnormal medical images.

Acknowledgments. This work was partially supported by the National Key Research and Development Program of China under Grant 2021YFA1000600, the National Natural Science Foundation of China under Grant 62072170, the Science and Technology Project of Department of Communications of Hunan Provincial under Grant 202101, the Key Research and Development Program of Hunan Province under Grant 2022GK2015, and the Open Research Fund of Hunan Provincial Key Laboratory of Network Investigational Technology under grant 2020WLZC001.

References

1. Bhatt, N., Prados, D.R., Hodzic, N., Karanassios, C., Tizhoosh, H.R.: Unsupervised detection of lung nodules in chest radiography using generative adversarial networks. In: 2021 43rd Annual International Conference of the IEEE Engineering in Medicine & Biology Society (EMBC). pp. 3842–3845. IEEE (2021)
2. Brock, A., Donahue, J., Simonyan, K.: Large scale gan training for high fidelity natural image synthesis. arXiv preprint arXiv:1809.11096 (2018)
3. Cai, J., Liang, W., Li, X., Li, K., Gui, Z., Khan, M.K.: Gtxchain: A secure iot smart blockchain architecture based on graph neural network. IEEE Internet of Things Journal 10(24), 21502 – 21514 (2023)
4. Creswell, A., White, T., Dumoulin, V., Arulkumaran, K., Sengupta, B., Bharath, A.A.: Generative adversarial networks: An overview. IEEE signal processing magazine 35(1), 53–65 (2018)
5. Dinh, L., Sohl-Dickstein, J., Bengio, S.: Density estimation using real nvp. arXiv preprint arXiv:1605.08803 (2016)
6. Dosovitskiy, A., Beyer, L., Kolesnikov, A., Weissenborn, D., Zhai, X., Unterthiner, T., Dehghani, M., Minderer, M., Heigold, G., Gelly, S., et al.: An image is worth 16x16 words: Transformers for image recognition at scale. arXiv preprint arXiv:2010.11929 (2020)
7. Esser, P., Rombach, R., Ommer, B.: Taming transformers for high-resolution image synthesis. In: Proceedings of the IEEE/CVF conference on computer vision and pattern recognition. pp. 12873–12883 (2021)
8. Gulrajani, I., Ahmed, F., Arjovsky, M., Dumoulin, V., Courville, A.C.: Improved training of wasserstein gans. Advances in neural information processing systems 30 (2017)
9. He, K., Zhang, X., Ren, S., Sun, J.: Deep residual learning for image recognition. In: Proceedings of the IEEE conference on computer vision and pattern recognition. pp. 770–778 (2016)
10. Ji, H., Xie, K., Wen, J., Zhang, Q., Xie, G., Liang, W.: Finemon: An innovative adaptive network telemetry scheme for fine-grained, multi-metric data monitoring with dynamic frequency adjustment and enhanced data recovery. Proc. ACM Manag. Data 2(1) (mar 2024), https://doi.org/10.1145/3639267
11. Karras, T., Laine, S., Aila, T.: A style-based generator architecture for generative adversarial networks. In: Proceedings of the IEEE/CVF conference on computer vision and pattern recognition. pp. 4401–4410 (2019)

12. Kingma, D.P., Welling, M.: Auto-encoding variational bayes. arXiv preprint arXiv:1312.6114 (2013)
13. Li, C., He, A., Wen, Y., Liu, G., Chronopoulos, A.T.: Optimal trading mechanism based on differential privacy protection and stackelberg game in big data market. IEEE Transactions on Services Computing 16(5), 3550–3563 (2023)
14. Li, C., Peng, Y., Liu, G., Li, Y., Yang, X., Chen, C.: Efficient vision transformer for human-centric aiot applications through token tracking assignment. IEEE Transactions on Consumer Electronics 70(1), 1029–1039 (2024)
15. Li, C., Zhu, D., Hu, C., Li, X., Nan, S., Huang, H.: Ecdx: Energy consumption prediction model based on distance correlation and xgboost for edge data center. Information Sciences 643, 119218 (2023), https://www.sciencedirect.com/science/article/pii/S0020025523008034
16. Liang, W., Li, Y., Xie, K., Zhang, D., Li, K.C., Souri, A., Li, K.: Spatial-temporal aware inductive graph neural network for c-its data recovery. IEEE Transactions on Intelligent Transportation Systems 24(8), 8431 – 8442 (2022)
17. Liang, W., Li, Y., Xu, J., Qin, Z., Zhang, D., Li, K.C.: Qos prediction and adversarial attack protection for distributed services under dlaas. IEEE Transactions on Computers 73(3), 669 – 682 (2023)
18. Liang, W., Liu, Y., Yang, C., Xie, S., Li, K., Susilo, W.: On identity, transaction, and smart contract privacy on permissioned and permissionless blockchain: A comprehensive survey. ACM Comput. Surv. 56(12) (jul 2024), https://doi.org/10.1145/3676164
19. Liu, Y., Liang, W., Xie, K., Xie, S., Li, K., Meng, W.: Lightpay: A lightweight and secure off-chain multi-path payment scheme based on adapter signatures. IEEE Transactions on Services Computing 17(4), 17 (2023)
20. Long, J., Liang, W., Li, K.C., Wei, Y., Marino, M.D.: A regularized cross-layer ladder network for intrusion detection in industrial internet of things. IEEE Transactions on Industrial Informatics 19(2), 1747–1755 (2022)
21. Mishra, P., Verk, R., Fornasier, D., Piciarelli, C., Foresti, G.L.: Vt-adl: A vision transformer network for image anomaly detection and localization. In: 2021 IEEE 30th International Symposium on Industrial Electronics (ISIE). pp. 01–06. IEEE (2021)
22. Pernet, C., Gorgolewski, K., Ian, W.: A neuroimaging dataset of brain tumour patients (2016)
23. Pinaya, W.H., Graham, M.S., Gray, R., Da Costa, P.F., Tudosiu, P.D., Wright, P., Mah, Y.H., MacKinnon, A.D., Teo, J.T., Jager, R., et al.: Fast unsupervised brain anomaly detection and segmentation with diffusion models. In: International Conference on Medical Image Computing and Computer-Assisted Intervention. pp. 705–714. Springer (2022)
24. Platt, J.: Sequential minimal optimization: A fast algorithm for training support vector machines (1998)
25. Puccio, B., Pooley, J.P., Pellman, J.S., Taverna, E.C., Craddock, R.C.: The preprocessed connectomes project repository of manually corrected skull-stripped t1-weighted anatomical mri data. Gigascience 5(1), s13742–016 (2016)
26. Radford, A., Metz, L., Chintala, S.: Unsupervised representation learning with deep convolutional generative adversarial networks. arXiv preprint arXiv:1511.06434 (2015)
27. Razavi, A., Van den Oord, A., Vinyals, O.: Generating diverse high-fidelity images with vq-vae-2. Advances in neural information processing systems 32 (2019)
28. Rezende, D., Mohamed, S.: Variational inference with normalizing flows. In: International conference on machine learning. pp. 1530–1538. PMLR (2015)
29. Roth, K., Pemula, L., Zepeda, J., Schölkopf, B., Brox, T., Gehler, P.: Towards total recall in industrial anomaly detection. arxiv 2021. arXiv preprint arXiv:2106.08265
30. Rudolph, M., Wandt, B., Rosenhahn, B.: Same same but differnet: Semi-supervised defect detection with normalizing flows. In: Proceedings of the IEEE/CVF winter conference on applications of computer vision. pp. 1907–1916 (2021)

31. Schlegl, T., Seeböck, P., Waldstein, S.M., Langs, G., Schmidt-Erfurth, U.: f-anogan: Fast unsupervised anomaly detection with generative adversarial networks. Medical image analysis 54, 30–44 (2019)
32. Schlegl, T., Seeböck, P., Waldstein, S.M., Schmidt-Erfurth, U., Langs, G.: Unsupervised anomaly detection with generative adversarial networks to guide marker discovery. In: International conference on information processing in medical imaging. pp. 146–157. Springer (2017)
33. Teng, Y., Li, H., Cai, F., Shao, M., Xia, S.: Unsupervised visual defect detection with score-based generative model. arXiv preprint arXiv:2211.16092 (2022)
34. Touvron, H., Cord, M., Douze, M., Massa, F., Sablayrolles, A., Jégou, H.: Training data-efficient image transformers & distillation through attention. In: International conference on machine learning. pp. 10347–10357. PMLR (2021)
35. Van Den Oord, A., Vinyals, O., et al.: Neural discrete representation learning. Advances in neural information processing systems 30 (2017)
36. Vaswani, A., Shazeer, N., Parmar, N., Uszkoreit, J., Jones, L., Gomez, A.N., Kaiser, Ł., Polosukhin, I.: Attention is all you need. Advances in neural information processing systems 30 (2017)
37. Woo, S., Park, J., Lee, J.Y., Kweon, I.S.: Cbam: Convolutional block attention module. In: Proceedings of the European conference on computer vision (ECCV). pp. 3–19 (2018)
38. Wyatt, J., Leach, A., Schmon, S.M., Willcocks, C.G.: Anoddpm: Anomaly detection with denoising diffusion probabilistic models using simplex noise. In: Proceedings of the IEEE/CVF Conference on Computer Vision and Pattern Recognition. pp. 650–656 (2022)
39. Xie, S., Xiao, L., Han, D., Xie, K., Li, X., Liang, W.: Hcvc: A high-capacity off-chain virtual channel scheme based on bidirectional locking mechanism. IEEE Transactions on Network Science and Engineering 11(5), 3995 – 4006 (2023)
40. Yu, J., Zheng, Y., Wang, X., Li, W., Wu, Y., Zhao, R., Wu, L.: Fastflow: Unsupervised anomaly detection and localization via 2d normalizing flows. arXiv preprint arXiv:2111.07677 (2021)
41. Zhou, S., Li, K., Chen, Y., Yang, C., Liang, W., Zomaya, A.Y.: Trustbcfl: Mitigating data bias in iot through blockchain-enabled federated learning. IEEE Internet of Things Journal 11(15), 25648–25662 (2024)
42. Zhu, J.Y., Park, T., Isola, P., Efros, A.A.: Unpaired image-to-image translation using cycle-consistent adversarial networks. In: Proceedings of the IEEE international conference on computer vision. pp. 2223–2232 (2017)
43. Zimmerer, D., Kohl, S.A., Petersen, J., Isensee, F., Maier-Hein, K.H.: Context-encoding variational autoencoder for unsupervised anomaly detection. arXiv preprint arXiv:1812.05941 (2018)

Yufeng Xiao received the B.Sc. and M.S. degrees in computer application technology from Hunan University in 2010 and 2013, respectively, and the Ph.D. degree in computer science and technology from the same school in 2020. He is an assistant professor at the School of Computer Science and Engineering, Hunan University of Science and Technology. His current research interests include speech information processing, image processing and deep learning.

Xueting Huang is currently pursuing a master's degree at Hunan University of Science and Technology, with research focused on enhancing the overall performance of blockchain through sharding technology, as well as on information security and privacy protection in blockchain systems.

Wei Liang received a Ph.D. degree in computer science and technology from Hunan University in 2013. He is a Postdoctoral Scholar at Lehigh University from 2014 to 2016.

He is currently a Professor at the School of Computer Science and Engineering, Hunan University of Science and Technology. His research interests include intelligent transportation, security of IoV, blockchain, embedded systems and hardware IP protection, and security management in wireless sensor networks.

Jingnian Liu received an M.Sc. from Hunan University of Science and Technology. He has published papers (EI-indexed) and holds one invention patent. His research interests focus on computer vision and deep learning.

Yuxiang Chen received a PhD degree in computer application from Hunan University in 2021. He worked as a postdoctoral fellow in the Department of Computing at Hunan University from 2021.7 to 2023.3. He is currently an assistant professor at Hunan University of Science and Technology. His research interests include network monitoring, network security, big data, and AI.

Rui Xie received his Bachelor's and Master's degrees in 2006 and 2010, respectively, and is currently pursuing his Ph.D. at Hunan University of Science and Technology. His research interests include network security, cloud and edge computing, and AI, with a particular focus on distributed computing, privacy protection, and embedded systems.

Kuanching Li received a Ph.D. degree in 2001. He has authored or co-authored papers in high-ranked journals and conferences, and serves as Associate and Guest editor for several scientific journals. His research interests include cloud and edge computing, Big Data, and blockchain.

Nam Ling received a B.Eng. degree from the National University of Singapore in 1981 and the M.S. and Ph.D. degrees from the University of Louisiana at Lafayette, USA, in 1985 and 1989, respectively. He is currently the Associate Dean for Research for the School of Engineering and the Wilmot J. Nicholson Family Chair Professor at Santa Clara University (SCU), California, USA. His topics of interest include video coding algorithms and architectures.

Received: February 27, 2024; Accepted: December 01, 2024.

Computer Science and Information Systems 22(1):239–257 https://doi.org/10.2298/CSIS240804005H

PSBD-EWT-EGAN: Heart Sound Denoising Using PSBD-EWT and Enhancement Generative Adversarial Network

Jianqiang Hu[1,2], Lin Chen[1], Miao Yang[1], Shigen Shen[3,⋆], and Xiao-Zhi Gao[4]

[1] School of Computer and Information Engineering, Xiamen University of Technology, 361024 Xiamen, P. R. China
hujianqiang@tsinghua.org.cn
275914270c@gmail.com
yangmiao1133@gmail.com
[2] Software School, Quanzhou University of Information Engineering, Quanzhou, P. R. China
[3] School of Information Engineering, Huzhou University, Huzhou, P. R. China
shigens@zjhu.edu.cn
[4] School of Computing, University of Eastern Finland, Kuopio, Finland
xiao-zhi.gao@uef.fi

Abstract. A heart sound signal (HSS) is sensitive to physiological noise and environmental noise, thereby degrading their quality, which makes the accurate diagnosis of machines or doctors difficult and unreliable. To this end, we present a heart sound denoising method using Parameterless Scale-space Boundary Detection (PSBD)-Empirical Wavelet Transform (EWT) and Enhancement Generative Adversarial Network (EGAN) to remove noises that corrupt HSSs in this paper. First, it introduces PSBD and kurtosis to find boundaries delimiting consecutive EWT modes. And then, it further selects the relevant modes on the Pearson's correlation coefficient between each of empirical modes and the original signal to reconstruct HSSs. Finally, EGAN is proposed to improve PSBD-EWT's generalization capacity with regard to different noises. Experimental validation is carried out on PASCAL, MHSDB and WUPHSD databases. The results show that our proposed method achieves significant improvements over state-of-the-art methods. In the case of white Gaussian noise with Signal Noise Ratio (SNR)=5dB, it obtains the best denoising performance under a SNR of 12.53dB and an Root Mean Square Error (RMSE) of 0.034.

Keywords: heart sound signals, denoising, empirical wavelet transform, heart sound signal enhancement.

1. Introduction

As reported by World Health Statistics 2023, in 2019, it is estimated that 17.9 million (UI: 13.4-22.9 million, 27%) people died of chronic diseases. There are 330 million Cardiovascular Disease (CVD) patients, including 11.39 million with Coronary Heart Disease

⋆ Corresponding author

(CHD), 8.9 million with Heart Failure (HF), 5 million with Pulmonary Heart Disease (PHD), and 4.87 million with Atrial Fibrillation (AF) in China [1]. Fortunately, the analysis of Heart Sound Signals (HSSs) has been the primary option for screening and early diagnosis of heart disease. This is because that heart sound contains a great number of biomedical signals related to cardiac activity, which can reveal many pathological heart conditions, such as HF, arrhythmia, and valvular heart disease (VHD).

Traditionally, heart sound was collected from a doctor with a stethoscope. However, manual auscultation brings about great uncertainty and diagnostic delay because it depends on the auscultation skills and experience. Challenges arise due to the presence of heart sound (below 600Hz) inaudible to the human ear. Therefore, Internet of Things (IoT)-based digital stethoscope, due to its non-invasive and easy-to-use nature, is developing rapidly. IoT-based digital stethoscope can record heart sounds and connect to edge clouds for real-time remote analysis and diagnosis [2]. Under uncontrolled environments, it is impossible to capture noise-free heart sound. Heart sounds are affected by respiratory sound, ambient noise and even signals from environments thereby degrading its quality. There is a significant overlapping frequency between heart sounds varying from 20Hz to 800Hz and respiratory sounds varying from 20Hz to 1600Hz. Besides, when people are walking or running, Motion Artifact (MA) is easily introduced to heart sounds. IoT Devices' circuits also may produce Powerline Interference (PLI) and Additive White Gaussian Noise (AWGN). These factors have seriously affected the outcomes of heart sound diagnosis. Due to the chaotic and non-stationary nature of heart sounds and their variability with changes in human body's physical conditions, heart sound denoising is a very complex problem and has become a research hotspot.

Over the past few decades, various techniques have been exploited to denoise heart sounds. First, various statistical methods, including Non-negative Matrix Decomposition (NMD) [3] and Singular Value Decomposition (SVD) [4], are usually used to distinguish HSSs from respiratory sounds, but these methods are difficult in dealing with the difference between the noise and murmurs [5]. Second, various time-domain methods, including conventional filters and auto-correlation methods are exploited to remove noise. Conventional filters such as Butterworth band-pass filters and Finite Impulse Response (FIR) filters can only remove noises outside the range of HSS frequency [6]. Empirical Mode Decomposition (EMD) [7] has good adaptability for non-linear decomposition of HSSs but suffers from modal aliasing and endpoint effect. Although Variational Modal Decomposition (VMD) can overcome modal aliasing but its decomposition performance decreases with the increase of noise intensity. Finally, various frequency-domain, including Wavelet transform (WT) [8], Fourier transform [9] and Empirical Wavelet Transform (EWT) [10] were exploited to denoise HSSs. Wavelet transform depends on predefined parameters including mother wavelet, threshold and DL. Similarly, Fourier transform needs fixed basis functions. Therefore, they lack self-adaptability and are difficult in suppressing the burst noise of HSSs. Compared to WT and Fourier transform, EWT is an adaptive technique which is more suitable to analyze the non-stationary signals. However, it has no improper segmentations of Fourier Transform spectrum due to noise interference, which directly leads to the failure of EWT decomposition. It is worth mentioning that the effectiveness of the above methods can be verified under the controlled clinical environment or simulated noisy conditions. In practice, there are irregular, unpredictable transient distortions of HSSs under uncontrolled environments. Moreover, in the exist-

ing techniques, there is no unified denoising method that can be suitable for multi-noise scenarios.

Notably, deep learning has attracted much attention in various signals denoising in biomedical engineering such as electrocardiogram (ECG) and electroencephalogram (EEG), but has rarely involved in the field of HSSs. To the best of our knowledge, only two works exist in the literature that have exploited deep learning-based denoising methods to remove noises from HSSs, i.e., Denoising Convolutional Neural Network (DnCNN) [11] and LU-Net [12]. DnCNN predicts the residual noise, which is the difference between the noisy HSSs and potential clean HSSs. A deep encoder-decoder-based denoising architecture, called LU-Net, was utilized to suppress respiratory sound and ambient noise that corrupt the heart sounds. Among them, sparse categorical cross-entropy and Mean Square Error (MSE) can be used as loss of useful information to measure the difference between noise-free and processed signals. In practice, the design of the loss function is difficult because of the requirement to capture as many details as possible in the fluctuations of HSSs.

In this work, we develop a new heart sound denoising method called PSBD-EWT-EGAN, using Parameterless Scale-space Boundary Detection (PSBD)-EWT and Enhancement Generative Adversarial Network (EGAN). First, it introduces PSBD and kurtosis to find boundaries delimiting consecutive EWT modes. And then, it selects the relevant modes on the Pearson's correlation coefficient between each of empirical modes and the original signal to reconstruct HSSs. Finally, EGAN architecture with an optimized loss function is presented to further suppress noises rather than directly outputting denoised HSSs of PSBD-EWT. Our proposed method combines the strengths of PSBD-EWT and EGAN in HSSs denoising. On one hand, PSBD-EWT decomposes HSSs to sub-band signals more discriminately than EWT. On the other hand, EGAN can improve PSBD-EWT's generalization capacity with regard to different noises, especially under low SNR (Signal Noise Ratio) environments.

Our contributions are summarized as follows:

- A heart sound denoising algorithm using PSBD-EWT is proposed, in which PSBD and kurtosis overcome the problem of noise component interference to sub-band segmentations of EWT, especially under varying temporal-spectral characteristics of environmental noises and physiological sounds.
- An EGAN architecture with an optimized loss function is proposed, which is capable of better preserving meaningful components of heart sounds while removing noise under a low SNR environment. EGAN makes the denoised HSSs as similar to the clean HSSs as possible, which is beneficial to avoid distortion and enhances the quality of HSSs.
- In order to verify the effectiveness of the proposed method, we have performed several experiments on PASCAL [13], MHSDB [14] and WUPHSD [15] databases. The experimental results show that the proposed method has advantages over the state-of-the-art methods. In the case of white Gaussian noise (WGN) with SNR=5dB, our proposed method obtains the best denoising performance under a SNR of 12.53dB and an RMSE (Root Mean Square Error) of 0.034.

In the following, related work of heart sounds denoising is reviewed in Section 2. Subsequent to this, Section 3 describes our proposed method. Later, the denoising performance of our proposed method is compared with several state-of-the-art methods on

publicly available heart sound datasets in Section 4. At the last, Section 5 concludes this paper.

2. Related work

Denoising methods have been explored in diverse branches of biomedical engineering, including ECG, EEG, respiratory sounds, and heart sounds.

(i) ECG Denoising. An adversarial denoising convolutional neural network (ADnCNN) [16] was exploited for a residual signal from noisy ECG to obtain a clean ECG. In a discriminator network, the denoised and clean signals were classified. The network was fed back to ADnCNN model for parameter adjustment. The work presented in paper [17] employed Convolutional Neural Network (CNN) based Generative Adversarial Network (GAN) model for ECG denoising, which was trained end-to-end using the noisy and clean ECG signals. Recently, a modified lightweight U-Net model called LUNet was exploited to handle various noises that corrupt ECG signals, including baseline wander, muscle artifacts, and AWGN [18]. In order to prevent the loss of effective information when the network is compressed, a deep-wave convolutional neural network called DW-CNN [19] replaces the simple complete layer with a convolutional layer to build an encoder and a decoder. Besides, a Cycle-consistent Generative Adversarial Network (Cycle-GANs) [20] was exploited to improve the quality of ECG recordings suffering from various artifacts, especially for an accurate arrhythmia diagnosis.

(ii) EEG Denoising. One Dimensional Residual Convolutional Neural Network (1D-ResCNN) [21] was exploited to remove the EEG artifacts, which included convolutional layers and Inception-ResNet mapping the noisy EEG signals to the clean ones. Because a single-channel approach might not extract specific spatial information, IC-U-Net [22] combined Independent Component (IC) and U-Net architecture to remove EEG artifacts. Furthermore, IC-U-Net is based on U-Net architecture with a loss function ensemble. Similarly, a framework based on GANs, called EEGANet [23], was applied to eliminate the ocular artifacts from EEG signals. In addition, 1D EEG signal denoising network with 2D transformer, called EEGDnet [24], offered a blend of local and nonlocal self-similarity in feed forward blocks to enhance the denoising performance.

(iii) Respiratory Sound Denoising. Respiratory sounds are recorded in noisy environments, which overlap with the different types of noises. A unique method, using EMD, hurst analysis and spectral subtraction, was proposed to denoise the lung sound [25]. Pouyani et al. [26] developed a method based on WT and Artificial Neural Networks (ANN) to remove noises from respiratory sound signals. Besides, singular spectrum analysis, combining with Discrete Cosine Transform (DCT), was applied to distinguishing BV signals from V signals, and finally enhance the quality of lung sounds [27].

(iv) PCG (Phonocardiogram) & HSSs Denoising. Band-pass filters and Butterworth band-pass filters are common methods of HSSs denoising, which can remove high-frequency and low-frequency noises with cut-off frequencies. WT, EMD, Power Law Algorithm (PLA), Hidden Markov Model (HMM) and Short-time Fourier Transform (STFT) [28] are usually used to denoise HSSs. In particular, WT has advantages in the time-frequency representation of HSSs, but selection of mother wavelet, threshold and DL is inevitable and excellent domain expertise is also crucial. These parameters of the wavelet threshold denoising method were optimized for HSSs. In [29], a noise reduction

method, fusing VMD and the wavelet soft threshold algorithm, was presented to suppress the noise contaminants from children's PCGs, especially crying noise. The method might effectively improve the performance of intelligent screening for CHD. In addition, an adaptive denoising algorithm, combining Time Delay Neural Networks (TDNN) and WT, was employed to denoise mobile PCG [30]. An adaptive noise cancellers-based filter was utilized to denoise and recover the PCG signal corrupted by Gaussian and pink noise [19]. In addition, the GAN-based architecture was used to generate synthetic HSSs, while EWT was used to denoise synthetic cardiac signal and decreased the computational cost that GAN requires [31].

Additionally, deep neural networks have achieved significant results in image noise reduction and speech enhancement, such as Residual Dense Generative Adversarial Network [32,33,34], and Speech Enhancement Generative Adversarial Network (SEGAN) [35][36], but rarely in the field of HSSs noise denoising.

Our work first exploits PSBD and kurtosis to find boundaries delimiting consecutive EWT modes. Furthermore, in the training phase, it takes the noisy and clean HSSs as input in a parallel mode instead of only noisy HSSs in an EGAN. From the above discussion, two novel points highlight the contributions to HSSs denoising.

(i) Our proposed method can separate meaningful and informative components from noisy HSSs, especially under varying temporal-spectral characteristics of environmental noises and physiological sounds.

(ii) The robustness of our proposed method will be better than the existing heart sound denoising methods. Quite a few heart sound denoising methods, such as [37,38], can achieve good performances in a strictly constrained environment. These methods only employ simple filters, such as Butterworth bandpass filtering, high-pass filter, etc., in the pre-processing stage, so their denoising capability is insufficient. PSBD-EWT-EGAN makes full use of clean HSSs and an optimized loss function to achieve heart sounds enhancement even under a low SNR environment.

3. Methodology

3.1. PSBD-EWT

EWT is an adaptive decomposition method in which empirical wavelet is used to decompose each signal into its modes. Because each mode revolves around a specific frequency, EWT can divide the normalized spectrum of each signal into N segmentations to extract the empirical modes. Extracting the bank of empirical wavelets is equivalent to finding a set of bandpass filters. In general, EWT determines boundaries of spectral segmentation based on the local maxima. However, Fourier spectrum is prone to noise and non-stationary factors. Once the segmentation boundaries are set incorrectly, it will directly lead to the failure of EWT decomposition.

In Consequence, we introduce PSBD [39] to find local maxima of time-frequency spectrum. The PSBD-EWT method exploits maxima on a kind of time-frequency spectrum based on the frequency-band segmentations, and the filter bank of orthogonal wavelet was constructed based on the sub-bands to perform EWT decomposition. The method of determining the boundaries of Fourier spectral segmentation is as follows:

Suppose that the classes of a given Fourier spectrum are represented in L levels, we have the total number of classes $N = n_1 + n_2 + \cdots + n_L$, where n_j is the number

of classes at level j. We adopt Otsu's method [40] to find the optimal threshold T such that the intra-class variances σ^2_{intra} of class A and class B are minimal while inter-class variances σ^2_{inter} are maximal. This is equivalent to maximizing σ^2_{intra} and its expression for intra-class variance is given by

$$\sigma^2_{intra} = w_A w_B (\mu_B - \mu_A)^2 \tag{1}$$

where the probabilities of class occurrence of A and B are $w_A = \frac{1}{N}\sum_{j=1}^{T} n_j$, $w_B = \frac{1}{N}\sum_{j=T+1}^{L} n_j$, respectively, and the class mean levels of A and B are $\mu_A = \frac{\sum_{j=1}^{T} jn_j}{\sum_{j=1}^{T} n_j}$, $\mu_B = \frac{\sum_{j=1}^{L} jn_j - \sum_{j=1}^{T} jn_j}{N(1-w_A)}$, respectively.

Obviously, the optimal threshold T is determined automatically in PSBD on the global characteristics of the given Fourier spectrum. Notably, one of the limitations of PSBD is segmentation boundaries under varying temporal-spectral characteristics of environmental noises and body sounds, such as breathing and intestinal sounds. These noises exhibit some important transient characteristics, including peak levels, peak intervals, and peak durations. Kurtosis [41] is a statistical measure, which can fully account for all the three transient characteristics. Therefore, kurtosis is introduced to PSBD-EWT to enhance the noises suppression under uncontrolled environments.

In order to describe a heart sound signals denoising algorithm using PSBD-EWT, we provides the following definitions.

Definition 1. *Empirical scaling $\theta_i(\varpi)$ and empirical wavelet $\varphi_i(\varpi)$ are expressed as*

$$\theta_i(\varpi) = \begin{cases} 1, & |\varpi| \le (1-\xi)\varpi_i \\ \cos(\frac{\pi}{2}\Phi(\xi,\varpi_i)), & (1-\xi)\varpi_i \le |\varpi| \le (1+\xi)\varpi_i \\ 0, & otherwise \end{cases} \tag{2}$$

$$\varphi_i(\varpi) = \begin{cases} 1, & (1+\xi)\varpi_i \le |\varpi| \le (1-\xi)\varpi_{i+1} \\ \cos(\frac{\pi}{2}\Phi(\xi,\varpi_{i+1})), & (1-\xi)\varpi_{i+1} \le |\varpi| \le (1+\xi)\varpi_{i+1}, \\ \sin(\frac{\pi}{2}\Phi(\xi,\varpi_i)), & (1-\xi)\varpi_i \le |\varpi| \le (1+\xi)\varpi_i \\ 0, & otherwise \end{cases} \tag{3}$$

where $\Phi(\xi,\varpi_i) = \Phi(\frac{|\varpi|-(1-\xi)\varpi_i}{2\xi\varpi_i})$, ξ ensures that there is no overlapping between the empirical scaling functions and empirical wavelets, and ϖ_i denotes i^{th} boundary frequency.

Algorithm 1:Heart sound denoising using PSBD-EWT

Input: An original heart sound signal $x(n)$

Output: A constructed heart sound signal $v(n)$

1. Convert an original heart sound signal x into Fourier spectrum ranging [0,π] by applying fast Fourier transform (FFT).
2. Apply EWT and PSBD to obtain N contiguous segmentations of Fourier spectrum, $\Delta_i = [\omega_{i-1}, \omega_i]$, $\sum_{i=1}^{N} \Delta_i = [0, \pi]$, $i = 1, 2, 3, \ldots, N$. For each ω_i, a transition phase T_i is with width $\tau_i = \xi\omega_i$. Two sequential areas are no overlap if and only if $0 < \xi < \min_i \frac{\Delta_{i+1} - \Delta_i}{\Delta_{i+1} + \Delta_i} < 1$.
3. Apply empirical scaling and wavelet functions over N contiguous segmentations to design bank-pass filters, and obtain detail coefficients D_i and approximation coefficients A_l of sub-bands with scaling function and empirical wavelet function given in Def. 1 [10], $i, l = 1, 2, ..., B$, where B represents the total number of detailed sub-bands.
4. Reconstruct time-domain components of N contiguous segmentations, where detail and approximation signals computed by $x_{D(i)}(n) = \sum_{j=1}^{N_j} D_i(j) W_i(n-j)$, $x_{A(l)}(n) = \sum_{j=1}^{N_l} A_l(j) S_l(n-j)$, where $x_{D(i)}(n)$, $x_{A(l)}(n)$ represents detail and approximation sub-band signals of i^{th} level [10], respectively.
5. Calculate kurtosis given in Def.2 on all the reconstructed time-domain components over N contiguous segmentations, and then find the frequency band with the maximum kurtosis and its overlapped frequency bands which are further divided. Set $i = i+1$, and repeat steps 2 to 4 util $i = N$. Finally, obtain the optimal boundary $\{\varpi'_1, \varpi'_2, ..., \varpi'_u\}$, and corresponding detail coefficients and approximation signals.
6. Obtain empirical modes by convolving the scaling function with the approximation coefficients and empirical wavelet functions with their corresponding detail coefficients, which is express as $e_1 = w_e(1,t) * \theta_1(t)$, $e_j = w_e(j,t) * \varphi_j(t)$, $j = 1, 2, \ldots, M$, M is the number of empirical modes.
7. Calculate the Pearson's correlation coefficient given in Def.3 on all the empirical modes, and select the n^{th} empirical modes e_n if and only if $C_{xe} > C_0$, where C_0 is an experimental parameter.
8. Reconstruct and obtain the denoised signal $v(n)$ using the sum of the denoised empirical modes.

Definition 2. *The expressions for Kurtosis are given by*

$$K[|x_h(n)|]^2 = \frac{E(|x_h(n)|^4)}{[E(|x_h(n)|^2)]^2} \tag{4}$$

$$E(|x_h(n)|^4) = \frac{1}{L_{\Delta(i)}} \sum_{n=t}^{t+L_{\Delta(i)}-1} ||x_h(n)\Delta(n-t)||^4 \tag{5}$$

$$[E(|x_h(n)|^2)]^2 = \{E[SE(x_h(n))]\}^2 \tag{6}$$

where $x(n)$ denotes the zero mean and amplitude normalized signal and $x_h(n)$ denotes its Hilbert transform; $SE(x_h(n))$ and $E(x_h(n))$ denotes absolute squared value and expectation of the signal $x(n)$, respectively, and $L_{\Delta(i)}$ denotes the length of the i^{th} contiguous segmentation $\Delta(i)$ of Fourier spectrum.

Definition 3. *For a sample of N values, the Person's correlation coefficient between the original signal and the empirical mode is defined as*

$$C_{xe} = \left| \frac{\sum_{n=1}^{N} (x(n) - \overline{x})(e_m(n) - \overline{e_m})}{\sqrt{\sum_{n=1}^{N} (x(n) - \overline{x})^2} \sqrt{\sum_{n=1}^{N} (e_m(n) - \overline{e_m})^2}} \right| \tag{7}$$

where $\overline{x}$ and $\overline{e_m}$ denote the average of heart sound signal $x(n)$ and the average of the m^{th} empirical mode $e_m(n)$, respectively.

The algorithm of heart sound signals denoising using PSBD-EWT is shown in Algorithm 1. It inspired from PSBD and kurtosis. On one hand, PSBD further enhances EWT's adaptive abilities to overcome noise interference. On the other hand, kurtosis improves EWT's robustness due to removal of noises with varying temporal-spectral characteristics, especially in the case of small fluctuations in places where heart sounds are not present. On basis of the above characteristics, PSBD-EWT can effectively decompose heart sounds under the noisy HSSs to the maximum extent.

3.2. Enhancement Generative Adversarial Network (EGAN)

Although PSBD-EWT can obtain the shape of HSSs well by decomposing the raw HSSs, its anti-aliasing ability are still insufficient. Especially under low SNR environments, the denoised HSSs of PSBD-EWT should be avoided distortion. To overcome such limitations, we here introduce EGAN to PSBD-EWT. It can further reduce the influence of different EWT mode selections.

The end-to-end architecture of EGAN is composed of a generator (G) and a discriminator (D). G network utilizes an encoder-decoder fully-convolutional structure. To obtain better performance of HSSs denoising, the encoder includes k convolutional layers with a kernel size 1×31 and a stride of 4, and Parameteric Rectified Linear Units (PReLUs). Correspondingly, the decoder has an anti-symmetric structure of the encoder. As the number of layers in the network is too deep, the features are easily lost. Consequently, a skip connection was needed between the encoder and decoder which can retain some important features and convey the details of HSSs. Moreover, it can avoid the vanishing gradients. The output of each layer of the encoder and the corresponding feature of the decoder are concatenated as input to the next layer of the decoder. The G network architecture of EGAN is shown in Fig. 1.

In EGAN, the input of G consists of a noisy HSS $\tilde{v}$, a clean HSS v and a random representation z from a distribution $P_z(z)$. The output of G is the denoised HSS $G(z, v)$. The received input of discriminator D is a pair of signals including a clean HSS and a noisy HSS $(x, \tilde{v})$, or a denoised HSS and a noisy HSS $(G(z, v), \tilde{v})$, respectively, and the output is 0 or 1. Actually, GANs chooses the sigmoid cross entropy as a loss function,

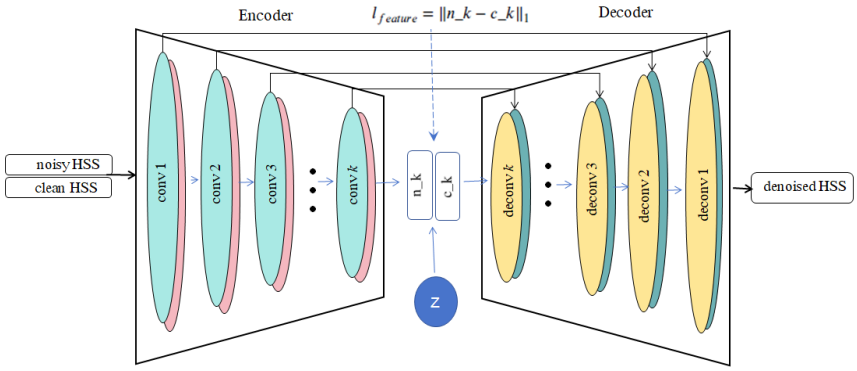

Fig. 1. The G network architecture of EGAN

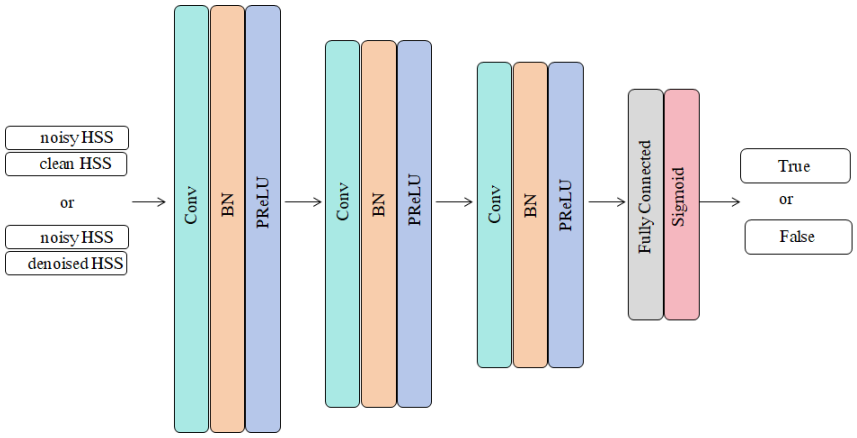

Fig. 2. The D network architecture of EGAN

which leads to vanishing gradients problem. Therefore, $L_2 - distance$ between a clean HSS v and a denoised HSS $G(z, \tilde{v})$ is introduced to the loss function, which can be defined as

$$l_{distance} = \sqrt{\sum_{j=1}^{k} |v - G(z, \tilde{v})|^2}. \tag{8}$$

In addition, the $L_1 - distance$ between a clean HSS v and a denoised HSS $G(z, \tilde{v})$ should be further introduced to the loss function, thereby generating the more realistic samples. It is expressed as

$$l_{samples} = \|v - G(z, \tilde{v})\|_1. \tag{9}$$

In low SNR environments, it is easy to bring about an incomplete feature representation due to difficulties in suppressing noise contaminations. Therefore, a clean HSS is needed to provide an important reference for the corresponding noisy HSS in the training

stage. Inspired by SEGAN [35], the clean HSSs and the noisy HSSs are compressed simultaneously and independently. They share the same network parameters, which can enhance the subsequence effect of reconstructed HSS. In practice, the noisy HSSs and clean HSSs are spliced at the same width and input into the network as two-dimensional vectors. Through layer-to-layer convolution operations, G network obtain a low-dimensional feature n_k of the noisy HSS and a low-dimensional feature c_k of the clean HSS from the decoder output. In order to force G to learn feature representations of HSSs, it is obvious that two features need to be as close to each other as possible. Therefore, the $l_{feature} - distance$ between n_k and c_k needs to be introduced to the loss function. It is expressed as

$$l_{feature} = \|n\_k - c\_k\|_1. \tag{10}$$

In this way, a new total loss function of G in EGAN can be represented as

$$\begin{aligned} \min_G V_{EGAN}(G) = \frac{1}{2} E_{z\sim P_z(z), v_c\sim Pdata(v_c)}[(D(G(z,\tilde{v}),\tilde{v})-1)^2] \\ +\lambda l_{samples} + \mu l_{feature} + \eta l_{distance} \end{aligned} \tag{11}$$

where $P_z(z)$ denotes the prior distribution of input variable z; $Pdata(v_c)$ denotes the distribution of the real data v_c; λ, μ and η denote the weight factors of $l_{samples}$, $l_{feature}$ and $l_{distance}$, respectively.

To obtain better denoising performance of HSSs, the network architecture for D is shown in Fig.2. D consists of 3 convolutional layers and 1 fully connected (FC) layer. Moreover, it employs a batch normalization (BN) and a PReLU activation function after each convolutional layer. Besides, D uses a sigmod activation function after FC to perform classification. The loss function of D in EGAN is expressed as

$$\begin{aligned} \min_D V_{EGAN}(G) = \frac{1}{2} E_{z\sim P_z(z), \tilde{v}\sim Pdata(\tilde{v})}[(D(G(z,\tilde{v}),\tilde{v}))^2] \\ +\frac{1}{2} E_{v,\tilde{v}\sim Pdata(\tilde{v})}[(D(v,\tilde{v})-1)^2] \end{aligned} \tag{12}$$

where $P_z(z)$ denotes the prior distribution of input variable z and $Pdata(\tilde{v})$ denotes the distribution of noisy HSS $\tilde{v}$.

In this way, EGAN has the following characteristics:

(i) In uncontrolled environments, especially in low SNR environments, it is difficult to obtain a complete feature representation from the noisy HSSs alone. EGAN can force the G network to learn the feature representations from the clean HSSs, thereby compensating for the loss of important components.

(ii) Through multi-layer convolution operations, the total loss function makes the denoised HSSs as similar to the clean HSSs as possible. More importantly, the noise contained in higher-level features is significantly eliminated in low-level features, which is more conducive to enhancing heart sounds in low SNR environments.

4. Experiment

4.1. Data Resources

Publicly available heart sound datasets are used to validate the effect of our proposed method. (i) PASCAL dataset. There are 176 files (Dataset A) and 656 files (Dataset B) collected from general public and clinical trials, respectively. Dataset A and B are gathered by iStethoscope Pro-iPhone app and digital stethoscope, DigiScope, respectively. (ii) Michigan Heart Sound and Murmur Database (MHSDB). There are 23 heart sound recordings with a total duration of 1496.8 seconds (iii) Washington University public heart sound dataset (WUPHSD). Heart sound records are collected from 50 patients, aged from 6 to 85 years. In addition, we utilize PyTorch 1.7 to implement deep learning architectures. The models are trained on the environments with Intel CPU, Nvidia GPU (RTX 2070Super), Ubuntu Server 22.04.

4.2. Performance metrics

SNR and RMSE are exploited to evaluate the noise reduction. SNR and RMSE are expressed as

$$SNR = 10 \lg \frac{\sum_{n=1}^{N} (v(n))^2}{\sum_{n=1}^{N} (v(n) - \hat{v}(n))^2}, \tag{13}$$

$$RMSE = \sqrt{\frac{1}{N} \sum_{n=1}^{N} (v(n) - \hat{v}(n))^2}, \tag{14}$$

respectively. Here, N denotes the number of HSS samples, $v(n)$ denotes the original HSS, $\hat{v}(n)$ denotes the denoised HSS.

4.3. Denoising Results of PSBD-EWT-EGAN

To verify whether our proposed method can perform noise reduction on HSSs in real-world scenarios, we use noisy HSSs from PASCAL dataset, which are polluted by various unavoidable entities. Take 201102201230.aif from PASCAL/A as an example, we first convert heart sound signal into Fourier spectrums and then apply EWT to obtain 97 contiguous segmentations. The resample points are set to 2000. Then, we exploit PSBD and kurtosis to merge the boundaries of contiguous segmentations and obtain 87 new segmentations. Finally, we exploit PSBD-EWT-EGAN to obtain the final constructed heart sound. Fig.3 show the segmentations of 201102201230.aif using EWT, PSBD and kurtosis, respectively. Some empirical modes are shown in Fig.4. Fig.5 clearly demonstrates the comparison the original HSS and the reconstructed HSS of PSBD-EWT-EGAN. It can be clearly observed that the noisy portions of the noisy HSS are effectively suppressed. Hence, PSBD-EWT-EGAN can denoise HSSs effectively under real-world noisy environments.

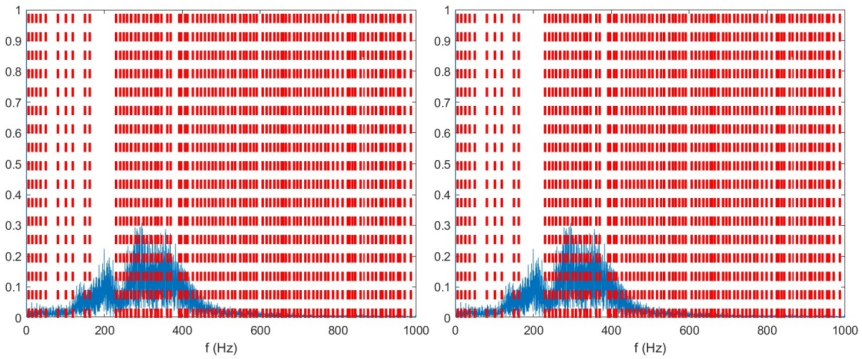

(a) The segmentations using EWT **(b)** The segmentations using PSBD kurtosis

Fig. 3. The segmentations of 201102201230.aif from PASCAL/A

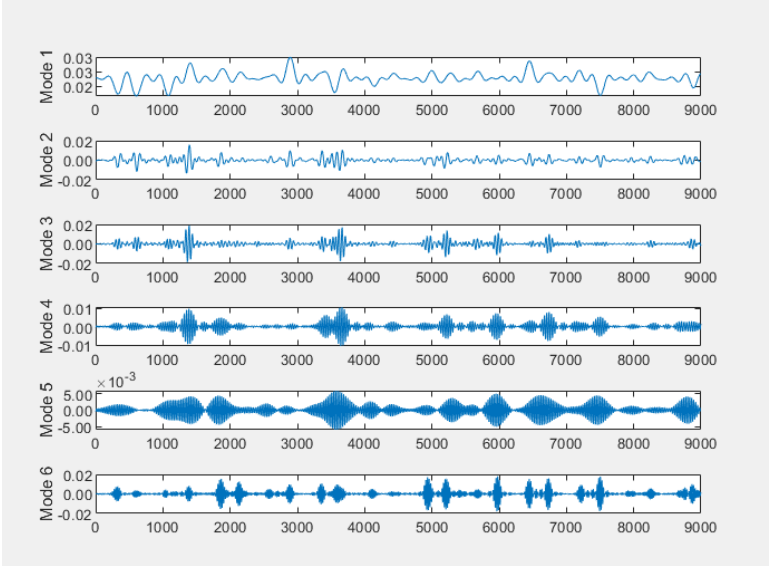

Fig. 4. The empirical modes of 201102201230.aif from PASCAL/A

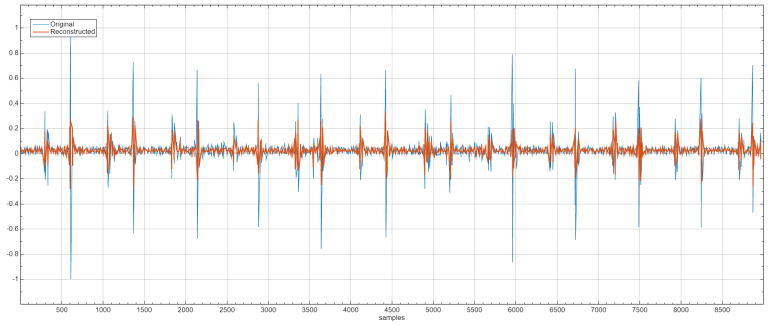

Fig. 5. The original HSSs and the reconstructed HSSs of PSBD-EWT-EGAN

4.4. Denoising Performance Comparisons

Under the same conditions, we evaluate noise reduction results of PSBD-EWT-EGAN compared to WT (constant threshold), EMD and AE-CGAN (autoencoder-Conditional Generative Adversarial Networks) [42]. WT and EMD are two frequently used tools for non-stationary signals. Compared with the EGAN, the generator network of AE-CGA only introduces $L_1 - distance$ to its loss function. The database of clean HSSs consists of the recordings from MHSDB and WUPHSD. The recordings were randomly divided two sets: the testing set and the training set, in a 1:4 ratio. The clean HSSs are mixed with WGN and pink noise at different SNRs (-5dB, -2.5dB, 0dB, 2.5dB, and 5dB) to get the noisy HSSs. All the recordings are partitioned into 3-second clips using the non-overlapping windows.

Figures 6 and 7 showcases the effects of noise reduction of normal HSSs from WUPHSD and aortic stenosis HSSs from MHSDB by four models when the HSSs are mixed with WGN noise and pink noise at SNRs=0dB, respectively. The resample points are set to 2000. The time-domain diagram is on the left and the time-frequency diagram is on the right. It can be seen that the WT denoising can not only remove most of the noise, but also eliminate meaningful components of the original HSSs, resulting in the waveform distortion of the denoised HSSs. Although EMD retains most of the original HSSs, it also retains components of the noise, and the denoised effect is not ideal. The main reasons for the above phenomenon are as follows:(i) The basis function of WT denoising is pre-selected and the parameters are fixed manually; (ii) The noise variance of EMD denoising is contained in the interval threshold, and even seriously destroys the structure of HSSs. Therefore, WT and EMD denoising of HSSs are difficult to accurately distinguish heart sounds and noises. Compared with WT and EMD, both AE-CGAN and PSBD-EWT-EGAN can retain more meaningful components of the original HSSs while removing noises in a low SNR environment. Notably, compared to AE-CGAN, PSBD-EWT-EGAN is more capable of preventing excessive distortion.

Table 1. Denoising performance comparison among WT, EMD, AE-CGAN and PSBD-EWT-EGAN

Noise Type	Input SNR(dB)	SNR(dB)				RMSE			
		WT	EMD	AE-CGAN	PSBD-EWT-EGAN	WT	EMD	AE-CGAN	PSBD-EWT-EGAN
White	-5	-4.08	-4.03	7.77	9.26	0.179	0.178	0.052	0.044
	-2.5	-1.69	-1.61	8.19	10.14	0.136	0.134	0.050	0.041
	0	0.68	0.85	8.63	11.24	0.103	0.101	0.049	0.037
	2.5	3.00	3.30	8.63	11.24	0.079	0.076	0.049	0.037
	5	5.28	5.75	9.04	12.53	0.061	0.058	0.047	0.034
Pink	-5	2.5	-3.25	5.63	6.46	0.084	0.162	0.067	0.063
	-2.5	3.64	-0.79	6.83	7.95	0.074	0.122	0.058	0.051
	0	4.89	1.62	7.64	9.10	0.064	0.093	0.053	0.046
	2.5	6.18	4.11	8.49	10.45	0.055	0.070	0.049	0.040
	5	7.56	6.51	8.83	11.54	0.047	0.053	0.048	0.037

Table 1 shows performance of different methods for different noise types and the input SNR levels, including WT, EMD, AE-CGAN and PSBD-EWT-EGAN. Compared with WT and EMD, our proposed method is advantageous in all aspects. In the case of WGN

SNR=5dB, our proposed method gains a best output SNR (dB) (12.53 vs.5.28 vs. 5.75) and an RMSE (0.034 vs. 0.061 vs. 0.058). In the case of pink noise SNR=5dB, PSBD-EWT-EGAN provides a best output SNR (dB) (11.54 vs. 7.56 vs. 6.51) and an RMSE (0.037 vs. 0.047 vs. 0.053). It demonstrates the superiority of exploiting PSBD-EWT-EGAN to enhance the quality of the HSSs. Besides, compared with AE-CGAN, PSBD-EWT-EGAN consistently outperforms AE-CGAN in output SNR and RMSE across all input SNRs. Overall, PSBD-EWT-EGAN has the highest anti-noise ability compared with WT, EMD and AE-CGAN. The main reason for the above results is that we replaced the cross-entropy loss with the least square loss. Moreover, the an optimized loss function of G combining $L_1 - distance$, $L_2 - distance$ and $l_{feature} - distance$ between the denoised HSS and the clean HSS is very effective.

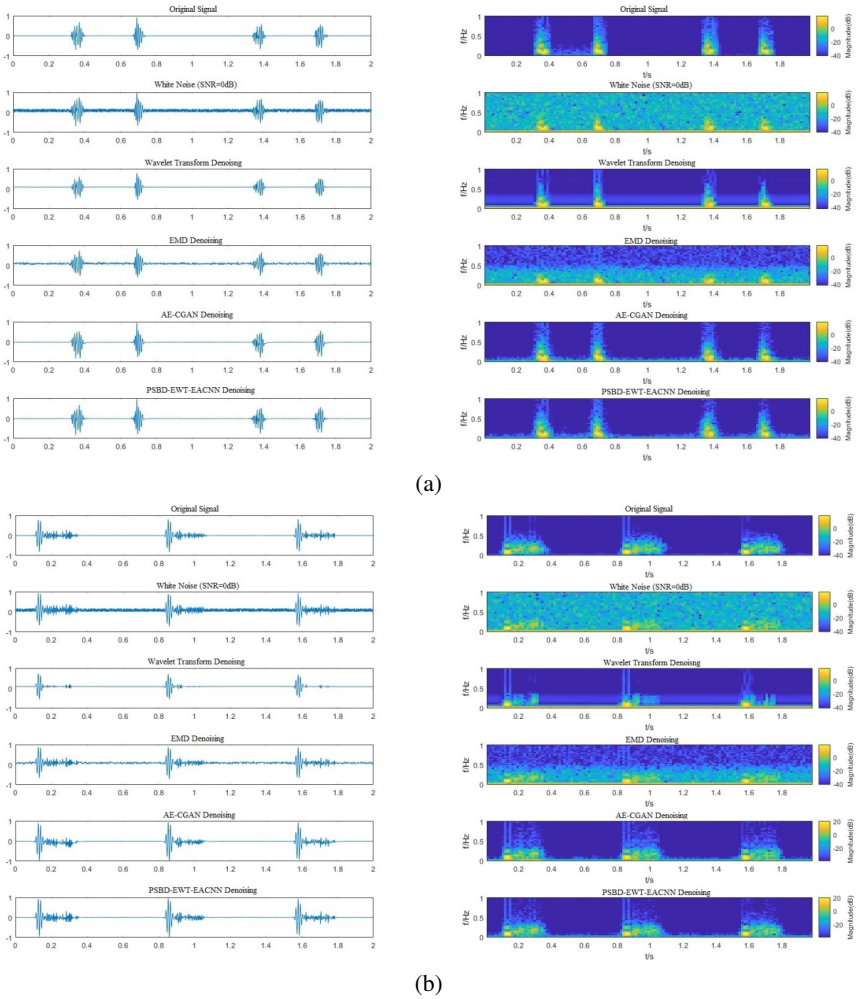

(a)

(b)

Fig. 6. The effects of four denoising methods on white noise SNR=0dB

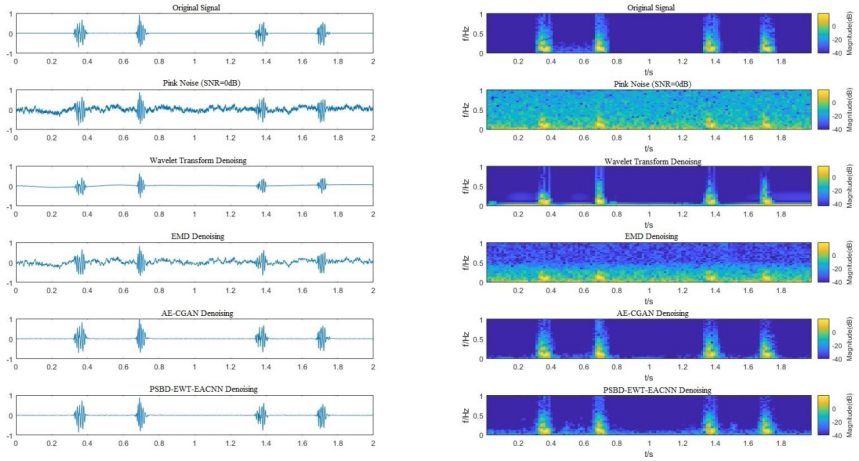

(c)

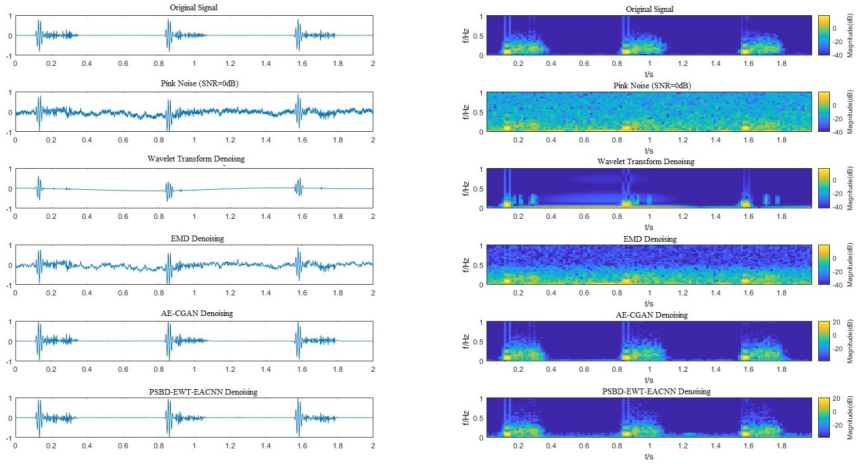

(d)

Fig. 7. The effects of four denoising methods on pink noise SNR=0dB

5. Conclusion

Under uncontrolled environments, various uncertain noises inherently corrupt HSSs. In this work, we take advantage of the interpretability of PSBD-EWT for HSSs denoising. Furthermore, we design EGAN architecture with an optimized loss function to improve PSBD-EWT's generalization capability with regard to different noises. Therefore, PSBD-EWT-EGAN has both stronger interpretability and higher generalization capability. Besides, we have validated it on PASCAL, MHSDB and WUPHSD databases, and both healthy and pathological recordings. Both normal and aortic stenosis HSSs contaminated with AWGN or pink noise at different levels of SNR, our approach achieves significant

improvements over state-of-the-art methods. In the case of WGN SNR=5dB, our proposed method obtains the best denoising performance, with a SNR of 12.53dB and an RMSE of 0.034.

PSBD-EWT-EGAN can play a vital role in resisting the noise interference for screening cardiac diseases in uncontrolled environments. The good effect of heart sound denoising lays the foundation for heart sound diagnosis, especially for non-invasive digital stethoscopes, which is conducive to accelerating the application and promotion of heart sound diagnosis in home healthcare monitoring.

Acknowledgments. This work was supported by Fujian Provincial Natural Science Foundation of China No. 2023J011426 and No. 2023J011428; Engineering Research Center for Big Data Application in Private Health Medicine of Fujian Universities, Putian University, Putian, Fujian 351100, China (MKF202408).

References

1. Organization, W.H., et al.: World health statistics overview 2019: monitoring health for the sdgs, sustainable development goals. Tech. rep., World Health Organization (2019)
2. Hadiyoso, S., Mardiyah, D.R., Ramadan, D.N., Ibrahim, A.: Implementation of electronic stethoscope for online remote monitoring with mobile application. Bulletin of Electrical Engineering and Informatics 9(4), 1595–1603 (2020)
3. Cañadas-Quesada, F.J., Ruiz-Reyes, N., Carabias-Orti, J., Vera-Candeas, P., Fuertes-Garcia, J.: A non-negative matrix factorization approach based on spectro-temporal clustering to extract heart sounds. Applied Acoustics 125, 7–19 (2017)
4. Zheng, Y., Guo, X., Jiang, H., Zhou, B.: An innovative multi-level singular value decomposition and compressed sensing based framework for noise removal from heart sounds. Biomedical Signal Processing and Control 38, 34–43 (2017)
5. Ali, A.M., Ghobashy, A.A., Sultan, A.A., Elkhodary, K.I., El-Morsi, M.: A 3d scaling law for supravalvular aortic stenosis suited for stethoscopic auscultations. Heliyon (2024)
6. Centracchio, J., Parlato, S., Esposito, D., Andreozzi, E.: Accurate localization of first and second heart sounds via template matching in forcecardiography signals. Sensors 24(5), 1525 (2024)
7. Sangeetha, B., Periyasamy, R.: Heart sound noise separation from lung sound based on enhanced variational mode decomposition for diagnosing pulmonary diseases. Biomedical Engineering: Applications, Basis and Communications 36(01), 2350035 (2024)
8. Hu, J., Hu, Q., Liang, M.: Heart sounds classification using adaptive wavelet threshold and 1d ldcnn. Computer Science and Information Systems 20(4), 1483–1501 (2023)
9. Xiao, F., Liu, H., Lu, J.: A new approach based on a 1d+ 2d convolutional neural network and evolving fuzzy system for the diagnosis of cardiovascular disease from heart sound signals. Applied Acoustics 216, 109723 (2024)
10. Gilles, J.: Empirical wavelet transform. IEEE transactions on signal processing 61(16), 3999–4010 (2013)
11. Sharan, T.S., Bhattacharjee, R., Sharma, S., Sharma, N.: Evaluation of deep learning methods (dncnn and u-net) for denoising of heart auscultation signals. In: 2020 3rd International Conference on Communication System, Computing and IT Applications (CSCITA). pp. 151–155. IEEE (2020)
12. Ali, S.N., Shuvo, S.B., Al-Manzo, M.I.S., Hasan, A., Hasan, T.: An end-to-end deep learning framework for real-time denoising of heart sounds for cardiac disease detection in unseen noise. IEEE Access 11, 87887–87901 (2023)

13. Everingham, M., Eslami, S.A., Van Gool, L., Williams, C.K., Winn, J., Zisserman, A.: The pascal visual object classes challenge: A retrospective. International journal of computer vision 111, 98–136 (2015)
14. Liu, C., Springer, D., Li, Q., Moody, B., Juan, R.A., Chorro, F.J., Castells, F., Roig, J.M., Silva, I., Johnson, A.E., et al.: An open access database for the evaluation of heart sound algorithms. Physiological measurement 37(12), 2181 (2016)
15. Grailu, H.: Compression of high-sampling-rate heart sound signals based on downsampling and pattern matching. Multimedia Tools and Applications 83(1), 201–226 (2024)
16. Hou, Y., Liu, R., Shu, M., Chen, C.: An ecg denoising method based on adversarial denoising convolutional neural network. Biomedical Signal Processing and Control 84, 104964 (2023)
17. Singh, P., Pradhan, G.: A new ecg denoising framework using generative adversarial network. IEEE/ACM transactions on computational biology and bioinformatics 18(2), 759–764 (2020)
18. Hu, L., Cai, W., Chen, Z., Wang, M.: A lightweight u-net model for denoising and noise localization of ecg signals. Biomedical Signal Processing and Control 88, 105504 (2024)
19. Jin, Y., Qin, C., Liu, J., Liu, Y., Li, Z., Liu, C.: A novel deep wavelet convolutional neural network for actual ecg signal denoising. Biomedical Signal Processing and Control 87, 105480 (2024)
20. Kiranyaz, S., Devecioglu, O.C., Ince, T., Malik, J., Chowdhury, M., Hamid, T., Mazhar, R., Khandakar, A., Tahir, A., Rahman, T., et al.: Blind ecg restoration by operational cycle-gans. IEEE Transactions on Biomedical Engineering 69(12), 3572–3581 (2022)
21. Sun, W., Su, Y., Wu, X., Wu, X.: A novel end-to-end 1d-rescnn model to remove artifact from eeg signals. Neurocomputing 404, 108–121 (2020)
22. Chuang, C.H., Chang, K.Y., Huang, C.S., Jung, T.P.: Ic-u-net: a u-net-based denoising autoencoder using mixtures of independent components for automatic eeg artifact removal. NeuroImage 263, 119586 (2022)
23. Sawangjai, P., Trakulruangroj, M., Boonnag, C., Piriyajitakonkij, M., Tripathy, R.K., Sudhawiyangkul, T., Wilaiprasitporn, T.: Eeganet: Removal of ocular artifacts from the eeg signal using generative adversarial networks. IEEE Journal of Biomedical and Health Informatics 26(10), 4913–4924 (2021)
24. Pu, X., Yi, P., Chen, K., Ma, Z., Zhao, D., Ren, Y.: Eegdnet: Fusing non-local and local self-similarity for eeg signal denoising with transformer. Computers in Biology and Medicine 151, 106248 (2022)
25. Haider, N.S.: Respiratory sound denoising using empirical mode decomposition, hurst analysis and spectral subtraction. Biomedical Signal Processing and Control 64, 102313 (2021)
26. Pouyani, M.F., Vali, M., Ghasemi, M.A.: Lung sound signal denoising using discrete wavelet transform and artificial neural network. Biomedical Signal Processing and Control 72, 103329 (2022)
27. Baharanchi, S.A., Vali, M., Modaresi, M.: Noise reduction of lung sounds based on singular spectrum analysis combined with discrete cosine transform. Applied Acoustics 199, 109005 (2022)
28. Yang, Y., Guo, X.M., Wang, H., Zheng, Y.N.: Deep learning-based heart sound analysis for left ventricular diastolic dysfunction diagnosis. Diagnostics 11(12), 2349 (2021)
29. Zhang, A., Wang, J., Qu, F., He, Z.: Classification of children's heart sounds with noise reduction based on variational modal decomposition. Frontiers in Medical Technology 4, 854382 (2022)
30. Gradolewski, D., Magenes, G., Johansson, S., Kulesza, W.J.: A wavelet transform-based neural network denoising algorithm for mobile phonocardiography. Sensors 19(4), 957 (2019)
31. Narváez, P., Percybrooks, W.S.: Synthesis of normal heart sounds using generative adversarial networks and empirical wavelet transform. Applied Sciences 10(19), 7003 (2020)
32. Gastineau, A., Aujol, J.F., Berthoumieu, Y., Germain, C.: A residual dense generative adversarial network for pansharpening with geometrical constraints. In: 2020 IEEE International Conference on Image Processing (ICIP). pp. 493–497. IEEE (2020)

33. Shen, S., Xie, L., Zhang, Y., Wu, G., Zhang, H., Yu, S.: Joint differential game and double deep q-networks for suppressing malware spread in industrial internet of things. IEEE Transactions on Information Forensics and Security 18, 5302–5315 (Aug 2023)
34. Hu, J., Wu, K., Liang, W.: An ipv6-based framework for fog-assisted healthcare monitoring. Advances in Mechanical Engineering 11(1), 1687814018819515 (2019)
35. Yang, F., Wang, Z., Li, J., Xia, R., Yan, Y.: Improving generative adversarial networks for speech enhancement through regularization of latent representations. Speech Communication 118, 1–9 (2020)
36. Feng, S., Zhao, L., Shi, H., Wang, M., Shen, S., Wang, W.: One-dimensional vggnet for high-dimensional data. Applied Soft Computing 135, 110035 (2023)
37. Li, J., Ke, L., Du, Q.: Classification of heart sounds based on the wavelet fractal and twin support vector machine. Entropy 21(5), 472 (2019)
38. Li, S., Li, F., Tang, S., Luo, F.: Heart sounds classification based on feature fusion using lightweight neural networks. IEEE Transactions on instrumentation and measurement 70, 1–9 (2021)
39. Gilles, J., Heal, K.: A parameterless scale-space approach to find meaningful modes in histograms—application to image and spectrum segmentation. International Journal of Wavelets, Multiresolution and Information Processing 12(06), 1450044 (2014)
40. Otsu, N., et al.: A threshold selection method from gray-level histograms. Automatica 11(285-296), 23–27 (1975)
41. Qiu, W., Murphy, W.J., Suter, A.: Kurtosis: a new tool for noise analysis. Acoust Today 16(4), 39–47 (2020)
42. Ge, F.: Brief review of recent researches in speech enhancement from filters to neural networks. In: 2020 International Conference on Computing and Data Science (CDS). pp. 260–264. IEEE (2020)

Jianqiang Hu is an associate professor in school of computer and information engineering, Xiamen University of Technology, China. He once worked as a postdoctoral researcher at Tsinghua University. He received his Ph.D. degree in computer science and engineering from National University of Defense Technology, China, in 2005. He is the author of more than 60 articles, and more than 8 inventions. His current research interests include Edge Computing, Biomedical Signal Processing, and Big Data Analytics.

Lin Chen is a master student at school of computer and information engineering, Xiamen University of Technology, China. His interest include Edge Computing and Biomedical Signal Processing.

Miao Yang received the B.S. degree from Jilin University, Changchun, China, in 2015, and the Ph.D. degree from the Shanghai Advanced Research Institute, Shanghai, and the University of Chinese Academy of Sciences, Beijing, China. He is currently with the Xiamen University of Technology, as a Lecturer. His current research interests include signal processing, federated learning, and edge AI.

Shigen Shen received the B.S. degree in fundamental mathematics from Zhejiang Normal University, Jinhua, China, in 1995, the M.S. degree in computer science and technology from Zhejiang University, Hangzhou, China, in 2005, and the Ph.D. degree in pattern recognition and intelligent systems from Donghua University, Shanghai, China, in 2013. He is a Professor with the School of Information Engineering, Huzhou University,

Huzhou, China. He has published more than 100 technical papers, including respected journals such as IEEE TRANSACTIONS ON INFORMATION FORENSICS AND SECURITY, IEEE TRANSACTIONS ON DEPENDABLE AND SECURE COMPUTING, IEEE TRANSACTIONS ON INDUSTRIAL INFORMATICS, IEEE TRANSACTIONS ON VEHICULAR TECHNOLOGY, and IEEE INTERNET OF THINGS JOURNAL. His current research interests include Internet of Things, cyber security, edge computing, and game theory.

Xiao-Zhi Gao received his B.Sc. and M.Sc. degrees from the Harbin Institute of Technology, China in 1993 and 1996, respectively. He obtained his D.Sc. (Tech.) degree from the Helsinki University of Technology (now Aalto University), Finland in 1999. He has been working as a professor at the University of Eastern Finland, Finland since 2018. He has published more than 450 technical papers in refereed journals and international conferences. His research interests are nature-inspired computing methods with their applications in optimization, data mining, machine learning, control, signal processing, and industrial electronics. Prof. Gao is currently serving on a number of prestigious editorial boards, such as Information Sciences, Applied Soft Computing, International Journal of Machine Learning and Cybernetics, Neural Computing and Applications, and Journal of Intelligent and Fuzzy Systems.

Received: August 04, 2024; Accepted: December 14, 2024.

Computer Science and Information Systems 22(1):259–278 https://doi.org/10.2298/CSIS240330008T

Academic research on Fuzzy Systems: A Country and Regional Analysis from its Origins in 1965 to 2023

Carlos J. Torres-Vergara[1], Víctor G. Alfaro-García[1], and Anna M. Gil-Lafuente[2]

[1] Facultad de Contaduría y Ciencias Administrativas, Universidad Michoacana de San Nicolás de Hidalgo,Morelia 58030, México
2146565g@umich.mx
victor.alfaro@umich.mx
[2] Facultat d'Economia i Empresa, Universitat de Barcelona, Barcelona 08034, Spain
amgil@ub.edu

Abstract. This study offers a bibliometric analysis to identify tendencies and trends and establish the most prolific and important countries in Fuzzy systems research and its evolution. The need for a robust mathematical approach that model human-like perceptions, values, and decision-making processes has made Fuzzy systems research grow significantly since its creation in 1965. This research had its epicentre originally in the USA and England and has moved first to Europe and then to Asia, following global trends in other fields of study. Data were retrieved from the scientific database Web of Science. A total of 185,673 documents were revised to identify tendencies and trends and establish the most prolific and influential countries.

Keywords: Fuzzy systems, Bibliometrics, Country analysis, Web of Science.

1. Introduction

Accurately representing uncertainty in statistical and probabilistic models is crucial in multiple fields of study, including finance, healthcare, engineering, and environmental science (Abdar et al., 2021). It ensures that predictions and decisions are based on realistic assessments of risk and variability, leading to more reliable and effective outcomes across diverse applications (Petropoulos et al., 2022). The valued logic introduced by Zadeh L. in 1965 in his paper Fuzzy sets (Zadeh, 1965) provided a useful tool to address and treat uncertainty and uncertain elements in a wide range of problems.

In his seminal paper, Zadeh analyzes the concept of Fuzzy systems, allowing classical Boolean sets to use a multi-valued logic in which the value of variables may be any real number between 0 and 1. This allows the concept of partial truth, where the truth value may range between completely true and false (Novák et al., 1999). At first, this research garnered minimal attention and faced substantial criticism within the scientific community (Zadeh, 2008). However, as the mid-1970s approached, and despite initial skepticism surrounding this novel theory, an increasing number of scientists began to analyze Zadeh's work and started applying it to his fields of study (Laengle et al., 2021).

Fuzzy systems were used first in engineering application (Wee & Fu, 1969; Asai & Kitajima, 1971) and were posteriorly applied to different areas such as mathematics

(Zadeh, 1971; De Luca & Termini, 1972), computer sciences (Ruspini, 1970; Zimmermann, 1978) or business economics (Basu, 1984) in order to manage in an effective way imprecise, incomplete vague or fragmentary information in humanlike dynamic systems (Jones et al., 1986).

Although these initial researchers come from different areas, they grouped to consolidate the field with the creation in 1978 of the first international journal exclusively for the international advancement of its theory and applications, Fuzzy Sets and Systems (Merigó et al., 2015). The journal is still active and relevant in 2023, publishing 340 works in 2022 that combine fuzzy concepts with other scientific disciplines as well as modern technologies and have an H-Index of 180 and an SJR index of 1.212 in 2022, which place it in the Q1 quartile both in Logic and Artificial Intelligence.

After this initial move, researchers from different areas of study such as Fu K.S., Bonissone P., Ruspini E., Bezdek J., Yager R. R. and Zadeh L. himself initiated endeavours to form a professional association dedicated to the study and application of Fuzzy Sets, establishing the North American Fuzzy Information Processing Society (NAFIPS) in 1985 in the state of California (Filev et al., 2009). Despite being officially created in 1985, annual meetings have been taking place since 1982, when the inaugural NAFIPS conference was hosted in Utah (USA[1]) on May 18-20.

The initial community of Fuzzy systems researchers was originally based in the USA but grew very quickly thanks to the attention received by Asian and European researchers since the 1970s (Blanco-Mesa et al., 2017). This attention globalized the Fuzzy community and led to the creation of the International Fuzzy Systems Association (IFSA), which held its first conference only 3 years later than the NAFIPS on July 1-6, 1985, in Palma de Mallorca (Spain).

From then on, Fuzzy systems publications grew in number and more specialized journals strictly dedicated to Fuzzy studies appeared. These publications include, among others: the Journal of Japan Society for Fuzzy Theory and Intelligent Informatics in 1989; the IEEE Transactions on Fuzzy Systems in 1993; the International Journal of Uncertainty, Fuzziness and Knowledge-Based Systems in 1993; the Journal of Intelligent & Fuzzy Systems in 1993; the Fuzzy Economic Review in 1995; the International Journal of Fuzzy Systems in 1999; Fuzzy Optimization and Decision Making in 2002; and the Iranian Journal of Fuzzy Systems in 2003 (Alfaro-García, Merigó, Pedrycz, et al., 2020).

Scientific production has increased exponentially in the last decades (Wuchty et al., 2007). This results in an overwhelming volume of new information and data, theories and conceptual developments that must be revised and classified quantitatively. From an academic perspective, it is important and necessary to classify all the papers published in a research field to find the leading trends and detect new lines of study and opportunities that help future investigations (Hicks et al., 2015).

In this scenario, bibliometrics studies offers a useful tool to provide a structured analysis to a large body of information, allowing one to infer trends over time and identify shifts in the boundaries of the research fields and detect the most productive and influential scholars, journals, and institutions, presenting a “big picture” of the existing

[1] Acronym: USA, United States of America

bibliography (Zupic & Čater, 2015). Thanks to the development of the internet and specialized computer software, bibliometric studies have become more viable, thus becoming a trend on its own (Ding et al., 2014). Bibliometric studies have become very common in the scientific community, within a wide range of research fields that include management (Vizuete-Luciano et al., 2021), medicine (Stenson et al., 2020), psychology (Arnett, 2008) or tourism (Jiang et al., 2019).

Production in Fuzzy systems research has increased greatly in the last years (Kumar et al., 2022) making necessary an update to previous bibliometric studies. This work tries to follow this lead and complement other works that have made a bibliometric approach to fuzzy research (Alfaro-García, Merigó, Alfaro Calderón, et al., 2020; Alfaro-García, Merigó, Pedrycz, et al., 2020; Merigó et al., 2015). Even though some of the published studies focus and analyzes specific characteristics of the Fuzzy area of study, there are no studies that analyzes Fuzzy systems research from a general perspective considering the most productive and influential countries in this academic field, being the scarce existing studies focused just in one specific region (Merino-Arteaga et al., 2022).

For that, the aim of this paper is to offer a bibliometric analysis to identify tendencies and trends and establish the most prolific and important countries in fuzzy research using the Web of Science (WoS) database and taking in account several bibliometric indicators. First, the study presents a regional analysis through time of the publications to see its evolution. Second, this paper presents a global table of nowadays Fuzzy research divided into countries with the highest number of articles, citations, and h-index. Third, we present different tables dividing the results of the previous table in periods of 10 years, in order to see how countries production evolved through time. Next, the study considers the most prolific authors and their countries, and finally introduces the most cited articles and their countries to establish a comparison between the most prolific countries and the most influential ones, which may differ. The main contribution of this approach is that it provides a general overview of the leading countries in Fuzzy research, allowing establish trends and to make comparisons between other scientific fields and geopolitics.

2. Methodology

This study classifies the data by using a bibliometric approach. Bibliometrics introduces a systematic and reproducible review process based on the statistical measurement of science, scientists, or scientific activity through a methodical quantification of the information concentrated in scientific databases (Broadus, 1987). To ensure that this review is neutral and informative, it's important to select the methods and tools that are going to be used (Merigó et al., 2015).

This paper reports on data drawn from the WoS database. WoS is currently owned by Clarivate Analytics and includes around 1.9 billion cited references from over 171 million records and over 20,000 scientific journals tracing back to the year 1900 (Birkle et al., 2020). Note that many other databases could be considered, including Google Scholar, SCOPUS and Microsoft Academic (Martín-Martín et al., 2018). Although Google Scholar and Microsoft Academic are the two most comprehensive bibliographic

data sources, they have several limitations in their search functionalities. These limitations include restricted support for Boolean and other advanced search operators, limited filtering capabilities, and non-transparent algorithms for processing queries and ranking documents on the results page, making them less suitable for bibliometric analyses (Martín-Martín et al., 2021). In this article, the focus will be given to WoS due to being one of the largest citation databases available in the market, providing a representative view of research and being the most used database in metanalysis over Scopus (Zhu & Liu, 2020).

The procedure for the retrieval of information is the following. We have used the keyword "fuzz*" for every title, abstract, and keyword. We have added all the papers published in some journals considered fuzzy systems oriented: Fuzzy Sets and Systems, IEEE Transactions on Fuzzy Systems, International Journal of Fuzzy Systems, Iranian Journal of Fuzzy Systems, Fuzzy Optimization and Decision Making, Advances in Fuzzy Systems and Fuzzy Information and Engineering. This list of journals was compiled using the bibliometric reviews conducted by Alfaro-García and García-Orozco on fuzzy logic journals (Alfaro-García, Merigó, Alfaro Calderón, et al., 2020; García-Orozco et al., 2022). The timespan of the search includes all the papers between 1965 to December 2021. This search was carried out in January 2023 and august 2024.

The advanced search for the replicability of this procedure is (((TS=(fuzz*)) OR SO=(fuzzy sets and systems OR ieee transactions on fuzzy systems OR international journal of fuzzy systems OR Iranian journal of fuzzy systems OR fuzzy optimization and decision making OR advances in fuzzy systems OR fuzzy information and engineering)) AND PY=(1965-2023)) AND DT=(Article OR Review OR Letter OR Note).

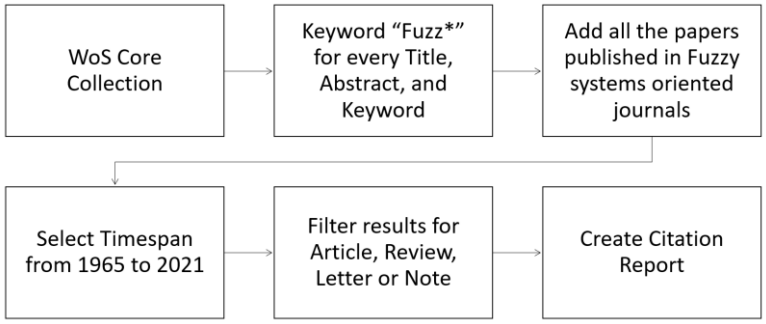

Fig. 1 Proposed search process

To measure scientific output of researchers is an increasingly important task for the scientific community (Zupic & Čater, 2015). In this study and for measure the influence of countries in the Fuzzy field of study, we rank the countries using the h-index and in the case of a tie, according to the number of citations. The h-index is a measure that aims to represent the importance of a set of papers defining the largest number of H for which an author has H papers with at least H citations each (Hirsch, 2005). For example, if an author has an h-index of 30, that means that 30 of the papers published by him have received at least 30 citations each. Since its introduction, the h-index has been extended and generalized by many authors, and it is considered a good method to value the

influence of and author or publication due to combining different metrics such as the total number of citations, the average number of citations per paper and the number and percentage of significant papers (Alonso et al., 2009). Although it has some weaknesses in measuring and analyzing very highly cited papers, it works quite well with huge volumes of publications, as is the case with a country analysis (Merigó et al., 2016).

Some papers are joint works of more than one author, some of them originally from different countries. We have made the search in the WoS database individually for each country, and the WoS database take in consideration the nationality of each of the authors to give proper data, so some papers had been counted various times. Although the search generates 185,673 documents, if we add the results of countries individually the number of papers is 235,075, reflecting this fact.

Each article is counted only once and is assigned to the country of the first author. Although it may cause some deviations, we consider that since each country has many researchers, the deviation this may cause in the overall results is minimal and may not affect the object of the study, which is to provide a general overview of the publishing countries and their evolution.

3. Results

This section presents the results of the study. Analyzing the data of the bibliometric retrieval, the results are classified by using a country study. The methodological procedure for the retrieval of information yields 185,673 documents. This contains all the publications covered by the WoS database and includes 181,631 articles, 8,236 proceeding papers, 4,061 book chapters, 3179 reviews, 529 letters, and 334 notes.

First, we group the countries utilizing the United Nations Regional Groups (United Nations Statistics Division, 2022) in Fig.2 and Fig. 3, dividing the world into 8 regions to observe the evolution of the publications of these regions throughout time (Mas-Tur et al., 2019) Following this first figure, we focused on individual countries, elaborating Table 1 which develops a global overview of the leading countries in Fuzzy research.

When conducting a country and regional analysis, some considerations must be attended. First, notable political changes took place during the timespan of the study, and some countries have changed their name, e.g. Soviet Union, Germany, and Czechoslovakia. In Table 1 we consolidated the data of the nonexistent regions to the actual territories. For example, the information of the German Democratic Republic and the Federal Republic of Germany that appears in Tables 2-3 have been unified into Germany in Tables 1-4-5-6 and 7.

Next, the results are divided into periods in Tables 2, 3, 4, 5, 6 and 7 to see the evolution of the leading countries throughout time. Same as the global overview of leading countries, due to political changes some countries disappear between tables. We grouped all the years between 1965 and 1980 because there is not much data compared to the other periods. Also, we grouped 2020 and 2023 in Table 7. It must be noted that these 4 years do not have enough time to be cited in comparison to the previous articles, causing a minor deviation in the analysis. Despite this, this table shows the tendencies for the last years and his analysis can be useful.

The work also develops an individual analysis of the most prolific authors in Fuzzy research in Table 8, so we can observe and analyze the origin of the authors. As some authors change their workplaces often, we took as criteria the last occupation and where they developed the majority of their career. We have included the Web of Science ID number of each of the authors to identify them. ORCID number is more reliable for this manner, but some of the authors who have been publishing long time as Pedrycz W. and Yagger R. R. do not have it. We have also included a time frame between his first article and the last one. Table 9 shows the most cited articles in Fuzzy research showing the year and the country of the first author with the same criteria as Table 8.

3.1. Analysis of Supranational Regions

Many regions are developing important research on Fuzzy around the World. Fig. 2 and Fig. 3 presents the number of articles published annually by 8 selected regions commented on above. Before 1991 it can be observed that Northern America was leading the field followed by Western Europe (including Scandinavian and southern countries), but then Asia took the lead and its production has risen significantly since then, with Western Europe overcoming Northern America in 1997. It is noticeable that the region including Northern Africa and Western Asia (we included Iran in this region) had remarkable growth since 2010, becoming the second-producing area in Fuzzy research in the world in 2023. We would like to emphasize the growth of Asia, especially since 2010, with his production being multiplied by 5. At the time of this article and according to the data retrieved, 101,229 out of 185,673 (which represents 54.52% of the papers produced historically worldwide) were produced in this region. This contrasts with the stagnation of production in Northern America, which had only increased by 60% in the last decade, passing from 795 papers to 1,278 according to the data.

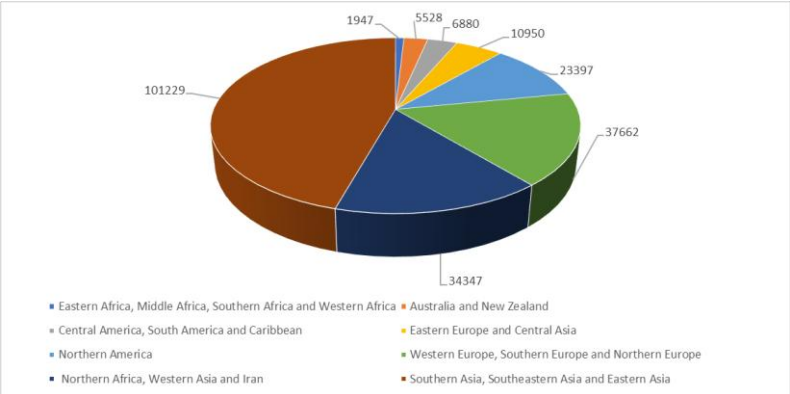

Fig. 2 Annual number of articles in Fuzzy systems published by each region

However, in terms of population, Southern, Southeastern, and Eastern Asia are one of the least productive areas. Even if these regions are the most productive regarding the

total number of papers, they are also the most populated areas in the world, with one-third of the world's entire population. Therefore, the productivity per person is very low compared to the rest of the areas of the analysis with countries like India with 14.32 papers per million inhabitants or People's Republic of China with 38.36 according to Table 1. This considered, Western Europe is the most productive area regarding its population with countries like Spain having 164.12 papers per million inhabitants or England with 130.24.

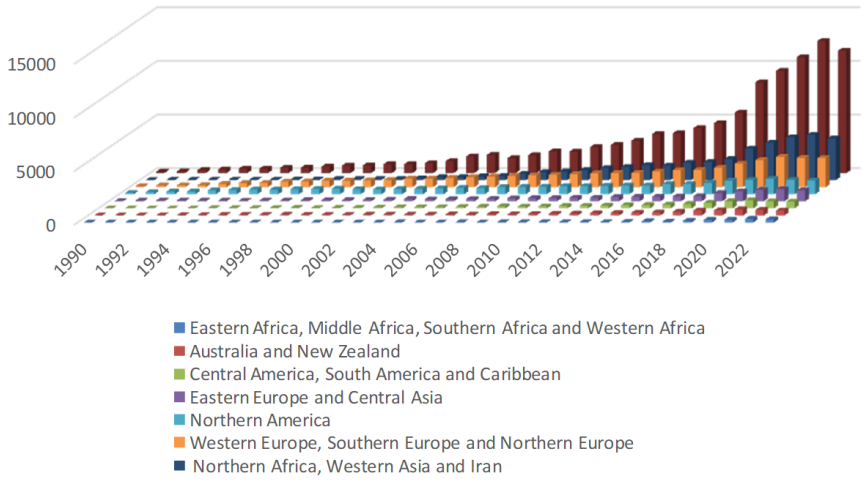

Fig. 3 Annual number of articles in Fuzzy systems published by each region

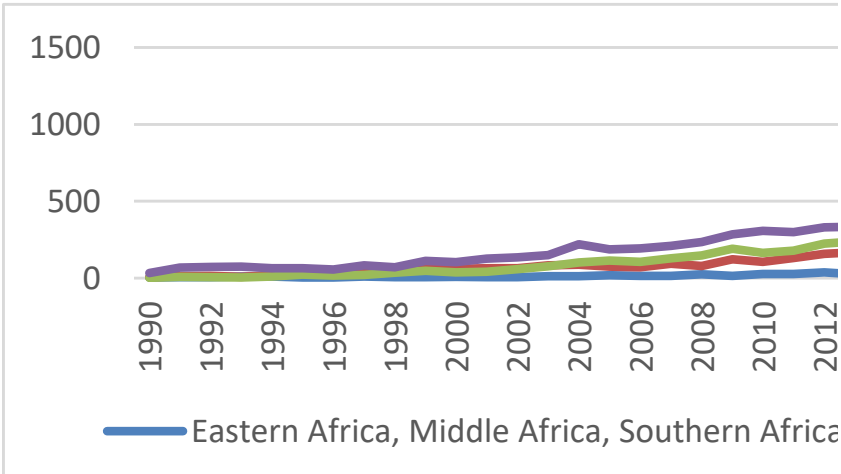

Fig. 4 Annual number of articles in Fuzzy systems published by less productive regions

Other regions not mentioned do not publish a significant number of articles and cannot be easily classified. Therefore, Fig. 4 presents a more specific analysis of the results of the less productive regions. Australia with 191.72 papers per million inhabitant and New Zealand with 109.87, for example, are publishing a relevant number

of papers according to their population, although the absolute numbers are not enough relevant as a region in Fig. 2. Central and South America (including the Caribbean) with countries like Brazil with 13.75 and México with 16.03 and Eastern Europe and Central Asia present similar total numbers and evolution, although Central and South America have twice the population, meaning that Eastern Europe with countries like Czech Republic with 174.29 papers per million inhabitant and Central Asia have a higher productivity per person. Africa (excluding North Africa) has the lowest total of papers and publications per capita with South Africa having 13.61 papers per million inhabitants being the most productive, with no other country in the region appearing in the top 50 countries.

3.2. Leading Countries in Fuzzy Systems Research

Fuzzy systems research articles are being produced by many countries. Table 1 presents the productivity and influence of the top 30 countries between 1965, when the first article about fuzzy systems was published, and 2023. The countries are ranked according to their number of publications, the total citations, the average article citations, the total number of papers per population, the total citations per population, and the total population are also included. Moreover, the table also includes the number of articles with more than 500, 250, 100, and 50 citations and the productivity per person.

The People's Republic of China is the most productive country attending to total papers with 29.45%, followed by India with 11.02, EEUU with 9.78, and Iran with 8.10. These 4 countries together represent more than 58% of total publications. Some smaller countries also obtain good results as Taiwan with 5.77%, Spain with 4.20%, England with 3.95%, Canada with 3,60% or South Korea with 3,33%

Regarding total citations, the People's Republic of China and the USA continue to obtain better results, followed at a significant distance by India, Iran, Taiwan, and England. This results in an average article citation of 41.34 for the USA and 39.32 for the Netherlands being the highest. England with 37.49, Singapore with 36.50, Belgium with 36.21 and Australia with 35.77 follows being the only countries with more than 35 average citations per article. The average article citation is an important indicator to measure the quality of the articles, especially when we compare articles of the same characteristics and fields of study (Waltman, 2016).

For having a proper overview of these indicators, it is important to compare the populations of the countries and the total articles and citations per population, as the country's characteristics have different impacts on how it can be researched (Man et al., 2003). Despite People's Republic of China having the most total publications and citations, compared to its population of 1,425.67 million, the number is not as high as it seems with 38.36 papers per million and 869.07 citations per million. The same can be observed by looking at the India data, with 14.32 articles per million inhabitants and 244.41 cites per million, despite being the fourth overall in total citations. On the other hand, Taiwan has the most articles per million inhabitants with 448.06 and 12,520.59 citations per million inhabitants. Singapore with 301.46 papers per million and 11,004.82 citations per million, Greece with 193.21 papers per million and 6,117.98 citations per million, Australia with 191.72 papers per million and 3,090.15 citations per

million and Canada with 172.51 articles per million and 6,858.09 citations per million also performs well in these indicators. The number of full-time researchers per million inhabitants has been included as a reference according to the UNESCO Science Report of 2021 (Schneegans et al., 2021) to give a better context, although some countries does not provide the information.

Lastly, Table 1 analyzes the number of articles with more than 500, 250, 100, and 50 citations. These indicators explain the impact that countries have on Fuzzy systems research, as the more articles with more than 500 and 250 citations a country has, the more influence they have in the research field and the more quality they have (Merigó et al., 2015). The USA is the most influential country in Fuzzy systems research with a total of 141 articles with more than 500 citations. China comes second with 69 articles with more than 500 citations. England with 35 and Spain with 28 and France with 24 complete the top 5. According to articles with more than 250 citations, China is the most influential country with 405 articles, followed by USA with 402, England with 140, Spain with 93, and Taiwan with 91.

Table 1. Most influential countries in Fuzzy systems research

R	R Name	TP-Fuzzy	TC-Fuzzy	AAC	%TP	TP/Pop	TC/Pop	Pop	R/Pop	>500	>250	>100	>50
1	P R CHINA	54,684	1,239,006	22.66	29.452	38.36	869.07	1,425.67	1,307	69	405	2,330	6,225
2	INDIA	20,459	349,167	17.07	11.019	14.32	244.41	1,428.63	253	23	89	1,823	1,244
3	USA	18,149	750,288	41.34	9.775	53.38	2,206.76	340.00	4,412	141	402	1,521	3,405
4	IRAN	15,032	384,534	25.58	8.096	168.57	4312.27	89.17	1,475	9	74	573	1,841
5	TAIWAN	10,719	299,530	27.94	5.773	448.06	12,520.59	23.92	N/A	23	91	586	1,602
6	SPAIN	7,799	228,546	29.30	4.200	164.12	4,809,57	47.52	3,001	28	93	353	1,089
7	TURKEY	7,406	208,229	28.12	3.989	86.30	2,426.46	85.82	1,379	12	60	409	1,130
8	ENGLAND	7,331	274,874	37.49	3.948	130.24	4,883.44	56.29	4,603	35	140	574	1,393
9	CANADA	6,690	216,060	32.30	3.603	172.51	5571.28	38.78	4,326	12	65	438	1,194
10	SOUTH KOREA	6,185	140,163	22.66	3.331	119.44	2706.69	51.78	7,980	6	38	234	699
11	ITALY	5,106	153,228	30.01	2.750	86.73	2,602.82	58.87	3,223	9	36	215	654
12	AUSTRALIA	5,069	181,321	35.77	2.730	191.72	6,858.09	26.44	N/A	12	86	381	981
13	SAUDI ARABIA	5,037	86,502	17.17	2.713	138.01	2370.11	36.50	N/A	3	27	138	430
14	JAPAN	4,658	139,458	29.94	2.509	37.78	1,131.10	123.29	5,331	21	71	233	611
15	FRANCE	4,547	153,408	33.74	2.449	70.22	2,369.02	64.76	6,419	24	61	288	719
16	GERMANY	4,426	120,438	27.21	2.384	53.14	1,445.94	83.29	7,539	9	47	219	617
17	PAKISTAN	3,915	68,397	17.47	2.109	16.28	284.41	240.49	336	3	14	76	294
18	POLAND	3,850	91,523	23.77	2.074	93.84	2,230.85	41.03	3,106	12	28	144	431
19	MALAYSIA	3,783	11,2000	29.61	2.037	110.27	3,264.54	34.31	2,397	9	49	197	591
20	BRAZIL	2,975	64,385	21.64	1.602	13.75	297.50	216.42	N/A	5	17	105	301
21	EGYPT	2,585	48,541	18.78	1.392	22.93	430.65	112.72	687	2	10	51	230
22	MEXICO	2,059	36,497	17.73	1.109	16.03	284.12	128.46	5,830	0	8	68	178
23	VIETNAM	2,018	56074	27.79	1087	20.41	567.22	98.86	315	0	17	112	331
24	GREECE	1,998	63266	31.66	1.076	193.21	6117.98	10.34	5,810	7	25	124	343
25	CZECH REPUBLIC	1,887	33457	17.73	1.016	174.29	3,090.15	10.83	708	1	5	47	157
26	SINGAPORE	1,813	66183	36.50	0.976	301.46	11004.82	6,01	6,803	4	33	145	372
27	RUSSIA	1,530	21333	13.94	0.824	10.59	147.69	144,44	2,784	1	9	32	71
28	BELGIUM	1,526	55262	36.21	0.822	130.58	4728.91	11,69	6,906	7	26	121	309
29	ALGERIA	1,489	27322	18.35	0.802	32.65	599.09	45,.61	819	1	6	44	141
30	NETHERLANDS	1,469	57755	39.32	0.791	83.38	3278.18	17.62	5,605	6	30	129	302

Acronyms: TP-Fuzzy, total papers in Fuzzy systems research. TC-Fuzzy, total citations in Fuzzy systems research. AAC, average article citation. %TP, percentage of total papers in Fuzzy systems research. TP/Pop, total papers per million inhabitants. TC/Pop, total citations per million inhabitants. Pop, Population in millions. R/Pop, Researchers per million inhabitants. >500, >250, >100 and >50, number articles with more than 500, 250,100 and 50 cites. PR CHINA, People's Republic of China. USA, United States of America.

3.3. Evolution of more Productive and Influential Countries in Fuzzy Systems Research

When analyzing the country rankings in a bibliometric study, the evolution through time becomes an interesting question (Merigó et al., 2016). This evolution depends on the economic and social situation of the country and the resources it invests in research (Man et al., 2003). Tables 2, 3, 4, 5, and 6 present the most productive and influential countries in fuzzy systems research divided into periods as explained previously. First, we have the most productive and influential countries in fuzzy research between 1980 in Table 2. The USA is by a large margin the most productive country with 153 papers. We can relate this early influence on the fact that fuzzy systems were created there in 1965. It must be highlighted that, even after producing just 28.10% of the articles the USA did, producing 43 papers, England has very similar citations with 10,804 vs the 11,853 citations of the USA. That results in an average article citation of 251.6 for England versus 77.47 for the USA. In contrast to England, Japan produced 20 papers in this period, which had only 702 citations regarding them, giving them an average of 35.3 citations per article. We should note that the average article citation in Table 2 is higher than the one in other periods due to the foundational and seminal articles of the area being created at that time. Regarding the h-Index USA has the highest number with 47, followed by England with 24, Canada with 13, and France and Japan with 10.

Table 3 follows the evolution of Fuzzy systems research between 1980 and 1989. USA continues leading the table in total papers with 598 representing 26.91% of the total, 43,500 citations, and an h-index of 94. Japan goes second with 193 total articles and 26,590 cites and an h-index of 50. The People's Republic of China started appearing on the list in third place with 163 articles but only 3,869 total cites. Poland and France also performed well with 135 and 121 total articles and 6,937 and 7,510 total citations respectively.

In Table 4 we can see that the article production in Fuzzy systems research between 1990 and 1999 greatly increased. If we add up the results of the top ten countries, we obtain 9,016 articles in comparison to the 1,655 produced between 1980 and 1989. The USA remains the most productive country and the one with the most citations, but it is noticeable how the People's Republic of China increased its total citations by 5.7 times. Taiwan also appears for the first time in the 4th place in total papers but is the second one in total citations with 34,014 and an h-index of 91. The tendency of European and northern American countries heading the rankings starts to change with Asian countries becoming more productive and producing articles with more quality.

Tables 5, 6, and 7 continue with this tendency, with the People's Republic of China being the most productive and influential country in the last 20 years. Its article production in the fuzzy research field increased dramatically every year to the point that between 2010 and 2019 the People's Republic of China produced more papers than the top ten countries in fuzzy research between 2000 and 2009 including himself. The USA falls to the 4 position overall, remaining a very influential and productive country in the field but not leading anymore. Taiwan, India, and Iran also perform well in the rankings, confirming that the center of the Fuzzy systems research has been displaced to the east, as can be seen in Fig. 2.

Table 2. Most influential countries in Fuzzy systems research before 1980

R	Name	TP-Fuzzy	TC-Fuzzy	AAC	% TP	H Index	TP/Pop	TC/Pop	Pop
1	USA	153	11,853	77,47	34.152	47	0.69	53.12	223.14
2	ENGLAND	43	10,804	251,26	9.598	24	0.92	230.92	46.79
3	JAPAN	26	959	36,88	5.804	10	0.22	8.15	117.62
4	FRANCE	19	2,988	157,26	4.241	10	0.35	55.63	53,71
5	CANADA	19	753	39,63	4.241	13	0.78	30.72	24,51
6	FED REP GER	12	1,129	94,08	2.009	8	0.19	18.31	61.66
7	BELGIUM	9	1,152	128,00	2.679	6	0.92	117.22	9.83
8	INDIA	9	446	49,56	2.009	6	0.01	0.64	696.83
9	POLAND	9	237	26,33	2.009	6	0.25	6.67	35.52
10	NETHERLANDS	9	1,966	218,44	2.009	8	0.64	139.14	14.13
11	ITALY	7	234	33,43	1.339	5	0.12	4.15	56.33
12	CZECHOSLOVAKIA	6	971	161,83	1.563	5	0.58	94.43	10.28
13	ISRAEL	6	23	3,83	1.339	3	1.60	6.14	3.74
14	AUSTRALIA	6	176	29,33	1.339	5	0.41	11.97	14.71
15	NEW ZEALAND	5	480	96,00	1.116	4	1.59	152.53	3.15
16	ROMANIA	4	51	12,75	0.893	3	1.27	16.21	22.125
17	GER DEM REP	4	13	3,25	0.893	2	0.24	0.78	16.74
18	GREECE	4	364	91,00	0.893	3	0.43	39.11	9.31
19	SPAIN	3	90	30,00	0.893	3	0.08	2.40	37.49
20	HUNGARY	3	19	6,33	0.670	3	0.28	1.78	10.70
21	IRAN	3	174	58,00	0.670	2	0.08	4.52	38.52
22	SOUTH AFRICA	3	121	40,33	0.670	3	0.10	4.11	29.46
23	BRAZIL	3	204	68,00	0.670	1	0.02	1.67	122.17
24	BUNDES REPUBLIK	3	18	6,00	0.670	1	0.18	1.08	16.74
25	DENMARK	2	1	0,50	0.446	1	0.39	0.20	5.13
26	DEUTSCH DEM REP	1	7	7,00	0.223	1	0.06	0.42	16.74
27	FINLAND	1	47	47,00	0.223	1	0.21	9.83	4.78
28	SWEDEN	1	240	240,00	0.223	1	0.12	28.88	8.31
29	UGANDA	1	0	0,00	0.223	0	0.08	0.00	13.28
30	USSR	1	6	6,00	0.223	1	0.00	0.02	270.00

Acronyms: H, h-index. FED REP GER, Federal Republic of Germany. GER DEM REP, German Democratic Republic. DEUTSCH DEM REP, Deutsche Demokratische Republik. USSR, Union of Soviet Socialist Republics

Table 3. Most influential countries in Fuzzy research between 1980 and 1989

R	Name	TP-Fuzzy	TC-Fuzzy	AAC	% TP	H Index	TP/Pop	TC/Pop	Pop
1	USA	598	43,500	70.22	26.913	94	2.44	177.58	244.95
2	JAPAN	193	26,590	147.26	8.686	50	1.57	215.71	123.27
3	PEOPLES R CHINA	163	3,869	22.69	7.336	27	0.14	3.41	1134.41
4	POLAND	135	6,937	48.53	6.076	40	3.56	182.85	37.94
5	FRANCE	121	7,510	64.92	5.446	36	2.15	133.70	56.17
6	INDIA	103	3,756	35.71	4.635	31	0.12	4.41	852.01
7	ENGLAND	102	3,887	32.02	4.590	31	2.15	81.74	47.55
8	ITALY	93	1,928	20.37	4.185	18	1.64	34.00	56.71
9	SPAIN	74	2,440	32.63	3.330	18	1.90	62.81	38.85
10	CANADA	73	3,099	38.4	3.285	27	2.68	113.75	27.24
11	FED REP GER	65	4,147	58.14	2.925	24	1.03	65.85	62.98
12	BELGIUM	58	2,001	33.12	2.610	25	5.84	201.37	9.94
13	USSR	52	356	6.6	2.340	10	0.18	1.22	290.93
14	GER DEM REP	37	547	14.5	1.665	15	2.25	33.28	16.43
15	CZECHOSLOVAKIA	35	443	12.82	1.575	9	3.38	42.75	10.36
16	FINLAND	34	3,072	83.61	1.530	14	6.85	618.86	4.96
17	AUSTRALIA	29	926	36.95	1.305	15	1.73	55.13	16.80
18	AUSTRIA	26	872	42.33	1.170	13	3.41	114.45	7.62
19	NETHERLANDS	25	3,287	140.55	1.125	16	1.68	221.35	14.85
20	GREECE	19	752	36.74	0.855	12	1.86	73.65	10.21
21	ROMANIA	19	290	15.82	0.855	8	0.83	12.73	22.79
22	EGYPT	18	321	19.06	0.810	10	0.32	5.76	55.77
23	HUNGARY	18	468	29.56	0.810	8	1.73	45.01	10.40
24	NORWAY	18	409	28.23	0.720	9	4.26	96.76	4.23
25	ISRAEL	18	1345	100.5	0.720	10	3.86	288.26	4.67
26	CZECH REPUBLIC	16	72	6.64	0.720	5	1.55	6.98	10.31
27	BULGARIA	11	13,501	1190.4	0.495	8	1.25	1,533.51	8.80
28	SWEDEN	11	132	11.9	0.495	5	1.29	15.52	8.50
29	SOUTH AFRICA	10	201	21.44	0.450	5	0.26	5.20	38.67
30	TURKEY	9	140	15.56	0.450	5	0.17	2.64	52.99

Table 4. Most influential countries in Fuzzy research between 1990 and 1999

R	Name	TP-Fuzzy	TC-Fuzzy	AAC	% TP	H Index	TP/Pop	TC/Pop	Pop
1	USA	3,038	168,309	55.40	25.440	164	10.88	602.87	279.18
2	JAPAN	1,156	32,448	28.07	9.680	80	9.13	256.39	126.56
3	PEOPLES R CHINA	838	22,200	26.49	7.017	70	0.67	17.68	1,255.43
4	TAIWAN	794	34,014	42.84	6.649	91	36.00	1542.10	22.06
5	GERMANY	685	15,854	23.14	5.736	63	8.40	194.39	81.56
6	INDIA	574	17,391	30.30	4.807	58	0.55	16.71	1,040.50
7	CANADA	536	23,475	43.80	4.488	73	17.63	772.23	30.40
8	ENGLAND	499	17,035	34.14	4.179	66	10.18	347.43	49.03
9	FRANCE	448	30,346	67.74	3.751	67	7.68	520.05	58.35
10	SOUTH KOREA	448	11,419	25.49	3.751	57	9.63	245.46	46.52
11	SPAIN	447	17,305	38.71	3.743	60	11.14	431.09	40.14
12	ITALY	406	12,365	30.46	3.400	53	7.13	217.14	56.95
13	AUSTRALIA	285	11,704	41.07	2.387	57	15.16	622.55	18.80
14	SINGAPORE	194	4,002	20.63	1.625	37	48.92	1,009.08	3.97
15	BELGIUM	184	7,541	40.98	1.541	45	18.00	737.58	10.22
16	POLAND	158	6,462	40.90	1.323	33	4.12	168.48	38.35
17	EGYPT	157	1,853	11,80	1.315	19	2.25	26.51	69.91
18	NETHERLANDS	138	6,882	49.87	1.156	42	8.73	435.24	15.81
19	RUSSIA	135	3,632	26.90	1.130	14	0.92	24.65	147.34
20	GREECE	125	4,200	33.60	1.047	36	11.37	382.06	10.99
21	BRAZIL	108	3,007	27.84	0.904	27	0.62	17.33	173.49
22	FINLAND	105	2,686	25.58	0.879	26	20.33	520.04	5.17
23	HUNGARY	105	4,027	38.35	0.879	32	10.26	393.65	10.23
24	CZECH REPUBLIC	99	1,860	18.79	0.829	23	9.63	180.88	10.28
25	AUSTRIA	98	2,825	28.83	0.821	29	12.26	353.52	7.99
26	YUGOSLAVIA	91	2,187	24.03	0.762	24	3.87	92.95	23.53
27	SCOTLAND	89	1,788	20.09	0.745	21	17.58	353.22	5.06
28	HONG KONG	87	2,897	33.30	0.729	29	13.10	436.23	6.64
29	ISRAEL	80	2,857	35.71	0.670	23	13.35	476.64	5.99
30	BULGARIA	77	2,415	31.36	0.645	21	9.43	295.88	8.16

Table 5. Most influential countries in Fuzzy research between 2000 and 2009

R	Name	TP-Fuzzy	TC-Fuzzy	AAC	% TP	H Index	TP/Pop	TC/Pop	Pop
1	PEOPLES R CHINA	4,865	184,504	37.92	16.212	184	3.63	137.78	1339.13
2	USA	4,204	229,159	54.51	14.009	197	13.63	742.79	308.51
3	TAIWAN	3,156	129,532	41.04	10.517	146	136.96	5621.07	23.04
4	SPAIN	1,589	64,694	40.71	5.295	112	34.27	1395.26	46.37
5	CANADA	1,530	61,497	40.19	5.098	113	45.55	1830.65	33.59
6	INDIA	1,530	62,285	40.71	5.098	113	1.25	50.90	1223.64
7	ENGLAND	1,470	81,178	55.22	4.899	135	28.16	1555.25	52.20
8	SOUTH KOREA	1,423	37,038	26.03	4.742	85	29.29	762.29	48.59
9	TURKEY	1,282	60,591	47.26	4.272	119	17.75	838.92	72.23
10	JAPAN	1,263	35,281	27.93	4.209	87	9.86	275.38	128.12
11	ITALY	1,240	39,482	31.84	4.132	90	20.82	662.87	59.56
12	GERMANY	1,031	37,091	35.98	3.436	89	12.69	456.45	81.26
13	FRANCE	1,030	38,663	37.54	3.432	94	16.59	622.66	62.09
14	IRAN	928	33,866	36.49	3.092	90	12.49	455.67	74.32
15	POLAND	813	27,247	33.51	2.709	73	21.09	706.70	38.56
16	AUSTRALIA	673	27,340	40.62	2.243	83	31.07	1262.23	21.66
17	GREECE	555	25,285	45.56	1.849	76	50.20	2287.20	11.06
18	BELGIUM	470	23,246	49.46	1.566	77	43.51	2152.21	10.80
19	SINGAPORE	463	21,814	47.11	1.543	80	92.42	4354.09	5.01
20	BRAZIL	429	17,563	40.94	1.430	60	2.21	90.29	194.52
21	CZECH REPUBLIC	367	11,565	31.51	1.223	58	34.99	1102.69	10.49
22	MEXICO	314	7,562	24.08	1.046	45	28.42	684.41	11.05
23	NETHERLANDS	305	17,647	57.86	1.016	72	18.44	1067.19	16.54
24	EGYPT	271	6,687	24.68	0.903	40	3.17	78.21	85.50
25	ROMANIA	255	6,474	25.39	0.850	43	12.46	316.33	20.47
26	FINLAND	218	7,885	36.17	0.726	45	40.84	1477.14	5.34
27	RUSSIA	214	3,350	15.65	0.713	25	1.49	23.40	143.16
28	AUSTRIA	212	7,535	35.54	0.706	51	25.41	903.26	8.34
29	MALAYSIA	190	4,912	25.85	0.633	40	6.73	174.08	28.22
30	HUNGARY	185	9,868	53.34	0.616	52	18.49	986.01	10.01

Table 6. Most influential countries in Fuzzy research between 2010 and 2019

R	Name	TP-Fuzzy	TC-Fuzzy	AAC	% TP	H Index	TP/Pop	TC/Pop	Pop
1	PEOPLES R CHINA	22,788	718,372	31.52	30.684	252	16.03	505.23	1421.86
2	IRAN	8,030	239,546	29.83	10.812	160	92.76	2767.27	86.56
3	INDIA	7,350	189,933	25.84	9.897	142	5.31	137.32	1383.11
4	USA	6,465	243,502	37.66	8.705	178	19.34	728.35	334.32
5	TAIWAN	4,471	107,853	24.12	6.020	118	188.04	4536.02	23.78
6	TURKEY	3,552	107,743	30.33	4.783	131	42.55	1290.63	83.48
7	SPAIN	3,467	117,516	33.90	4.668	138	73.56	2493.39	47.13
8	ENGLAND	2,714	118,441	43.64	3.654	143	48.22	2104.23	56.29
9	CANADA	2,683	96,221	35.86	3.613	129	71.50	2564.39	37.52
10	SOUTH KOREA	2,396	60,502	25.25	3.226	104	46.25	1167.92	51.80
11	AUSTRALIA	2,164	105,362	48.69	2.914	146	85.34	4155.14	25.36
12	ITALY	1,959	57,914	29.56	2.638	97	32.80	969.65	59.73
13	MALAYSIA	1,906	81,468	42.74	2.566	124	58.10	2483.48	32.80
14	FRANCE	1,868	61,252	32.79	2.515	105	29.01	951.13	64.40
15	GERMANY	1,595	52,776	33.09	2.148	101	19.18	634.72	83.15
16	POLAND	1,487	36,909	24.82	2.002	81	38.63	958.85	38.49
17	SAUDI ARABIA	1,318	46,788	35.50	1.775	102	36.79	1305.94	35.83
18	BRAZIL	1,279	32,300	25.25	1.722	77	6.04	152.52	211.78
19	JAPAN	1,211	34,715	28.67	1.631	83	9.63	275.97	125.79
20	PAKISTAN	1,163	32,323	27.79	1.566	83	5.21	144.76	223.29
21	MEXICO	990	20,494	20.70	1.333	69	7.91	163.83	125.10
22	CZECH REPUBLIC	818	15,355	18.77	1.101	53	77.36	1452.15	10.57
23	GREECE	806	26,898	33.37	1.085	77	75.38	2515.48	10.69
24	EGYPT	745	21,639	29.05	1.003	70	7.05	204.88	105.62
25	ALGERIA	732	17,441	23.83	0.986	68	17.14	408.41	42.71
26	SERBIA	706	16,319	23.11	0.951	61	95.39	2204.97	7.40
27	SINGAPORE	691	32,191	46.59	0.930	86	117.80	5487.73	5.87
28	ROMANIA	664	13,429	20.22	0.894	62	34.01	687.82	19.52
29	VIETNAM	624	26,943	43.18	0.840	88	6.52	281.31	95.78
30	NETHERLANDS	599	23,540	39.30	0.807	76	34.50	1355.76	17.36

Table 7. Most influential countries in Fuzzy research between 2020 and 2023

R	Name	TP-Fuzzy	TC-Fuzzy	AAC	% TP	H Index	TP/Pop	TC/Pop	Pop
1	PEOPLES R CHINA	26,027	310,061	11.91	38.977	140	18.25	217.45	1425.89
2	IRAN	6,024	74,650	12.39	16.313	82	68.51	849.04	87.92
3	INDIA	4,923	110,216	22.39	9.021	91	3.50	78.30	1407.56
4	USA	3,690	53,965	85.00	5.526	53	10.95	160.13	337.00
5	SAUDI ARABIA	3,564	43,442	12.19	5.337	71	99.14	1208.40	35.95
6	PAKISTAN	2,705	34,975	12.93	4.051	65	11.69	151.14	231.40
7	ENGLAND	2,502	43,362	17.33	3.747	79	44.29	767.62	56.49
8	TURKEY	2,488	37,809	15.20	3.726	72	29.26	444.59	85.04
9	TAIWAN	2,289	27,310	11.93	3.428	62	95.94	1144.64	23.86
10	SPAIN	2,219	26,397	11.90	3.323	62	46.73	555.89	47.49
11	AUSTRALIA	1,912	35,813	18.73	2.863	76	73.76	1381.62	25.92
12	SOUTH KOREA	1,910	27,532	14.41	2.860	67	36.85	531.20	51.83
13	CANADA	1,848	30,909	16.73	2.768	71	48.43	810.09	38.16
14	MALAYSIA	1,671	25,150	15.05	2.502	66	49.77	749.11	33.57
15	ITALY	1,400	20,512	14.65	2.097	61	23.63	346.25	59.24
16	EGYPT	1,396	17,962	12.87	2.091	56	12.78	164.39	109.26
17	VIETNAM	1,337	27,531	20.59	2.002	76	13.72	282.46	97.47
18	POLAND	1,248	13,632	10.92	1.869	46	32.58	355.86	38.31
19	BRAZIL	1,151	11,184	9.72	1.724	44	5.37	52.18	214.33
20	GERMANY	1,099	14,717	13.39	1.646	51	13.18	176.45	83.41
21	FRANCE	1,061	12,649	11.92	1.589	45	16.44	196.01	64.53
22	JAPAN	809	11,191	13.83	1.551	52	6.49	89.81	124.61
23	IRAQ	789	9,465	12.00	1.212	45	18.12	217.42	43.53
24	RUSSIA	780	6,471	8.30	1.182	35	5.38	44.60	145.10
25	MEXICO	732	7,833	10.70	1.168	39	5.78	61.82	126.71
26	SERBIA	689	10,171	14.76	1096	47	94.44	1394.05	7.30
27	ALGERIA	619	4,484	7.24	1032	28	14.01	101.50	44.18
28	THAILAND	616	5,247	8.52	0.927	33	8.60	73.28	71.60
29	CZECH REPUBLIC	592	4,563	7.71	0.923	31	56.25	433.58	10.52
30	GREECE	489	5,696	11.65	0.887	33	46.82	545.33	10.45

3.4. Most Productive Authors in Fuzzy Systems Research

We included Table 8 with the most prolific researchers in the Fuzzy field. 15 out of 30 produced their work in the People's Republic of China, which we can relate to China being the most productive country. 20 out of 30 authors come from Asia. Despite this, the most prolific author is Pedrycz W. from Canada with 1,011 papers, way more than the other authors. Wang J. from Liverpool University is the second most prolific author with 735 articles, but Xu, Z. is the most cited one with 44,169 articles. The first USA author is Yager R. R. in the 14th position with 403 papers published but the third one on the total citation. It must be noted that Iran, being one of the most productive countries in Table 2 doesn't have any author in this top 30.

Looking at the period of activity of the authors, the majority of them started publishing in the 1990s, when the first point of growth in the area of study occurred. Garg. H. from India is the most recent author in the table, having his first article published in 2012. In future analysis, other authors that started publishing in the 2010s will probably appear, as pointed out in Fig.2 and Table 6, that decade shows the bigger expansion of the Fuzzy systems field. It is also remarkable that some authors that showed interest and started publishing very early like Pedrycz W. and Yager R. R. are still active in 2021, meaning that they have a very long career of more than 40 years.

Table 8. Most productive authors in Fuzzy research

R	Name	Country	TP-Fuzzy	TC-Fuzzy	H-Fuzzy	Active Period	WoS ID
1	Pedrycz W.	CANADA	1,011	33,041	83	1981-2023	FPE-7309-202
2	Wang J.	ENGLAND	735	22,944	81	1993-2023	AAX-4516-20
3	Zhang Yingmiao	PEOPLES R CHINA	707	12,922	54	1988-2023	GSC-0345-202
4	Liu Yang	PEOPLES R CHINA	693	13,557	57	1999-2023	AAD-5667-20
5	Xu Z.	PEOPLES R CHINA	621	44,169	103	2002-2023	N-8908-2013
6	Wang Y.	PEOPLES R CHINA	597	11,291	56	1999-2023	BBC-2658-202
7	Li Yue	PEOPLES R CHINA	578	11,545	50	1996-2023	DBQ-8192-20
8	Kumar A.	INDIA	513	10,232	51	1994-2023	DCA-4254-20
9	Wang L.	PEOPLES R CHINA	507	10,651	49	1992-2023	EFM-4090-20
10	Liu Jun	PEOPLES R CHINA	455	9,325	47	1996-2023	C-1338-2011
11	Li J.	PEOPLES R CHINA	443	8,614	46	1997-2023	FIA-2393-202
12	Zhang J.	PEOPLES R CHINA	428	8,132	43	1995-2023	ABT-0791-20
13	Zhang L.	SINGAPORE	417	9,676	51	1997-2023	EIW-2267-202
14	Yager R. R.	USA	403	28,619	73	1977-2023	GKQ-0038-20
15	Huang G.	CANADA	391	11,406	53	1993-2023	H-5306-2011
16	Li Xiang	PEOPLES R CHINA	382	7,589	46	1996-2023	DDJ-7834-202
17	Castillo O.	MEXICO	379	12,957	67	1999-2023	I-5578-2019
18	Akram M.	PAKISTAN	379	10,156	50	2008-2023	N-3369-2014
19	Garg H.	INDIA	375	16,201	73	2012-2023	C-6063-2012
20	Li Y.	PEOPLES R CHINA	365	20,644	70	1999-2023	F-8379-2016
21	Zhang H.	PEOPLES R CHINA	358	8,151	48	1999-2023	GLM-3140-20
22	Tong S.	PEOPLES R CHINA	343	28,47	94	1994-2023	JCM-4762-202
23	Kahraman C.	TURKEY	338	16,347	70	1999-2023	N-9259-2013
24	Mesiar R.	SLOVAKIA	326	9,246	51	1989-2023	DZI-2965-202
25	Wang H.	PEOPLES R CHINA	285	5,046	38	1998-2023	EGI-7701-202
26	Shi Peng	AUSTRALIA	279	23,281	93	2004-2023	EOZ-7086-202
27	Melin P.	MEXICO	274	8,849	57	1994-2023	B-3611-2013
28	Herrera-Viedma	SPAIN	270	27,414	84	2006-2023	FWR-4541-20
29	Zhang Q.	PEOPLES R CHINA	265	4,7	35	1994-2023	ABU-1212-20
30	Herrera F.	SPAIN	261	39,96	102	2006-2023	K-9019-2017

3.5. Most Cited Articles in Fuzzy Research

Lastly, we included Table 9 with the most cited articles in the Fuzzy systems research area. None of the authors shown in Table 8 appear in Table 9, despite some of them like Pedrycz W., Xu Z., Yager, R.R., Tong S. or Herrera F. having more than 20,000 citations. The country with the most contributions to the list is the USA with 12 out of 30 articles, followed by England with 3 and Taiwan, Bulgaria, Australia, and Spain with 2. People's Republic of China only have 1. The total number of articles from Northern America and England is 16, showing that this area is the most important one, in contrast to what is shown in Table 8 where China and Asia were leading.

Table 9. Most cited articles in Fuzzy research

R	Article Title	Authors	TC	Year	Country
1	Fuzzy Sets	Zadeh, LA	54,314	1965	USA
2	Fuzzy identification of systems and its applications to modeling and control	Takagi, T; Sugeno, M	13,808	1985	Japan
3	ANFIS - Adaptative-Network-Based Fuzzy Inference System	Jang, JSR	10,963	1993	Taiwan
4	Intuitionistic Fuzzy-Sets	Atanassov, KT	9,983	1986	Bulgaria
5	Fuzzy nanoassemblies: Toward layered polymeric multicomposites	Decher, G	9,237	1997	Germany
6	Enrichr: a comprehensive gene set enrichment analysis web server 2016 update	Kuleshov, MV; Jones, MR; Rouillard, AD	5,462	2016	USA
7	Experiment in linguistic synthesis with a fuzzy logic controller	Mamdani, EH; Assilian, S	4,435	1975	England
8	FCM - The Fuzzy C-means clustering-algorithm	Bezdek, JC; Ehrlich, R; Full, W	4,192	1984	Australia
9	Survey of clustering algorithms	Xu, R; Wunsch, D	3,665	2005	USA
10	Core affect and the psychological construction of emotion	Russell, JA	3,393	2003	USA
11	Fuzzy-Logic in control-systems - Fuzzy-Logic controller .1.	Lee, CC	3,124	1990	USA
12	Soft set theory - First results	Molodtsov, D	3,026	1999	Russia
13	Survey over image thresholding techniques and quantitative performance evaluation	Sezgin, M; Sankur, B	2,969	2004	Turkey
14	Applications of the extent analysis method on fuzzy AHP	Chang, DY	2,949	1996	USA
15	Hesitant Fuzzy Sets	Torra, V	2,942	2010	Spain
16	Building Better Causal Theories: A Fuzzy Set Approach to typologies in organization research	Fiss, PC	2,767	2011	USA
17	Fuzzy identity-based encryption	Sahai, A; Waters, B	2,762	2005	USA
18	Validation of the theoretical domains framework for use in behaviour change and implementation research	Cane, J; O'Connor, D; Michie, S	2,576	2012	England
19	Extensions of the TOPSIS for group decision-making under fuzzy environment	Chen, CT	2,452	2000	Taiwan
20	Interval Valued Intuitionistic Fuzzy-Sets	Atanassov, K; Gargov, G	2,395	1989	Bulgaria
21	On digital soil mapping	McBratney, AB; Santos, MLM; Minasny, B	2,350	2003	Australia
22	Decision-Making in a Fuzzy Environment	Bellman, RE; Zadeh, LA	2,333	1970	USA
23	A review on image segmentation techniques	Pal, NR; Pal, SK	2,322	1993	India
24	A validity measure for Fuzzy clustering	Xie, XLL; Beni, G	2,296	1991	PR China
25	Application of Fuzzy algorithms for control of simple dynamic plant	Mamdani, EH	2,273	1974	England
26	Gene trees in species trees	Maddison, WP	2,209	1997	Canada
27	A 2-tuple fuzzy linguistic representation model for computing with words	Herrera, F; Martinez, L	2,146	2000	Spain
28	Fuzzy hierarchical analysis	Buckley, JJ	2,146	1985	USA
29	Fuzzy cognitive maps	Kosko, B	2,132	1986	USA
30	Fuzzy logic equals Computing with words	Zadeh, LA	2,043	1996	USA

4. Conclusion

The aim of this paper is to offer a bibliometric analysis to identify tendencies and trends and establish the most prolific and important countries in Fuzzy systems research. For that, an analysis of research documents focused on Fuzzy systems using bibliometric tools and techniques has been presented. The analysis is focused on the most productive and influential countries between 1965 and 2023. The results obtained show that the last decade has been the most prolific both in articles and citations, representing that the average article citation is getting lower every decade.

First, we made a supranational analysis in **Fig. 2** and **Fig. 3** aiming to see from a global perspective how fuzzy research is distributed in the world and how evolved throughout time. All the regions increased the number of publications with Southern Asia, Southeastern Asia and Eastern Asia leading after multiplying per 3.77 his publications in 10 years, going from 3,023 in 2013 to 11,411 in 2023. Northern America was leading before the 1990s, but its production has not increased at the same rhythm as the other regions changing from 795 in 2013 to 1,278 in 2023. Northern Africa and Iran holds second position, and their production is currently increasing significatively, especially in the last decade going from 1,231 to 3,891. Western Europe, which follows Northern America also increased its production significantly, but not enough to match Asia, Western Africa, and Iran.

Looking at individual countries, the conclusions are the same. The epicentre of the Fuzzy systems research production moved from the USA and England (with Canada and the rest of Europe being very important as well) to Asia with People's Republic of China, India and Iran leading the change. The expectations for the future are that Asia production will continue growing, and Western countries will not be able to match them. It is important to highlight that, even the epicenter of production is changing, the most important and influential papers are from the USA and England.

It should be underlined that this tendency change must not be seen as a rarity that happens just in the fuzzy systems field, as other science fields, especially the ones that are related to computer sciences are following the same path, where countries like People's Republic of China, India and Iran are surpassing USA and Western Europe, who were the traditional leaders in the field (Huang et al., 2015), and other countries start to match them. This is happening due to different reasons, but the governments of these countries are investing lots of resources into it to reduce their dependence on foreign countries as they develop (Ong, 2021).

Development priorities have aligned over the last years, with countries of all income levels prioritizing their transition to digital economies, convinced that their future economic competitiveness will depend upon how quickly they transition to digital. In order to achieve this development, countries need to improve their infrastructure and industrialization on a parallel path to its research, chronic underspending on research and development means they are largely a recipient of foreign scientific expertise and technology (Bonilla et al., 2015).

Although this work shows the tendencies and leading countries in fuzzy research, it has its limitations. As mentioned above in point 3, many authors work abroad and it's not easy to classify and evaluate the research of a country. English-speaking countries receive a large number of researchers from other countries, and that means that they can place higher in the rankings than other countries that count only on their citizens. If we

took the birth nationality as the main nationality to this study, some of the results will change, as some scholars prefers to work in more competitive institutions abroad.

Another important limitation related to this is that WoS gives each author only one country of reference. Some authors can work for different institutions in different countries in their lifetime, causing some deviations in the study. However, a country includes many researchers, and therefore, from a statistical point of view, the deviations should be equilibrated when considering a high volume of data and should not affect the final conclusions.

Also, the vast majority of the papers published in WoS are written in English, and non-English-speaking countries may also publish their research in other languages and therefore are not included in WoS. However, we must consider that the material included in WoS is sufficiently representative of the most important works so we can identify the trends and obtain conclusions.

We consider that the country and regional analysis provided in this article can be useful for different works that may be performed in the future, not only in the fuzzy research field, but also in other areas of study such as computer sciences. This article forms a preliminary stage to that may allow to identify trends in geopolitical studies, giving and overview of the focus and point of interest from different countries.

Acknowledgment. This work was (partially) supported by Programa Iberoamericano de Ciencia y Tecnología para el Desarrollo (CYTED) (through Red SIEMCI 522RT0130)

References

1. Abdar, M., Pourpanah, F., Hussain, S., Rezazadegan, D., Liu, L., Ghavamzadeh, M., Fieguth, P., Cao, X., Khosravi, A., Acharya, U. R., Makarenkov, V., & Nahavandi, S. (2021). A review of uncertainty quantification in deep learning: Techniques, applications and challenges. Information Fusion, 76, 243–297. https://doi.org/10.1016/j.inffus.2021.05.008
2. Alfaro-García, V. G., Merigó, J. M., Alfaro Calderón, G. G., Plata-Pérez, L., Gil-Lafuente, A. M., & Herrera-Viedma, E. (2020). A citation analysis of fuzzy research by universities and countries. Journal of Intelligent and Fuzzy Systems, 38(5), 5355–5367. https://doi.org/10.3233/JIFS-179629
3. Alfaro-García, V. G., Merigó, J. M., Pedrycz, W., & Gómez Monge, R. (2020). Citation Analysis of Fuzzy Set Theory Journals: Bibliometric Insights About Authors and Research Areas. International Journal of Fuzzy Systems, 22(8), 2414–2448. https://doi.org/10.1007/s40815-020-00924-8
4. Alonso, S., Cabrerizo, F. J., Herrera-Viedma, E., & Herrera, F. (2009). h-Index: A review focused in its variants, computation and standardization for different scientific fields. Journal of Informetrics, 3(4), 273–289. https://doi.org/10.1016/j.joi.2009.04.001
5. Arnett, J. J. (2008). The neglected 95%: Why American psychology needs to become less American. American Psychologist, 63(7), 602–614. https://doi.org/10.1037/0003-066X.63.7.602
6. Asai, K., & Kitajima, S. (1971). A method for optimizing control of multimodal systems using fuzzy automata. Information Sciences, 3(4), 343–353. https://doi.org/10.1016/S0020-0255(71)80014-2
7. Basu, K. (1984). Fuzzy revealed preference theory. Journal of Economic Theory, 32(2), 212–227. https://doi.org/10.1016/0022-0531(84)90051-6

8. Birkle, C., Pendlebury, D. A., Schnell, J., & Adams, J. (2020). Web of Science as a data source for research on scientific and scholarly activity. Quantitative Science Studies, 1(1), 363–376. https://doi.org/10.1162/qss_a_00018
9. Blanco-Mesa, F., Merigó, J. M., & Gil-Lafuente, A. M. (2017). Fuzzy decision making: A bibliometric-based review. Journal of Intelligent & Fuzzy Systems, 32(3), 2033–2050. https://doi.org/10.3233/JIFS-161640
10. Bonilla, C. A., Merigó, J. M., & Torres-Abad, C. (2015). Economics in Latin America: a bibliometric analysis. Scientometrics, 105(2), 1239–1252. https://doi.org/10.1007/s11192-015-1747-7
11. Broadus, R. N. (1987). Toward a definition of "bibliometrics." Scientometrics, 12(5–6), 373–379. https://doi.org/10.1007/BF02016680
12. De Luca, A., & Termini, S. (1972). Algebraic properties of fuzzy sets. Journal of Mathematical Analysis and Applications, 40(2), 373–386. https://doi.org/10.1016/0022-247X(72)90057-1
13. Ding, Y., Rousseau, R., & Wolfram, D. (Eds.). (2014). Measuring Scholarly Impact. Springer International Publishing. https://doi.org/10.1007/978-3-319-10377-8
14. Filev, D. P., Barone, J. M., & Reformat, M. (2009). A brief message on the twenty-fifth anniversary of NAFIPS. NAFIPS 2009 - 2009 Annual Meeting of the North American Fuzzy Information Processing Society, 1–2. https://doi.org/10.1109/NAFIPS.2009.5156376
15. García-Orozco, D., Alfaro-García, V. G., Merigó, J. M., Espitia Moreno, I. C., & Gómez Monge, R. (2022). An overview of the most influential journals in fuzzy systems research. Expert Systems with Applications, 200, 117090. https://doi.org/10.1016/j.eswa.2022.117090
16. Hicks, D., Wouters, P., Waltman, L., de Rijcke, S., & Rafols, I. (2015). Bibliometrics: The Leiden Manifesto for research metrics. Nature, 520(7548), 429–431. https://doi.org/10.1038/520429a
17. Hirsch, J. E. (2005). An index to quantify an individual's scientific research output. Proceedings of the National Academy of Sciences, 102(46), 16569–16572. https://doi.org/10.1073/pnas.0507655102
18. Huang, C., Su, J., Xie, X., Ye, X., Li, Z., Porter, A., & Li, J. (2015). A bibliometric study of China's science and technology policies: 1949–2010. Scientometrics, 102(2), 1521–1539. https://doi.org/10.1007/s11192-014-1406-4
19. Jiang, Y., Ritchie, B. W., & Benckendorff, P. (2019). Bibliometric visualisation: an application in tourism crisis and disaster management research. Current Issues in Tourism, 22(16), 1925–1957. https://doi.org/10.1080/13683500.2017.1408574
20. Jones, A., Kaufmann, A., & Zimmermann, H.-J. (Eds.). (1986). Fuzzy Sets Theory and Applications. Springer Netherlands. https://doi.org/10.1007/978-94-009-4682-8
21. Kumar, S., Sahoo, S., Lim, W. M., Kraus, S., & Bamel, U. (2022). Fuzzy-set qualitative comparative analysis (fsQCA) in business and management research: A contemporary overview. Technological Forecasting and Social Change, 178, 121599. https://doi.org/10.1016/j.techfore.2022.121599
22. Laengle, S., Lobos, V., Merigó, J. M., Herrera-Viedma, E., Cobo, M. J., & De Baets, B. (2021). Forty years of Fuzzy Sets and Systems: A bibliometric analysis. Fuzzy Sets and Systems, 402, 155–183. https://doi.org/10.1016/j.fss.2020.03.012
23. Man, J. P., Weinkauf, J. G., Tsang, M., & Sin, J. H. D. D. (2003). Why do Some Countries Publish More Than Others? An International Comparison of Research Funding, English Proficiency and Publication Output in Highly Ranked General Medical Journals. European Journal of Epidemiology, 19(8), 811–817. https://doi.org/10.1023/B:EJEP.0000036571.00320.b8
24. Martín-Martín, A., Orduna-Malea, E., Thelwall, M., & Delgado López-Cózar, E. (2018). Google Scholar, Web of Science, and Scopus: A systematic comparison of citations in 252 subject categories. Journal of Informetrics, 12(4), 1160–1177. https://doi.org/10.1016/j.joi.2018.09.002

25. Martín-Martín, A., Thelwall, M., Orduna-Malea, E., & Delgado López-Cózar, E. (2021). Google Scholar, Microsoft Academic, Scopus, Dimensions, Web of Science, and OpenCitations' COCI: a multidisciplinary comparison of coverage via citations. Scientometrics, 126(1), 871–906. https://doi.org/10.1007/s11192-020-03690-4
26. Mas-Tur, A., Modak, N. M., Merigó, J. M., Roig-Tierno, N., Geraci, M., & Capecchi, V. (2019). Half a century of Quality & Quantity: a bibliometric review. Quality & Quantity, 53(2), 981–1020. https://doi.org/10.1007/s11135-018-0799-1
27. Merigó, J. M., Cancino, C. A., Coronado, F., & Urbano, D. (2016). Academic research in innovation: a country analysis. Scientometrics, 108(2), 559–593. https://doi.org/10.1007/s11192-016-1984-4
28. Merigó, J. M., Gil-Lafuente, A. M., & Yager, R. R. (2015). An overview of fuzzy research with bibliometric indicators. Applied Soft Computing, 27, 420–433. https://doi.org/10.1016/j.asoc.2014.10.035
29. Merino-Arteaga, I., Alfaro-García, V. G., & Merigó, J. M. (2022). Fuzzy systems research in the United States of America and Canada: A bibliometric overview. Information Sciences, 617, 277–292. https://doi.org/10.1016/j.ins.2022.10.116
30. Novák, V., Perfilieva, I., & Močkoř, J. (1999). Mathematical Principles of Fuzzy Logic. Springer US. https://doi.org/10.1007/978-1-4615-5217-8
31. Ong, S. (2021). Southeast Asian countries join forces for scientific strength. Nature, 591(7850), S30–S32. https://doi.org/10.1038/d41586-021-00670-3
32. Petropoulos, F., Apiletti, D., Assimakopoulos, V., Babai, M. Z., Barrow, D. K., Ben Taieb, S., Bergmeir, C., Bessa, R. J., Bijak, J., Boylan, J. E., Browell, J., Carnevale, C., Castle, J. L., Cirillo, P., Clements, M. P., Cordeiro, C., Cyrino Oliveira, F. L., De Baets, S., Dokumentov, A., … Ziel, F. (2022). Forecasting: theory and practice. International Journal of Forecasting, 38(3), 705–871. https://doi.org/10.1016/j.ijforecast.2021.11.001
33. Ruspini, E. H. (1970). Numerical methods for fuzzy clustering. Information Sciences, 2(3), 319–350. https://doi.org/10.1016/S0020-0255(70)80056-1
34. Schneegans, S., Lewis, J., & Straza, T. (2021). UNESCO Science Report: the race against time for smarter development.
35. Stenson, P. D., Mort, M., Ball, E. V., Chapman, M., Evans, K., Azevedo, L., Hayden, M., Heywood, S., Millar, D. S., Phillips, A. D., & Cooper, D. N. (2020). The Human Gene Mutation Database (HGMD®): optimizing its use in a clinical diagnostic or research setting. Human Genetics, 139(10), 1197–1207. https://doi.org/10.1007/s00439-020-02199-3
36. United Nations Statistics Division. (2022). Statistical yearbook 2022. 65th issue.
37. Vizuete-Luciano, E., Boria-Reverter, S., Merigó-Lindahl, J. M., Gil-Lafuente, A. M., & Solé-Moro, M. L. (2021). Fuzzy Branch-and-Bound Algorithm with OWA Operators in the Case of Consumer Decision Making. Mathematics, 9(23), 3045. https://doi.org/10.3390/math9233045
38. Waltman, L. (2016). A review of the literature on citation impact indicators. Journal of Informetrics, 10(2), 365–391. https://doi.org/10.1016/j.joi.2016.02.007
39. Wee, W., & Fu, K. (1969). A Formulation of Fuzzy Automata and Its Application as a Model of Learning Systems. IEEE Transactions on Systems Science and Cybernetics, 5(3), 215–223. https://doi.org/10.1109/TSSC.1969.300263
40. Wuchty, S., Jones, B. F., & Uzzi, B. (2007). The Increasing Dominance of Teams in Production of Knowledge. Science, 316(5827), 1036–1039. https://doi.org/10.1126/science.1136099
41. Zadeh, L. A. (1965). Fuzzy sets. Information and Control, 8(3), 338–353. https://doi.org/10.1016/S0019-9958(65)90241-X
42. Zadeh, L. A. (1971). Quantitative fuzzy semantics. Information Sciences, 3(2), 159–176. https://doi.org/10.1016/S0020-0255(71)80004-X
43. Zadeh, L. A. (2008). Is there a need for fuzzy logic? Information Sciences, 178(13), 2751–2779. https://doi.org/10.1016/j.ins.2008.02.012

44. Zhu, J., & Liu, W. (2020). A tale of two databases: the use of Web of Science and Scopus in academic papers. Scientometrics, 123(1), 321–335. https://doi.org/10.1007/s11192-020-03387-8
45. Zimmermann, H.-J. (1978). Fuzzy programming and linear programming with several objective functions. Fuzzy Sets and Systems, 1(1), 45–55. https://doi.org/10.1016/0165-0114(78)90031-3
46. Zupic, I., & Čater, T. (2015). Bibliometric Methods in Management and Organization. Organizational Research Methods, 18(3), 429–472. https://doi.org/10.1177/1094428114562629

Carlos Javier Torres Vergara obtained his MBA from EAE Business School and is currently pursuing a Ph.D. in Administration at the Universidad Michoacana de San Nicolás de Hidalgo, México. He serves as an Associate Professor at the University of Barcelona. His research interests include family businesses, organizational resilience, and soft skills. He is also an active researcher in the SIEMCI project, (Project No. 522RT0130) under the Ibero-American Program on Science and Technology for Development (CYTED) contributing to the development of innovative approaches in his fields of expertise.

Víctor G. Alfaro-García obtained his Ph.D. in Business from the Universitat de Barcelona, Spain. He currently serves as a Professor and Researcher at the School of Accounting and Managerial Sciences, Universidad Michoacana de San Nicolás de Hidalgo, in Morelia, México. His research interests include fuzzy systems, intelligent and expert systems, bibliometric studies, and their applications in business, innovation management, and regional development. He actively participates as an organizer and committee member in various international research projects and conferences. He is a member of the National Researchers System (SNII) under the Secretaría de Ciencia, Humanidades, Tecnología e Innovación (Secithi) and serves as the leader for Mexico in the SIEMCI network (Project No. 522RT0130) under the Ibero-American Program on Science and Technology for Development (CYTED).

Anna Maria Gil Lafuente is a Full Professor at the Faculty of Economics and Business at the University of Barcelona, where she earned her Ph.D. in Economic Sciences in 1992. Her research focuses on financial analysis, operational management techniques, multivalued analysis, and the economics of uncertainty. She actively contributes to various research initiatives, including projects assessing the multiplier effect of light innovation capabilities in companies and their impact on progress and well-being in Ibero-America. She also serves as the coordinator of the SIEMCI network (Project No. 522RT0130) under the Ibero-American Program on Science and Technology for Development (CYTED), fostering collaboration across multiple research institutions. Additionally, she leads the UB-Fundació Mutua Madrileña Chair of Corporate Sustainability, promoting sustainability in business practices aligned with the United Nations' Sustainable Development Goals.

Received: March 30, 2024; Accepted: September 09, 2024.

Computer Science and Information Systems 22(1):279–310 https://doi.org/10.2298/CSIS240701009D

Mapping-Based Approach to Integration of Technical Spaces

Vladimir Dimitrieski[1], Slavica Kordic[1], Sonja Ristic[1], Heiko Kern[2], and Ivan Lukovic[3]

[1] Faculty of Technical Sciences, Trg Dositeja Obradovića 6, 21000 Novi Sad, Serbia
{dimitrieski, slavica, sdristic}@uns.ac.rs
[2] Institute for Applied Computer Science, Goerdelerring 9, 04109 Leipzig, Germany
kern@infai.org
[3] Faculty of Organizational Sciences, Jove Ilića 154, 11000 Belgrade, Serbia
ivan.lukovic@fon.bg.ac.rs

Abstract. In the contemporary business landscape, the seamless integration of software components and systems is vital for ensuring the unimpeded flow of information, which is key to achieving success in the market. While addressing integration issues using standardized communication interfaces is generally preferred, standards are often adjusted or disregarded due to business goals or market strategies. Consequently, developers often resort to the manual development of integration adapters. This process is time-consuming, error-prone and persists as a significant cost factor. In this paper, we address integration issues and introduce a novel mapping-based approach for structured, automated, and reusable integration. We present an automated development process for the integration adapters at a higher level of abstraction, based on model-driven software development principles. We also present a tool called AnyMap and a visual domain-specific modeling language for specifying mappings and generating adapters, and we demonstrate the approach in a practical use case.

Keywords: mapping-based integration, technical spaces, model transformations, model-driven software development, Industry 4.0.

1. Introduction

The modern business landscape is characterized by its open, dynamic, and almost limitless nature, presenting many new challenges. Key features of this landscape include globalization, intensified competition, technological innovation, rapid development cycles, flexibility, resource efficiency, decentralized production, and individualized demand. Companies are not only required to be the first to market their own products but also to offer a high degree of customization to meet the unique needs of individual buyers. Consequently, companies are rapidly adapting and engaging in collaborative processes, which necessitates the integration of their hardware and software [1–4].

Integrated systems enhance competitive advantage by providing unified and efficient access to information [5], leading to the necessity of integrating information systems (IS). The decentralization of production has given rise to new forms of partnership,

allowing companies visibility into their respective business partners' operations. For instance, in a factory with integrated systems, partners may gain insight into the production status of a specific product. This shift has also fostered new client relationships, enabling customers to monitor the progress of their products from manufacturing to delivery. Continuous data exchange is essential for implementing standardized business processes as part of integration.

One defining aspect of modern businesses is the emphasis on technological innovation, encompassing the Internet of Things (IoT) with its Radio-Frequency IDentification (RFID) tags, sensors, actuators, and mobile phones, Cyber-Physical Systems (CPS), Internet of Services (IoS), and Smart Factory. These advancements have given rise to the concept of Industry 4.0. “Industry 4.0 is a collective term for technologies and concepts of value chain organization. Within the modular structured Smart Factories of Industry 4.0, CPSs monitor physical processes, create a virtual copy of the physical world, and make decentralized decisions. Over the IoT, CPSs communicate and cooperate with each other and humans in real time. Via IoS, internal and cross-organizational services are offered and utilized by value chain participants” [6]. Introducing protocols and data formats for device communication by market entrants can create integration challenges.

An entire company's supply chain, encompassing levels such as material procurement, manufacturing, storage, transportation, and sales, is orchestrated through an information system (IS). Each level requires data from the level below to provide services and information to end users, making integration between levels a critical concern. Therefore, seamless information flow must be facilitated through device and IS integration to ensure the company's smooth operation across all levels. In general, integration in system and software development can be defined as “the process of linking separate computing systems into a whole so that these elements can work together effectively” [7]. Developers of ISs face the challenge of connecting the machines at a software level with the existing machine landscapes and IoT.

In contemporary manufacturing systems, integrating different devices and software components can be a complex task due to the use of various data formats and communication protocols. Manufacturers often opt for proprietary protocols over standardization for various business and market reasons, which complicates integration. As a result, integration engineers are required to create adapters to facilitate smooth communication and data exchange between these devices and software components. Data formats, which are either implicitly defined or explicitly expressed by data schemas, and the tools used to handle them constitute a Technical Space (TS). Adapting data from one TS to another, such as from Comma Separated Values (CSV) to Extensible Markup Language (XML), requires the development of specific adapters for each combination of TSs. This challenge, termed inter-space heterogeneity or data model heterogeneity [8], persists despite industry standards and remains a significant cost factor [9]. Manual development of adapters for each pair of technical spaces is time-consuming, error-prone, expensive, and labor-intensive.

Despite numerous approaches and tools to solving problems in the data integration domain, there remains a significant space for improvement. Most existing tools provide just one visual concrete syntax, graphical or tabular, with no exposed or explicitly defined abstract syntax. The graphical syntax is suitable for integration scenarios with low to medium complexity, while tabular syntax is suitable for scenarios with high complexity. Having multiple syntaxes could provide different views on top of the same

abstract syntax. Thus, the tool can be used in a variety of scenarios, enabling automated model validation and reasoning and easier development of code generators. Another important issue is the granularity level of reusable components. Many integration tools provided the reuse of one of the following concepts: user-defined functions, TS specifications, or mapping specifications. The most important type of reuse is the mapping specification reuse, but it is the hardest to accomplish. With this type of reuse, whole mappings could be reused and adapted to a new integration scenario, resulting in the (semi-)automation of the integration process. This requires the reuse and adaptation at the level of individual element mappings, not just at the level of whole mapping, as is the case with most tools.

Our goal is to address the inefficiency when creating integration adapters by introducing an innovative approach for the structured, automated, and reusable integration of different TSs. In this paper, we propose an automated development process for software integration adapters at a higher level of abstraction, rather than manually crafting adapters at the data level. In our approach, we distinguish between the transformation logic and its implementation. This differentiation is facilitated by leveraging Model-Driven Software Development (MDSD) principles. As stated in [10], MDSD is a "methodology for applying the advantages of modeling to software engineering activities". It is grounded in explicitly specifying models considered first-class artifacts of all software engineering activities. Consequently, any software-related artifact is viewed as a model or a component of a larger model. The encouragement examples of successful MDSD principles' application in industry are encountered: in the development and management of Cyber–Physical Systems (CPSs) and smart manufacturing [11], in the fields of Internet of Things (IoT), and multi-agent systems [12] and in the development of software for robots [13].

MDSD approaches are usually centered around a language that is specific to a certain domain of application [14, 15]. Such languages are called Domain-Specific Modeling Language (DSML). We have developed a visual DSML aimed at specifying transformation models, known as mappings, between diverse technical spaces and their schemas. This language allows expressing of expert knowledge with a set of domain-specific concepts and appropriate models to facilitate the creation of high-abstraction-level mappings between the elements of the integrated technical spaces. These mappings are considered the fundamental units of integration and can be conveniently reused when building new transformation models. Segregating the transformation logic by creating platform-independent mappings enables transformation knowledge to be translated to different scenarios and integration platforms. We have developed two algorithms aimed at automation of transformation model's specification – a reuse algorithm and an alignment algorithm. The reuse algorithm identifies reuse candidates amongst previously specified and stored mappings by detecting similarities between the new schema elements and the elements within the existing mappings. The alignment algorithm compares pairs of source and target schemas to estimate their similarity and proposes the best matching pairs. We have developed various comparators, which can be combined to enhance the algorithms' precision. Output for both algorithms is a set of mappings that can be automatically applied to the new schema.

The executable transformation code, an integration adapter, is generated automatically from mappings for supported execution environments. This automation minimizes development effort and increases the quality of adapters.

To implement our approach, we have developed a tool called AnyMap [16, 17] for specifying mappings and generating adapters. This tool provides the following functionalities: (i) importing existing technical space data schemas or automatically deducing a simplified schema from a schema-less data file, (ii) creating mappings between the schema elements based on a DSML, (iii) reusing existing mappings based on those stored in a reuse repository, and (iv) generating executable adapters to transform the data. Adapters are generated for different target environments and programming languages, so they can be used immediately after generation on the provided source data files. Currently, a code generator is provided for our custom-built, Java-based microservice execution environment.

Therefore, our research's main contributions include our integration approach, the AnyMap tool with the developed DSML, and the implemented reuse mechanism. They are intended for software engineers of various profiles and domain experts participating in integration processes. We offer a highly generic solution that allows that concept to be applied in any business, economic, or problem domain. Following the MDSD principles and providing a formal abstract syntax for the DSML, we can specify more than one concrete syntax and automate model validation and code generation. In addition, this solution enables the reuse and adaptation of individual element mappings, not limited to whole mappings, leading to a substantial increase in the level of mapping specification automation. Finally, the automatic generation of integration adapters speeds up work, reduces the number of errors, increases quality, and reduces costs of adapter development.

The paper is structured as follows. In Section 2, we discuss related work. Section 3 presents our integration approach in detail with the developed DSML and reuse mechanisms. Afterward, we briefly present the AnyMap tool in Section 4. After that, we illustrate a use case in Section 5 and conclude this paper in Section 6 with a summary and suggestions for future work.

2. Related Work

Various methods exist for integrating TSs or system components. We focus on transferring data between interfaces or components with disparate data structures. This form of integration is commonly referred to as interconnectivity. The interconnectivity integration approaches mentioned in the literature can be categorized into two main types: standardization and transformation-based. Standardization approaches aim to provide standard solutions, protocols, and processes for different layers of the integration process. In cases where a standard is not available, fully developed, or not adhered to by a company, a proprietary protocol and integration adapters may be used to integrate desired TSs. These integration adapters are created by following a transformation-based approach, transforming input data to target data based on a set of transformation rules. This section focuses on transformation-based approaches, as our approach can also be classified under this category.

There are three main sub-categories of transformation-based approaches found in the literature: (i) schema-based integration approaches, (ii) model-driven integration approaches, and (iii) ontology-based integration approaches. What is known as schema mapping or schema matching in the database and artificial intelligence domains, in the

semantic web community is known under the name ontology alignment or ontology matching. Some of the approaches from Sections 2.2 and 2.3 also share this view and are based on ontologies, so no clear line separates these approaches and fits them into a single, separate category. Therefore, in the rest of the section, we will only focus on the schema-based and model-driven approaches.

Schema matching, as defined in the book [18], involves finding semantic correspondences between elements of two schemas. On the other hand, schema mapping, as described by Ten Cate et al. [19], is a high-level, declarative specification of the relationship between the source schema and the target schema. Visual notation is commonly used to specify schema mappings, allowing for manual specification, and may also include schema matching modules to aid in finding suitable mapping candidates. Therefore, schema matching focuses on (semi-)automatically providing a set of mapping elements, while schema mapping involves a tool for manually specifying mappings between source and target schemas, which serves as input for executable code generators.

Agreste et al. [20] provided a survey on XML schema matching. The authors expanded the scope of existing surveys on general matching approaches by describing new techniques tailored specifically for the XML domain. They argued that for the best matching technique in the XML domain, the matching tools should be specialized for that domain and utilize all its peculiarities. This approach leads to more efficient matches better suited to the XML domain, allowing for more precise identification of schema element semantics.

In their work, Bernstein et al. [21, 22] present a solution for adapting the schema mapping technique to an industrial setting. They introduce a prototype of a customizable schema matcher called PROTOtype PLAtform for Schema Matching (PROTOPLASM). This tool consists of three layers: (i) an import layer where mapped artifacts are transformed into a common internal representation based on XML, (ii) an operation layer containing the necessary concepts to construct a schema-matching strategy, and (iii) a graphical language layer used to combine graphical representations of operational concepts into matching strategy scripts for execution. Similarly, Raghavan et al. [23] propose SchemaMapper, which utilizes a hyperbolic tree instead of a linear tree representation. According to their findings, the hyperbolic tree supports faster human-performed searches for elements required during the matching process.

In their work, Alexe et al. [24, 25] present a schema mapping approach for integrating relational database schemas. Unlike traditional solutions that involve loading entire source and target schemas and creating high-level mappings between them, Alexe's "divide-design-merge" approach advocates splitting source and target schemas into smaller parts, establishing mappings between these parts and then merging all partial mappings into a comprehensive whole as the final step. The approach is accompanied by three tools developed by the authors.

Duchateau and Bellahsene introduce Yet Another Matcher (YAM) [26], a self-tuning, machine-learning-based, and extensible matcher factory tool in their work. YAM generates a best-fit schema-matching algorithm tailored to a specific integration scenario. The generated algorithm identifies schema element matches and proposes them to the user. The self-tuning feature allows the production of a matcher with user-defined characteristics for a given scenario, while the extensible feature enables users to add new similarity measures, enhancing the system's overall effectiveness. Similar

techniques are found in MatchPlanner [27], utilizing decision tree methods, and eTuner [28], which employs synthetic matching scenarios to create matches.

Model-driven software development facilitates the development of software systems at different levels of abstraction, with DSMLs playing a crucial role in reducing development costs. In MDSD, transformations are defined at the meta-model level, wherein data schema and transformation rules can be interpreted as schema-matching rules. Büttner et al. [29] have introduced a model-driven approach for integrating data among government institutions in Germany. The approach emphasizes standardizing the messages, interfaces, and data models exchanged. Adherence to these standards is overseen by a central governing body that defines meta-models (data formats) for various sectors within the German government. Given different standards, integrating data becomes a crucial task for enabling exchange. This integration process operates at the meta-model level, allowing for the transformation of messages and facilitating communication with other German or European institutions.

Authors of [30, 31] have introduced a meta-modeling approach for integrating heterogeneous distributed IT systems, known as Berlin Brandenburg Business Process Integration and Evolution framework BIZYCLE. The BIZYCLE integration process relies on multilevel modeling abstractions. Initially, the integration scenario is modeled at the computation-independent level, covering the business aspects, and then refined at the platform-specific level to describe the technical interfaces of the integrated systems. A platform-specific model is created for each supported platform. The integration process is automated through model extraction, systematic conflict analysis, and code generation. The BIZYCLE Repository [32] supports reuse at the model level, allowing interface descriptions, transformation rules, and semantic annotations to be stored and shared between projects and users.

There are various DSMLs and frameworks that are not directly linked to schema mapping but are better suited to the fields of schema matching and enterprise application integration. Vuković et al. [33, 34] have introduced a language called Semantic-Aided Integration Language (SAIL). This language allows the description, generation, and use of matching components within their framework without requiring implementation in a general-purpose programming language. The developed matching framework aims to automate certain steps in conflict resolution during the matching process. Interfaces and their elements can be semantically described using ontologies to facilitate this automation. Although the approach is based on ontology alignment principles, the SAIL domain-specific language is used to specify matching algorithms and adheres to the principles of the MDSD methodology. Similarly, with the IS modeling approach based on MDSD principles and the form type concept, Luković et al. [35, 36] propose integrated modeling of disparate parts of an IS.

The FUSE (Federated User Exchange) approach [37] is a domain-aware method for achieving user model interoperability. It involves manual mapping and automatic translation processes, each utilizing two domain-aware mechanisms: (i) a canonical user model and (ii) user model mapping transformations tailored to specific domains. All mappings are initially made with the canonical user model as the target, which serves as a consistent shared user model. The user model mapping transformations are components designed specifically for mapping between different user models via the canonical model. This approach differentiates itself from generic approaches by integrating domain knowledge into new processes and tools, supporting complex user model interoperability tasks across overlapping domains.

In summary, despite the availability of numerous schema-matching approaches, only a small subset of them is actively being developed and maintained. Most accompanying tools were created as prototypes to validate the approach, making them outdated or inapplicable for real-world scenarios. Also, these approaches focus on schema-matching in relational databases and XML domains, traditionally seen as the training ground for schema-based integration algorithms. However, only a few identified approaches have been applied outside these domains, with the most notable instance mentioned in [12] being in the industrial domain. In contrast to these approaches, which mainly focus on matching source and target elements, our approach takes a broader view of the integration problem. It encompasses all the steps preceding the specification of rules and incorporates both manual and automatic integration mechanisms. As observed in the surveyed approaches, our tool can leverage schema and ontology-matching algorithms to facilitate process automation.

Some of the fundamental elements of our approach, such as the previous iterations of DSML, our integration tool, execution environment, and the reuse algorithm, have been outlined throughout our previous work [16, 17, 38, 39]. However, this paper marks the first time we have formulated and presented our integration approach in its entirety, also encompassing all the updated details since the previous publications. The meta-model of our DSML has been enriched with additional concepts to offer broader domain coverage. Based on the results of applying the language in several use cases, existing concepts have been also fine-tuned to better fit the domain. In addition, the automation feature now incorporates an alignment algorithm that does not rely on previously created mappings to streamline developer efforts. This notably enhances the level of automation in cases where the reuse repository has not yet been populated with previously created mappings, thereby rendering the reuse algorithm inapplicable. Lastly, we present a realistic, more intricate industrial integration example covering all aspects of this improved approach.

3. Mapping-based integration approach

In this section, we present our mapping-based integration approach, which is the main aspect of our research. The approach focuses on enabling interconnectivity, which maintains the existing system functionality while enabling data-level integration. It employs a common data structure onto which all other data formats are mapped to facilitate the integration. This common data structure can be seen as a TS model. Adhering to the MDSD principles, each model is treated as a first-class citizen, and all necessary operations are specified and performed on top of them. These TS models are directly utilized in the development process of integration adapters by establishing transformations between source and target TS model elements at a higher level of abstraction. We denote these transformations as mappings, and they are created utilizing a visual DSML. Once all the relevant mappings are specified, based on these abstract yet formal specifications of integration adapters, code generators can be used to generate executable integration adapters.

While the entire integration adapter can be manually developed in a chosen programming language, this process is usually overly repetitive, time-consuming, and error prone. Offering an integration tool to support the adapter development increases

the level of automation in this process, yielding better development times and fewer errors. Therefore, the description of the approach in this section assumes that the integration with our approach is carried out with the support of an integration tool.

Each activity of the integration development approach can be performed either by the adapter developer, automatically by the tool, or semi-automatically with the developer and tool participating in the activity execution. To reflect this, all diagrams depicting process steps in this section have two swimlanes. The first swimlane is for the developer, where all the integration process steps are performed by the developer. The second swimlane is for the integration tool, where all the integration process steps are performed in an automated manner by the tool without any developer intervention. Any process steps that can be performed by the developer, the tool, or both are drawn at the border between the two swimlanes.

To facilitate the automated development of integration adapters, our approach can be divided into three phases:

1. *Import of TSs*: An adapter developer imports all participating TSs into an integration tool.
2. *Mapping specification*: The developer specifies the source-to-target mappings between the TSs imported in the previous phase. Specification may be completed manually, using our DSML, or in an automated way, using a supported mapping automation facility.
3. *Generation of an integration adapter*: The executable adapter code is generated for a chosen execution environment based on the mapping specification created in the previous phase.

3.1. Phase 1: Import of TSs

To enable data-level integration between two TSs, i.e., interconnectivity, developers must first provide data schemas and data files from those TSs. These files are the input to the *Import TSs* phase presented in Fig. 1.

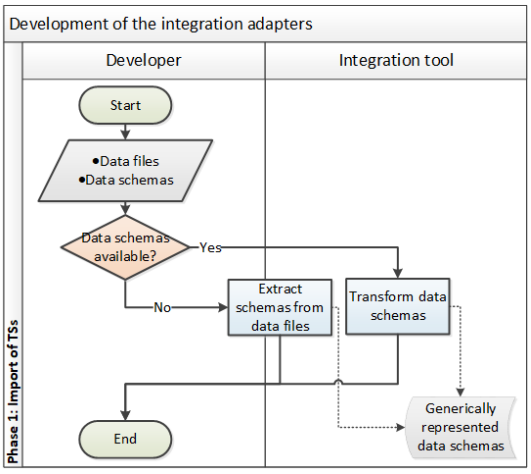

Fig. 1. Activity diagram for the *Import of TSs* phase

Data files serve a dual purpose. First, they are used during the adapter execution as they are transformed into another file corresponding to the target TSs. Second, if no data schema is available, they can be used as examples to partially or fully construct the schema. These data files are referred to as example data files.

Data schemas are essential for the integration adapter development as they define the structure for creating mappings. If the data schema exists, it is imported via the *Transform data schemas* process step. If a data schema is missing, a developer can use example data files as input for the (semi-)automatic extraction of schemas (*Extract schemas from data files*). This presents a challenging task, akin to inferring DSML context-free grammars from example models written in that DSML [40]. By having enough example data files, an inferred schema may closely match the original. Nonetheless, even a small subset of example data files can yield a simplified schema with sufficient information for integration. Therefore, for some TSs, schema extraction is a straightforward process and can be performed automatically, for some TSs, user input is required to adequately construct the schema document. Therefore, we classify this step as (semi-)automatic and put it in the middle between the two swimlanes in Fig. 1.

For the integration process to be applied consistently, imported data schemas must be represented in a common, generic manner, irrespective of the TSs being integrated and their specificness. We view each data schema as a graph of nodes and links describing their relationships, as introduced in [41] and described in short in the rest of the text. A schema can be represented as a graph with a single root element and multiple child elements. The root element can either be explicitly specified in the schema or be a part of the shared substructure and referential constraints. We have used a tree representation for all schemas to make it easier to handle and represent schemas. General graph schemas are converted into tree schemas by flattening the graph structure. During the flattening, relationships between elements at the same level or between upper and lower levels of the tree can be represented as tree elements with non-trivial types. This can be achieved by copying referenced structures to the referenced place or introducing a special reference element type for representing references where copying is not an option, as it would introduce recursive and infinite structures. Flattening is done at the TS importer level. The importer's developer is responsible for converting the original schema structure to the generic tree representation. The flattening can be implemented in many ways and algorithms, one of which is described in more detail in [41]. This generic schema representation is the output of *Extract schemas from data files* and *Transform data schemas* process steps and serves as a base structure for creating mappings. Concepts used to represent this generic schema structure are a part of the meta-model of the developed DSML and are presented in more detail in Section 3.2.

3.2. Phase 2: Mapping specification

Once the generic schema structures are created, transformations are specified as mappings between schema elements. In our approach, this is done by utilizing a custom-made DSML and an expression language, described in detail later in this subsection. To start the mapping creation, a developer performs the *Mapping specification* phase of the approach, depicted in Fig. 2.

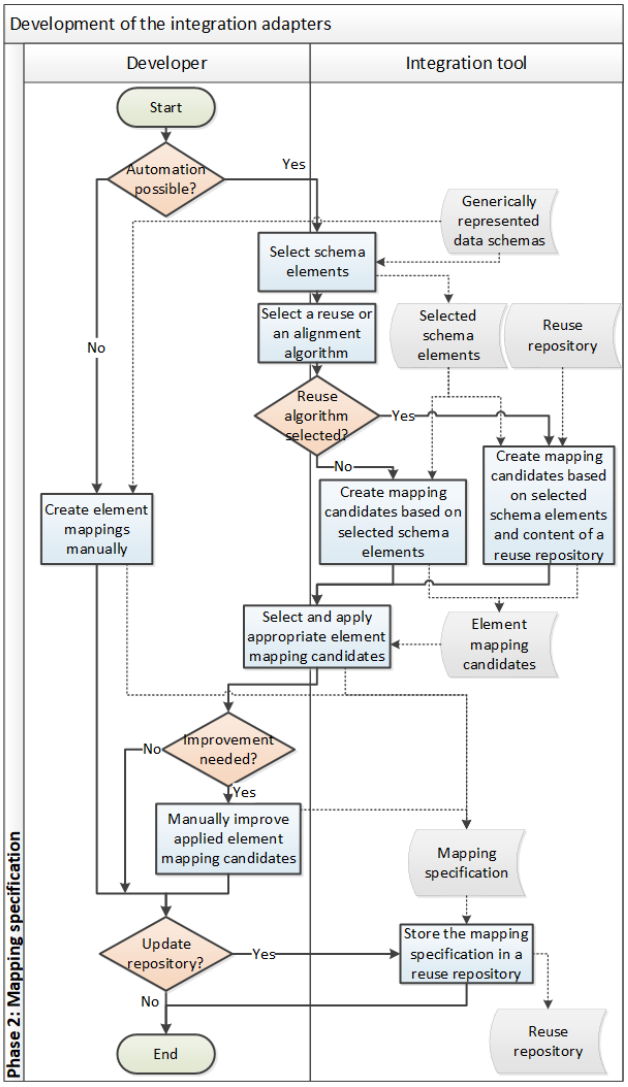

Fig. 2. Activity diagram for the *Mapping specification* phase

Although our integration approach promotes using automated facilities for mapping specification, we also acknowledge some cases where a manual specification utilizing our DSML is required. For example, one automation facility reuses previously defined mappings stored in the reuse repository and tries to apply them to the current integration scenario. Manual mapping is required when there is not enough historical data for reuse to autonomously and with high precision conclude the best possible mappings for the current pair of TSs. Therefore, this section discusses the three ways of specifying mappings between the generic schema structures: manual, semi-automatic, and fully automatic. Regardless of the chosen way, the mappings are created by utilizing the

provided DSML, and the result is a mapping specification used to generate the executable adapter code.

The manual way of creating mappings (*Create element mappings manually*) allows developers to use our DSML to manually connect the source and target schema elements and provide additional transformation expressions that will later be used at execution time. It must be noted that this is different from manual adapter development in a programming language, as in this case, the developer uses the DSML to formally create such an adapter without the integration tool's automation mechanisms in use.

Implementing automation at the schema level allows multiple data files to be easily transformed using the same mapping, making automation more efficient. However, mapping reuse is restricted as there is significant variability at the data level, even for data that conforms to the same schema element. Conversely, if a mapping is specified at the schema level, it can be easily adapted to another schema element and transform all instances of both the new schema element and the original schema element.

There are two approaches to automating the creation of mapping specifications: fully automatic and semi-automatic. In the case of a fully automatic approach, all schema elements are passed to the automation algorithm as it tries to specify all possible mappings that make sense for the two TSs in hand. As this way of mapping specification takes time to calculate the possible mappings, a developer might choose the semi-automatic method due to the usually large search space comprising many source and target schema elements. If a developer chooses this way for mapping specification, the first step is to select a subset of source and target schema elements that need to be mapped (*Select schema elements*). While this step is not always necessary, it may significantly speed up the automation process for large schemas.

Regardless of the automation method, fully or semi-automatic, a developer must choose an automation algorithm to proceed, either a reuse algorithm or an alignment algorithm (*Select reuse or an alignment algorithm*), both introduced later in this section. Executing the alignment (*Create mapping candidates based on selected schema elements*) or reuse algorithms (*Create mapping candidates based on selected schema elements and content of a reuse repository*) requires a set of source and target elements as input and produces a set of mapping candidates as output.

In the next step (*Select and apply appropriate element mapping candidates*), some or all candidates are applied to the current mapping context, becoming the final mappings from which the integration adapter is generated. In the case of the fully automatic method, the offered candidates are all applied to the current integration context, which considerably speeds up the development process and reduces errors as the developer does not need to interfere with the process. In the semi-automatic method, users may choose which mapping candidates will become new mappings applied to the mapping context. If they decide so, developers might also perform the *Manually improve applied element mapping candidates* process step to achieve higher precision in the automation process in cases when the precision of the automation algorithm is low because of the scarce mapping history it operates on. A developer creates use-case-specific element mappings missed by the automation algorithms creating more complete mapping specifications.

The result of performing the *Mapping specification* phase is a formally defined mapping specification, which is serialized and saved to storage. The mapping specification is later used in the *Generation of Integration Adapters* phase, presented in the following subsection.

The DSML for mapping specification

We developed a new DSML that is a core component of our approach. Initially, we identified the essential concepts necessary for creating mappings by thoroughly examining existing literature and numerous integration tools available at the time. As it is stated in [42], domain experts are essential for producing reliable results when constructing, making decisions, and evaluating a language. Therefore, a preliminary set of concepts was then discussed with domain experts across various integration domains, primarily focusing on industrial manufacturing where this issue is particularly significant. Fig. 3 shows its current meta-model based on previous versions presented in [16, 17, 38]. Generically represented data schemas serve as the foundation or recipe for creating integration adapters and, therefore, are part of the DSML meta-model. Concepts used to represent data schemas are represented as rectangles with gray filling. Once the data schemas have been identified and represented in a generic manner, the mapping specification process can begin. Concepts used for the element mapping specification are represented as rectangles with a white filling. In the rest of the section, the names of meta-model concepts are given in italics.

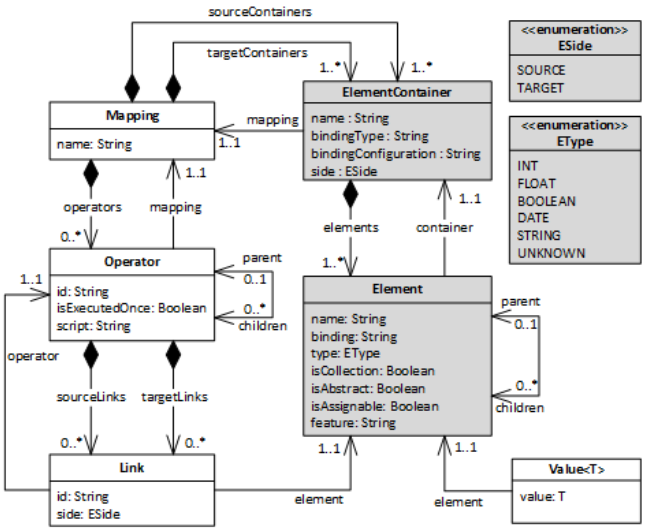

Fig. 3. The mapping DSML meta-model

A single element container (*ElementContainer*) is created when a data schema is loaded. It is given a name (*name*) to distinguish it from other containers. Depending on whether the container represents a source or a target schema, the side attribute (*side*) is set to either *SOURCE* or *TARGET*. These are both literal values defined as part of the *ESide* enumeration. Each container is contained by a single mapping specification (*mapping*), either as a source container (*sourceContainers*) or a target container (*targetContainers*).

The concept of binding refers to the link between the imported, generic schema element and the original schema element from which it originates. These bindings create a two-way connection between the original data schema and the generic schema

structure. This connection is crucial for the adapter execution process because the mapping specification process occurs on top of the generic schema representation, while the resulting adapters must be executed based on the data files with the original schema definitions. By following these bindings, the code generator can accurately produce code that accesses the original elements of the schema documents and their associated data files. These bindings are established when a TS is imported into the tool, hence why we refer to these TS importers as binders.

Therefore, at the level of an element container, a binding type (*bindingType*) and a binding configuration (*bindingConfiguration*) attribute must be set. The binding type identifies the binding component responsible for reading the data schema and handling data file read/write operations. Based on the binding type attribute, a generator can package the appropriate binder component with the integration adapter for execution. The binding configuration attribute is a storage for schema-level configuration during data schema import by the identified binder, based on the binding type. Since different binders may format this attribute differently, it's binder-specific. The binding configuration is essential for recreating the element tree during adapter execution, as the adapter only has access to the mapping file.

Each container in the system consists of one or more data schema elements (*Element*). The name (*name*) and binding string (*binding*) are an element's two most important attributes. The name of an element corresponds to the name of the corresponding imported schema element. The binding string is a binder-specific unique identifier that stores the path of the schema element in the imported data schema document. In addition to the binder-specific configuration, a binder may set an additional feature (*feature*) for the element that will be used later in the adapter execution process.

A binder can set values for each element that specify the element's type (*type*) and properties. These properties specify whether the element is a collection (*isCollection*), abstract (*isAbstract*), or assignable (*isAssignable*). By setting these values, the binder limits the number of functions that can be applied to these elements, which helps to prevent inappropriate mappings from being specified in the first place. If an element is a collection, usual collection operators can be applied. Abstract elements are placeholders or grouping elements and cannot be used as source or target elements of an element mapping. Finally, non-assignable elements can only be used as a source but not as target elements of an element mapping.

The element type attribute is only set for primitive elements, with possible values defined by the EType enumeration. Complex types, like objects, are represented as sub-trees within their element container (*children*). Each element representing an object property has a parent relationship (*parent*) pointing to the element representing the object.

The main meta-model concept used for the mapping specification is *Mapping*, which represents a single mapping specification used in the adapter generation process. Each mapping has a name (*name*) and a set of source and target element containers representing loaded data schemas. Additionally, a set of element mapping specifications (*Operator* and *Link*) specifies transformation rules at a higher abstraction level.

In addition to the language representing the connections between source and target schema elements, i.e., element mappings, it is important to have an expression language for expressing algorithms to manipulate the input values. For each operator that represents a high-level element mapping, we specify the value-level transformation

logic in the *script* property using the expression language. This expression language can be either custom-developed as a Domain-Specific Language (DSL) or adapted from a chosen general-purpose language. In our approach, the expression language is created by adapting an existing general-purpose programming language. This is achieved by specifying one or more integration-specific structures and application programming interfaces (APIs) and using the standard programming language mechanisms on top of these structures. This process is similar to building an embedded or internal DSL [43], where we use the syntax of the host language and add domain-specific elements, such as an integration-specific structure. From the point of our DSML, the transformation code written in the *script* property is related to the target framework or libraries used for the execution of the generated adapter code.

The advantage of using an existing language is that all its mechanisms, statements, and expressions are available for defining the transformation logic. To create a structure that can be used in any general-purpose programming language, we have designed a value encapsulation structure using the generic *Value<T>* concept (illustrated in Fig. 3). The template parameter *T* represents the type of the value (*value*) received as input, corresponding to the schema element (*element*). Therefore, this structure encapsulates values and schema elements, allowing expressions to be made at both meta-data and data levels. Furthermore, the *Value<T>* structure and the connected *Element* concept can be easily translated to a structure in any target scripting language, provided the language supports generics or a similar concept (e.g. if the target language is dynamically typed).

When an operator is connected through input and output links, input and output variables are automatically created in the script. These variables are instances of *Value<T>*, where *T* represents the type of the schema element connected by the link. The expression language can use these variables to specify the transformation logic. Additionally, transformation rules can be implemented in an arbitrary construct from a general-purpose language on top of these variables.

Automating the mapping specification

As introduced earlier in this subsection, users can utilize the DSML to manually specify the transformation logic or use a mapping automation facility to help them in that endeavor. The mapping automation facility is developed in response to the existence of variability in input and output data schemas. In the realms of MDSD and DSMLs, a language developer can choose to either introduce new language concepts and adjust code generators to handle newly encountered variations [42, 44] or employ automatic model refinement and creation algorithms that do not change the DSML while assisting users based on implicit or stored domain knowledge. Our approach to automatic variability handling aligns with the latter category.

There are two kinds of automation algorithms to apply to their current integration context. Fig. 4 visually represents the difference between these two algorithms. The left side of the figure depicts the alignment process. This process uses a schema-matching algorithm to identify similarities between the source schema elements ($Es_i..Es_k$) and the target schema elements ($Et_j..Et_l$). The matching algorithm compares each pair of source and target schema elements and returns a similarity score.

The reuse process is depicted on the right side of the figure. Though in a slightly different role, the matching algorithms can also be used in this process. Instead of comparing the source (Es_i...Es_k) and target (Et_j...Et_l) schema elements directly, the matching algorithms compare schema elements with the schema elements from a mapping repository, (Ers_i...Ers_k) and (Ert_j...Ert_l) respectively, to find previously created element mappings that are similar and can be reused and applied in the current integration scenario. This results in a probability that the repository mapping fits the current integration scenario. Defining a minimum probability threshold is possible to simplify choosing the appropriate repository mapping. This threshold is used to exclude any unnecessary element mappings. Throughout the rest of the text, we will simply refer to this threshold as "probability".

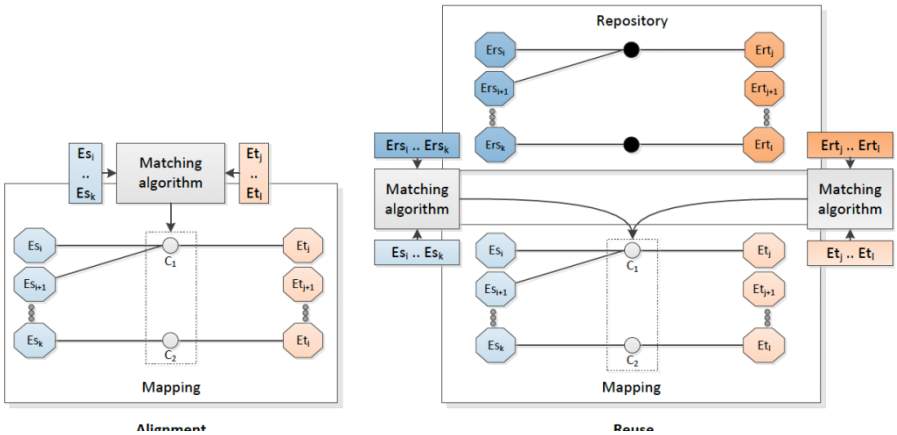

Fig. 4. Comparison of the alignment and reuse algorithms

Independent of the chosen automation algorithm, the result is always a collection of mapping candidates that can be applied to the current integration context to create mapping specifications. Such formal mapping specifications conform to the presented DSML's meta-model. As such, it possesses intrinsic value for reuse in future integration adapter developments as it is formally and generically specified. Therefore, a developer may want to improve the reuse process by adding the created mapping specification to a *Reuse repository* (cf. Fig. 2). There are two types of repositories: local and global. Local repositories are deployed on a single machine and maintained by a developer or group of developers who typically work on the same integration issues. By focusing on a single integration domain, local repositories can improve the accuracy of the reuse algorithm for that domain. However, local repositories tend to have a small number of mapping specifications, which means that the reuse algorithm cannot provide element mapping candidates for newly introduced elements with no previous similar elements in the domain. In such situations, a global repository may be more suitable. Developers from different integration domains store their mapping specifications in a global repository. Depending on the tool and data security policies, a global repository may be deployed at a company level or worldwide. More details about the automation algorithms may be found in our papers [38, 39].

3.3. Phase 3: Generation of Integration Adapters

After completing the previous process steps, a mapping specification is created. It represents an abstract specification of the integration adapter. If developers are satisfied with the mapping specification, they can generate an executable integration adapter for a specific execution platform. In Fig. 5 we present the activity diagram for the *Generation of integration adapters* phase.

Our approach envisions having multiple code generators, each responsible for generating code that runs on a different execution platform or environment. Developers can choose and invoke the most suitable code generator for their integration needs (*Select and invoke a code generator*). The integration tool executes the entire code generation process (*Generate code*) by taking a formal mapping specification as input, parsing its contents, and producing an executable integration adapter code as output. The executable integration adapter serves as the output of the entire presented integration process.

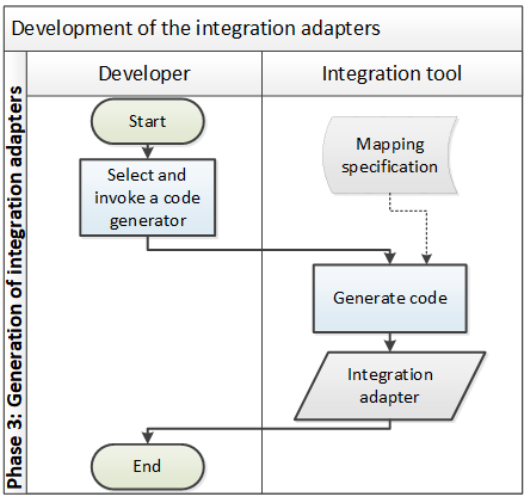

Fig. 5. Activity diagram for the *Generation of integration adapters* phase

4. The AnyMap Tool

We have developed an easily extendable integration tool named AnyMap to support our integration approach. AnyMap is the primary interaction point with the user and encompasses all activities, from reading and parsing data schemas to specifying mappings and generating an integration adapter. The tool helps us to realize and validate our approach to real-world problems. The architecture of the tool is illustrated in Fig. 6.

The AnyMap tool comprises five modules: Core, Binding, Mapping Editor, Reuse, and Generator. Within each module, one or more plug-ins adhere to the interface outlined in the core module. To add new plug-ins to a module, it is necessary to

implement the appropriate interface from the core module and register their execution with the Eclipse IDE (Integrated Development Environment) runtime engine. The Eclipse IDE is a widely used IDE for Java developers who create web and desktop applications. With Eclipse, it's easy to create plug-ins that add functionality to the IDE, allowing fast and agile development. All plug-ins are implemented in Java and Xtend programming languages.

The **Core** module is a fundamental part of the tool, including basic components used throughout the other modules. These core components have been developed to provide only the most essential functionality, allowing easy extension of other modules. The Core module comprises concepts such as the mapping language, expression language, and interfaces for implementing binders and generators. It includes all the necessary interfaces required to extend any of the other modules.

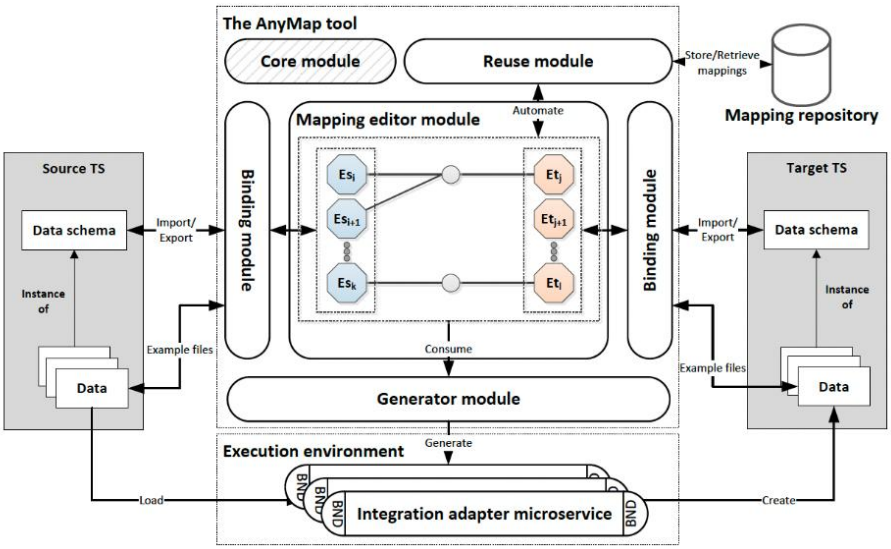

Fig. 6. Architecture of the AnyMap tool

The **Binding** module contains plug-ins representing TS binders used for importing and exporting data and data schemas of a specific TS. These binders can transform schemas into generic element trees and store reverse links from generically represented schema elements to the original schema elements. Each binder plug-in has an appropriate GUI (Graphical User Interface) that provides user interaction with the binders. For instance, when importing a new file from a TS, users can set up the binder parameters through a GUI wizard. Therefore, each binder is designed to support all the process steps presented in Fig. 1.

The **Mapping Editor** module is a crucial component in the AnyMap tool, serving as the main point of interaction between users and the system. This module offers a graphical concrete syntax for the mapping language and a textual concrete syntax for the expression language. It also provides all the necessary GUI classes, such as event listeners, commands, and menu items, to ensure seamless interaction between the user and the tool.

Currently, the Mapping Editor module implements a graphical concrete syntax of the mapping language, which we believe is the most appropriate syntax for the integration domain we are interested in. This syntax provides a comprehensive view of the mapping specification, making it easy to learn and understand. A disadvantage of the graphical concrete syntax is that the diagram becomes overcrowded when many mappings are created. However, we feel that the benefits of this syntax outweigh its drawbacks.

Our tool supports the textual concrete syntax for the expression language, as we chose Java as our expression language. We have limited the possible number of functions that can be used in creating expressions, and each expression can only be defined on top of an object that is an instance of the *Value<T>* class presented in Fig. 3.

The **Reuse** module consists of various plug-ins that work together to facilitate aligning and reusing schema elements. These plug-ins use different algorithms to calculate similarities between schema elements and generate a list of element-mapping candidates as an output. Users can then review this list and their probabilities and select the most appropriate element candidates for their specific integration scenario. Once selected, the AnyMap tool will automatically apply these chosen element mappings to the current mapping specification and store them for future reuse in the **Mapping repository**.

The **Generator** module consists of plug-ins that can be used to create executable transformations for a specific execution environment. The main function of each plug-in is to analyze a mapping file, extract the necessary mappings, and generate executable transformation code based on these mappings. Each plug-in is designed to improve the tool's capabilities in generating code for different execution environments. We have only implemented a generator for our custom-made execution environment.

We have developed a custom **execution environment** to support the execution of generated adapters in a scalable and transparent way. Although a user can provide different generators for the AnyMap tool to generate adapters for different execution environments, we have implemented an execution environment based on the microservice architecture. We chose this architecture to demonstrate that integration adapters can be generated as stateless code components and run on demand when a new file needs to be transformed. This environment has been developed in the Java programming language and using the Spring Cloud library. These components can be instantiated on-demand depending on the frequency of input data reception [38].

5. Example Usage

To illustrate the applicability of our approach, we have applied it to a typical device-to-information-system integration scenario in an industrial context. Such a scenario is frequently encountered and entails slight variations in integrated technical spaces, which is perfect for effectively demonstrating the full power of our approach. The presented use case involves integrating a sensor that measures various characteristics of semiconductor wafers and an IS module for data visualization. The integration is performed between CSV and XML TSs. The sensors gather data and send it as a CSV document. The information system visualizes the data using the JavaScript Chart (JSChart) library and expects it to be formatted according to a predefined XML schema.

The import mechanism must overcome technical (inter-space) and functional (intra-space) heterogeneity to import CSV and XML documents. Functional complexity is caused by different measurement methods that can result in variability in the structure of CSV documents, which means that an IS vendor needs a set of different adapters for integrating sensors that use different measuring methods. However, manual implementation is often time-consuming, costly, and error-prone. Our approach is used to simplify the specification of adapters in the presence of the two heterogeneity problems steps, and the tool modules used in this use case are outlined in Fig. 7.

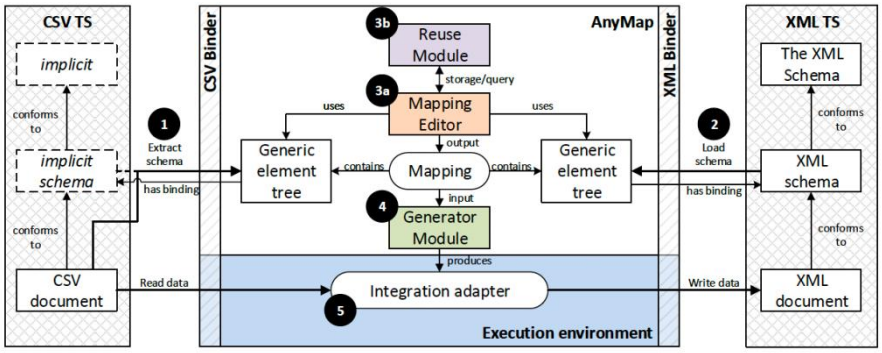

Fig. 7. Importing CSV and XML technical spaces using the AnyMap tool

Fig. 7 displays the five main steps to merge CSV and XML, numbered in black circles. The rest of this section gives a detailed explanation of the steps. In Fig. 8 we present the input CSV file and the target XML schema to which the CSV file must be transformed.

Step 1. To work with CSV files, which do not have an explicit schema definition language, the schema must be extracted from an example data file. This is done using the CSV binder to read the data file and extract schema information. The schema can be extracted by reading column names from the file header or by manually specifying column names and types.

Step 2. Creating a generic element tree from an XML schema structure is a simple way to load the schema. With the help of the XML binder, a developer can easily convert an existing XML Schema Definition (XSD) document into a generic tree representation. Unlike the CSV binder, the XSD binder is very simple. A developer only provides a path to an XSD document and the mapping side on which this TS participates.

Step 3. After importing data schemas from both technical spaces, the tool provides a blank canvas for mapping creation with a generic element tree present on both sides of the canvas. In Fig. 9 we captured a mapping state from an ongoing mapping specification based on these imported data schemas.

Meas. Nr.	Ord. Nr.	Weight	Radius	Thickness	Pos. Before	Pos. After	Fallback
1048	1	7570	7205	19.772	25.601	-0.001	0
1048	2	7279	6932	20.002	4.734	0.031	0
1048	3	7175	6837	20.248	5.528	0.112	0
1048	4	7200	6863	20.395	-5.572	-0.204	0
1048	5	7300	6957	20.262	-6.628	-0.130	0
1048	6	7555	7198	20.177	-2.361	-0.165	0
1048	7	7880	7500	19.752	100.840	0.228	0
1048	8	7669	7301	19.868	-2.013	-0.049	0
1048	9	7278	6926	19.681	-19.475	-0.175	0
...	...	...	...	...	...	...	...

```
<?xml version="1.0" encoding="UTF-8" standalone="no"?>
<xs:schema xmlns:xs="http://www.w3.org/2001/XMLSchema"
    attributeFormDefault="unqualified"
    elementFormDefault="qualified">
    <xs:element name="JSChart">
        <xs:complexType>
            <xs:sequence>
                <xs:element maxOccurs="unbounded" name="dataset">
                    <xs:complexType>
                        <xs:sequence>
                            <xs:element maxOccurs="unbounded" name="data">
                                <xs:complexType>
                                    <xs:attribute name="unit" type="xs:int"/>
                                    <xs:attribute name="value" type="xs:int"/>
                                </xs:complexType>
                            </xs:element>
                        </xs:sequence>
                        <xs:attribute name="type" type="xs:string"/>
                        <xs:attribute name="id" type="xs:string"/>
                    </xs:complexType>
                </xs:element>
            </xs:sequence>
        </xs:complexType>
    </xs:element>
</xs:schema>
```

Fig. 8. CSV document and XML schema examples

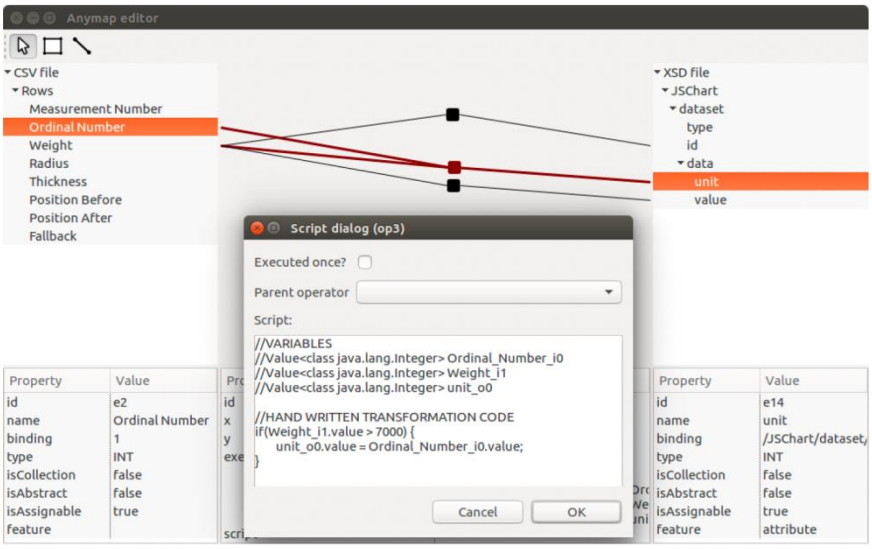

Fig. 9. The mapping specification process

On the left side of Fig. 9, there is an element container labeled "CSV file." This container holds just one element called *Rows*, which is an abstract element representing the data payload of the CSV document. By payload, we mean the rows that show measured values from the System Under Supervision (SUS). Additionally, a CSV document may have other top-level meta-attributes that don't represent measured values, but instead provide information about the protocol, sensor configuration, and manufacturer. If these elements appear in the document, they will be created on the same level as the *Rows* element. Each child element of *Rows* represents a single column from the CSV document, and these elements are not abstract. They can be used in the mapping specification, and their type is inferred during the binding process. Their binding, or reverse link to the original schema element, is an ordinal number of the column they represent. You can see these properties in Fig. 9 in the property view located below the generic element tree. The property views displayed show the properties of the Ordinal Number and Unit elements.

On the right side of Fig. 9, there is an element container that is based on the XSD document that has been imported. This element container is named "XSD file". The only child element of this container is the "JSChart" element. The "JSChart" element is created from the "JSChart" root element of the XSD document in Fig. 8. All other child elements are created from the XSD sub-elements and their attributes. The binding values are XML Path Language (XPath) expressions uniquely identifying each XSD document element.

To create element mappings, the developer must first create the generic element representations for both the source and target meta-models. Element mappings are comprised of two components - operators and links, which are specified separately. Operators are represented as rectangles and must be created first. They are then linked to generic tree elements via links, which are represented as lines. Every link connected to an operator introduces a new variable that can be used in the operator script when writing expressions using the Expression language. The variable name is derived from the element name by adding a single character that represents the side of the link in comparison to the operator (i.e. "i" for input and "o" for output) and an ordinal number of the link at its side of the operator. Examples of link names can be seen in Fig. 9 in the opened *Script* dialog.

The first few lines of the script are comments with variable names which provide a good operator overview to developers. For example, the highlighted rule which is marked red on the canvas has two inputs and one output link and therefore has three variables: (i) *Ordinal_Number_i0*, first input variable corresponding to the Ordinal Number element, (ii) *Weight_i1*, second input variable corresponding to the Weight element, and (iii) *unit_o0*, first output variable corresponding to the unit element. Types of these variables are inferred from imported schemas and example data files. The types are then passed instead of the generic type *T* in *Value<T>* (cf. Fig. 2). The Script dialog in Fig. 9 provides an example of the script specification. This transformation rule should be executed only when a value of the Weight column is greater than 7000 in the same CSV row.

In the Script dialog, developers can specify whether an operator is executed only once or multiple times for each input document. This can be done by checking or unchecking the *"Executed once?"* checkbox in the Script dialog. Operators can be executed multiple times for each input document in cases where a single document is divided into smaller data units. A data unit refers to an atomic piece of data that is

provided as a single input to a transformation system. For instance, in the CSV TS, each row of the payload can be sent independently and transformed to a desired target structure. However, in many cases, an XML document must be sent to be properly interpreted and transformed.

In the Script dialog, a developer can select an operator from a *Parent operator* combo box and set it as the parent to the current operator. This is necessary when an operator's execution depends on another previously specified operator (parent). By creating operator hierarchies, a developer can specify groups of operators executed in a particular order.

We should note that in Fig. 9, the manual specification step is denoted as 3a, covering the described process. On the other hand, 3b denotes mapping specification using the automation facility and is presented in Section 5.1.

Step 4: Invoke the microservice code generator to generate the microservice code. Upon completion, the mapping specification will serve as input to the Generator module, which generates an executable integration adapter.

Step 5 To initiate the integration adapter, it may effortlessly be launched within the execution environment. The adapter will then read the input data through the CSV binder and apply the relevant transformations based on the generated rules. Once the data is transformed, it is written to the target TS. To ensure that the data is written in correctly, the adapter utilizes the XML binder in compliance with the specified XML schema.

The left-hand side of Fig. 10 presents the XML document that contains the values generated after executing the generated code on top of the CSV file. To avoid repetition, we have excluded lines with the same structure as those shown in lines 4-8. The values are generated from the columns of the CSV document displayed in the top section of Fig. 8. The information system can use the generated XML document to create a line chart with the JSChart library. The right-hand side of Fig. 10 shows an example of this chart.

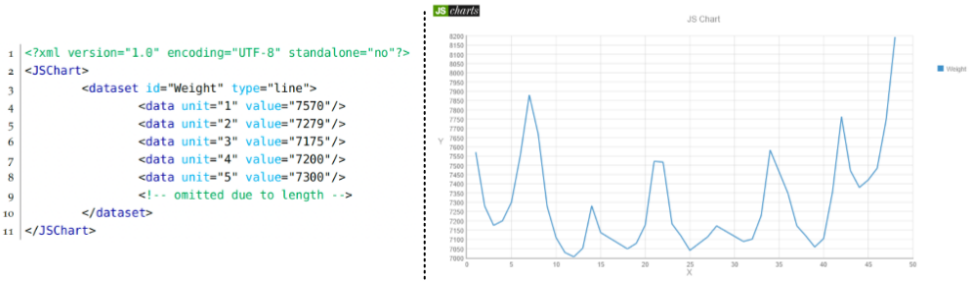

Fig. 10. The output XML file (left) and the line chart (right) of the single-layered measurement data

5.1. Automating the Device-to-information-system Integration

In Industry 4.0, variations in data schema often arise within the same integration scenario. This can result from using devices from different vendors or different

operation modes of the same device. Adapting existing adapters or creating new ones to handle these variations can be laborious and error prone. However, our approach provides a more efficient and user-friendly solution, as illustrated in this subsection.

In certain scenarios, the measurement device in wafer production employs a second measuring method as it is considered preferable and potentially ensures higher production quality, but at the cost of network utilization since it requires more data to be sent. Devices utilizing this measurement method require different configuration than those using the first measurement method. This configuration change necessitates the development or adaptation of an integration adapter, which can recognize the new data structure and transform it into the desired target technical space.

The new CSV document being sent is called a double-layered CSV, and an example is shown in Fig. 11. The wafer's weight is represented by columns titled Weight_A and Weight_B, among others. Some column names have been abbreviated in Fig. 11 due to space limitations. The full schema element names in the AnyMap tool screenshots are provided. In our use case, we require mapping double-layered CSV documents onto the same XML schema shown in Fig. 8.

Meas. Nr.	Ord. Nr.	Weight_A	Radius_A	Th._A	Pos.Pass_A	Fall.T.	Error_A	Fall._A	Weight_B	Radius_B	Th._B	Pos.Pass_B	Fall._B	Error_B
91	1	7041	6256	8	0.089	0	-9999	0	7113	6323	8	-0.182	0	-9999
91	2	6816	6059	8	-0.073	0	-9999	0	6839	6079	8	-0.091	0	-9999
91	3	6762	6014	8	-0.554	0	-9999	0	6756	6007	8	-0.062	0	-9999
91	4	6659	5926	8	-0.844	0	-9999	0	6638	5906	8	-0.058	0	-9999
91	5	3711	5314	3	10000	R	-9999	R	6621	5891	8	-47.542	U	-9999
91	6	6640	5912	8	0.051	0	-9999	0	6634	5909	8	-0.147	0	-9999
...	...	...	...	...	...	...	...	...	...	...	...	...	...	...

Fig. 11. Double-layered CSV document example

There are a few ways to specify a mapping for integration. The first option is a manual specification, where the developer can specify the mapping from scratch, as described in Step 3. The second option is a semi-automatic specification, where the developer can rely on a mapping repository and automation algorithms. They can provide a set of element mapping candidates, and the developer can select the most suitable ones for the current integration task. This approach requires some manual intervention from the developer, but the degree of involvement is far lower than with the manual specification. The third option is an automatic specification. This requires the least amount of user involvement, as all tasks are performed automatically by the AnyMap tool based on predefined heuristics. However, for the automatic specification to yield satisfactory results, a mapping repository must be populated with enough mappings from that domain to steer the process in the right direction.

As we want to present the automation process in our double-layered example, we will present the mapping specification that follows the semi-automatic approach and uses the reuse automation algorithm.

To initiate the mapping specification process, the first step is to load the double-layered CSV and XML schemas into the AnyMap tools. Once both schemas are loaded, the developer selects the reuse automation mechanism and sets it up through a dialog box on the left side of Fig. 12.. This can be an alternative to Step 3, as described earlier.

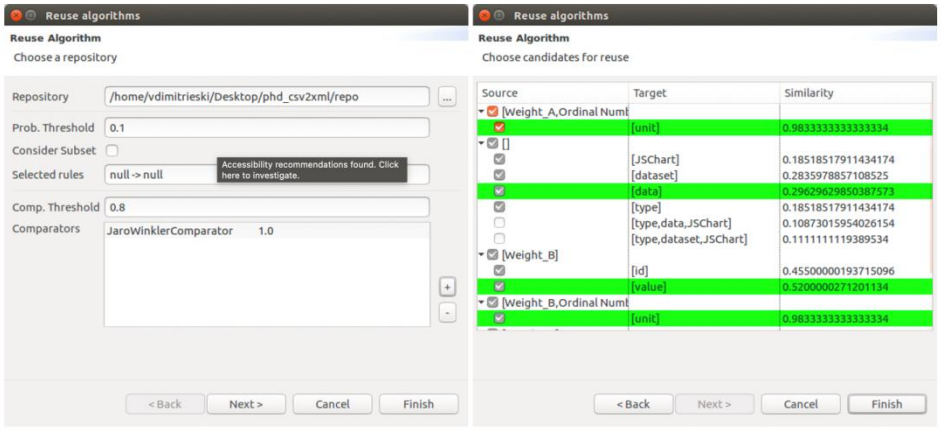

Fig. 12. The reuse configuration (left) and the element mapping candidates (right) dialogs

The first section of the dialog box defines the path to the reuse repository. In this example, a local repository is used. In the second section of the dialog box, the developer sets the probability threshold that defines a minimum probability at which an element mapping candidate is presented to the developer. If the *Consider Subset* checkbox is checked, the algorithm will provide element mapping candidates comprising a subset of schema elements the developer selects. Otherwise, only a superset or an equal set to the one provided as an input is considered a candidate. Selected schema elements provided as input to the algorithm are presented in the Selected rules textbox.

The third section of the dialog box allows the selection and configuration of schema matchers (comparators). Schema matchers are used to detect similarities between current schema elements and repository schema elements. These similarities are later used by the reuse algorithm and combined into a probability of a specific element mapping being appropriate for the current mapping context. Schema matchers can detect element similarity based on the structure or semantics of the elements.

In our particular use case, the data sent by the sensors follows strict naming rules. If a property is measured multiple times by a single sensor in a single measurement pass, a new letter is appended to the property name for each measurement. Therefore, the similarity between CSV columns (source schema elements) in this use case can be measured using a string comparison mechanism. In Fig. 12, the Jaro-Winkler [45] string comparison algorithm is selected as it is the most suitable for short names and strings.

AnyMap tool enables developers to select multiple schema matchers and use them simultaneously. Each selected matcher is assigned a weight value, which modifies the result of each comparator. In Fig. 12 there is one matcher, and its weight is set to 1.0. Additionally, the developer can set a Comp. threshold value, which determines the minimum similarity required for a matcher to report two elements as similar. In this example, elements are considered similar if they have a similarity score of 80% (0.8) or higher.

Once the configured reuse algorithm is executed, a dialog appears on the right side of Fig. 12, which displays the calculated element mapping candidates. These candidates are grouped by the source schema elements. Each group presents target schema

elements of the element mapping candidates and their probability of being a suitable fit for the current integration scenario. The element mapping candidates highlighted in green have the highest probability.

The developer chooses the most appropriate element mapping candidates for the current integration scenario. If an automatic algorithm were used, the candidates highlighted in green would be automatically selected. In either case, the selected candidates are applied automatically in the mapping canvas. The resulting mapping specification is presented in Fig. 13. The element trees on the left and right sides of the mapping canvas are created from the double-layered CSV document shown in Fig. 11 and the XSD document presented in the bottom part of Fig. 8, respectively. Compared to Fig. 9, we can observe that more mappings are created, representing the same relationships but, in this case, twice as the CSV has two layers of measurements.

The generated integration adapter takes the CSV document from Fig. 11 as input and produces the XML document from the left-hand side of Fig. 14 as output. We have omitted repetitive lines. Once the information system receives the XML document, it presents the content as a line graph, as shown on the right-hand side of Fig. 14.

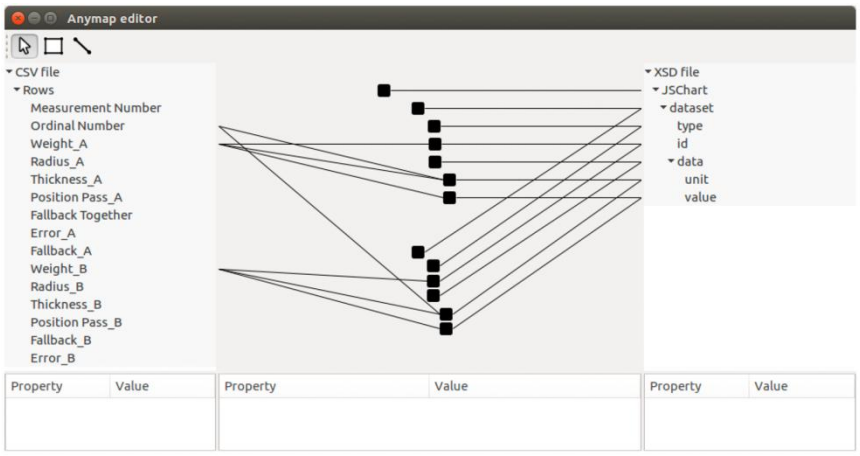

Fig. 13. The double-layered CSV2XML mapping specification

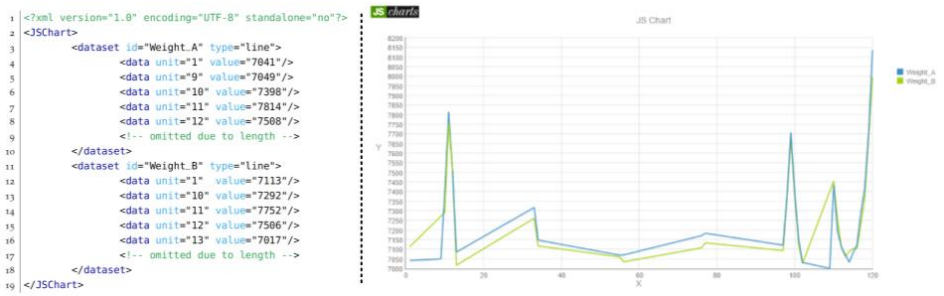

Fig. 14. The output XML file (left) and the line chart (right) of the double-layered measurement data

6. Conclusion

In this paper, we propose an approach to specifying and implementing integration adapters for any pair of TSs. Our approach employs a common data format to facilitate integration across diverse system components. Initially, we established a universal data structure onto which all other data formats can be mapped based on the core principles of MDSD. Each TS involved in integration is represented as a generic data model. Subsequently, integration experts and developers create transformations, i.e., mappings, using a declarative mapping DSML with a graphical notation. This allows the connection of structures from the source and target TS models, thus representing required mappings between them. Ultimately, the integration adapter is automatically generated from the mappings, leading to expedited development and reduced errors.

One notable aspect of this approach involves reusing existing mappings and creating new mappings based on those stored in a repository. Including knowledge and derivation functionality also allows for the automated specification of a new mapping. This reusability accelerates the integration process and simplifies the development process for integration engineers.

We have developed an integration tool called AnyMap to support our approach. This tool consists of the following components: TS importers (binders), a DSML for the specification of mappings, alignment and reuse algorithms, and code generators. AnyMap allows integration developers to specify mappings between systems at a higher level of abstraction and then use code generators to create executable adapters for a specific execution environment. In addition to the AnyMap tool, we have also developed a microservice-based scalable execution environment in which adapters are executed. However, creating other code generators that will generate regular, stand-alone Java or C adapters is possible. We have successfully applied our integration approach to integrate devices communicating via CSV with ISs communicating via XML.

The tool can be very useful to various software engineers and experts from different domains who need to integrate arbitrary TSs and do not have an adequate mechanism for mutual data exchange. With the tool, users can integrate arbitrary TSs uniformly, allowing users to learn the approach and become accustomed to the tooling support once and afterward, just spending time on performing the integration tasks without learning the implementation and serialization details of each one. AnyMap allows users to specify integration adapters at the level of data schemas using a custom DSML. As concepts of such a language on a highly abstraction level are tailored to non-programmers' needs and skills, by using these concepts, a user does not need to be experienced in any of the contemporary programming languages. Also, the reuse and alignment algorithms offered by AnyMap alleviate a user of the tedious, error-prone, and time-consuming process of creating repetitive mapping (transformation) rules.

Our approach has a limitation, as it can only be applied to three-level meta-models with a graph structure that can be transformed into a tree without losing significant semantic properties. This restricts its utility to schemas that can be flattened, i.e., schemas without infinite recursions of their elements. However, in our experience, we have seldom encountered infinite recursion in the cases where we have used our approach. Moreover, in instances where infinite recursion has been encountered at the schema level, flattening the structure to a desired depth and breaking the recursion with stub elements has proven to be an effective solution. We plan to address this limitation as a part of future work by investigating schema representation approaches and their implementation possibilities.

One potential avenue for future research is the development of more advanced and effective element-matching algorithms. At present, automation relies on simple matching algorithms that gauge element similarity and probability based on individual element information without considering the context or relationships of the element when determining the probability of it being the right candidate for a new mapping. An enhancement could involve semantically describing TSs using a shared ontology or a set of ontologies and automatically identifying semantic correspondences between source and target elements using ontology alignment methods.

We also plan to establish metrics and an evaluation framework for qualitative and quantitative assessment of our approach in future research endeavors. The research

community widely recognizes [46, 47] that evaluating an MDSD approach and measuring the quality of DSML are challenging tasks, and to date, only a limited amount of research has been conducted on these issues.

To advance the development of the AnyMap tool, it is essential to implement various enhancements to improve its usability, efficiency, and domain coverage. Introducing new TS binders would expand the tool's applicability across various use cases. This, in turn, would lead to a greater number of mappings in the reuse repository, fostering improved mapping automation. Our strategy involves developing binders for the most widely used protocols in the Industrial IoT (IIoT) domain, such as Open Platform Communications Unified Architecture (OPC UA), Message Queue Telemetry Transport (MQTT), and Modbus. With the addition of these protocols to the existing support for SEMI Equipment Communications Standard/Generic Equipment Model (SECS/GEM), CSV, and XML, we will achieve comprehensive coverage for many common use cases in the industrial environment.

Furthermore, we intend to enhance the tool by integrating a real-time execution engine. This functionality will allow users to promptly execute specified mappings and observe the results directly within the tool. This improvement will enhance debuggability and shorten the feedback loop. Additionally, expanding the tool with the new concrete syntaxes and allowing users to customize the graphical syntax for specifying the mappings could help increase the developers' efficiency.

We also need to expand our generator and execution environments. Although our current microservice execution environment offers the necessary flexibility and scalability, there are industrial settings where the speed of transformation execution is crucial. We intend to create a generator for optimized adapters using C or C++ programming languages to address this. These adapters will be executed directly on the industrial PCs connected to the devices. Running near the machines, these adapters will enable real-time or near-real-time data transformation. It's important to note that optimizing these adapters is crucial due to the limited resources on which they often run.

An additional enhancement would involve upgrading the tool to enable the transformation of streaming data, as opposed to data transferred in files. This enhancement would necessitate a comprehensive repository of predefined mappings within the domain of the receiving data stream. The tool would need to operate in a "headless" manner, without any GUI elements, and in a fully automated mode that does not require any user intervention. It would apply existing mappings to all compliant data packages within a stream, thereby promptly producing the output data. In the event that new, unknown variations of input data are encountered, for which suitable mappings are not already executed within the tool, the tool would autonomously create new mappings using alignment and reuse algorithms. These newly created mappings would then be applied to the input data, ensuring uninterrupted stream processing.

Acknowledgements. This research has been supported by the Ministry of Science, Technological Development and Innovation (Contract No. 451-03-65/2024-03/200156), the Faculty of Technical Sciences, University of Novi Sad, through project “Scientific and Artistic Research Work of Researchers in Teaching and Associate Positions at the Faculty of Technical Sciences, University of Novi Sad” (No. 01-3394/1) and by Faculty of Organizational Sciences, University of Belgrade.

References

1. Pourmirza, S., Peters, S., Dijkman, R., Grefen, P.: BPMS-RA: A Novel Reference Architecture for Business Process Management Systems. ACM Trans. Internet Technol. 19, 1–23 (2019). https://doi.org/10.1145/3232677.
2. Todorovic, N., Vjestica, M., Todorovic, N., Dimitrieski, V., Lukovic, I.: A Novel Approach and a Language for Facilitating Collaborative Production Processes in Virtual Organizations Based on DLT Networks. In: Proceedings of the 2nd International Conference on Innovative Intelligent Industrial Production and Logistics (IN4PL 2021). pp. 197–208. , Online (2021). https://doi.org/10.5220/0010720900003062.
3. Vještica, M., Dimitrieski, V., Pisarić, M., Kordić, S., Ristić, S., Luković, I.: Production processes modelling within digital product manufacturing in the context of Industry 4.0. Int. J. Prod. Res. 61, 6271–6290 (2023). https://doi.org/10.1080/00207543.2022.2125593.
4. Shamsuzzoha, A., Toscano, C., Carneiro, L.M., Kumar, V., Helo, P.: ICT-based solution approach for collaborative delivery of customised products. Prod. Plan. Control. 27, 280–298 (2016). https://doi.org/10.1080/09537287.2015.1123322.
5. Juric, M.B. ed: SOA approach to integration: XML, Web services, ESB, and BPEL in real-world SOA projects. Packt Publ, Birmingham (2007).
6. Hermann, M., Pentek, T., Otto, B.: Design principles for Industrie 4.0 scenarios: a literature review. Technische Universität Dortmund, Dortmund (2015).
7. Linthicum, D.S.: Enterprise application integration. Addison-Wesley Professional (2000).
8. Wortmann, A., Barais, O., Combemale, B., Wimmer, M.: Modeling languages in Industry 4.0: an extended systematic mapping study. Softw. Syst. Model. 19, 67–94 (2020). https://doi.org/10.1007/s10270-019-00757-6.
9. Pulier, E., Taylor, H.: Understanding enterprise SOA. Manning Greenwich, Conn (2006).
10. Brambilla, M., Cabot, J., Wimmer, M.: Model-Driven Software Engineering in Practice. Morgan & Claypool Publishers, San Rafael (2012).
11. Mohamed, M.A., Challenger, M., Kardas, G.: Applications of model-driven engineering in cyber-physical systems: A systematic mapping study. J. Comput. Lang. 59, 100972 (2020). https://doi.org/10.1016/j.cola.2020.100972,.
12. Sebastián, G., Gallud, J.A., Tesoriero, R.: Code generation using model driven architecture: A systematic mapping study. J. Comput. Lang. 56, 100935 (2020). https://doi.org/10.1016/j.cola.2019.100935.
13. de Araújo Silva, E., Valentin, E., Carvalho, J.R.H., da Silva Barreto, R.: A survey of Model Driven Engineering in robotics. J. Comput. Lang. 62, 101021 (2021). https://doi.org/10.1016/j.cola.2020.101021.
14. Mernik, M., Heering, J., Sloane, A.M.: When and how to develop domain-specific languages. ACM Comput. Surv. CSUR. 37, 316–344 (2005).
15. Kelly, S., Tolvanen, J.-P.: Domain-specific modeling: enabling full code generation. John Wiley & Sons (2008).
16. Kern, H., Stefan, F., Dimitrieski, V., Čeliković, M.: Mapping-Based Exchange of Models Between Meta-Modeling Tools. In: Proceedings of the 14th Workshop on Domain-Specific Modeling. pp. 29–34. ACM, New York, NY, USA (2014). https://doi.org/10.1145/2688447.2688453.
17. Kern, H., Stefan, F., Fähnrich, K.-P., Dimitrieski, V.: A Mapping-Based Framework for the Integration of Machine Data and Information Systems. In: Proceedings of 8th IADIS International Conference on Information Systems 2015. pp. 113–120. International Association for Development of the Information Society, Madeira, Portugal (2015).
18. Bellahsene, Z., Bonifati, A., Rahm, E., others: Schema matching and mapping. Springer (2011).
19. Ten Cate, B., Kolaitis, P.G., Tan, W.-C.: Schema mappings and data examples. In: Proceedings of the 16th International Conference on Extending Database Technology. pp. 777–780. ACM (2013).

20. Agreste, S., De Meo, P., Ferrara, E., Ursino, D.: XML matchers: approaches and challenges. Knowl.-Based Syst. 66, 190–209 (2014).
21. Bernstein, P.A., Melnik, S., Petropoulos, M., Quix, C.: Industrial-strength schema matching. ACM SIGMOD Rec. 33, 38–43 (2004).
22. Bernstein, P.A., Madhavan, J., Rahm, E.: Generic schema matching, ten years later. Proc. VLDB Endow. 4, 695–701 (2011).
23. Raghavan, A., Rangarajan, D., Shen, R., Gonçalves, M.A., Vemuri, N.S., Fan, W., Fox, E.A.: Schema mapper: a visualization tool for DL integration. In: Digital Libraries, 2005. JCDL'05. Proceedings of the 5th ACM/IEEE-CS Joint Conference on. pp. 414–414. IEEE (2005).
24. Alexe, B., Tan, W.-C.: A New Framework for Designing Schema Mappings. In: Tannen, V., Wong, L., Libkin, L., Fan, W., Tan, W.-C., and Fourman, M. (eds.) In Search of Elegance in the Theory and Practice of Computation. pp. 56–88. Springer Berlin Heidelberg (2013). https://doi.org/10.1007/978-3-642-41660-6_4.
25. Golshan, B., Halevy, A., Mihaila, G., Tan, W.-C.: Data Integration: After the Teenage Years. In: Proceedings of the 36th ACM SIGMOD-SIGACT-SIGAI Symposium on Principles of Database Systems. pp. 101–106. ACM, Chicago Illinois USA (2017). https://doi.org/10.1145/3034786.3056124.
26. Duchateau, F., Bellahsene, Z.: YAM: A Step Forward for Generating a Dedicated Schema Matcher. In: Hameurlain, A., Küng, J., and Wagner, R. (eds.) Transactions on Large-Scale Data- and Knowledge-Centered Systems XXV. pp. 150–185. Springer Berlin Heidelberg (2016). https://doi.org/10.1007/978-3-662-49534-6_5.
27. Duchateau, F., Bellahsene, Z., Coletta, R.: A flexible approach for planning schema matching algorithms. In: On the Move to Meaningful Internet Systems: OTM 2008. pp. 249–264. Springer (2008).
28. Lee, Y., Sayyadian, M., Doan, A., Rosenthal, A.S.: eTuner: tuning schema matching software using synthetic scenarios. VLDB Journal— Int. J. Very Large Data Bases. 16, 97–122 (2007).
29. Büttner, F., Bartels, U., Hamann, L., Hofrichter, O., Kuhlmann, M., Gogolla, M., Rabe, L., Steimke, F., Rabenstein, Y., Stosiek, A.: Model-driven standardization of public authority data interchange. Sci. Comput. Program. 89, 162–175 (2014). https://doi.org/10.1016/j.scico.2013.03.009.
30. Kutsche, R., Milanovic, N., Bauhoff, G., Baum, T., Cartsburg, M., Kumpe, D., Widiker, J.: BIZYCLE: Model-based Interoperability Platform for Software and Data Integration. In: Proceedings of the MDTPI at ECMDA (2008).
31. Milanovic, N., Cartsburg, M., Kutsche, R., Widiker, J., Kschonsak, F.: Model-Based Interoperability of Heterogeneous Information Systems: An Industrial Case Study. In: Paige, R.F., Hartman, A., and Rensink, A. (eds.) Model Driven Architecture - Foundations and Applications. pp. 325–336. Springer Berlin Heidelberg (2009). https://doi.org/10.1007/978-3-642-02674-4_24.
32. Milanovic, N., Kutsche, R., Baum, T., Cartsburg, M., Elmasgünes, H., Pohl, M., Widiker, J.: Model&Metamodel, Metadata and Document Repository for Software and Data Integration. In: Czarnecki, K., Ober, I., Bruel, J.-M., Uhl, A., and Völter, M. (eds.) Model Driven Engineering Languages and Systems. pp. 416–430. Springer Berlin Heidelberg (2008). https://doi.org/10.1007/978-3-540-87875-9_30.
33. Vuković, Ž., Milanović, N., Bauhoff, G.: Prototype of a Framework for Ontology-aided semantic conflict resolution in enterprise integration. In: Proceedints of 5th International Conference on Information Society and Technology. Society for Information Systems and Computer Networks, Kopaonik, Serbia (2015).
34. Vuković, Ž., Milanović, N., Vaderna, R., Dejanović, I., Milosavljević, G.: SAIL: A Domain-Specific Language for Semantic-Aided Automation of Interface Mapping in Enterprise Integration. In: On the Move to Meaningful Internet Systems: OTM 2015 Workshops. pp. 97–106. Springer (2015).

35. Luković, I., Čeliković, M., Kordić, S., Vještica, M.: An Approach to the Information System Conceptual Modeling Based on the Form Types. In: Karagiannis, D., Lee, M., Hinkelmann, K., and Utz, W. (eds.) Domain-Specific Conceptual Modeling. pp. 589–614. Springer International Publishing, Cham (2022). https://doi.org/10.1007/978-3-030-93547-4_26.
36. Čelikovic, M., Luković, I., Aleksić, S., Ivančević, V.: A MOF based meta-model and a concrete DSL syntax of IIS*Case PIM concepts. Comput. Sci. Inf. Syst. 9, 1075–1103 (2012). https://doi.org/10.2298/CSIS120203034C.
37. Walsh, E., O'Connor, A., Wade, V.: The FUSE domain-aware approach to user model interoperability: A comparative study. In: Information Reuse and Integration (IRI), 2013 IEEE 14th International Conference on. pp. 554–561. IEEE (2013).
38. Kern, H., Stefan, F., Dimitrieski, V.: Intelligent And Self-Adapting Integration Between Machines And Information Systems. Iadis Int. J. Comput. Sci. Inf. Syst. 10, 47–63 (2015).
39. Dimitrieski, V., Čeliković, M., Igić, N., Kern, H., Stefan, F.: Reuse of Rules in a Mapping-Based Integration Tool. In: Intelligent Software Methodologies, Tools and Techniques. pp. 269–280. Springer, Naples, Italy (2015). https://doi.org/10.1007/978-3-319-22689-7.
40. Črepinšek, M., Mernik, M., Bryant, B.R., Javed, F., Sprague, A.: Inferring context-free grammars for domain-specific languages. Electron. Notes Theor. Comput. Sci. 141, 99–116 (2005).
41. Madhavan, J., Bernstein, P.A., Rahm, E.: Generic schema matching with cupid. In: VLDB. pp. 49–58 (2001).
42. Djukić, V., Popović, A.: Handling complex representations in visual modeling tools for MDSD/DSM by means of code generator languages. J. Comput. Lang. 75, 101208 (2023). https://doi.org/doi.org/10.1016/j.cola.2023.101208.
43. Fowler, M.: Domain-specific languages. Pearson Education (2010).
44. Djukić, V., Popović, A., Luković, I., Ivančević, V.: Model variations and automated refinement of domain-specific modeling languages for robot-motion control. Comput. Inform. 38, 497–524 (2019).
45. Winkler, W.E.: String Comparator Metrics and Enhanced Decision Rules in the Fellegi-Sunter Model of Record Linkage. (1990).
46. Ozkaya, M., Akdur, D.: What do practitioners expect from the meta-modeling tools? A survey. J. Comput. Lang. 63, 101030 (2021).
47. Kahraman, G., Bilgen, S.: A framework for qualitative assessment of domain-specific languages. Softw. Syst. Model. 1–22 (2013).

Vladimir Dimitrieski works as an associate professor at the University of Novi Sad, Faculty of Technical Sciences, Serbia. There, he went through all the academic education levels, receiving a Ph.D. in computer science in 2018. Currently, he is a lecturer in several courses at the Faculty of Technical Sciences that cover domains of (meta-) modeling, domain-specific languages, and data engineering. With a strong background in the domain of Industry 4.0, (meta-)modeling and data engineering, he has been part of multiple national, international, and industrial projects in these domains.

Slavica Kordić received her M.Sc. degree from the Faculty of Technical Sciences, at University of Novi Sad. She completed her Mr (2 year) and Ph.D. degrees, both from Faculty Technical Sciences, University of Novi Sad. Currently, she works as an associate professor at the Faculty of Technical Sciences at the University of Novi Sad, where she lectures in several Computer Science and Informatics courses. Her research interests are related to Information Systems, Database Systems, Business Intelligence Systems, Data Reengineering and Model Driven Software Engineering. She is the

author or co-author of over 60 papers, and several industry projects and software solutions in the area.

Sonja Ristić works as a full professor at the University of Novi Sad, Faculty of Technical Sciences, Serbia. She received her bachelor's degree (Hons.) in Mathematics from the Faculty of Science, University of Novi Sad, Serbia, in 1983. The bachelor's degree (Hons.) in Economics, M.Sc degree in Informatics (former Mr, two years) and Ph.D degree in Informatics she received from the Faculty of Economics, University of Novi Sad, in 1989, 1994, and 2003, respectively. From 1984 until 1990 she worked with the Novi Sad Cable Company NOVKABEL – Factory of Electronic Computers. From 1990 till 2006 she was with Novi Sad School of Business, and since 2006 she has been with the University of Novi Sad, Faculty of Technical Sciences. Her research interests include Database Systems, Software Engineering, Model Driven Engineering, Domain Specific Languages, and production system modelling in the context of Industry 4.0/Industry 5.0. She is the author or co-author of over 100 papers, and 10 industry projects and software solutions in the area.

Heiko Kern receiving a Ph.D. in computer science in 2016. His research interests include Model-Driven Engineering, especially modeling and meta-modeling, model transformations as well as tool interoperability. He has experience in national and international funded research projects. Currently, he works as senior researcher at Institute of Applied Informatics at University of Leipzig, Germany and is head of the research group Software and System Integration.

Ivan Luković received his diploma degree (5 years) in Informatics from the Faculty of Military and Technical Sciences in Zagreb in 1990. He completed his M.Sc (former Mr, 2 years) degree at the University of Belgrade, Faculty of Electrical Engineering in 1993, and his Ph.D. at the University of Novi Sad, Faculty of Technical Sciences in 1996. Currently, he works as a Full Professor at the Faculty of Organizational Sciences of the University of Belgrade, where he lectures in several Computer Science and Informatics courses. His research interests are related to Database Systems, Business Intelligence Systems, and Software Engineering. He is the author or co-author of over 200 papers, 4 books, and 30 industry projects and software solutions in the area. He created a new set of B.Sc. and M.Sc. study programs in Information Engineering, i.e., Data Science, at the Faculty of Technical Sciences. The programs were accredited for the first time in 2015. Currently, he is a chair of the M.Sc. study program in Information Engineering at the Faculty of Organizational Sciences, as well as the chair of the Managing Board of the Computer Science and Information Systems (ComSIS) journal.

Received: July 01, 2024; Accepted: October 30, 2024.

Computer Science and Information Systems 22(1):311–325 https://doi.org/10.2298/CSIS241107010C

Linear Projection-Based Noise Filtering Framework for Image Denoising

Congyin Cao, Yangjun Deng, Menglong Yang, and Xinghui Zhu*

School of Information and Intelligence, Hunan Agricultural University,
Changsha 410128, China
19913809590@stu.hunau.edu.cn
dyj2012@yeah.net
y602367035@163.com
zhuxh@hunau.net

Abstract. Image denoising remains a fundamental challenge in digital image processing due to the inevitable presence of noise during image acquisition and transmission. While existing noise filtering methods predominantly focus on local spatial information, they often overlook crucial structural information from other perspectives, such as local manifold and global structures. To address this limitation, we propose a novel linear projection-based noise filtering (LPNF) framework grounded in linear projection learning theory. This framework innovatively learns a linear projection for noise filtering by incorporating multiple structural information sources - local spatial, local manifold, and global structures - through well-defined criteria. We present two specialized implementations of the LPNF framework: PCA-based LPNF (LPNF-PCA) and LPP-based LPNF (LPNF-LPP). The LPNF-PCA simultaneously leverages local spatial and global information, while LPNF-LPP integrates both local manifold and spatial information for enhanced denoising performance. Comprehensive experiments conducted on four standard test images with various noise types demonstrate that both LPNF-PCA and LPNF-LPP consistently outperform state-of-the-art denoising methods in terms of both quantitative.

Keywords: Image denoising, linear projection-based noise filtering framework, principle component analysis, locality preserving projection.

1. Introduction

In the era of rapid technological advancement, digital imaging has become increasingly prevalent across various domains. The surge in artificial intelligence research has positioned digital image processing as a critical focus in computer vision applications. Digital images play instrumental roles in diverse applications, ranging from face recognition and satellite television to computed tomography. However, the quality of these images is invariably compromised by various types of noise, primarily due to sensor material limitations and environmental interference during image acquisition and transmission. Common noise types affecting digital images include Gaussian noise, Salt-and-Pepper noise, Scattering noise, Poisson noise, and various combinations thereof [3,15,20,26]. Consequently, image denoising has emerged as both a fundamental challenge and an essential preprocessing step in image processing applications.

* Corresponding author

Image denoising methods can be broadly categorized into two fundamental approaches: spatial domain and frequency domain techniques [5,13]. Among these, spatial domain filtering methods have reached a higher level of theoretical maturity and practical application. Representative approaches in the spatial domain include Gaussian filtering, mean filtering, and non-local mean filtering [6,10], which form the foundation of modern denoising techniques. Recent advances in this domain have led to significant improvements in denoising performance. For instance, Gao et al. [2] developed an innovative Gaussian filtering approach utilizing random weighting, which addresses the limitations of traditional Gaussian filtering in nonlinear system state estimation through adaptive noise characteristic estimation. Zhang et al. [28] introduced a fast combined median and mean filtering method that effectively suppresses both impulse and Gaussian noise simultaneously, representing a significant advancement in multi-noise suppression. Further innovations include the adaptive switching weight mean filter (ASWMF) proposed by Thanh et al.[21], specifically designed for salt-and-pepper noise removal, and an enhanced adaptive median filtering method developed by Tang et al. [19] that overcomes the limitations of conventional median filtering techniques in structured light image denoising. Huang and Ji [8] proposed an image denoising method that combines diffusion probability and dictionary learning. The approach aims to improve edge clarity during noise removal, addressing issues where traditional methods may blur edge information. These spatial domain methods have demonstrated remarkable effectiveness in noise removal and have gained widespread adoption across various image processing applications.

In the frequency domain, digital filtering methods have evolved significantly since the introduction of Fourier transform-based techniques, with low-pass and high-pass filters serving as foundational approaches [18]. Recent years have witnessed substantial advancements in frequency domain filtering algorithms. For instance, Zhang et al. [27] enhanced the optimal computation of center weight by incorporating a Wiener filter into the calculation process, achieving superior denoising results compared to traditional nonlocal mean methods. A notable contribution by Liu et al. [12] introduced the parallelizable Fast Multi-channel Wiener Filter (FMWF) algorithm, representing a significant advancement in computational efficiency. In addressing the specific challenges of hyperspectral imaging, Aswathy et al. [1] developed an innovative sparsity-based denoising strategy that effectively processes each band of hyperspectral images (HSI), demonstrating particular efficacy in this specialized domain. Further expanding the theoretical framework, Selesnick et al. [17] proposed an integrated approach combining low-pass filtering with total variation modeling, establishing a more comprehensive basis for frequency domain denoising.Yang and Li [25] proposed a method that enhances wavelet domain features to improve noisy image segmentation,the techniques discussed could be relevant to noise filtering applications.

Despite the advances in existing noise filtering methods, a significant limitation persists: these approaches typically consider image data from a single perspective, overlooking valuable information from other structural aspects. To address this limitation, we propose a novel linear projection-based noise filtering (LPNF) framework, grounded in projection learning theory. This framework innovatively integrates multiple structural aspects - local spatial information, local manifold structure, and global structure - through well-defined criteria to learn an optimal linear projection for noise filtering.

The proposed LPNF framework demonstrates remarkable flexibility, as it can accommodate various projection learning criteria commonly used in feature extraction for denoising purposes. We present two specific implementations of this framework: Principal Component Analysis-based LPNF (LPNF-PCA) and Locality Preserving Projection-based LPNF (LPNF-LPP). These implementations leverage the established criteria of PCA and LPP, respectively, to learn effective linear projections for noise filtering. Notably, LPNF-PCA achieves simultaneous consideration of both local spatial and global information, while LPNF-LPP effectively preserves the local manifold structure while maintaining spatial information integrity.

To rigorously evaluate the effectiveness of our proposed framework, we conduct comprehensive experiments on four standard test images corrupted with various types of noise. These experiments are designed to assess both the quantitative performance and visual quality of the denoising results.

2. Related Works

2.1. Principal Component Analysis

Principal Component Analysis (PCA) is a widely used dimensionality reduction technique in data science and machine learning, introduced by Pearson [14] and later formalized by Hotelling [7]. It transforms a dataset into a new coordinate system, where the axes (principal components) represent directions of maximum variance. PCA is particularly effective for simplifying data, reducing redundancy, and visualizing high-dimensional datasets. PCA works by computing the eigenvalues and eigenvectors of the covariance matrix of the data, where the eigenvectors define the principal components, and the eigenvalues represent the variance captured by each component. By retaining components with the largest eigenvalues, PCA minimizes information loss while reducing dimensionality. This property makes it valuable in fields like image compression, facial recognition, and gene expression analysis [11]. A key strength of PCA lies in its unsupervised nature and computational efficiency. However, it assumes linear relationships in the data, limiting its effectiveness for datasets with nonlinear structures. Variants like Kernel PCA address this limitation by mapping data into higher-dimensional feature spaces [16].

Despite its simplicity, PCA remains foundational in data analysis. Its applications extend across disciplines, including computer vision, finance, and biology, offering insights by emphasizing the most significant patterns in complex datasets.Principal Component Analysis (PCA) is a fundamental unsupervised dimensionality reduction and feature extraction technique that has garnered significant attention across various domains of data analysis and machine learning. The core principle of PCA is to transform high-dimensional data into a lower-dimensional subspace while maximizing variance and minimizing the correlation between features [23].

Mathematically, given an observation data matrix $[x_i] \in R^{(d\times n)}$, where $x_i \in R^d$ represents individual data points, d denotes the feature dimension, and n indicates the number of samples, PCA aims to find an optimal projection matrix P that minimizes the reconstruction error [24]. This optimization problem can be formally expressed as:

$$\min_{P} \sum_{i=1}^{n} \left\| x_i - PP^T x_i \right\|_2^2 \quad s.t. P^T P = I. \tag{1}$$

2.2. Classical Image Noise Filtering Methods

Classical image noise filtering methods include mean filter, bilateral filter, and median filter, etc. These are foundational techniques in image denoising, widely used for their simplicity and effectiveness in reducing noise while preserving image quality to varying degrees.The mean filter is a linear smoothing technique that replaces each pixel with the average value of its surrounding pixels. This method effectively reduces random noise but often blurs edges and fine details, making it less suitable for images where edge preservation is critical [4].The bilateral filter, introduced by Tomasi and Manduchi [22], is a nonlinear method that combines spatial proximity and pixel intensity differences to preserve edges while removing noise. By weighting nearby pixels based on both their spatial distance and intensity similarity, the bilateral filter avoids the over-smoothing associated with linear filters and is especially effective for images with fine textures.The median filter is another nonlinear approach, replacing each pixel with the median value of its neighborhood. This method excels in removing impulse noise (e.g., salt-and-pepper noise) without blurring edges, making it ideal for applications requiring robust noise suppression and edge preservation [9].In general, those methods can be summarized in a common framework as presented in Algorithm 1.

Problem Formulation: Given:

Input noisy image $Q = [q_{ij}] \in R^{a \times b}$

where a and b represent image dimensions $k \times k$ denotes the size of sliding window.

Objective:

Generate denoised image $Q' = [q_{ij}]$ through spatial convolution operations General Framework:

Window Operation:

For each pixel q_{ij} in Q

Apply $k \times k$ sliding spatial window

Generate local patch $I_{ij} \in R^{k \times k}$

Filtering Process:

Compute weight matrix W_{ij} specific to each method

Perform convolution: $q'_{ij} = W_{ij} * I_{ij}$

where * denotes convolution operation.

Specifically, in Algorithm 1, the different definitions of weight matrix W_{ij} represent different noise filters. For example, the mean filter is related the weight matrix whose elements are all equal to $\frac{1}{k2}$. The formula for constructing the weight matrix of the bilateral filter is:

$$W_{ij} = \omega s \times \omega r \tag{2}$$

where $\omega s = e^{\left(-\frac{(i-k)^2+(j-l)^2}{2\sigma_s^2}\right)}$ is the spatial distance factor and $\omega r = e^{\left(-\frac{\|I_{ij}-I_{kl}\|^2}{2\sigma_r^2}\right)}$ is the difference factor of grayscale. σ_s and σ_r are the filter parameters.

Algorithm 1: Classical noise filtering methods
Input: Noisy image $Q = [q_{ij}] \in R_{a\times b}$
for $i \leq a$ do
  for $j \leq b$ do
  Step 1: Generate a local patch $I_{ij} \in R^{k\times k}$ around each pixel q_{ij}
  with a $k \times k$ sliding spatial window.
  Step 2: For each patch I_{ij}, compute a corresponding weight matrix $W_{ij} \in R^{k\times k}$.
  Step 3: Convolution operation on pixel q_{ij} to get denoised pixel
  $q'_{ij} = W_{ij} * I_{ij}$, where * is a convolution operation.
  end
end
Step 4: Restore the denoised image $Q' = \left[q'_{ij}\right] \in R^{a\times b}$.
Output: Denoised image Q'

3. Methodology

3.1. Linear Projection-Based Noise Filtering Framework

Digital image acquisition and transmission processes are inherently susceptible to various types of noise, stemming from both imaging equipment limitations and environmental interference. These noise artifacts significantly degrade image quality, making image denoising a crucial preprocessing step in numerous computer vision applications. While traditional image filtering approaches employ sliding window-based convolution operations for noise reduction, they primarily focus on local spatial information, overlooking other valuable structural characteristics such as local manifold relationships and global image patterns.

To address these limitations, we propose a novel Linear Projection Noise Filtering (LPNF) framework that approaches image denoising from a data transformation perspective using linear projection theory. This framework uniquely integrates multiple structural aspects of image data:

- Local spatial information for detail preservation
- Local manifold structure for neighborhood relationships
- Global structure for overall image coherence

The detailed architecture of our proposed LPNF framework, illustrated in Fig 1, demonstrates how these different information sources are systematically integrated to achieve superior denoising performance.

In particular, assume

$Q = [q_{ij}] \in R^{a\times b}$ is a nosiy image and the size of the sliding window is $k \times k$,the detailed procedure of the proposed LPNF contains four steps. Namely,

Step1. For each pixel q_{ij}, a sliding window with size of $k \times k$ is employed to generate a local patch $I_{ij} \in R^{k\times k}$ around the center pixel q_{ij}, where $0 < i \leq a$ and $0 < j \leq b$.

Step2. Obtain data matrix X by vectorizing each patch I_{ij} into a row vector x_n, where $n = i + (j-1) \times a$. The data matrix X contains the local spatial information of image.

Step3. Construct a certain criterion to compute a linear projection $P \in R^{m\times k^2}$, $\left(m < k^2\right)$ for noise filtering.

Step4. Compute each noise filtered center pixel q'_{ij} by the following equation:

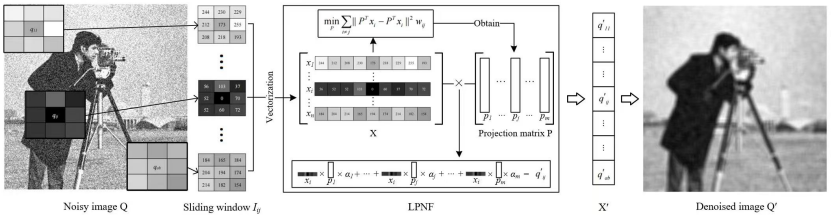

Fig. 1. The flowchart of LPNF framework

$$q'_{ij} = x_i * \sum_{j=1}^{m} p_j \alpha_j \tag{3}$$

where $p_j \in R^{k^2}$ is the column vector of linear projection P . Then, the denoised image Q' can be obtained by reorganizing the transformed data into a matrix of $a \times b$.

3.2. The Computation of Projection Matrix P

In our proposed LPNF framework, the selection and formulation of projection learning criteria play a pivotal role in determining denoising performance. The framework's flexibility allows for the incorporation of various projection learning approaches, particularly those developed within the graph embedding paradigm. Drawing from extensive literature review, we can formulate a generalized objective function for projection learning as follows:

$$\begin{aligned} \tilde{P} &= arg \min_{P^T X L_p X^T P} \sum_{i \neq j} \left\| P^T x_i - P^T x_j \right\|^2 \omega_{ij} \\ &= arg \min_{P^T X L_p X^T P} tr\left(P^T X L X^T P \right), \end{aligned} \tag{4}$$

where L is the Laplacian matrix of the intrinsic graph $G, L = D - W$, W is the graph weight matrix, D is a diagonal matrix with the ith diagonal element being $Dii = \sum_{j=1}^{n} w_{ij}$, and L_p may be the Laplacian matrix of the penalty graph G_p or a simple scale normalization constraint. By taking the structure information from different aspects into consideration, the weighted matrix W can be defined with different criteria.

The optimal solution of the minimizing problem (4) is equivalent to the generalized eigenvectors of the following generalized eigen-decomposition problem.

$$XLX^T p = \lambda X L_p X^T p \tag{5}$$

Thus, the optimal $\tilde{P}$ consists of the generalized eigenvectors corresponding to the m smallest nonzero eigenvalues of (5).

3.3. LPNF-PCA and LPNF-LPP

The objective function in our projection learning framework can be formulated using different criteria, primarily distinguished by their approaches to constructing the weight matrix W. We present two specialized implementations of LPNF, each representing a distinct methodology for capturing different aspects of image structure.

1) LPNF-PCA Implementation:

This first variant employs Principal Component Analysis (PCA) criteria for computing the linear projection. The weight matrix W is constructed as: $w_{ij} = 1/n$, for $j \neq i$

where:

- w_{ij} represents the $(i, j) - th$ element of matrix W
- n is the total number of samples
- The condition $j \neq i$ ensures proper handling of self-connections

This formulation enables LPNF-PCA to simultaneously capture:

- Local spatial relationships
- Global structural patterns
- Overall data distribution characteristics

2) LPNF-LPP Implementation: The second variant utilizes Locality Preserving Projection (LPP), an unsupervised approach that integrates both local manifold structure and spatial information. The weight matrix construction follows:

$$\omega_{ij} = \begin{cases} \exp\left(\frac{-\|x_i - x_j\|^2}{t}\right), & if\ x_i\ and\ x_j\ are\ neighbours\ of\ each\ other \\ 0, & otherwise \end{cases} \tag{6}$$

where:

- t is the heat kernel parameter
- Neighborhood relationship is defined by geometric proximity
- The exponential term preserves local manifold structure

4. Experiments

4.1. Experimental Setup

To rigorously evaluate the effectiveness of our proposed methods (LPNF-PCA and LPNF-LPP), we conducted comprehensive experiments using a diverse set of benchmark images under various noise conditions.

Experimental Setup:

1) Test Images: Four widely-used benchmark images (Fig 2):

- Cameraman
- Peppers
- Barbara
- Goldhill

Fig. 2. From left to right, the images are Cameraman, Peppers, Barbara, and Goldhill

2) Noise Scenarios:
- Gaussian noise contamination
- Mixed noise contamination

3) Comparative Methods:
Classical Approaches:
-Mean filter
-Median filter
-Bilateral filter
Advanced Techniques:
-Robust Principal Component Analysis (RPCA)
-Weighted Schatten p-norm Minimization (WSNM)

4)Performance Metrics:
Quantitative Evaluation:
Peak Signal-to-Noise Ratio (PSNR)
-Measures overall reconstruction quality
-Evaluates pixel-level accuracy

Structural Similarity Index (SSIM)
-Assesses structural preservation
-Quantifies perceptual quality

Normalized Mean Square Error (NMSE)
-Provides normalized error measurement
-Enables cross-image comparison

Qualitative Assessment:
-Visual comparison of restored images
-Analysis of detail preservation
-Evaluation of artifact suppression

4.2. Experimental Results and Analysis

First, we evaluate the performance of our proposed denoising methods using the Cameraman and Peppers images contaminated with zero-mean Gaussian noise at two different variance levels (0.2 and 0.3). The comprehensive denoising results for both images across different methods are presented in Tables 1 through 4.

Analysis of the Cameraman image results (Tables 1 and 2) demonstrates that our proposed methods achieve superior performance compared to competing approaches across nearly all evaluation metrics and scenarios. Specifically, both LPNF-PCA and LPNF-LPP show significant improvements over traditional filtering approaches such as mean, median, and bilateral filters. The quantitative gains are substantial, with minimum improvements of 0.04 in NMSE, 1.35 dB in PSNR, and 0.09 in SSIM. These consistent improvements across multiple metrics indicate the robust performance of our proposed methods in handling Gaussian noise at different intensity levels.

For the Peppers image (Tables 3 and 4), the LPNF-LPP variant demonstrates particularly impressive performance across both noise variance levels (0.2 and 0.3). The method maintains its effectiveness even at higher noise intensity, showcasing its robustness and stability in challenging denoising scenarios. The superior performance is consistent across all evaluation metrics, indicating that our method successfully preserves image structure while effectively removing noise. This comprehensive performance improvement over existing methods validates the effectiveness of our proposed approach in handling various types of image content and noise levels.

In summary, both LPNF-PCA and LPNF-LPP demonstrate clear advantages over existing methods across all three evaluation metrics (NMSE, PSNR, and SSIM). These consistent improvements across different images and noise levels validate the effectiveness and robustness of our proposed framework in image denoising applications.

Table 1. Performance comparison of different methods on the Cameraman polluted by Gaussian noise with variance of 0.2

Methods	NMSE	PSNR	SSIM
RPCA	0.1563±0.0006	13.64±0.02	0.3971±0.0027
WSNM	0.1733±0.0005	13.20±0.01	0.2930±0.0001
Mean filter	0.1606±0.0004	13.53±0.01	0.4893±0.0011
Median filter	0.1614±0.0006	13.50±0.02	0.3449±0.0013
Bilateral filter	0.1736±0.0004	13.19±0.01	0.2933±0.0012
LPNF-PCA	0.1147±0.0014	14.99±0.06	0.5805±0.0022
LPNF-LPP	0.1142±0.0038	15.02±0.14	0.5812±0.0024

To further validate the effectiveness of our proposed methods, we conducted a comprehensive evaluation using Barbara and Goldhill images contaminated with mixed noise conditions. The noise model combines zero-mean Gaussian noise (variance = 0.3) with Salt-and-Pepper noise (density = 0.2), representing a more challenging and realistic denoising scenario.

The experimental results for the Barbara image (Table 5) demonstrate the superior performance of our proposed methods compared to other state-of-the-art approaches.

Table 2. Performance comparison of different methods on the Cameraman polluted by Gaussian noise with variance of 0.3

Methods	NMSE	PSNR	SSIM
RPCA	0.2749±0.0004	11.19±0.01	0.3994±0.0041
WSNM	0.3245±0.0008	10.47±0.01	0.3019±0.0013
Mean filter	0.3053±0.0009	10.74±0.01	0.4852±0.0017
Median filter	0.3242±0.0010	10.47±0.01	0.3584±0.0014
Bilateral filter	0.3244±0.0010	10.47±0.01	0.3018±0.0010
LPNF-PCA	0.2113±0.0014	12.33±0.03	0.5653±0.0016
LPNF-LPP	0.2111±0.0021	12.34±0.04	0.5655±0.0020

Table 3. Performance comparison of different methods on the Peppers polluted by Gaussian noise with variance of 0.2

Methods	NMSE	PSNR	SSIM
RPCA	0.2001±0.0002	13.61±0.00	0.3148±0.0010
WSNM	0.2267±0.0002	13.07±0.00	0.2163±0.0004
Mean filter	0.1830±0.0002	14.00±0.00	0.6201±0.0010
Median filter	0.2013±0.0002	13.58±0.00	0.3305±0.0009
Bilateral filter	0.2213±0.0004	13.17±0.01	0.2430±0.0007
LPNF-PCA	0.1213±0.0019	15.78±0.07	0.6703±0.0018
LPNF-LPP	0.1200±0.0017	15.83±0.06	0.6710±0.0014

Both LPNF-PCA and LPNF-LPP achieve significant quantitative improvements, with notable gains of approximately 0.18 in NMSE and 4.32 dB in PSNR compared to competing methods. These substantial improvements indicate the robust capability of our methods in handling complex mixed noise scenarios while preserving important image details.

Similarly, the results for the Goldhill image (Table 6) corroborate these findings, showing consistent performance improvements across all evaluation metrics. The ability of our methods to maintain superior performance across different image content and mixed noise conditions demonstrates their robustness and general applicability.

In summary, both LPNF-PCA and LPNF-LPP consistently outperform existing comparative methods when applied to Barbara and Goldhill images contaminated with mixed noise. This superior performance in challenging mixed noise scenarios further validates the effectiveness of our proposed framework in real-world denoising applications.

Table 4. Performance comparison of different methods on the Peppers polluted by Gaussian noise with variance of 0.3

Methods	NMSE	PSNR	SSIM
RPCA	0.3945±0.0003	10.66±0.00	0.4396±0.0014
WSNM	0.4225±0.0002	10.36±0.00	0.2105±0.0006
Mean filter	0.3877±0.0004	10.74±0.00	0.5712±0.0007
Median filter	0.4126±0.0003	10.47±0.00	0.3213±0.0008
Bilateral filter	0.4244±0.0003	10.34±0.00	0.2447±0.0006
LPNF-PCA	0.2286±0.0019	13.03±0.04	0.6317±0.0012
LPNF-LPP	0.2255±0.0027	13.09±0.05	0.6334±0.0014

Table 5. Performance comparison of different methods on the Barbara with mixed noise

Methods	NMSE	PSNR	SSIM
RPCA	0.4095±0.0004	10.29±0.01	0.2634±0.0008
WSNM	0.5767±0.0006	8.80±0.01	0.0953±0.0007
Mean filter	0.2908±0.0008	11.77±0.01	0.3763±0.0020
Median filter	0.4522±0.0006	9.85±0.01	0.2304±0.0017
Bilateral filter	0.5770±0.0004	8.80±0.00	0.0952±0.0009
LPNF-PCA	0.1035±0.0040	16.26±0.16	0.3796±0.0015
LPNF-LPP	0.1077±0.0023	16.09±0.09	0.3815±0.0012

Table 6. Performance comparison of different methods on the Goldhill with mixed noise

Methods	NMSE	PSNR	SSIM
RPCA	0.3867±0.0007	10.49±0.01	0.2775±0.0015
WSNM	0.5659±0.0007	8.84±0.01	0.0654±0.0005
Mean filter	0.2806±0.0009	11.89±0.01	0.3936±0.0020
Median filter	0.4371±0.0005	9.96±0.01	0.1881±0.0020
Bilateral filter	0.5661±0.0007	8.84±0.01	0.0651±0.0007
LPNF-PCA	0.0880±0.0074	16.93±0.36	0.4035±0.0015
LPNF-LPP	0.0887±0.0060	16.90±0.31	0.4042±0.0024

Examining the qualitative results presented in Figure 3, our proposed methods demonstrate superior visual performance compared to existing denoising approaches when applied to images contaminated with zero-mean Gaussian noise (variance = 0.2). While established methods such as WSNM, median filter, and bilateral filter show significant residual noise in their recovered images, both LPNF-PCA and LPNF-LPP achieve more effective noise suppression while maintaining image fidelity.

The visual superiority of our methods is particularly evident in their ability to preserve crucial image details while effectively removing noise artifacts. Both LPNF-PCA and LPNF-LPP excel at retaining facial features and fine structural details of the original image, achieving a better balance between noise reduction and detail preservation. The recovered images show enhanced edge sharpness and more natural texture reproduction compared to the results from competing methods.

These qualitative improvements are characterized by clearer facial feature definition, better preservation of subtle texture details, and more balanced noise reduction without over-smoothing artifacts. The results maintain the natural contrast and overall visual characteristics of the original image while successfully eliminating noise contamination. These visual outcomes strongly complement our quantitative findings, demonstrating that our proposed methods not only achieve superior numerical metrics but also produce more visually appealing and faithful image reconstructions.

Figure 4 presents a comprehensive visual comparison of various denoising methods applied to the Barbara image contaminated with mixed noise (Gaussian noise with variance 0.3 and salt-and-pepper noise with density 0.2). The traditional filtering approaches demonstrate significant limitations in handling this complex noise scenario. Specifically, the mean filter tends to blur important image details while only partially removing noise. The median filter, while effective against salt-and-pepper noise, struggles to address the

Fig. 3. Visual comparison of different denoising methods on the Cameraman with Gaussian noise (variance is 0.2). From left to right and top to bottom, the images are the Original image, Noisy image, and the denoised images obtained by RPCA, WSNM, Mean filter, Median filter, Bilateral filter, LPNF-PCA, and LPNF-LPP, respectively

Fig. 4. Visual comparison of different denoising methods on the Barbara with mixed noise. From left to right and top to bottom, the images are the Original image, Noisy image, and the denoised images obtained by RPCA, WSNM, Mean filter, Median filter, Bilateral filter, LPNF-PCA, and LPNF-LPP, respectively

Gaussian noise component, resulting in loss of fine texture details. The bilateral filter preserves edges but fails to adequately remove the mixed noise, particularly in regions with complex textures.

In contrast, our proposed methods (LPNF-PCA and LPNF-LPP) demonstrate superior denoising performance in several aspects:

- Better preservation of fine texture details, particularly visible in the fabric patterns
- More effective removal of both Gaussian and salt-and-pepper noise components
- Improved edge preservation and structural integrity
- Enhanced visual clarity without introducing significant artifacts

– Better maintenance of the original image contrast and brightness

This visual comparison clearly demonstrates the advantages of our proposed methods in handling complex mixed noise scenarios while preserving important image details and structures.

5. Conclusions

In this study, we present a novel linear projection-based noise filtering (LPNF) framework for image denoising. The framework is innovatively constructed from the perspective of linear projection learning and demonstrates the ability to comprehensively utilize multiple structural information, including local spatial information, local manifold structure, and global structure, through the construction of diverse criteria for linear projection learning. Within this framework, two specialized implementations (i.e., LPNF-PCA and LPNF-LPP) were developed by incorporating the projection learning objective functions of Principal Component Analysis (PCA) and Locality Preserving Projection (LPP), respectively. Extensive experimental evaluations conducted on four standard test images with various noise types demonstrate that the proposed methods consistently outperform several state-of-the-art denoising approaches in terms of both quantitative metrics and visual quality. The superior performance validates the effectiveness and robustness of our proposed framework in image denoising applications.

Acknowledgments. This work was supported in part by the Hunan Provincial Key Research and Development Program under Grant 2023NK2011 and in part by the Hunan Provincial Natural Science Foundation of China under Grant 2022JJ40189.

References

1. Aswathy, C., Sowmya, V., Soman, K.: Hyperspectral image denoising using low pass sparse banded filter matrix for improved sparsity based classification. Procedia Computer Science 58, 26–33 (2015)
2. Gao, Z., Gu, C., Yang, J., Gao, S., Zhong, Y.: Random weighting-based nonlinear gaussian filtering. IEEE Access 8, 19590–19605 (2020)
3. Gholami Bahador, F., Mokhtary, P., Lakestani, M.: Mixed poisson-gaussian noise reduction using a time-space fractional differential equations. Information Sciences 647, 119417 (2023)
4. Gonzalez, R.C., Woods, R.E.: Digital Image Processing (3rd Edition). Pearson Education (2008)
5. Goyal, B., Dogra, A., Agrawal, S., Sohi, B.S., Sharma, A.: Image denoising review: From classical to state-of-the-art approaches. Information fusion 55, 220–244 (2020)
6. He, L., Zhang, Q., Yang, X., Wang, Y., Wang, C.: Sln-red: Regularization by simultaneous local and nonlocal denoising for image restoration. IEEE Signal Processing Letters (2023)
7. Hotelling, H.: Analysis of a complex of statistical variables into principal components. Journal of Educational Psychology 24(6), 417–441 (1933)
8. Huang, J., Jin, Z.: Enhanced image denoising with diffusion probability and dictionary learning adaptation. Technical gazette 31(3), 774–783 (2024)
9. Huang, T.S., Yang, G.J., Tang, G.Y.: A fast two-dimensional median filtering algorithm. IEEE Transactions on Acoustics, Speech, and Signal Processing 27(1), 13–18 (1997)

10. Jebur, R.S., Der, C.S., Hammood, D.A., Weng, L.Y.: Image denoising techniques: An overview. AIP Conference Proceedings 2804(1), 020002 (09 2023)
11. Jolliffe, I.T.: Principal Component Analysis (2nd Edition). Springer (2002)
12. Liu, J., Sun, H., Wu, M., Yang, J.: Gpu implementation of a fast multichannel wiener filter algorithm for active noise control. IEEE Signal Processing Letters (2024)
13. Mafi, M., Martin, H., Cabrerizo, M., Andrian, J., Barreto, A., Adjouadi, M.: A comprehensive survey on impulse and gaussian denoising filters for digital images. Signal Processing 157, 236–260 (2019)
14. Pearson, K.: On lines and planes of closest fit to systems of points in space. Philosophical Magazine 2(11), 559–572 (1901)
15. Saadia, A., Rashdi, A.: A speckle noise removal method. Circuits, Systems, and Signal Processing 37, 2639–2650 (2018)
16. Schölkopf, B., Smola, A., Müller, K.R.: Nonlinear component analysis as a kernel eigenvalue problem. Neural Computation 10(5), 1299–1319 (1997)
17. Selesnick, I.W., Graber, H.L., Pfeil, D.S., Barbour, R.L.: Simultaneous low-pass filtering and total variation denoising. IEEE Transactions on Signal Processing 62(5), 1109–1124 (2014)
18. Susladkar, O., Deshmukh, G., Nag, S., Mantravadi, A., Makwana, D., Ravichandran, S., Chavhan, G.H., Mohan, C.K., Mittal, S., et al.: Clarifynet: A high-pass and low-pass filtering based cnn for single image dehazing. Journal of systems architecture 132, 102736 (2022)
19. Tang, J., Wang, Y., Cao, W., Yang, J.: Improved adaptive median filtering for structured light image denoising. In: 2019 7th International conference on information, communication and networks (ICICN). pp. 146–149. IEEE (2019)
20. Thanh, D., Surya, P., et al.: A review on ct and x-ray images denoising methods. Informatica 43(2) (2019)
21. Thanh, D.N., Hien, N.N., Kalavathi, P., Prasath, V.S.: Adaptive switching weight mean filter for salt and pepper image denoising. Procedia Computer Science 171, 292–301 (2020)
22. Tomasi, C., Manduchi, R.: Bilateral filtering for gray and color images. In: Proceedings of the Sixth International Conference on Computer Vision (ICCV). pp. 839–846. IEEE, Bombay, India (1998)
23. Uddin, M.P., Mamun, M.A., Hossain, M.A.: Pca-based feature reduction for hyperspectral remote sensing image classification. IETE Technical Review 38(4), 377–396 (2021)
24. Wang, J., Wu, Y., Li, B., Yang, Z., Nie, F.: Fast anchor graph preserving projections. Pattern Recognition 146, 109996 (2024)
25. Yang, R., Li, D.: Adaptive wavelet transform based on artificial fish swarm optimization and fuzzy c-means method for noisy image segmentation. Computer Science and Information Systems 19(3), 1389–1408 (2022)
26. Zhang, J., Li, Z.y., Wang, L.z., Chen, Y.p.: Salt-and-pepper denoising method for colour images based on tensor low-rank prior and implicit regularization. IET Image Processing 17(3), 886–900 (2023)
27. Zhang, X.: Center pixel weight based on wiener filter for non-local means image denoising. Optik 244, 167557 (2021)
28. Zhang, X., Liao, H., Du, X., Xu, B.: A fast hybrid noise filtering algorithm based on median-mean. In: 2018 IEEE International Conference on Mechatronics and Automation (ICMA). pp. 2120–2125. IEEE (2018)

Congyin Cao received the B.S. degree in software engineering from Zhongyuan University of Technology, Zhengzhou, China, in 2022. He is currently working toward the M.Agr. degree in agricultural engineering and information technology with the College

of Information and Intelligence, Hunan Agricultural University, Changsha, China. His research interests include remote sensing image processing and analysis field, especially remote sensing image feature extraction and classification technology.

Yangjun Deng received the Ph.D. degree in signal and information processing from the School of Information Science and Technology, Southwest Jiaotong University, Chengdu, China, in 2020. From 2018 to 2019, he was a Visiting Scholar along with Prof. Qian Du at Mississippi State University, Starkville, MS, USA, to study on the dimensionality reduction of hyperspectral images. He is currently a associate professor with the College of Information and Intelligence, Hunan Agricultural University, Changsha, China. His research interests include pattern recognition, remote sensing image processing, and agricultural information processing.

Menglong Yang received the B.S. degree in computer science and technology and M.Agr. degree in agricultural engineering and information technology from Hunan Agricultural University, Changsha, China, in 2021 and 2024, respectively. He is currently pursuing the Ph.D. degree in forestry engineering with the School of Central South University of Forestry and Technology. His research interests include machine learning and pattern recognition.

Xinghui Zhu received the M.S. degree in computer science and technology from National University of Defense Technology, Changsha, China, in 2004. He received the Ph.D. degree in land resources and information technology from Hunan Agricultural University, Changsha, China, in 2018. From 2016 to 2023, he served as dean with the College of Information and Intelligence, Hunan Agricultural University, Changsha, China. He is currently a member of the National Steering Committee of Agricultural Graduate Education, vice chairman of Hunan Provincial Computer Specialized Committee, and executive director of Hunan Computer Federation. His research interests include Artificial Intelligence, Big Data, Smart Agriculture, etc. He has already won one first prize of Hunan Provincial Scientific and Technological Progress in related fields, and has presided over four national projects such as the National Science and Technology Support Program and the National Key Research and Development Program, as well as eight provincial and ministerial projects such as the Hunan Provincial Natural Science Foundation and the Hunan Provincial Key Research and Development Program. He has more than 60 publications in these areas.

Received: November 07, 2024; Accepted: December 17, 2024.

Computer Science and Information Systems 22(1):327–344 https://doi.org/10.2298/CSIS241110011Y

Multimodal Deep Learning-based Feature Fusion for Object Detection in Remote Sensing Images

Shoulin Yin[1], Qunming Wang[2], Liguo Wang[3], Mirjana Ivanović[4], and Hang Li[5]

[1] College of Information and Communication Engineering, Harbin Engineering University
Harbin, 150001 China
yslin@synu.edu.cn
[2] College of Surveying and Geo-informatics, Tongji University
[3] College of Information and Communications Engineering, Dalian Minzu University
Dalian, 116600, China
wangliguo@hrbeu.edu.cn
Corresponding author:Liguo Wang
[4] Faculty of Sciences, University of Novi Sad, Serbia
mira@dmi.uns.ac.rs
[5] Software College, Shenyang Normal University
Shenyang, 110034 China
lihang@synu.edu.cn

Abstract. Object detection is an important computer vision task, which is developed from image classification task. The difference is that it is no longer only to classify a single type of object in an image, but to complete the classification and positioning of multiple objects that may exist in an image at the same time. Classification refers to assigning category labels to the object, and positioning refers to determining the vertex coordinates of the peripheral rectangular box of the object. Therefore, object detection is more challenging and has broader application prospects, such as automatic driving, face recognition, pedestrian detection, medical detection etc,. Object detection can also be used as the research basis for more complex computer vision task such as image segmentation, image description, object tracking and action recognition. In traditional object detection, the feature utilization rate is low and it is easy to be affected by other environmental factors. Hence, this paper proposes a multimodal deep learning-based feature fusion for object detection in remote sensing images. In the new model, cascade RCNN is the backbone network. Parallel cascade RCNN network is utilized for feature fusion to enhance feature expression ability. In order to solve the problem of different segmentation shapes and sizes, the central part of the network adopts multi-coefficient cascaded hollow convolution to obtain multi-receptive field features without using pooling mode and preserving image information. Meanwhile, an improved self-attention combined receptive field strategy is used to obtain both low-level features with marginal details and high-level features with global semantics. Finally, we conduct experiments on DOTA set including ablation experiments and comparison experiments. The experimental results show that the mean Average Precision (mAP) and other indexes have been greatly improved, and its performance is better than the state-of-the-art detection algorithms. It has a good application prospect in the remote sensing image object detection task.

Keywords: Object detection, remote sensing image, multimodal deep learning, feature fusion.

1. Introduction

In recent years, with the development of remote sensing technology, object detection technology based on remote sensing image has attracted wide attention. Object detection can locate the object of interest on the ground from a distance and identify its category. It has a wide range of applications and prospects in the fields of military defense and civil aviation [1,2]. In particular, the classification and detection of aircraft/airport objects in the application of high-resolution remote sensing images can provide some new solutions for the more efficient and scientific organization and management of civil aviation, military and national defense research and other fields [3].

With the rapid development of deep learning, object detection algorithms based on deep learning are widely used in various fields. At present, the mainstream object detection algorithms are divided into two categories: (1) two-stage object detection algorithm based on candidate regions; (2) single-stage object detection algorithm based on direct regression. Single-stage detection algorithm can achieve a balance in accuracy and running speed, which is a kind of detection framework widely used in object detection at present [4].

Single-stage object detection algorithms mainly include SSD [5] series and YOLO [6] series. Zhong et al. [7] proposed a single-stage rotating object detection method based on anchor frame transformation. Based on YOLOv3, a new feature extraction Network Darknet-53-Dense was designed in this algorithm to improve the feature extraction ability. In addition, an Anchor Transformation Network (ATN) [8] was proposed for the detection head network. The initial horizontal anchor frame was transformed into a rotating anchor frame to improve the accuracy of object detection. Cao et al. [9] proposed an algorithm for object detection based on Dilated convolution pyramid, introducing different sizes of hollow convolution layers into Feature Pyramid Networks (FPN). It built a Hybrid Receptive Field Module (HRFM). By increasing the receptive field to obtain more global feature information, the problem of object occlusion was solved. Murthy et al. [10] proposed an anti-residual object detection algorithm, which was based on YOLOv4. An efficient Lightweight Ghost Convolution model (LGC) was proposed to obtain more feature maps with fewer parameters to improve the network's ability to extract global feature information and improve the overall object detection performance. Zhao et al. [11] proposed a object detection algorithm based on improved YOLOv3, added convolutional layer module to the network structure to classify the object background of samples, and adjusted the size of the anchor frame on the feature map. After the object background probability was output, the samples whose background probability value was lower than the set threshold were filtered out, so as to solve the imbalance of the ratio of positive and negative samples in the original algorithm.

Kumar et al. [12] proposed an improved object detection algorithm (Single Shot multibox Detector (SSD) based on DenseNet [13] and feature fusion. On the basis of SSD network, DenseNetS-31-1 feature extraction network was designed according to DenseNet dense connection to enhance the feature extraction ability of the model. In the multi-scale detection part, the fusion mechanism of multi-scale feature layer was introduced to combine the low-level semantic features and high-level semantic features in the network structure, and then improved the model performance.

The two-phase object detection algorithms mainly use RCNN [14] as a series. Xiao et al. [15] proposed an improved object detection algorithm for Faster RCNN, which

improved the accuracy of the model by introducing two difficult sample mining strategies and alternate training. Jiang et al. [16] proposed an improved Faster R-CNN algorithm for multi-scale object detection. By adopting multi-level feature extraction strategy to extract multi-scale object features and using multi-channel method to generate multi-scale object candidate boxes, the accuracy of the object detection algorithm could be improved to some extent. Detection based on the above single or two stage methods can improve the accuracy of object detection. However, the above improved algorithms have low detection accuracy when the detection object is different, the background is complex and the object is blocked. For example, it can be seen from Figure 1 that the scales of Big Ben, dogs and crowds in the three images from Figure 1(a) to Figure 1(c) are from large to small. The two images shown in Figure 1(d) both contain objects of multiple scales. For MSCOCO data sets commonly used in detection tasks, if the scale of all instances is statistically and sorted according to the pixel ratio of object mask to image, it will be found that 10% of objects in the data set have a scale smaller than 0.0207, and 10% of objects have a scale larger than 0.345, with a large scale span.

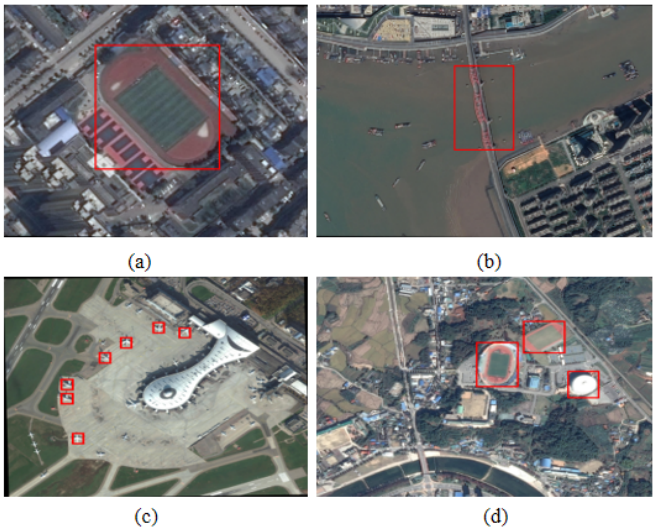

Fig. 1. Remote sensing image objects at different scales. (a) big object; (b) medium object; (c) small object; (d) Multi-scale object

Object detection includes two sub-tasks: object location and classification. The scaling problem lies in the fact that, in the process of deepening convolutional neural networks [17], the ability to express abstract features becomes stronger and stronger, but the shallow spatial information is also relatively lost.

In reference [18], deconvolution layer was added to CNN to fuse the deep and shallow features of CNN network for the detection of buildings in remote sensing images. In reference [19], optimized ResNet model was introduced to solve the significance detection problem of remote sensing images. In reference [20], CNN features with moderate sen-

sitivity field were selected according to the aircraft imaging size in the image, and deep CNN features and shallow CNN features were sampled for superposition fusion. In reference [21], Markov random fields and full convolutional neural networks were introduced to generate high-quality candidate regions. In reference [22], multi-layer CNN features were integrated to describe vehicle objects in remote sensing images, and the hierarchical boost classifier was used to discriminate and achieves good results. Reference [23] used features of different layers of CNN to detect objects of different scales respectively, and improved the detection effect by combining context information. Reference [24] expanded the sample data and combined the object context features to detect aircraft objects in remote sensing images. It can be seen that, for the problem of object scale diversity and small object in remote sensing images, it is a good idea to integrate the corresponding features of different convolutional layers in CNN network, that is, to integrate the detailed information rich in shallow convolutional layer and the semantic information rich in deep convolutional layer in CNN network for feature extraction. However, the use of dimension splicing or pixel-by-pixel addition/multiplication to fuse multi-layer features rarely considers the distribution and scale differences of features of different layers, so feature fusion is still a difficult research task. In addition, the background complexity of remote sensing image has great interference on object detection, so it is necessary to pay more attention to the influence of context information on object detection.

Therefore, according to the above analysis, this paper proposes a multimodal deep learning-based feature fusion for object detection in remote sensing images. In the new model, cascade RCNN is the backbone network. In the multi-scale object detection task, the proposed method makes full use of the features of different scales for fusion, which can greatly improve the robustness of the algorithm.

Our main contributions for this paper are as follows:

1. Parallel cascade RCNN network is utilized for feature fusion to enhance feature expression ability.
2. In order to solve the problem of different segmentation shapes and sizes, the central part of the network adopts multi-coefficient cascaded hollow convolution to obtain multi-receptive field features without using pooling mode and preserving image information.
3. Meanwhile, an improved self-attention combined receptive field strategy is used to obtain both low-level features with marginal details and high-level features with global semantics.

The organizational structure of this paper is assigned as follows. This paper summarizes recent developments in detecting remote sensing objects using deep learning techniques in section 2. The proposed object detection architecture via multi-modal deep learning is presented in Section 3. Section 4 presents experiments including various situations. Section 5 presents the conclusion and future works.

2. Related Works

In order to quantify the scale of the object, usually the area occupied by the object instance (i.e. the number of pixels occupied by the mask) is divided by the area of the image and the result obtained is taken as the relative scale of the object instance (between 0-1), which

is referred to as the scale. Therefore, the relative scales of objects in different images are very different, or the sizes of multiple objects in the same image are very different, which is called the scaling problem. It has always been one of the core challenges that affect the accuracy of object detection.

Table 1 lists the detection results of some object detection algorithms on MSCOCO test set. The "++" symbol indicates that the model uses an image pyramid when inferring. Where, AP refers to the average accuracy when the thresholds of IoU are 0.50:0.05:0.95. AP50 and AP75 are the accuracy when the IoU threshold is 0.50 and 0.75, respectively. APS, APM and APL refer to small, medium and large object AP respectively.

It can be seen from the data in Table 1 that the detection accuracy of small objects of early detectors such as SSD, YOLOv2 and FPN is less than half of that of medium and large objects [25]. In recent two years, the size of detectors has been improved, but there is still an obvious gap between the accuracy of small objects and that of medium and large objects, which seriously affects the improvement of the overall accuracy. Therefore, how to make detectors better cope with objects of different scales (especially small objects) is still an important problem in current object detection research.

Table 1. Different object detection models

Model	Skeleton network	Year	AP	AP50	AP57	APS	APM	APL
Faster RCNN	VGGNet-16	2015	21.9	42.7	–	–	–	–
SSD512	VGGNet-16	2016	28.8	48.5	30.3	10.9	31.8	43.5
Faster RCNN+++	ResNet-101	2016	34.9	55.7	37.4	15.6	38.7	50.9
R-FCN	ResNet-101	2016	29.9	51.9	–	10.8	32.8	45.0
Cascade R-CNN	ResNet-101	2018	42.8	62.1	46.3	23.7	45.5	55.2
DES512	VGGNet-16	2018	32.8	53.2	34.6	13.9	36.0	47.6
TridentNet	ResNet-101	2019	42.7	63.6	46.5	23.9	46.6	56.6
YOLOv3	DarkNet-53	2019	43.9	64.1	49.2	27.0	46.6	53.4
ATSS	ResNet-101	2020	46.3	64.7	50.4	27.7	49.8	58.4
Dynamic R-CNN	ResNet-101	2020	42.0	60.7	45.9	22.7	44.3	54.3
YOLOv4	CPSDarkNet-53	2020	43.5	65.7	47.3	26.7	46.7	53.3

In this paper, we mainly focus on the cascade RCNN to perfect the proposed method in remote sensing images. Cascade RCNN Network consists of feature extraction network (ResNet101), feature pyramid network (FPN), Region Proposal Network (RPN) layer, and cascade detector. Feature extraction network ResNet101 is used to extract image features. The original image is convolved by Conv1, Conv2, Conv3, Conv4 and Conv5 and features of different levels are fused to obtain feature images P2, P3, P4 and P5 of different scales. Then, the feature maps of different scales P2, P3, P4 and P5 are input into RPN to obtain candidate object regions. After the ROI Align [26] operation on the obtained candidate object region, the feature map of Region of Interest (ROI) with uniform size is obtained. Figure 2 shows the Cascade RCNN network structure.

In the detection stage, different from Faster RCNN, Cascade RCNN uses cascade detector for detection, and three detectors set different thresholds respectively for detection. Each detector consists of ROI Align, full connection layer, classification score C and frame regression position coordinate B. During detection, the candidate object region is

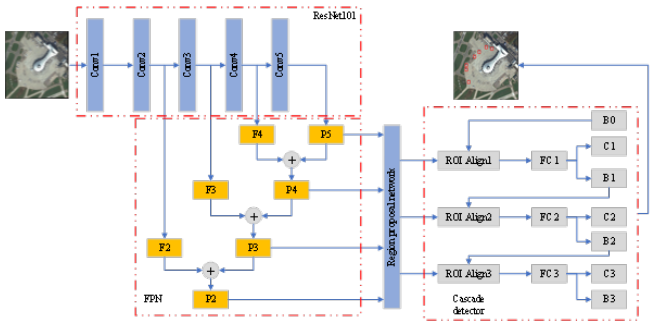

Fig. 2. Cascade RCNN network structure

re-sampled through the frame regression B output by the detector in the previous stage, and the new classification score C and frame regression B are obtained by gradually improving the IoU threshold training, and finally the sample quality and network training effect are improved.

In the process of frame regression, annotated frame P is the predefined anchor, annotated frame G is the object frame, and annotated frame G' is the forecast frame output by the model, whose ultimate purpose is to bring the forecast frame closer to the object frame. When the IoU of candidate box and object box is large, the transformation $d(\cdot)$ from candidate box to prediction box can be regarded as an approximate linear transformation. Define the object box center (G_x, G_y), width and height (G_w, G_h), candidate box center (P_x, P_y), width and height (P_w, P_h), and establish a regression model, as shown in equation (1).

$$\begin{cases} G'_x = & P_x + P_w d_x(P) \\ G'_y = & P_y + P_h d_y(P) \\ G'_w = & P_w exp(d_h(P)) \\ G'_h = & P_h exp(d_h(P)) \\ d_x(P) = & W_*^T \phi(P) \end{cases} \tag{1}$$

Here, $\phi(P)$ is the feature of the candidate frame, and is the parameter to be learned.

The loss function of Cascade RCNN mainly consists of two parts, namely classification error and coordinate regression error, as shown in equation (2).

$$L(p_i, t_i) = \frac{1}{N_{cls}} \sum_i L_{cls}(p_i, p_i^*) + \lambda \frac{1}{N_{reg}} \sum_i p_i^* L_{reg}(t_i, t_i^*). \tag{2}$$

Where p_i is the probability that anchor prediction is the object. p_i^* is the probability of the real box. $t_i = [t_x, t_y, t_w, t_h]$ is a vector representing the four parameterized coordinates of the prediction box. t_i^* is the coordinate vector of the real box, N_{cls} and N_{reg} both represent the total number of samples, λ is the weight balance factor.

In Formula (2), $L_{cls}(p_i, p_i^*)$ is the error between the predicted class confidence and the object class, and the loss function is the cross entropy loss function. $L_{reg}(t_i, t_i^*)$ is frame regression loss, Smooth is adopted as loss function, as shown in equations (3)-(5).

$$L_{cls}(p_i, p_i^*) = -\log[p_i^* p_i + (1 - p_i^*)(1 - p_i)]. \tag{3}$$

$$L_{reg}(t_i, t_i^*) = Smooth_{L1}(t_i - t_i^*). \tag{4}$$

$$Smooth_{L1}(x) = \begin{cases} 0.5x^2, |x| < 1 \\ |x| - 0.5, others \end{cases} \tag{5}$$

3. Multimodal Deep Learning-based Feature Fusion for Object Detection

Aiming at the problems of low detection rate and object occlusion in Cascade RCNN network, this paper proposes an improved Cascade RCNN network structure diagram, as shown in Figure 3. The improved Cascade RCNN algorithm introduces a Dilated convolution module in ResNet101, which carries out multi-scale feature extraction and enhances the robustness of the model for slices with different sizes. The coordinate attention mechanism is introduced into ResNet101 residual network [27]. The low level features with edge details and high level features with global semantics are obtained by using axial self-attention combined with receptive field strategy to improve the accuracy of object detection.

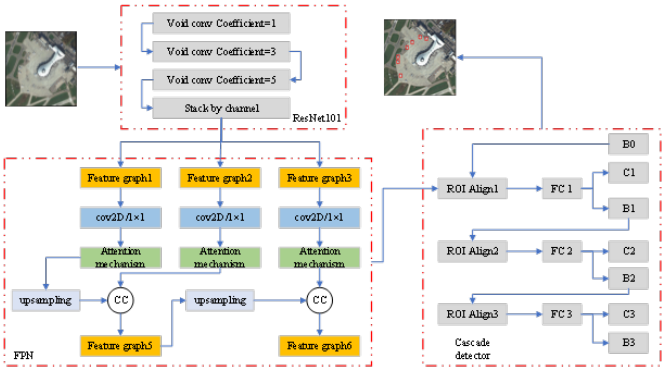

Fig. 3. Proposed object detection structure. CC is Channel-wise Concat.

3.1. Dilated Convolution Module

Considering the complexity of remote sensing images, the correlation of the whole image and the difference of the original resolution distribution of each data sample, it is of great significance to improve the sensing range of the features in the central part of the network and the feature fusion of multiple receptive fields. Pooling can effectively improve the

receptive field of the feature map, but at the same time, important spatial information will be lost due to the decrease of the resolution of the feature map. Therefore, a 3-layer dilated convolution module (3DCM) with skip connection is designed in the central part of FPN to obtain the features of three receptive fields. The structure of this module is shown in Figure 4. C represents the number of output channels of the encoder. It is specifically defined as:

$$d = \varphi(C(\sigma(g_1); \sigma(g_2); \sigma(g_3))). \tag{6}$$

Where g_i represents the output of the $i-th$ layer dilated convolution. σ is the activation function of ELU (exponential linear units). In this paper, the adjustable parameter α of the activation function is set as 1. C represents the stacked feature graphs by channel. $\varphi \in R^{1\times1\times N/2}$ is the convolutional parameter matrix, where N is the feature graph size of input 3DCM module.

Dilated convolution effectively improves the receptive field without introducing new parameter number by injecting holes into the convolution kernel, which is specifically defined as:

$$g[x, y] = \sum_{i}^{M} \sum_{j}^{M} f[x + r \times i, y + r \times j] \cdot h[i, j]. \tag{7}$$

Where x and y represent the coordinates of feature points. i and j are the coordinates of the convolution point. M is the size of the convolution kernel. r is the void coefficient, $r = 1$ in the standard convolution operation. f is the input feature, h is the convolution kernel and g is the output feature.

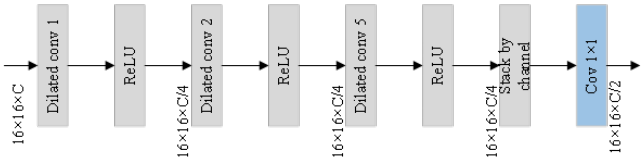

Fig. 4. One kernel

However, if the dilated coefficient is set in the continuous dilated convolution layer without mutual prime, the problem of sampling discontinuity of the feature graph, that is, grid effect, will be generated, and a large amount of feature information will be lost. In order to avoid this effect and take into account the segmentation effect of large and small objects, the dilated coefficient of 3DCM follows the design structure of hybrid dilated convolution (HDC). The dilated coefficients of three layers are set as 1, 2 and 5 respectively. The size of convolution kernel is 3×3 and the step is 1. In this way, the adjacent information of the feature map can be obtained by the 3DCM module and the recognition ability of small object can be improved. In addition, it can also obtain deep receptive field similar to the feature map and improve the recognition ability of large objects.

The receptive field is calculated as:

$$l_k = l_{k-1} + (f_k - 1) \times \prod_{i=1}^{k-1} s_i. \tag{8}$$

Where l_k is the receptive field of each point in the $k-th$ layer. f_k is the size of the $k-th$ convolution kernel. s_i is the convolution step of the $i-th$ layer. According to Formula (8), the actual receptive fields of each layer relative to the output feature map of the encoder are respectively 3, 7 and 17. Since the size of the output feature graph of the encoder is 16×16, the feature points of layer 3 cavity convolution will cover relatively complete information in the input feature graph of 3DCM module. In addition, after stacking channels for feature graphs of different receptive fields, 3DCM uses 1×1 convolution instead of channel addition, which improves the ability of the network to adjust feature weights of different receptive fields adaptively and promotes information fusion.

3.2. Receptive Field Enhancement in Axial Self-attention

In image segmentation, many researchers are studying how to extract low-level features with edge details and global semantic high-level features at the same time. Although self-attention can better achieve the above purposes, this method requires a huge amount of computation, and axial attention solves the above two problems to a certain extent. Therefore, based on this, and combining with the receptive field block (RFB) [28] strategy, this paper designs an axial self-attention receptive field module, as shown in Figure 5. First, the input feature graphs are respectively passed through the receptive field path of 1×3, 1×5, 1×7, 1×1 convolution layer. Secondly, the receptive field is expanded by the cavity convolution layer with cavity rates of 3, 5, 7, 1 respectively, and then the axial self-attention module is entered. Finally, the channel is spliced with the feature map of 1×1 receptive field path and output. Among them, axial self-attention is shown in Figure 6.

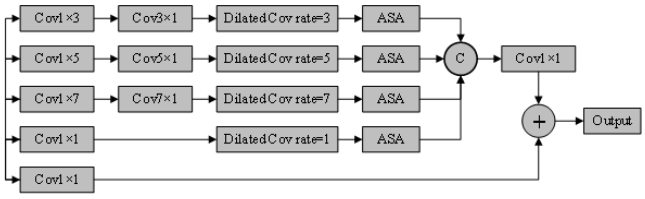

Fig. 5. Axial self-attention field enhancement module

This module is used to build a rich context-dependent model for local features, model the remote dependency relationship, and improve the feature representation of remote sensing image segmentation. Since its purpose is to enhance the features of relatively small objects, this paper selects parallel strategies to compute both horizontal and vertical directions for non-local operations to construct axial attention. At the same time, since the horizontal direction and the vertical direction contribute equally to the output, this paper

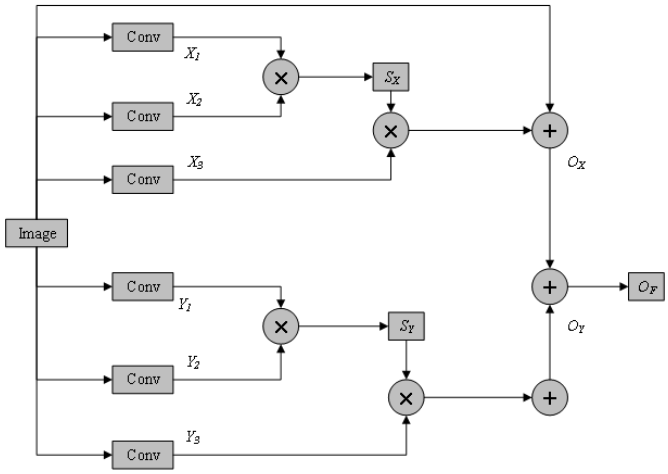

Fig. 6. Axial self-attention module

adopts the method of element by element addition to aggregate the feature maps. The local feature maps are first sent to the convolution layer to generate feature maps, which are reconstructed and transposed into $H \times C \times W$ and $W \times H \times C$ respectively in the horizontal direction (X-axis) to obtain X_1 and X_2. The horizontal space feature maps S_X are calculated by Softmax. i and j represent the position of pixel space. The influence of the $j - th$ position on the pixel of the $i - th$ position can be expressed as:

$$S_{ij} = \frac{e^{(X_{1i}, X_{2j})}}{\sum_{i=1}^{N} e^{(X_{1i}, X_{2j})}}. \tag{9}$$

The more similar the feature representations of the two locations, the stronger the correlation between them. After matrix multiplication of and the feature map reconstructed as $W \times H \times C$, the feature map in the horizontal direction can be obtained by adding the original local feature element by element.

$$O_X = \sum_{i=1}^{N} S_{ij} X_{3i}. \tag{10}$$

Similarly, in the vertical direction (Y-axis), they are reconstructed and transposed as $W \times C \times H$ and $H \times W \times C$, the vertical spatial feature graph S_Y is calculated by Softmax. After matrix multiplication with the reconstructed feature graph $H \times W \times C$, the vertical feature graph O_Y is obtained by adding the original local feature element by element. Finally, it outputs O_F by adding the feature graphs horizontal axis and vertical axis.

4. Experiment Results and Analysis

4.1. Data Set and Experiment Setting

In order to test the performance of the multi-modal deep learning model, 200 high-resolution remote sensing images containing different object categories are collected in the DOTA data set published by Wuhan University [29]. The scale of the original remote sensing image ranges from 800×800 pixels to 4000×4000 pixels. These remote sensing images include roads, trees, houses and other types of complex backgrounds. The spatial resolution range is 0.1-0.3m. Before training, we use DOTA_devkit tools to cut the image into 600×600 pixels, Stride size=100. After data enhancement processing, the images are divided into three sets, of which 4157 are used as the training set, 1064 as the verification set and 1234 as the test set. The model is trained on the training set and tested on the test set. The Non-maximum-suppression (NMS) method with IOU threshold=0.1 is adopted for the final test results to discard repeated detection.

The experimental operating environment is Intel(R) Core (TM) i79700CPU 3.00GHz processor, NIVDIA RTX 30608 GB GDDR6 graphics card 64 GB-DDR4 memory. The environment settings are Cuda10.1 and Cudnn 7.6.4. The network frameworks for deep learning are Pytorch 1.7.1, Python 3.8.8. During training, batch size is set to 4, learning rate to 1.25×10^{-4} and num_epochs to 80. In order to accelerate the model convergence speed, the pre-training weight of ResNet50 on the ImageNet classification task is also introduced as transfer learning.

In this paper, Mean Average Precision (mAP) and Frame Per Second (FPS) are used as evaluation indexes of the model. mAP represents the percentage of the number of correctly recognized single objects in the total number of recognized objects, which is used to measure the overall comprehensive performance of the model. FPS is positively correlated with the speed of model detection.

4.2. Ablation Experiments

In order to verify the effectiveness of multi-scale feature fusion module and spatial and channel attention module in multi-modal deep learning networks, ablation experiments are conducted on DOTA remote sensing data sets, and the experimental results are shown in Table 2.

Table 2. Ablation experiments

Backbone	3DCM	Attention	mAP/%	FPS/s
ResNet101	NO	NO	89.64	1.72
ResNet101	YES	NO	89.98	1.32
ResNet101	NO	YES	90.27	1.37
ResNet101	YES	YES	92.76	1.25

After the introduction of dilated convolution and self-attention multi-scale feature fusion modules, the mAP of the model increases by 3.12% when the backbone network is ResNet101. After adding the self-attention module, the model detection mAP increases

by 0.63% when the backbone is ResNet101. Through the analysis of experimental data, it is found that the introduction of multi-scale feature fusion module and attention module increases the complexity of the whole model, resulting in a 0.47 frame/s FPS reduction, but the model detection speed can still meet the requirements of real-time detection. Some results based on the proposed method are shown in Figure 7.

Fig. 7. Detection results

4.3. Comparison Experiments

To verify the effectiveness of the object detection algorithm in this paper, it is compared with other advanced object detection algorithms containing MSFYOLO, RFEB, ADIR and MSDA. Under the same training and test data sample conditions, $IOU > 0.5$ indicates that the detection is correct, and mAP and FPS are used as evaluation indicators. Tables 3,4,5 show the comparison of detection results between the proposed algorithm and other algorithms on DOTA data sets. To display the intuitionally results, figures 8,9,10 give the objective results.

As shown in Table 3, in the DOTA data set, the detection model presented in this paper has the best detection effect on airport targets, and the detection accuracy reaches 93.87%. In addition, compared with MSFYOLO, RFEB, ADIR and MSDA, the detection model proposed in this paper increases the average accuracy mAP by 12.33%, 9.63%, 5.88%,

Table 3. Comparison experiments on airports

Model	mAP/%	FPS/s
MSFYOLO	81.54	1.97
RFEB	84.24	1.22
ADIR	88.19	2.07
MSDA	90.64	1.73
Proposed	93.87	1.46

Table 4. Comparison experiments on harbors

Model	mAP/%	FPS/s
MSFYOLO	80.81	1.62
RFEB	76.92	1.84
ADIR	82.13	1.45
MSDA	86.95	2.28
Proposed	91.49	1.27

and 3.23%, respectively. Compared with B algorithm, the detection speed of the model is increased by 0.24 frame/s. Due to the introduction of void convolution and self-attention multi-scale feature fusion modules, the model complexity is relatively high, resulting in a relatively slow model detection speed compared with similar models.

From table 4 and table 5, the mAP values of proposed model are 91.49% and 95.58% on harbor and aircraft object respectively. It also illustrates the better detection effect on DOTA.

5. Conclusion

In this paper, an object detection model based on multi-modal deep learning feature fusion in remote sensing images is proposed. A multi-scale feature fusion module is constructed by integrating dilated convolution and self-attention mechanism to enrich the spatial and semantic information of objects and further improve the effectiveness of model detection. Compared with the traditional detection algorithm ResNet101, the accuracy is improved by about 3.12%, which proves the effectiveness of the proposed detection algorithm. Although the detection effect of the method in this paper has been significantly improved on the test set, some problems still exist, and this is also the direction of future research. 1) The detection is time-consuming. Although the detection accuracy of this method has

Table 5. Comparison experiments on aircraft

Model	mAP/%	FPS/s
MSFYOLO	83.83	1.66
RFEB	86.52	1.95
ADIR	88.27	2.84
MSDA	94.84	1.67
Proposed	95.58	1.48

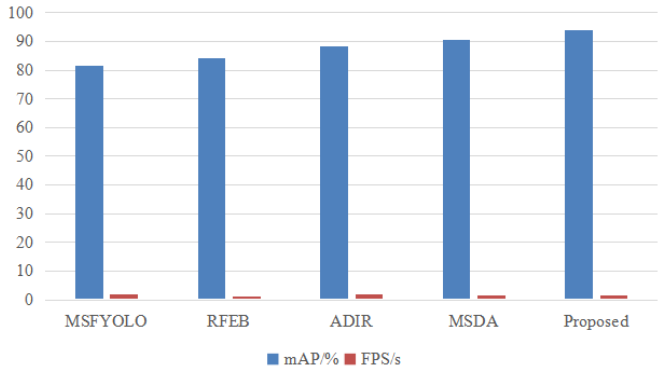

Fig. 8. Visualization result for airports

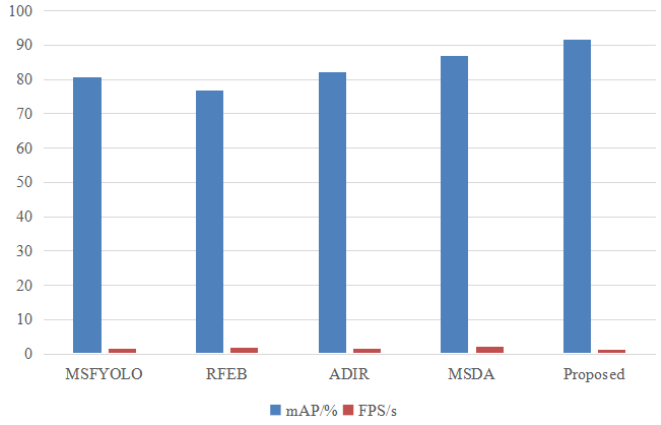

Fig. 9. Visualization result for harbors

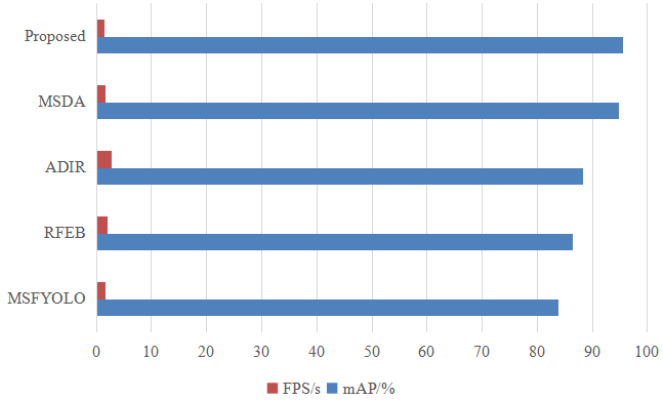

Fig. 10. Visualization result for aircraft

been significantly improved, the calculation amount is relatively large. 2) Context is not used enough. For example, the distribution of objects such as aircraft and oil-tanks has certain linear and clustered characteristics. Better use of these characteristics may further improve the detection accuracy. In the following work, the method of candidate region generation will be studied to improve the quality of candidate region generation and reduce the amount of calculation. At the same time, the application of context information will be deeply mined to explore the distribution correlation between objects and the use of context information in position regression, so as to further improve the accuracy of optical remote sensing image object detection.

Acknowledgments. This work was supported by the Liaoning Province science and technology plan joint project. Project name ”Research on key technologies of object recognition and interpretation in high resolution remote sensing images under complex scenes”.

References

1. Y. Pi, N. D. Nath, H. A. Behzadan, Convolutional neural networks for object detection in aerial imagery for disaster response and recovery, Advanced Engineering Informatics, vol. 43, pp. 101009, 2020.
2. M. R. Marshall et al., ”3-D Object Tracking in Panoramic Video and LiDAR for Radiological Source Object Attribution and Improved Source Detection,” IEEE Transactions on Nuclear Science, vol. 68, no. 2, pp. 189-202, Feb. 2021, doi: 10.1109/TNS.2020.3047646.
3. S. Yin, L. Wang, M. Shafiq, L. Teng, A. A. Laghari and M. F. Khan, ”G2Grad-CAMRL: An Object Detection and Interpretation Model Based on Gradient-Weighted Class Activation Mapping and Reinforcement Learning in Remote Sensing Images,” IEEE Journal of Selected Topics in Applied Earth Observations and Remote Sensing, vol. 16, pp. 3583-3598, 2023, doi: 10.1109/JSTARS.2023.3241405
4. Y. Tao, Z. Zongyang, Z. Jun, C. Xinghua and Z. Fuqiang, ”Low-altitude small-sized object detection using lightweight feature-enhanced convolutional neural network,” Journal of Systems Engineering and Electronics, vol. 32, no. 4, pp. 841-853, Aug. 2021, doi: 10.23919/JSEE.2021.000073.
5. A. Kumar, S. Srivastava, Object detection system based on convolution neural networks using single shot multi-box detector, Procedia Computer Science, vol. 171, pp. 2610-2617, 2020.
6. T. Diwan, G. Anirudh, V. J. Tembhurne, Object detection using YOLO: Challenges, architectural successors, datasets and applications, Multimedia Tools and Applications, vol. 82, no. 6, pp. 9243-9275, 2023.
7. B. Zhong, K. Ao, Single-stage rotation-decoupled detector for oriented object, Remote Sensing, vol. 12, no. 19, pp. 3262, 2020.
8. F. Zhao, J. Li, J. Zhao and J. Feng, ”Weakly Supervised Phrase Localization with Multi-scale Anchored Transformer Network,” 2018 IEEE/CVF Conference on Computer Vision and Pattern Recognition, Salt Lake City, UT, USA, 2018, pp. 5696-5705, doi: 10.1109/CVPR.2018.00597.
9. D. Cao, S. Yang, A Method based on Faster RCNN Network for Object Detection, Recent Advances in Computer Science and Communications (Formerly: Recent Patents on Computer Science), vol. 15, no. 9, pp. 1239-1244, 2022.
10. B. C. Murthy,F. M. Hashmi, G. A. Keskar, EfficientLiteDet: a real-time pedestrian and vehicle detection algorithm, Machine Vision and Applications, vol. 33, no. 3, pp. 47, 2022.
11. L. Zhao, S. Li, Object detection algorithm based on improved YOLOv3, Electronics, vol. 9, no. 3, pp. 537, 2020.

12. A. Kumar, S. Srivastava, Object detection system based on convolution neural networks using single shot multi-box detector, Procedia Computer Science, vol. 171, pp. 2610-2617, 2020.
13. K. Zhang, Y. Guo, X. Wang, J. Yuan and Q. Ding, "Multiple Feature Reweight DenseNet for Image Classification," IEEE Access, vol. 7, pp. 9872-9880, 2019, doi: 10.1109/ACCESS.2018.2890127.
14. L. Wang, S. Yin, A. Hashem, et al., A novel deep learning-based single shot multibox detector model for object detection in optical remote sensing images,Geoscience Data Journal, 2022. https://doi.org/10.1002/gdj3.162
15. Y. Xiao, X. Wang, P. Zhang, et al., Object detection based on faster R-CNN algorithm with skip pooling and fusion of contextual information, Sensors, vol. 20, no. 19, pp. 5490, 2020.
16. D. Jiang, G. Li, C. Tan, et al., Semantic segmentation for multiscale target based on object recognition using the improved Faster-RCNN model, Future Generation Computer Systems, vol. 123, pp. 94-104, 2021.
17. S. Yin and H. Li, "Hot Region Selection Based on Selective Search and Modified Fuzzy C-Means in Remote Sensing Images," IEEE Journal of Selected Topics in Applied Earth Observations and Remote Sensing, vol. 13, pp. 5862-5871, 2020, doi: 10.1109/JSTARS.2020.3025582.
18. G. A. Tsihrintzis, P. M. Johansen and A. J. Devaney, "Buried object detection and location estimation from electromagnetic field measurements," IEEE Transactions on Antennas and Propagation, vol. 47, no. 11, pp. 1742-1744, Nov. 1999, doi: 10.1109/8.814957.
19. G. Cheng, Y. Si, H. Hong, X. Yao and L. Guo, "Cross-Scale Feature Fusion for Object Detection in Optical Remote Sensing Images," IEEE Geoscience and Remote Sensing Letters, vol. 18, no. 3, pp. 431-435, March 2021, doi: 10.1109/LGRS.2020.2975541.
20. D. Ortego, J. C. SanMiguel and J. M. Martanez, "Long-Term Stationary Object Detection Based on Spatio-Temporal Change Detection," IEEE Signal Processing Letters, vol. 22, no. 12, pp. 2368-2372, Dec. 2015, doi: 10.1109/LSP.2015.2482598.
21. C. R. del-Blanco, F. Jaureguizar and N. Garcia, "An efficient multiple object detection and tracking framework for automatic counting and video surveillance applications," IEEE Transactions on Consumer Electronics, vol. 58, no. 3, pp. 857-862, August 2012, doi: 10.1109/TCE.2012.6311328.
22. X. Yu, J. Yang, Z. Lin, J. Wang, T. Wang and T. Huang, "Subcategory-Aware Object Detection," IEEE Signal Processing Letters, vol. 22, no. 9, pp. 1472-1476, Sept. 2015, doi: 10.1109/LSP.2014.2299571.
23. L. Pan, W. -S. Chu, J. M. Saragih, F. De la Torre and M. Xie, "Fast and Robust Circular Object Detection With Probabilistic Pairwise Voting," IEEE Signal Processing Letters, vol. 18, no. 11, pp. 639-642, Nov. 2011, doi: 10.1109/LSP.2011.2166956.
24. Q. Hu, S. Paisitkriangkrai, C. Shen, A. van den Hengel and F. Porikli, "Fast Detection of Multiple Objects in Traffic Scenes With a Common Detection Framework," IEEE Transactions on Intelligent Transportation Systems, vol. 17, no. 4, pp. 1002-1014, April 2016, doi: 10.1109/TITS.2015.2496795.
25. Z. -Q. Zhao, P. Zheng, S. -T. Xu and X. Wu, "Object Detection With Deep Learning: A Review," IEEE Transactions on Neural Networks and Learning Systems, vol. 30, no. 11, pp. 3212-3232, Nov. 2019, doi: 10.1109/TNNLS.2018.2876865.
26. Y. Lin, H. He, Z. Yin and F. Chen, "Rotation-Invariant Object Detection in Remote Sensing Images Based on Radial-Gradient Angle," IEEE Geoscience and Remote Sensing Letters, vol. 12, no. 4, pp. 746-750, April 2015, doi: 10.1109/LGRS.2014.2360887.
27. Z. Cai and N. Vasconcelos, "Cascade R-CNN: High Quality Object Detection and Instance Segmentation," IEEE Transactions on Pattern Analysis and Machine Intelligence, vol. 43, no. 5, pp. 1483-1498, 1 May 2021, doi: 10.1109/TPAMI.2019.2956516.
28. Q. Yao, X. Hu and H. Lei, "Multiscale Convolutional Neural Networks for Geospatial Object Detection in VHR Satellite Images," IEEE Geoscience and Remote Sensing Letters, vol. 18, no. 1, pp. 23-27, Jan. 2021, doi: 10.1109/LGRS.2020.2967819.

29. J. Ding et al., "Object Detection in Aerial Images: A Large-Scale Benchmark and Challenges," IEEE Transactions on Pattern Analysis and Machine Intelligence, vol. 44, no. 11, pp. 7778-7796, 1 Nov. 2022.
30. Z. Song, Y. Zhang, Y. Liu, K. Yang and M. Sun, "MSFYOLO: Feature fusion-based detection for small objects,"IEEE Latin America Transactions, vol. 20, no. 5, pp. 823-830, May 2022, doi: 10.1109/TLA.2022.9693567.
31. X. Dong, R. Fu, Y. Gao, Y. Qin, Y. Ye and B. Li, "Remote Sensing Object Detection Based on Receptive Field Expansion Block," IEEE Geoscience and Remote Sensing Letters, vol. 19, pp. 1-5, 2022, Art no. 8020605, doi: 10.1109/LGRS.2021.3110584.
32. Z. Wu, J. Wen, Y. Xu, J. Yang and D. Zhang, "Multiple Instance Detection Networks With Adaptive Instance Refinement," IEEE Transactions on Multimedia, vol. 25, pp. 267-279, 2023, doi: 10.1109/TMM.2021.3125130.
33. X. Dong et al., "Multiscale Deformable Attention and Multilevel Features Aggregation for Remote Sensing Object Detection," IEEE Geoscience and Remote Sensing Letters, vol. 19, pp. 1-5, 2022, Art no. 6510405, doi: 10.1109/LGRS.2022.3178479.

Shoulin Yin received the M.A. degree from Shenyang Normal University, Shenyang, China, in 2015. He is currently pursuing the Ph.D. degree with the College of Information and Communication Engineering, Harbin Engineering University, Harbin. His research interests are remote sensing image processing and object detection.

Liguo Wang received his M.A. degree in 2002 and Ph.D. degree in signal and information processing in 2005 from Harbin Institute of Technology, Harbin, China. He held postdoctoral research position from 2006 to 2008 in the College of Information and Communications Engineering, Harbin Engineering University. He is currently a Professor with Information and Communications Engineering, Dalian Minzu University, Dalian, China. His research interests are remote sensing image processing and machine learning. He has published three books, 27 patents, and more than 200 papers in journals and conference proceedings. Email: wangliguo@hrbeu.edu.cn.

Qunming Wang received the Ph.D. degree from The Hong Kong Polytechnic University, Hong Kong, in 2015. He is currently a Professor with the College of Surveying and Geo-Informatics, Tongji University, Shanghai, China. From 2017 to 2018, he was a Lecturer (Assistant Professor) with Lancaster Environment Centre, Lancaster University, Lancaster, U.K., where he is currently a Visiting Professor. Prof. Wang is an Editorial Board Member for Remote Sensing of Environment, and serves as an Associate Editor for Science of Remote Sensing (sister journal of Remote Sensing of Environment) and Photogrammetric Engineering & Remote Sensing.

Mirjana Ivanovic (Member, IEEE) has been a Full Professor with the Faculty of Sciences, University of Novi Sad, Serbia, since 2002. She has also been a member of the University Council for informatics for more than 10 years. She has authored or coauthored 13 textbooks, 13 edited proceedings, 3 monographs, and of more than 440 research articles on multi-agent systems, e-learning and web-based learning, applications of intelligent techniques (CBR, data and web mining), software engineering education, and most

of which are published in international journals and proceedings of high-quality international conferences. She is/was a member of program committees of more than 200 international conferences and general chair and program committee chair of numerous international conferences. Also, she has been an invited speaker at several international conferences and a visiting lecturer in Australia, Thailand, and China. As a leader and researcher, she has participated in numerous international projects. She is currently an Editor-in-Chief of Computer Science and Information Systems Journal.

Hang Li received the B.S., M.S., and Ph.D. degrees in computer applications technology from Dalian Fisheries University, Dalian, China, Shenyang Institute of Technology, Shenyang, China, Northeastern University, Shenyang, China, in 1999, 2002, and 2005, respectively. In 2002, he joined Software College as a Teacher. He is a full Professor and Master Supervisor. He is an Outstanding Young Backbone Teacher of Liaoning General Institutions of Higher Learning (Liaoning Education Department). His research interests include image analysis and processing, big data, and cloud computing. Dr. Li won the Second Prize of National Defense Science and Technology Award of The Commission of Science, Technology and Industry for National Defense (National Defense Science, Technology and Industry Commission 2005GFJ2126-6) and First Prize of Science and Technology Award of China North Industries Group Corporation (2005-BQJ-1-0019-6).

Received: November 10, 2024; Accepted: January 01, 2025.

Computer Science and Information Systems 22(1):345–368 https://doi.org/10.2298/CSIS231101013L

Improved Session Recommendation Using Contrastive Learning based Tail Adjusted Repeat Aware Graph Neural Network

Daifeng Li[1], Tianjunzi Tian[2], Zhaohui Huang[1], Xiaowen Lin[1,⋆], Dingquan Chen[1,⋆], and Andrew Madden[3]

[1] School of Information Management, Sun Yat-sen University, 51006 Guangzhou, China
lidaifeng@mail.sysu.edu.cn
huangzhaohui27@mail2.sysu.edu.cn
linxw26@mail2.sysu.edu.cn
gzchendq@163.com
[2] Department of Information Management, Nanjing University, 210023 Nanjing, China
tiantjz@smail.nju.edu.cns
[3] University of Sheffield, S10 2TN South Yorkshire, England
admadden@hotmail.com

Abstract. Session-based recommendation using graph neural networks (GNN) is a popular approach to model users' behaviors and attributes of items from the perspective of user-item interaction sequence. However, current researches seldom incorporate the unique attributes of items to delve into a comprehensive analysis of user behaviors. In addition, GNN faces three problems when encounting complex modeling scenarios: long-range dependencies, order information loss, and data sparsity, which are essential to modeling long-tail items. We study the interactions between users and items from a new perspective. A novel Contrastive Learning based Tail Adjusted Repeat Aware Graph Neural Network (CLTAR-GNN) is proposed to tackle the problems. A Tail Adjusted Repeat (TAR) mechanism captures users' repeat-explore behaviors in both short-head and long-tail session items based on graph neural networks. Through the TAR, we are able to further understand the underlying graph-based mechanisms that influence user-item interactions. A Self-Attention (SA) network with position embedding is incorporated to overcome the sequence information loss issues, which may be caused by the complex user behaviors and item characteristics modeling. Finally, a mutli-task learning framework is employed to combine TAR, SA and a contrastive learning model into a unified framework to enhance model performance by collaboratively training graph and sequence-based embeddings. Experimental results show that CLTAR-GNN outperforms the state-of-the-art session-based recommendation methods significantly. The average improvement compared with all baselines are 17.5% (HR@20) and 22.5% (MRR@20) on both experimental datasets.

Keywords: Session-based Recommendation, Contrastive Learning, Self-Attention Networks, Tail Adjusted Repeat.

⋆ Corresponding authors

1. Introduction

Recommendation systems alleviate the issue of information overload by providing users with relevant information. These systems usually rely on user identity and historical behavior data, but for anonymous browsing sessions, recommendations must be based on short-term behavior records. The challenge of session-based recommendation is to obtain high-quality sequence representations. Traditional classic methods such as Markov chain-based methods can model the intrinsic correlations of sequence data [7]. However, there is still significant room for improvement in traditional methods regarding memory enhancement, learning and generalization capabilities, discovery of complex nonlinear sequence patterns, and computational efficiency [9]. With the rapid development of deep learning technology, approaches such as recurrent neural networks (RNN) [10] and graph neural networks (GNN) have applied deep learning methods to session-based recommendations, RNN-based methods that incorporating attention mechanism could be used to model a long session sequence [11], but RNN-based methods have two significant limitations [26]: could not accurately estimate user representations and seldom consider complex interactions between session items. GNN-based methods model sessions as graph-structured data and are able to capture complex transitions of items [18,13], which can be used to investigate users' behavior patterns in sessions by constructing user-item sequence-based graphs [19,16]. For example, Ren et al [19] focus on investigating users' different behaviors in session-based recommendation scenarios. Liu et al [16] constructed new networks to improve the performance of session-based recommendation by considering different characteristics of items.

Different from previous researches, we mainly focus on studying how patterns of repeat-explore behavior differ depending on whether they are associated with long-tail or short-head items. We define repeat-explore, long-tail and short-head as follows: Repeat behavior means the next item which user will click during a session process has already existed in the current session, otherwise it is Explore behavior. Long-tail means unpopular items, the number of which may account for a large proportion, and generate a long-tail effect [31]. In contrast, short-head means popular items, which occupies the head position of sales. The main idea of modelling repeat-explore behavior, long-tail and short-head items into a unified framework is essential important for further understanding users' future actions based on his/her historical behaviors. More importantly, incorporating the attributes of long-tail and short-head items can help better understand users' potential demands by explicitly considering users' preference patterns towards items with different popularity. Besides, long-tail items can provide more diversified information to further satisfy users' demands. It is also meaningful to promote the transformation of high-quality long-tail items into short-head items in an e-commerce system.

However, there exists two challenging problems when constructing a unified model framework: The first problem is How to mine patterns from session sequence while modelling user behavior and the intrinsic associations of items. Existing session recommendation models mainly focus on using GNN with L layers to capture $L - hop$ relations of items in a graph. The use of GNN-based methods has led to significant improvements in session recommendations. However, this solution may cause over-fitting and over-smoothing because of stacking too many layers [2]. In another aspect, when sessions are converted to graphs, the information within item orders in a session may be lost. Although combining sequence attention model can reduce the negative influence of in-

formation loss, existing methods are ineffective in capturing sequence patterns due to the complexity of user behavior modelling. Another important factor affecting the quality of session representations is the problem of data sparsity, especially for long-tail items. A deep learning model usually has a large number of parameters that need to be optimized. However, in two public datasets for session-based recommendations (Yoochoose and Diginetica), there are items that appear many times but there are also long-tail items that rarely appear. Due to lack of training data, the accuracy of session recommendations with long-tail items will be relatively low, and there will exist big biases towards popular short-head items. To address these problems, we propose a novel model called Contrastive Learning based Tail Adjusted Repeat Aware Graph Neural Network (CLTAR-GNN), which is designed to improve recommendations by capturing more of the rich information contained in sessions. The main contributions of our work can be summarized as follows:

- A novel Tail Adjusted Repeat Aware Graph Neural Network (TAR-GNN) is proposed to investigate user repeat-explore patterns in both short-head and long-tail session items. These can improve model performance by further understanding users' behaviors towards different items, while can increase the item diversity of the recommendation list.
- The re-designed Repeat-Explore and Factor Generating module consider both long-term global and short-term local dependencies between items in a session.
- By integrating self-attention with position embedding, the model can consider both order information and complex high-order relations between session items, which can further optimize the modelling of users' repeat-explore behaviors by mining sequence patterns from sessions.
- A multi-task learning framework is proposed to collaboratively learn users' repeat-explore behaviors towards items with different level of popularity and item sequence patterns. In addition, a contrastive learning framework is also Incorporated to deal with data sparsity problem caused by long-tail items.

The code could be found in: `https://github.com/Linxw718/CLTAR-GNN`

2. Related Work

2.1. Conventional Recommendation Methods

In traditional recommendation systems, where users can be identified, neighborhood-based methods have been widely used [22]. Such methods do not directly optimize the ranking of items, though Rendle et al [20] present a generic optimization criterion derived from the maximum posterior estimator for optimal Bayesian personalized ranking based on matrix factorization. However, the method seldom considers the context of a session item. Early methods for session-based recommendation borrow the idea of neighborhood-based methods. For instance, Davidson et al [4] calculate the similarity between items using the co-occurrence between them. They recommend items that are most similar to those in the current session. Neighborhood-based methods are limited by the problem of data sparsity, and do not take the order information of the session into consideration. Methods based on Markov chains [21] are capable of capturing order information, but when more preceding items are considered, the state size becomes unmanageable, making such methods unsuitable for capturing complex high-order sequential information within a session.

2.2. Deep Learning Based Methods

With the rapid development of deep learning technology, many new methods for session-based recommendation have been proposed. Hidasi et al [8] use RNN to model session sequences. These are able to leverage historical information from the session and take item order into account. Nevertheless, in long sessions, RNN-based methods cannot capture the complex dependencies between items. Li et al [12] point out that previous studies only model users' sequential behavior, and do not emphasize the user's main purpose. They propose a model based on attention mechanism, which uses a local encoder and a global encoder to model the users' behavior sequences with a view to infer the user's main purpose. Liu et al [15] consider both global and current interests of the user in the session.

In recent years, many researches have applied GNN to session-based recommendation. Wu et al [27] transformed sessions into a directed graph, in which nodes represent items and edges represent the sequential relationship of items. Item vectors are obtained through a gated GNN, after which, session vectors can be obtained by combing the item vectors using an attention network. On the basis of this research, Yu et al [32] proposed a target attentive GNN model able to generate different session representations for the same session with respect to different target items. Gupta et al [6] point out that GNN-based methods are subject to popularity bias, causing these methods to recommend popular items over long-tail items which is related to the norm of the learned items and their session-graph representations. Chen and Wong [2] spotted two information loss problems in the GNN-based methods: namely loss of long-range dependencies of items and loss of order information. They addressed these problems by adding EOPA to preserve order-information and SGAT to capture long-term dependencies. Instead of GNN, Fang [5] used self-attention networks to encode sessions that capture long-range dependencies.

The aforementioned research does not thoroughly explore the modeling of user behavior and item characteristics. In addition, enhancing the model with more detailed analysis would improve the complexity of the model, which could inadvertently compromise its inherent ability to capture and represent sequential patterns effectively. In this research, we model users' repeat-explore behaviors and item popularity into a unified framework, and incorporate self-attention with POS embedding to enhance the model capability in mining sequence patterns from sessions.

2.3. Contrastive Learning

As a kind of self-supervised learning, contrastive learning has achieved excellent performance in Computer Vision (CV) area. SimCLR [3], which stands for Similarity Constrastive Learning Representation, is a typical contrastive learning framework that generates different views of images using data-augmentation methods such as random rotation. It is designed to learn useful representations from unlabeled data by maximizing the similarity between augmented views of the same image and minimizing the similarity between different images. It produces different views of the same image close and keep views of different images away in the feature space by optimizing a loss function called NT-Xent loss. The feature representations of images obtained from SimCLR can then be applied to other downstream tasks.

In recommendation area, SimCLR can effectively learn representations of items or users without relying heavily on labeled data. Some researchers have tried to apply the

idea of contrastive learning. Zhou et al [34] used a self-supervised learning method to learn the internal relationship among items, item attributes and item sequences by designing different contrastive loss functions. Xie et al [28] applied contrastive learning to sequential recommendations. Unlike sequential recommendation, user identity is usually unknown in session-based recommendations, and more attention is paid to a user's short-term preferences, which is apparent from the shorter session sequences.

In this paper, we apply contrastive learning to session-based recommendation by mining self-supervised signals, we can capture intrinsic features of the session by considering both order-information and complex correlations between items. Therefore, the model could obtain high-quality session representations, especially long-tail item representations, for making more accurate recommendations based on repeat-explore behaviors.

3. Model Descriptions

3.1. Model Overview

Session-based recommendation aims to predict the next item that a user may click based on the sequence of items clicked earlier in the current session. Let $V = \{v_1, v_2, \ldots, v_{|V|}\}$ denotes the set of $|V|$ items that have appeared in all sessions. Assume SS is the set of N sessions, a session $S \in SS$ can be represented as a list $S = [v_{s1}, v_{s2}, \ldots, v_{sn}]$, where $v_{si} \in V$ denotes an item has been clicked in the ith position or at the ith timestamp by the same user in session S. n is the length of session S, and for different sessions S, the values of n are different. For the current session S at the nth timestamp, the objective of session-based recommendation is to predict $v_{s(n+1)}$ at the $n+1$ timestamp. The main idea is that we use the CLTAR-GNN model to calculate the score $\hat{y}_i$ (a real number) of each candidate item $v_i \in V$ based on the session S. The formula can be seen as below:

$$\begin{aligned} &\hat{y}_i = \mathrm{CLTAR} - \mathrm{GNN}(v_i, S), i \leq |V| \\ &\hat{y} = \{\hat{y}_1, \hat{y}_2, \ldots, \hat{y}_{|V|}\} \end{aligned} \tag{1}$$

All the scores $\hat{y}_i$ ($i \leq |V|$) generate a score vector $\hat{y}$, where $\hat{y}_i$ is the score of item v_i, which is calculated by CLTAR-GNN. The top K items with the highest score from $\hat{y}$ will be recommended to the user. The architecture of the proposed CLTAR-GNN is shown in Figure 1. There are eight major components in CLTAR-GNN, including a Data Augmentation module, a Gated Graph Neural Network (GGNN) embedding layer, a Session Generation module, a Repeat-Explore component, an Item Factor Generating module, a Self-Attention network, a Contrastive Loss (CL) framework and a Multi-Task Learning strategy. The Data Augmentation module can generate new sessions by leveraging existing ones, thereby enhancing the training dataset for sessions involving long-tail items. The initial session embedding are generated by using GGNN model. The Session Generation module, Repeat-Explore module and Item Factor Generating module are collaboratively incorporated to model users' repeat-explore behaviors based on short-head and long-tail items. We define the model consists of the three modules as Tail Adjust Repeat Aware (TAR) mechanism. In addition, a Self-Attention module is also combined with TAR module to enhance the model capability in mining sequence patterns. Contrastive losses are calculated for different session augmentations. The contrastive task and recommendation task are jointly training using a Multi-Task Learning framework.

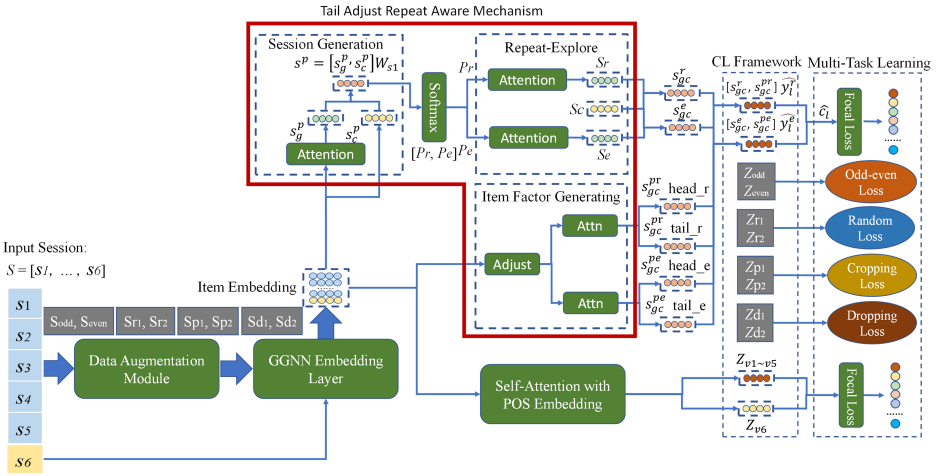

Fig. 1. A representation of the architecture of CLTAR-GNN

3.2. Data Augmentation Module

The Data Augmentation module can generate two new sessions for each existing session through augmentation operations. The two new sessions are similar to the existing ones, and will be used as a positive pair in Contrastive Learning, while any two augmented sessions generated from different sessions are used as a negative pair. CLTAR-GNN adopts four data augmentation operations, including Odd-Even augmentation, Random augmentation, Cropping augmentation and Dropping augmentation [28,34]. Assume there exists N sessions, then each augmentation can generate $2N$ new sessions, which are prepared for the Contrastive Learning module.

As seen in Figure 1, the output of Odd-even augmentation is S^{odd} and S^{even}, which can be treated as a positive pair for odd-even contrastive learning (Odd-Even loss); the output of Random Augmentation is S^{r1} and S^{r2}, which can be treated as a positive pair for random contrastive learning (Random loss); the output of Cropping Augmentation is S^{p1} and S^{p2}, which can be treated as a positive pair for cropping contrastive learning (Cropping loss); the output of Dropping Augmentation is S^{d1} and S^{d2}, which can be treated as a positive pair for dropping contrastive learning (Dropping loss).

3.3. GGNN Embedding Layer

In this research, Gate Graph Neural Network (GGNN) is adopted as the embedding layer [13]. The advantage of GGNN over traditional sequence-based embedding methods, such as LSTM or GRU, is that it can capture high-order graph-based correlations among items. For a session $S = [s_1, s_2, \ldots, s_n]$, its in-degree and out-degree adjacency matrices are defined as E^{in} and $E^{out} \in R^{n \times n}$. We define $E \in R^{n \times 2n}$ as the concatenate of E^{in} and E^{out}. Assuming that there exists t iterations, then for node i in session S at t, its node

embedding at $t+1$ could be represented as:

$$m_i^{t+1} = \sum_{v \in N_i} M_t(h_i^t, h_v^t | E, S) \tag{2}$$

$$h_i^{t+1} = U_t(h_i^t, z_i^t, r_i^t | m_i^{t+1}) \tag{3}$$

where M_t is message propagation operation, and indicates the correlation between i and its neighbors $v \in N_i$. h_i^t and h_v^t denote item embedding at t. z_i^t controls forget information and r_i^t controls the influence of newly generated information. U_t is similar to GRU, and is used to update the embedding of item i at $t+1$. The length of h_i^t is defined as d.

3.4. Tail Adjust Repeat Aware Mechanism (TAR)

In this section, a TAR mechanism is proposed to collaboratively model users' repeat-explore behavior patterns on short-head and long-tail items. The mechanism consists of three modules: A Session Generation module is designed to calculate the probabilities [P_r,P_e] of users selecting different behaviors. The Repeat-Explore module calculates the preference score for each candidate item under different behaviors of a user. The Item Factor Generating module is used to encode items with different level of popularity (short-head and long-tail). Finally, a Focal Loss based Repeat-Tail loss function is designed to provide optimization strategy for TAR.

Session Generation Module. The main target of the session generation module is to adopt an attention mechanism that captures a user's main preference in session S. This mechanism can then be used to discover the probability distributions of users' behavior patterns. Existing researches often use probability distributions to describe users' preferences towards different behaviors [19,30]. In this article, we focus mainly on two types of user behavior pattern: repeat and explore. We define the probability of users' repeat patterns as P_r and explore patterns as P_e. Formulas for P_r and P_e are shown below:

$$s_g^p = \sum_{i=1}^{n} a_i^g h_i^t; \quad s_c^p = h_n^t \tag{4}$$

$$s^p = [s_g^p, s_c^p] W_{s1} \tag{5}$$

$$[P_r, P_e] = softmax(W_{s2} \times s^p) \tag{6}$$

where a_i^g is the attention weight of item i in session S, which is utilized to determine the influence of a user's historical click behaviors on items to his/her current state at timestamp n. $W_{s1} \in R^{2d \times d}$, $W_{s2} \in R^d$ means weight matrices. Different from previous studies [19], inspired by long-short term modules which are widely applied in sequence processing [15], we consider both long-term global dependencies s_g^p and short-term local dependencies s_c^p by calculating h_n^t. In formula 6, the P_r and P_e of users' repeat-explore behaviors for selecting the $(n+1)$th item in session S are mainly determined by s^p, which is the concatenate of s_g^p and s_c^p. P_r and P_e are two probabilities, which are used to determine whether the user will adopt repeat or explore behaviors at $(n+1)$th timestamp.

Repeat-Explore Module. The Repeat-Explore module is used to re-calculate session representations based on two behavior patterns: repeat and explore. Assume $I_s \in V$ is the item set, and that each item appears in session S. x represents item embedding and $T(x)$ represents item id which x represents. Then the indicator function $H(x, y)$ is defined in formula 7. $y = 0$ represents repeat mode, $y = 1$ represents explore mode. The idea of using indicator function to encode different user behaviors are discussed in existing researches [1,17,33]. We design a repeat-explore function: for an arbitrary item l in V, its score of whether a user will click it at $n + 1$ in session S is represented in formula 8.

$$H(x, y) = \begin{cases} 1 - y, T(x) \in I_s \\ y, \quad T(x) \notin I_s \end{cases} \tag{7}$$

$$\begin{aligned} &\textbf{Repeat:} \quad \hat{y}_l^r = H(e_l, 0) e_l (s_{gc}^r)^T \\ &\textbf{Explore:} \quad \hat{y}_l^e = H(e_l, 1) e_l (s_{gc}^e)^T + \gamma \cdot \frac{\sum_{i \in S} sim(e_l, e_i)}{len(S)} \end{aligned} \tag{8}$$

where s_g^r and s_g^e are global session representation of repeat and explore with attention weight [15,5] as a_i^r and a_i^e respectively (Similar to formula 4, $s_g^r = \sum_{i=1}^n a_i^r h_i^t$ and $s_g^e = \sum_{i=1}^n a_i^e h_i^t$). s_{gc}^r and s_{gc}^e are combination of global and local representations of Repeat and Explore patterns respectively (similar to formula 5, $s_{gc}^r = [s_g^r, s_c^p] W_{r1}$ and $s_{gc}^e = [s_g^e, s_c^p] W_{e1}$). $\hat{y}_l^r$ is the score of item l in a repeat pattern, $\hat{y}_l^e$ is the score of item l in a explore pattern. e_l is the embedding of item l with its size as d, the initial value of which is pre-trained by neural network embedding (pytorch nn.Embedding). In our study, explore pattern led to item recommendations that have fewer interactions (ex. Co-occurrence in all sessions) with items in session S, while ignores that in many cases, users prefer to click new items that have high co-occurrences with existing items in a session [17,32,33]. To resolve this issue, we added $\sum_{i \in S} sim(e_l, e_i)/len(S)$ to the **Explore** formula in formula 8, and γ is the weight to control the influence of item correlations.

Item Factor Generating. The main target of item factor is to generate session embeddings and their influence factors by consider both long-tail and short-head items. Similar to previous studies, which model items according to their unique characteristics [1,16,25], we used Pareto rules to identify short-head popular and long-tail less popular items by counting each item's click frequency. Assume I_S^T, I_S^H represent the set of long-tail and short-head items which appear in session S. We re-define item embedding as:

$$F(x) = \begin{cases} x + [1, 1, 1, \ldots, 1], T(x) \in I_S^T \\ x + [0, 0, 0, \ldots, 0], T(x) \in I_S^H \end{cases} \tag{9}$$

where $F(x)$ is adjust function. x represents item embedding and $T(x)$ represents item id of x. $F(x)$ could adjust x based on its short-head or long-tail characters. Vector $[1, 1, 1, \ldots, 1]$ and $[0, 0, 0, \ldots, 0]$ have the same length as x. Based on the adjust function $F(x)$, attention mechanisms [23,29] are then adopted to obtain long-term global session representations s_g^{pr} and s_g^{pe}, which are corresponding to repeat and explore behaviors respectively. The expressions of global sessions could be seen in formula 10. Short-term local representations of s_c^{pr} and s_c^{pe}, which are corresponding to repeat and explore behaviors, could be

seen in formula 11. Finally, based on formulas 10 and 11, the combinations of long-short term global and local session representations s^{pr} and s^{pe}, which are corresponding to repeat and explore behaviors, could be seen in formula 12.

$$s_g^{pr} = \sum_{i=1}^{n} a_i^{pr} F(h_i^t); \quad s_c^{pr} = F(h_n^t) \tag{10}$$

$$s_g^{pe} = \sum_{i=1}^{n} a_i^{pe} F(h_i^t); \quad s_c^{pe} = F(h_n^t) \tag{11}$$

$$s_{gc}^{pr} = [s_g^{pr}, s_c^{pr}]W_{pr1}; \quad s_{gc}^{pe} = [s_g^{pe}, s_c^{pe}]W_{pe1} \tag{12}$$

where a_i^{pr} and a_i^{pe} are attention weights. W_{pr1} and $W_{pe1} \in R^{2d \times d}$ are weight matrices. s_{gc}^{pr} and s_{gc}^{pe} are used to generate four item factors: R_{head}^r and R_{head}^e are for short-head items, which are associated with repeat and explore behaviors. R_{tail}^r and R_{tail}^e are for long-tail items, which are associated with repeat and explore behaviors (formula 13, 14).

$$R_{head}^r = sigmoid(W_{p2} \cdot s_{gc}^{pr}); \quad R_{tail}^r = 1 - R_{head}^r \tag{13}$$

$$R_{head}^e = sigmoid(W_{p3} \cdot s_{gc}^{pe}); \quad R_{tail}^e = 1 - R_{head}^e \tag{14}$$

where W_{p2} and $W_{p3} \in R^d$ are the weight matrices. R_{head}^r and R_{tail}^r are item factors which are used to calculate the probabilities of users' selections for short-head or long-tail items when engaging in repeat behaviors. R_{head}^e and R_{tail}^e are item factors which are used to calculate the probabilities of users' selections for short-head or long-tail items when engaging in explore behaviors.

Repeat-Tail Loss. We design repeat-tail loss l_{rt-rec} to investigate users' different repeat-explore patterns for both long-tail and short-head items. For an arbitrary item $v_l \in V$, we have already obtained its repeat and explore pattern probability for session S, which are P_r and P_e respectively, through formula 6; while the item's recommendation score under repeat and explore patterns, which are $\hat{y}_l^r$ and $\hat{y}_l^e$, could be obtained through formula 8. Then the item l's recommendation score $\hat{c}_l$ could be represented as:

$$\hat{c}_l = P_r \hat{y}_l^r T(l, 1) + P_e \hat{y}_l^e T(l, 0) \tag{15}$$

where $T(x, y)$ is an indicator function to determine which factors should be adopted to item l according to its unique characters and its correlations with session S. $T(x, y)$ could be represented as in formula 16.

$$T(x, y) = \begin{cases} R_{head}^r, x \in I^H, y = 1 \\ R_{tail}^r, x \in I^T, y = 1 \\ R_{head}^e, x \in I^H, y = 0 \\ R_{tail}^e, x \in I^T, y = 0 \end{cases} \tag{16}$$

where I_H and I_T are the set of short-head and long-tail items. For all candidate items $[v_1, v_2, \ldots, v_{|V|}]$, the recommendation score could be $\hat{c} = [\hat{c}_1, \hat{c}_2, \ldots, \hat{c}_{|V|}]$, then vector $\hat{y}_c = softmax(\hat{c})$ is the vector of final recommendation scores based on probability

distributions. It denotes the probability of each candidate item to be clicked next at $n+1$ for session S. The cross-entropy loss $l_{rt-ce}(\hat{y}_c)$ between the predicted probability and the ground-truth is calculated as:

$$\begin{aligned} \hat{y}_c &= softmax(\hat{c}) = [\hat{y}_{c1}, \hat{y}_{c2}, \ldots, \hat{y}_{c|V|}] \\ l_{rt-ce}(\hat{y}_c) &= -\sum_{l=1}^{|V|}(y_l \times log(\hat{y}_{cl}) + (1-y_l) \times log(1-\hat{y}_{cl})) \end{aligned} \tag{17}$$

where y_l is the one-hot embedding denoting the ground-truth item (It denotes which item was truly clicked at $n+1$ timestamp). $\hat{y}_{cl}$ is the lth element in $\hat{y}_c$. It denotes the probability of item l to be clicked at timestamp $n+1$ in session S. Due to the imbalanced data of sessions, we use focal loss [14] in CLTAR-GNN. Focal loss could increase the impact of hard samples and decrease the impact of easy samples in the process of model optimization. Hence, focal loss can help make more accurate recommendations of long-tail items. The focal loss based repeat-tail loss $l_{rt-rec}(\hat{y}_c)$ is formulated as:

$$l_{rt-rec}(\hat{y}_c) = (1 - exp(-l_{rt-ce}(\hat{y}_c)))^{\gamma} l_{rt-ce}(\hat{y}_c) \tag{18}$$

where γ is the focusing parameter and we set it as to 2. The repeat-tail loss $l_{rt-rec}(\hat{y}_c)$ can predict the next likely-to-be-clicked short-head or long-tail item within a session when operating under the repeat-explore behaviors, with the objective of aligning the predicted value as closely as feasible to the actual value (the item that is genuinely clicked).

3.5. Self-Attention Network (SA)

The TAR mechanism mainly focuses on modelling user different behaviors towards items with different popularity, which can detect more complex interaction patterns from a session. However, this mechanism is chiefly concerned with the design of theoretical models that address intricate relationships between users and items, which may consequently reduce the model's inherent capability for sequence modeling. In another aspect, GGNN is adopted as embedding layer for capturing high-order correlations among items, while its limitations would be that GGNN could not capture order information and long-range dependencies in a session. Though there exists related researches optimized existing GGNN-based methods to solve the problems mentioned above to a certain extent [2], it is challenge to incorporate more complex user-item interaction models, such as TAR, into existing researches, because modelling complex interactions between user-item may compromise the sequential modelling capabilities of the model.

In this research, we find that sequential modelling is very important to the accuracy of recommendation results. Thus, we design a Self-Attention (SA) network specifically for sequential modelling, and then adopt a multi-task learning framework to collaboratively train the model and TAR in a unified framework. For a session $S = [v_{s1}, v_{s2}, \ldots, v_{sn}]$, its t iteration item embedding through GGNN could be represented as $E' = [h_1^t, h_2^t, \ldots, h_n^t]$ with dimension size as d. In order to take the order information of the session into account, we stack position embeddings $P = [p_1, p_2, \ldots, p_n]$ for each item in the session, where p_i denotes the position embedding of item v_{si} . The input E for self-attention networks is:

$$E = E' + P \tag{19}$$

Self-attention [23] are composed of multi-head attention and feed-forward networks. Multi-head attention could capture different information from the session. Assume H heads are assigned, then the output F of multi-head attention could be seen in formula 20. $W^O \in R^{Hd \times d}$ is the projection matrix. Then F is passed through a two-layer fully connected feed-forward network (FFN) with activation functions (σ) to obtain output as $H_S = [h_1, h_2, \ldots, h_n]$. According to experiments, we find that using the average of the last two item vectors (h_{n-1} and h_n) as session representation z can produce better results.

$$\begin{aligned} F &= Concat(head_1(E), \ldots, head_H(E))W^O + E \\ H_S &= \sigma(\mathrm{FFN}(\mathrm{FFN}(F))) = [h_1, h_2, ..., h_n] \\ z &= \frac{h_{n-1} + h_n}{2} \end{aligned} \tag{20}$$

After getting the session representation z, we can calculate the items that should be recommended to users. For each candidate item $v_l \in V$, its corresponding recommendation score is calculated as $g_l = z \cdot e_l$, where e_l is the vector of item v_l (e_l is calculated by using pytorch nn.Embedding). Let $g = [g_1, g_2, \ldots, g_{|V|}]$ denotes the recommendation scores of all items. $\hat{y}_s = softmax(g)$ is the vector of final recommendation scores. It denotes the probability of each candidate item to be clicked next for session S. The cross-entropy between the predicted probability and the ground-truth is calculated as:

$$\begin{aligned} &g = [g_1, g_2, \ldots, g_{|V|}] \quad where \quad g_l = z \cdot e_l \quad and \quad l \leq |V| \\ &\hat{y}_s = softmax(g) = [\hat{y}_{s1}, \hat{y}_{s2}, \ldots, \hat{y}_{s|V|}] \\ &l_{sa-ce}(\hat{y}_s) = -\sum_{l=1}^{|V|}(y_l \times log(\hat{y}_{sl}) + (1 - y_l) \times log(1 - \hat{y}_{sl})) \end{aligned} \tag{21}$$

where y_l is the one-hot embedding denoting the ground-truth item. $\hat{y}_{sl}$ is the lth element in $\hat{y}_s$. $\hat{y}_{sl}$ denotes the probability of item l to be clicked next at $n+1$ for session S. Similar to formula 18, the focal loss based self-attention loss $l_{sa-rec}(\hat{y}_s)$ is formulated in 22, where γ is the focusing parameter and we set it as to 2.

$$l_{sa-rec}(\hat{y}_s) = (1 - exp(-l_{sa-ce}(\hat{y}_s)))^{\gamma} l_{sa-ce}(\hat{y}_s) \tag{22}$$

3.6. Contrastive Loss Function

Session embeddings of S from different modules are summarized as: **Repeat-Explore**: s^r_{gc}, s^e_{gc} (Formula 8). **Item Factor**: s^{pr}_{gc}, s^{pe}_{gc} (Formula 12). **Self-Attention**: z (Formula 20). We merge all representations into a unified vector as $sz = [s^r_{gc}, s^e_{gc}, s^{pr}_{gc}, s^{pe}_{gc}, z]$. Assume a training batch contains N sessions $S_1, S_2, \ldots, S_N$. Data augmentation strategies from Odd-even, Random, Cropping, Dropping are used to generate positive instances for each session S_i. For each session S_i, each strategy could generate two positive instances, which are S^{odd}_i and S^{even}_i for Odd-even, S^{r1}_i and S^{r2}_i for Random, S^{p1}_i and S^{p2}_i for Cropping, S^{d1}_i and S^{d2}_i for Dropping. The representations of all instances are sz^{odd}_i and sz^{even}_i, sz^{r1}_i and sz^{r2}_i, sz^{p1}_i and sz^{p2}_i, sz^{d1}_i and sz^{d2}_i respectively. Then for all sessions, we adopt SimCLR framework for contrastive learning and use **NT-Xent** loss (Normalized Temperature-Scaled Cross-Entropy Loss) to generate contrastive loss [3], which are odd-

even loss $l_{cl}^{odd-even}$, random loss l_{cl}^{r1-r2}, cropping loss l_{cl}^{p1-p2} and dropping loss l_{cl}^{d1-d2}:

$$\begin{aligned} l_{cl}^{odd-even} &= \sum_{i=1}^{N} \mathrm{NT-Xent}(S_i, S_i^{odd}, S_i^{even}) \\ l_{cl}^{r1-r2} &= \sum_{i=1}^{N} \mathrm{NT-Xent}(S_i, S_i^{r1}, S_i^{r2}) \\ l_{cl}^{p1-p2} &= \sum_{i=1}^{N} \mathrm{NT-Xent}(S_i, S_i^{p1}, S_i^{p2}) \\ l_{cl}^{d1-d2} &= \sum_{i=1}^{N} \mathrm{NT-Xent}(S_i, S_i^{d1}, S_i^{d2}) \end{aligned} \tag{23}$$

3.7. Predictions

In previous sections, we introduced the calculation methods for repeat-tail loss $l_{rt-rec}(\hat{y}_c$ (formula 18), self-attention loss $l_{sa-rec}(\hat{y}_s)$ (formula 22), contrastive loss $l_{cl}^{odd-even}$, l_{cl}^{r1-r2}, l_{cl}^{p1-p2} and l_{cl}^{d1-d2} (formula 23). In this section, a multi-task learning strategy is adopted to obtain the final loss l_{cltar} of CLTAR-GNN. The loss function could be seen as below in formula 24:

$$l_{cltar} = \alpha \cdot l_{rt-rec} + \beta \cdot l_{sa-rec} + \gamma(l_{cl}^{odd-even} + l_{cl}^{r1-r2} + l_{cl}^{p1-p2} + l_{cl}^{d1-d2}) \tag{24}$$

where α, β and γ are weight parameters to control the contributions of each loss. Based on grid search of hyperparameter, we assign α as 0.3, β as 0.7 and γ as 1. Finally, for a session $S = [v_{s1}, v_{s2}, \ldots, v_{sn}]$, the probability score $\hat{y}_i$ for each candidate item v_i ($i \leq |V|$) that could be clicked at timestamp $n+1$ is as follows:

$$\hat{y}_i = \alpha \times \hat{y}_{ci} + \beta \times \hat{y}_{si} \tag{25}$$

4. Experiments

4.1. Experiment Settings

Two widely-used public datasets Yoochoose and Diginetica are selected to test the performance of the model. Yoochoose is from RecSys Challenge 2015, which contains the click sequence of users on an e-commerce website within six months. Because the Yoochoose dataset is too large, only the latest 1/64 part of it is used, as done in [27]. Diginetica is from CIKM Cup 2016 challenge. The statistics of datasets are shown in Table 1.

Evaluation Metrics In order to compare with other models for session-based recommendation, two evaluation metrics HR@20 and MRR@20 are used.

HR@20 (Hit Rate): This metric indicates the proportion of correctly predicted sessions in all testing sessions. Correctly predicted n_{hit} means that the ground-truth item is among the top 20 items with the highest recommendation scores calculated by the model.

Table 1. Statistics of datasets used in the experiment

Statistics	Yoochoose 1/64	Diginetica
# of clicks	557,248	982,961
# of training sessions	369,859	719,470
# of test sessions	55,898	60,858
Average length	6.16	5.12

In formula 26, n_{hit} represents sessions that have been correctly predicted, and N denotes the number of all testing sessions.

$$HR@20 = \frac{n_{hit}}{N} \tag{26}$$

MRR@20 (Mean Reciprocal Rank): This metric denotes the average of reciprocal ranks of the ground-truth items. When the ground-truth item is not among the top-20 recommended items, the reciprocal rank is set to 0. In formula 27, S denotes the set of correctly predicted sessions, and $rank_i$ denotes the rank of ground-truth item for session i.

$$MRR@20 = \frac{1}{N}(\sum_{i \in S} \frac{1}{rank_i}) \tag{27}$$

Baseline Methods The proposed model CLTAR-GNN will be compared with the following representative baseline methods on Yoochoose and Diginetica datasets.

- Item-KNN [22] recommends similar items of the previous clicked item in the session based on cosine similarity.
- BPR-MF [20] optimizes a pairwise ranking objective function via stochastic gradient descent.
- FPMC [21] models next-basket recommendation. The user feature is removed since it is unavailable in session-based recommendation.
- GRU4REC [8] models user sequences for session-based recommendation using RNN.
- NARM [12] employs a local encoder and a global encoder with an attention mechanism to model the user's sequential behavior and capture the user's main purpose.
- STAMP [15] captures users' general interests of session context and user's current interests of last click.
- RepeatNet [19] takes repeat-explore consumption behaviors into account and uses GNN to model users' repeat and explore behaviors.
- CSRM [24] incorporates collaborative modeling into session-based recommendation with an end-to-end model.
- SR-GNN [27] models session sequences into graph-structure data and uses graph neural networks to capture complex item transitions.
- GC-SAN [29] integrates self-attention layers with graph neural networks to learn long-range dependencies.
- TAGNN [32] proposes a target attentive network which could discover the relevance of target item with graph neural networks.
- LESSR [2] designs two new graph neural network based layers, which are EOPA and SGAT to solve the information loss problems.

- SR-SAN [5] captures long-range dependencies between items using self-attention networks.
- NISER [6] normalizes the item and session-graph representations to improve the recommendation accuracy of long-tail items.

Hyperparameter Setup Following [16], for sessions with length ¿ 10, we consider only the most recently clicked 10 items. The dimensions of both item embeddings and position embeddings are set as 300 (Hyper-parameter studies of embedding size could be seen in Figure 2). The batch size is set to 100. Following [13], The Adam optimizer is adopted with the initial learning rate 0.001. Decay rate is set as 0.1 per 3 epochs. We use dropout probability of 0.1 and attention heads of 4 on self-attention networks. The focusing parameter for focal loss is set to 2. The weight of contrastive loss in multi-task learning is set to 1, which make it have the same impact for the model optimization with the loss of recommendation task. We use the normalization strategy as introduced in [16] and set the scale factors as 16 following the paper. The number of training epochs is set to 30, and we adopt the early stopping strategy. When the performance does not improve after 10 consecutive epochs, the training will be terminated.

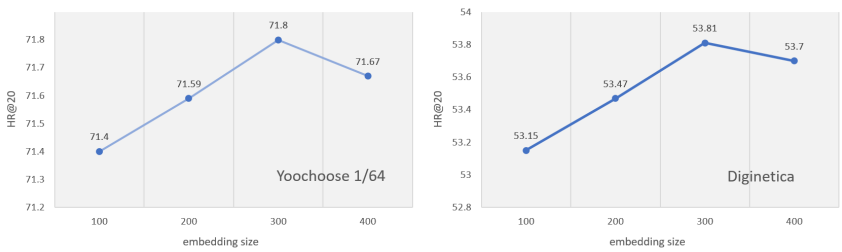

Fig. 2. The performance of CLTAR-GNN with different embedding sizes

Another important hyper-parameter is split-ratio, which decides the proportion of long-tail items in training dataset. We assign the split-ratio as $sr \in 0.5, 0.6, 0.7, 0.8, 0.9$, and use sr to divide all items in V into long-tail and short-head groups. Then we test different sr to find the best results, which is evaluated by HR@20, MRR@20. Experimental results of selecting sr could be seen in Figure 3. The proposed CLTAR-GNN could obtain the best HR@20 and MRR@20 on Yoochoose 1/64 when sr = 0.7; while for Diginetica, the best sr is 0.6. The training process could be seen in Figure 4, the loss of the CLTAR-GNN is small compared with other three baselines during the training process, while the performance on validation datasets in terms of HR@20 and MRR@20 keeps a relatively high score.

4.2. Overall Performance Comparison

Results and Observations To evaluate the performance of CLTAR-GNN, we compare it with 14 state-of-the-art baselines introduced above. Table 2 summarizes the best results

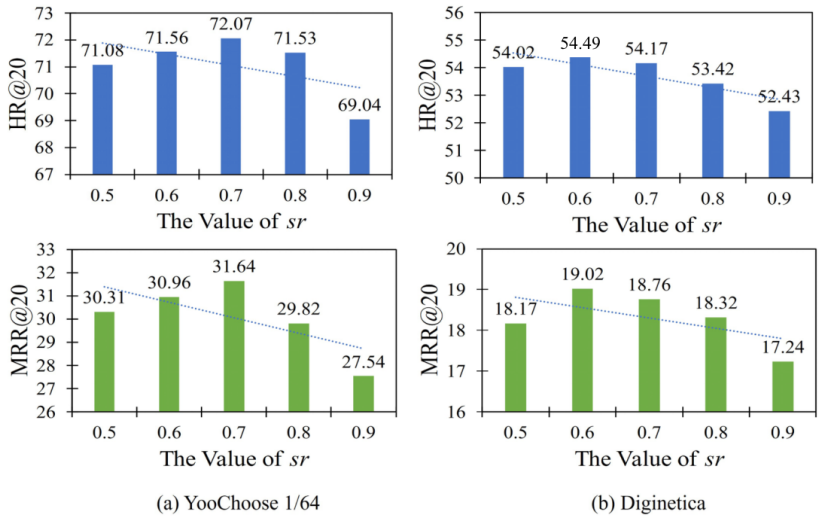

Fig. 3. The Performance of sr on Yoochoose 1/64 and Diginetica

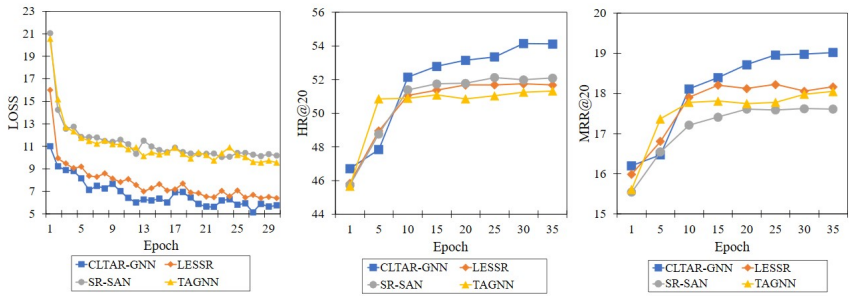

Fig. 4. The Training Process of CLTAR-GNN in terms of LOSS, HR@20 and MRR@20

of all models. As seen in Table 2, Traditional recommendation methods including Item-KNN, BPR-MF and FPMC obtain the lowest performance score. These methods make recommendations only based on the similarities or transitions between items, which are unable to leverage other important information such as the order of items. Compared with traditional methods, GRU4REC applies RNN to session-based recommendation and outperforms traditional methods. Both NARM and STAMP consider the current interest and global interest of the user, and thus get better results. RepeatNet considers users' repeated-explore patterns, and has better performance than other RNN-based methods. CSRM applies collaborative neighbor information to current session, and it's performance on Yoochoose dataset is very competitive.

The GNN-based methods generally perform better than the methods mentioned above. SR-GNN firstly model the session sequences as graphs and then consider the transitions of items, obtaining better results than RNN-based methods. TAGNN is an improved version

Table 2. The performance of CLTAR-GNN and its variants compared with 14 state-of-the-art Baseline

Methods	Yoochoose 1/64		Diginetica	
	HR@20	MRR@20	HR@20	MRR@20
Item-KNN	51.60	21.81	35.75	11.57
BPR-MF	31.31	12.08	5.24	1.98
FPMC	45.62	15.01	26.53	6.95
GRU4REC	60.64	22.89	29.45	8.33
NARM	68.32	28.63	49.70	16.17
STAMP	68.74	29.67	45.64	14.32
RepeatNet	70.71	31.03	47.79	17.66
CSRM	71.45	30.06	50.55	16.38
SR-GNN	70.57	30.94	50.73	17.59
GC-SAN	70.66	30.04	51.70	17.61
TAGNN	71.02	31.12	51.31	18.03
LESSR	70.64	30.97	51.71	18.15
SR-SAN	71.74	31.58	52.04	17.61
NISER	71.27	<u>31.61</u>	53.39	18.72
TAR-GNN w/o sa	69.85	30.76	51.73	18.22
TAR-GNN w/o $sa - ls$	69.46	30.45	51.52	18.03
TAR-GNN	<u>71.73</u>	31.17	<u>53.92</u>	<u>18.98</u>
CLTAR-GNN w/o sa	70.31	30.98	52.65	18.66
CLTAR-GNN w/o $sa - ls$	70.12	30.82	52.49	18.31
CLTAR-GNN	**72.07**	**31.67**	**54.49**	**19.02**

of SRGNN. By adding a target attentive module, its performance is better than SRGNN in all the metrics. LESSR proposes two new layers on the basis of graph neural networks to solve the information loss problem, which outperforms TAGNN on Diginetica dataset. GC-SAN outperforms SR-GNN since it applies self-attention mechanism and combines it with graph neural network to capture long-range dependencies, however, the information of global dependencies between items may be lost during the process of neighbor item aggregations. SR-SAN mainly uses self-attention networks to replace GNN for session encodings, and achieves the second place on Yoochoose dataset in term of HR@20. Though NISER uses GNN to get session encodings, it adopts optimal normalization representation method to obtain more accurate item and session embeddings, it greatly improves the performance of long-tail items recommendations and achieves the second place on Yoochoose dataset in term of MRR@20. The proposed method CLTAR-GNN outperforms all baselines on both datasets in terms of all metrics, proving its effectiveness in the session-based recommendations task. Specifically, CLTAR-GNN outperforms the best baseline by average 1.2% (HR@20) and 0.9% (MRR@20) on Yoochoose and Diginetica datasets. The average improvement compared with all baselines are 17.5% (HR@20) and 22.5% (MRR@20) on both datasets. In order to better illustrate the effectiveness of the proposed model, five variants are proposed, which are TAR-GNN, TAR-GNN w/o sa, TAR-GNN w/o $sa - ls$, CLTAR-GNN w/o sa, CLTAR-GNN w/o $sa - ls$.

- **TAR-GNN**: CLTAR-GNN does not contain contrastive learning.
- **TAR-GNN w/o** sa: TAR-GNN does not contain self-attention.

- **TAR-GNN w/o** $sa - ls$: TAR-GNN does not contain both self-attention and long-short term mechanism.
- **CLTAR-GNN w/o** sa: CLTAR-GNN does not contain self-attention.
- **CLTAR-GNN w/o** $sa - ls$: CLTAR-GNN does not contain both self-attention and long-short term mechanism.

Based on the performance analysis of the proposed CLTAR-GNN and its variants, our findings are summarized in four aspects:

- **Considering users' repeat-explore patterns in both short-head and long-tail items could improve the performance compared with RepeatNet, GC-SAN and TA-GNN.** TAR-GNN w/o $sa - ls$ could make an average improvement of 7.8% and 2.1% in terms of HR@20 and MRR@20 on Diginetica compared with RepeatNet, while the performance on Yoochoose 1/64 is not as good as RepeatNet. One main reason is that the number of sessions in Diginetica is bigger than Yoochoose 1/64, so Diginetica could provide more training instances with long-tail items and reduce the negative influence of data sparsity. Compared with GC-SAN and TA-GNN, the average improvements of TAR-GNN are 3.8% (HR@20) and 4.1% (MRR@20) on two datasets, which indicates that on the premise of incorporating self-attention network at the same time, the investigation of behavior patterns could bring more advantages in session recommendations.
- **Incorporating long-short term module into TAR could make further improvement.** Compared with TAR-GNN w/o $sa - ls$, the average improvements of TAR-GNN w/o sa are 0.5% and 1.1% on two datasets. Experimental results indicate the effectiveness of the proposed long-short term module. Besides, compared with NARM and STAMP, which considers both general and current interests of users, TAR-GNN w/o sa could also have an average improvement of 7% and 12% in terms of HR@20 and MRR@20.
- **Self-attention module is important for capturing order-information, which could not be well captured by only using GNN based methods.** Compared with TAR-GNN w/o sa, TAR-GNN could obtain a more significant improvement in terms of two metrics. Besides, TAR-GNN outperformances SR-GNN and TAGNN by average 3.5% (HR@20) and 3% (MRR@20) on two datasets. Experimental results illustrate that TAR-GNN could better leverage order information derived from self-attention to improve the performance. Compared with LESSR, which adopts optimized GNN and GRU for capturing long-term dependencies and order information, TAR-GNN incorporating self-attention could also obtain a better result.
- **Data sparsity limits the ability of the proposed model to process long-tail items, while the contrastive learning could better solve the problem to a certain extent.** SR-SAN and NISER exhibits strong competitiveness in the task of session recommendation, and outperformance TAR-GNN in terms of two metrics. We consider the potential reasons that limit the ability of TAR-GNN could be the lack of training samples of long-tail items. Adding contrastive learning validates our motivations that it is necessary to use data augmentation strategies to improve the performance. Experimental results show that incorporating CL could significantly improve the performances of TAR-GNN and CLTAR-GNN outperformances the two competitive baselines by average 1.5% (HR@20) and 1.2% (MRR@20) on both datasets.

Performance based on Popularity Threshold As illustrated in [6], popularity threshold is an indicator to evaluate whether an item is popular or not. The indicator could help better evaluate the performance of CLTAR-GNN on the task of long-tail item recommendations. The popularity of an item could be defined as $popularity = \frac{\varphi(i)}{max\varphi(i)}$, where $\varphi(i)$ is the number of times item i appears in all sessions. In order to evaluate the performance of long-tail recommendations, we should firstly construct a long-tail testing dataset L. For a session $S = [s_1, s_2, \ldots, s_n]$ in the testing dataset, if its $n+1$th clicked item is non-popular ($popularity \leq threshold$), then we set $S \in L$. We set the threshold as 0.01, 0.05, 0.1, 0.5, 1, and obtain five long-tail testing datasets, the performances of the proposed model and four other baselines on the five datasets are summarized in Figure 5.

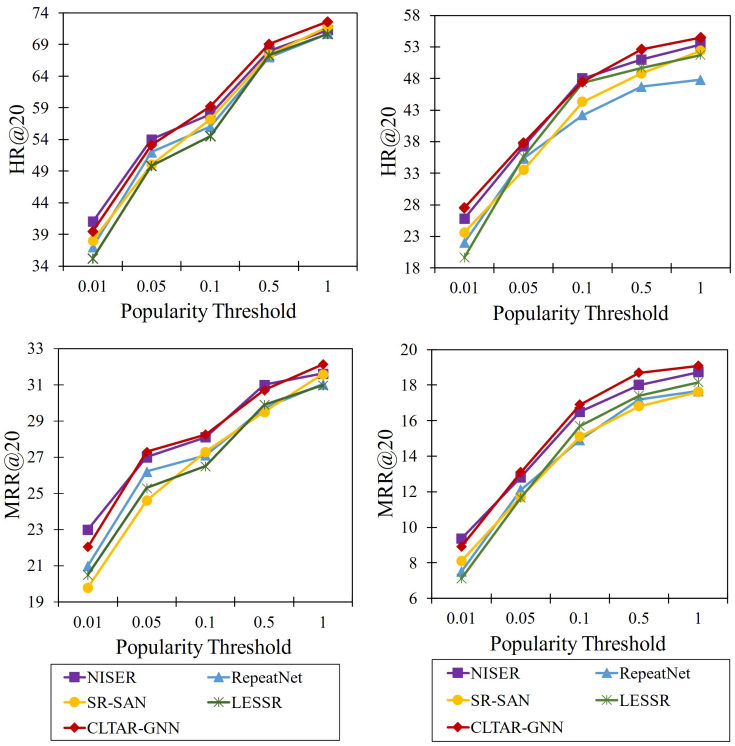

(a) YooChoose 1/64 (b) Diginetica

Fig. 5. The performance of long-tail item recommendations on Yoochoose 1/64 and Diginetica

In Figure 5, when the threshold is small, the target items of all sessions in the long-tail testing dataset are non-popular. The proposed CLTAR-GNN outperforms the other four baselines significantly for those sessions filtered by threshold with long-tail items as target. While for RepeatNet, SR-SAN and LESSR, there are no mechanisms for them to

identify whether current session is a long-tail or short-head recommendation task. Though NISER is a competitive model for the task of long-tail item recommendations, CLTAR-GNN outperformances NISER by average 1.2% and 0.8% improvement on two datasets in terms of HR@20 and MRR@20. One main reason is that CLTAR-GNN uses item factor to decide whether short-head or long-tail items are taken as recommendation targets.

Performance based on Repeat-explore Patterns In this section, a new experiment is conducted to investigate the models' performance on users' repeat and explore behaviors separately. Repeat behavior means repeating click a item that has already existed in a session, explore means a new item will be clicked in the session. According to the definition of repeat and explore, we could divide all sessions in the testing dataset into repeat sessions and explore sessions, and evaluate the performance of the proposed model on the two types of sessions. Experimental results could be seen as in Table 3.

Table 3. The performance of repeat-explore

Methods		Yoochoose 1/64		Diginetica	
		HR@20	MRR@20	HR@20	MRR@20
CLTAR-GNN	R	**93.55**	**64.85**	**91.87**	**58.28**
	E	**64.35**	19.26	**44.60**	8.82
RepeatNet	R	91.71	57.65	87.43	49.33
	E	61.27	27.81	39.69	**8.89**
SR-GNN	R	92.25	63.08	86.14	52.26
	E	62.55	19.04	42.10	8.74
SR-SAN	R	92.93	64.37	86.86	51.53
	E	64.11	**19.31**	43.02	8.45

As seen in Table 3, "R" represents Repeat sessions, and "E" represents Explore sessions. In both Yoochoose 1/64 and Diginetica datasets, the percentage of Repeat sessions is about 30% and that of Explore sessions is about 70%. RepeatNet is a research to investigate users' repeat-explore behaviors, CLTAR-GNN obtains better performance compared with RepeatNet because the proposed model could capture more accurate repeat-explore patterns. The proposed CLTAR-GNN also outperformances SR-GNN and SR-SAN significantly. The two baselines represent GNN-based and Attention-based session recommendation models respectively.

4.3. Ablation Test

An ablation study was conducted to help determine the contribution of each component of the proposed model. Variations of CLTAR-GNN are tested, in which specific components were removed or replaced. These assignments were as follows:

- **-CL**: Contrastive learning removed.
- **-GGNN**: Use neural network embeddings to replace GGNN.
- **-RE**: Repeat-explore removed.
- **-HR**: Item factor generating removed.

- **-LS**: Long-short term removed.
- **-SA**: Self-attention removed.
- **-PE**: Position embedding removed.
- **-FL**: Use entropy loss to replace focal loss.
- **+PH**: Add projection head to CLTAR-GNN.

As for +PH, the main idea is from the study of SimCLR, which adds a projection head (PH) to improve the performance. The projection head is a MLP layer which projects session vectors into a different feature space to calculate the contrastive loss. The test results are evaluated using HR@20 and MRR@20, and are summarized in Table 4.

Table 4. Ablation results for CLARE

Methods	Yoochoose 1/64		Diginetica	
	HR@20	MRR@20	HR@20	MRR@20
CLTAR-GNN	**72.07**	**31.67**	**54.49**	**19.02**
-CL	71.73	31.17	53.92	<u>18.98</u>
-GGNN	71.97	31.26	54.33	18.89
-RE	72.01	31.14	54.31	18.91
-HR	71.95	31.15	54.25	18.82
-LS	71.95	31.21	<u>54.36</u>	18.88
-SA	70.31	30.98	52.65	18.66
-PE	70.69	29.40	53.54	18.65
-FL	71.82	31.04	54.23	18.88
+PH	71.66	<u>31.55</u>	53.75	18.96

As seen in Table 4, self-attention (-SA) and position embedding (-PE) have the highest contribution on the performance of CLTAR-GNN, which is consistent with our previous experimental conclusion. Besides, contrastive learning (-CL) also has a great impact on the performance of CLTAR-GNN. The impact of focal loss (-FL) is relatively smaller, but also make positive contributions to the performance, which indicate that focal loss could help resolve data imbalance problem. Projection head (+PH) cannot improve the performance in session-based recommendation.

4.4. Comparison with Different Model Variant

Different variants of the proposed CLTAR-GNN are also verified in this section. Six variants are summarized as below:

- **CLTAR-GNN-AVG**: Use the average of self-attention output as the representation of session embedding.
- **CLTAR-GNN-N1**: Use the last item embedding of self-attention output as the representation of session embedding.
- **CLTAR-GNN-N2**: Use average of the last two item embeddings of self-attention output as the representation of session embedding.
- **CLTAR-GNN-S**: Only use single attention mechanism in item generating module.
- **CLTAR-GNN-M:** The session embeddings in session generation layer will share weights with adjust function in item factor generating module.

– **CLTAR-GNN-SM**: The structure considers both single attention design and weight sharing strategy.

CLTAR-GNN-S is used to evaluate whether the design of two attention mechanisms in item factor generating module is necessary. CLTAR-GNN-M investigates whether incorporating repeat-explore and head-tail modules in early stage will obtain better performances. In order to verify those assumptions, experiments are conducted based on CLTAR-GNN and its six variants, and the results could be seen in Table 5.

Table 5. Experimental results for different variants

Methods	Yoochoose 1/64		Diginetica	
	HR@20	MRR@20	HR@20	MRR@20
CLTAR-GNN-AVG	71.46	30.54	53.61	18.55
CLTAR-GNN-N1	71.72	31.43	53.54	18.66
CLTAR-GNN-N2	**72.07**	**31.67**	**54.43**	**19.02**
CLTAR-GNN-S	71.56	30.02	53.49	18.37
CLTAR-GNN-M	68.36	27.62	51.98	17.44
CLTAR-GNN-SM	68.64	27.36	51.35	17.10

As shown in Table 5, CLTAR-GNN-N2 is the best choice for calculating session embeddings. CLTAR-GNN-AVG may be unable to make accurate recommendations because it focuses on the global interest, and CLTAR-GNN-N1 only uses one item vector which may be unrepresentative. Therefore, CLTAR-GNN-N2 is a better choice which doesn't have these problems. Besides, different structure-based variants of CLTAR-GNN (S, M, SM) could not obtain better results in terms of HR@20 and MRR@20 on both datasets, which further indicates the effectiveness of the proposed CLTAR-GNN.

5. Conclusion

In this paper, we propose a novel model called Contrastive Learning based Tail Adjusted Repeat Graph Neural Network (CLTAR-GNN) for Session-based Recommendation. We design a series of innovations, which include: incorporate self-attention, position embedding and graph neural network into a unified framework to consider both long-term order information and high-order complex correlations among items; incorporate repeat-explore and head-tail into a unified framework to consider users' different behavior patterns in long-tail and short-head items; consider long-short term correlations for all session representation modelling; use contrastive learning to extract self-supervised signals from raw data, thus get high-quality session representations and make more accurate recommendations. Extensive experiments conducted on two public datasets Yoochoose 1/64 and Diginetica show that CLTAR-GNN evidently outperforms the state-of-the-art session-based recommendation methods. Besides, Experiments also exhibit that self-attention with position embedding is essential important for the proposed model to capture long-term dependencies and order information. The negative influence of data sparsity and data imbalance problems in session recommendations have also been confirmed through extensive ex-

periments, and contrastive learning framework is verified as a good solution to solve the above problems to a certain extent.

In future, it would be worth exploring and employing different contrastive learning frameworks in CLTAR-GNN. In another aspect, users' behavior patterns will be further investigated from the perspective of consumer behavior theory. With the guidance of domain theory, prior knowledge of users and sessions will be also taken into considerations to further improve the performance and make the results more explainable.

Acknowledgments. This research was supported by Guangdong Natural Science Foundation General Project under Grant No. 2024A1515011793.

References

1. Benson, A., Kumar, R., Tomkins, A.: Modeling user consumption sequences. In: WWW '16: In Proceedings of the 25th International Conference on World Wide Web. pp. 519–529 (2016)
2. Chen, T., Wong, R.C.W.: Handling information loss of graph neural networks for session-based recommendation. In: Proceedings of the 26th ACM SIGKDD International Conference on Knowledge Discovery & Data Mining. pp. 1172–1180 (2020)
3. Chen, T., Kornblith, S., Norouzi, M., Hinton, G.: A simple framework for contrastive learning of visual representations. In: International conference on machine learning. pp. 1597–1607. PMLR (2020)
4. Davidson, J., Liebald, B., Liu, J., Nandy, P., Van Vleet, T., Gargi, U., Gupta, S., He, Y., Lambert, M., Livingston, B., et al.: The youtube video recommendation system. In: Proceedings of the fourth ACM conference on Recommender systems. pp. 293–296 (2010)
5. Fang, J.: Session-based recommendation with self-attention networks. arXiv preprint arXiv:2102.01922 (2021)
6. Gupta, P., Garg, D., Malhotra, P., Vig, L., Shroff, G.: Niser: Normalized item and session representations to handle popularity bias. arXiv preprint arXiv:1909.04276 (2019)
7. He, R., McAuley, J.: Fusing similarity models with markov chains for sparse sequential recommendation. In: In Proceedings of 2016 IEEE 16th International Conference on Data Mining (ICDM'16), pp. 191–200 (2016)
8. Hidasi, B., Karatzoglou, A., Baltrunas, L., Tikk, D.: Session-based recommendations with recurrent neural networks. arXiv preprint arXiv:1511.06939 (2015)
9. Hidasi, B., Karatzoglou, A., Baltrunas, L., Tikk, D.: Session-based recommendations with recurrent neural networks. In: In Proceedings of 2016 International Conference on Learning Representation (ICLR'16) (2016)
10. Hidasi, B., Quadrana, M., Karatzoglou, A., Tikk, D.: Parallel recurrent neural network architectures for feature-rich session-based recommendations. In: Proceedings of the 10th ACM conference on recommender systems, pp. 241–248 (2016)
11. Li, J., Ren, P., Chen, Z., Ren, Z., Lian, T., Ma, J.: Neural attentive session-based recommendation. In: Proceedings of the 2017 ACM on Conference on Information and Knowledge Management, pp. 1419–1428 (2017)
12. Li, J., Ren, P., Chen, Z., Ren, Z., Lian, T., Ma, J.: Neural attentive session-based recommendation. In: Proceedings of the 2017 ACM on Conference on Information and Knowledge Management. pp. 1419–1428 (2017)
13. Li, Y., Tarlow, D., Brockschmidt, M., Zemel, R.: Gated graph sequence neural networks. arXiv preprint arXiv:1511.05493 (2015)
14. Lin, T.Y., Goyal, P., Girshick, R., He, K., Dollár, P.: Focal loss for dense object detection. In: Proceedings of the IEEE international conference on computer vision. pp. 2980–2988 (2017)

15. Liu, Q., Zeng, Y., Mokhosi, R., Zhang, H.: Stamp: short-term attention/memory priority model for session-based recommendation. In: Proceedings of the 24th ACM SIGKDD international conference on knowledge discovery & data mining. pp. 1831–1839 (2018)
16. Liu, S., Zheng, Y.: Long-tail session-based recommendation. In: Fourteenth ACM conference on recommender systems. pp. 509–514 (2020)
17. Pang, Y., Wu, L., Shen, Q., Zhang, Y., Wei, Z., Xu, F., Chang, E., Long, B., Pei, J.: Heterogeneous global graph neural networks for personalized session-based recommendation (2022)
18. Perozzi, B., Al-Rfou, R., Skiena, S.: Deepwalk: Online learning of social representations. In: Proceedings of the 20th ACM SIGKDD international conference on Knowledge discovery and data mining, pp. 701–710 (2014)
19. Ren, P., Chen, Z., Li, J., Ren, Z., Ma, J., De Rijke, M.: Repeatnet: A repeat aware neural recommendation machine for session-based recommendation. In: Proceedings of the AAAI Conference on Artificial Intelligence. vol. 33, pp. 4806–4813 (2019)
20. Rendle, S., Freudenthaler, C., Gantner, Z., Schmidt-Thieme, L.: Bpr: Bayesian personalized ranking from implicit feedback. arXiv preprint arXiv:1205.2618 (2012)
21. Rendle, S., Freudenthaler, C., Schmidt-Thieme, L.: Factorizing personalized markov chains for next-basket recommendation. In: Proceedings of the 19th international conference on World wide web. pp. 811–820 (2010)
22. Sarwar, B., Karypis, G., Konstan, J., Riedl, J.: Item-based collaborative filtering recommendation algorithms. In: Proceedings of the 10th international conference on World Wide Web. pp. 285–295 (2001)
23. Vaswani, A., Shazeer, N., Parmar, N., Uszkoreit, J., Jones, L., Gomez, A.N., Kaiser, Ł., Polosukhin, I.: Attention is all you need. Advances in neural information processing systems 30 (2017)
24. Wang, M., Ren, P., Mei, L., Chen, Z., Ma, J., de Rijke, M.: A collaborative session-based recommendation approach with parallel memory modules. In: Proceedings of the 42nd international ACM SIGIR conference on research and development in information retrieval. pp. 345–354 (2019)
25. Wang, S., Zhang, Q., Hu, L., Zhang, X., Wang, Y., Aggarwal, C.: Sequential/session-based recommendations: Challenges, approaches, applications and opportunities (2022)
26. Wu, S., Tang, Y., Zhu, Y., Wang, L., Xie, X., Tan, T.: Session-based recommendation with graph neural networks. In: Proceedings of the AAAI conference on artificial intelligence, vol. 33, pp. 346–353 (2019)
27. Wu, S., Tang, Y., Zhu, Y., Wang, L., Xie, X., Tan, T.: Session-based recommendation with graph neural networks. In: Proceedings of the AAAI conference on artificial intelligence. vol. 33, pp. 346–353 (2019)
28. Xie, X., Sun, F., Liu, Z., Wu, S., Gao, J., Ding, B., Cui, B.: Contrastive learning for sequential recommendation. In: In Proceedings of IEEE 38th International Conference on Data Engineering. pp. 1259–1273 (2022)
29. Xu, C., Zhao, P., Liu, Y., Sheng, V.S., Xu, J., Zhuang, F., Fang, J., Zhou, X.: Graph contextualized self-attention network for session-based recommendation. In: IJCAI. vol. 19, pp. 3940–3946 (2019)
30. Yang, L., Luo, L., Li, F., Zhang, X., Zhang, X.: Dagnn: Demand-aware graph neural networks for session-based recommendation. In: SIGIR (2022)
31. Yin, H., Cui, B., Li, J., Yao, J., Chen, C.: Challenging the long tail recommendation. In: In Proceedings of the VLDB Endowment. vol. 5 (2012)
32. Yu, F., Zhu, Y., Liu, Q., Wu, S., Wang, L., Tan, T.: Tagnn: target attentive graph neural networks for session-based recommendation. In: Proceedings of the 43rd international ACM SIGIR conference on research and development in information retrieval. pp. 1921–1924 (2020)
33. Zhong, S., Qin, J., Huang, Z., Li, D.: Cem:machine-human chatting handoff via causal-enhance module (2022)

34. Zhou, K., Wang, H., Zhao, W.X., Zhu, Y., Wang, S., Zhang, F., Wang, Z., Wen, J.R.: S3-rec: Self-supervised learning for sequential recommendation with mutual information maximization. In: Proceedings of the 29th ACM International Conference on Information & Knowledge Management. pp. 1893–1902 (2020)

Daifeng Li is a professor at School of Information Management, Sun Yat-sen University (SYSU). He has working experience at Tsinghua University as post phd and Baidu as Senior Engineer. His research interests include Information Sciences, Data Science, Information Systems and Artificial Intelligent.

Tianjunzi Tian is a master student at Department of Information Management at Nanjing University, majoring in information science. Her research interests include data mining, data analysis and management science.

Zhaohui Huang is an undergraduate student at School of Information Management, Sun Yat-sen Univeristy (SYSU), majoring in information science. His research interests include software engineering, data mining, data analysis and management science.

Xiaowen Lin is a master student at Department of Information Management at Nanjing University, majoring in information science. Her research interests include data mining, data analysis and management science.

Dingquan Chen is a professor at School of Information Management, Sun Yat-sen University (SYSU). His research interests include Library and Information Science.

Andrew Madden began his research career as an agricultural ecologist, but became interested in Information Science after working on a project to develop computer-based materials for teaching about land use. He has worked as a researcher at the UK's Natural Resources Institute, Sheffield Hallam University, Sheffield University, and a senior researcher in the School of Information Management at Sun Yat-sen University. His current research interests are in information behavior, the evolution of decision-making systems and information literacy.

Received: November 01, 2024; Accepted: December 02, 2024.

Computer Science and Information Systems 22(1):369–399 https://doi.org/10.2298/CSIS240411012A

Unraveling the Organisational Debt Phenomenon in Software Companies*

Muhammad Ovais Ahmad[1], Osama Al-Baik[2], Abdelrahman Hussein[3], and Mwaffaq Abu-Alhaija[4]

[1] Department of Computer Science, Karlstad University,
Karlstad, Sweden
{ovais.ahmad}@kau.se
[2] Department of Software Engineering, Princess Sumaya University for Technology
Amman, Jordan
o.albaik@psut.edu.jo
[3] Department of Software Engineering, Al-Ahliyya Amman University
Amman, Jordan
a.husein@ammanu.edu.jo
[4] Department of Computer Science, Applied Science Private University
Amman, Jordan
m_abualhaija@asu.edu.jo

Abstract. Organizational debt (OD) is a major challenge to software organizations that seek to maintain agility, adaptability and sustainable competitiveness in the dynamic business environment. OD can be refers to suboptimal decisions, outdated procedures, misaligned structures and cultural barriers that limit an organization's ability to adapt and innovate quickly. This multifaceted process includes several factors, including ineffective workflows, knowledge silos, cultural issues, and inadequate resource utilization. When organizations are focused on short-term gains at the expense of long-term organizational health, the symptoms of organizational dysfunction may manifest themselves as reduced output, reduced quality and customer satisfaction. This study aims at assessing the extent of knowledge, factors, and consequences of organizational maladjustment in software organizations. A survey performed in three organizations identified several highly visible issues such as complex code, inconsistent UI, unclear requirements, and outdated processes. These themes often emerge due to exponential growth, prioritizing speed over quality, lack of cooperation and coordination, and outdated processes. The adverse effects of OD are comparable to technical debt, affecting the maintainability, user experience, and project management. This study also offers strategies for identifying, assessing, and mitigating OD through a combination of quantitative metrics, user feedback, and interdepartmental collaboration. By fostering a culture of continuous improvement, open communication, and cross-functional alignment, organizations can proactively address OD and create an environment conducive to innovation, quality, and customer-centricity.

Keywords: Organisational debt, software development, technical debt, process debt, nontechnical debt, agile, organisational agility.

* This is an extended version of our conference paper [6].

1. Introduction

The software development landscape is in a constant state of flux, demanding that organizations remain agile, adaptable, and competitive. Tight deadlines often lead to prioritizing features over code quality, and inadequate documentation creates a technical debt burden [2] [33], [34]. As market needs evolve and technological advancements accelerate, companies must navigate a complex interplay of technical and non-technical factors to sustain innovation and deliver value to customers [2]. Maintaining software in a suboptimal state, both technically and non-technically, can compromise its reliability and efficiency [33] [50] [2].

Short-term gains and a series of less-than-ideal decisions (e.g., prioritizing speed over proper documentation) can lead to the accumulation of "organizational debt" (OD) [2]. While technical debt (TD) has been extensively explored in academic literature [2][49][16], non-technical debt (NTD) remains less understood [33] [2][4][9]. NTD encompasses process debt, social debt, and people debt [13]. OD extends beyond TD and encompasses NTD, including process, social, and people debts. Liu et al. define "organizational debt" more narrowly, encompassing only social and process debt [36]. While TD focuses on codebase and architecture, OD covers broader organizational inefficiencies such as outdated processes and misaligned structures. NTD represents the unintended consequences of prioritizing short-term expediency over long-term sustainability [37]. This results in a gradual accumulation of outdated processes, misaligned structures, and cultural barriers within an organization. OD refers to the difference between a company's strategic plans and its actual ability to implement them in view of the ever-changing market needs [6] focusing on both technical and non-technical barriers to agility and innovation. This multifaceted concept extends beyond technical debt, encompassing a broad range of factors that can hinder an organization's ability to adapt, innovate, and maintain a competitive edge [36] [33][34][6]. As software companies grapple with the challenges posed by OD, a comprehensive understanding of its causes, consequences, and potential mitigation strategies becomes crucial. Recognizing the various manifestations of OD, such as inefficient workflows, knowledge silos, cultural misalignments, and inadequate resource allocation, allows organizations to take proactive steps. These steps can foster an environment conducive to continuous improvement, open communication, and cross-functional collaboration.

This study expands on the findings of our previous multivocal literature review (MLR) presented at the 39th ACM/SIGAPP Symposium on Applied Computing, Track on Lean and Agile Software Development [6]. This study seeks to provide insight into the impact of OD on software companies by investigating IT professionals' views on this issue. To this end, we will use data collected from a survey conducted in three different organizations in different fields. Moreover, this research aims to explore the ways of detecting, evaluating, and managing OD by using a set of quantitative measures, feedback from the users, and collaboration between departments. When an organization encourages learning and development, communication, and collaboration, they can prevent OD and establish a culture that supports change, quality, and customer focus. Finally, this approach can help achieving sustainable business performance and market sustainability in the context of the software development industry.

This study is organized into seven sections. Section 2 provides background information relevant to the research goal. Section 3 details the research methodology employed,

including research design, data collection methods, and data analysis procedures. Section 4 presents result of our study. Section 5 addresses potential limitations of the study that could affect the validity of findings. Section 6 provides a discussion of results, interpreting them in the context of existing knowledge and highlighting their significance. Finally, Section 7 offers concluding remarks, summarizing the key findings and outlining potential future research directions.

2. Background

Software development is a complex process. Its complexity arises from the relationships and interactions among a large number of stakeholders, which have unpredictable behaviour. Additionally, each project is unique, with specific challenges stemming from the diverse backgrounds of individuals involved and the problem domain. Since technology and organisational processes are constantly evolving, these factors interact in unpredictable ways. Agile and Lean processes prioritize frequent delivery of value to customers by eliminating waste that hinders productivity and quality [10] [7] [11]. Treating team members as interchangeable 'resources' and constantly swapping them in and out of projects is ineffective [85]. In addition, they often blame the team for not following the process when problems occur. The "Just get it done" approach is the primary driver of debt in software development.

In 1992, Cunningham [21] introduced the concept of technical debt (TD) and described how "Shipping first-time code is like going into debt. A small debt accelerates development as long as it is promptly paid back with a rewrite... The danger occurs when the debt is not repaid. Every minute spent on a not-quite-right code counts as interest on the debt. Entire engineering organizations can be brought to a standstill under the debt load of an unconsolidated implementation." Avgeriou et al. [15] elaborated on this definition as TD is a collection of design or implementation constructs that are expedient in the short term but set up a technical context that can make future changes more costly or impossible. TD represents an actual or contingent liability whose impact is limited to internal system qualities, primarily maintainability and evolvability. Other types of TD include architectural debt, code debt, and test debt [33][34].

Extensive research has been carried out on TD from a wide range of perspectives, including efforts, tools, types, management strategies, architectural aspects, agile development and prioritisation [2][49][40]. Rios et al. [50] reported 78 causes and 66 effects of TD. The main reported causes were deadlines, obsolete or incomplete documentation, lack of technical knowledge, inappropriate planning, lack of knowledge of technology, a focus on higher production at the expense of quality, and lack of a well-defined process. Avgeriou et al. [15][16] conducted comparisons of tools used for measuring TD, assessing their features, popularity, and empirical validity, and found that TD results in reduced maintainability and quality, amplified project costs, financial losses, bad code refactoring, team overload, difficulties in implementing the system and stakeholder dissatisfaction. Matkovic et al. [42] highlighted challenges contributing to technical debt, such as inadequate identification, monitoring, and refactoring of non-functional requirements, emphasizing the importance of business analysis and architectural decisions. Marjanović et al. [39] emphasized the need for updating organizational processes, developer training, and tools to improve application security. Poth et al. [47] discussed the issue of organizational

silos in large enterprises, proposing self-service kits as a potential solution for scaling knowledge to autonomous teams.

Khomyakov et al. [31] specifically explored TD measurement and analysis tools, focusing on quantitative methods that could be automated. Besker et al. [18] address architectural TD and combined research efforts to produce new insights with a specific interest in the topic. The findings indicate a lack of efficient management principles for architectural debt. In agile software development, Behutiye et al. [17] stress the significance of timely delivery and design matters, which may precipitate TD pitfalls. The adverse outcomes of TD in agile software development comprise reduced output, system quality, and escalated maintenance costs. Lenarduzzi et al. [34] found that code debt and architectural debt are the most common types of TD studied. Nevertheless, research into other types of TD, including test debt and requirement debt, was limited.

The Danish government faced challenges as a third of its critical IT systems were inadequate, lacking proper documentation, security, and requiring software and hardware upgrades [26]. Sweden's government agencies also struggled with outdated IT systems, affecting 70 percent of their setups [14]. According to Klinger et al. [33] "the decision to acquire TD is not made by technical architects, but rather by non-technical stakeholders who cause the project to acquire new technical debt or discover existing TD that wasn't previously visible" (p. 35). Klinger's highlight an important aspect of OD, which is that non-technical stakeholders play a crucial role in the accumulation of debt within organizations. Software project success or failure depends on both technical and non-technical factors. TD has received more attention in research and practice compared to non-technical debt (NTD) in software development [2].

NTD refer to a range of debt types that can arise in software companies, including process, social, people, cultural [2] [8] [6]. NTD stems from suboptimal decisions that prioritise short-term gains over long-term sustainability, which can impede software development activities. In recent systematic review [2] to explore NTD in software engineering, focusing on social, process, and people debt. Their study analyzed 42 primary studies and identified 29 causes and 31 effects of NTD. It is highlighted that NTD is often interconnected and can significantly influence software development activities. The study revealed that NTD can lead to reduced productivity, decreased software quality, and increased development costs. It is important address NTD alongside TD for more effective software development and propose strategies for managing NTD, including improved communication, knowledge sharing, and process optimization. Our literature review provided detailed background to various NTD types such as social, process, and people debts in software engineering [2] [8] [8] [6]. Appendix B provided glossary of various debt types, below we only highlight definitions and key leading causes, we reported details in [2].

Process debt is a "suboptimal action or event with short-term advantages but long-term detrimental effects" [17]. Teams incur process debt when conducting stand-up meetings solely for status updates to leaders, limiting the meetings' full potential. The leading causes of process debt are lack of process competencies, process divergence, and external dependencies (i.e. technology, tools and external trends) [2].

People debt refers to "people issues that, if present in the software organization, can delay or hinder some development activities", for example, expertise focussed on a few personnel, as an effect of delayed training and hiring [2]. People's debt causes examples

are lack of knowledge, experience, commitment and lack of psychological safety, inadequate management decisions and low developer morale [2].

"Cultural debt is a technical decision that borrows against the organization's culture. Such decisions can introduce team divisions, deteriorate communication or even weaken leadership effectiveness". The leading causes of cultural debt include hiring the wrong people, dismissing complaints, charging discrepancies, and giving unequal rewards.

Social debt refers to "the presence of sub-optimality in the development community, which causes a negative effect on software development" [52]. An example of social debt is lone wolf, and radio silence/bottleneck [2] [5]. Social debt causes are communication, collaboration and coordination challenges, and community smells [2] [9].

Introducing new policies for hybrid work can expose managers to the potential of incurring OD [37]. These policies have the power to shape the norms that develop among employees. If managers fail to address unfavourable norms promptly, they will be faced with the consequences of this OD in future. Liu et al [37] research identified 23 mechanisms, grouped into eight general coordination categories, and assessed their impact on aspects such as shared mental models, team coordination, team cohesion, and team learning.

3. Research Method

In this section, we present the methodology used for our research. Our initial step involved conducting a multivocal literature review (MLR) focused on OD within software companies, as we previously reported in our work [6].

MLR typically encompass a wide array of easily accessible material. Given that this approach incorporates diverse perspectives, including non-academic sources, it is crucial to establish a clear objective before proceeding. In our case, the primary aim of the MLR was to gain insight into how software industry professionals conceptualize and describe the phenomenon of "organizational debt".

We adhered to the MLR guidelines proposed by Garousi and Mantyla [6][7] [12] [53]. Considering the novelty of "organizational debt" as a topic and the scarcity of academic literature, we opted to use Google search engine rather than traditional academic databases (such as SpringerLink, ACM, or IEEE eXplore). Google search capabilities proved effective in locating relevant grey literature. In June 2023, we conducted our search using the query ("organizational debt" OR "organisational debt" AND "software"). This search string was based on our study scope, incorporating both "population" and "intervention" terms. We included "software" to ensure coverage of studies discussing software, its development, engineering aspects, or software-intensive products, services, and systems. The term ("organizational debt" OR "organisational debt") was employed to capture all OD-related papers.

From the search results, we examined the first 120 sources. This approach aligns with Haddaway et al. [27] observation that grey literature researchers often focus on the top 50 results. We scrutinized each link, recording relevant findings in a Microsoft Excel spreadsheet. We excluded sources that were non-English, videos, advertisements, catalogs, duplicates, research profiles, or outside the software engineering domain. Our final selection comprised 22 blog posts out of the initial 120 sources, which are documented in [6]. Notably, our search strategy did not yield any relevant scientific articles.

For data analysis, we employed thematic analysis techniques, focusing on four key themes: OD definitions, causes, consequences, and mitigation strategies. Within each theme, we conducted an open analysis of the data. It is worth noting that we didn't use pre-defined themes or codes for causes, effects, and mitigation strategies; instead, these emerged organically from the data. The initial MLR findings were published in [6]. Building upon this foundation, we subsequently expanded our research through an exploratory survey.

The survey instrument itself was developed based on our OD literature review in software engineering, as reported [6]. The development process adhered to best practices for exploratory survey design, as suggested by Kitchenham and Pfleeger [32]. To ensure methodological rigor, the survey followed a structured series of steps, including expert reviews and pilot testing. These steps were crucial in refining the survey's content and ensuring its alignment with the study's objectives. However, it is important to clarify that the pilot testing was distinct from the main survey and was conducted solely to test the clarity and reliability of the instrument, not to collect final survey data.

Expert reviews were conducted by professionals with over ten years of experience in software engineering and project management, ensuring that the instrument was reviewed by domain experts. Their feedback resulted in adjustments to question phrasing, the inclusion of additional response categories, and refinement of the open-ended questions. The profile of these experts included senior software engineers and project managers. Experts recommended rephrasing some of the closed-ended questions to avoid ambiguity, improving the clarity of operational definitions related to OD, and expanding the scope of questions to cover a broader range of organizational levels (e.g., operational, managerial, executive). Additionally, they suggested restructuring open-ended questions to encourage more detailed and insightful responses from participants.

After incorporating the experts' feedback, the survey was subjected to pilot testing with a small sample of participants to assess the overall clarity and usability of the instrument. The pilot test focused on understanding whether participants could easily interpret the questions and provide responses that align with the survey objectives. Importantly, the data collected from the pilot test were not included in the final survey results, as the purpose of this phase was to refine the instrument rather than to gather actionable data. Adjustments based on pilot test feedback included simplifying technical jargon and restructuring several questions to improve response accuracy.

The respondent pool included project managers, senior managers, and other key stakeholders in software organizations, ensuring a broad representation of perspectives within the software engineering industry. The survey consisted of 17 questions divided into six sections:

1. Participants background
2. Organizational Information,
3. Awareness and Identification of Organizational Debt
4. Causes and Consequences of Organizational Debt
5. Mitigation Strategies and Practices
6. Additional Comments and Feedback.

The survey included a mix of closed-ended questions and open-ended questions to gather both quantitative and qualitative data (See Appendix A, for survey questions).

The survey was distributed electronically to nine different software organizations across various regions. The organizations were selected based on their size (medium-sized) and willingness to participate in the study. Responses were received from five of the nine organizations contacted. Two organizations were excluded from the analysis due to an insufficient number of responses (three or fewer responses received). The remaining three organizations were located in Jordan (JoOrg), Canada (CaOrg), and the United States (UsOrg). These organizations were categorized based on international definitions for company size, where medium-sized companies are defined as having between 100 and 500 employees, as outlined in Table 3. In addition to the steps outlined in the research

Table 1. Participating Organizations

ID	Size	Responses	Included responses	Domain	Location
JoOrg	200-250	16	13	Education Technology	Jordan
CaOrg	300-350	21	16	E-Commerce	Canada
UsOrg	200-250	18	13	Healthcare	United States

method, the study also addressed validity threats by implementing strategies such as peer debriefing and member checking. Peer debriefing involved discussions with colleagues in software engineering to validate the coding framework, while member checking ensured that the participants' responses were accurately interpreted by returning initial results to a subset of respondents for verification. Furthermore, data triangulation was employed, comparing qualitative insights with MLR data to improve the robustness of the analysis.

3.1. Data Coding and Analysis

The closed-ended responses were coded numerically for quantitative analysis. In accordance with best practices for survey analysis in software engineering research [32], descriptive statistics such as frequencies and percentages were employed to provide an initial quantitative overview of the data. For open-ended questions, a thematic analysis approach was employed to identify common themes and patterns in the responses. We applied a deductive thematic analysis, as described by Kitchenham and Pfleeger [32] and Braun and Clarke [20], which allows researchers to analyze data using predefined theoretical frameworks to guide the process. This approach is particularly useful when examining data through the lens of established theories. In contrast to inductive methods, where themes emerge directly from the data, deductive analysis facilitates a more targeted examination of key research questions and theoretical constructs [3][20].

We compared these themes with the original ones that were reported by Ahmad and Al-Baik [6] focusing on their relevance to OD. Specifically, the open-ended responses were first read thoroughly to gain familiarity with the data. In line with qualitative research guidelines, the initial coding process involved identifying recurring ideas, concepts, or patterns in participants' responses, which were then organized into codes. These codes were subsequently refined and consolidated into broader themes that aligned with the study's research objectives. The coding process was iterative, with codes and themes being revised as new insights emerged from the data. In order to ensure the robustness

of our findings, methodological triangulation was applied, as recommended by Kitchenham and Charters [32]. This involved comparing and integrating data from MLR and open-ended survey responses to generate a holistic understanding of OD in software organizations.

To enhance the credibility and trustworthiness of the qualitative research, peer debriefing and member-checking procedures were rigorously applied. Peer debriefing involved discussions with an independent coder knowledgeable in OD, allowing for the verification of the identified themes and codes, thereby improving the credibility and confirmability of the analysis. Additionally, a purposive sample of participants was asked to review the interpretations of their responses and provide feedback, a process known as member checking. This step further strengthened the validity of the qualitative data by ensuring that the interpretations accurately reflected participants' perspectives. Moreover, efforts were made to improve the reliability of the analysis by adhering to a systematic process of comparison between qualitative and quantitative data. This methodological approach, recommended by Kitchenham and Pfleeger [32], allows for a more nuanced understanding of the phenomenon under investigation and ensures a reliable synthesis of both qualitative and quantitative data. By using both data types, the study was able to address the research questions comprehensively, reducing bias and enhancing the validity of the conclusions.

4. Results

In this section, we first review the trends of OD awareness and try to refine the definition of OD that was established in our MLR [6]. Secondly, we discuss OD causes and effects as reported by the survey participants and examine the alignment to the ones that were previously reported in Ahmad and Al-Baik [6]. Thirdly, we discuss OD identification, assessment metrics, and mitigation strategies as reported by the research participants. Finally, we provided future directions and potential OD research agenda.

4.1. Results from Literature Review

OD Concept and Definition In our conference papers, we systematically assembled twenty-two blog postings centred on OD, authored by software engineering professionals. The concept of OD has gained increasing attention in recent years, as evidenced by the growing number of publications on the topic. A clear pattern emerges as six out of 13 articles were written in the past couple of years 2020-2023, highlighting the increasing discussion surrounding the OD phenomenon.

The conceptual roots of OD trace back to 2015 when Steve Blank extended the metaphor of TD and characterized OD as "worse" [19]. Notably, this idea finds antecedents in Ben Horowitz's conceptualization of "management debt" dating back to 2012 [6]. Subsequent contributors like Dignan broadened the scope, asserting that OD is not confined to start-ups but holds significance on a broader organizational scale. The MLR results [6] offer a plethora of OD definitions, reflecting the nuanced perspectives of software industry professionals; Table 1 below shows a summary of these definitions.

We synthesis these definitions and proposed: "OD refers to the difference between a company's strategic plans and its actual ability to implement them in view of the ever-changing market needs" [6]. OD, however, is a multifaceted phenomenon that encompasses a wide range of technical and non-technical aspects within an organization. While

TD primarily refers to the accumulation of shortcuts and compromises made in the codebase, OD encompasses a broader scope that includes inefficient processes, outdated policies, cultural misalignments, and suboptimal organizational structures. This reveals a nuanced understanding of OD that goes beyond the traditional concept of TD.

OD Causes and Consequences: As reported by Ahmad and Al-Baik [6], Table 2, summarises the OD causes, consequences and mitigation strategies. It was also reported that OD is not frequently measured in software organizations, nor valued because it's extremely expensive [46]. Organisations that are not responsive to change accumulate OD: decreased agility, reduced competitiveness, negative effect on employee morale and increased resistance to change, and eventually lead to inefficiency and bureaucracy [6]. At a higher level, OD manifests itself in two ways:

1. Obsolescence occurs when structures and policies become unfit for purpose. While rules and structures may have initially served the organisation well, they can become entrenched and inflexible, impeding adaptability and innovation.

2. Accumulation occurs when policies and procedures are constantly added but never removed. When employees are unsure of their responsibilities and accountabilities, it leads to confusion and inefficiency. Overcompensating some employees while neglecting others can create perceptions of unfairness, leading to demotivated teams and reduced overall productivity.

OD Mitigation Strategies: Identifying and mitigating organisational debt requires a systematic approach given its multifaceted nature. Organisational debt symptoms can be spotted through regular performance monitoring, employee surveys, and audits of processes [6]. A comprehensive evaluation of various organisational components is vital for deeper insights.

Quantitative performance metrics offer warning signs such as prolonged declines in productivity, increasing software defects, lags in new feature releases, product quality issues, and rising customer complaints. Comparing metrics over time and against competitors highlights underperformance. Periodic audits help assess process efficiency, redundancy, and alignment with objectives. Surveys and interviews to gather employee perspectives on pain points complement the top-down analysis. The utilization of both quantitative and qualitative data allows for the cross-validation of findings regarding the state of organizational components.

4.2. Practitioners Survey Results

Demographics: A total of 54 responses were collected from Jordan (JoOrg), Canada (CaOrg), and the United States (UsOrg). Majority of the responses were from 21 responses from CaOrg, followed by 18 responses from UsOrg and 16 responses from JoOrg. However, 3 responses from JoOrg, 5 responses from CaOrg, and 5 responses from UsOrg were excluded due to incomplete responses, resulting in a final sample of 42 included responses. The study included a diverse group of participants from various roles (See Table 4).

Table 2. OD Definitions, adopted from our MLR [6]

Proposed Definition in Grey Literature	Year
“OD is all the people/culture compromises made to ‘just get it done’ in the early stages of a start-up”	2015
“Organizational debt is any structure or policy that no longer serves an organization”	2020
“Organizational debt is the accumulation of changes and decisions leaders should have made but did not”	2016
“The interest companies pay when their structure & policies stay fixed and/or accumulate as the world changes”	2016
“Management Debt is incurred when you make an expedient, short-term management decision with an expensive, long-term consequence”	2022
“Organizations may intentionally or unintentionally incur organizational debt through management actions, governance process changes, internal process changes, or large-scale organizational changes when short-term advantages are sought at the expense of ’doing things right”	2017
“Organizational debt is the baggage that prevents people from delivering astonishing results”	2015
“Organizational debt - our organizations are also a good excuse to avoid changes, as we often look for someone who is going to help us, but we do not really want to give him or her the power to implement the changes”	2019
“Organizational debt is sibling of technical debt, for example a toxic culture, struggling leader etc.”	2020
“Organizational debt: things that should’ve been done to ensure health & efficiency, but weren’t”	2021
“Organizational debt, an analogy! During the execution of organizational changes (transformations, reorganizations, changes in ways of working etc.) shortcuts are taken that lead to frustration, more time and money etc. It’s the same thing as technical debt”	2021
“Organizational Debt is the interest companies pay when their structure and policies 1) stay fixed and/or 2) accumulate as the world changes”	2016
“Organizational debt is a holistic concept, and it is more than technical debt and also different from bureaucracy. Organizational debt is a networked concept that fosters the blame-free identification of cross-functional and cross-department weak points”	2023

Table 3. OD Causes, Consequences, and Mitigation Strategies from MLR [6]

Theme	Cause	Consequences	TD Analogy	Mitigation Strategies
Pressure to "Just Get It Done"	Root cause is urgency to complete tasks	Reduced Organizational Effectiveness: Decreased speed, capacity, engagement, flexibility, and innovation	Rushed to suboptimal solutions	Avoid rigid organizational charts, set work-in-progress limits, and use Kanban.
Organizational Growth Challenges	Compromises in personnel, culture, and leadership practices	Decline in Key Performance Metrics: Decreased agility, slow delivery, reduced competitiveness	Rapid growth without proper scalability measures	Encourage individual workers to tailor their roles for flexibility and adaptation
Cost and Measurement Issues	OD not frequently measured or valued due to perceived high cost	Diminished Agility, Slow Adaptation, and Reduced Competitiveness: Hinders responsiveness and efficiency	Avoiding investments in tools and processes.	Establish a feedback culture, nurturing internal trust and encouraging open feedback
Poorly Managed Change	Inadequate adaptation or ineffective change management initiatives	Poorly managed changes lead to resistance and ineffectiveness	Quick, temporary fixes instead of comprehensive changes	Practice continuous participatory governance: Involve people in co-designing roles, structures, and policies
Lack of Collaboration Culture	Failure to seek input from stakeholders during change initiatives	Structures and policies become unfit, hindering adaptability	Lack of collaboration, outdated systems and processes	Regularly monitor performance, behavioral, and innovation metrics
Siloed Change Efforts	Independent change efforts without coordination	Fragmentation, duplicated efforts, and lack of synergy due to independent change efforts	Fragmented solutions that don't integrate well	Implement programs like "process bounty" to encourage to highlight hindrances, fostering a culture of identifying and rectifying OD sources.
Leadership Decisions Avoiding Disruption	Hesitation to address underperforming employees and avoiding necessary changes	Mediocrity and resistance become accepted norms, hindering necessary changes	Leadership avoids necessary improvements	Offer leadership training, change management, etc.

The largest groups were Project Managers and Product Owners, each comprising 14.29% of the sample (6 participants each), and CEOs (4.76%). This focus on managerial-level participants ensures understanding of OD from a strategic perspective. Other roles included Software Developers (11.90%) and Quality Engineers (9.52%). This distribution highlights the variety of perspectives included in the study, ensuring a well-rounded view of challenges faced by different levels within software organizations.

Table 4. Participant Titles and Demographics

Title	N	Percentage
Quality Engineer	4	9.52%
Graphic Designer	2	4.76%
Network Engineer	3	7.14%
Project Manager	6	14.29%
UX Researcher	2	4.76%
Software Developer	5	11.90%
Business Analyst	4	9.52%
Security Officer	3	7.14%
Product Owner	6	14.29%
Customer Support Team Lead	2	4.76%
CEO	2	4.76%
Marketing Professional	3	7.14%
Total	42	100%

Table 5 provide an over of demographic characteristics of our survey participants. The majority of participants were male (66.67%), with females making up 33.33% of the sample. This distribution reflects the current gender disparity often seen in the software engineering industry. A significant proportion of participants held Graduate degree

Table 5. Demographic profile of respondents (N=42)

	Characteristic	Frequency	Percentage
Gender	Male	28	66.67%
	Female	14	33.33%
Age (years)	22-25	10	23.81%
	26-29	12	28.57%
	30-33	8	19.05%
	34 and above	12	28.57%
Education Level	Graduation (Bachelor)	22	52.38%
	Post-Graduation(Masters/MPhil)	14	33.33%
	Doctorate	6	14.29%
Software Development (Years)	Less than 1	4	9.52%
	1-2	8	19.05%
	3-5	12	28.57%
	6-7	10	23.81%
	7+	8	19.05%

(52.38%). Those with Post-Graduation degrees (Masters/MPhil) made up 33.33% of the sample, and 14.29% held Doctorate degrees. This variety in educational background underscores the breadth of expertise represented in the study. Participants' experience in software development varied widely.

The largest group had 3-5 years of experience (28.57%), followed by those with 6-7 years (23.81%). This mix of experience levels ensures that the study encompasses both relatively new and experienced professionals, providing a comprehensive view of how OD affects in their work.

The survey results also provide a view of OD awareness across various organizational levels. A significant proportion of respondents (60%) indicated familiarity with the concept of OD, highlighting a growing recognition of the term within the software industry. However, 25% of participants reported only partial familiarity, and 15% were entirely unfamiliar with OD. This suggest that while awareness is increasing, there remain knowledge gaps that could hinder effective OD identification and mitigation.

Moreover, when asked to describe their organization's current level of OD, 50% of respondents identified OD at the operational level, indicating that day-to-day processes, workflows, and procedures are where inefficiencies are most prevalent. 35% reported OD at the managerial level, suggesting that mid-level management also grapples with decision-making inefficiencies and misaligned structures.

Only 15% recognized OD at the executive level, reflecting that strategic misalignment exists, it is less prevalent compared to operational and managerial layers. These findings underscore the need for targeted OD mitigation strategies that focus on operational and managerial inefficiencies, where the debt is most concentrated, while ensuring alignment at the executive level to drive long-term organizational adaptability and competitiveness.

Table 6 presents a comprehensive overview of OD based on practitioners' survey. It outlines five key themes related to OD: complex codebase, inconsistent UI, unclear requirements, outdated content, and inability to adapt to change. For each theme, the table details the causes, consequences, TD analogies, and mitigation strategies. In the following sections, we will discuss each of these themes in detail.

We will present the specific causes that lead to OD, the consequences, and strategies that practitioners recommend for mitigating these challenges. This analysis will provide valuable insights into the nature of OD and offer practical approaches for addressing it in software development organizations.

OD Concept from Practitioners Survey: From a developers' perspective, OD can manifest as complex and poorly documented codebases, siloed knowledge, and a lack of clear code ownership, hindering maintainability and the integration of new features. As developers mentioned, "*Difficulty integrating new features due to complex code structure" (Jo8), "Difficulty meeting sprint goals due to last minute feature additions or changes*" (Us12), and "*Long code review times due to a large codebase*" are indicators of OD (Ca15).

For designers, OD may present itself as inconsistencies in the user interface, outdated design guidelines, and a lack of user research, leading to design debt and usability issues. A UX designer noted, "*Inconsistency in user interface (UI) elements across different parts of the application can indicate design debt*." (Ca8) and "*Inconsistent brand application*

Table 6. OD Causes, Consequences, and Mitigation Strategies Based on Practitioners Survey

Themes	Causes	Consequences	TD Analogy	Mitigation Strategies
Complex codebases, Siloed knowledge, unclear code ownership	Rapid uncontrolled growth, prioritization of speed over quality, lack of clear communication & collaboration, outdated processes and structures	Reduced maintainability, difficulty integrating new features, longer development cycles	Impacting code quality & maintainability	Dedicating time for code refactoring, implementing code reviews, investing in test automation
Inconsistent UI, outdated design guidelines, lack of user research	Rapid growth, prioritization of speed over quality, lack of communication between design & development teams	Design debt leading to usability issues, user frustration	Impacting the user experience	Fostering collaboration between design and development teams, integrating user research findings into development process
Unclear requirements, inefficient communication	Lack of clear collaboration and cooperation, outdated processes and structures	Missed deadlines, frustrated teams, difficulty adapting to changes	Process debt impacting project management & communication	Streamlining workflows, establishing knowledge management practices, collaborating with product teams
Outdated content, misaligned messaging	Prioritization of speed over quality, limited resources	Ineffective communication, difficulty aligning content with product features	Process debt impacting content creation & management	Investing in content creation tools, establishing clear content creation workflows
Inability to adapt & change, hindered innovation	Lack of agility and understanding agile concepts, limited resources and competing priorities	Reduced competitiveness, difficulty responding to market shifts	Accumulated debt across various aspects hindering overall agility	Fostering a culture of continuous improvement, invest in staff training, promoting user-centric mindset

across different platforms, potentially indicating outdated design assets or style guides." (Jo4).

Project managers often grapple with OD in the form of unclear requirements, scope creep, and inefficient communication between stakeholders. In response to what symptoms of OD exist in the participating organizations, a project manager from CaOrg stated, "*Frequent scope creep and missed deadlines due to unclear project requirements*" (Ca5), while a project manager from JoOrg mentioned "*Frustration among team members due to inefficient workflows or unclear priorities.*" (Jo5), and from the UsOrg, a project manager stated "*Project teams struggling to adapt to changes due to inflexible project management methodologies.*" (Us5).

As for marketing and content writer specialists working in the software domain, OD can manifest as outdated content, misalignment between messaging and product features, and inefficient content creation workflows. A marketing professional from CaOrg mentioned, "*Difficulty aligning marketing campaigns with new product releases due to slow content creation workflows*" as an indicator of OD (Ca6), while another marketing professional from JoOrg mentioned "*Inconsistent branding across different platforms due to outdated style guides or lack of clear communication.*" as a symptom of OD (Jo7).

While TD primarily impacts the maintainability, evolvability, and quality of the codebase, OD has far-reaching consequences that can affect an organization's ability to adapt to change, innovate, and remain competitive in the market. OD encompasses a broader range of factors, including suboptimal decisions, outdated processes, misaligned structures, and cultural barriers, which collectively hinder an organization's agility and overall performance. Each of these terms within the OD definition can be understood as follows: Suboptimal decisions refer to short-term choices that prioritize immediate gains at the cost of long-term sustainability. Outdated processes reflect workflows and procedures that no longer align with current organizational goals or market demands. Misaligned structures refer to organizational hierarchies or teams that are no longer optimal for innovation and flexibility.

Finally, cultural barriers involve resistance to change or a lack of openness to new ideas, which stifles innovation. Understanding how each element of OD (suboptimal decisions, outdated processes, etc.) influences organizational behavior is crucial for developing holistic approaches that address both technical and non-technical challenges. By refining management practices to account for OD, organizations can incorporate strategies that specifically target these inefficiencies.

Considering the above discussion and definitions, OD is define as the accumulation of suboptimal decisions, outdated processes, misaligned structures, and cultural barriers that impede an organization's ability to adapt and innovate effectively. The inclusion of 'and' in the definition does not imply that all components must coexist for OD to be present. This definition integrates the technical and non-technical aspects of debt, making it applicable in practice. Rather, each component represents a potential source of OD, which can be assessed individually. For instance, an organization may assess its OD by evaluating its decision-making processes, structural efficiency, and adaptability to market changes. The organization's ability to adapt effectively can be defined as its capacity to restructure processes, workflows, and team dynamics in response to internal and external changes. Innovation, on the other hand, can be defined as the organization's capacity to

introduce new products, services, or processes that deliver value in line with evolving market demands.

The gradual build-up of unresolved decisions and unimplemented actions that should have been undertaken by leaders. This accumulation results in structures, policies, and processes that no longer align with the organisation's objectives, ultimately impeding its progress and adaptability in the face of changing circumstances. This accumulation hinders an organization's ability to maintain optimal performance, agility, and responsiveness. As a result, OD exacerbates the gap between its intended strategic plans and the practical capacity to meet evolving market demands. The means that OD encompasses a broader range of organizational factors compared to TD and NTD. While TD focuses on code quality and maintainability, OD extends beyond technical aspects to include organizational inefficiencies that limit agility and competitiveness. This expanded view helps identify and mitigate debt beyond technical aspects, integrating social, process, and structural considerations.

OD Causes and Consequences: The survey results highlight that OD significantly affects an organization's agility, adaptability, and competitiveness. Agility refers to the ability to respond quickly to market changes, while adaptability denotes the capacity to adjust processes and structures in response to internal and external pressures. Competitiveness is defined as the organization's ability to maintain or improve its position relative to competitors. Rapid growth and the prioritization of speed over quality emerged as significant contributors to the accumulation of OD across multiple departments.

The survey found that organizations burdened by OD were less agile and adaptable, often facing challenges in maintaining competitiveness due to outdated processes and misaligned structures. Participants noted that OD led to slow decision-making, reduced innovation, and lower responsiveness to customer needs, further highlighting its detrimental impact on organizational performance.

In the development realm, respondents reported a primary cause of technical debt as Ca15 cited "*Rapid growth leading to pressure to ship features quickly, sometimes at the expense of code quality*" and Us1 testified "*In my experience, rapid feature releases with tight deadlines can lead to technical debt as corners are sometimes cut*" (Us1). Similarly, Ca7, a product owner, mentioned that "*Rapid feature releases with tight deadlines can lead to technical debt due to shortcuts taken*." Even in the marketing department, Ca6 noted that "*Limited resources might lead to slow content creation and outdated materials*," indicating that the pressure of rapid growth can contribute to process debt.

Lack of clear communication and collaboration was another recurring theme highlighted by respondents from various roles. Ca5, a project manager, pointed out that ". *Us6, a UX researcher, stated that "Outdated user personas that don't reflect the current user base could cause the product to miss user needs*," suggesting a lack of communication between user research and development teams. Ca14, a customer support team lead, mentioned that "*Lack of clear communication between development and customer support teams could be hindering the creation of user-friendly self-service options*," leading to process debt in customer support. Us9, a network engineer stated that "*Limited communication between network operations and development teams can lead to mismatched network requirements*," resulting in debt that impacts performance and scalability.

Outdated processes and structures were also identified as significant contributors to organizational debt. Ca15, a software developer, noted that "*Lack of clear code ownership makes refactoring and maintaining code quality challenging*," indicating outdated processes for code management. Ca11, a business analyst, mentioned "*A lack of standardized processes across departments, potentially resulting in redundancies and inefficiencies*," as a potential source of process debt. Ca10, a security officer, cited "*Difficulty keeping up with the evolving threat landscape due to outdated security tools*," as a contributor to security debt.

Limited resources and competing priorities were frequently cited as factors hindering efforts to address organizational debt. Developers like Ca15 mentioned "*Limited resources and time for code refactoring and technical debt reduction*" as a factor contributing to technical debt accumulation. Ca16, a quality engineer, stated that "*Limited resources and time for QA to develop and maintain automated tests*" led to testing debt. Ca4, a graphic designer, noted that "*Limited time and resources for the design team to undertake large-scale organization initiatives*" hindered efforts to mitigate design debt. The limited resources were also reported on both, human and non-human resources, Us9 a network engineer from UsOrg, stated "*Frequent network slowdowns, bottlenecks during peak usage periods, and difficulty integrating new applications due to limited network capacity.*" and "L*imited staff resources might make network modernization a complex and time consuming process*."

Lack of agility and inability to adapt to market changes were also reported to introduce insufficient flexibility and incapacity to adjust to shifts in the market. The organization's outdated legacy systems and bloated processes hinder its ability to stay up with more agile competitors, making it slow and inflexible. The CEO of JoOrg attested that "Reduced agility and adaptability to changing requirements due to technical limitations" is a major OD impact on the organization (Jo2). The CEO of CaOrg acknowledged that "*I believe a strong focus on employee development and training on new technologies will help us stay agile and adapt to changing market demands*" (Us2).

These observations from various departments and roles illustrate the multifaceted nature of OD and highlight how factors such as rapid growth, communication barriers, outdated processes, and resource constraints can contribute to the accumulation of different types of OD within software organizations.

OD Identification Identifying the presence of OD within an organization often involves recognizing various indicators and symptoms across different domains. One key area is inefficient processes and outdated policies, where teams might encounter "*Difficulty finding clear and up-to-date documentation for internal systems" or "Repetitive tasks that could potentially be automated"* (Ca3), or "*Outdated design tools or asset libraries requiring workarounds and slowing down workflows*" (Jo4). Project managers may also observe "*Frequent scope creep and missed deadlines due to unclear project requirements*" (Ca5) or "*...team members struggle to adapt to changes due to inflexible project management methodologies*" (US5).

Technical debt and code quality issues can also serve as indicators of OD. Developers might face "*Difficulty integrating new features due to complex code structure*" (Ca7) or experience "*Long code review times due to a large codebase*" (Ca1). Additionally, teams

may encounter "*difficulty troubleshooting issues caused by legacy code or features not documented clearly*" (Us11), further highlighting the presence of technical debt.

User experience and customer satisfaction issues can be telling signs of OD as well. Design teams might receive "*User complaints about unintuitive features or cluttered interface*" (Ca8) or "*Difficulty getting timely feedback on design concepts, leading to revisions and delays*" (Jo4), or "*Inconsistent brand application across different platforms due to lack of design guidelines*" (Us4).

QA teams could struggle with "*Difficulty reproducing reported bugs due to insufficient test data or unclear defect documentation*" (Ca16). Customer support personnel might encounter "*Frequent reports of slow loading times or bugs in the software*" (Ca13) experience "*Long resolution times for complex customer inquiries due to limited knowledge base information*" (Ca14), or experience "*Frequent escalations to developers due to lack of readily available solutions in the internal knowledge base*" (Us11).

Moreover, employee frustration and morale concerns can be indicative of OD within an organization. This might manifest as "*Employee surveys indicate frustration with slow internal tools and processes"* (Ca2), or *"Frustration among developers due to inconsistent coding standards and legacy code*" (Ca5). Support teams could also face *"Difficulty accessing clear and up-to-date product information"* (Ca13), while development teams may show signs of *"decreased developer morale and productivity due to rework caused by last-minute changes"*(Us12), contributing to overall employee dissatisfaction.

OD Assessment: To effectively assess and monitor OD levels, organizations can implement various metrics and processes. Project data analysis can involve *"Track[ing] project metrics like cycle time, defect escape rates, and time spent on bug fixes versus new feature development"* (Jo1, Jo5, Jo9, Ca5, Ca12, Us5, and Us6) or *"Analyz[ing] project data to identify potential bottlenecks, delays, and inefficiencies"* (Ca12) or *"... track[ing] project metrics like schedule variances, defect rates, and team member utilization..."* (Jo5).

User feedback and experience metrics can be gathered through "*regular user surveys and interviews*" (Ca9), tracking "*user task completion rates, error messages, and usability issues*" (Ca9), or monitoring "*website traffic, engagement metrics, and competitor marketing strategies*" (Ca6).

Customer satisfaction and support metrics can provide valuable insights, such as tracking "*customer satisfaction surveys and identify[ing] recurring pain points"* (Ca14), monitoring *"customer service ticket volume regarding repetitive issues"* (Ca2), or analyzing or *"website traffic and user engagement with different content"* (Us7).

Interdepartmental collaboration and knowledge sharing can be facilitated by *"establish[ing] clear communication channels and protocols for collaboration between departments*" (Ca11), conducting *"workshops and retrospectives to identify areas for process improvement"* (Ca12), and encouraging *"open feedback loops and knowledge sharing across teams and departments"* (Us1).

Additionally, organizations should focus on security and compliance monitoring by *"track[ing] the number of unpatched vulnerabilities and time taken to address them"* (Ca10), *"conduct[ing] regular penetration testing to identify potential security weaknesses"* (Ca10), and monitoring *"compliance with security regulations and industry best practices"* (Ca10).

By leveraging a combination of these metrics and processes, organizations can gain valuable insights into potential sources of organizational debt, identify areas that require improvement, and monitor the effectiveness of their OD mitigation strategies over time, enabling them to make informed decisions and implement targeted interventions to address organizational debt proactively.

OD Mitigation Strategies: Identifying and mitigating organisational debt requires a systematic approach given its multifaceted nature. Organizations can dedicate specific time periods for *"addressing technical debt and code refactoring"* (Ca15) to incrementally improve their codebase. Implementing rigorous "*code reviews with a focus on code quality, maintainability, and identifying potential issues early on*" (Ca1) can prevent the accumulation of future technical debt. Furthermore, "*investing in test automation tools and frameworks*" (Ca16) can reduce manual testing workloads and improve overall test coverage, ensuring better quality assurance.

Fostering practices that promote knowledge-sharing and collaboration among developers is also crucial. Respondents highlighted the benefits of " *focus on collaboration across teams is essential to prevent knowledge silos and maintain a healthy codebase*" (Us1), and the CEO of JoOrg stated "*Clearer communication and collaboration across teams could be beneficial*" for facilitating knowledge transfer and enabling better collaboration on codebase maintenance.

Addressing process debt often involves optimizing processes and improving knowledge management practices. "*Conducting process optimization workshops*" (Ca14) can help organizations streamline workflows, eliminate redundancies, and improve overall efficiency. Establishing "*robust knowledge management practices, such as creating comprehensive documentation, centralized knowledge bases, and facilitating knowledge sharing across teams*" (Us3) can mitigate process debt stemming from knowledge gaps and inefficient information flow.

Moreover, "*collaborating with product teams to identify opportunities for improving self-service resources based on customer feedback*" (Ca14) can reduce the burden on support teams and enhance the overall customer experience. "*Integrating user research findings into the product development process and establishing user research libraries*" (Ca9) can ensure that user needs are adequately addressed, preventing the accumulation of user experience-related debt.

Mitigating cultural debt requires fostering an environment that promotes continuous improvement, open communication, and cross-functional collaboration. "*Encouraging open communication, feedback loops, and cross-functional collaboration across teams and departments*" (Ca1) can break down silos, promote transparency, and leverage collective expertise to address organizational challenges holistically.

Additionally, "f*ostering a culture of continuous improvement through practices like retrospectives, workshops, and encouraging participatory decision-making*" (Ca12) and "*Conducting regular reviews to identify areas for improvement*" (Jo5), enables organizations to proactively identify areas for improvement and adapt to changing needs and requirements.

"*Investing in employee training and development programs*" (Ca2) can help upskill teams on new technologies, methodologies, and best practices, ensuring they remain agile and adaptable. Promoting a "*user-centric mindset by incorporating user research, design*

thinking workshops, and prioritizing user experience throughout the product development lifecycle" (Ca8,) can prevent the accumulation of design debt and ensure a superior user experience.

To mitigate security debt, organizations should prioritize "*implementing security awareness training programs for all employees*" (Ca10) to promote best practices and reduce vulnerabilities. "*Piloting automated security patching processes*" (Ca10) can address vulnerabilities promptly and reduce the risk of security breaches. Furthermore, "*integrating security considerations earlier in the development lifecycle and investing in modern security tools and resources*" (Ca10) can enhance the overall security posture of the organization.

Across all these mitigation strategies, the importance of fostering a culture of continuous improvement, open communication, and cross-functional collaboration cannot be overstated. By embracing these principles, organizations can effectively combat organizational debt, improve operational efficiency, enhance product quality, and better adapt to changing market demands and customer needs.

4.3. Future Research Directions

While this study consolidated understanding of OD, several fruitful avenues exist for further investigation based on current knowledge gaps:

- Develop metrics to quantify OD, enabling rigorous tracking and benchmarking. Combine productivity data with indicators of culture, innovation, and TD. Establish validated scales to measure dimensions like employee engagement, psychological safety, organizational agility, and leadership effectiveness [24] [45] [38]. Statistical modelling can relate these metrics to OD.
- Conduct empirical studies on the impact of OD on workforce motivation, attrition, fatigue, and burnout [35] [44] [41]. Use questionnaires and ethnographic methods to gather insights. Relate debt to tangible individual performance metrics like productivity, absenteeism, and error rates.
- Investigate through case studies the relationship between OD and customer satisfaction [22] [13], especially in software-intensive service organizations. Survey data can correlate debt to metrics like call resolution times, complaint rates, churn, and net promoter scores.
- Examine through controlled experiments the role of OD in software project success/failure. Vary team structures and processes to reveal optimal configurations. Productivity, quality, cost, and schedule metrics assess performance.
- Estimate the economic costs of OD through case studies and cost modelling across software companies [30] [25]. Assess opportunity costs from delayed innovations. Relate to the total cost of ownership models.
- Explore whether TD quantification techniques [15][16][40] can be extended to provide estimates of OD. Comparative studies could be conducted to evaluate the precision of these techniques when applied to different types of debt within software organizations.
- Organizational forgetting [29],a concept largely overlooked in this research stream. Organizational forgetting refers to the processes through which an organization intentionally or unintentionally loses knowledge, practices, or routines that no longer

serve its strategic goals [29]. In the context of OD, fostering deliberate organizational forgetting can be instrumental in reducing debt by eliminating outdated processes, suboptimal decisions, and misaligned structures. Future work could explore how organizational forgetting can be systematically applied to debt reduction efforts, improving organizational adaptability and performance.

– Design field studies of interventions such as restructured teams, revised workflows, and new planning processes to validate OD mitigation techniques [43]. These studies should measure the before-and-after effects of such interventions to determine their efficacy in reducing OD. However, it is important to recognize that OD, especially when accumulated in the early phases of an organization's lifecycle, is often difficult to address without external engagement. Engaging external consultants [1], even in a limited capacity such as providing strategic nudges or asking critical questions, can play a pivotal role in mitigating debt that is deeply ingrained in organizational structures and processes. To minimize OD effectively, future research should explore the role of external consultants in the early stages of a company's lifecycle.

Further research to address these gaps will provide more rigorous, empirically grounded insights to guide debt management in practice. It represents an emerging interdisciplinary arena spanning management science, organizational behaviour, anthropology, and software engineering [54]. Collaboration between academics and industry practitioners is needed to develop context-specific strategies rooted in both theory and pragmatism [48]. There are rich possibilities for cross-pollination between disciplines to uncover novel solutions [23]. With organizational agility and adaptability growing more crucial in turbulent conditions [28], understanding how to minimize friction and debt represents the key to sustaining innovation and competitiveness [51].

5. Validity Threats and Limitations

The study presented in this manuscript has several potential validity threats and limitations that should be acknowledged. One significant threat is the external validity, which stems from the relatively small sample size, with only 42 responses obtained from three software organizations. Although these responses provided valuable insights into OD, a larger and more diverse sample, spanning different industries and geographical regions, would improve the generalizability of the findings.

The survey relied on self-reported data from participants, which may be subject to personal biases, perceptions, and interpretations. According to Kitchenham and Pfleeger [32], reliance on self-reported data introduces a potential threat to internal validity, as participants' responses may not always accurately reflect the true state of OD within their organizations. To mitigate construct validity threats, we employed several strategies, including peer debriefing, which was conducted with subject matter experts from diverse sectors of software engineering. These experts provided critical feedback on the coding and interpretation of the survey data, ensuring a robust analysis. Furthermore, member checking was performed by sharing the coded data with a subset of participants to validate the accuracy of the interpretation and ensure alignment with their original responses. This procedure enhanced the credibility of the qualitative findings. Additionally, data triangulation was applied by comparing the qualitative data from open-ended survey questions

with the MLR results. Triangulating these two data sources helped corroborate the findings, although the inherent subjectivity in qualitative data analysis—where researchers' interpretation might introduce bias—cannot be entirely eliminated [32].

The study provided a cross-sectional snapshot of OD at a certain period of time. Kitchenham and Pfleeger [32] suggests, a cross-sectional design may limit the ability to observe long-term trends or changes in OD over time. A longitudinal study, where organizations are observed over an extended period, would provide a deeper understanding of how OD evolves and the long-term effectiveness of mitigation strategies. This is particularly relevant as OD is a dynamic construct that fluctuates with organizational and environmental changes. Therefore, the findings of this study are valid for the period during which the research was conducted, but future studies may need to revisit and update the results over time.

Despite these limitations, the study offers insights into the awareness, causes, consequences, and mitigation strategies for OD in software organizations. Future research should address these limitations by incorporating a larger, more diverse sample, utilizing multiple data collection sources, and adopting longitudinal research designs to better capture the evolving nature of OD and its effects on organizations.

6. Discussion

The notion of OD has attracted more attention by the software organizations as they face difficulties in sustaining the key values such as flexibility, adaptability, and competitiveness in the context of the changing environment. This paper set out to investigate the level of awareness, factors, impacts, and risk management measures of OD within software organizations so as to confirm the findings of Ahmad and Al-Baik [6].

The results of this study show that OD has far-reaching consequences beyond TD, particularly in its impact on organizational agility and competitiveness. Organizations that accumulate OD tend to have outdated structures and processes, which slow down their ability to respond to market changes and customer demands. Agility is reduced as organizations struggle to implement changes efficiently, while competitiveness suffers because of their inability to innovate and adapt quickly. Addressing OD through continuous improvement and cross-functional collaboration is crucial for maintaining organizational performance and market relevance. As for the issues, participants pointed out several signs and manifestations of OD in different areas such as ineffective workflows, outdated procedures, poor code quality, user interface and experience problems, and dissatisfied employees. This goes to show that OD affects an organization's performance and its capacity to create value for clients in a profound way. Table 7, offered omparison of literature review and survey results.

The factors that contributed to the development of OD were numerous, which included growth, poor communication and coordination, obsolete methods and structures, and resource constraints as some of the frequently mentioned reasons. The following factors lead to the creation of various types of debts like technical, process, and cultural debts that affect an organization's ability to be agile [2]. Interestingly, OD have negative impacts not only in technical domains but also in other domains like competitiveness, employee morale, resistance to change and inefficiency. This observation stresses the need for han-

Table 7. Comparison of literature review and survey results

Themes	Causes from review	Causes from survey	Similarities	Differences
Rapid Growth	Organizational growth challenges	Rapid uncontrolled growth	Both acknowledge rapid growth as a cause	Table 2 focuses on general organizational growth challenges, while Table 5 emphasizes uncontrolled growth
Poor Communication and Collaboration	Lack of collaboration culture, siloed change efforts	Lack of clear communication and collaboration	Both emphasize poor communication	Table 2 mentions siloed change efforts, while Table 5 highlights lack of communication between specific teams
Urgency to Complete Tasks	Pressure to "Just Get It Done"	Prioritization of speed over quality	Both recognize urgency as a cause	Table 2 refers to general urgency, while Table 5 focuses on speed over quality
Measurement and Cost Issues	OD not frequently measured or valued due to perceived high cost	Not found	Not found	Survey does not mention measurement and cost issues explicitly
Ineffective Change Management	Poorly managed change, leadership decisions avoiding disruption	Outdated processes and structures	Both address change management	Literature includes leadership decisions, while survey focuses on outdated processes
Technical and Design Debt	Not found	Complex codebases, inconsistent UI, outdated design guidelines	Both acknowledge technical aspects	Survey provides detailed technical causes not mentioned in the review

dling OD preventatively as it tends to spread throughout the organisation and threaten its sustainability.

This paper also sought to find out different approaches of recognizing, evaluating, and managing OD. People stressed the need to use number indicators, consumers' responses, and customer satisfaction rates to identify potential causes of OD, as well as, collaborate with different departments. These findings support previous studies that have been done on the best practices for the management of NTDs [2]. Additionally, fostering a culture of continuous improvement, open communication, and cross-functional collaboration emerged as crucial elements in combating OD effectively. Mitigating TD involved practices such as dedicated time for code refactoring, rigorous code reviews, and investment in test automation, consistent with established software engineering best practices [34]. Addressing debt required process optimization, robust knowledge management practices, and collaboration with product teams. Mitigating cultural debt necessitated promoting open communication, fostering a culture of continuous improvement, and prioritizing user experience throughout the product development lifecycle.

The findings of this study contribute to the growing body of knowledge on OD and provide valuable insights for software organizations seeking to enhance their long-term success. By recognizing the multifaceted nature of OD and implementing proactive mitigation strategies, organizations can minimize the accumulation of debt and foster an environment conducive to innovation, quality, and customer satisfaction. However, it is important to acknowledge the limitations of this study, such as the relatively small sample size, reliance on self-reported data, and the potential for response biases.

Future research should aim to address these limitations by employing larger and more diverse samples, triangulating data from multiple sources, and conducting longitudinal studies to further strengthen the understanding of OD and its implications. Additionally, the evolving nature of OD necessitates ongoing research to keep pace with the dynamic landscape of software development and organizational practices. Exploring the quantification of OD, estimating its economic costs, and examining the relationship between OD and factors such as workforce motivation, customer satisfaction, and project success could provide valuable insights for effective debt management. Collaboration between academia and industry practitioners is crucial in this endeavour, as it fosters the integration of theoretical frameworks and practical insights, ultimately leading to the development of context-specific strategies rooted in both rigour and pragmatism.

7. Conclusion

This study demonstrates that OD extends beyond technical debt, encompassing a broad range of organizational inefficiencies, including outdated processes, misaligned structures, and cultural barriers. OD integrates both technical and non-technical debt, influencing organization's ability to maintain agility, adaptability, and competitiveness. The accumulation of OD hinders decision-making, slows innovation, and weakens the organization's competitive edge. By recognizing and addressing OD through proactive measures such as interdepartmental collaboration and continuous improvement, organizations can reduce their debt and create an environment conducive to long-term success. This study has shed light on the multifaceted nature of OD, its causes, consequences, and potential mitigation strategies within software organizations.

The survey findings revealed a growing awareness of OD among software professionals, recognizing its impact on various aspects of an organization, including inefficient processes, code quality issues, user experience challenges, and employee frustration. The causes of OD were found to be diverse, with rapid growth, communication barriers, outdated processes, and resource constraints contributing to the accumulation of different types of debt, such as technical debt, process debt and cultural debt.

Notably, the consequences of OD extend beyond technical aspects, affecting an organization's competitiveness, employee morale, adaptability, and overall efficiency. This underscores the importance of proactively addressing OD to ensure long-term success and sustainability. The study explored various strategies for identifying, assessing, and mitigating OD, emphasizing the importance of leveraging quantitative metrics, user feedback, customer satisfaction data, and interdepartmental collaboration. Fostering a culture of continuous improvement, open communication, and cross-functional collaboration emerged as crucial elements in combating OD effectively.

Mitigating technical debt involved practices such as dedicated time for code refactoring, rigorous code reviews, and investment in test automation. Addressing process debt required process optimization, robust knowledge management practices, and collaboration with product teams. Mitigating cultural debt necessitated promoting open communication, fostering a culture of continuous improvement, and prioritizing user experience throughout the product development lifecycle. While this study contributes to the growing understanding of OD, it is essential to acknowledge its limitations and the need for further research. Future studies should aim to address these limitations by employing larger and more diverse samples, triangulating data from multiple sources, and conducting longitudinal studies to provide a more comprehensive and dynamic understanding of OD. Additionally, exploring the quantification of OD, estimating its economic costs, and examining its relationship with factors such as workforce motivation, customer satisfaction, and project success could yield valuable insights for effective debt management. Collaboration between academia and industry practitioners is crucial in this endeavour, fostering the integration of theoretical frameworks and practical insights to develop context-specific strategies rooted in both rigour and pragmatism.

In conclusion, the concept of organizational debt represents a critical challenge for software organizations striving for agility, adaptability, and long-term success. By recognizing the multifaceted nature of OD, implementing proactive mitigation strategies, and fostering a culture of continuous improvement and open communication, organizations can minimize the accumulation of debt and foster an environment conducive to innovation, quality, and customer satisfaction. Ongoing research and collaboration between academia and industry are essential to further advance the understanding and effective management of organizational debt in the software development domain.

Acknowledgments. This work was supported by the KK-stiftelsen (grant no. 20200253), Helge Axson Johnsons Stiftelse, and STINT - Swedish Foundation for International Cooperation in Research and Higher Education (IB2020-8720).

References

1. Adizes, I., Cudanov, M., Rodic, D.: Timing of proactive organizational consulting: difference between organizational perception and behaviour. Amfiteatru Economic 19(44), 232 (2017)

2. Ahmad, M.O., Gustavsson, T.: The pandora's box of social, process, and people debts in software engineering. Journal of Software: Evolution and Process p. e2516 (2022)
3. Ahmad, M.O.: A deep dive into self-regulated learning: Reflective diaries role and implementation strategies. Communications of the Association for Information Systems 54(1), 868–888 (2024)
4. Ahmad, M.O.: Psychological safety, leadership and non-technical debt in large-scale agile software development. In: 2023 18th Conference on Computer Science and Intelligence Systems (FedCSIS). pp. 327–334. IEEE (2023)
5. Ahmad, M.O.: 5g secure solution development and security master role. In: Proceedings of the 28th International Conference on Evaluation and Assessment in Software Engineering. pp. 629–633 (2024)
6. Ahmad, M.O., Al-Baik, O.: Beyond technical debt unravelling organisational debt concept. In: Proceedings of the 39th ACM/SIGAPP Symposium on Applied Computing. pp. 802–809 (2024)
7. Ahmad, M.O., Dennehy, D., Conboy, K., Oivo, M.: Kanban in software engineering: A systematic mapping study. Journal of Systems and Software 137, 96–113 (2018)
8. Ahmad, M.O., Gustavsson, T.: Nexus between psychological safety and non-technical debt in large-scale agile enterprise resource planning systems development. In: Conference on Practical Aspects of and Solutions for Software Engineering. pp. 63–81. Springer (2023)
9. Ahmad, M.O., Gustavsson, T., Saeeda, H.: Customised roles in scrum teams for the development of secure solution. In: 2023 49th Euromicro Conference on Software Engineering and Advanced Applications (SEAA). pp. 362–369. IEEE (2023)
10. Al-Baik, O., Miller, J.: Kaizen cookbook: The success recipe for continuous learning and improvements. In: 2016 49th Hawaii International Conference on System Sciences (HICSS). pp. 5388–5397. IEEE (2016)
11. Al-Baik, O., Miller, J.: Integrative double kaizen loop (idkl): towards a culture of continuous learning and sustainable improvements for software organizations. IEEE transactions on Software Engineering 45(12), 1189–1210 (2018)
12. Al-Tarawneh, A.M.: An analysis of the positive and negative effects of cyberpsychotherapy: A systematic review. In: 2024 2nd International Conference on Cyber Resilience (ICCR). pp. 1–4. IEEE (2024)
13. Anderson, E.W., Sullivan, M.W.: The antecedents and consequences of customer satisfaction for firms. Marketing science 12(2), 125–143 (1993)
14. Audit, T.S.N.: Föråldrade it-system–hinder för en effektiv digitalisering (2019)
15. Avgeriou, P., Kruchten, P., Ozkaya, I., Seaman, C.: Managing technical debt in software engineering (dagstuhl seminar 16162). Dagstuhl reports 6(4) (2016)
16. Avgeriou, P.C., Taibi, D., Ampatzoglou, A., Fontana, F.A., Besker, T., Chatzigeorgiou, A., Tsintzira, A.A.: An overview and comparison of technical debt measurement tools. IEEE software 38(3), 61–71 (2020)
17. Behutiye, W.N., Rodríguez, P., Oivo, M., Tosun, A.: Analyzing the concept of technical debt in the context of agile software development: A systematic literature review. Information and Software Technology 82, 139–158 (2017)
18. Besker, T., Martini, A., Bosch, J.: Managing architectural technical debt: A unified model and systematic literature review. Journal of Systems and Software 135, 1–16 (2018)
19. Blank, S.: Organizational debt is like technical debt–but worse (2015)
20. Braun, V., Clarke, V.: Thematic analysis. American Psychological Association (2012)
21. Cunningham, W.: The wycash portfolio management system. In: Addendum to the Proceedings on Object-oriented Programming Systems, Languages, and Applications (Addendum). ACM, Vancouver, British Columbia, Canada (1992)
22. DeLone, W.H., McLean, E.R.: The delone and mclean model of information systems success: a ten-year update. Journal of management information systems 19(4), 9–30 (2003)

23. Dodgson, M., Gann, D.M., Phillips, N.: Organizational learning and the technology of foolishness: The case of virtual worlds at ibm. Organization science 24(5), 1358–1376 (2013)
24. Edmondson, A.: Psychological safety and learning behavior in work teams. Administrative science quarterly 44(2), 350–383 (1999)
25. Ernst, N.A., Bellomo, S., Ozkaya, I., Nord, R.L., Gorton, I.: Measure it? manage it? ignore it? software practitioners and technical debt. In: Proceedings of the 2015 10th Joint Meeting on Foundations of Software Engineering. pp. 50–60 (2015)
26. of Finance, D.M.: Regeringens kasseeftersyn på it-området (2017)
27. Haddaway, N.R., Collins, A.M., Coughlin, D., Kirk, S.: The role of google scholar in evidence reviews and its applicability to grey literature searching. PloS one 10(9), e0138237 (2015)
28. Helfat, C.E., Finkelstein, S., Mitchell, W., Peteraf, M., Singh, H., Teece, D., Winter, S.G.: Dynamic capabilities: Understanding strategic change in organizations. John Wiley & Sons (2009)
29. Holan, P.M.D., Phillips, N.: Organizational forgetting. Handbook of organizational learning and knowledge management pp. 433–451 (2012)
30. Kemerer, C.F., Slaughter, S.: An empirical approach to studying software evolution. IEEE transactions on software engineering 25(4), 493–509 (1999)
31. Khomyakov, I., Makhmutov, Z., Mirgalimova, R., Sillitti, A.: Automated measurement of technical debt: A systematic literature review. In: International Conference on Enterprise Information Systems. pp. 95–106 (2019)
32. Kitchenham, B.A., Pfleeger, S.L.: Personal opinion surveys. In: Guide to advanced empirical software engineering, pp. 63–92. Springer (2008)
33. Klinger, T., Tarr, P., Wagstrom, P., Williams, C.: An enterprise perspective on technical debt. In: Proceedings of the 2nd Workshop on managing technical debt. pp. 35–38 (2011)
34. Lenarduzzi, V., Besker, T., Taibi, D., Martini, A., Fontana, F.A.: A systematic literature review on technical debt prioritization: strategies, processes, factors, and tools. Journal of Systems and Software 171, 110827 (2021)
35. LePine, J.A., Podsakoff, N.P., LePine, M.A.: A meta-analytic test of the challenge stressor–hindrance stressor framework: An explanation for inconsistent relationships among stressors and performance. Academy of management journal 48(5), 764–775 (2005)
36. Liechti, O., Pasquier, J., Reis, R.: Supporting agile teams with a test analytics platform: a case study. In: 2017 IEEE/ACM 12th International Workshop on Automation of Software Testing (AST). pp. 9–15. IEEE (2017)
37. Liu, Z., Stray, V., Sporsem, T.T.: Organizational debt in large-scale hybrid agile software development: A case study on coordination mechanisms. In: Agile Processes in Software Engineering and Extreme Programming–Workshops: XP 2022 Workshops, Copenhagen, Denmark, June 13–17, 2022, and XP 2023 Workshops, Amsterdam, The Netherlands, June 13–16, 2023, Revised Selected Papers. Springer (2023)
38. Luthans, F., Youssef-Morgan, C.M.: Psychological capital: An evidence-based positive approach. Annual review of organizational psychology and organizational behavior 4(1), 339–366 (2017)
39. Marjanović, J., Dalčeković, N., Sladić, G.: Blockchain-based model for tracking compliance with security requirements. Computer Science and Information Systems 20(1), 359–380 (2023)
40. Martini, A., Besker, T., Bosch, J.: Process debt: a first exploration. In: 27th Asia-Pacific Software Engineering Conference. pp. 316–325. IEEE (2020)
41. Maslach, C., Schaufeli, W.B., Leiter, M.P.: Job burnout. Annual review of psychology 52(1), 397–422 (2001)
42. Matkovic, P., Maric, M., Tumbas, P., Sakal, M.: Traditionalisation of agile processes: Architectural aspects. Computer Science and Information Systems 15(1), 79–109 (2018)
43. Morgeson, F.P., Hofmann, D.A.: The structure and function of collective constructs: Implications for multilevel research and theory development. Academy of management review 24(2), 249–265 (1999)

44. Mowday, R.T., Porter, L.W., Steers, R.M.: Employee—organization linkages: The psychology of commitment, absenteeism, and turnover. Academic press (2013)
45. Nadler, D.A., Tushman, M.L.: A model for diagnosing organizational behavior. Organizational Dynamics 9(2), 35–51 (1980)
46. Piqueres, C.: Managing debt: Organizational debt (2021), https://carlos-piqueres.medium.com/managing-debt-organizational-debt-a7a1578235f3
47. Poth, A., Kottke, M., Riel, A.: Self-service kits to scale knowledge to autonomous teams-concept, application and limitations. Computer Science and Information Systems 20(1), 229–249 (2023)
48. Rainer, A., Hall, T.: Key success factors for implementing software process improvement: a maturity-based analysis. Journal of Systems and Software 62(2), 71–84 (2002)
49. Rios, N., de Mendonca Neto, M.G., Spinola, R.O.: A tertiary study on technical debt: types, management strategies, research trends, and base information for practitioners. Information Software Technology 102, 117–145 (2018)
50. Rios, N., Spinola, R.O., Mendonça, M., Seaman, C.: The practitioners' point of view on the concept of technical debt and its causes and consequences: a design for a global family of industrial surveys and its first results from brazil. Empirical Software Engineering 25, 3216–3287 (2020)
51. Senge, P.M.: The fifth discipline: The art and practice of the learning organization. Broadway Business (2006)
52. Tamburri, D.A., Kruchten, P., Lago, P., Vliet, H.V.: Social debt in software engineering: insights from industry. Journal of Internet Services and Applications 6(1), 1–17 (2015)
53. Turab, N., Abu Owida, H., Al-Nabulsi, J.I.: Harnessing the power of blockchain to strengthen cybersecurity measures: a review. Indonesian Journal of Electrical Engineering and Computer Science 3(1), 593–600 (July 2024)
54. Wasserman, S., Faust, K.: Social network analysis: Methods and applications (1994)

APPENDIX A: Survey questions

Category	**Questions**
Participants background	What is your sex?
	What is your title?
	What is your age?
	How many years of experience do you have?
Organizational Information	What is your organization size?
	What domain is the organization operating in?
Awareness and Identification of Organizational Debt	Are you familiar with the concept of organizational debt (OD)?
	How would you describe your organization's current level of OD? (Operational, Managerial, Executive)
	What indicators or symptoms do you use to identify the presence of OD in your organization? (e.g., inefficient processes, outdated policies, employee dissatisfaction)
	Do you have any specific processes or methods in place to assess and monitor OD levels?
Causes and Consequences of Organizational Debt	In your opinion, what are the primary causes or factors contributing to the accumulation of OD in your organization? (e.g., rapid growth, lack of communication, outdated structures)
	What impact has OD had on your organization? (e.g., decreased productivity, employee turnover, difficulty adapting to change)
Mitigation Strategies and Practices	Does your organization have any strategies or practices in place to mitigate or reduce OD?
	If yes, please describe the strategies or practices you use to mitigate OD.
	How effective have these strategies or practices been in mitigating OD? (Very effective, Somewhat effective, Not effective)
	What challenges or obstacles have you faced in implementing strategies to mitigate OD?
Additional Comments and Feedback	Do you have any additional comments, suggestions, or insights regarding the identification, impact, or mitigation of organizational debt in software organizations?

APPENDIX B: Definition of various types of debt [2] [6]

Debt type	Definition
Technical debt	The debt incurred through the speeding up of software project development which results in a number of deficiencies ending up in high maintenance overheads
Non-technical debt	It is an umbrella term to cover a combination of social and technical aspects, such as process, social, and people debt.
Process debt	Refers to inefficient processes, for example, what the process was designed to handle may be no longer appropriate
Social debt	Social debt is analogous to technical debt in many ways: It represents the state of software development organizations as the result of "accumulated" decisions. In the case of social debt, decisions are about people and their interactions.
People debt	People debt Refers to people issues that, if present in the software organization, can delay or hinder some development activities. An example of this kind of debt is expertise concentrated in too few people, as an effect of delayed training and/or hiring
Organisational debt	OD refers to the difference between a company's strategic plans and its actual ability to implement them in view of the ever-changing market needs

Muhammad Ovais Ahmad is an associate professor at Karlstad University Sweden and adj. professor at the University of Oulu, Finland. He received his PhD and MSc degree in Information Processing Science from University of Oulu, Finland. Previously, he worked as a Professor of software engineering at the Gdansk University of Technology, Poland; research fellow and programme coordinator of the European Masters Programme in Software Engineering at the University of Oulu, Finland. Dr. Ahmad's research interests are focused on software development methodologies, evidence based software engineering, process assessment and improvement, software engineering curriculum and pedagogy, technology and digital services adoption and diffusion. He has published in journals such as the Journal of Systems and Software, Software Quality Journal, Information & Software Technology, Information Systems Frontiers, Information Technology and People, IET Software, Journal of Software: Evolution and Process, Journal of Cleaner Production, Transforming Government: People, Process and Policy, e-Informatica Software Engineering Journal.

Osama Al-Baik is a quality-oriented professional with over 20 years of experience and technical expertise in diverse range of technologies within multiple industry settings. He has held senior positions in international and domestic organizations. Dr. Osama received his Doctorate degree in Software Engineering and Intelligent Systems from University of Alberta, Canada; Master Degree in Software Engineering and Project Management from DePaul University, USA. Dr. Osama has also a PGP in AI and Machine Learning from University of Texas at Austin, USA. Dr. Osama's research interests have been in Software Engineering, Health Information Systems, Lean Operations, Process improvements and Optimization, Lean Product Development, Lean Service Excellence, and the Sociocultural aspects of Software Engineering.

AbdelRahman Hussein is an Associate Professor at the Department of Computer Science at Al-Ahliyya Amman University, Jordan. He received his first degree in Computer Science from Jordan University of Science and Technology, Jordan, in July 2000, master degree in Computer Science from Jordan University, Jordan in July 2003, and Ph.D. from the Anglia Ruskin University ARU), UK in 2010. His main research interests lie in the areas of VoIP, mobile Ad-Hoc networking, and E-learning.

Mwaffaq Abu Alhija is an Associate Professor at the Department of Computer Science, Applied Science Private University, Amman, Jordan. His main research interests lie in the areas of operating system design, distributed computing systems, multimedia communication and networking, mobile and wireless networks, data and network security, wireless sensor networks, Cybersecurity, and parallel computing.

Received: April 11, 2024; Accepted: December 20, 2024.